PHYS

VOLUME 61

THE PHYSICAL REVIEW

A journal of experimental and theoretical physics established by E. L. Nichols in 1893

Published by the American Institute of Physics
for the
AMERICAN PHYSICAL SOCIETY

Officers

President

I. I. RABI
Columbia University
New York, New York

Vice-President

C. C. LAURITSEN
California Institute of Technology
Pasadena, California

Secretary

K. K. DARROW
Bell Telephone Laboratories
Office:
Columbia University
New York 27, New York

Treasurer

G. B. PEGRAM
Columbia University
New York 27, New York

Local Secretary
for the Pacific Coast

J. KAPLAN
University of California at Los Angeles
Los Angeles, California

Managing Editor

E. L. HILL
University of Minnesota
Minneapolis, Minnesota

BOARD OF EDITORS

Editor

E. L. HILL

Assistant Editor

J. W. PEARL

Associate Editors

S. A. GOUDSMIT — W. E. LAMB, JR. — HARVEY BRINKMAN
E. M. PURCELL — R. G. HERB — R. F. CHRIST
V. F. WEISSKOPF — J. BARDEEN — ERWIN HAHN

Manuscripts for publication should be submitted to E. L. Hill, University of Minnesota, Minneapolis, Minnesota. The authors' institution is requested to pay a publication charge of $8 per page which, if honored, entitles them to 100 free reprints. Instructions will be sent with galley proof.

Proof and all correspondence concerning papers in the process of publication should be addressed to the Publication Manager, American Institute of Physics, 57 East 55 Street, New York 22, New York.

Subscription Price

United States and Canada $25.00
Elsewhere $27.00

Back Numbers[1]

Yearly back number rate when complete year is available:
Prior to 1949: $20.00
Thereafter: $27.00
Single copies: $2.00 each, prior to July, 1929;
$1.00 each, July, 1929–December, 1941;
$2.00 each, January, 1942–December, 1946;
$1.00 each, January, 1947–December, 1948;
$1.25 each, thereafter.
General Index, 1893–1920: $1.00.

Subscriptions, renewals, and orders for back numbers should be addressed to the American Institute of Physics, 57 East 55 Street, New York 22, New York.

Changes of address in the case of members of the American Physical Society should be addressed to the Treasurer; in the case of other subscribers to the American Institute of Physics.

[1] For Sale: Librarian of Physics Department, Cornell University, Ithaca, New York.

The Physical Review is published semi-monthly at Prince and Lemon Streets, Lancaster, Pennsylvania.

Entered as second-class matter March 6, 1917, at the Post Office at Lancaster, Pennsylvania, under the Act of March 3, 1879.

Acceptance for mailing at special rate of postage provided for in paragraph (d-2), section 34.40, P. L. & R. of 1948, authorized January 23, 1925.

THE
PHYSICAL REVIEW

A journal of experimental and theoretical physics established by E. L. Nichols in 1893

SECOND SERIES, VOL. 81, NO. 3 FEBRUARY 1, 1951

Nuclear Magnetic Moments and Atomic Hyperfine Structure

AAGE BOHR*
Department of Physics, Columbia University, New York, New York
(Received August 7, 1950)

The asymmetric nuclear model discussed in a previous paper provides the basis for a more detailed interpretation of nuclear magnetic moments than the single particle model permits. The structure of the moment which the model implies may be tested by a study of the influence of the finite size of the nucleus on the atomic h.f.s. This effect was investigated previously in cooperation with Weisskopf, and is considered more closely in the present paper with the assumption that the nuclei in question can be described in terms of a single particle moving in an asymmetric nuclear core. The K-isotopes should be well represented by this model, and for these nuclei the theoretical value obtained for the h.f.s. is in close agreement with the observed data. Also for the Rb-isotopes the agreement is satisfactory.

I. INTRODUCTION

IN a recent article[1] a nuclear model was discussed in which the individual nucleons are assumed to move in an average nuclear field which deviates from spherical symmetry. This so-called asymmetric model contains many of the characteristic features of the single particle model, and at the same time incorporates such collective types of nuclear motion as are manifested in the existence of the large electric quadrupole moments.

The asymmetric model implies that the nuclear core possesses rotational degrees of freedom. The character of a nuclear state, and its magnetic moment in particular, is therefore not determined uniquely by the quantum numbers of the single particle motion, but depends also on the coupling of this motion to the asymmetric nuclear core and on the rotational state of the nucleus. For a given total angular momentum of the nucleus the magnetic moment may have any value, within certain limits, corresponding to the observed behavior of nuclear magnetic moments.

In the present state of our knowledge of the coupling of angular momenta in the nucleus, it is in general difficult to make quantitative predictions regarding the value of the magnetic moment. By means of the empirical value of the moment it is possible, however, to determine the character of the nuclear state in question, at any rate for the simplest type of nuclei, those which can be described in terms of a single nucleon moving in a nuclear core which possesses no intrinsic angular momentum.

A detailed model of the nucleus is thereby obtained which can be tested in its relation to other nuclear properties. One such test is provided by an accurate measurement of the atomic hyperfine structure. Because of the distribution of the magnetic moment over the finite volume of the nucleus, the h.f.s. splitting differs slightly from the value corresponding to a point-dipole at the nuclear center. This deviation, the h.f.s. anomaly, depends not only on the size of the nucleus, but also on the intrinsic structure of the moment. Effects of this type have been observed in a number of cases.[2-5]

A theoretical treatment of the h.f.s. anomaly for the case of heavy nuclei was given previously by Weisskopf and the writer.[6] It was found that the part of the nuclear moment due to the intrinsic spin of the nucleons, and the part due to orbital motion in the nucleus, will contribute differently to the h.f.s. anomaly. The effect is therefore especially sensitive to the distribution of the

* On leave from the Institute of Theoretical Physics, Copenhagen, Denmark. The writer is indebted to Columbia University for a fellowship enabling him to take part in research work in the Physics Department. The publication is assisted by the Ernest Kempton Adams Fund for Physical Research.

[1] A. Bohr, Phys. Rev. **80**, 134 (1951). Referred to in the following as A. See also J. Rainwater, Phys. Rev. **79**, 432 (1950).

[2] J. E. Nafe and E. B. Nelson, Phys. Rev. **73**, 718 (1948).
[3] F. Bitter, Phys. Rev. **76**, 150 (1949).
[4] P. Kusch and A. K. Mann, Phys. Rev. **76**, 707 (1949).
[5] Ochs, Logan, and Kusch, Phys. Rev. **78**, 184 (1950).
[6] A. Bohr and V. Weisskopf, Phys. Rev. **77**, 94 (1950). Referred to in the following as B.

nuclear moment on these two types of magnetic moment.

Since no model was then available which could account in detail for the nuclear moments, an approximate estimate of the h.f.s. anomaly was made on the basis of very general assumptions regarding the structure of the nucleus. In the following, we shall attempt a more accurate treatment based on the asymmetric nuclear model. For simplicity, we shall assume that the nuclei in question can be represented in terms of a single nucleon moving with respect to the nuclear core.

II. ANGULAR DISTRIBUTION OF THE SPIN MOMENT

In order to evaluate the h.f.s. anomaly for the spin part of the moment, the assumption was made in **B** that this part of the moment can be represented by a spherically symmetric distribution function. Such an assumption is justified for nuclear models, like the uniform model,[7] which ascribe no exceptional spatial distribution to the nucleons carrying the spin moment. The single particle model, or the asymmetric model, however, implies in general pronounced angular asymmetries in the spin distribution, which may have a considerable influence on the h.f.s. anomaly.

The effect of such asymmetries is given by formula (**B**7). It follows from [**B**(6, 8, and 12)] that the quantity κ_s—representing the anomaly in the spin part of the h.f.s.—must be replaced by κ_s' given by

$$\kappa_s' = \kappa_s + \zeta(\kappa_s - \kappa_L), \tag{1}$$

where

$$\zeta = \frac{-1}{(s_z)_{kk}}((s_x\cos\varphi + s_y\sin\varphi)\tfrac{3}{2}\cos\vartheta\sin\vartheta + s_z(\tfrac{3}{2}\cos^2\vartheta - \tfrac{1}{2}))_{kk}, \tag{2}$$

the averages to be taken for the spin and angular distribution of the odd nucleon in the nucleus.

Extreme Single Particle Model

We first consider the extreme single particle model according to which the total nuclear angular momentum is possessed by the odd nucleon.

The angular distribution and the spin direction of this nucleon are given by the wave functions

$$\psi_+ = Y_{I-\frac{1}{2}}^{I-\frac{1}{2}}(\vartheta, \varphi)\chi^+ \tag{3a}$$

and

$$\psi_- = \frac{1}{(2I+2)^{\frac{1}{2}}} Y_{I+\frac{1}{2}}^{I-\frac{1}{2}}(\vartheta, \varphi)\chi^+ - \left(\frac{2I+1}{2I+2}\right)^{\frac{1}{2}} Y_{I+\frac{1}{2}}^{I+\frac{1}{2}}(\vartheta, \varphi)\chi^- \tag{3b}$$

for the cases of parallel and antiparallel spin and orbital moment, respectively. The total angular momentum is denoted by I, and we are considering the magnetic substate $M=I$. The angular wave functions Y_l^m are the normalized spherical harmonics[8] representing a particle with angular momentum l and magnetic quantum number m. The spin functions χ^+ and χ^- correspond to the eigenvalues $s_z=\frac{1}{2}$ and $s_z=-\frac{1}{2}$, respectively.

The evaluation of ζ gives

$$\zeta = (2I-1)/4(I+1), \quad (I=l+\tfrac{1}{2}) \tag{4a}$$

and

$$\zeta = (2I+3)/4I, \quad (I=l-\tfrac{1}{2}) \tag{4b}$$

for the states (3a) and (3b), respectively.

The asymmetry expressed by the quantity ζ is partly due to the fact that, for $I>\frac{1}{2}$, the particle density is not isotropic, but is a maximum for $\vartheta=\pi/2$. Thus, it is evident from the expressions (2) that ζ approaches the value $\frac{1}{2}$ for large I.

In the case of antiparallel **l** and **s**, an additional effect arises from the fact that the direction of the spin depends on the polar angles of the particle. By means of the recursion formula

$$Y_{I+\frac{1}{2}}^{I-\frac{1}{2}} = -(2I+1)^{\frac{1}{2}}\cot\vartheta\cdot e^{-i\varphi}\cdot Y_{I+\frac{1}{2}}^{I+\frac{1}{2}} \tag{5}$$

the wave function (3b) may be written:

$$\psi_- = f(\vartheta, \varphi)\{\cos\vartheta e^{-\frac{1}{2}i\varphi}\chi^+ + \sin\vartheta e^{\frac{1}{2}i\varphi}\chi^-\}. \tag{6}$$

It follows that the direction of the spin is characterized by the polar angles 2ϑ and φ. It is easily seen that this effect tends to increase ζ by making the magnetic field inside the nucleus depart more strongly from the field produced by a dipole at the nuclear center.

Asymmetric Model. Extreme Coupling Cases

For the asymmetric model, the nuclear wave function is not determined uniquely by the values of I and M, even if we restrict ourselves to the ground state of the nucleus. As discussed in **A**, a number of different coupling cases may arise, depending on the strength of the spin-orbit coupling as compared with the coupling of the nucleon to an axis of the nucleus and the rotational level-spacing of the nucleus.

In the case B_2 (see **A**), of very strong spin-orbit coupling, the particle wave function is again given by (3), except for the fact that the polar angles of the particle are now defined with respect to the axis of the nucleus, and that the spin functions represent states for which the spin is quantized parallel or antiparallel to the nuclear axis. We assume that the asymmetry of the nuclear core is not too large, and that l therefore is a good quantum number. To obtain the wave functions for the entire nucleus, the expressions (3) must be multiplied by the symmetrical top wave function

[7] H. Margenau and E. Wigner, Phys. Rev. **58**, 103 (1940).

[8] The phase factors are those used in E. U. Condon and G. H. Shortley, *The Theory of Atomic Spectra* (Cambridge University Press, 1935).

describing the motion of the nuclear axis, whose polar angles we denote by θ and ϕ.

It is easily seen from (2) that the value of ζ for a nuclear state of this type is equal to the value obtained from the single particle model. In fact, the numerator as well as the denominator of (2) represent the z-component of a vector. If we first keep θ and ϕ fixed, and average over the motion of the particle with respect to the nuclear axis, these two vectors must, for symmetry reasons, have the direction of the nuclear axis. Their ratio is equal to (4), and is not affected by the subsequent averaging with respect to θ and ϕ.

If the spin-orbit coupling is smaller than the coupling of $\mathbf{l}$ to the nuclear axis, but larger than the rotational level spacing of the nucleus, we have the coupling case B_1. The wave function describing the motion of the nucleon with respect to the nuclear axis is given by

$$\psi_+ = Y_{I-\frac{1}{2}}^{I-\frac{1}{2}}(\vartheta', \varphi')\chi^+ \quad (I=l+\tfrac{1}{2}) \tag{7a}$$

and

$$\psi_- = Y_{I+\frac{1}{2}}^{I+\frac{1}{2}}(\vartheta', \varphi')\chi^- \quad (I=l-\tfrac{1}{2}), \tag{7b}$$

where ϑ' and φ' are the polar angles of the particle in the nuclear coordinate system.

In case of parallel $\mathbf{l}$ and $\mathbf{s}$, the coupling cases B_1 and B_2 are identical, but for antiparallel $\mathbf{l}$ and $\mathbf{s}$ the spin direction given by (7b) does not have the dependence on the polar angles which is characteristic of the wave function (3b). The value of ζ for the state (7b) is simply obtained from (4a) by replacing I with $I+1$. Thus

$$\zeta = (2I-1)/4(I+1), \quad (I=l+\tfrac{1}{2}) \tag{8a}$$

and

$$\zeta = (2I+1)/4(I+2), \quad (I=l-\tfrac{1}{2}) \tag{8b}$$

for the states (7a) and (7b), respectively. For small I, the expression (8b) gives values for ζ much smaller than those obtained from (4b).

Finally, if the spin-orbit coupling is smaller than the nuclear rotational level-spacing, we have the coupling case A. The nuclear wave function is given by an expression of the type (3) except that the spherical harmonics must be replaced by wave functions which describe the rotation of the nuclear core as well as the orbital motion of the particle with respect to the nuclear axis.

We first consider the parallel case corresponding to (3a). From (2) it follows that ζ is given by

$$\zeta = -(\tfrac{3}{2}\cos^2\vartheta - \tfrac{1}{2})_{Av}, \tag{9}$$

where ϑ is the polar angle of the nucleon with respect to the fixed z-axis. In order to evaluate (9) it is convenient to express ϑ in terms of the polar angle ϑ' with respect to the nuclear axis. One finds

$$\zeta = -(\tfrac{3}{2}\cos^2\vartheta' - \tfrac{1}{2})_{Av}(\tfrac{3}{2}\cos^2\theta - \tfrac{1}{2})_{Av}, \tag{10}$$

which leads to

$$\zeta = (I-1)(2I-1)^2/4(2I+1)(I+1)^2 \tag{11a}$$

for the state in question.

For antiparallel $\mathbf{l}$ and $\mathbf{s}$, corresponding to (3b), the coupling cases A and B_1 are identical. The value of ζ is therefore given by (8b).

Asymmetric Model. Intermediate Coupling Cases

The empirical nuclear magnetic moments do not, in general, coincide with either of the values corresponding to the three extreme coupling cases considered above. As was pointed out in **A**, it is possible, however, at any rate for the simplest types of nuclei, to account for the magnetic moments in terms of intermediate coupling cases. For the following applications we shall consider coupling cases between B_1 and B_2.

The case of $l=I-\frac{1}{2}$, in which the two models B_1 and B_2 coincide, needs no further treatment. For $l=I+\frac{1}{2}$, the wave function describing the motion of the particle with respect to the nuclear axis will be of the general form:

$$\psi_- = \text{const.}(Y_{I+\frac{1}{2}}^{I-\frac{1}{2}}\chi^+ + \beta Y_{I+\frac{1}{2}}^{I+\frac{1}{2}}\chi^-). \tag{12}$$

The value of β depends on the strength of the l–s coupling compared with the coupling of $\mathbf{l}$ to the nuclear axis.

An evaluation of (2) leads to

$$\zeta = \frac{1}{4(I+2)}\,\frac{1}{\beta^2-1}\{\beta^2(2I+1) - 6\beta(2I+1)^{\frac{1}{2}} + 5 - 2I\}. \tag{13}$$

It will be noted that, for $\beta = -(2I+1)^{\frac{1}{2}}$ and $\beta = \infty$, expression (13) coincides with (4b) and (8b), respectively.

III. THE ORBITAL ANGULAR MOMENTUM

The expression given in **B** for κ_L—representing the anomaly in the orbital part of the h.f.s.—has a simple interpretation if the orbital angular momentum can be ascribed to a single particle. It is therefore immediately applicable to the extreme single particle model.

According to the asymmetric model, the nuclear core also contributes to $\mathbf{L}$. For the corresponding part of the nuclear magnetic moment, the value of κ can be obtained from an expression like (**B**12) if only the radial average is performed for the radial distribution of the orbital magnetic moment in the nuclear core.

Since the contribution of the nuclear rotation to the magnetic moment of the nucleus is in general small, one obtains a first approximation by neglecting the difference between the distribution of the orbital magnetic moment in the core and the radial density distribution of the single particle. The expression (**B**12) can then be used for the total orbital magnetic moment of the nucleus. It must be taken into account, however, that, due to the contribution of the nuclear core, the effective orbital g-factor, g_L, differs somewhat from the single particle value.

IV. RADIAL AVERAGES

According to (**B**18), the radial averages of κ, and κ_L involve essentially the mean value of $(R/R_0)^2$ for the

density distribution of the odd particle. The nuclear radius is denoted by R_0.

On the average, for all the particles in the nucleus, this mean value equals $\frac{3}{5}$, if the nuclear density is constant. For the individual nucleons, however, $(R/R_0)^2_{Av}$ will depend on the kinetic energy and angular momentum and may differ appreciably from $\frac{3}{5}$.

As an indication of the trend of $(R/R_0)^2_{Av}$, it may be noted that in the semiclassical approximation, valid for large quantum numbers, one obtains, for a particle confined within a sphere of constant potential,

$$(R/R_0)^2_{Av}=\tfrac{1}{5}+\tfrac{2}{5}(l^2\hbar^2/2MTR_0^2) \qquad (14)$$

where T is the kinetic energy of the particle, M its mass.

In individual cases, an estimate of $(R/R_0)^2_{Av}$ can be made by assuming the orbit to have the quantum numbers given by the single particle model on the basis of the nuclear spin and the empirical value of the magnetic moment. If the potential is assumed to vanish for $R>R_0$, and for $R<R_0$ to be a constant, which can be determined from the empirical value of the binding energy, the entire particle wave function can then be constructed.

If the odd nucleon is a proton, the influence of the Coulomb forces should be taken into account. This effect is in general rather small, and, since the electrostatic potential does not vary greatly over the region in which the particle spends most of its time, the potential can be approximated by a constant equal to the Coulomb potential at the nuclear surface. This amounts to the introduction of an effective binding energy given by the energy which the proton must acquire in order to be able to leave the nucleus by passing over the barrier.

V. FORMULAS FOR THE H.F.S. ANOMALY

From (1) and (B18), one gets the following expression:

$$\epsilon=-\{(1+0.38\zeta)\alpha_s+0.62\alpha_L\}(R/R_0)^3 \qquad (15)$$

for the h.f.s. anomaly as a fraction of the h.f.s. for a point nucleus. The quantity b is a function of Z and R_0 and is tabulated in **B**.

The fractions of the nuclear moment of spin type and orbital type are denoted by α_s and α_L, respectively. These quantities are given by (B20) in terms of the nuclear g-factors. For the asymmetric model, however, the orbital g-factor depends on the contribution of the nuclear core to the magnetic moment of the nucleus and must itself be determined from the empirical value of the nuclear moment.

We shall in particular consider nuclei for which the angular momentum coupling falls between that of the cases B_1 and B_2. The contribution of nuclear rotation to the magnetic moment is then given by (A1). In the extreme cases, B_1 and B_2, the value of g_0 is given by (A2) and (A3) respectively, but more generally we have

$$Ig_0=\sigma g_s+(I-\sigma)g_l, \qquad (16)$$

where σ represents the average value of the odd particle spin component along the nuclear axis. This quantity is given by

$$\sigma=(1-\beta^2)/2(1+\beta^2) \qquad (17)$$

in terms of the coefficient β in the wave function (12).

From (16) and (A1) one obtains

$$\sigma=[(I+1)g_I-g_R-Ig_L]/(g_s-g_l), \qquad (18)$$

where g_R is the g-factor for the nuclear rotation. Its value is somewhat uncertain, but is expected to be of the order of Z/A.

Expression (18) gives σ in terms of the empirical value of g_I. The quantities α_s and α_L are then determined by

$$\alpha_s=\sigma g_s/(I+1)g_I, \quad \alpha_L=1-\alpha_s. \qquad (19)$$

Moreover, (17) gives the value of β from which ζ can be found by means of (13).

It should be noted that (17) gives only the numerical value of β, while ζ depends also on the sign of β. For a particle moving in a field of cylindrical symmetry, there are two eigenstates of the type (12), one with positive and one with negative β. It is easily seen that if the spin orbit coupling favors large j (parallel coupling of **l** and **s**), the state of positive β has the lowest energy. If the sign of the spin orbit coupling is reversed, β must be taken to be negative for the state of lowest energy.

VI. DISCUSSION OF EXPERIMENTAL DATA

K

A particularly instructive example of h.f.s. anomalies is provided by the recent accurate measurement by Ochs, Logan, and Kusch[5] of the nuclear moments of the odd K-isotopes and of the h.f.s. of the ground states of the corresponding atoms. In fact, the K-nuclei ($Z=19$) contain just one proton less than the number required for a closed shell. These nuclei are expected to be well represented by the model of a single particle moving in a nuclear core of no intrinsic angular momentum. Their magnetic moments can be accounted for in terms of a coupling case between B_1 and B_2.

The ground states of the isotopes K^{39} and K^{41} have $I=\frac{3}{2}$. The odd particle (formally the proton lacking in a closed shell configuration) is expected to be in a $3d$ state. For an effective binding energy (see Section IV) of 12 Mev, one finds a value for $(R/R_0)^2_{Av}$ of 0.66. It may be noted that this value is only changed by about 1 percent if the effective binding is altered by 2 Mev.

From (18), one finds for $g_R=\frac{1}{2}$ the values $\sigma=-0.294$ and $\sigma=-0.359$ for K^{39} and K^{41}, respectively. The corresponding values of α_s obtained from (19) are -2.52 and -5.59. According to the considerations in Section V, the sign of β is negative. In fact, the spin-orbit coupling is assumed to favor large j, but the sign of this coupling is formally reversed for a particle lacking in a closed shell configuration. From (17) one thus finds

$\beta=-1.96$ and -2.46 for K^{39} and K^{41}, respectively, leading by means of (13) to the ζ values 1.02 and 0.79.

The table in **B** gives a value for b of 0.19 percent and from (15) one finally obtains

$$\epsilon(K^{39})=0.165 \text{ percent}, \quad \epsilon(K^{41})=0.396 \text{ percent}, \quad \Delta=\epsilon_{39}-\epsilon_{41}=-0.23 \text{ percent}. \tag{20}$$

The experimental value of Δ is $-(0.226\pm0.010)$ percent.

The model of the K^{39} nucleus is not quite consistent, since β is found to be slightly smaller, numerically, than the value $-(2I+1)^{\frac{1}{2}}=-2$ corresponding to a wave function for the limiting coupling case B_2. The value obtained for β corresponds to an eigenstate only if the coupling of **l** to the nuclear axis favors small values of Ω, in contradiction to the assignment $\Omega=\frac{3}{2}$ for the ground state of the nucleus.

As already mentioned, however, the choice $g_R=\frac{1}{2}$ is rather uncertain, and a slight increase of g_R suffices to make $|\beta|$ exceed 2. It may be added that even a large increase of g_R has a very small influence on Δ. For $g_R=1$, one finds $\epsilon_{39}=0.194$ percent, $\epsilon_{41}=0.432$ percent, and $\Delta=-0.24$ percent.

On the basis of the asymmetric model it thus appears to be possible to account simultaneously for the nuclear moments and for the h.f.s. anomalies of the K-isotopes.

Rb

A h.f.s. anomaly has also been observed for the Rb isotopes.[8] If, as a first approximation, these nuclei are described by the model of a single proton moving in an asymmetric nuclear core, Rb^{85} may be considered in complete analogy to the K-isotopes. For $g_R=\frac{1}{2}$, one finds $\sigma=-0.49$, $\beta=-1.7$, $\zeta=1.25$ and, $\alpha_s=-0.71$, which leads to a vanishing value of ϵ_{85}.

The magnetic moment of Rb^{87} ($I=\frac{3}{2}$) comes close to the value corresponding to the extreme coupling case B_1. For $g_R=0.8$, this coincidence would be exact; for $g_R=0.5$, a coupling case tending slightly towards A would need to be assumed. With a sufficient accuracy ζ can be obtained from (8a), giving $\zeta=0.2$. The value of α_s is close to 0.6 and is not very sensitive to the choice of g_R.

The odd particle is expected to be in a $3p$ state. For an effective binding energy of 15 Mev the value of $(R/R_0)^2_{hw}$ is found to be 0.49. The table in **B** gives $b=0.58$ percent, and one thus obtains $\epsilon_{87}=-0.26$ percent and, consequently, $\Delta=\epsilon_{85}-\epsilon_{87}=0.26$ percent. This value is to be compared with the empirical value of 0.33 ± 0.05 percent.

The agreement is presumably as close as could be expected since the nuclei in question may need to be considered in terms of the motion of several equivalent protons.

Other Elements

Apart from the light elements H and Li, for which the nuclear models here discussed do not apply and for which special considerations are necessary,[9] K and Rb constitute the only elements for which experimental evidence has so far been obtained regarding the effect on the h.f.s. of the intrinsic structure of the nuclear moment. Additional evidence would be of value as a further test of nuclear models.

There exist a number of other elements for which the effect, as in the two above-mentioned cases, can be determined by an accurate measurement of the h.f.s. ratio in the atomic ground state for two isotopes.

For the heavy elements, for which the h.f.s. anomaly may become very large, of the order of five percent, it may be possible to detect the effect in the h.f.s. of a single isotope if the electronic wave function can be determined with sufficient accuracy.[10]

---

[9] A. Bohr, Phys. Rev. **73**, 1109 (1948); F. Low, Phys. Rev. **77**, 361 (1950).

[10] M. F. Crawford and A. Schawlow, Phys. Rev. **76**, 1310 (1949); A. Bohr and A. Schawlow (in preparation).

The Existence of Different Capture Levels in the Formation of Nuclear Isomers by Slow Neutron Irradiation

P. C. CAPRON AND A. J. VERHOEVE-STOKKINK*
Institut Inter-Universitaire de Physique Nucléaire, University of Louvain, Louvain, Belgium
(Received June 23, 1950)

Experiments have been performed on the formation of bromine and rhodium isomers, by thermal as well as resonance neutrons, in order to study capture levels. With slow neutrons of variable energies obtained from a Ra–Be source in a slowing-down medium of paraffin, we have studied: (a) the relative formation of the isomeric pairs as a function of the distance from the source and (b) the migration distances for each isomer.

The experimental results show that for bromine isomers produced by resonance neutrons as well as for rhodium isomers produced by resonance and *C*-neutrons, the ratio of the activities of the fundamental state to the metastable state is a function of the distance from the source. Moreover, at each point this ratio is different for resonance and for *C*-neutrons. The migration distances corresponding to each of the isomers formed by resonance neutrons on bromine, or by *C*-neutrons on rhodium, are found to be different.

This leads to the assumption of the existence of more than one capture level in the formation of the bromine and rhodium isomers. It may be suggested that for rhodium the resonance levels extend within the region defined by the *C*-neutrons.

I. INTRODUCTION

THE question of whether nuclear isomers, such as the isomers of Br^{80}, Rh^{104}, or In^{119} arise from one or more capture levels, is still undecided.[1–9] In order to elucidate this problem, we have investigated the formation of two of these isomeric pairs by means of slow neutrons irradiation by the reactions

$$\text{Br}^{79}(n,\gamma)\text{Br}^{80*}\begin{cases}\nearrow \text{Br}^{80}(4.4\text{ hr})\\ \searrow \text{Br}^{80}(18\text{ min})\end{cases},$$

$$\text{Rh}^{103}(n,\gamma)\text{Rh}^{104*}\begin{cases}\nearrow \text{Rh}^{104}(4.2\text{ min})\\ \searrow \text{Rh}^{104}(44\text{ sec})\end{cases}.$$

The object was to examine separately "resonance" and "thermal" capture levels for both isomers and to work with a sufficiently high precision to decide whether neutron capture levels corresponding to nuclear isomers are simple or multiple.

Using a Ra–Be neutron source in a slowing-down medium of paraffin, we studied: (a) the relative formation of the isomeric pairs as a function of decreasing neutron energy (increasing distance from the source), (b) the migration distances of the neutrons in the paraffin for each isomer.

A variable ratio for the activities of the two isomers, as well as a difference between their migration distances, would give an indication in favor of the multiplicity of the capture levels.

II. PROCEDURE

The slow neutrons were produced by a Ra–Be neutron source fixed in the center of a paraffin block 50 cm high and 40 cm in diameter. The bromine or rhodium detectors were placed in the paraffin block at increasing distances from the source.

In one part of the experiments the detectors were wrapped in a Cd shield, so that activation was only due to "resonance" neutrons; *viz.* all the effective neutrons had energies higher than the Cd resonance energy (0.17 ev). The second part concerned experiments without Cd, the difference of the two series giving the activation of "*C*-neutrons," which are considered practically to be the neutrons in the thermal region (0.028 ev).

The bromine sample was irradiated for 15 hours by a one-Curie Ra–Be source. The detector consisted of a square, 3 cm per side, of carbon tetrabromide, 0.2 g/cm² wrapped in Cellophane.

Activity[10] due to the Br^{82} (34 hr) was eliminated, so that the remaining activity corresponded to the isomers Br^{80}(4.4 hr) and Br^{80}(18 min).

The rhodium sample was irradiated for 70 min. The activity caused by the isomer of 44-sec period is nearly ten times as high as that of the 4.2-min period, so that when we take the activity of the latter sufficiently high to be counted with good accuracy, the activity of the short-lived isomer is so high that the corrections for the resolving time of the counting apparatus would preclude

* Research physicist of the Laboratoire de Recherches Physiques des Ateliers de Constructions Electriques de Charleroi (A.C.E.C.), at Charleroi, Belgium.

[1] E. Segrè, Ricerca sci. **VII**, 389 (1936).
[2] E. Amaldi and E. Fermi, Phys. Rev. **50**, 899 (1936).
[3] R. Fleischmann, Z. f. Physik **107**, 205 (1937).
[4] Frisch, Koch, and von Halban, Congrès du Palais de la Découverte 119, October 1937, Paris.
[5] B. Pontecorvo, Nature **141**, 785 (1938).
[6] P. Capron, Bull. acad. roy. Belg. **27**, 524 (1941).
[7] Goldsmith and Rasetti, Phys. Rev. **50**, 328 (1936).
[8] Mitchell and Langer, Phys. Rev. **53**, 505 (1938).
[9] Keller and Preiswerk, Helv. Phys. Acta **11**, 372 (1938).
[10] See the Segrè chart in *The Science and Engineering of Nuclear Power*, Ed. Clark Goodman (Cambridge, 1947), for the half-lives.

good accuracy. We found, indeed, that the resolving time may vary with the activity, as has already been stated by others.[11] Thus, in a first series of experiments we measured only the activity of the 4.2-min period as a function of the distance from the source. We therefore used a one-Curie source and a square metallic Rh sample 2.4 cm per side, of 0.123 g/cm².

In a second series of experiments we determined only the ratio of the activities of the two isomers, as a function of the distance from the source. This time a 200-millicurie source was used, the samples being squares with areas increasing (from 0.71 to 2.4 cm per side) with the distance from the source. In this manner we obtained approximately equal initial activities at each point in the paraffin. The activity was kept sufficiently low that no correction for resolving time would be necessary. The statistical error was reduced to about one percent by repetition of the measurements.

The combination of the two series gave us the activities of both isomers as functions of the distance from the source, referred to a one-Curie source and a standard sample of surface $(2.4)^2$ cm².

For rhodium as well as for bromine, the distances in the paraffin were corrected for the sizes of the source and the sample in a manner similar to that of Rush.[12]

The irradiation times were practically infinite for the different half-lives, except for the 4.4-hr activity, which was corrected for infinite irradiation. The resulting counting-rates were measured by a Geiger-Müller counting system.

The initial counting rates, *viz.* the activities of both isomers at the end of the irradiation time, were determined from the total measured activity in the classical way. The counting times were long compared with the half-lives. In this way, the statistical errors were minimized,[13] because the deviation for a simple element is of the form:

$$\sigma = \{A_{1,2} \exp[-\lambda(t_1 - t_2)]\}^{\frac{1}{2}},$$

where $A_{1,2}$ is the total activity measured in the time from t_1 to t_2, so that the exponential is much smaller than unity if the time interval is large.

The determination of the mean square of the migration distance: $\langle r^2 \rangle_{Av}$, was based on the classical formulas, fitted to each isomer:[2,12]

$$\langle r^2 \rangle_{Av} = \left(\int_0^\infty \mathrm{Ar}^4 dr \right) \Big/ \left(\int_0^\infty \mathrm{Ar}^3 dr \right),$$

where A is the activity, and r is the distance from the source. These integrals are resolved into two parts. First, a graphical integration on the experimental points between 0 and 9 cm. For further distances the $\mathrm{Ar}^2(r)$ curve is considered to be exponential of the form e^{-ur}.

[11] C. O. Muehlhause and H. Friedman, Rev. Sci. Instr. **17**, 506 (1946).
[12] H. J. Rush, Phys. Rev. **73**, 271 (1948).
[13] G. Friedlander and J. W. Kennedy, *Introduction to Radiochemistry* (John Wiley and Sons, Inc., New York, 1949), p. 207.

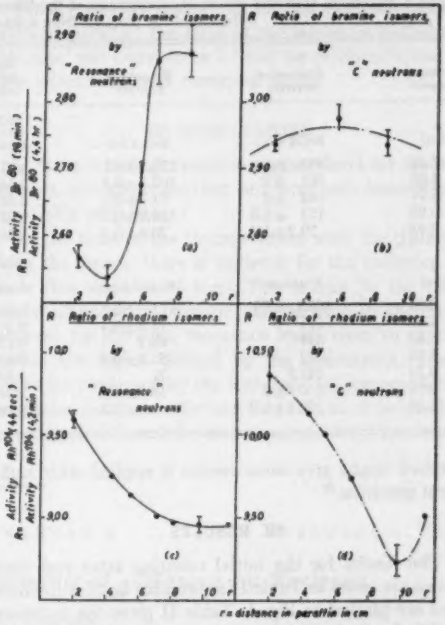

FIG. 1. Ratio of the saturated activities of the nuclear isomers of Br^{80} and Rh^{104} produced by resonance and by C-neutrons as a function of the distance from a Ra–Be neutron source in a paraffin medium. Distances are corrected for the sizes of the source and the sample. The indicated deviations are the probable statistical errors.

For bromine we used $u = 0.123$ cm^{-1} which is deduced from data by Rush.[12] For rhodium this coefficient was determined from our own experiments, where $u = 0.090$ cm^{-1} which is comparable to the data by Bakker.[14] This is why our values $\langle r^2 \rangle_{Av}$ for Br and Rh are not directly comparable, but we are only interested here in the relative values for each isomer.

It would be interesting to find the real values of the resonance energy corresponding to each of the isomers, but this is not possible in our case, for the known relation:[2,15]

$$\ln(W/W') = [\langle r'^2 \rangle_{Av} - \langle r^2 \rangle_{Av}]/6\lambda\lambda'$$

will not give sufficient precision because of the importance of the possible errors in the absolute value of $\langle r^2 \rangle_{Av}$, as well as the uncertainty in the values of the mean free paths λ, λ' corresponding to the resonance energies. Different authors give values fluctuating between 0.56 and 1.1 cm.[2,16–21] Probably the boron

[14] C. J. Bakker, Physica **IV**, 723 (1937).
[15] E. Fermi, Ricerca Sci. **VII**, 13 (1936).
[16] H. A. Bethe, Rev. Mod. Phys. **9**, 127 (1937).
[17] D. Yost and R. C. Dicksenson, Phys. Rev. **50**, 128 (1936).
[18] Goldhaber and Briggs, Proc. Roy. Soc. **162A**, 137 (1937).
[19] L. Simmons, Det. Kgl. Danske Videnskabernes Selskab, Math. fys. Meddelser. **XVII**, 7 (Kobenhavn, 1940).
[20] Cohen, Goldsmith, and Schwinger, Phys. Rev. **55**, 106 (1939).
[21] Pontecorvo and Munn, Can. J. Research **A25**, 143 (1947).

TABLE I. Saturated activities and ratio of activities of the isomers of Br^{80} and Rh^{104} produced by resonance and by *C*-neutrons, as a function of the distance from a Ra–Be neutron source in a paraffin medium.

Corrected distance	Resonance activity	Resonance activity	Ratio of resonance activities	Thermal activity	Thermal activity	Ratio of thermal activities
			Br(18 min)			Br(18 min)
r (cm)	Br(18 min)	Br(4.4 hr)	Br(4.4 hr)	Br(18 min)	Br(4.4 hr)	Br(4.4 hr)
2.22	395 ±4	153.5±0.7	2.57±0.02	1297 ±7	435 ±1	2.94±0.01
4.03	261 ±2	102.5±0.4	2.54±0.02			
5.97	144 ±2	53.7±0.4	2.68±0.03	790 ±6	265 ±1	2.98±0.02
6.95	112 ±1.8	38.9±0.3	2.87±0.04			
8.93	59.2±1.7	20.6±0.3	2.88±0.04	454.4±4	154.4±0.8	2.94±0.02
			Rh(44 sec)			Rh(44 sec)
r (cm)	Rh(44 sec)	Rh(4.2 min)	Rh(4.2 min)	Rh(44 sec)	Rh(4.2 min)	Rh(4.2 min)
2.04	1065 ±10	111 ±0.5	9.60±0.05	8480±128	817 ±6	10.38±0.12
4.36	677	73.2±0.4	9.24	7042	695 ±3	10.14
5.42	549	60.2	9.12	5747	575	10.00
7.11	322	35.7±0.3	9.02	4055	416.5±1.4	9.74
8.11	242.5	27	8.89	3321	348.5	9.53
9.77	150.5±2	16.8±0.2	8.96±0.05	2154±35	233.3±0.4	9.23±0.10
11.49	98.1±1.9	9.9±0.2	8.96±0.16	1411	148	9.53

method might give some results if applied with sufficient precision.[22]

III. RESULTS

The results for the initial counting rates and their ratios are given in Table I for bromine and for rhodium and are plotted in Fig. 1. Table II gives the cadmium ratio's for both elements at increasing distances.

Our conclusions from these results are as follows.

For *bromine* activated by the *resonance neutrons*, the ratio of the activities of the two isomers varies from 2.57±0.02 to 2.88±0.04 as the distance in the paraffin goes from 2 to 9 cm. As this ratio undoubtedly varies with the neutron energy, this seems to confirm the existence of more than one capture level. Furthermore, we can say that the lower capture level favors the formation of the ground state bromine isomer (18 min), in the energy region investigated, because the ratio increases with decreasing energy. These views are confirmed by finding two different values for the mean square migration distances, corresponding to each of the isomers:

$$\langle r^2\rangle_{Av} = 97.8 \text{ cm}^2 \text{ for Br(18 min)},$$
$$\langle r^2\rangle_{Av} = 94.4 \text{ cm}^2 \text{ for Br(4.4 hr)},$$

the first of which corresponds to the lowest resonance energy.

The activation of bromine by *C-neutrons* results in a ratio of activities which remains quite constant as the distance in the paraffin goes from 2 to 9 cm. This again is confirmed by the values of the mean square distances, which are quite the same for the two isomers.

However, a difference certainly exists between the relative activations of both isomers, on one side by thermal neutrons and on the other side by resonance neutrons. This result confirms a previous paper[6] and indicates that capture levels in the nucleus may be multiple.

In the case of *rhodium*, for the *resonance neutrons*, the ratio of activities of isomer Rh(44 sec) to Rh(4.2 min) varies from 9.60±0.05 to 8.96±0.05 at distances from the source from 2 to 10 cm. This indicates, as for bromine, but less precisely, the existence of more than one capture level, in agreement with Goldsmith and Rasetti,[7] who found by the boron method resonance energies of 1.16 ev for Rh(44 sec) and about 1 ev for Rh(4.2 min).

Here, in contrast to the case of bromine, the ratio of activities decreases with increasing distances from the source, so that it is the upper capture level which favors the formation of the ground-state isomer, Rh(44 sec), in the inspected region.

On the other hand, different authors[1,2,4,6] assume the existence of only one capture level, but they consider that the ratio of activities is the same with and without Cd. However, in these experiments only one distance in the paraffin appears to have been used. In our case too, at 10 cm the values of the "thermal" and the "resonance" ratio are nearly equal, but at other distances they differ.

For the corresponding $\langle r^2\rangle_{Av}$ values we find a very small difference, but come to the same conclusions as above.

TABLE II. The cadmium ratio C_R=activity without Cd/activity with Cd for the isomers of Br^{80} and Rh^{104}, as a function of the distance from a Ra–Be neutron source in a paraffin medium.

r (cm)	Cd ratio Br(18 min)	Cd ratio Br(4.4 hr)	r (cm)	Cd ratio Rh(44 sec)	Cd ratio Rh(4.2 min)
2.22	4.23	3.84	2.04	8.96	8.36
—	—	—	4.36	11.40	10.49
—	—	—	5.43	11.47	10.50
5.97	6.49	5.94	7.11	13.59	12.66
—	—	—	8.11	14.69	13.91
—	—	—	9.77	15.32	14.89
8.93	8.68	8.50	11.49	16.84	15.89

[22] (To be published later by the authors.)

The action of the *C-neutrons* on rhodium gives an unexpected result. Within the thermal region, the ratio of activities varies from 10.38 ± 0.12 to 9.23 ± 0.10 for paraffin-distances from 2 to 10 cm. This shows the existence of different capture levels in the *C*-neutron band, which seems to be due to resonances within the thermal region. Such resonances have already been proposed by others[7] and seem to be the more probable for Rh as this element has a resonance level at 1.33 ev which is close to the thermal region.

In this part of the experiments too, the ground state is favored by the higher energies, which is the same as observed in the resonance region.

The existence of different *C*-neutron capture levels seems to be confirmed by the different values obtained for the mean square distance of each isomer

$\langle r^2\rangle_{Av}=267.0$ cm^2 for the 4.2-min Rh isomer,
$\langle r^2\rangle_{Av}=263.1$ cm^2 for the 44-sec Rh isomer,

this value corresponding to the highest energy.

Finally we may notice that for fast neutrons (source without paraffin) the ratio of the isomer activities for bromine[6] was found to be 2.1 and for rhodium[5] about 6. The latter value was confirmed by us.

IV. CONCLUSIONS

If there is a single neutron capture level for nuclear isomers, this single level can but form both isomers in a invariable proportion.

As the ratio of the isomers varies with the distance from the source, there is evidence for the existence of *more than one* capture level. This is true for the resonance neutrons in bromine and perhaps in rhodium, whereas for rhodium, resonance levels seem to extend within the region defined by the *C*-neutrons. These views are confirmed by the fact that: (a) corresponding migration distances differ and (b) the ratio of the isomers certainly is different for resonance and for *C*-neutrons.

PHYSICAL REVIEW VOLUME 81, NUMBER 3 FEBRUARY 1, 1951

An Experiment on the Anomalous Scattering of μ-Mesons by Nucleons

E. AMALDI AND G. FIDECARO
Istituto di Fisica della Università, Centro di Studio per la Fisica Nucleare del C.N.R., Rome, Italy
(Received August 7, 1950)

Large angle scattering of fast μ-mesons by an iron plate, 6 cm thick, has been investigated by means of a counter-hodoscope which recorded separately two energy bands: from 200 Mev to 320 Mev kinetic energy, and from 320 Mev to infinity. About half a million incident μ-mesons were counted. Upper limits for the cross sections for anomalous scattering were obtained: about 4.5×10^{-29} cm^2/nucleon for the low energy band; about 2.3×10^{-30} cm^2/nucleon for the high energy band. Also an upper limit for the cross section for production of penetrating showers by μ-mesons at sea level is given. We found a cross section of 10^{-30} cm^2/nucleon for showers of at least two particles of which at least one is emitted at an angle larger than 20° with a range of at least 7 cm Fe+5 cm Pb.

I. INTRODUCTION

IN a previous paper[1] we pointed out that the investigation of anomalous scattering of μ-mesons by nucleons seems unnecessary because of the well known experiment of Conversi, Pancini, and Piccioni, which showed that μ-mesons at rest interact very weakly with nucleons. However, it is not evident that the conclusions regarding the nuclear interactions between μ-mesons almost at rest and nucleons can be extrapolated to the case of μ-mesons with kinetic energy around several hundred Mev. In fact, Evans and George, and George and Trent,[2] working at sea level, under a clay thickness equivalent to 60 m water, found a local production of stars and penetrating showers which had to be due to μ-mesons. The corresponding cross section for these effects turned out to be of the order of 10^{-29} cm^2/nucleon; i.e., a value enormously larger than that expected according to the calculations of Fermi, Teller, and Weisskopf[3] on the capture of slow mesons by light nuclei. It is still smaller, however, than the lowest value yet obtained by means of direct observation of the anomalous scattering.[4] For these reasons we thought the anomalous scattering of mesons at sea level to be worthy of investigation. Some of the results reported here have already been published elsewhere.[1]

[1] E. Amaldi and G. Fidecaro, Helv. Phys. Acta **23**, 93 (1950).
[2] T. Evans and E. P. George, Nature **164**, 20 (1949); E. P. George and P. T. Trent, Nature **164**, 838 (1949). We thank Mr. George for sending a manuscript of an extensive paper by himself and Evans, which will appear in the Proc. Roy. Soc.
[3] Fermi, Teller, and Weisskopf, Phys. Rev. **71**, 314 (1947); see also B. Ferretti, Nuovo Cimento **5**, 325 (1948); H. Frölich, Nature **160**, 255 (1947); **162**, 450 (1948).
[4] P. M. S. Blackett and J. G. Wilson, Proc. Roy. Soc. **A165**, 209 (1938); J. A. Vargus, Phys. Rev. **56**, 480 (1939); J. G. Wilson, Proc. Roy. Soc. **A174**, 73 (1940); F. L. Code, Phys. Rev. **59**, 229 (1941); R. P. Shutt, Phys. Rev. **61**, 6 (1942); **69**, 128 (1946); **69**, 261 (1946); M. S. Sinha, Phys. Rev. **68**, 153 (1945); W. T. Scott and H. S. Snyder, Phys. Rev. **73**, 1260 (1948).

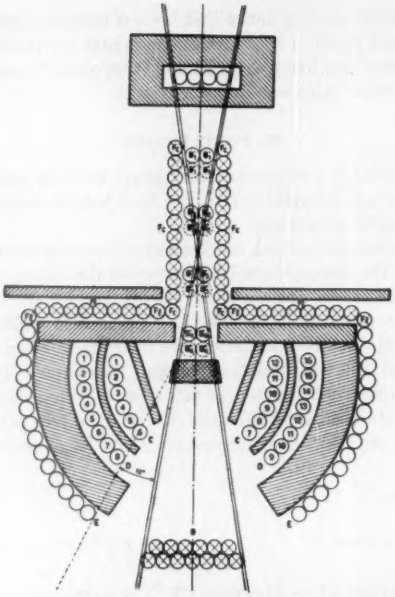

FIG. 1. A scale diagram of the experimental setup.

II. PROCEDURE

The equipment used is shown in Fig. 1. The solid angle of the incident particles was defined by either of two telescopes, B' or B'', placed one behind the other. These trays were mounted in this way in order to increase the intensity without increasing too much the lack of angular definition in the direction perpendicular to the plane of the figure. Counters A were in parallel and were placed under 15 cm Pb and above 5 cm Pb, so that the soft component was eliminated. F_c+F_l was an anticoincidence set of counters for lateral protection. The 6-cm thick scatterer covered almost exactly the solid angle defined by the two telescopes B' and B''. The counters of C and D were connected to a hodoscope of neon lamps which gave some rough information concerning the direction of motion of the scattered particles. A layer of Pb 2.5 cm thick was placed in front of counters C and a second layer of 2.5-cm Pb was placed between counters C and D. Counters E were all in parallel and separated from counters D by 10 cm of Pb. Counters G were connected in parallel.

By means of suitable circuits we counted the following types of events:

$$N_1 \rightarrow A+B' \text{ (or } B'')+(C+D)-F-G.$$
$$N_2 \rightarrow A+B' \text{ (or } B'')+G+(C+D)-F.$$
$$N_3 \rightarrow A+B' \text{ (or } B'')+G-F.$$
$$N_4 \rightarrow A+B' \text{ (or } B'')+(C+D)+E-F-G.$$

Pictures of the neon lamps of the hodoscope were taken for all events of types N_1, N_2, and N_4. N_2 represents the total number of particles crossing either of the telescopes B' or B'', and the scatterer. N_1 and N_4 are the numbers of particles scattered at angles larger than 18°, N_1 including all particles that had a minimum range of ~7 cm Fe+5 cm Pb after the collision, N_4 including those that had a minimum range of ~7 cm Fe+15 cm Pb. If the scattered particles were μ-mesons, the corresponding minimum kinetic energies before the collision are $T_\mu \simeq 200$ Mev and $T_\mu \simeq 320$ Mev.

III. RESULTS

The results of three sets of measurements are given in Table I. In the first set we used a Pb scatterer in order to have an appreciable multiple Coulomb scattering. In the third set of measurements the incident mesons were filtered with a brick layer about 200 g/cm² thick, sufficiently wide to insure that the solid angle defined by the two telescopes B' and B'' was completely covered.

Before trying to use the data of Table I to give an upper limit to the anomalous scattering cross section of μ-mesons by nucleons, we must consider several other effects which could contribute to the number of scattered particles (Table II). The geometry of the equipment was so chosen that the multiple Coulomb scattering[5] was quite appreciable in the case of Pb but negligible in the case of Fe. The single Coulomb scattering has been calculated under two assumptions: we considered, first, Fe and Pb nuclei of finite size,[5] and second, individual point charge protons as scatterers. The number of scattered protons is rather uncertain, because its calculation involves the number[6] and energy spectrum[7] of protons present in the cosmic radiation at sea level, and their differential cross section for elastic collisions against nucleons.[8]

TABLE I. Experimental results.

Set of measurements	Absorber	Scatterer 6 cm thick	Total time, t, in hours	Number of incident particles per min, N_3/t	Total number of incident particles, N_3	Total number of scattered particles: $200 \leq T_\mu \leq 320$ Mev N_1-N_4	Total number of scattered particles: $T_\mu \geq 320$ Mev N_4
1	...	Pb	230 hr 16 min	5.33±0.02	73,769	13	0
2	...	Fe	765 hr 10 min	5.44±0.01	249,168	3	3
3	200 g/cm²	Fe	706 hr 23 min	4.84±0.01	204,914	1	0

[5] E. J. Williams, Proc. Roy. Soc. **A169**, 531 (1939).
[6] Adams, Anderson, Lloyd, Rau, and Saxena, Rev. Mod. Phys. **20**, 334 (1948); B. Rossi, Rev. Mod. Phys. **20**, 537 (1948).
[7] B. Ferretti, Nuovo Cimento **6**, 379 (1949).
[8] Hadley, Kelly, Leith, Segrè, Wiegand, and York, Phys. Rev. **75**, 351 (1949); F. Rohrlich and J. Eisenstein, Phys. Rev. **75**, 705 (1949).

From Table II we see that it is possible that none of the very few particles scattered by Fe were μ-mesons; rather, all were protons. In order to state an upper limit for the anomalous scattering cross section of μ-mesons by nucleons it would be necessary to know the expected number, $\bar{N}_p$, of scattered protons for each of the two bands of energy. We think that a conservative evaluation of such an upper limit is obtained if we assume for $\bar{N}_p$ the values given in Table III. With this assumption and from the observed number of incident μ-mesons, one can conclude that it is very improbable that the anomalous scattering cross section is larger than the following values:

$$\text{for } 200 \leq T_\mu \leq 320 \text{ Mev} = 4.5 \times 10^{-29} \text{ cm}^2/\text{nucleon},$$
$$\text{for } 320 \leq T_\mu = 2.3 \times 10^{-30} \text{ cm}^2/\text{nucleon}.$$

Such a conclusion is correct provided that the hypothetical anomalous scattering of μ-mesons does not deviate too strongly from an isotropic distribution in the center-of-mass system.

TABLE II. Number of counts expected as a result of events which are different from anomalous scattering of μ-mesons by nucleons.

	Pb, first set of measurements		Fe, second set of measurements		Fe, third set of measurements	
Observed counts	Low energy band 13	High energy band 0	Low energy band 3	High energy band 3	Low energy band 1	High energy band 0
Expected counts due to: (calculated)						
Chance coincidences	0.01	0.04	0.04	0.13	0.04	0.10
Multiple Coulomb scattering	7	0	<0.04	0	0	0
Single Coulomb scattering by nuclei	0.07	0.007	0.26	0.026	0.21	0.021
Single Coulomb scattering by protons	0.18	0.23	0.48	0.62	0.39	0.51
Scattered protons	1.3	0.6	3	1.5	0.9	0.4

We now consider the events of type N_2, which have not yet been discussed. An event N_2 is recorded when one or more particles cross the telescope $A+B$ (or B') $+G$ and not the anticoincidence F, and give rise in the scatterer to at least one particle crossing the hodoscope $C+D$. The particle crossing the hodoscope must be emitted at an angle of at least 20° with an energy large enough to cross at least 5 cm Pb.

Three types of events contribute to N_2; electronic secondaries of single penetrating particles, penetrating showers generated by protons, and penetrating showers generated by μ-mesons. Adding together the results of the second and third sets of measurements, we have $N_2 = 39$ for about 4.5×10^5 incident mesons of $T_{0\mu} \geq 100$ Mev.

While the correction for chance coincidence is quite small for events of type N_1 and N_4 (Table II), in the case of events of type N_2 such a correction reduces the observed value of N_2 by about one-half. An upper limit

TABLE III. Numbers used for the mean values of the scattered protons.

	$\bar{N}_p$	
	Low energy band	High energy band
Second set of measurements	2	1
Third set of measurements	0	0

of the value of the cross section for the production of penetrating showers by μ-mesons can be obtained by assuming that the contribution to N_2 from secondary electrons and penetrating showers generated by fast protons is negligible. Under this assumption one obtains $\sigma \sim 10^{-30}$ cm^2/nucleon for production, by μ-mesons, of penetrating showers with at least two particles of which at least one is emitted at an angle larger than ~20° with a range larger than ~7 cm Fe+5 cm Pb.

In this calculation we have used the total number of incident mesons, i.e., all mesons for which $T_\mu \geq 100$ Mev. It is evident that mesons of this low energy cannot produce events of the type N_2. We note, however, that the μ-meson spectrum is flat in the region of a few hundred Mev and that a shift of 100 Mev of the minimum kinetic energy, $T_{0\mu}$, corresponds to an increase in the given cross section of only 5 percent. Thus the upper limits for the cross sections would have to be increased by perhaps 20 percent. This correction would be beyond our limits of accuracy.

The cross sections for anomalous scattering and for the production of showers by μ-mesons can be compared with the results of Evans and George, and of George and Trent.[2] Our cross sections are appreciably lower than those given by these authors. The difference, however, could be due to the much higher energy of the incident μ-meson in the experimental conditions of these authors. Under a layer equivalent to 60 m of water, the mean energy of μ-mesons is about 1.4×10^{10} ev while at sea level it is of the order of 0.9×10^9 ev.

George and Evans[2] interpret their results as due to the electromagnetic interaction of the incident μ-meson with the nuclear meson field. According to this scheme one would expect a cross section for μ-mesons at sea level at least 10 times smaller than at 60 m water equivalent.

A more detailed account of the experimental arrangement and of the evaluation of the measurements will be published elsewhere.[9]

Our thanks are due M. Ageno and G. Bernardini for their contributions to the present work and B. Ferretti for many valuable discussions. Dr. M. A. Tuve, Director of the Department of Terrestrial Magnetism of the Carnegie Institution of Washington, has given us a part of the radio equipment used in this experiment. We thank the Innocenti Company for having kindly supplied the iron structure on which our experimental device was mounted.

[9] E. Amaldi and G. Fidecaro, Nuovo Cimento (1950) (in press).

Relative Photo-Fission Cross Sections of Several Fissionable Materials*

J. McElhinney† and W. E. Ogle
Los Alamos Scientific Laboratory, Los Alamos, New Mexico
(Received September 25, 1950)

Relative cross sections for the photo-fission of several fissionable elements have been measured using a "catcher" method. The results indicate the following cross sections with respect to U^{238}: U^{235}, 2.49; U^{233}, 1.49; Pu^{239}, 2.51; Th^{232}, 0.257; and Io^{230}, 0.847.

I. INTRODUCTION

A SUGGESTION has been made by Teller[1] that the relative photo-fission cross sections of various fissionable materials would be of help in the theoretical interpretation of the photo-fission process. This work is the result of that suggestion. A measurement of the photo-fission yield of U^{233}, U^{235}, Pu^{239}, Th^{232}, and Io^{230}, relative to the photo-fission yield of U^{238}, has been made as a function of bremsstrahlung peak energy, using the Los Alamos 22-Mev betatron as the source of x-rays.

II. EXPERIMENTAL METHOD

The relative photo-fission yields of the different materials with respect to U^{238} were measured by a "catcher" method. The experimental set-up is shown in Fig. 1. X-rays from the betatron passed through a carbon wall 4 in. thick into a cadmium-shielded foil holder. The carbon block was sufficiently thick to block out electrons coming directly from the betatron.

A top view of the foil holder is shown in Fig. 2. It consists of nine $\frac{1}{16}$-in. thick aluminum plates held by slots in an aluminum frame such that the distance between plates is $\frac{1}{8}$ in. The plates are numbered as shown in the diagram. To one side of each plate, except number 9, is fastened fissionable material. A one-mil thick aluminum foil is held against the other side of each plate by $\frac{1}{8}$-in. aluminum frames or spacers. The aluminum foil on one plate then acts as the catcher for fission fragments from the plate next to it. Thus the foil on plate number 2 catches fragments from plate number 1, etc. Between each aluminum foil and its backing plate another one-mil foil was placed to prevent any fragments that might penetrate the first foil from contaminating the backing plate. These foils were changed after each run. Two extra background aluminum foils were in the foil holder on each run in order to measure the activity induced in the aluminum itself. These foils were between the second foil mentioned above and the aluminum backing plate. Aluminum catcher foils were used because of the small activity induced in the foil during the irradiation to which it was subjected.

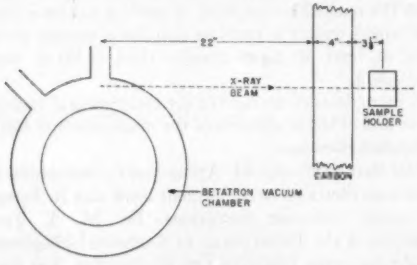

FIG. 1. Irradiation geometry for relative photo-fission yields.

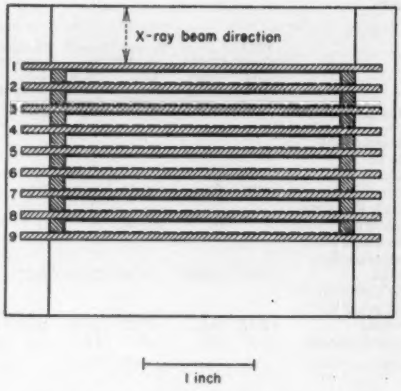

FIG. 2. Foil holder.

Eight fissionable material samples were used, of which three were U^{238}.

Two runs were made at each energy setting of the betatron, one with the beam incident on Plate No. 1 (Fig. 2) and the other with the beam incident on Plate No. 9. The results of these two runs were averaged in order to minimize the effect of inverse square loss and absorption loss due to the different positions of the foils. In every case the samples were irradiated for twenty minutes, and counting began four minutes after

* This document is based on work performed at the Los Alamos Scientific Laboratory of the University of California under Government Contract.
† Now at the National Bureau of Standards, Washington, D. C.
[1] E. Teller, private communication.

the irradiation and continued for a 30-min counting interval.

The catcher foils were counted on glass-walled counter tubes, Model 10A, Mark I, made by the Radiation Counter Laboratories. Ten counter and scaler set-ups were used on each run so that the foils collecting fission fragments from any particular fissionable material were always counted on the same counter. The counters were intercalibrated by means of a radioactive arsenic sample that had the same area as the fission foils counted. The net activity recorded was the total number of counts in 30 minutes minus the counter background, minus the aluminum activity, and corrected to one counter.

III. RESULTS

Relative Fission Yields

Table I lists the weights and sizes of the fissionable materials used, and the positions of the foils in the sample holder. The subscripts on the U^{238} notations

TABLE I. Fissionable material foils.

Sample	Position	Weight (grams)	Area (cm^2)	g/cm^2
U_I^{238}	1	0.002536	23.5	1.08×10^{-4}
U_{II}^{238}	5	0.002356	24.0	0.982×10^{-4}
U_{III}^{238}	8	0.002485	24.5	1.014×10^{-4}
Pu^{239}	4	0.001367	13.8	0.9906×10^{-4}
Io^{230} *	2	0.001042	11.9	0.8756×10^{-4}
Th^{232} *		0.003276		2.7530×10^{-4}
$Th^{232}O_2$	7	0.00290 (0.00255 Th)	24.3	1.049×10^{-4}
$(U^{234})_4O_9$	3	0.00307 (0.00261 U^{234})	27.3	0.956×10^{-4}

* These weights derived from the original data of a total alpha-decay rate of 45,687,000 per minute in 100 percent geometry and 25 percent ionium by weight.

indicate the three different uranium samples. All samples were considered to be thin compared to the fission fragment ranges with the exception of the ionium sample. Thus, no correction was made for self-absorption of the fission fragments except in the case of the ionium foil where a four percent correction was applied.

The activity per atom of the fission fragments from the various fissionable materials relative to U^{238} is given in Table II as a function of the peak bremsstrahlung energy for each run. In order to obtain the ratios given in Table II, the net activity of each sample was divided by the number of atoms of fissionable material in the corresponding foil and this number was compared with the net activity per atom obtained from the U^{238} foils. Since the activity obtained at low energies was in general small, the background and aluminum activity corrections became rather large so that the possible error on the low energy ratios given in Table II is larger than at higher energies. The absence of any obvious trend with energy allows us to assume the same photo-

TABLE II. Relative activity per atom.

X-ray energy	U^{235}/U^{238}	Pu^{239}/U^{238}	U^{233}/U^{238}	Th^{232}/U^{238}	Io^{230}/U^{238}
12.4 Mev	1.45	2.70	3.26	0.218	1.645
14.3	1.59	2.74	2.87	0.247	0.836
16.1	1.59	2.54	2.68	0.276	0.907
17.1	1.44	2.24	3.01	0.352	0.466
18.0	1.57	2.70	2.22	0.254	0.783
18.9	1.47	2.60	2.06	0.260	0.672
19.8	1.43	2.39	2.13	0.209	0.894
20.8	1.31	2.06	1.90	0.227	0.602
21.7	1.54	2.65	2.29	0.273	0.816
Average	1.49 ± 0.02*	2.51 ± 0.05*	2.49 ± 0.11*	0.257 ± 0.010*	0.847 ± 0.075*

* This error is the probable error of the mean assuming thar the individual numbers are all measurements of the same quantity. As seen from Table III there may be an additional systematic error as great as 15 percent.

fission cross-section shape with energy for all fissionable materials observed. Thus, we can assume that the ratio of the activity from a fissionable substance to the activity obtained from U^{238} should be a constant independent of energy. On this basis the average ratio in each case was calculated and is shown at the bottom of Table II. The error shown is the probable error of the mean assuming that the individual numbers are all measurements of the same quantity.

In order to obtain a measure of the error in the experiment three U^{238} foils were used. The ratios of activity per atom between the different foils is shown in Table III as a function of energy. Since this is the relative activity per atom the ratio in all cases should be one. Thus, the variation from one is a measure of the systematic error in the experiment. The error shown on the average is the probable error of the mean as calculated from the individual values. It is seen that while the error due to statistical variations is rather small, of the order of two or three percent, the average values themselves differ from one by as much as 15 percent. Thus, it must be concluded that these measurements of the ratios of the photo-fission yields, relative to U^{238}, may have a systematic error as large as 10 or 15 percent.

IV. DISCUSSION

It is to be noted that the ratio of the ionium activity to U^{238} activity given in Table II has an appreciably larger error than that quoted on any of the other ratios.

TABLE III. Uranium activity comparison.

X-ray energy (Mev)	U_I^{238}/U_{II}^{238}*	$U_{II}^{238}/U_{III}^{238}$*	U_{III}^{238}/U_I^{238}*
12.4	1.30	1.15	0.671
14.3	1.20	1.12	0.741
16.1	1.09	1.12	0.818
17.1	1.03	0.995	0.976
18.00	1.13	1.04	0.856
18.9	1.00	0.998	1.001
19.8	1.11	1.04	0.866
20.8	1.23	0.867	0.937
21.7	1.00	1.28	0.784
Average	1.12 ± 0.02	1.07 ± 0.03	0.850 ± 0.025

* The subscripts I. II. and III indicate the different uranium foils.

The main reason for this large error is that the ionium was not pure but rather was only 25 percent by weight of a sample containing mostly thorium. Thus, the pro-rated thorium activity for each point had to be subtracted from the total activity in order to obtain numbers proportional to the ionium activity. Hence, any errors in the thorium curve were multiplied in the ionium curve.

It is also to be noted that we obtain a ratio for the thorium to uranium activity of approximately $\frac{1}{4}$, whereas Baldwin and Klaiber[2] observed a ratio of $\frac{1}{2}$. It appears that part of this discrepancy is due to the fact that Baldwin and Klaiber's fissionable material foils were all assumed to be completely thick compared with the fission fragment range; however, from the numbers that they quote it appears that their uranium sample was not completely thick. This difference might change their ratio to approximately 1 to 3, which would still leave a discrepancy between the two observed values.

The authors would like to express their appreciation to Messrs. R. D. England and A. N. Carson for their very considerable help in carrying out the above work.

[2] G. C. Baldwin and G. S. Klaiber, Phys. Rev. **71**, 3 (1947).

PHYSICAL REVIEW VOLUME 81, NUMBER 3 FEBRUARY 1, 1951

The Resonance Photo-Fission Cross Section for U^{238}*

W. E. OGLE AND J. McELHINNEY*
Los Alamos Scientific Laboratory,† Los Alamos, New Mexico
(Received September 25, 1950)

An attempt has been made to determine the shape of the U^{238} photo-fission cross section up to a gamma-ray energy of 22 Mev by an analysis of the excitation function obtained by varying the peak energy of the bremsstrahlung from a 22-Mev betatron. A resonance for the photo-fission process is indicated in the region of 15 Mev.

I. INTRODUCTION

THE work of Baldwin and Klaiber[1] on photo-fission in heavy elements aroused considerable interest in the possibility of a resonance photo-fission cross section.[2] This work is an attempt to measure the shape of the U^{238} cross section up to 22 Mev by an analysis of the photo-fission excitation function obtained by varying the peak energy of the bremsstrahlung from a 22-Mev betatron.

II. EXPERIMENTAL METHOD

The arrangement used to observe the excitation function of U^{238} consisted essentially of a standard 22 Mev Allis Chalmers betatron to produce the x-ray spectrum and a fission chamber containing U^{238} to observe the number of fissions as a function of energy. The physical set-up of the experiment required that the x-ray beam from the betatron go through approximately $\frac{3}{8}$ in. of porcelain (the vacuum chamber wall), $\frac{3}{4}$ in. of wood, and 1.4 in. of aluminum before reaching the detecting system itself. In order to establish equilibrium between the primary gamma-rays and the secondary electrons a 4-in. thick layer of carbon was placed in the x-ray beam just in front of the ion chamber.

The detector was a flat plate ion chamber in which one surface was a thick uranium sample and the other a copper collecting plate. The uranium was in the form of a 5-mil thick disk 3 in. in diameter. The gap between the uranium and the collecting plate was $\frac{1}{4}$-in. The chamber was filled with argon at atmospheric pressure. In order to partially cancel the pulse due to the x-ray burst, a bucking chamber was placed behind the fission chamber in the x-ray beam. The bucking chamber was connected in such a manner that the output was of the opposite sign to that of the fission chamber. No fissionable material was in the bucking chamber. The output of the bucking chamber was then mixed with the output of the fission chamber and the result amplified and passed into a gating circuit which allowed only those pulses occurring within ± 5 μsec of the x-ray burst from the betatron to pass through. The output of the gating circuit was then fed into a discriminator and scaler where the pulses were counted. Two $\frac{1}{4}$-*R*-thimbles were placed in front of the fission chamber but enough to one side that the chamber was not shadowed by the *R*-thimbles. The betatron was then run at various energies and the number of fission counts per Roentgen unit of radiation was recorded. Since the ion chamber and *R*-thimbles were approximately 15 meters from the betatron the detectors received uniform intensity radiation, so that no correction for different angular spread of the beam at different energies was necessary.

The energy calibration of the betatron was based upon a measurement of the observed threshold of the

* Now at the National Bureau of Standards, Washington, D. C.
† This document is based on work performed at the Los Alamos Scientific Laboratory of the University of California under Government Contract.
[1] G. C. Baldwin and G. S. Klaiber, Phys. Rev. **71**, 3 (1947).
[2] M. Goldhaber and E. Teller, Phys. Rev. **74**, 1046 (1948).

TABLE I. Number of fissions per Roentgen unit observed as a function of the peak bremsstrahlung energy from the betatron.

X-ray energy (Mev)	Counts/R
8.75	42± 42
10.59	883± 32
12.4	1726± 75
14.3	3010± 37
16.1	4375± 69
17.1	4756±150
18.0	4918± 55
18.9	5443± 78
19.8	5434±148
20.8	5971±157
21.2	5663±182
21.7	5995±163

$N^{14}(\gamma,n)N^{13}$ reaction. The value of this threshold was calculated[3] to be 10.54 Mev.

III. RESULTS

The results of the measurement of the photo-fission excitation curve in U^{238} measured with a fission ion chamber are given in Table I. This lists the peak bremsstrahlung energy settings at which the betatron was run and the number of fissions per Roentgen unit observed at that energy where the number of fissions per Roentgen unit is the average of several runs. The errors quoted in Table I represent the probable error of the mean from the several runs at each point.

TABLE II. Data interpolated from Table I and used for the purposes of calculation.

X-ray energy (Mev)	Counts/R
7.5	0
8.5	0± 60
9.5	320± 60
10.5	790± 70
11.5	1280±100
12.5	1840±100
13.5	2420±100
14.5	3120±100
15.5	3880±100
16.5	4480±120
17.5	4900±150
18.5	5220±170
19.5	5480±200
20.5	5720±220
21.5	5920±220

For the purposes of calculation the data of Table I were interpolated to give the number of counts per Roentgen unit at 1-Mev intervals from 7½- to 21½-Mev peak bremsstrahlung energy. These numbers are shown in Table II. In order to determine the shape of the photo-fission cross section as a function of gamma-ray energy from these data it is necessary to know the relative number of quanta in each energy interval striking the uranium foil for each R recorded by the R-thimble. The initial x-ray spectrum emerging from the target was calculated[4,5] on the assumption of an effective target thickness of 1.5 Mev, using an equation derived by Schiff and Stehle.[6] That spectrum was then corrected for all absorbing materials between the target and the uranium foil. The response of the R-thimble was calculated assuming that it responded only to the secondary electrons coming out of the carbon which were in equilibrium with the primary gamma-rays. From these two calculations the number of gamma-rays per unit energy interval hitting the uranium per Roentgen unit was calculated. Using these numbers an attempt was made to derive the photo-fission cross-section shape from the observed excitation curve.

The equation for the excitation curve can be written as

$$\left(\frac{\text{counts}}{R}\right)_{E_m}=\frac{A\int_0^{E_m}\sigma(k)N(k,E_m)dk}{\int_0^{E_m}R(k)N(k,E_m)dk},$$

where $\sigma(k)$ is the cross section at energy k, $R(k)$ is the R-thimble response, and $N(k,E_m)dk$ is the number of photons in energy interval dk when the peak of the bremsstrahlung is E_m, and A is a constant having to do with the number of atoms of uranium in the counting system and the counting efficiency.

In principle, if one knows the photo-fission excitation curve exactly and the gamma-ray spectrum exactly, one can arrive at a unique solution for the photo-fission cross section as a function of energy. However, comparatively small errors in the excitation curve lead to very large errors in the deduced cross-section curve. Thus, a more sensible procedure seemed to be to assume various cross-section shapes and to try to fit these to the excitation curve. In practice this consisted of assuming a function for $\sigma(k)$, inserting the values in the above equation, performing the numerical integration with 1-Mev intervals, and arriving at a calculated excitation curve.

Although many shapes were assumed for the photo-fission cross section as a function of energy none would give an excitation function similar to that observed unless a maximum in the cross-section value were assumed in the neighborhood of 15 Mev.

A solution was attempted using the resonance formula

$$\sigma=A/[B+(E-E_0)^2].$$

It was found necessary, in order to make a proper fit to the observed excitation curve, to cut off the cross-section curve obtained from the above equation below 8 Mev and allow only a small value of the cross section at 8 Mev. The equation finally obtained which gave

[3] J. Mattauch, *Nuclear Physics Tables*, Interscience Publishers Inc. (1946).

[4] McElhinney, Hanson, Becker, Duffield, and Diven, Phys. Rev. 75, 542 (1949).

[5] L. I. Schiff, Phys. Rev. 70, 89 (1946).

[6] L. I. Schiff and P. Stehle, MDDC-43, unpublished.

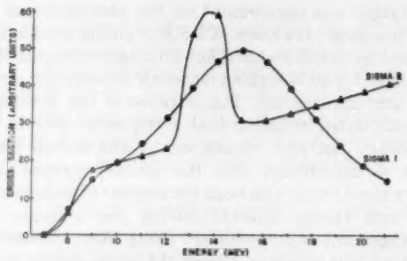

FIG. 1. Possible U^{238} photo-fission cross-section curves. $Sigma_1$ fits a resonance equation. (In the figure, 1 and 2 should be subscripts to sigma.)

an excitation curve that fell within the limits of error of Table II is

$$\sigma = 771.88/[15.625+(E-15)^2]$$

where E is the gamma-ray energy in Mev. The above equation does not imply that we know the cross-section shape to five significant figures. The numbers shown are simply those which will give a fit within the errors of the excitation curve. Attempts to fit the observed excitation curve using the above resonance formula are unsuccessful if the resonance peak is chosen more than $\frac{1}{2}$ Mev different from the 15 Mev assumed. A plot of this cross-section curve is shown in Fig. 1 and the exact values used are given in Table III listed under $Sigma_1$. $Sigma_2$, also listed in Table III and shown in Fig. 1, is another cross-section shape leading to an excitation curve that fits the observed data.

No correction has been applied to any of the data of this work for possible fission due to fast neutrons coming from the betatron. However, absorption and time-of-flight measurements have indicated that neutron-induced fission does not contribute appreciably above 8- or 9-Mev peak bremsstrahlung energy.

It should be emphasized that the experimental excitation curve arrived at in this work does not and cannot lead to unique photo-fission cross-section curves. However, the data should be sufficiently good to check on a theoretically derived cross-section shape.

A more complete description of this experiment giving the actual calculations of the bremsstrahlung spectrum incident on the U^{238} fission chamber, detailed calculations of the R-thimble response, and detailed calculations of the possible cross-section shapes, is given in the Los Alamos Report LADC-654.

TABLE III. Possible photo-fission cross-section shapes for U^{238}.

X-ray energy (Mev)	$Sigma_1$*	$Sigma_2$*
0 to 7	0	0
8	6.690	6.00
9	14.95	17.40
10	19.00	19.40
11	24.40	21.2
12	31.34	23.2
13	39.34	54.0
14	46.42	59.0
15	49.40	30.8
16	46.42	31.0
17	39.34	32.8
18	31.34	34.8
19	24.40	36.8
20	19.00	38.6
21	14.95	40.6

* Arbitrary units.

The authors would like to express their appreciation to Mr. A. N. Carson and Mr. R. D. England for their considerable help in performing this experiment.

Boundary Conditions for the Description of Nuclear Reactions

MARCOS MOSHINSKY
Institutos de Física y Geofísica, Universidad de México, México, D.F.
(Received June 22, 1950)

The present paper deals with a phenomenological description of nuclear reactions by means of boundary conditions. The several stages of the reaction (initial particles, compound nucleus, etc.) are described in their respective configuration spaces; and the state representing the whole system is given by a wave function in Fock space. The wave equations and the boundary conditions are deduced with the help of an analogy to vibration problems. The interaction leading to the nuclear reaction appears as a boundary condition between the different components of the Fock type wave function. A discussion is given of elastic scattering and of two-particle nuclear reactions, showing that the present procedure gives the same dependence of the cross sections on energy as the Breit-Wigner resonance formula and its generalizations. A sketch is given of the extension of the present ideas to multiple particle reactions. The whole treatment is nonrelativistic.

I. INTRODUCTION

OVER a wide range of energies of the incident particles, it is useful to follow the progress of a nuclear reaction in the following three stages:

(1) the presence of the initial nucleus and the incident particle,
(2) the formation of a single particle (compound nucleus) after the collision,
(3) the appearance of two or more particles as a result of the disintegration of the compound system.

The possibility of contemplating these three stages of the reaction stems from the relatively long lifetime of the compound nucleus, for a large range of collision energies, which makes it fruitful to consider it as a separate entity.[1]

The usual description of the nuclear reaction processes represents all three stages of the reaction in the configuration space of the nucleons which constitute the incident particle and the initial nucleus.[2] The complexity of the problem, particularly in the absence of a definite theory of nuclear forces, has made it useful to consider the coordinates of the center of mass and the relative position of the two initial particles as six of the coordinates of the configuration space of the nucleons, and to include the rest in the internal coordinates of the particles. By an appropriate division of this configuration space, Wigner and Eisenbud[3] and others developed a method for the description of two-particle reactions which takes into account the general features of the phenomenon.

In the present paper we will develop a description of nuclear reactions which will not use the configuration space of all the nucleons present, but the configuration space of the reacting particles and of the compound particle, all of which will be considered as elementary particles.

The three stages of the nuclear reaction will not be represented in the same configuration space. The first stage, corresponding to the presence of the two initial particles, will be described in the 6-dimensional configuration space corresponding to them by the wave function $\psi_1(\mathbf{r}_1,\mathbf{r}_2,t)$. The second stage, in which a single particle (the compound nucleus) is present, will be represented by the wave function $\psi_2(\mathbf{r}_1,t)$ in 3-dimensional configuration space. Finally, the third stage, in which we have, let us say, n-particles, which are produced in the disintegration of the compound system, will be described in their $3n$-dimensional configuration space by the wave function $\psi_3(\mathbf{r}_1,\mathbf{r}_2,\cdots,\mathbf{r}_n,t)$. The reaction products will be described in a different configuration space from that of the initial particles, even if $n=2$, except when we have only elastic scattering. In this case, only the first two spaces are needed to describe the reaction.

As the state of the system that is undergoing a nuclear reaction may be in any of the three stages mentioned above, it is clear that its complete description can be achieved only by a wave function of the type introduced by Fock,[4] in connection with states in which the number of particles is not a constant of the motion. For our problem, the appropriate wave function, which will be referred to from now on as the Fock wave function of the state, is given by the vector:

$$\Psi=\begin{bmatrix}\psi_1(\mathbf{r}_1,\mathbf{r}_2,t)\\ \psi_2(\mathbf{r}_1,t)\\ \psi_3(\mathbf{r}_1,\mathbf{r}_2,\cdots,\mathbf{r}_n,t)\end{bmatrix}. \tag{1}$$

The scalar product of two Fock wave functions is defined by:

$$(\Psi,\Psi')=\int\int\psi_1^*\psi_1'd\mathbf{r}_1d\mathbf{r}_2+\int\psi_2^*\psi_2'd\mathbf{r}_1+\int\cdots\int\psi_3^*\psi_3'd\mathbf{r}_1\cdots d\mathbf{r}_n \tag{2}$$

[1] H. A. Bethe, *Elementary Nuclear Theory* (John Wiley and Sons, Inc., New York, 1947), p. 109. Also L. Eisenbud, Princeton dissertation, 1946, and E. P. Wigner, Am. J. Phys. 17, 99 (1949).
[2] See reference 1 and H. A. Bethe, Revs. Modern Phys. 8, 107 (1936).
[3] E. P. Wigner and L. Eisenbud, Phys. Rev. 72, 29 (1947) and E. P. Wigner, Phys. Rev. 70, 15 (1946). This article also contains references to earlier literature.
[4] V. Fock, Z. Physik 75, 622 (1932). Also L. Landau and R. Peierls, Z. Physik 62, 188 (1930).

and the Fock wave function is normalized when $(\Psi,\Psi)=1$.

The interpretation given to the components of (1) is the following: $\psi_1^*(\mathbf{r}_1,\mathbf{r}_2,t)\psi_1(\mathbf{r}_1,\mathbf{r}_2,t)d\mathbf{r}_1d\mathbf{r}_2$ represents the probability of finding, at time t, the state in the form of the two initial particles in the neighborhood of $\mathbf{r}_1,\mathbf{r}_2$, and similarly for the other components.

Our problem is now to determine the wave equations satisfied by the Fock wave function, as well as to describe the flux of probability which takes place in the course of time, from the configuration space of the initial particles to that of the particles produced in the reaction.

To guide us in this problem we consider the analogous problem of the vibration of continuous media.

II. ANALOGY WITH VIBRATION PROBLEMS

The usefulness of the analogy between vibration problems in continuous media and the above description of nuclear reactions rests on the following considerations:

(a) the equations obeyed by the displacements in the vibration problem are similar to those (Schroedinger or Klein-Gordon) which the wave functions in configuration space satisfy.

(b) The probability density in configuration space, which is the quadratic form $\psi\psi^*$, can be compared to the energy density in the vibration problem, which is also a quadratic form of the derivatives of the displacement. In both cases we have conservation theorems. In the vibration problem, the total energy of the vibrating medium is constant, while in configuration space, the total probability equals unity for normalized wave functions, and is independent of time.

(c) For a state represented by a Fock wave function, such as the nuclear reaction above, there will be a flux of probability between the configuration spaces of different dimensions. A similar problem appears when we consider vibrations of continuous media of different dimensions which are in contact, and where we observe a transfer of energy between the media.

A simple example of vibrating media of different dimensions in contact is given by the two semi-infinite strings **I** and **III** of linear densities ρ_1, ρ_3, and tension T, which are coupled at $x=0$ by the mass point **II** of mass M_2 (Fig. 1).

We have in this case one-dimensional continuous media represented by the two strings, in contact with the zero-dimensional mass point **II**. When the system is set into vibration, there is a continuous exchange of energy between the strings and the mass point.

If a disturbance is produced in **I**, all the energy of the system will be concentrated there; but, in the course of time, some of the energy is communicated to the mass point **II**, which, in turn, passes it to **III** and gives some back to **I** in the form of a reflected wave.

In the Fock space picture, something similar happens

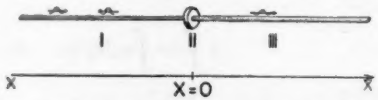

FIG. 1. One-dimensional elastic system composed of two strings (I and III) coupled by a mass (II).

in the description of a nuclear reaction. At the beginning, all the probability is concentrated in the configuration space of the two initial particles. Later on, there is a flow into the configuration space of the compound system, and finally, into the configuration space of the particles produced in the reaction.

A spontaneous disintegration of a particle, such as the α-decay, would correspond in the vibration picture to the energy of the system being concentrated initially in the mass point **II**. This energy would be communicated to the strings, and it can be seen easily that, because of this radiation of energy, the amplitude of the vibrations of **II** suffers an exponential decrease with time.

We designate by $u_1(x,t)$ the lateral displacement of the string **I** and by $u_3(x,t)$ the lateral displacement of string **III**, the displacement of the mass point **II** is given by $u_2(t)$. The "state" of the vibrating system is given by the vector:

$$U=\begin{bmatrix}u_1(x,t)\\u_2(t)\\u_3(x,t)\end{bmatrix}. \tag{3}$$

The equations of motion for the strings when $x\neq 0$ will be the ordinary wave equations:

$$\rho_1(\partial^2u_1/\partial t^2)-T(\partial^2u_1/\partial x^2)=0$$

and

$$\rho_3(\partial^2u_3/\partial t^2)-T(\partial^2u_3/\partial x^2)=0. \tag{4}$$

The equation of motion of the particle **II** will no longer be that of a free particle, and a simple way to find it is through the principle of conservation of energy. The total energy of the vibrating system is given by

$$H=\tfrac{1}{2}\int_{-\infty}^{0}[\rho_1(\partial u_1/\partial t)^2+T(\partial u_1/\partial x)^2]dx+\tfrac{1}{2}M_2(du_2/dt)^2$$
$$+\tfrac{1}{2}\int_{0}^{\infty}[\rho_3(\partial u_3/\partial t)^2+T(\partial u_3/\partial x)^2]dx. \tag{5a}$$

Assuming that u_1,u_3 vanish appropriately for $x=\pm\infty$, and using the wave equations (4), we obtain

$$dH/dt=T(\partial u_1/\partial x)_{x=0}(\partial u_1/\partial t)_{x=0}$$
$$+M_2(d^2u_2/dt^2)(du_2/dt)$$
$$-T(\partial u_3/\partial x)_{x=0}(\partial u_3/\partial t)_{x=0}=0. \tag{5b}$$

If the coupling between the wires and the mass point **II** is such that the displacement of the wires is equal to that of **II**, we have

$$u_1(0,t)=u_2(t) \quad \text{and} \quad u_2(t)=u_3(0,t). \tag{6}$$

From Eqs. (5b) and (6), the equation of motion of the particle **II** becomes

$$M_2(d^2u_2/dt^2)+T(\partial u_1/\partial x)_{x=0}-T(\partial u_3/\partial x)_{x=0}=0. \tag{7}$$

We see that the equation of motion of the particle is modified by the presence of terms due to the action of the higher dimensional media. Furthermore, the interaction between **I** and **III** takes place through the

boundary conditions (6) and (7) at $x=0$ and in no way through the equation of motion of the strings. In fact, with the help of Eq. (6), we can eliminate u_2 from Eq. (7) and obtain direct boundary conditions between u_1 and u_2 and their derivatives at $x=0$.

The properties of the vibration problem, suggest the following procedure for the Fock wave function in configuration space:

(*a*) The wave functions for the initial and final particles satisfy free-particle Schroedinger wave equations everywhere except at the point of coincidence of the particles.

(*b*) The wave equation for the compound system ψ_2 will be modified by the wave functions of the higher dimensional configuration spaces, similarly to what happens in Eq. (7).

(*c*) The theorem of conservation of probability could guide us in the determination of the boundary conditions of the problem.

We will proceed to apply these considerations to several types of nuclear reaction problems, starting with elastic scattering.

III. ELASTIC SCATTERING

For the description of elastic scattering, our Fock wave function will have only two components corresponding to the initial particles and the compound system, respectively, as those are the only stages in which our state can be found. We restrict our state to zero total momentum, i.e., we choose the center-of-mass reference frame.

The Fock wave function becomes then

$$\Psi=\begin{bmatrix}\psi_1(\mathbf{r},t)\\ \psi_2(t)\end{bmatrix}, \tag{8}$$

where $\psi_1(\mathbf{r},t)$ is the wave function representing the two initial particles with $\mathbf{r}=\mathbf{r}_1-\mathbf{r}_2$ being the relative position vector, and $\psi_2(t)$ is the wave function for the compound particle.

When there is no interaction between the components of the Fock wave function, they should obey the free particle Schroedinger equations:

$$-i\hbar\partial\psi_1/\partial t+(m_1+m_2)c^2\psi_1=(\hbar^2/2\mu)\nabla^2\psi_1, \tag{9}$$

$$-i\hbar(\partial\psi_2/\partial t)+Mc^2\psi_2=0, \tag{10}$$

where m_1, m_2 are the masses of the two initial particles, $\mu=m_1m_2/(m_1+m_2)$ the reduced mass, and M the mass of the compound particle. The energy operator $E=i\hbar\partial/\partial t$ represents here, for reasons which will be apparent later, the total energy and not, as usual, the kinetic energy alone.

In case there are interactions between the configuration spaces of different dimensions of ψ_1 and ψ_2, we can still consider that ψ_1 satisfies Eq. (9) as long as $r\neq 0$. On the other hand, the analogy with the vibration problem suggests that ψ_2 can no longer satisfy Eq. (10), and also that the theorem of conservation of probability could give a clue to the modifications we have to impose on Eq. (10).

From Eq. (2) we have

$$P(t)\equiv(\Psi,\Psi)=\int\psi_1^*(\mathbf{r},t)\psi_1(\mathbf{r},t)d\mathbf{r}+\psi_2^*(t)\psi_2(t), \tag{11}$$

which represents the probability of finding at time t the state (8) in any of its stages. This probability should be a constant, and equal to unity in case the Fock wave function is properly normalized.

We assume now that the wave function $\psi_1(\mathbf{r},t)$ is regular at $\mathbf{r}=\infty$, and we surround the point $\mathbf{r}=0$ where the wave function is singular by the sphere $r^2=a^2$ whose radius $a\to 0$. If we evaluate dP/dt, making use of the wave equation (9) in the region outside the sphere $r^2=a^2$, we obtain

$$\frac{\hbar}{i}\frac{dP}{dt}=\lim_{a\to 0}\int_0^{\pi}\int_0^{2\pi}\frac{\hbar^2}{2\mu}\left[\left(\psi_1\frac{\partial\psi_1^*}{\partial r}-\psi_1^*\frac{\partial\psi_1}{\partial r}\right)r^2\right]_{r=a}$$
$$\times\sin\theta d\theta d\varphi+\psi_2^*\left(\frac{\hbar}{i}\frac{\partial\psi_2}{\partial t}+Mc^2\psi_2\right)$$
$$-\psi_2\left(\frac{\hbar}{i}\frac{\partial\psi_2}{\partial t}+Mc^2\psi_2\right)^*=0. \tag{12}$$

The Fock wave function that satisfies Eq. (12) must represent a state for which the conservation of probability holds. We restrict ourselves to an initial state in which the particles have zero relative angular momentum, as otherwise the law of conservation of angular momentum would require that the compound particle represented by ψ_2 should have a spin. Furthermore, if relation (12) is satisfied for the wave function

$$\Psi=\begin{bmatrix}\psi_1\\ \psi_2\end{bmatrix}\quad\text{and}\quad\Psi'=\begin{bmatrix}\psi_1'\\ \psi_2'\end{bmatrix},$$

the general principles of quantum mechanics require that it should be satisfied by any linear superposition of Ψ and Ψ', and this implies that Eq. (12) becomes the bilinear relation:

$$\frac{2\pi\hbar^2}{\mu}\left(\frac{\partial r\psi_1}{\partial r}\right)_{r=0}^*(r\psi_1')_{r=0}-(r\psi_1)_{r=0}^*\frac{2\pi\hbar^2}{\mu}\left(\frac{\partial r\psi_1'}{\partial r}\right)_{r=0}$$
$$+\psi_2^*\left(\frac{\hbar}{i}\frac{\partial\psi_2'}{\partial t}+Mc^2\psi_2'\right)$$
$$-\left(\frac{\hbar}{i}\frac{\partial\psi_2}{\partial t}+Mc^2\psi_2\right)^*\psi_2'=0. \tag{13}$$

This bilinear form is of the familiar type:

$$x_1^*y_3-x_3^*y_1+x_2^*y_4-x_4^*y_2=0, \tag{14}$$

which appears in many boundary value problems,[5] and

[5] E. L. Ince, *Ordinary Differential Equations* (Dover Publications, New York, 1944), Chapter IX.

it is known[6] that the general linear self-adjoint equations which make Eq. (14) vanish are:

$$x_3=C_{11}x_1+C_{12}x_2, \quad x_4=C_{21}x_1+C_{22}x_2, \tag{15}$$

where $\mathbf{C}=\|C_{ij}\|$ is a constant Hermitian matrix.

From Eqs. (13) and (15) we obtain the linear equations:

$$(r\psi_1)_{r=0}=C_{11}(2\pi\hbar^2/\mu)(\partial r\psi_1/\partial r)_{r=0}+C_{12}\psi_2, \tag{16a}$$

$$(\hbar/i)(\partial\psi_2/\partial t)+Mc^2\psi_2 =C_{21}(2\pi\hbar^2/\mu)(\partial r\psi_1/\partial r)_{r=0}+C_{22}\psi_2. \tag{16b}$$

Equations (16a) and (16b) give us the coupling between the wave functions of the initial particles and the compound particle. The constant C_{12} is a measure of the coupling, because the interaction between ψ_1 and ψ_2 disappears if $C_{12}=C_{21}^*=0$.

When there is no coupling, Eq. (16b) should reduce to Eq. (10); and this implies that $C_{22}=0$. If we now assume that our state corresponds to a definite energy E, we have $-i\hbar\partial\psi_2/\partial t=-E\psi_2$ and eliminating ψ_2 between Eqs. (16a) and (16b) we obtain

$$(r\psi_1)_{r=0}=[4\pi\hbar C_{12}^2/(Mc^2-E)+4\pi\hbar C_{11}] \times(\hbar/2\mu)(\partial r\psi_1/\partial r)_{r=0}. \tag{17}$$

This equation is the boundary condition which characterizes the elastic scattering, and the term in the square bracket corresponds to the single term of Wigner's[3] **R**-matrix.

The energy E corresponds to the total energy of the initial pair of particles, so that:

$$E-Mc^2=E_k-[M-(m_1+m_2)]c^2=E_k-E_0 \tag{18}$$

where E_k is the kinetic energy of the relative motion of the two initial particles, and E_0 is the binding energy of the compound system. Thus the **R**-matrix, which is in this case one-dimensional, becomes

$$\mathbf{R}=[4\pi\hbar|C_{12}|^2/(E_0-E_k)]+4\pi\hbar C_{11}. \tag{19}$$

This result is identical to the form of the **R**-matrix for single-level elastic scattering, and we see that in the present phenomenological description it is only a consequence of the theorem of conservation of probability.

IV. MANY-LEVEL ELASTIC SCATTERING

The formation of a single compound particle has led to the single-level Breit-Wigner formula for elastic scattering. We shall obtain the many-level formula by assuming that the collision process may give rise to any of $n-1$ compound particles. The Fock wave function then becomes

$$\Psi=\begin{bmatrix}\psi_1(\mathbf{r},t)\\ \psi_2(t)\\ \cdots\\ \psi_n(t)\end{bmatrix}. \tag{20}$$

This implies that our system can be in the state in which the two initial particles are present, or in the $n-1$ other states in which single particles of masses M_2, M_3, $\cdots M_n$ are present instead.

By applying the theorem of the conservation of probability to the Fock wave function (20), we arrive at the bilinear relation:

$$\sum_{i=1}^{n}(x_i^*y_{n+i}-x_{n+i}^*y_i)=0, \tag{21}$$

where for all $i=2, 3, \cdots, n$,

$$x_1=(2\pi\hbar^2/\mu)(\partial r\psi_1/\partial r), \quad x_{n+1}=(r\psi_1)_{r=0},$$
$$x_i=\psi_i, \quad x_{n+i}=-i\hbar(\partial\psi_i/\partial t)+M_ic^2\psi_i$$

and the y's have a similar significance with respect to a second wave function.

The linear self-adjoint equations which make this bilinear form vanish, are

$$x_{n+i}=\sum_{j=1}^{n}C_{ij}x_j \tag{22}$$

where $\mathbf{C}=\|C_{ij}\|$ is, as before, a constant Hermitian matrix.

There should be no coupling between the wave functions of the compound particles themselves, but only between them and the wave function for the initial two particles. This implies that only $C_{i1}=C_{1i}^*\neq 0$ for $i=2, 3, \cdots, n$ and the linear relations (22) become

$$x_{n+1}=\sum_{i=1}^{n}C_{1j}x_j$$

and $x_{n+i}=C_{i1}x_1$ for $i=2, 3, \cdots, n$.

If we now assume a definite energy E for the state, we can eliminate, as in the one-level case, the ψ_i $(i=2, 3, \cdots, n)$ and obtain

$$(r\psi_1)_{r=0}=\left(\sum_{i=2}^{n}\frac{4\pi\hbar|C_{i1}|^2}{E_{0i}-E_k}+4\pi\hbar C_{11}\right)\frac{\hbar}{2\mu}\left(\frac{\partial r\psi_1}{\partial r}\right)_{r=0}, \tag{23}$$

where $E_{0i}=[M_i-(m_1+m_2)]c^2$ represents the binding energy of the ith compound particle.

Equation (23) is the many-level formula for elastic scattering.

V. TWO-PARTICLE NUCLEAR REACTIONS

The nuclear reaction in which the compound particle can disintegrate into either of two pairs of particles can be described by the Fock wave function:

$$\Psi=\begin{bmatrix}\psi_1(\mathbf{r},t)\\ \psi_2(t)\\ \psi_3(\mathbf{r},t)\end{bmatrix}. \tag{24}$$

Both wave functions ψ_1, ψ_3, for the initial and final particles, satisfy the free particle wave equation (9) with reduced masses μ_1 and μ_3, as long as $\mathbf{r}\neq 0$. If we apply the principle of conservation of probability, the same reasoning which we used in the case of elastic scat-

[6] This will be proved in the Appendix.

tering leads to the bilinear form

$$\sum_{i=1}^{3}(x_i^* y_{3+i} - x_{3+i}^* y_i) = 0, \tag{25}$$

where x_1, x_2, x_4, x_5 are given as in Eq. (21) for $n=3$, and

$$x_3 = (2\pi\hbar^2/\mu_3)(\partial r\psi_3/\partial r)_{r=0}, \quad x_6 = (r\psi_3)_{r=0}. \tag{26}$$

The linear self-adjoint equations which guarantee the vanishing of Eq. (25) have again the form (22), with $n=3$. We shall assume that in the present problem there is no direct coupling between the initial and final wave functions, but only a coupling through the compound state. The Hermitian matrix then has the form

$$\mathbf{C} = \begin{vmatrix} C_{11} & C_{12} & 0 \\ C_{21} & 0 & C_{23} \\ 0 & C_{32} & C_{33} \end{vmatrix}. \tag{27}$$

For a definite energy E of the system, we can again eliminate ψ_2 from the linear equations (22). We thus obtain the relations

$$(r\psi_i)_{r=0} = R_{i1}(\hbar/2\mu_1)(\partial r\psi_1/\partial r)_{r=0} + R_{i3}(\hbar/2\mu_3)(\partial r\psi_3/\partial r)_{r=0} \text{ (with } i=1,3), \tag{28}$$

where the matrix $\mathbf{R} = \|R_{ij}\|$, $i,j=1,3$ has the form:

$$\mathbf{R} = \frac{4\pi\hbar}{E_0 - E_k}\begin{bmatrix} C_{12}C_{21} & C_{12}C_{23} \\ C_{32}C_{21} & C_{32}C_{23} \end{bmatrix} + 4\pi\hbar\begin{bmatrix} C_{11} & 0 \\ 0 & C_{33} \end{bmatrix}.$$

The matrix $\mathbf{R}$ is clearly Hermitian and equivalent to the one obtained by Wigner for the single-level two-alternative reaction.

Our phenomenological description could deal with many-level, many-alternative, two-particle nuclear reations if we assumed a Fock wave function which could take into account all of the possible stages of the nuclear reaction.

VI. β-DISINTEGRATION

As a last example we shall deal with a process in which one particle decomposes into three particles. A process of this nature is the β-decay such as the disintegration of a neutron into a proton-electron-neutrino triplet. Unfortunately, since the neutrino mass is zero, the energy distribution of the disintegration products given by the present nonrelativistic theory will not be directly comparable with the actual energy distribution. However, it will be possible to make the comparison on the basis of a remark of Uhlenbeck and Goudsmit.[7]

The vibration analog is illustrated in Fig. 2. The configuration space for the final particles is of higher dimensionality than that for the initial particle; and, in order to represent it, we need a vibrating medium of higher dimension, such as the plane **II** in Fig. 2. The original system, i.e., the neutron, is represented by the mass point **I**.

[7] See G. E. Uhlenbeck and S. Goudsmit, article in "Pieter Zeeman" (M. Nijhoff, 'S-Gravenhage, 1935), p. 201.

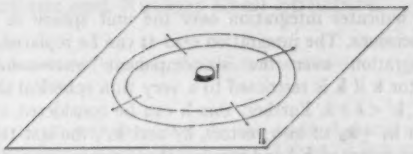

FIG. 2. Elastic system composed of a membrane (II), and a mass (I).

In Fig. 2, we would expect that the vibration set up in the region **II** will have circular symmetry; i.e., will correspond to the lowest "spherical harmonic" in two dimensions. Similarly, in the six-dimensional space of the relative coordinates of the disintegration products, the wave function will be an outgoing wave which is independent of the angular coordinates in that space,

$$\psi \approx R^{-2}H_2(kR)\exp(-iEt/\hbar). \tag{29}$$

In Eq. (29), $k=(2ME/\hbar^2)^{\frac{1}{2}}$ is the generalization of wave number for the six-dimensional space in which ψ is defined, H_2 is the outgoing Hankel function of order 2, and R is the analog of the radius vector of the particle; also, for six-dimensional configuration space,

$$R^2 = \sum_{s=1}^{3}(m_s/M)(\mathbf{r}_s - \mathbf{r})^2, \tag{29a}$$

with $\mathbf{r}$ the center of mass of the system,

$$\mathbf{r} = \sum m_s\mathbf{r}_s/\sum m_s, \quad M = \sum_{s=1}^{3} m_s, \tag{29b}$$

The three values 1,2,3 of the index s refer to the three reaction products: proton, electron, and neutrino. Since the theory here presented is nonrelativistic, it was necessary to attribute a finite mass even to the neutrino. However, since the proton mass m_1 is very much larger than the other masses, we can use the approximation for Eq. (29a),

$$R^2 = (m_2\mathbf{r}_2^2 + m_3\mathbf{r}_3^2)/M. \tag{29c}$$

The same approximation is customarily made in β-theory; hence our result is made more easily comparable with the usual theory if we introduce the approximation involved in Eq. (29c).

For $kR \gg 1$, the wave function (29) becomes asymptotically

$$\psi \approx R^{-5/2}\exp(ikR - iEt/\hbar). \tag{30}$$

This asymptotic expression can be considered as a superposition of plane waves of equal intensity in all directions in six-dimensional space:

$$\psi \approx \int \exp\{i\mathbf{k}\Omega\cdot[(m_2/M)^{\frac{1}{2}}\mathbf{r}_2 + (m_3/M)^{\frac{1}{2}}\mathbf{r}_3] - iEt/\hbar\}d\Omega. \tag{31}$$

In this, Ω is a unit vector in six-dimensional space, and

$d\Omega$ indicates integration over the unit sphere in six dimensions. The integration over Ω can be replaced by integration over the six-component wave-number vector $\mathbf{k}$ if $\mathbf{k}$ is restricted to a very thin spherical shell $k<|\mathbf{k}|<k+\delta$. Further, this $\mathbf{k}$ can be considered as a sum $\mathbf{k}_2'+\mathbf{k}_3'$ of two vectors, $\mathbf{k}_2'$ and $\mathbf{k}_3'$, the last three components of $\mathbf{k}_2'$ and the first three components of $\mathbf{k}_3'$ being zero. This gives

$$\psi\approx\delta^{-1}\int d\mathbf{k}_2'd\mathbf{k}_3'\exp[i\mathbf{k}_2'(m_2/M)^{\frac{1}{2}}\cdot\mathbf{r}_2]\times\exp[i\mathbf{k}_3'(m_3/M)^{\frac{1}{2}}\cdot\mathbf{r}_3]\exp(-iEt/\hbar).$$

The integration herein is to be extended over the shell $k^2<\mathbf{k}_2'^2+\mathbf{k}_3'^2<(k+\delta)^2$. Introducing $\mathbf{k}_2=(m_2/M)^{\frac{1}{2}}\mathbf{k}_2'$, $\mathbf{k}_3=(m_3/M)^{\frac{1}{2}}\mathbf{k}_3'$, we have

$$\psi\approx\delta^{-1}\exp(-iEt/\hbar)\int\exp(i\mathbf{k}_2\cdot\mathbf{r}_2)d\mathbf{k}_2\times\int\exp(i\mathbf{k}_3\cdot\mathbf{r}_3)d\mathbf{k}_3, \quad (32)$$

where the integration is subject to the condition

$$k^2/M<(\mathbf{k}_2^2/m_2)+(\mathbf{k}_3^2/m_3)<(k+\delta)^2/M. \quad (32a)$$

We are interested in the probability that the energy of the electron $\epsilon_2=\hbar^2\mathbf{k}_2^2/2m_2$ is in unit neighborhood of ϵ_2. This will be proportional to that part of the volume of the ellipsoidal shell (32a), for which

$$\epsilon_2<\hbar^2\mathbf{k}_2^2/2m_2<\epsilon_2+d\epsilon_2. \quad (32b)$$

This is easily calculated to be proportional to

$$[(\hbar^2k^2/2M)-\epsilon_2]^{\frac{1}{2}}\epsilon_2^{\frac{1}{2}}d\epsilon_2. \quad (33)$$

Hence, the energy distribution of the β-disintegration products becomes proportional to the square roots of the energies of the two light particles which are emitted, i.e., proportional to the volume available in phase space. According to Uhlenbeck and Goudsmit,[7] this is also the result in relativistic theory.[8]

[8] The transition from Eq. (29) to Eq. (33) can be carried out also by means of an identity in the theory of Bessel functions.

VII. CONCLUSIONS

The principal new point raised in the present paper is the analogy between vibration problems in which bodies of different dimensionality are involved on the one hand, and quantum-mechanical problems in which the number of particles is not constant, on the other. The formalism here proposed, which amounts to a prescription of boundary conditions in Fock space,[9] yields the same energy dependence for reaction cross sections as the ordinary theory and yields, for three particle disintegrations, an energy distribution between the product particles which is very similar to that to which the customary β-disintegration theory leads.

I want to express my thanks to Professor E. P. Wigner to whom I am indebted for many discussions and suggestions concerning the present work. It is a pleasure also to acknowledge the support given to the present research by the Comisión Impulsora y Coordinadora de la Investigación Cientffica.

APPENDIX

We are given the bilinear form:

$$\sum_{i=1}^{n}(x_i^*y_{n+i}-x_{n+i}^*y_i),$$

and we want to find n linear equations between the $2n$ variables x such that combined with the same linear equations for the y, they make the above bilinear form vanish identically.

Let us assume that the n linear equations are

$$x_{n+i}=\sum_{j=1}^{n}C_{ij}x_j.$$

Substituting this into the above bilinear form we obtain

$$\sum_{i=1}^{n}x_i^*(y_{n+i}-\sum_{j=1}^{n}C_{ji}^*y_j).$$

This will vanish if the y's satisfy the equations

$$y_{n+i}=\sum_{j=1}^{n}C_{ji}^*y_j.$$

Since the x and y should satisfy the same equations, the $\mathbf{C}$ matrix must be Hermitian. Conversely, every connection between the x_i and x_{n+i} of the above form, with an arbitrary Hermitian $\mathbf{C}$, guarantees the vanishing of our bilinear form.

[9] M. Moshinsky and E. P. Wigner, Phys. Rev. **74**, 1212 (1948) and **75**, 1322 (1949), also M. Moshinsky, Princeton dissertation, 1949.

Neutron Binding Energies from (d, p) Reactions and Nuclear Shell Structure*

J. A. HARVEY
Laboratory for Nuclear Science and Engineering, Massachusetts Institute of Technology, Cambridge, Massachusetts
(Received September 21, 1950)

Using 14-Mev deuterons from the M.I.T. cyclotron, proton spectra have been measured for many heavy and medium atomic weight elements. The range of the protons was measured in aluminum foils by the method of "peaking" with a triple proportional counter. From the Q-value of the ground-state proton group (measured relative to a Q-value of 5.50 Mev for the aluminum ground-state group), the neutron binding energy of the residual nucleus has been obtained. These values are compared to the maximum gamma-ray energy obtained from thermal neutron capture. A few neutron binding energies have been measured from the (d, t) reaction and are compared with values obtained from the (γ, n) threshold. Several neutron binding energies have been computed from radioactive decay energies and measured neutron binding energies. All neutron binding energies have been compared with the values predicted from the semi-empirical mass formula. A sharp drop in neutron binding energy of about 2.2 Mev occurs at the completion of the closed shell of 126 neutrons. A drop, a little greater than 2 Mev, occurs at 50 neutrons. There is also a decrease in the region of 82 neutrons. There also seems to be a decrease of about 1 Mev in the region of 29 neutrons, but this is not very conclusive.

The differential cross section of the ground-state peaks from even Z, odd A isotopes at forward angles are much smaller (about a factor of ten) than the differential cross sections of the ground-state peaks from the same Z but even A isotopes. The ground-state peaks from Sn^{117} and Pb^{207}, however, are about 50 percent that of the even A isotopes.

I. INTRODUCTION

TO explain observed properties of nuclei, two models have been used, (a) the independent particle concept, and (b) the strong interaction viewpoint. Although the strong interaction picture successfully accounts for many nuclear phenomena, the single-particle model has received much attention by many writers.[1–7] Recently, many nuclear properties such as the natural abundances of the stable isotopes,[1] spins,[2] magnetic moments,[3] radioactive transitions,[2] isomerism,[2] quadrupole moments,[3] neutron capture cross sections,[4] and nuclear fission[5] have been analyzed in the light of a shell model and the existence of "magic numbers" has been definitely established.

It has also been pointed out[1, 8–16] that when a shell is completed, we should expect a nucleus of particular stability. When a new shell is begun, the binding energy of newly added particles will be less than that of the particles which completed the shell. This was shown[8] to be true for O^{16}. Considering only the masses of $A=4n$ nuclei, Smart[9] concluded that closed shells occur at mass numbers of 20 and 32. From a careful study of decay energies of the natural radioactive series and the semi-empirical mass formula, the binding energy of the last neutron and of the last proton has been predicted in the lead region.[10–15] Upon completion of the closed shell of 126 neutrons there is a decrease in neutron binding of about 2 Mev, and a decrease in proton binding energy of the order of 2.5 Mev after completing a closed shell of 82 protons. From a consideration of the nuclear stability in the region of 82 neutrons, Mayer[1] has suggested a drop in neutron binding energy of the order of 2 Mev after filling up the shell of 82 neutrons. Also Hanson *et al.*[17] have explained the high values of the (γ, n) thresholds in Zr^{90} and Mo^{92} as due to the particular stability of 50 neutrons. Recently,[18] precise mass measurements have indicated a sudden break in the packing fraction curve in the neighborhood of Zr^{90}, and possibly in the region of 28 neutrons. Masses in the region of calcium do not show any shell effect[19] with the exception of Ca^{40}.

II. METHODS OF MEASURING NEUTRON BINDING ENERGIES

The binding energy of the last neutron can be measured in many ways which can be conveniently divided into two groups. The first group includes the measurement of the energy required to remove a neutron from a stable nucleus represented by the threshold of the

* Part of a thesis submitted in partial fulfillment of the requirements for the degree of Doctor of Philosophy in Physics in the Graduate School of the Massachusetts Institute of Technology. This work was supported by the joint program of the ONR and the AEC. Some of these results were reported at the New York Meeting (February, 1950) and the Washington Meeting (April, 1950) of the American Physical Society.

[1] Maria G. Mayer, Phys. Rev. 74, 235 (1948); W. D. Harkins and M. Popelka, Jr., Phys. Rev. 76, 989 (1949).
[2] E. Feenberg, Phys. Rev. 75, 320 (1949); E. Feenberg and K. C. Hammack, Phys. Rev. 75, 1877 (1949); L. W. Nordheim, Phys. Rev. 75, 1894 (1949); Feenberg, Hammack, and Nordheim, Phys. Rev. 75, 1968 (1949).
[3] W. Gordy, Phys. Rev. 76, 139 (1949); R. D. Hill, Phys. Rev. 76, 998 (1949); Townes, Foley, and Low, Phys. Rev. 76, 1415 (1949); J. Rainwater, Phys. Rev. 79, 432 (1950).
[4] D. J. Hughes and D. F. Sherman, Phys. Rev. 78, 632 (1950).
[5] D. C. Brunton, Phys. Rev. 76, 1798 (1949); L. E. Glendenin, Phys. Rev. 77, 755 (1950).
[6] Maria G. Mayer, Phys. Rev. 75, 1969 (1949); Haxel, Jensen, and Suess, Phys. Rev. 75, 1766 (1949).
[7] E. Feenberg, Phys. Rev. 76, 1275 (1949); E. Feenberg, Phys. Rev. 77, 771 (1950); Maria G. Mayer, Phys. Rev. 78, 16, 22 (1950).
[8] H. A. Bethe and R. F. Bacher, Revs. Modern Phys. 8, 171 (1936).
[9] J. S. Smart, Phys. Rev. 76, 439 (1949).
[10] W. Elsasser, J. phys. radium 5, 635 (1934).
[11] A. Berthelot, J. phys. radium (VIII) 3, 17 (1942).
[12] S. von Flügge and J. Mattauch, Physik. Z. 44, 181 (1943).
[13] M. Stern, Revs. Modern Phys. 21, 316 (1949).
[14] K. Way, Phys. Rev. 75, 1448 (1949).
[15] A. H. Wapstra, Physica 16, 33 (1950).
[16] Perlman, Ghiorso, and Seaborg, Phys. Rev. 77, 27 (1950).
[17] Hanson, Duffield, Knight, Diven, and Palevsky, Phys. Rev. 76, 578 (1949).
[18] Duckworth, Woodcock, and Preston, Phys. Rev. 79, 198 (1950).
[19] C. H. Townes and W. Low, Phys. Rev. 79, 198 (1950).

(γ, n)[17,20–26] or the $(n, 2n)$ reaction,[27] the Q-value of the ground-state group from a (p, d) reaction[28] or a (d, t) reaction.[29] Nearly 40 neutron binding energies have been obtained from photo-neutron thresholds. The reported values are measured relative to the Cu^{63} threshold at 10.9 Mev and are accurate to 100 or 200 kev. The only $(n, 2n)$ threshold reported is that of Cu^{63}, giving a value of 11.2 ± 0.3 Mev in good agreement with the photo-neutron threshold. The (p, d) reaction has been observed with low energy protons on beryllium and with high energy protons on carbon.[28] The Q-value for a (d, t) reaction is only slightly negative, since the binding energy of the last neutron in a triton is over 6 Mev. Triton groups have been observed in several heavy elements and the neutron binding energy derived from the Q-value of the highest energy group agrees with (γ, n) threshold measurements. If the residual nucleus is not left in its ground state, then only an upper limit to the neutron binding energy is obtained by these methods.

The second group consists in the measurement of the energy released on the addition of a neutron to a stable nucleus by the gamma-rays from thermal neutron capture or the Q-value of the ground-state proton group from a (d, p) reaction. A search for high energy gamma-rays has been made by Kubitschek and Dancoff,[30] using an absorption method, and by Kinsey *et al.*,[31–33] using a pair spectrometer. The resolution obtained with the spectrometer is about 100 kev and gamma-ray energies can be measured to an accuracy of 10–20 kev. For targets containing more than one isotope the highest energy gamma-ray is assigned to the lowest odd A isotope in the target. Results obtained by this method will be compared to the results obtained from the (d, p) method. Since a (d, p) reaction is simply the transfer of a neutron from the deuteron to the target nucleus, the Q-value for the reaction is equal to the difference between the neutron binding energy in the residual nucleus and the deuteron binding energy. Prior to the present research very little work[34–38] had been done with nuclei heavier than calcium and then only up to arsenic ($A = 75$). Both of these methods measure the neutron binding energy in the residual nucleus, which has one more neutron than the target nucleus. Also, if the residual nucleus is not left in the ground state then only a lower limit for the neutron binding energy is obtained. The (d, p) method has the advantage, in principle at least, that coincidences between protons and gamma-rays can be searched for, and if no coincidences are found, then it can be concluded that the proton group observed truly leaves the nucleus in its ground state. However, the counting rates are very low and the work done to date is not conclusive.

If the neutron binding energy measured by the (d, p) or (n, γ) method agrees with the value obtained by the (γ, n) or (d, t) method, then we know that this value is the true value. Using decay energies of neighboring isobars we can also check several other values measured by the (d, p) and (γ, n) methods. A few cycles can be completed to check several values as a group; for example, the cycle involving the alpha-decay energy of Po^{210} or the mass difference of Fe^{54} and Fe^{56} from mass spectrographic measurements.[39]

In a few cases, neutron energies can be computed from decay energies and a measured neutron binding energy. However, it is necessary that the total decay energy be known or else one obtains only an upper or a lower limit. This method is very useful in the lead region where the total decay energies of nearly all the elements are well known.

III. DESCRIPTION OF APPARATUS

The equipment is the same as that described by Boyer, *et al.*,[40] and only the details pertinent to the accurate measurement of Q-values shall be given here. The 15.5-Mev deuteron beam from the cyclotron is "piped" from the cyclotron and focused at the center of the target chamber about 12 feet from the cyclotron. Targets are mounted in small aluminum frames 1 inch square at the center of the target chamber. The targets can be retracted into the target holder and inserted into the deuteron beam by compressed air. A target can also be inserted into the deuteron beam through a side port and alternate runs can be taken on the two targets and one target can be used for a reference. The targets used were about 20 mg/cm² thick. The deuteron beam was uniformly spread over ½ inch square on the target. The protons were detected by a triple proportional counter and their range measured in aluminum absorbers by the principle of "peaking," so that only protons ending their range in the third counter were counted. The triple counter and absorbers can be rotated in angle, and thus the proton spectrum can be

[20] G. C. Baldwin and H. W. Koch, Phys. Rev. **67**, 1 (1945).
[21] McElhinney, Hanson, Becker, Duffield, and Diven, Phys. Rev. **75**, 542 (1949).
[22] H. Palevsky and A. O. Hanson, Phys. Rev. **79**, 242 (1950).
[23] W. E. Ogle and R. E. England, Phys. Rev. **78**, 63 (1950.)
[24] Ogle, Brown, and Carson, Phys. Rev. **78**, 63 (1950).
[25] R. W. Parsons and C. H. Collie, Proc. Phys. Soc. London **A63**, 839 (1950).
[26] R. W. Parsons, *et al.*, Proc. Phys. Soc. London **A63**, 915 (1950).
[27] J. L. Fowler and J. M. Slye, Jr., Phys. Rev. **77**, 787 (1950).
[28] Levinthal, Martinelli, and Silverman, Phys. Rev. **78**, 199 (1950).
[29] J. A. Harvey, Phys. Rev. **79**, 241 (1950).
[30] H. E. Kubitschek and S. M. Dancoff, Phys. Rev. **76**, 531 (1949).
[31] Kinsey, Bartholomew, and Walker, Phys. Rev. **78**, 77 (1950).
[32] Kinsey, Bartholomew, and Walker, Phys. Rev. **78**, 481 (1950).
[33] Bartholomew, Kinsey, and Walker, Phys. Rev. **79**, 218 (1950); also private communications.
[34] A. B. Martin, Phys. Rev. **56**, 1062 (1939).
[35] W. L. Davidson, Phys. Rev. **57**, 568 (1940).
[36] A. B. Martin, Phys. Rev. **72**, 378 (1947).
[37] W. D. Whitehead and N. P. Heydenburg, Phys. Rev. **79**, 99 (1950).
[38] W. O. Bateson and E. Pollard, Phys. Rev. **79**, 241 (1950).
[39] Duckworth, Woodcock, and Preston, Phys. Rev. **78**, 479 (1950); H. E. Duckworth and R. S. Preston, Phys. Rev. **79**, 402 (1950); also private communications.
[40] Boyer, Gove, Harvey, Livingston, and Deutsch, to be published.

measured at any angle. The solid angle of the counter was defined by a rectangular slit $\frac{3}{4}$ in. high and 0.4 in. wide, 4 in. from the target. A parallel plate ionization chamber was located at the entrance of the target chamber in order to monitor the deuteron beam, and this reduced the deuteron energy to about 14.0 Mev.

IV. DETERMINATION OF Q-VALUES

A. Experimental Procedure

Deuteron and proton energies cannot be measured precisely by the range technique because of the difficulty in measuring the exact range and the uncertainty in the range energy curve. Thus, the Q-values are measured relative to an accurately known Q-value such as the Q-value of the aluminum ground-state proton peak. The Q-equation for a (d, p) reaction for a deuteron of energy E_d, a proton of energy E_p at an angle θ, and a residual nucleus with a mass number A is approximately

$$Q=(1+1/A)E_p-(1-2/A)E_d-(2/A)(2E_pE_d)^{\frac{1}{2}}\cos\theta.$$

From the Q-equation for two proton groups from targets of mass numbers A_1 and A_2 we have

$$\begin{aligned}Q_1-Q_2=&(E_{p1}-E_{p2})-(E_{d1}-E_{d2})\\&-[2A_1^{-1}(2E_{p1}E_{d1})^{\frac{1}{2}}\cos\theta_1-2A_2^{-1}(2E_{p2}E_{d2})^{\frac{1}{2}}\cos\theta_2]\\&+(E_{p1}+2E_{d1})A_1^{-1}-(E_{p2}+2E_{d2})A_2^{-1};\end{aligned}$$

and, hence, the error would be

$$\begin{aligned}\Delta(Q_1-Q_2)=&\Delta(E_{p1}-E_{p2})-\Delta(E_{d1}-E_{d2})\\&+[(2/A_1)(2E_{p1}E_{d1})^{\frac{1}{2}}\sin\theta_1\Delta\theta_1\\&-(2/A_2)(2E_{p2}E_{d2})^{\frac{1}{2}}\sin\theta_2\Delta\theta_2]+\text{terms of order}\\&(\Delta E_{p1}/A_1,\ \Delta E_{d1}/A_1,\ \Delta E_{p2}/A_2,\ \Delta E_{d2}/A_2).\end{aligned}$$

Thus, it is not necessary to measure accurately the deuteron and proton energies but only the difference in energy between the two proton groups and the difference in deuteron energy at the center of each target, since the targets are of different thicknesses. The Q-values are calculated at the center of the target, since a thick target introduces a rectangular spread centered about the protons produced at the center of the target.

The aluminum ground-state peak was selected as a standard, since the ground-state peak is well separated from lower energy groups, thin foils are readily available, and the Q-values to be measured are expected to be in this region. The Q-value adopted for the ground-state peak was 5.50 Mev. The Q-values obtained from range measurements are as follows: Allan and Clavier:[41] 5.50±0.06; Pollard, Sailor, and Wyly:[42] 5.45±0.05; and Whitehead and Heydenburg:[37] 5.71. Recent measurements with magnetic analysis results[43] in a Q-value of 5.50±0.01 Mev with a low lying excited level at 30 kev.

Tests were made to determine how sensitive the deuteron energy was to the various controls of the cyclotron. By keeping the controls within reasonable limits it is estimated that the deuteron energy can be kept constant to 20 to 30 kev.

Data for the light and medium weight elements were run at some forward angle, usually 30°, and the heavy elements at an angle of 50° to 60°. A careful search was made for high energy proton groups of very weak intensities. In many cases, if there had been a peak the order of 1 percent of the highest energy peak observed, it would have been detected. The high energy section of the spectrum was then taken at several angles up to 90° to check that the peaks shifted correctly with angle corresponding to the mass of the target. In many cases, with targets having several isotopes, one isotope is quite abundant (greater than 60 percent) and the ground-state proton peak can be identified from its intensity. Since a lighter isotope will have a higher energy ground-state peak, it can usually be identified. An angle such as 30° was selected and alternate spectra of the aluminum ground-state peak at 30° and the proton peaks from the target were taken. About 10 to 15 points were taken on the aluminum ground-state peak; each point took about 10 seconds. A spectrum of the protons from the other target took about 5 minutes. Several alternate measurements were taken to average out any fluctuation in the deuteron energy or drift in the gate settings. When the alternate spectra showed a fluctuation in range of more than 1 or 2 mg/cm² of Al (about 30 kev), the data were taken again. These alternate spectra were averaged, and the difference in the ranges of the two peaks was measured; and thus the difference in energy of the two proton groups determined. We must also correct for the proton energy loss in the target.

The procedure for computing the Q-value from the target was as follows. From the mean range of the aluminum ground-state protons (corrected for a half-target thickness) we obtain the proton energy at the center of the target, and then we compute the deuteron energy from the Q-equation. Correcting for the deuteron energy loss in a half-target thickness we obtain the incident deuteron energy. We now compute the deuteron energy and the proton energy at the center of the other target and then calculate the Q-value of the other peak. Because we are dealing with quite high energies, one might expect that it would be necessary to use the relativistic Q-equation. For the aluminum ground peak at 90° the difference amounts to 11 kev, but is only 1 kev at 30°. The difference is negligible for heavy elements. Also we have used the mass number A instead of the exact mass M. For the aluminum ground-state peak at 90° the difference is 13 kev; but at 30° it is only 2 kev. This difference is also negligible for heavy elements.

[41] H. R. Allan and C. A. Clavier, Nature 158, 832 (1946).
[42] Pollard, Sailor, and Wyly, Phys. Rev. 75, 725 (1949).
[43] High Voltage Lab., M.I.T., private communication.

B. Analysis of Experimental Uncertainties

Counter Angle θ

Assuming that Q_2 is the accurately known Q-value, then the error in Q_1 due to the uncertainty in the counter angle θ is

$$(\Delta Q_1)_\theta = (2/A_1)(2E_{p1}E_{d1})^{\frac{1}{2}} \sin\theta_1 \Delta\theta_1 - (2/A_2)(2E_{p2}E_{d2})^{\frac{1}{2}} \sin\theta_2 \Delta\theta_2.$$

Thus for a given error in θ, the minimum error in Q for a heavy nucleus is obtained for small angles for a heavy reference nucleus. However, elements heavier than aluminum either do not have well-resolved ground-state peaks or their Q-values are not accurately known. This is the reason for selecting aluminum for a reference and choosing an angle of 30°. The counter can be aligned to the deuteron beam to an accuracy of about 1°. There are two small effects that change the effective angle of the counter. One effect, owing to the finite solid angle and size of the deuteron beam on the target, increases the angle. At 30° the effective counter angle is increased by about 0.5°. The other small effect is a result of the angular distribution of the protons. Since for light elements the distribution is strongly forward, the effective angle is less than the measured angle. However, since the aluminum ground-state peak has a maximum[44] at 30°, this second effect is not present. For the aluminum ground-state peak at 30° with 13.9-Mev deuterons and 19-Mev protons, an error in angle of 1.5° results in an error in the Q-value for a heavy nucleus of 20 kev.

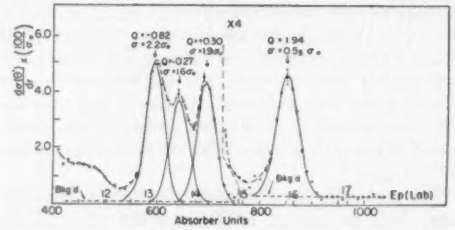

FIG. 1. Proton spectrum at $\theta = 50°$ from a 10-mg/cm² bismuth target bombarded with 14-Mev deuterons from the reaction $Bi^{209}(d, p)Bi^{210}$. The ordinate is the differential cross section in the center-of-mass system per absorber unit in terms of the ground-state proton peak from aluminum $(\sigma_0)\cdot\sigma_0 = 2.5\pm1.0\times10^{-27}$ cm²/steradian. θ' is the angle measured in the center-of-mass system. The abscissa is in units of 0.416 mg/cm² of Al. The proton energy in the laboratory system is also given. The vertical bar represents the square root of the number of counts.

Range of Protons R

The center of the proton peak is chosen as a measure of the mean range of the proton group, since this corresponds to the protons produced at the center of a thick target. The range is measured in absorber units, which are then converted into mg/cm² of aluminum by the conversion factor that 1 absorber unit = 0.416 mg/cm² of aluminum. To the range measured in the foil changer must be added the thickness of foils and gas in the triple counter (10 mg/cm²). There are two other small corrections to be applied to the range. By changing the gate settings, the peak can be made to shift in range. This correction can be approximately determined by comparing a differential and an integral run. For the gate settings used, this correction amounted to about 4 mg/cm². The other small effect is due to the large solid angle and the size of the deuteron beam on the target. Thus, the protons do not pass through the foils exactly at right angles. The average angle is about 4° from the normal, resulting in a correction of 1.5 mg/cm² for the aluminum ground-state peak. The mean range is accurate to a few mg/cm². The difference between the range of 2 proton peaks is accurate to 1 mg/cm² (20 kev).

Range-Energy Curve

The range-energy curve used is that calculated by Smith.[45] Assuming that the computed values for the energy loss per mg/cm² are accurate to 1 percent, the difference in energy of the two proton groups will be accurate to 1 percent.

Energy Loss in Target

In order to obtain sufficient counting rates, targets were of the order of 20 mg/cm² thick. Since the center of the proton peak is taken as a measure of the proton energy, Q-values must be calculated at the center of the target. Bethe and Livingston[46] have calculated the atomic stopping power of various elements at different proton energies. This can be converted into mg/cm² of the various elements equivalent to 1 mg/cm² of aluminum. For a 20-mg/cm² lead target, the deuteron energy loss is about 200 kev in reaching the center of the target and the proton energy loss another 100 kev. Thus, it is necessary that the measured mass/cm² and the calculated conversion values be accurate to 5 percent. Therefore, it was decided to measure the thickness of all targets for 14-Mev deuterons and for high energy protons. This was done by inserting the target in the deuteron beam or the ground-state aluminum protons and measuring the shift of the aluminum ground-state peak at 30°. Since in both cases the target thickness is measured over the same central region as is bombarded, this eliminates errors due to the non-uniformity of the foils. The target thickness for the deuteron beam and for the protons can be measured to 20 kev, and thus the half-target thickness is accurate to 10 kev. The error due to uncertainty in the target angle is negligible.

C. Factors Contributing to the Spread

Since the proton peaks are broad (full width at half-maximum is 500 kev for the aluminum ground-state

[44] H. E. Gove, Phys. Rev. **81**, 364 (1951).

[45] J. H. Smith, Phys. Rev. **71**, 32 (1947).

[46] M. S. Livingston and H. A. Bethe, Revs. Modern Phys. **9**, 272 (1937).

peak), a careful study must be made of the factors which contribute to the spread to justify the choice of the center of the peaks as a measure of the proton energy for all targets. If the observed high energy peak is too broad, then it must be resolved into two peaks, as will be shown in detail later. In order to determine how the width of the proton peak will vary with proton energy and the different targets, one must know the factors which cause the spread and how they vary. For a thin aluminum target, the half-width at $1/e$ of the maximum is 34 absorber units. The factors contributing to this spread are as follows: straggling[47]—23.5, deuteron energy—11, solid angle spread—8, gate settings—14, and other effects—15. The distributions are approximately Gaussian and the numbers are the half-widths in absorber units at $1/e$ of the maximum. When thick targets are used, there is another spread in range introduced, since the (d, p) reaction can occur at any depth of the target. Assuming a constant cross section, the target thickness introduces a rectangular spread centered about the protons produced at the center of the target. This rectangular distribution must be combined with a Gaussian distribution. A 20-mg/cm^2 aluminum target has been run, and the calculated curve fits the observed points very well. The Q-value for the thick target agreed to within 10 kev of the Q-value for a thin target.

D. Differential Cross Sections

Since alternate spectra were taken on the aluminum ground-state peak and the target proton peak, the differential cross section can be evaluated readily in terms of the differential cross section of the aluminum ground-state peak. The relative cross sections are accurate to about 20 percent. The absolute differential cross section (σ_0) of the aluminum ground-state peak at 30° has been measured by Gove[48] and is $2.5\pm1.0\times10^{-27}$ cm^2/steradian/atom. Counting rates have been converted into a scale of differential cross section/absorber unit/atom of the target.

E. The Ground-State Peaks of $C^{13}(d, p)C^{14}$ and $N^{14}(d, p)N^{15}$

In order to test the method for determining the width of the peaks and for calculating Q-values for thick targets where the Q-values are several Mev different from the aluminum ground-state Q-value, the ground-state peaks of carbon and nitrogen were measured. Thick targets of polyethylene and nylon were run at 30°. The calculated curves fit the observed points very closely. The Q-values calculated from the center of the peaks are 2.70 ± 0.03 and 8.63 ± 0.03 Mev. These agree with the accurately measured Q-values of 2.717 ± 0.004 and 8.615 ± 0.006 Mev.[49]

[47] H. A. Bethe, *The Properties of Atomic Nuclei II*, (Brookhaven National Laboratory, June 1, 1949), unpublished.
[48] H. E. Gove and K. Boyer, Phys. Rev. 79, 241 (1950).
[49] B. Malm, Doctor's thesis, M.I.T., May, 1950.

V. EXPERIMENTAL RESULTS

The nuclei investigated have been grouped into three regions: nuclei containing approximately 126 neutrons, 50–82 neutrons, and approximately 28 neutrons. Preliminary results have been reported previously.[50]

A. Nuclei Containing Approximately 126 Neutrons

The proton energy spectra from nuclei containing almost the magic number of 126 neutrons and very

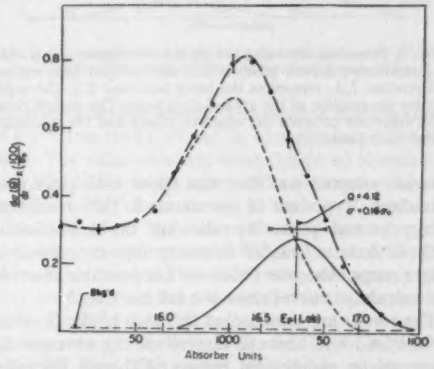

FIG. 2. High energy section of the proton spectrum at $\theta=50°$ from a 20-mg/cm^2 gold target from the reaction $Au^{197}(d, p)Au^{198}$. In this and all succeeding figures of proton spectra the ordinate and the abscissa are the same as for Fig. 1. The lower and upper limits for the position of the ground-state peak are also shown.

nearly the magic number of 82 protons are quite different from spectra of other heavy elements such as gold. The level spacing seems to be quite large in these nuclei near magic number, since the proton spectra from Bi^{209}, Pb^{208}, Pb^{207}, and Pb^{206} targets can be resolved into a few proton groups as shown in Fig. 1. A single peak can be fitted to the long-range proton group from these four targets, as was done for the carbon and nitrogen ground-state peaks. However, in other heavy elements such as tantalum, platinum, gold, thallium, and uranium, the levels are much closer together and the ground-state peak is not well resolved (Fig. 2).

The positions of the ground-state peaks for these cases are determined as follows. One first determines the lower limit for the position of the proton peak by requiring that the calculated curve fit the observed points on the high energy side. When one subtracts this curve from the experimental points, the resultant curve must not drop off more rapidly than the calculated shape. If one fits a curve of shorter range than this lower limit, the calculated curve drops too rapidly on the high-energy side, as shown in Fig. 3.

The upper limit is determined so that the ground-state peak should have a reasonable intensity. The

[50] J. A. Harvey, Phys. Rev. 79, 241 (1950).

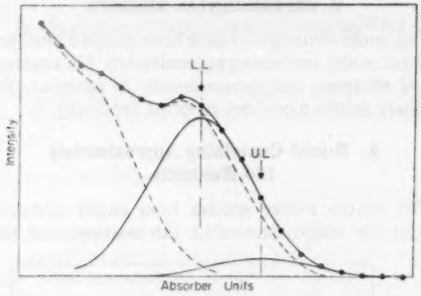

FIG. 3. Procedure for fitting the ground-state proton peak when the ground-state proton group is not well resolved from excited level protons. L.L. represents the lower limit and U.L. the upper limit for the position of the ground-state peak. The dashed curve is the difference between the observed points and the calculated ground-state peak.

criterion adopted was that this upper limit peak contain about 10 percent of the counts in the broad high energy proton peak. By allowing the ground-state peak to have a smaller intensity one can obtain a longer range. Also, the difference between the observed and calculated curves must not fall too steeply.

The results are summarized in Table I. The Q-values for the lead and bismuth targets are the averages for many angles and several targets. Although the other targets have been run at several angles, only one angle was analyzed, since the error in the Q-value depends on this analysis. Table I also contains the differential cross sections for a given angle.

The lead targets were enriched isotopes obtained from the Isotopes Division, Oak Ridge.[51] The Pb^{208} was enriched to 96 percent, the Pb^{207} to 67 percent, and the Pb^{206} to 71 percent. For any target the contributions due to the other two isotopes can be subtracted, since their percentages are known. The thallium target contained 70 percent Tl^{205} and 30 percent Tl^{203}. The observed spectrum has been resolved, so that the ground-state peaks from the two isotopes should have about the same cross section.

B. Nuclei Containing from 50–82 Neutrons

The proton spectra from nuclei with 50 neutrons, such as Sr^{88} and Zr^{90} (Fig. 4), are different from other nuclei in this region such as columbium, molybdenum, rhodium, silver, indium, tin, and antimony (Fig. 5). Again this light nucleus appearance is probably due to the closed shell of 50 neutrons. Table I summarizes the results.

The ground-state peak due to Sr^{88} can be identified, since this is the abundant isotope. A small peak about 2 Mev higher in energy is assigned to Sr^{86}. The ground-state protons due to Sr^{87} would have about 2 Mev higher energy than the Sr^{86} ground-state protons as

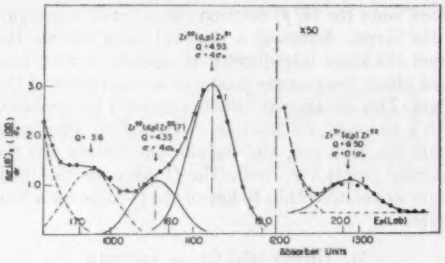

FIG. 4. The high energy section of the proton spectrum at $\theta=20°$ from a 20-mg/cm² zirconium target from the reaction $Zr^{A}(d,p)Zr^{A+1}$.

estimated from the semi-empirical mass formula. This region has been searched and no peak has been found. Thus, we can set an upper limit to its cross section at $0.02\ \sigma_0$.

The ground-state peak of Zr^{90} can be identified readily because of its intensity (Fig. 4). There is also a low intensity peak on the high energy side of the Zr^{90} peak which is assigned to Zr^{91}. If one assumes that

TABLE I. Summary of experimental results for nuclei containing approximately 126 neutrons, 50 and 82 neutrons, and 28 neutrons

Approx. 126 neutrons				Approx. 50 and 82 neutrons				Approx. 28 neutrons			
Target	Angle (θ)	σ/σ_0	Average Q-value	Target	Angle (θ)	σ/σ_0	Average Q-value	Target	Angle (θ)	σ/σ_0	Average Q-value
Bi^{209}	50°	0.55	1.91±0.03	Sr^{88}	30°	1.0	4.32±0.2	Ti^{48}	30°	0.4	5.92±0.05
Pb^{208}	50°	0.6	1.64±0.05	Sr^{86}	30°	0.15	6.29±0.2	Ti^{47}	30°	0.06	8.82±0.4
Pb^{207}	50°	0.10	5.14±0.03	Zr^{90}	20°	4	4.93±0.05	Ti^{46}	30°	0.6	6.51±0.10
Pb^{206}	50°	0.18	4.48±0.03	Zr^{91}	20°	0.1	6.50±0.10	V^{51}	30°	0.6	5.02±0.05
Tl^{205}	30°	0.2	3.93±0.15	Zr^{92}(?)	20°	4	4.33±0.10	Fe^{56}	30°	0.8	5.42±0.10
Tl^{203}	30°	0.2	4.29±0.15	Cb^{93}	30°	0.5	5.03±0.10	Fe^{54}	30°	0.5	7.11±0.05
Ta^{181}	30°	0.13	3.80±0.15	Mo^{92}	30°	0.5	6.08±0.2	Co^{59}	15°	0.8	5.43±0.2
Au^{197}	50°	0.16	4.12±0.15	Rh^{103}	30°	0.5	4.58±0.2	Ni^{58}	30°	0.5	6.78±0.10
U^{238}	60°	0.1	2.40±0.15	Ag^{107}	30°	0.5	4.78±0.2	Cu^{63}	15°	0.6	5.55±0.2
Pt^{194}	30°	0.5	3.91±0.2	In^{115}	30°	0.7	4.36±0.2	Zn^{64}	30°	0.7	5.69±0.05
Pt^{196}(?)	30°	0.05	5.74±0.2	Sn^{117}	30°	0.3	7.14±0.2				
				Sn^{120}	30°		4.0 ±0.3				
				Sb^{121}	30°	0.6	4.41±0.2				
				Ba^{138}	90°		3.0 ±0.3				

[51] Supplied by Carbide and Carbon Chemical Division, Oak Ridge National Laboratory, Oak Ridge, Tennessee.

the proton spectrum from Zr^{90} is similar to that from Sr^{88}, in that the first excited level to occur will be separated from the ground-state by about 1 Mev, then a peak may be assigned to the ground-state group from Zr^{92}.

The ground-state peaks for other elements in this region were analyzed as explained for gold. Figure 5 shows the proton spectrum from an indium target. Preliminary results have also been obtained from a Sn^{120} target[81] and a barium target.

C. Nuclei Containing Approximately 28 Neutrons

The proton spectra from odd Z isotopes like cobalt and copper indicate a much smaller level spacing than in even Z nuclei like iron, nickel, and zinc. Table I summarizes the results.

The Ti^{48} ground-state peak can be identified by its intensity. A small peak on the high energy side of this peak is assigned to Ti^{46}. Higher energy protons of low intensity result from the odd mass isotopes. The high energy proton spectrum from the Fe^{56} isotope has been resolved into two peaks as shown in Fig. 6. The small high energy peak is assigned to Fe^{54}. The nickel spectrum is very similar to that of iron and gives an excited level in Ni^{59} at 0.4 Mev. Zn^{64} shows a well-resolved ground-state peak. Higher energy peaks from Zn^{67} are not detected.

Figure 7 shows the proton spectrum from a cobalt

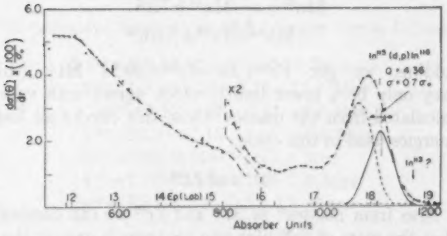

FIG. 5. Proton spectrum at $\theta=30°$ from a 10-mg/cm² indium target from the reaction $In^{115}(d, p)In^{116}$.

target. The ground-state peaks for cobalt and copper were analyzed as explained for gold. The ground-state peak for vanadium was well resolved with the first excited level at 0.8 Mev.

VI. DISCUSSION OF RESULTS

A. Checks for Neutron Binding Energies

Pb^{208}, Pb^{207}, Pt^{195}, *and* Zr^{91}

It was pointed out that the neutron binding energy obtained from the (d, p) method might be only a lower limit. However, if we can also measure the neutron binding energy of the same nucleus from the (γ, n) threshold, or a (d, t) reaction, which set an upper limit, and if the two values agree, then this value must be

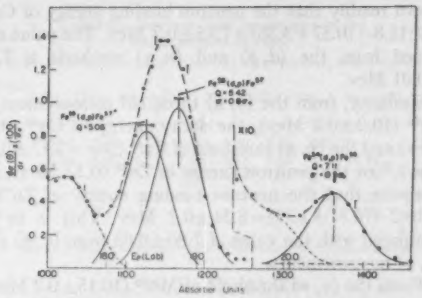

FIG. 6. High energy section of the proton spectrum at $\theta=30°$ from a 20-mg/cm² iron target from the reaction $Fe^{4}(d, p)Fe^{4+1}$.

the correct binding energy. The neutron binding energy of Pb^{208} from the (d, p) and (n, γ) methods is 7.38±0.01 Mev. The value obtained from the (γ, n) threshold is 7.44±0.10 Mev, which agrees. Also the neutron binding energy of Pb^{207} from the (d, p) and (n, γ) method is 6.74±0.01 Mev. The values obtained from the (d, t) and (γ, n) reactions are 6.70±0.05 and 6.93±0.10 Mev, respectively. The (γ, n) measurement is 0.19 Mev too high; but, since the (d, t) value agrees, we can again conclude that this value is correct. The neutron binding energy of Pt^{195} from the (d, p) method is 6.14±0.2 Mev. This agrees with the (γ, n) threshold value of 6.1±0.1 Mev. Finally, the neutron binding energy of Zr^{91} from the (d, p) method is 7.16±0.05 Mev, and from the (γ, n) threshold 7.2±0.4 Mev.

Cu^{64}, Zn^{68}, Fe^{58}, Sn^{121}, *and* Tl^{206}

If we use decay energies[82] or (p, n) thresholds, we can also check several other values. For example, the neutron binding energy for Cu^{64} can be checked as follows. From (γ, n) measurements the neutron binding energy of Zn^{64} is 11.8±0.2 Mev (this may only be an upper limit). From the decay energy of Cu^{64} (0.57 Mev) and the positron energy of Zn^{63} (2.36 Mev) it can be

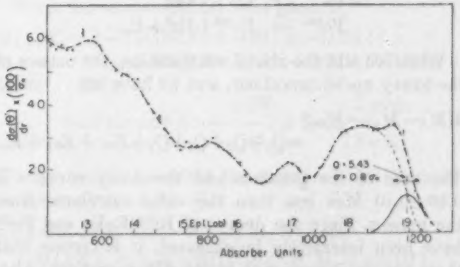

FIG. 7. Proton spectrum at $\theta=15°$ from a 17-mg/cm² cobalt target from the reaction $Co^{59}(d, p)Co^{60}$.

[82] J. Mattauch and A. Flammersfeld, Isotopic Report (1949); G. T. Seaborg and I. Perlman, Revs. Modern Phys. 20, 585 (1948); D. H. Frisch, M.I.T. Lab. Nuclear Science and Engineering, Technical Report No. 43, table compiled by I. Goldin.

shown readily that the neutron binding energy of Cu^{64} is $\leqq 11.8-(0.57+3.38)=7.85\pm0.2$ Mev. The value obtained from the (d, p) and (n, γ) methods is 7.91 ±0.01 Mev.

Similarly, from the (γ, n) threshold measurement of Cu^{65} (10.2$\pm$0.2 Mev), the decay energy of Cu^{64} (0.57 Mev) and the (p, n) threshold of Cu^{65} ($Q=-2.17\pm0.01$ Mev),[58] or the positron energy of Zn^{65} (0.32 Mev), we compute that the neutron binding energy of Zn^{65} is $\leqq 10.2-(0.57+1.39)=8.24\pm0.2$ Mev. This is to be compared with the value of 7.86$\pm$0.03 from (d, p) and (n, γ) measurements.

From the (γ, n) threshold of Mn^{55} (10.15$\pm$0.2 Mev), the (p, n) threshold[54] of Mn^{55} ($Q=-1.16\pm0.02$ Mev) and the neutron binding energy of Fe^{55} (9.28$\pm$0.03 Mev), we can predict the β'-energy of Mn^{54} $E_{\beta'}\leqq 10.15-(9.28+0.38)=0.49\pm0.2$ Mev. It has been reported[55] that there are electrons $\sim$1 Mev, but this is not in agreement with the computed value.

From the neutron binding energy of Sb^{121} (9.25 $\pm$0.2 Mev), the Sn^{121} β-energy (0.38 Mev), and the Sb^{120} positron energy (1.53 Mev), we compute the neutron binding energy of $Sn^{121}\leqq 9.25-(0.38+2.55)=6.32$ $\pm$0.2 Mev. The value obtained from the (d, p) reaction is 6.2$\pm$0.3 Mev.

Finally, from the neutron binding energies of Pb^{206} (8.15$\pm$0.10 Mev) and Tl^{206} (6.23 Mev), and the β-decay energy of Tl^{206} (1.70 Mev), we can predict the energy difference between Pb^{205} and Tl^{205} (0.22 Mev). Thus, Pb^{205} decays by K-capture.

Pb^{209} *and* Bi^{210}

In order to check the values for Pb^{209} and Bi^{210} we can close the following cycle:

$$\begin{aligned}
&Pb^{206}(d, p)Pb^{207}+Q_1\\
&Pb^{207}(d, p)Pb^{208}+Q_2\\
&Pb^{208}(d, p)Pb^{209}+Q_3\\
&Pb^{209}\xrightarrow{\beta'} Bi^{209}+E_{\beta_1'}\\
&Bi^{209}(d, p)\ Bi^{210}+Q_4\\
&Bi^{210}\xrightarrow{\beta'} Po^{210}+E_{\beta_2'}\\
&Po^{210}\xrightarrow{\alpha} Pb^{206}+He^4+E_\alpha.
\end{aligned}$$

When we add the above relationships, the masses of the heavy nuclei cancel out, and we have left

$$4(M_d-M_p)-M_{He^4}=Q_1+Q_2+Q_3+Q_4+E_{\beta_1'}+E_{\beta_2'}+E_\alpha.$$

The sum of the Q-values and the decay energies is 0.40$\pm$0.10 Mev less than the value calculated from the masses. Since the decays of Bi^{210}(RaE) and Po^{210} have been intensively investigated, it is certain that there are no gamma-rays in the disintegrations. Also, it has been reported[52] that there are no gamma-rays in the Pb^{209} β-decay. Preliminary investigations[56] indicate there may be some energy in addition to the β-ray energy. The neutron binding energies predicted by Wapstra[15] agree very well with values derived from Q_1, Q_2, and Q_3. (The maximum difference is 0.19 Mev.) However, Wapstra's computed neutron binding energy of Bi^{210} is 0.55 Mev higher than that derived from Q_4. Since he assumed the decay energy of Pb^{209} to be 0.69 Mev, this indicates that either Q_4 or the Pb^{209} decay energy is not correct. Also, Kinsey, *et al.*,[31] report that the bismuth gamma-ray from neutron capture is broader than expected, and this may be caused by low lying levels in Bi^{210}. There is a level known at 0.047 Mev from the β-decay of Pb^{210}. Thus, it appears that the error is in the Pb^{209} decay. It would be very useful to measure (d, α), (p, α), or (α, p) Q-values in order to check other cycles.

Fe^{55} *and* Mn^{56}

We can also check a few neutron binding energies from mass spectroscopic data. For example, the difference in mass[39] between Fe^{56} and Fe^{54} is 1.99621 amu, from which we calculate that the binding energy of the last two neutrons in Fe^{56} is 20.24$\pm$0.3 Mev. Now we can check the neutron binding energies for Fe^{55} and Mn^{56} by the following cycle.

$$\begin{aligned}
&Fe^{54}+n\rightarrow Fe^{55}+9.28\\
&Fe^{55}\rightarrow Mn^{55}+0.38\\
&Mn^{55}+n\rightarrow Mn^{56}+7.25\\
&Mn^{56}\xrightarrow{\beta,\gamma} Fe^{56}+3.63.[57]
\end{aligned}$$

Adding, we get $Fe^{54}+2n\rightarrow Fe^{56}+20.54$ Mev (this may only be a lower limit), which agrees with value calculated from the masses. Thus, this checks all four energies used in this cycle.

Sr^{89} *and* Zr^{90}

Also from masses[39] of Sr^{88} and Zr^{90} we can compute that the mass of Sr^{88} plus two neutrons is greater than the mass of Zr^{90} by 18.5$\pm$0.8 Mev. Thus, from the cycle

$$\begin{aligned}
&Sr^{88}+n\rightarrow Sr^{89}+6.55\\
&Sr^{89}\xrightarrow{\beta} Y^{89}+1.46\\
&2.05+Y^{89}\leftarrow Zr^{89}\\
&-12.0+Zr^{89}+n\leftarrow Zr^{90},
\end{aligned}$$

we get

$$Sr^{88}+2n\rightarrow Zr^{90}+18.0\ \text{Mev}.$$

This value checks the value calculated from the masses. However, it does not necessarily prove that the four values used are correct, since two values used allow it to be a lower limit and two values permit it to be an upper limit.

[52] Shoupp, Jennings, and Jones, Phys. Rev. **73**, 421 (1948).
[54] H. T. Smith and R. V. Richards, Phys. Rev. **74**, 1257 (1948).
[55] J. D. Kurbatov and D. Gideon, Phys. Rev. **75**, 328 (1949); Emmerich, Balhueg, and Kurbatov, Phys. Rev. **76**, 1891 (1949).
[56] K. Shure and M. Deutsch, private communication.
[57] K. Siegbahn as reported by Mitchell, Revs. Modern Phys. **22**, 36 (1950).

A few other cycles can be completed but are not of sufficient value to be presented.

B. Computed Neutron Binding Energies

Fe^{56} *and* Ni^{65}

From the neutron binding energy of Mn^{56} (7.25 Mev), the decay energy of Mn^{56} (3.63 Mev), and the mass difference of Fe^{55} and Mn^{55} (0.38 Mev) we can readily compute the neutron binding energy of Fe^{56} as follows:

$$E_n \geqq 7.25+0.38+3.63=11.26 \text{ Mev}.$$

Similarly, the neutron binding energy Ni^{65} is $\leqq 10.2-(2.10+1.68)=6.4$ Mev. In the case of Fe^{56} this might only be a lower limit and in Ni^{65}, only an upper limit.

Rb^{87}, Y^{89}, Sr^{90}, Sr^{91}, Y^{91}, $(Rb^{88}-Sr^{88})$

The neutron binding energies for the above elements have been computed from the neutron binding energies in Sr^{87}, Sr^{89}, Zr^{90} and Zr^{91} and the following total decay energies (in Mev):

Rb^{86}	1.82[58]	Sr^{91}	3.2 ± 0.1[58]
Rb^{87}	0.3 ± 0.1[58]	Y^{88}	~ 3.72[61]
Rb^{88}	5.1[62]	Y^{90}	2.180 ± 0.007[59]
Sr^{89}	1.463 ± 0.005[59]	Y^{91}	1.537 ± 0.007[59]
Sr^{90}	0.54[60]	Zr^{89}	2.05[62].

The computed neutron binding energies are as follows:

$$Rb^{87}=8.5+1.82-0.3=10.0 \text{ Mev}$$
$$Y^{89} \geqq 6.55+1.46+3.72=11.7 \text{ Mev}$$
$$Sr^{90}=7.8+1.46-0.54=8.7 \text{ Mev}$$
$$Y^{90} \leqq 12.0-(2.18+2.05)=7.8 \text{ Mev}$$
$$Sr^{91}=7.8+0.54-3.2=5.1 \text{ Mev}$$
$$Y^{91}=7.16+2.18-1.54=7.8 \text{ Mev}$$
$$Sr^{88}-Rb^{88}=5.1-0.3=4.8 \text{ Mev}.$$

The value for Y^{89} may only be a lower limit and the value for Y^{90} may be an upper limit. The other values may be upper or lower limits, depending on which decay energy is in error.

La^{139}

The neutron binding energy for La^{139} can be computed from the value for Ba^{139}, the decay energy of Ba^{139} (3.5 Mev), and the decay of La^{138}. It has been reported[62] that a 1-Mev γ-ray occurs in the K-capture of La^{138}; thus, this represents a lower limit to the energy. Then the neutron binding energy in $La^{139} \geqq 5.2+(3.5+1.0)=9.7$ Mev.

[58] Zaffarano, Kern, and Mitchell, Phys. Rev. **74**, 682 (1948).
[59] L. M. Langer and H. Clay Price, Phys. Rev. **76**, 640 (1949).
[60] L. J. Laslett, Phys. Rev. **79**, 412 (1950).
[61] W. C. Peacock and J. W. Jones, reported in G. T. Seaborg and I. Perlman, reference 52.
[62] Pringle, Standil, and Roulston, Phys. Rev. **78**, 303 (1950).

TABLE II. Neutron binding energies in the neighborhood of lead.

Z \ N+1	122	123	124	125	126	127	128	129	130	131
81	6.54	7.48	6.23	6.97	3.86	5.08	3.00			
82	6.49	8.15	6.74	7.38	3.87	5.20	3.75	5.21		
83				7.44	4.17	5.09	4.41	5.31	3.36	
84			6.71	7.77	4.56	6.01	4.32	5.87	4.08	
85								5.89	4.57	
86									4.7	

Tl, Pb, Bi, Po, At, Em

The neutron binding energies in this region have been predicted by many writers.[10–15] Table II has been computed from the decay energies listed by Wapstra[5] on the assumption that the 0.40-Mev error in closing the lead cycle is due to the Pb^{209} decay. The computed values are not changed if the error is due to the Bi^{210} neutron binding energy. The underlined values are observed values.

C. The Closed Shells of 126, 82, 50, and 28 Neutrons

The neutron binding energy of a nucleus depends on many factors and fluctuates by several Mev, excluding the closed shell effect. For example, nuclei with an even number of neutrons such as Cu^{62} ($E_n=10.9$ Mev) and Cu^{65} ($E_n=10.2$ Mev) have higher neutron binding energies than does a nucleus with an odd number of neutrons such as Cu^{64} ($E_n=7.9$ Mev). This is the θ-term in the semi-empirical mass formula, which gives a value of 3.0 Mev. The semi-empirical mass formula also has a term proportional to $(\frac{1}{2}A-Z)^2$. Thus, the neutron binding energy is greater in the lighter nucleus. For example, the calculated neutron binding energy in Cu^{63} is greater than that in Cu^{65} by 1.0 Mev. Other small effects are caused by the change in the Coulomb energy and the fluctuation in the surface energy. These effects can also be estimated from the semi-empirical mass formula.

From the semi-empirical mass formula,[63]

$$M(A,Z)=A-0.00081Z-0.00611A+0.014A^{\frac{1}{3}}+0.083(\tfrac{1}{2}A-Z)^2A^{-1}+0.000627Z^2A^{-\frac{4}{3}}+\theta,$$

where

$$\delta=0 \text{ for odd } A=\mp\frac{0.036}{A^{\frac{1}{3}}} \quad A \text{ even}\begin{cases} Z \text{ even} \\ Z \text{ odd}. \end{cases}$$

We can readily calculate the neutron binding energy for the nucleus $(A+1, Z)$

$$E_n(A+1,Z) \text{ in Mev}=931[M(A,Z)+M_n-M(A+1,Z)]=0.931[15.04+14[A^{\frac{1}{3}}-(A+1)^{\frac{1}{3}}]+83\{(\tfrac{1}{2}A-Z)^2/A-[\tfrac{1}{2}(A+1)-Z]^2/(A+1)\}+0.627Z^2[A^{-\frac{1}{3}}-(A+1)^{-\frac{1}{3}}]+\delta],$$

[63] C. F. v. Weizsacker, Z. Physik **96**, 431 (1935); N. Bohr and J. A. Wheeler, Phys. Rev. **56**, 426 (1939); E. Fermi, *Nuclear Physics* (The University of Chicago Press, 1950), p. 7.

TABLE III. Neutron binding energies.

$N+1$ No. of neutrons	$A+1$	Z	(γ, n) thresholds	(n, γ) Kinsey, *et al.*	(d, p) reaction	$(E_n)_{cal}$ B.W.	$(E_n)_{exp} - (E_n)_{cal}$
24	46	22	13.3 ±0.2			12.79	0.4
25	47	22			8.74±0.1	8.24	0.5
26	48	22			11.05±0.4	11.24	−0.2
26	50	24	13.4 ±0.2			12.88	0.5
27	49	22			8.15±0.05	6.91	1.3
28	54	26	13.8 ±0.2			12.96	0.8
29	52	23		7.30	7.25±0.05	6.58	0.7
29	55	26		9.28	9.34±0.05	8.95	0.4
30	55	25	10.15±0.2			10.92	−0.8
30	56	26			≧11.3 (cal.)	11.62	≧−0.3
30	58	28	11.7 ±0.2			13.04	−1.3
31	56	25		7.25	7.2[a]	7.03	0.2
31	57	26		7.63	7.65±0.10	7.76	−0.1
31	59	28		9.01	9.01±0.10	9.23	−0.2
33	60	27		7.73	7.66±0.2	7.43	0.3
34	63	29	10.9 ±0.2			11.31	−0.4
34	64	30	11.8 ±0.2			11.93	−0.1
35	64	29		7.91	7.78±0.2	7.79	0.1
35	65	30		7.86	7.92±0.05	8.43	−0.6
36	65	29	10.2 ±0.2			10.26	−0.1
37	65	28			≦6.4 (cal.)	6.20	≦0.2
40	70	30	9.2 ±0.2			8.97	0.2
42	75	33	10.3 ±0.2			9.78	0.5
44	79	35	10.7 ±0.2			10.00	0.7
46	81	35	10.2 ±0.2			9.22	1.0
48	82	34	9.8 ±0.5			7.99	1.8
49	87	38		8.42	8.52±0.2	7.18	1.3
50	87	37			≈10.0 (cal.)	8.74	≈1.3
50	89	39			≦11.7 (cal.)	9.64	≦2.1
50	90	40	12.0 ±0.2			10.10	1.9
50	92	42	13.28±0.15			11.00	2.3
(50–51)	(88)	(38–37)			≈(4.8 cal.)	(3.2)	≈(1.6)
51	89	38			6.55±0.2	6.53	0.0
51	90	39			≦7.8 (cal.)	7.02	≦0.8
51	91	40	7.2 ±0.4		7.16±0.05	7.46	−0.3
51	93	42			8.31±0.2	8.39	−0.1
52	90	38			≈8.7 (cal.)	8.47	≈0.2
52	91	39			≈7.8 (cal.)	8.94	≈−1.1
52	92	40			8.73±0.10	9.40	−0.7
53	91	38			≈5.1 (cal.)	5.92	≈−0.8
53	93	40			6.56±0.10(?)	6.83	−0.3(?)
53	94	41			7.26±0.10	7.29	0.0
55	97	42	7.1 ±0.3			7.11	0.0
59	104	45			6.81±0.2	7.22	−0.4
60	107	47	>9.5			9.77	>−0.3
61	108	47			7.01±0.2	7.47	−0.5
62	109	47	9.3 ±0.5			9.20	0.1
65	113	48	6.44±0.15			6.80	−0.4
66	115	49	9.5 ±0.5			8.85	0.6
67	116	49			6.59±0.2	6.69	−0.1
68	118	50		9.33	9.37±0.2	8.68	0.7
69	119	50	6.51±0.15			6.57	−0.1
70	121	51	9.25±0.2			8.54	0.7
71	121	50			6.2±0.3	6.12	0.1
71	122	51		7.02	6.64±0.2	6.47	0.2
74	124	50	8.50±0.15			7.30	1.2
74	127	53	{9.3 ±0.2 9.45±0.2			8.27	1.1
82	139	57			≧9.7 (cal.)	7.78	≧1.9
82	141	59	{9.4 ±0.1 9.8 ±0.3			8.39	1.2
83	139	56			5.2±0.3	5.63	−0.4
90	150	60	7.4 ±0.2			7.16	0.2
108	181	73	7.7 ±0.2			7.49	0.2
109	182	73		6.07	6.03±0.15	5.98	0.1
117	195	78	6.1 ±0.1		6.14±0.2	6.02	0.1
118	196	78			8.0±0.2(?)	7.17	0.8(?)
118	197	79	{8.00±0.15 8.10±0.10			7.38	0.6
119	198	79		6.54	6.35±0.15	5.98	0.5
121	201	80	{6.25±0.2 6.6 ±0.2			5.94	0.4

TABLE III.—(*Continued*).

$N+1$ No. of neutrons	$A+1$	Z	(γ, n) thresholds	(n, γ) Kinsey, *et al.*	(d, p) reaction	$(E_n)_{sm}$ B.W.	$(E_n)_{exp} - (E_n)_{sm}$
123	204	81		6.54	6.52±0.15	5.89	0.6
124	205	81	7.48±0.15 7.3 ±0.25		7.7±0.2[a]	7.02	0.5
124	206	82	8.25±0.10		8.10±0.10[a]	7.21	1.0
125	206	81		6.23	6.16±0.15	5.65	0.6
125	207	82	6.95±0.10 6.9 ±0.1	6.737±0.01	6.71±0.03 6.70±0.05[a]	5.85	0.9
126	208	82	7.44±0.10	7.38±0.01	7.37±0.03	6.96	0.4
126	209	83	7.45±0.2 7.2 ±0.1		7.44±0.05[a]	7.16	0.3
127	209	82			3.87±0.05	5.62	−1.75
127	210	83		4.17 ±0.015	4.14±0.03	5.82	−1.65
142	232	90	6.0 ±0.15			6.62	−0.6
143	233	90			4.9±0.2[b]	5.3	−0.4
146	238	92	5.8 ±0.15		5.9±0.2[b]	6.59	−0.7
147	239	92			4.63±0.15	5.34	−0.7

[a] These values are from the (d, t) reaction.
[a] W. D. Whitehead and N. P. Heydenburg, Phys. Rev. 79, 99 (1950).
[b] Preliminary result added in proof.

where

$$\delta = \mp \frac{36}{A^{\frac{1}{2}}} \quad A \text{ even} \begin{cases} Z \text{ even} \\ Z \text{ odd} \end{cases}$$

$$= \pm \frac{36}{(A+1)^{\frac{1}{2}}} \quad A \text{ odd} \begin{cases} Z \text{ even} \\ Z \text{ odd.} \end{cases}$$

Table III contains the neutron binding energies determined from (γ, n) threshold measurements,[17,20–26] from the gamma-ray energies in neutron capture,[21–23] and from the (d, p) reaction. Also included in the (d, p) column are a few values from the (d, t) reaction noted by asterisks and the computed values. The calculated values from the semi-empirical mass formula are also listed. The last column is the difference between the observed and the calculated values.

The results are plotted in Fig. 8. Since the (n, γ) measurements are in agreement with the (d, p) measurements, the (n, γ) data have not been plotted. Also, (γ, n) values have not been plotted where (d, t) Q-values were measured. Figure 8 shows sharp discontinuities at 126 and 50 neutrons. The binding energy of the 127th neutron is about 2.2 Mev less than the binding energy of the 126th neutron. Also, the binding energy of the 50th neutron is a little more than 2 Mev greater than the binding energy of the 51st neutron. We can also see that there is another drop in the region of 82 neutrons. In the region of 28 neutrons, there does seem to be a decrease of about 1 Mev. However, this decrease is between 29 and 30 neutrons. If one considers only the (γ, n) data, the decrease is almost 2 Mev. The evidence of the closed shell of 28 neutrons is not very conclusive.

D. The Low Intensity of Ground-State Peaks from Even Z, Odd A Nuclei

The differential cross section of the ground-state peak from an even Z, odd A isotope at forward angles is much smaller than that from an isotope of the same Z but an even A. For the targets where the ground-state peak from an odd isotope was sufficient to be detected (Pt^{195}, Zr^{91}, $Ti^{47,49}$), the differential cross section of the ground-state peak was only about 10 percent that of an even A isotope. Also, for other targets where the intensity was too low to be detected (Sr^{87}, $Mo^{95,97}$, Fe^{57}, and Zn^{67}), we can set an upper limit for their differential cross sections at 10 percent that of an even A isotope. The ground-state peaks from Sn^{117} and Pb^{207}, however, have differential cross sections about one-half

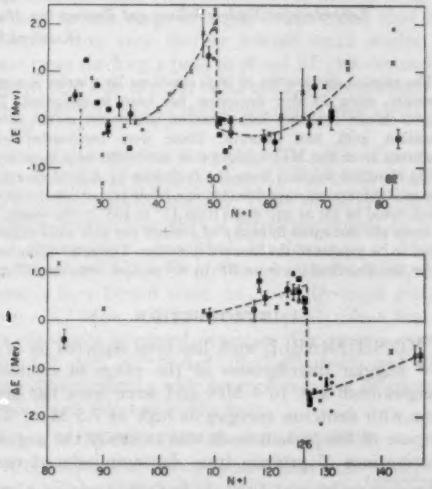

FIG. 8. ΔE is the difference between the observed neutron binding energy for a nucleus with $N+1$ neutrons and the neutron binding energy calculated from the semi-empirical mass formula, plotted *vs* the number of neutrons $N+1$. ■(d, p) reaction with 14-Mev deuterons. ▲(d, t) reaction with 14-Mev deuterons. ×(γ, n) thresholds. ● computed from decay energies.

those of the even Z isotopes. This may be a result of the closed shells of 50 and 82 protons.

The differential cross sections for these even Z, odd A ground-state peaks are low for probably two reasons. First, since the Q-values for these nuclei are larger than for even Z, even A nuclei, their proton energies will be higher. High energy protons are less probable because of the momentum distribution of the proton in the deuteron. The second reason is that the neutron from the deuteron may not pair up with the odd neutron in the target nucleus for nuclear reasons.

The author is indebted to Professors M. Deutsch and M. S. Livingston under whose direction this research was carried out. He would also like to thank M. Deutsch for many helpful criticisms in the preparation of this paper for publication. The equipment was built in collaboration with K. Boyer and H. E. Gove, with whom the author has had many valuable discussions. The cooperation of all the personnel of the Cyclotron Laboratory, Mr. F. J. Fay, Mr. R. W. Kilson, Mr. E. Pulster, and Mr. E. F. White, is gratefully acknowledged. Many of the targets were rolled foils supplied through the kindness of Dr. J. R. Low of the Knolls Atomic Power Laboratory. The chemistry on the separated lead isotopes was done by Mrs. E. Backofen.

APPENDIX

RELATIVE STOPPING POWER OF VARIOUS ELEMENTS

The relative stopping power (relative to aluminum) was measured for 19-Mev protons and 14-Mev deuterons for nearly all of the targets. The values were plotted *vs* Z and a straight line drawn through the points. A few values are compared to values computed from Livingston and Bethe and also to values obtained by Kelly[44] using 28-Mev alpha-particles.

$E_p = 19.0$ Mev

No. of mg/cm^2 = 1 mg/cm^2 Al

Element	Experimental	L. and B.	Percent difference
Au	1.82±0.02	1.96	7
Ag	1.42±0.03	1.55	9
Cu	1.20±0.03	1.26	5

$E_d = 14$ Mev

No. of mg/cm^2 = 1 mg/cm^2 of Al

Element	Experimental	L. and B.	Percent difference	$E_\alpha = 28$ Mev Kelly
Au	2.045±0.01	2.10	2.5	1.99
Ag	1.54 ±0.02	1.61	4.5	1.54
Cu	1.26 ±0.02	1.29	2.5	1.28

[44] E. L. Kelly, Phys. Rev. 75, 1006 (1949).

PHYSICAL REVIEW VOLUME 81, NUMBER 3 FEBRUARY 1, 1951

Angular Distributions of (d,p) Reactions Using 14-Mev Deuterons*

H. E. GOVE

Laboratory for Nuclear Science and Engineering, Massachusetts Institute of Technology, Cambridge, Massachusetts

(Received September 21, 1950)

The angular distribution of (d,p) reactions for a series of target elements, using 14-Mev deuterons has been investigated. The targets chosen were thin foils of carbon, aluminum, nickel, silver, tantalum, gold, and bismuth. These were bombarded with deuterons from the MIT cyclotron in the center of a large scattering chamber shielded from the cyclotron by 4 ft of concrete. The emitted protons were detected in a triple proportional counter which could be set at any angle from 15° to 135° to the beam. In all cases the measured intensity of protons per unit solid angle is found to be greater in the forward direction. The ratio of the area under the distributions from 20° to 90° to that between 90° and 140° varies from 1.6 to 13. For a given element this ratio increases with proton energy. In addition, for carbon and aluminum, in which individual groups can be resolved, the intensity of protons in a given group, in some cases, exhibits maxima at various angles. In the three elements of highest atomic number the intensity rises from back angles to a maximum at some forward angle and then drops off towards zero degrees. The position of this "turn over" angle appears to increase slowly with atomic number. The general features of the distributions appear to be explainable on a stripping picture rather than that of a compound nucleus.

I. INTRODUCTION

CONSIDERABLE work has been reported on (d,p) angular distributions in the range of deuteron energies from zero to 4 Mev and some work has been done with deuteron energies as high as 7.5 Mev. The purpose of the present work was to study the angular distributions of protons from deuteron-induced reactions at a fixed deuteron energy of 14 Mev over a wide range of atomic number. Detailed studies of (d,p) reactions in the energy range near 15 Mev have been largely neglected and to the best of our knowledge there has been no previous work of this nature reported.

Heydenburg and Inglis[1] have investigated the excitation curves and the angular distributions of proton groups from $O^{16}(d,p)O^{17}$ leaving O^{17} in its ground, and first excited state for deuteron energies between 0.6 and 3 Mev. The excitation curves indicate resonances. The

* Part of thesis submitted in partial fulfillment of the requirements for the degree of Doctor of Philosophy at the Massachusetts Institute of Technology. This work has been assisted by the joint program of the ONR and the AEC. Some of the results have been previously reported at the New York meeting, February, 1950, and the Washington meeting, April, 1950, of the American Physical Society.

[1] N. P. H. Heydenburg and D. R. Inglis, Phys. Rev. 73, 230 (1948).

character of the asymmetry about 90° of the angular distributions seems to be a rather random function of the deuteron energy except that the distributions show a tendency to become more nearly symmetric about 90° as the deuteron energy approaches that of the peaks in the excitation curve. In some later work Heydenburg, Inglis, Whitehead, and Hafner[2] studied the reaction $C^{12}(d,p)C^{13}$ for deuteron energies from 1 to 3.5 Mev. In this case the excitation curve shows resonances which agree with energy levels in N^{14} found by measuring γ resonances. Although the angular distributions at various energies were not investigated in such great detail, the results were similar to those from $O^{16}(d,p)O^{17}$ as regards the variation in the character of the asymmetry about 90° with deuteron energy. The angular distribution of protons from $N^{14}(d,p)N^{15}$ leaving N^{15} in its ground and first excited states has been investigated by Wyly[3] for deuteron energies between 1.5 and 3 Mev. The long range group is slightly forward over the whole energy range while the short range group is spherically symmetric. No excitation functions were obtained and there were no marked variations in the distributions with energy. The angular distribution of two proton groups from the reaction $O^{16}(d,p)O^{17}$ and five groups from $Al^{27}(d,p)Al^{28}$ have been reported by Nemilov and Funshtein[4] for 3.9-Mev deuterons. The distributions are markedly forward in all cases except for the two long range groups which are isotropic. The lower energy proton groups are progressively more forward than the high groups; other than this the variation with angle is quite smooth. The angular distribution of the long range proton group from $B^{10}(d,p)B^{11}$ has been investigated by Redman[5] for deuterons between 1 and 3.7 Mev. The distributions when analyzed in an expansion of Legendre polynomials show the presence of a P_1-term giving a forward asymmetry at all but the lowest energy. The highest term required to fit the data was P_2. Whaling and Bonner[6] have studied the disintegration of Li^6 by deuterons. In particular, for the $Li^6(d,p)Li^7$ process the excitation curve for the long and short range proton groups shows no resonance structure for energies up to 1.8 Mev. The angular distributions of these two groups taken at energies between 0.4 and 1.4 Mev show the presence of terms in the Legendre polynomial as high as P_6. Again there is a reasonably smooth change in the shape of the distributions with deuteron energy.

Since the present work was completed the angular distribution of various portions of the proton spectrum from the reaction $Al^{27}(d,p)Al^{28}$ between 25° and 140° has been reported by Holt and Young.[7] Using deuteron energies of 4.6, 5.8, and 7.5 Mev, they find that the distributions are forward in all cases. The angular distribution of the long range proton group for this reaction as measured by the author at 13.8 Mev, and by Holt and Young at 7.5, 5.8, and 4.6, is discussed later in this paper and is illustrated in Fig. 16.

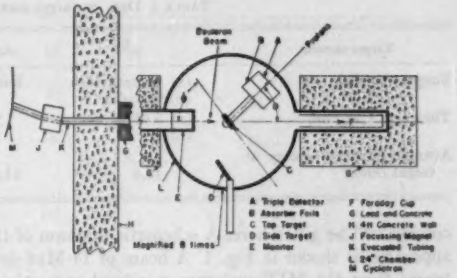

FIG. 1. Schematic diagram of apparatus for measuring angular distributions using a triple proportional counter.

There has been some work done by Helmholz, McMillan, and Sewell[8] on (d,n) angular distributions using very high energy deuterons (about 200 Mev). The distributions are very strongly peaked in the forward direction having angular widths at half maximum around 10°.

Substantial work has been done by Falk[9] on the angular distributions of (d,n) reactions using 15-Mev deuterons. Nine elements ranging from Be to Au were used and the thick target yield of neutrons with angle was measured using the radioactivity produced in silver by the $(n,2n)$ reaction with a threshold of 11 Mev. The measurements were made on both sides of 0° up to 50° and in this range of angle it was found that the intensity rose very sharply toward small angles, in some cases reaching a peak at about 10° and decreasing toward zero and in other cases reaching a maximum at zero. The width at half maximum varies from about 20° to 50°.

This paper reports the yield with angle of protons from reactions in which the neutron was left in a bound state in the residual nucleus. These would be protons of range greater than that of elastic deuterons. In fact, it is quite easy to show that, for deuterons of energy greater than 8 Mev, protons emitted leaving the neutron in a bound state, i.e., with Q-values greater than -2.2 Mev, will have ranges greater than that of the elastically scattered deuteron. The targets chosen were C^{12}, Al^{27}, $Ni^{58,60}$ $Ag^{107,109}$, Ta^{181}, Au^{197}, and Bi^{209} since these covered a wide range of values of Z and were available in thin foil or film form.

II. EXPERIMENTAL ARRANGEMENT

A description of the equipment used in these experiments will be published shortly[10] and only a brief dis-

[2] Heydenburg, Inglis, Whitehead, and Hafner, Phys. Rev. **75**, 1147 (1949).
[3] L. D. Wyly; Phys. Rev. **76**, 104 (1949).
[4] Y. A. Nemilov and B. L. Funshtein, Inst. of Radium, USSR Academy of Science **66**, 609 (1949).
[5] W. C. Redman, Phys. Rev. **79**, 6 (1950).
[6] W. Whaling and T. W. Bonner, Phys. Rev. **79**, 258 (1950).
[7] J. R. Holt and C. T. Young, Proc. Phys. Soc. (London) **A63**, 833 (1950).
[8] Helmholz, McMillan, and Sewell, Phys. Rev. **72**, 1003 (1947).
[9] C. E. Falk, Carnegie Inst. of Tech., Tech. Rep. 5 (July 1, 1950) (to be published).
[10] Boyer, Gove, Harvey, Livingston, and Deutsch (to be published).

TABLE I. Data on target materials, thickness, and deuteron energy.

Target element	$_6C^{13}$	$_{13}Al^{27}$	$_{28}Ni^{58,60}$	$_{47}Ag^{107,109}$	$_{73}Ta^{181}$	$_{79}Au^{197}$	$_{83}Bi^{209}$
Target material	(a) polyethylene (b) aquadag	foil	foil	foil	foil	(a) foil (b) foil	evaporated film
Thickness (mg/cm²)	(a) 3.95 (b) 1	1.9	4	7.3	15.5	(a) 24 (b) 6.6	12
Average deuteron energy at target center	13.8	13.8	13.8	13.8	13.9	13.6	13.8

cussion will be given here. A schematic diagram of the apparatus is shown in Fig. 1. A beam of 14-Mev deuterons from the MIT cyclotron was used to bombard thin targets in the center of a large evacuated chamber located about 12 ft from the cyclotron and separated from it by a 4-ft thick concrete wall. At the entrance to the chamber the deuteron beam passed through a parallel plate ionization chamber which was provided with lead slits, placed before and after, to ensure that all deuterons passing through it struck the target. The output current from this monitor was integrated electronically so that counts were measured for a constant number of deuterons incident on the target. The emitted protons were detected in a triple proportional counter arrangement, the three sections of which were placed in triple coincidence, and which could be set at any angle from 15° to 135° with respect to the deuteron beam. The detector and the associated electronic circuits were designed to count only those protons whose ranges terminated in the detector. A system of graded aluminum foils set in front of the detector was used to scan the spectrum of the emitted protons, and between these and the target an aperture 0.4 in. wide and 0.75 in. high defined a solid angle of 0.013 steradian. The target to be investigated was placed in a target holder inserted through to top lid of the chamber. Fragile targets were mounted in thin aluminum frames large enough so that no deuterons could strike the frame. A separate target holder which could be introduced through the side of the chamber was provided, and an element was chosen for this side target which gave a well-resolved proton group upon deuteron bombardment. This could be used both to line up the equipment initially and to check on drifts. In general it was a 1.9 mg/cm² aluminum foil which gives a fairly well-resolved long range proton group from the reaction $Al^{27}(d,p)$, $Q=5.5$ Mev (Fig. 4). Another convenient side target material was found to be polyethylene of thickness 3.95 mg/cm² carbon content which gives a very well-resolved proton group from the reaction $C^{13}(d,p)$, $Q=2.7$ Mev (Fig. 2).

III. PROCEDURE

The target to be investigated was placed in the top target holder and the discriminator gate settings and amplifier gains for the three sections of the triple chamber were adjusted so that a plot of triple coincidences *vs* range gave a narrow symmetrical peak from the side target. The side target was then removed, the top target inserted, and a plot of triple coincidences *vs* range was recorded for all protons with range greater than that of the elastic deuterons at a series of angles between 15 and 135. The counting time for each point on these plots of the energy spectrum was determined by integrating the deuteron beam current produced in the monitor. Between each run at a given angle on the top target, the side target would be inserted and a plot of the normalization peak would be taken. The top target run would be repeated if the area under this normalization peak had changed more than 10 percent during the run. The target and counter angles are indicated in Fig. 1.

The following relationsip between θ and ϕ was maintained for the reflection and transmission cases

$$\text{for } \theta \lesssim 90^\circ \quad \phi = 90 - \theta/2$$
$$\text{for } \theta \gtrsim 90^\circ \quad \phi = 180 - \theta/2.$$

In all of the elements studied, with exception of carbon and the long range proton group from aluminum, the close level spacing and the poor resolution inherent in range measurements made it impossible to resolve individual groups. In these cases angular distributions of segments of the spectrum were measured. This was accomplished by marking on the abscissa which is linear in range (mg/cm² Al), the values of the energy in the center of mass system. These will be nonlinear in the proper way so that the area under the curve measured between any two limits of center of mass energy will be the same as would be the case if the spectrum had been replotted on a scale linear in E with the ordinate multiplied by $\Delta R/\Delta E$. The areas are then multiplied by a factor $\sin\phi$ to compensate for varying thickness presented by the target to the deuteron beam as the angle is varied and a normalization factor N which is the mean area of the normalization peak taken before and after the run to compensate for drift. The third factor applied compensates for the fact that the solid angle in which the protons are accepted by the counter, while constant in the laboratory system of coordinates, varies with angle and energy in the center of mass system. This correction, which has been discussed by several authors,[1] is given by

$$g(\theta) = \frac{\text{center of mass intensity}}{\text{laboratory intensity}} = \frac{\sin\theta d\theta}{\sin\theta' d\theta'},$$

where θ and θ' are the counter angles in the laboratory and center of mass system. This can be written as

$$g(\theta)=[1-2\cos\theta/K(\theta)+1/K^2(\theta)]^{\frac{1}{2}}[1-\cos\theta/K(\theta)],$$
$$K(\theta)=\cos\theta+(\cos^2\theta+G)^{\frac{1}{2}}, \quad (1)$$
$$G=M_c[M_2(1+Q/E_1)-m_1]/m_1m_2.$$

Here m_1, M_c, m_2, M_2 are the masses of the bombarding particle, the "compound" nucleus, the emitted particle, and the residual nucleus, respectively. E_1 is the energy of the bombarding particle in the laboratory system and Q is the reaction energy. For cases of medium atomic number where $G>1$ the expression reduces to

$$g(\theta)\simeq 1-(2\cos\theta/G^{\frac{1}{2}}). \quad (2)$$

For large atomic numbers such as gold, $g(\theta)\sim 1$, and can be ignored.

The areas corrected in this way are plotted against the center of mass angle given by the relation

$$\tan\theta'=K\sin\theta/(K\cos\theta-1). \quad (3)$$

Again for $G>1$ this reduces to $\theta'=\theta$.

Because of the rapid variation of intensity with angle the intensity has been plotted on a logarithmic scale on the ordinates of the figures shown in order that several angular distributions could be displayed on one figure.

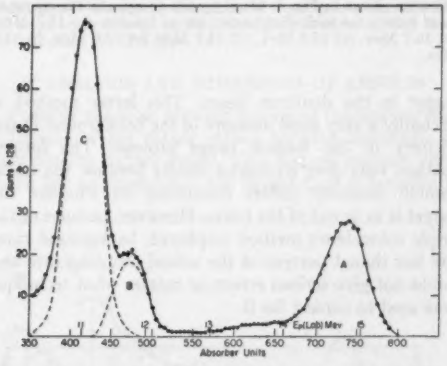

FIG. 2. Proton spectrum from the reaction $C^{12}(d,p)C^{13}$ taken at $\theta=60°$. The ordinate gives the triple coincidence counts on a scale of 128 and the abscissa gives the thickness of absorber inserted between the target and detector in units of 0.416 mg/cm² of aluminum. Also marked on the abscissa is the proton energy in Mev in the laboratory system.

IV. RESULTS

Table I lists the target elements used, along with the target material and thickness and the average deuteron energy at the target center. The measured intensities per unit solid angle for various segments of the emitted proton spectra for the seven elements studied are shown in Figs. 3, 5, 7, 9, 11, 13, and 15. In these figures the intensity has been plotted on a logarithmic scale against the center of mass angle θ' as abscissa or against laboratory angle θ where the difference is negligible.

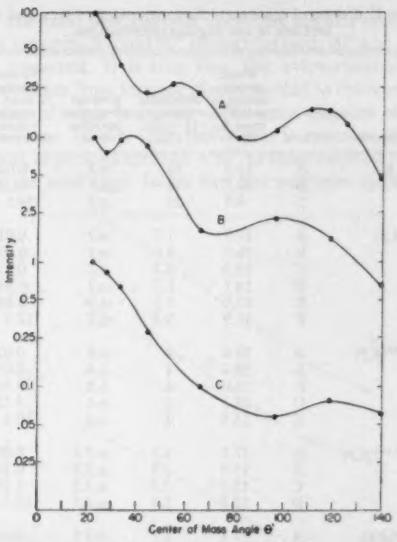

FIG. 3. The angular distributions of protons from the reaction $C^{12}(d,p)C^{13}$ for the three proton groups shown in Fig. 2. The abscissa is proportional to the number of protons emitted at a given angle per unit solid angle. The proton energies for each distribution are the following: (a) 13.5 Mev, (b) 10.7 Mev, (c) 9.9 Mev in the center of mass system.

Typical spectra at one angle for each of the seven targets are shown in Figs. 2, 4, 6, 8, 10, 12, and 14. The choice of segments is shown in each case and lettered alphabetically, corresponding to the lettering on the angular distributions.

Table II lists the mean proton energy in the center of mass system for each of the angular distributions, the average percentage probable error in any of the points plotted on the angular distributions, and finally a factor by which all the points plotted in a given distribution should be multiplied to obtain the differential cross section in units of σ_1, where σ_1 is the differential cross section at 30° for the reaction $Al^{27}(d,p)$; $Q=5.5$ Mev. The absolute value of σ_1 has been measured by the author[11] to be roughly 2.4 millibarns/atom-steradian. The probable error was obtained from the average variation in area of the normalization peak taken before and after a run at a given angle, or where runs have been repeated, from the average variations in the repeated values. Because of the extremely high counting rates, statistical errors can be neglected in most cases. There are, however, two other sources of possible error which cannot be estimated accurately. The first occurs principally at small forward angles and is caused by the presence on the target of carbon and oxygen contamination. These contaminant peaks must be excluded when the area is measured and this introduces some

[11] H. E. Gove and K. Boyer, Phys. Rev. 79, 241A (1950).

TABLE II. Center of mass correction, percentage errors, and cross sections of the angular distributions.

Reaction	Curve	Mean proton energy in center of mass E_p (Mev)	Maximum value of $\lvert 1-g(\theta)\rvert$ (%)	Average percentage probable error	To obtain cross section in units of σ_1 multiply values on each curve by
$C^{12}(d,p)$	A	13.5	16	±3	0.0266
	B	10.7	18	±5	0.226
	C	9.9	20	±5	19.1
$Al^{27}(d,p)$	A	17.7	7.7	±2	0.010
	B	16.7	8.0	±2	0.020
	C	15.5	8.3	±2	0.155
	D	14.1	8.7	±2	0.849
	E	13.0	9.1	±2	5.04
	F	11.9	9.5	±2	12.5
$Ni^{58,60}(d,p)$	A	19.6	4	±4	0.0297
	B	18.4	4	±4	0.0744
	C	16.9	4	±4	0.561
	D	15.3	4	±4	3.73
	E	13.5	4	±4	10.3
$Ag^{107,109}(d,p)$	A	17.1	2.5	±2.5	0.0348
	B	15.0	2.5	±2.5	0.179
	C	13.5	2.5	±2.5	1.21
	D	12.5	2.5	±2.5	15.3
$Ta^{181}(d,p)$	A	17.1	1.7	±3.5	0.0318
	B	15.8	1.7	±3.5	0.296
	C	14.7	1.7	±3.5	1.63
	D	13.4	1.7	±3.5	6.06
	E	12.1	1.7	±3.5	37.5
$Au^{197}(d,p)$	A	17.2	1.5	±5.0	0.0864
	B	15.8	1.5	±2.5	0.169
	C	14.4	1.5	±2.5	0.826
	D	13.3	1.5	±2.5	5.95
	E	11.9	1.5	±2.5	7.85
$Bi^{209}(d,p)$	A	15.3	1.4	±2	0.0403
	B	13.7	1.4	±2	4.06
	C	12.7	1.4	±2	41.1

uncertainty. The second effect is that of background. As a rule this is measured in two ways, first by raising the target and measuring the counting rate, and secondly by continuing to measure the counting rate well beyond the longest range proton group with the target in the deuteron beam. This latter method is probably a very good measure of the background in the vicinity of the longest range protons. The former method may give erroneous results because the background intensity differs depending on whether the target is in or out of the beam. However, because of the triple coincidence method employed, background rates are less than 1 percent of the actual counting rate and could not give serious errors no matter what technique was used to correct for it.

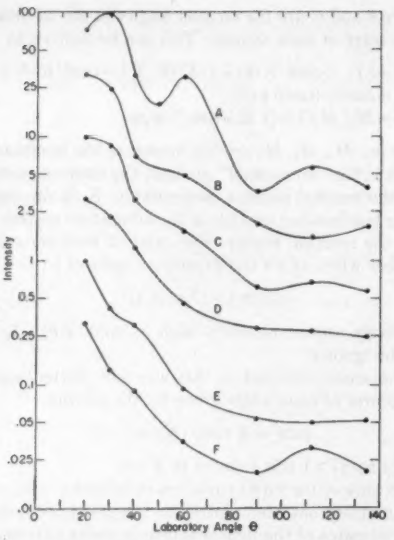

FIG. 5. Angular distributions of protons from the reaction $Al^{27}(d,p)Al^{28}$ for the long range proton group and the segments of spectrum shown in Fig. 4. Mean proton energies in the center of mass system for each distribution are as follows: (a) 17.7 Mev, (b) 16.7 Mev, (c) 15.5 Mev, (d) 14.1 Mev, (e) 13.0 Mev, (f) 11.9 Mev.

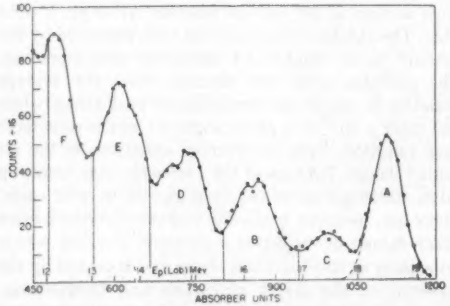

FIG. 4. Proton spectrum from the reaction $Al^{27}(d,p)Al^{28}$ taken at $\theta = 60°$. For this and all subsequent figures of proton spectra the abscissa scale is in units of 0.416 mg/cm² and the proton energy scale is given in Mev in the laboratory system.

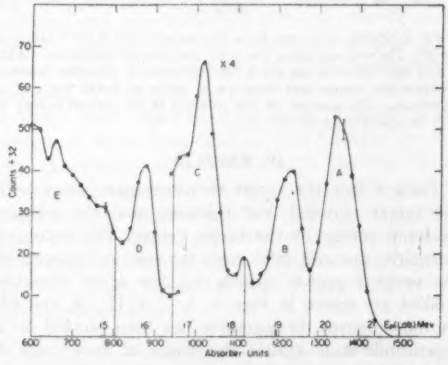

FIG. 6. Proton spectrum from the reaction $Ni^{58,60}(d,p)Ni^{59,61}$ taken at $\theta = 30°$.

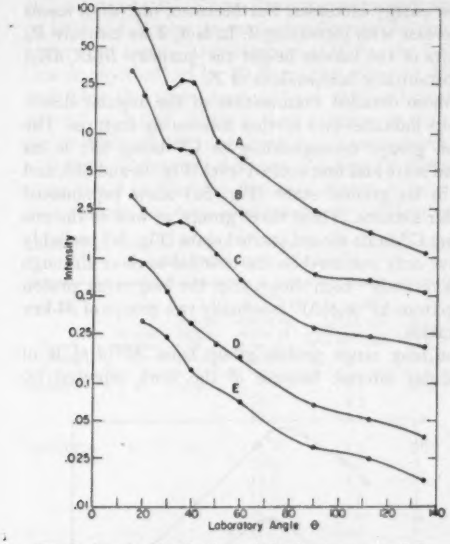

FIG. 7. Angular distributions of the five segments of the proton spectrum shown in Fig. 6 for the reaction $Ni^{58,60}(d,p)Ni^{59,61}$. Mean proton energies in the center of mass system for each distribution are as follows: (a) 19.6 Mev, (b) 18.4 Mev, (c) 16.9 Mev, (d) 15.3 Mev, (e) 13.5 Mev.

V. ANALYSIS AND DISCUSSION OF RESULTS

Possibly the most striking feature of the angular distributions is the rather strong forward intensity, at least for the lighter nuclei. This feature appears very much less pronounced in the figures than it actually is

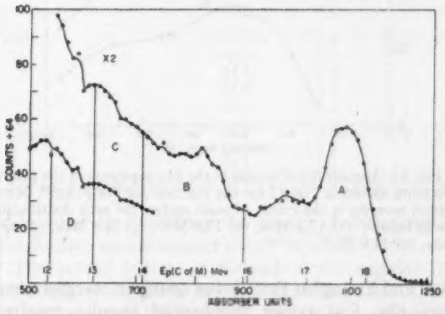

FIG. 8. Proton spectrum from the reaction $Ag^{107,109}(d,p)Ag^{108,110}$ taken at $\theta=30°$.

because of our method of plotting the *logarithm* of the observed intensity per unit solid angle.

A gross measure of the character of this asymmetry about 90° can be obtained by measuring the ratio of the area under the plot of intensity per unit solid angle against angle for $\theta<90°$ to the area for $\theta>90°$. Since the measurements were made in general between 20° and 140° the ratio R of the area under the angular distributions between 20° and 90° to that between 90° and 140° was measured. It is true that this overestimates the contribution from forward directions due to the unequal division of angle but it provides some measure of the asymmetry. Notice that this is not a measure of the number of protons emitted $<90°$ to those emitted $>90°$ since the solid angle factor $\sin\theta$ has not been included.

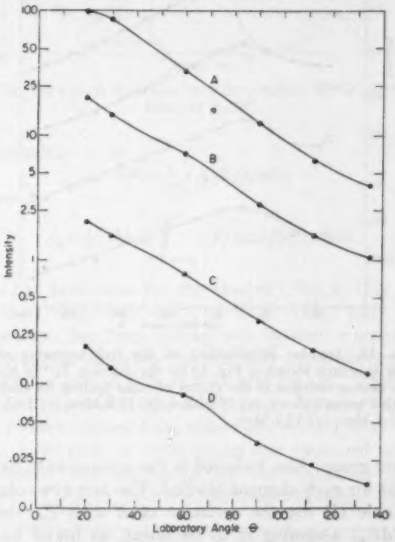

FIG. 9. Angular distributions of the four segments of the proton spectrum shown in Fig. 8 for the reaction $Ag^{107,109}(d,p)Ag^{108,110}$. Mean proton energies in the center of mass system for each distribution are as follows: (a) 17.1 Mev, (b) 15.0 Mev, (c) 13.5 Mev, (d) 12.5 Mev.

It is merely some measure of the asymmetry of the distributions as they are normally plotted; i.e., intensity per unit solid angle as ordinate. This quantity R is listed in Table III with the corresponding mean proton energy in the center of mass system for each segment or

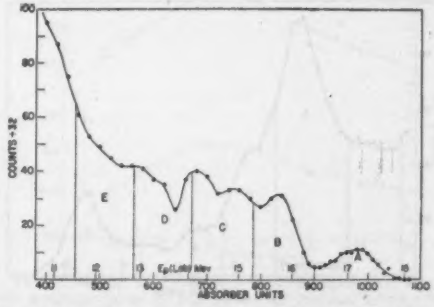

FIG. 10. Proton spectrum from the reaction $Ta^{181}(d,p)Ta^{182}$ taken at $\theta=90°$.

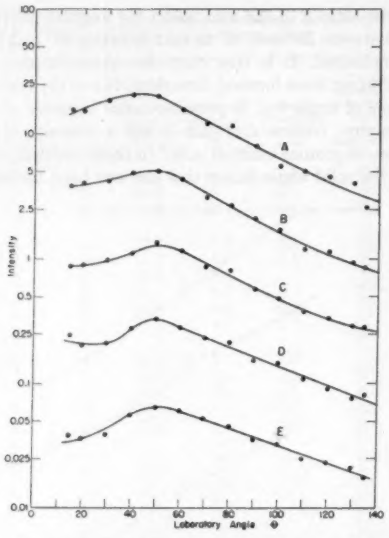

FIG. 11. Angular distributions of the five segments of the proton spectrum shown in Fig. 10 for the reaction $Ta^{181}(d,p)Ta^{182}$. Mean proton energies in the center of mass system for each distribution are as follows: (a) 17.1 Mev, (b) 15.8 Mev, (c) 14.7 Mev, (d) 13.4 Mev, (e) 12.1 Mev.

proton group. Also included is the approximate barrier height for each element studied. The last two columns in Table III list the variation of R with E_p, that is (dR/dE_p) assuming it to be linear, as found by the method of least squares and the product of (dR/dE_p) and barrier height B.

The ratio R measured in this way turns out to be considerably greater than unity in most cases, varying from 1.6 in gold to 13 in nickel. Even if one takes account of the unequal division in the abscissa, the ratio is greater than unity in *all* cases.

For all elements except the lightest one, carbon, the ratio R increases in essentially a linear fashion as the proton energy increases. Furthermore, (dR/dE_p) seems to decrease with increasing Z. In fact, if we measure E_p in units of the barrier height the quantity $B(dR/dE_p)$ is substantially independent of Z.

A more detailed examination of the angular distributions indicates two further interesting features. The proton groups corresponding to C^{13} being left in its ground state and first excited level (Fig. 3a and 3b), and Al^{28} in its ground state (Fig. 5a) show pronounced angular maxima. These three groups as well as the one leaving C^{13} in its second excited state (Fig. 3c) probably involve only one level in the residual-nucleus although it has recently[12] been shown that the long range proton group from $Al^{27}(d,p)Al^{28}$ is actually two groups of 30-kev separation.

The long range proton group from $Al^{27}(d,p)$ is of particular interest because of the work reported by

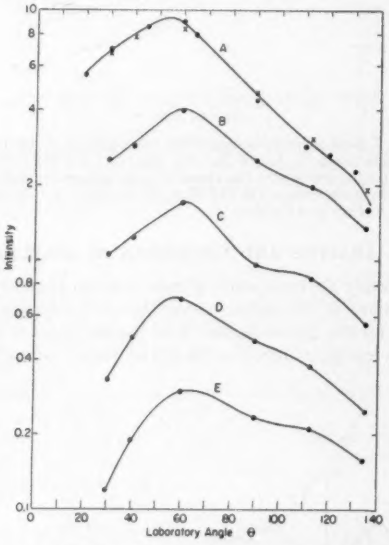

FIG. 13. Angular distributions of the five segments of the proton spectrum shown in Fig. 12 for the reaction $Au^{197}(d,p)Au^{198}$. Mean proton energies in the center of mass system for each distribution are as follows: (a) 17.2 Mev, (b) 15.8 Mev, (c) 14.4 Mev, (d) 13.3 Mev, (e) 11.9 Mev.

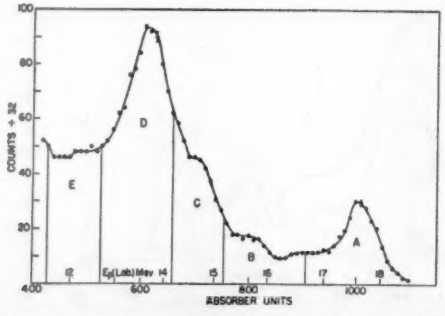

FIG. 12. Proton spectrum from the reaction $Au^{197}(d,p)Au^{198}$ taken at $\theta = 30°$.

Holt and Young[7] at three lower deuteron energies where they also find rather pronounced angular maxima. Figure 16 shows a plot of the distributions for the four energies. Nemilov and Funshtein[4] find that the long range group from this reaction is emitted with spherical symmetry within the limits of accuracy of their results for 3.9-Mev deuterons. At 4.6 Mev a single maximum appears at about 60° with a rise at forward energies. At 5.8 Mev there are three maxima at about 50°, 85°, and 135°. At 7.5 Mev these maxima have shifted forward to

[12] Preliminary measurements, MIT High Voltage Laboratory.

40°, 80°, and 130°. These three measurements are due to Holt and Young. In each case the distribution rises at forward angles. The intensity at 0° for the 7.5-Mev case is reported[7] to be 30 times the value at 25°. At 13.8 Mev the three maxima have shifted forward to 30°, 60°, and 120°. There is some evidence to show that the intensity at 15° is again rising. These maxima give a definite impression of waves of intensity advancing along the θ axis as the deuteron energy is increased. This analogy has been used previously by Heydenburg and Inglis[1] in describing the results of their angular distribution measurements for $O^{16}(d,p)O^{17}$.

TABLE III. Analysis of data in terms of the proton energy, the ratio R and the barrier height.

Target element	Atomic number Z	Barrier height B (Mev)	Mean proton energy in center of mass E_p (Mev)	Ratio $\frac{\text{area } 20°\text{–}90°}{\text{area } 90°\text{–}140°}$ R	Slope $\frac{dR}{dE_p}$	$B\frac{dR}{dE_p}$
Carbon	6	3.0	9.9	9.1	Neg.	
			10.7	4.6		
			13.5	3.4		
Aluminum	13	4.5	11.9	4.0	0.79	3.5
			13.0	6.2		
			14.1	5.3		
			15.5	7.8		
			16.7	7.6		
			17.7	10.4		
Nickel	28	7.3	13.5	6.6	0.61	4.4
			15.3	7.4		
			16.9	6.5		
			18.4	10.0		
			19.6	13.0		
Silver	47	9.8	12.5	5.6	0.87	8.5
			13.5	7.0		
			15.0	7.7		
			17.1	9.6		
Tantalum	73	12.8	12.1	2.7	0.45	5.7
			13.4	3.2		
			14.7	3.7		
			15.8	4.4		
			17.1	4.5		
Gold	79	13.4	11.9	1.6	0.32	4.2
			13.3	2.9		
			14.4	2.3		
			15.8	2.4		
			17.2	3.6		
Bismuth	83	13.9	12.7	2.0	0.39	5.4
			13.7	2.5		
			15.3	3.1		

The second feature is evident in the angular distributions of the three heaviest elements, Ta, Au, and Bi. In these cases the intensity, instead of continuing to rise with decreasing angle, reaches a maximum between 40° and 60° and then falls as the angle decreases. In this respect the results bear a resemblance to the work of Falk[9] who found a similar effect for (d,n) distributions except that in all cases the "turn over" angle is about 10°.

A conventional method of evaluating the complexity of angular distributions is to expand the observed intensity per unit solid angle $I(\theta)$ in terms of Legendre polynomials.

$$I(\theta)=\sum_l A_l P_l(\cos\theta), \tag{4}$$

where

$$A_l=\tfrac{1}{2}(2l+1)\int_{\theta=0}^{\pi} I(\theta)\sin\theta P_l(\cos\theta)d\theta. \tag{5}$$

This has been done for the case of $C^{12}(d,p)$ (Fig. 2a), $Al^{27}(d,p)$ (Fig. 4a), and $Au^{197}(d,p)$ (Fig. 12a). The integration has been carried out by first multiplying the observed intensity by $\sin\theta$ and extrapolating the resultant curve to zero at $\theta=0$ and $\theta=180°$. Intervals of θ of 5° were taken and the quantity $I(\theta)\sin\theta P_l(\cos\theta)$ was plotted against θ for values of l from 0 to 11. The area under each of these curves was measured with a planimeter and multiplied by the statistical factor $(2l+1)$. Table IV lists the coefficients obtained for the

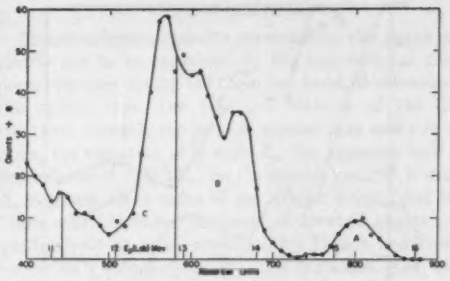

FIG. 14. Proton spectrum from the reaction $Bi^{209}(d,p)Bi^{210}$ taken at $\theta=90°$.

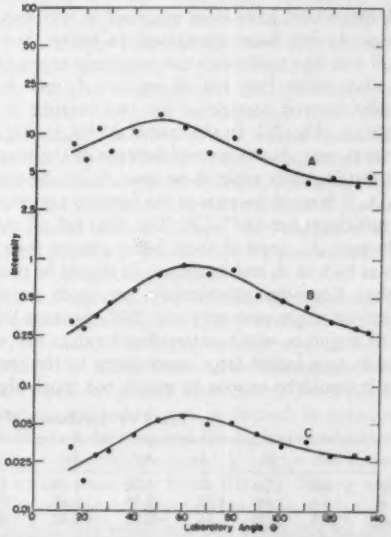

FIG. 15. Angular distributions of the three segments of the proton spectrum shown in Fig. 14 for the reaction $Bi^{209}(d,p)Bi^{210}$. Mean proton energies in the center of mass system for each distribution are as follows: (a) 15.3 Mev, (b) 13.7 Mev, (c) 12.7 Mev.

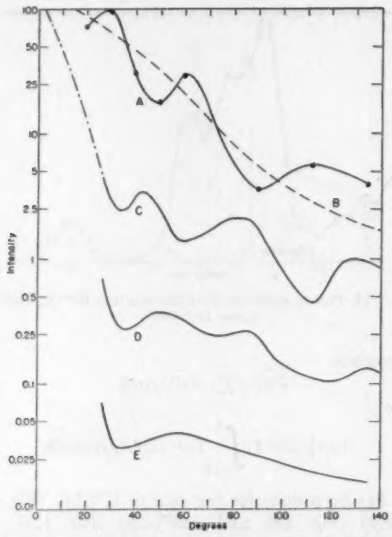

FIG. 16. Comparison of the angular distribution of the long range proton group from the reaction $Al^{27}(d,p)Al^{28}$ taken at 13.8 Mev (curve A) with the theoretical prediction of French and Goldberger (curve B) and with the experimental results of Holt and Young at deuteron energies of 7.5 Mev (curve C), 5.8 Mev (curve D), and 4.6 Mev (curve E). The dotted portion of curve C is based on the measurements made by Holt and Young of the ratio of the intensity at 0° to that at 25° which they found to be 30. At 3.9 Mev Nemilov and Funshtein find the distribution to be spherically symmetric.

distributions that have been analyzed in this way. In all cases A_0 has been normalized to unity. For the $C^{12}(d,p)$ case the coefficients are relatively constant up to A_7 after which they fall off rapidly. A_3 and A_6 are especially favored because of the two maxima in the distribution (Fig. 2a). In the case of $Al^{27}(d,p)$ (Fig. 4a) coefficients near A_3 are favored because of the maxima in the distributions while those near A_5 are depressed. Again A_1 is favored because of the forward asymmetry. The coefficients for $Au^{197}(d,p)$ (Fig. 12a) fall off rather rapidly past A_1, none of them being greater than A_0; values as high as A_3 are significant. It should be pointed out that Legendre polynomials are quite sensitive functions of angle near zero and 180°. Because this is just the region in which extrapolated values are used, this leads to a rather large uncertainty in the results. Hence it would be unwise to attach too much significance to any analysis of this nature. In spite of this, it is probably safe to say that the presence of terms in the expansion as high as P_7 to P_9 indicates that at least g-wave deuterons are effective in the reactions.

VI. THEORY

The emission of protons from deuteron-induced reactions can be described by two different models. The first model is based on the Bohr[13] concept of the compound nucleus and the second on the Oppenheimer-Phillips[14] stripping process.

Let us first consider the compound nucleus case. When the deuteron enters the target nucleus a compound nucleus of rather high excitation energy is formed (about 28 Mev for deuterons of 14-Mev energy). This energy is quickly shared among the constituent particles. For excitation energies of this magnitude the levels in the compound nucleus would be expected to be broad and overlapping so that even for a monoenergetic deuteron beam a rather large number of values of total angular momentum would be involved in the compound nucleus. Recent calculations have been made by Wolfenstein[15] on the angular distribution of deuteron-induced reactions in the region of deuteron energy. In this work he assumed the formation of a compound nucleus. Since, for all l-values of the incoming deuterons only three m-values are permitted, the angular momentum of the compound nucleus will be polarized. He concludes that this will result in an anisotropy in the angular distribution of the outgoing particles. It will, however, be characteristically symmetric about 90°. This latter condition presumably results from the assumption that many levels in the compound nucleus may be effective and that for every case of two levels differing in parity which interfere to give a forward distribution there will be some other combination of interfering levels which give a backward distribution. The net result gives the required anisotropy required by the polarization, but still maintaining the symmetry about 90°. The condition is somewhat different when lower energy deuterons and lighter target nuclei are employed. Here the presence of resonances in the excitation functions indicates that more widely spaced levels in the compound nucleus are involved. The proton angular distributions show a tendency to become more symmetric about 90° at deuteron energies corresponding to resonances in the excitation curve since one value of l for the compound nucleus will predominate over all others at such an energy. In the regions between resonances the distribu-

TABLE IV. Coefficients of the expansion in Legendre polynomials.

Reaction	Figure	A_0	A_1	A_2	A_3	A_4	A_5	A_6	A_7	A_8	A_9	A_{10}	A_{11}
$C^{12}(d,p)$	2A	1.00	1.37	1.26	1.64	1.19	1.03	1.52	0.72	0.07	0	−0.39	−0.18
$Al^{27}(d,p)$	4A	1.00	1.78	1.55	0.89	0.22	−0.06	−0.04	−0.81	−1.28	−1.01	−0.49	0.61
$Au^{197}(d,p)$	12A	1.00	0.85	−0.20	−0.42	−0.38	−0.10	0.16	0.41	0.41	−0.14	−0.12	−0.12

[13] N. Bohr, Nature **137**, 344 (1936).
[14] J. R. Oppenheimer and M. Phillips, Phys. Rev. **48**, 500 (1935).
[15] L. Wolfenstein, Phys. Rev. **78**, 322A (1950).

tions show either forward or backward asymmetry in a somewhat random fashion due to interference effects between two levels of different parity. Analyzing the distributions in terms of either an expansion in powers of $\cos\theta$, or of Legendre polynomials, gives some indication of the possible values of angular momentum of the incoming deuteron involved in the reaction and, in a few simple cases, of the total angular momentum of the excited level in the compound nucleus.

The second possible mode of reaction for (d,p) and (d,n) processes was first proposed by Oppenheimer and Phillips.[14] Subsequent considerations of this process have been made by several authors, in particular by Volkoff.[16] In this article references can be found to previous theoretical work on this subject. Application to high energy deuterons was made by Serber[17] to explain the results of Helmholz *et al.*[8] An explanation of deuteron excitation functions for a wide range of atomic number and for deuteron energies up to 15 Mev using the stripping model has been proposed by Peaslee.[18] An extension of the Peaslee stripping theory to the angular distribution of protons from (d,p) reactions at 14 Mev has been made by French and Goldberger.[19] In this model the deuteron is pictured as breaking up, with the neutron at the surface of the target nucleus (where it must be in order that there exist an appreciable probability for it to be captured) and the proton of the order of a deuteron diameter away. At breakup the proton's momentum consists of a contribution from the forward momentum of the deuteron and a contribution from the internal motion of the deuteron. It has been shown[19] that under these conditions the angular distribution would manifest a strong preference for forward directions. Furthermore, it turns out that this preference increases with proton energy. On the other hand, it is rather unlikely that protons will be emitted at zero degrees because both the incoming deuteron and the outgoing proton are deflected by the Coulomb potential of the target nucleus. Hence at some forward angle the rising intensity must reach a maximum and there decline towards 0°. Clearly this angle at which the "turn-over" occurs will increase for increasing atomic number. It is true, of course, that one can designate this assembly of particles comprising the target nucleus and the deuteron at breakup as a compound system, but it differs from the conventional concept of the compound nucleus in two respects, first, there is no thorough sharing of energy among all the particles, and, secondly, the possible values of total angular momentum of the system will be somewhat greater in consequence of the larger size. This latter difference is actually just a question of degree whereas the former is a real difference which would not allow the character of the asymmetry about 90° of the proton distribution to vary in a random fashion as the deuteron energy is changed.

[16] G. M. Volkoff, Phys. Rev. 57, 866 (1940).
[17] R. Serber, Phys. Rev. 72, 1008 (1947).
[18] D. C. Peaslee, Phys. Rev. 74, 1001 (1948).
[19] J. B. French and M. Goldberger (to be published).

VII. CONCLUSIONS

The experimental results presented in this paper are clearly not to be explained by the conventional compound nucleus model. On the other hand, if we exclude the carbon case, the principal features of the distribution, namely, the ratio R greater than unity in all cases, the variation of R with E_p, the apparent lack of dependence of (dR/dE_p) on the atomic number Z when E_p is measured in units of the barrier height, and the "turn over" in heavy elements at forward angles are, qualitatively at least, explained by French and Goldberger on a stripping model. The tantalum, gold, and bismuth cases indicate that this "turn-over" angle does increase with Z as predicted. It will however be necessary to measure the position of this angle for lighter Z-elements which involves the use of targets in the rare earth region of atomic numbers and some method for measuring proton intensity for angles from 15° to zero.

The results in the case of carbon are not completely compatible with the stripping picture because the higher energy protons are less forward than the lower energy ones. This same result was found at much lower energy by Nemilov and Funshtein which, similarly, does not lend itself to interpretation by a stripping model.

The rather sharp angular maxima which are observed in the proton distributions from lighter target nuclei have not yet been satisfactorily explained due, no doubt, to the fact that deuterons are not in general very amenable to theoretical interpretation. It is conceivable that these maxima may not be incompatible with the stripping concept. On the other hand, they may be attributable to the competing compound nucleus process. The agreement between theory[19] and experiment for 14-Mev deuterons is shown for the long range proton groups from $Al^{27}(d,p)$ in Fig. 16a.

The effect of these maxima shifting toward smaller angles as the energy of the deuterons is increased can be attributed to an effect of the Coulomb potential. The same intensity maximum would be expected to occur at more forward angles as the deuteron energy increases since both the higher energy deuterons and protons will suffer smaller deflections from the Coulomb field. Such an effect points again to a stripping picture rather than that of a compound nucleus.

It is a sincere pleasure to acknowledge the guidance and encouragement provided by Professor M. Deutsch and Professor M. S. Livingston throughout this investigation. The many informative discussions with Dr. J. B. French are greatly appreciated. The building and testing of equipment was performed in collaboration with Dr. J. A. Harvey and Dr. K. Boyer who have provided a considerable amount of advice and assistance. The writer wishes to thank Mr. K. Huang and Mr. M. Zimmerman for their assistance in analyzing some of the data. He would also like to express his gratitude to the personnel of the cyclotron laboratory, in particular to Mr. F. J. Fay, Mr. R. W. Kilson, and Mr. E. F. White who have assisted in the work in innumerable ways.

The Angular Distribution of High Energy Neutrons from Targets Bombarded by 330-Mev Protons*

RICHARD D. MILLER, DUANE C. SEWELL, AND ROBERT W. WRIGHT
Radiation Laboratory, Department of Physics, University of California, Berkeley, California
(Received October 9, 1950)

The angular distribution of neutrons with energies above 20 Mev produced by bombardment with the 330-Mev proton beam in the 184-in. cyclotron of Be, Al, Cu, and U targets has been measured with carbon detectors. The full widths at half-maximum obtained are 54° for Be, 59° for Al and Cu, and 58° for U. Experimental details and the resulting curves are given.

I. INTRODUCTION

WHEN the 184-in. cyclotron was converted to accelerate protons, a beam of high energy neutrons was obtained, as had been the case previously with deuteron acceleration. Preliminary measurements by Hadley of the energy spectrum of the neutrons in the forward direction from a beryllium target bombarded by 345-Mev protons show a distribution extending from about 150 Mev up to 345 Mev with a broad maximum at about 270 Mev.

These neutrons were presumed to be obtained primarily by a single charge exchange collision inside the target nucleus. The n–p scattering data[1] at 90 Mev give evidence of such exchange collisions in approximately 50 percent of the n–p collisions. At the presently available proton energies of greater than 300 Mev, the free particle model of the nucleus as proposed by Serber[2] should be considerably better than it was for the highest previously available nucleon energies of about 100 Mev. There was consequently some hope that the neutron angular distribution could be accounted for by a suitable modification of the free n–p exchange cross section to take into account the effects of binding.

The experiment performed was similar to the measurement of the angular distribution of neutrons from deuteron bombardment by Helmholz, McMillan, and Sewell,[3] which gave results in accord with Serber's stripping theory.[4]

II. EXPERIMENTAL

Detecting System

Relative neutron intensities were measured by the 20.5-min C^{11} beta-activity produced in polystyrene disks $1\frac{1}{16}$ in. in diameter and $\frac{1}{8}$-in. thick. These detectors were mounted on the back of a wall of lead bricks which was sufficiently thick to stop the protons that were also present. It was shown by experiments to be described later that the effects of secondary reactions in the lead absorber were not appreciable.

After a 20- to 40-min bombardment, the eight to ten detecting disks were each counted at two different times on a standard end-window beta-counter. Actual counting rates varied from 500 to 2000 counts/min. After the usual corrections for counter dead time and background, the decay corrections were made using the accepted 20.5-min half-life. Several times the decay of a detector was followed for three half-lives; no evidence of any other activity was found, and the half-life always agreed with the accepted value.

Two further corrections to the weighted average of the two corrected counting rates for each detector were necessary to obtain the relative neutron intensities. The first was the inverse square target distance correction, and the second was the correction for the variation in attenuation of the neutrons by the absorbing lead wall. This latter variation was caused by the slight variation in neutron path length through the absorber with the angle from the target, and the maximum correction for this variation was only three percent.

General Arrangements

Two different arrangements were used. The one with which most of the data were obtained is illustrated schematically in Fig. 1. Protons accelerated in the 184-in. cyclotron impinged on the edge of the target, which was mounted on a probe running into the vacuum tank. The target was set at the 80-in. radius, corresponding to a nominal proton energy of 330 Mev; however, radial oscillations of the protons reduce the mean incident energy by perhaps 10 Mev. A "beam clipper" consisting of two horizontal copper bars, $1\frac{1}{4}$-in. thick and 2 in. apart, and oriented so that it intercepted protons whose vertical oscillations were greater than 2 in., was mounted on a probe on the opposite side of the cyclotron. The purpose of this clipper was to reduce the possibility of an appreciable contribution of neutrons being produced by protons hitting the dee. The center of the neutron beam produced in the target passed through the $1\frac{3}{4}$-in. thick steel wall of the vacuum tank at 10 degrees from the normal.

The 4-in. thick wall of lead and the detectors were placed in a horizontal row against the outside of the tank wall as indicated in Fig. 1. The angles from the target, relative to the incident proton beam direction, at which

* This work was performed under the auspices of the AEC.
[1] Hadley, Kelly, Leith, Segrè, Wiegand, and York, Phys. Rev. 75, 351 (1949).
[2] R. Serber, Phys. Rev. 72, 1114 (1947).
[3] Helmholz, McMillan, and Sewell, Phys. Rev. 72, 1003 (1947).
[4] R. Serber, Phys. Rev. 72, 1007 (1947).

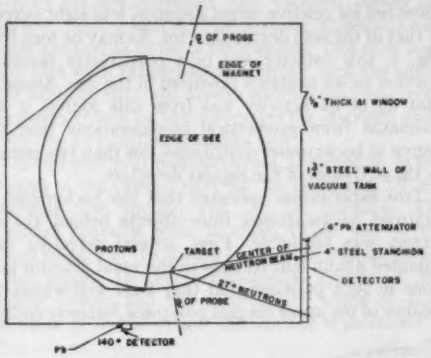

FIG. 1. Schematic drawing of the experimental arrangement.

detecting disks were placed were 0°, 8°, and 12° and at 3° intervals to 27°. No data could be obtained with this arrangement at greater angles because of scattering from the corner of the vacuum tank, and at angles between 0° and 8° because of the absorption and scattering from a stiffening stanchion just inside the tank wall at about the 4 degree position.

The second arrangement was used to obtain data between 0° and 8°, and also, in conjunction with other experiments, to set an upper limit on the contribution of the proton flux to the detector activities because of secondary reactions in the absorber. In this arrangement the positions of the target and "beam clipper" were interchanged, and the direction of the proton beam was reversed. The center of the neutron beam from the target then came out through a ⅛-in. thick, spun aluminum window in the vacuum tank wall. The only other change was that the lead absorber was made 6 in. thick instead of 4 in.

Data were taken with four different targets: beryllium, aluminum, copper, and uranium. In order to obtain reasonable counting rates, the targets were made as thick as possible consistent with the requirements that the energy loss of the incident protons be small compared with the incident energy, and that they be "thin" for the neutrons produced. The thicknesses used were: beryllium, $2\frac{5}{8}$ in.; aluminum, $1\frac{13}{16}$ in.; copper, $\frac{11}{16}$ in.; and uranium, $\frac{3}{8}$ in. These were all 35 Mev thick for 330-Mev protons. The effective thicknesses, however, were probably smaller, especially for beryllium and aluminum, because of possible deviations of the target edge from tangency to the proton orbits. The nominal thicknesses are all less than 20 percent of the mean free paths, corresponding to the total cross sections for neutrons in the forward direction produced by 345-Mev protons on beryllium, as measured by De Juren.[5] However, for 90-Mev neutrons the total cross sections are larger;[6] for the worst case, beryllium, the nominal thickness was 35 percent of the mean free path. The rms Coulomb multiple scattering of the proton beam in all the targets and the spread caused by radial oscillations of the beam were less than one degree.

Auxiliary Experiments

Absorption cross section of lead. The value of the absorption cross section of lead used in making the path length corrections was measured directly for the neutrons at four different angles from 8 to 27 degrees. An additional wall of 4 in. of lead and 4 additional detectors were mounted directly behind the usual detectors. The ratio of the activity of the detector behind the second absorber to that of the corresponding detector in front of the second absorber was the same at all four positions to within the counting probable errors of two percent. This ratio corresponds to a mean free path of 8.9 in. or a cross section of 1.2 barns. The corresponding cross section of iron was taken by interpolation from the values of De Juren,[5] since the maximum correction caused by the tank wall was only one percent.

Neutron Production in the Lead Absorber

To determine whether or not the protons incident on the lead absorber produced an appreciable number of detectable neutrons in the absorber, three results were necessary: first, the activity produced behind the absorber relative to that in front of it by the mixture of neutrons and protons which were present in the arrangements used; second, the relative activities behind and in front of the same absorber produced by a beam of neutrons only; and third, the relative activities by a beam of protons only.

The second result is that obtained in the neutron attenuation experiment described in the previous paragraph.

The first result was obtained using the second general arrangement described, in which the center of the neutron beam passed through the ⅛-in. thick aluminum window instead of the steel tank wall. This arrangement was necessary in order not to ignore the neutrons produced in the tank wall. The activity of the detector behind the 6-in. lead absorber was 24 percent of that of the detector in front, at the zero degree position.

To obtain a beam of protons only, it was necessary to use the external, deflected beam of the cyclotron. Since this beam consists of 345-Mev protons, the number of neutrons produced in the absorber in this experiment should be greater than the number produced by the protons in the original arrangements. There, the protons were not over 330 Mev, and were probably about 295 Mev, because of the target thickness. The deflected beam is not large enough in area to perform a "bad geometry" experiment as in the previous cases, so it was necessary to use a number of detectors behind the lead and integrate the distribution of activity to

[5] J. De Juren, Phys. Rev. **81**, 458 (1951).
[6] Cook, McMillan, Peterson, and Sewell, Phys. Rev. **75**, 7 (1949).

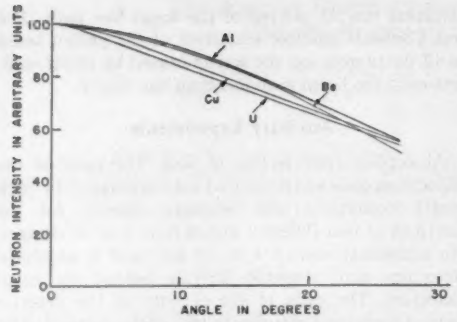

FIG. 2. Angular distributions of neutrons from Be, Al, Cu, and U.

find the total activity which an infinite detector behind the absorber would have received. The incident proton beam was one inch in diameter and was all well within the area of the detector in front of the lead. The integrated activity behind the lead was 3.5 ± 1 percent of the activity of the detector in front.

These three data give the result that at the zero degree position 8.3 ± 2.4 percent of the normal detector activity was due to the protons incident on the absorber. This figure is only an upper limit for three reasons. First, the neutron production in the absorber was measured for 345-Mev protons instead of 295 Mev. Second, the protons that were present were, in all probability, those that were scattered by the target through sufficiently wide angles to escape the magnetic field of the cyclotron. They were then incident on the absorber at rather oblique angles, and the effective absorber thickness for these protons was thus definitely greater than for the neutrons. Third, it should be expected that the substitution of the steel tank wall for the initial part of the lead absorber would produce fewer neutrons. This is because the number of neutrons, in iron nuclei, per unit area of the tank wall, is less than the number per unit area of an equivalent stopping thickness of lead. Also, the proportion of detector activity due to the protons should be greatest at the zero degree position, since the protons at the wider angle detector positions would have to have been scattered through wider angles by the target.

Possible Background Sources of Neutrons

There were three possible sources of background neutrons in these experiments: first, neutrons produced in the cyclotron dee by scattered protons; second, neutrons scattered from the concrete radiation shielding and other objects which were behind the detectors; and third, neutrons scattered from the pole pieces of the cyclotron magnet.

In one run with the beryllium target a detector was placed behind 4 in. of lead on an adjacent wall of the vacuum tank at a position corresponding to 140° from the incident proton beam. Its activity, after being corrected for relative target distance, was eight percent of that of the zero degree detector. As may be seen from Fig. 1, this detector was in a particularly favorable position to see neutrons produced in the dee. Assuming that all of its activity was from this source, it was estimated from geometrical considerations that this source of background contributed less than two percent to the activities of the regular detectors.

Two experiments indicated that the background of neutrons backscattered from objects behind the detectors was negligible. First, several detectors were mounted about four feet above the usual detector positions in such positions that they were well within the shadow of the upper magnet pole piece, but were entirely

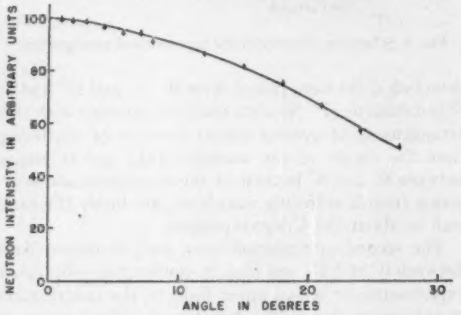

FIG. 3. Angular distribution of neutrons from beryllium with data. Data below 8° were obtained with the reversed beam arrangement.

open to any scattered radiation from the rear. Their activities were all less than 0.5 percent of that of the zero degree detector. Second, it was found that placing an additional 4 in. of lead behind some of the usual detectors did not change their activities measurably.

There is no direct experimental evidence proving that scattering from the pole pieces was negligible. Unfortunately, lack of sufficient intensity makes a measurement of the differential scattering cross sections with these detectors impracticable. However, a computation of the geometrical factors involved in the evaluation of the scattered intensity at the detector positions shows that it is extremely unlikely that this scattered intensity is appreciable. The smallest angle by which any neutron could have been scattered by the magnet into any detector is 22°. For comparison, the first zero in the calculated diffraction scattering pattern of 250-Mev neutrons by iron is at 14°. Detailed calculations showed that in order for the scattered intensity to be three percent of the direct intensity, the scattering cross section per unit solid angle at angles greater than 22° would have to be greater than $1/4\pi$ times the absorption cross section.

III. RESULTS

The resulting angular distributions are shown in Fig. 2. The experimental points and errors due to counting

statistics for the beryllium and uranium curves are shown in Figs. 3 and 4. The data for aluminum and copper are similar to those for uranium. Two runs were made with each target except uranium, and the agreement between runs was always within counting errors. The errors shown on the curves are the standard deviations due to counting statistics only.

The full widths at half-maximum, obtained by extrapolation of the curves, were 54° for beryllium, 59° for aluminum and copper, and 58° for uranium. The estimated probable error in these values due to the extrapolation and the scatter of the experimental points is one degree. In the center-of-mass system of the incident proton and the nucleus, the width at half-maximum of the beryllium distribution is increased to 59°.

IV. DISCUSSION

The dependence of the efficiency of the present detecting system on the neutron energy is the principal uncertainty in these measurements. The variation with energy of the neutron absorption cross section of lead is fairly well known,[5,6] the cross section at 270 Mev being about 30 percent lower than at 45 Mev with most of the decrease occurring above 90 Mev. However, there are no experimental data for the excitation function of the $C^{12}(n,2n)C^{11}$ reaction. Theoretical predictions of this excitation function have been made by Heckrotte and Wolff,[7] and by Baumhoff.[8] The theoretical curves

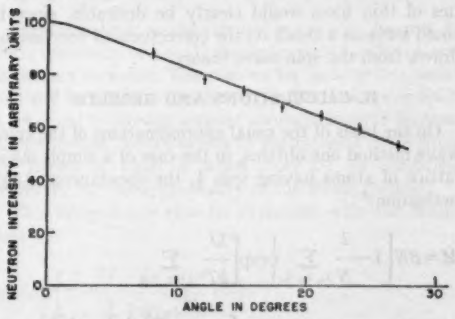

FIG. 4. Angular distributions of neutrons from uranium with data.

show a peak at about 40 Mev, and only a very gradual decrease above 100 Mev. Baumhoff's curve shows a decrease of 25 percent between 100 Mev and 350 Mev. Since this decrease opposes the decrease in the absorption cross section in its effect on the efficiency of the detecting system, it is felt that the detector efficiency is flat to within 15 percent for neutron energies above 100 Mev. It is probable, however, that the detection efficiency for neutrons with energies in the range of 30 to 60 Mev is considerably higher.

[7] W. Heckrotte and P. Wolff, Phys. Rev. 73, 265 (1948).
[8] L. Baumhoff, private communication.

TABLE I. Nuclear radii divided by the mean free path in nuclear matter.[a]

	Be	Al	Cu	U
90 Mev	0.64	0.91	1.2	1.9
270 Mev	0.4	0.6	0.8	1.3

[a] These values are given by $R=1.37\times10^{-13}A^{\frac{1}{3}}$ cm, $\lambda_{90}=4.5\times10^{-13}$ cm, $\lambda_{270}=6.7\times10^{-13}$ cm.

The most striking feature of the present distributions is their large widths. Using any reasonable momentum distribution for the nucleons in the target nucleus, it appears to be impossible to account for the widths found with the assumption that the detected neutrons were produced in single nucleon-nucleon collisions and escaped the nucleus without further interactions. For instance, the width at half-maximum, due only to the target nucleon momentum distribution, was calculated to be only 36° for a Fermi distribution with the upper limit as high as 30 Mev. The preliminary n–p scattering data[9] at 270 Mev indicate that the exchange collision protons have a width of only about 10°, and thus this source of width contributes only slightly to the total width.

The most obvious further source of broadening is the effect of secondary collisions in the same nucleus in which the initial collision takes place. That this source should be expected to be important is shown in the values of the ratio of nuclear radius to mean free path in nuclear matter given in Table I. The 90-Mev values in this table are those derived by Fernbach, Serber, and Taylor[10] from the 90-Mev neutron cross section data. While they have not been able to fit the 270-Mev data as well with their model, they estimate that the mean free path is about 50 percent greater at this energy.

The low energy partner of the initial collision is particularly likely to suffer further interactions, and thus may escape as a neutron at a wide angle from the incident proton. It is also possible that an appreciable fraction of the incident protons produce more than one detectable neutron, thus emphasizing further the lower energy and wider angle components.

It is of interest to compare the present angular distributions with the angular distributions of protons from targets bombarded by 90-Mev neutrons as measured by Hadley and York.[11] They found the following full widths at half-maximum for protons with energies greater than 20 Mev: 44° for carbon; 46° for copper; and 48° for lead. That the present distributions are wider even though the bombarding momentum is nearly doubled, is strong evidence that secondary collisions are a major source of the width.

It would be of interest to repeat this experiment with higher threshold detectors. It seems likely that the

[9] Kelly, Leith, Segrè, and Wiegand, Phys. Rev. 79, 96 (1950).
[10] Fernbach, Serber, and Taylor, Phys. Rev. 75, 1352 (1949).
[11] J. Hadley and H. York, Phys. Rev. 80, 345 (1950).

angular distributions of neutrons with energies greater than say 90 percent of the incident proton energy should be due principally to the target nucleon momentum distribution, and that consequently such measurements would yield considerable information concerning momentum distributions in nuclei.

The authors wish to express their appreciation to Professor Edwin M. McMillan for his interest and advice, to Dr. Geoffrey Chew and Mr. Lester Baumhoff for valuable discussions on the theoretical aspects of the experiment, and to Mr. James Vale and the cyclotron operating crew for their cooperation and assistance.

PHYSICAL REVIEW VOLUME 81, NUMBER 3 FEBRUARY 1, 1951

Thin Ferromagnetic Films*

MARTIN J. KLEIN AND ROBERT S. SMITH
Department of Physics, Case Institute of Technology, Cleveland, Ohio
(Received June 15, 1950)

The magnetic properties of thin films of ferromagnetic materials have been studied by means of the Bloch spin-wave theory. The spontaneous magnetization depends upon the number of atomic layers, G_z, in the film. For thicknesses below a "critical" thickness, which depends on the temperature and film dimensions, the spontaneous magnetization decreases rapidly as the number of atomic layers is decreased. The temperature dependence of the spontaneous magnetization varies from a $T^{\frac{3}{2}}$ law for very thick films to a linear function of T for a monolayer film. The spontaneous magnetization, at fixed temperature and film thickness, decreases as the film dimension increases.

I. INTRODUCTION

IT has been shown by Bloch[1] that one- and two-dimensional lattices, in contrast to three-dimensional lattices, should not exhibit spontaneous magnetization, even when the exchange integral is positive. This conclusion was reached by the use of the spin-wave method, which was introduced by Bloch as an approximate way of treating the Heisenberg[2] model of a ferromagnet. The spin-wave method provides a reasonable approximation to the lowest energy states of the system, as shown by Bethe,[3] but only for these; and conclusions reached by this method are therefore expected to be valid only at low temperatures when the magnetization is near its saturation value. It should be mentioned that Bloch's result on the absence of spontaneous magnetization in two-dimensional lattices has been substantiated by the calculations of Weiss[4] using the Bethe-Peierls method;[5] on the other hand, recent work by Ekstein[6] contradicts this result, leaving this point in doubt.

If one accepts Bloch's result, it follows that the magnetic properties of a slab of ferromagnetic material should vary with the thickness of the slab and should show a transition from ferromagnetic behavior for thick slabs to paramagnetic behavior for sufficiently thin films. We have studied the dependence of the spontaneous magnetization on the thickness of the sample, using the method of spin-waves, in order to determine the nature of the transitional behavior to be expected. An experimental investigation of the magnetic properties of thin films would clearly be desirable, since it could serve as a check on the correctness of conclusions drawn from the spin-wave theory.

II. CALCULATIONS AND RESULTS

On the basis of the usual approximations of the spin-wave method one obtains, in the case of a simple cubic lattice of atoms having spin $\frac{1}{2}$, the spontaneous magnetization:[7]

$$M=\beta N\left[1-\frac{2}{N}\sum_{\lambda_x,\lambda_y,\lambda_z}\left\{\exp\left[\frac{2J}{kT}\sum_{i=x,y,z}\times\left(1-\cos\frac{2\pi\lambda_i}{G_i}\right)\right]-1\right\}^{-1}\right]. \quad (1)$$

Here $2\pi\lambda_x/G_x$ is the x component of the spin-wave vector: G_x is the x dimension of the crystal in units of the lattice parameter and λ_x is an integer ($\lambda_x=0, 1, 2, \cdots G_x-1$). β is the Bohr magneton, J is the exchange integral between nearest neighbors, and N is the total number of atoms in the crystal ($N=G_xG_yG_z$).

If G_x, G_y, G_z are large numbers, then the variables $K_\lambda{}^{(x)}=2\pi\lambda_x/G_x$, etc., change by small steps and one can approximate the sums by integrals. Thus, for a three-

* This work was supported in part by the ONR.

[1] F. Bloch, Z. Physik **61**, 206 (1930).
[2] W. Heisenberg, Z. Physik **49**, 619 (1928). J. H. Van Vleck, Revs. Modern Phys. **17**, 27 (1945).
[3] H. Bethe, Z. Physik **71**, 205 (1931). A. Sommerfeld and H. Bethe, *Handbuch der Physik*, Band 24, Teil 2, p. 601–613.
[4] P. Weiss, Phys. Rev. **74**, 1493 (1948).
[5] H. Bethe, Proc. Roy. Soc. (London) **A150**, 552 (1935). R. Peierls, Proc. Cambridge Phil. Soc. **32**, 477 (1936).
[6] H. Ekstein, Phys. Rev. **80**, 122 (1950).
[7] See Sommerfeld and Bethe, reference 3. T. Holstein and H. Primakoff, Phys. Rev. **58**, 1098 (1940).

dimensional crystal the standard treatment[7] gives

$$M^{(3\text{ dim})}=\beta N\left[1-\frac{2(4\pi)}{(2\pi)^3}\int_0^\infty \frac{K^2dK}{\exp(JK^2/kT)-1}\right]$$
$$=\beta N[1-0.13(kT/J)^{\frac{3}{2}}]. \quad (2)$$

(The cosines have been expanded to first order.) This is the Bloch $T^{\frac{3}{2}}$ formula for the spontaneous magnetization. Similarly, for a two-dimensional lattice:

$$M^{(2\text{ dim})}=\beta N\left[1-\frac{2(2\pi)}{(2\pi)^2}\int_0^\infty \frac{KdK}{\exp(JK^2/kT)-1}\right]. \quad (3)$$

This integral diverges at the lower limit, a result which is interpreted to mean that the plane lattice has no spontaneous magnetization. For this case, the basic assumption of the Bloch theory, that the magnetization is close to the saturation value, is invalid.

In the case of a thin film (thin in the z direction) G_z and G_y are large numbers, taken equal to G for convenience; and, therefore, one can integrate over λ_x and λ_y but not over λ_z. One obtains

$$M=\beta N\left\{1-\frac{2G^2(2\pi)}{N(2\pi)^2}\sum_{\lambda_z=0}^{G_z-1}\int_{2\pi/G}^\infty \times\frac{KdK}{\exp(J/kT)[K^2+2-2\cos(2\pi\lambda_z/G_z)]-1}\right\}. \quad (4)$$

The lower limit on the integral is not zero, because in the original sum of Eq. (1) the states with $\lambda_x=\lambda_y=\lambda_z=0$ have been excluded. The reasons for making this omission will be discussed in the Appendix. The upper limit is set equal to infinity without appreciable error because the important contributions to the integral come from the region of small K when $J/kT\gg 1$, (a condition necessary for the applicability of the Bloch method).

This integral can now be evaluated with the result that

$$M=\beta N\left[1-\frac{kT}{J}\frac{1}{2\pi G_z}\sum_{\lambda_z=0}^{G_z-1}(-) \times\ln\left\{1-\left(1-\frac{J}{kT}\frac{4\pi^2}{G^2}\right)\exp[-f(\lambda_z)]\right\}\right], \quad (5)$$

where

$$f(\lambda_z)=(2J/kT)[1-\cos(2\pi\lambda_z/G_z)]. \quad (6)$$

Only the first-order term in $\exp[(J/kT)\cdot(4\pi^2/G^2)]$ has been retained.

We have carried out the summation in Eq. (5) by numerical methods for films varying in thickness from 1 to 128 layers of atoms. Representative results are plotted in Fig. 1, which shows the relative magnetization M/M_0 as a function of the reduced temperature T/T_B for different values of G_z, the thickness expressed in atomic layers. Here, $M_0=\beta N$, the magnetic moment for complete saturation; and T_B is the characteristic temperature determined from the Bloch $T^{\frac{3}{2}}$ law Eq. (2); i.e.,

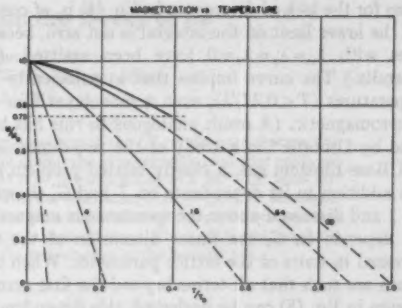

FIG. 1. The relative magnetization M/M_0 as function of the reduced temperature T/T_B for films of different thickness. The integers on the curves represent the number of layers of atoms. The film is square, 2×10^7 atoms on a side. The dashed line at $M/M_0=0.75$ indicates that the predictions of the theory are not expected to be valid below this limit. The value 0.75 is arbitrary.

$$T_B^{\frac{3}{2}}=(1/0.13)(J/k)^{\frac{3}{2}}; \quad T_B=3.9J/k. \quad (7)$$

The curve for $G_z=\infty$ is a plot of Eq. (2). G, the linear dimension of the film in units of the lattice parameter has been taken as 2×10^7 in Fig. 1.

It will be noted that the curves have been drawn dashed for magnetizations less than $0.75M_0$. This is to stress the point that valid conclusions cannot be drawn from the spin-wave theory unless the magnetization[8] is near its saturation value M_0.

Perhaps the most important conclusion to be drawn from Fig. 1 is that, for the assumed values of the parameters, significant deviations from the three-dimensional spontaneous magnetization occur for films less than about 60 atomic layers in thickness. At any given temperature the spontaneous magnetization decreases rapidly with decreasing film thickness below this "critical" number of atomic layers. Furthermore, for these sufficiently thin films the spontaneous magnetization falls off more sharply with increasing temperature than $T^{\frac{3}{2}}$, approaching a linear function of temperature.[9]

It should be noted that we include a curve for $G_z=1$, i.e., the two-dimensional lattice. This curve has been calculated from Eq. (4) rather than from Eq. (3). The

[8] For example, the curve for $G_z=\infty$, the $T^{\frac{3}{2}}$ law does not correspond to experimental curves except at low temperatures, below about $\frac{1}{3}$ the Curie temperature. See the curves in R. H. Fowler, *Statistical Mechanics* (The Macmillan Company, New York, 1936), pp. 500–501.

[9] The curve drawn for a monolayer film is strictly of the form $M/M_0=1-aT$. This is incompatible with Nernst's theorem which requires that $(\partial M/\partial T)_{T=0}=0$. The reason for the discrepancy is that the integration over λ_x and λ_y is not permitted at very low temperatures ($kT\leqq 2\pi J/G$) and the magnetization should then be calculated directly from Eq. (1). The authors would like to thank Dr. Charles Kittel for raising this question.

reason for the lack of divergence in Eq. (4) is, of course, that the lower limit on the integral is not zero, because states with $\lambda_x=\lambda_y=\lambda_z=0$ have been omitted. (See Appendix.) The curve implies that at sufficiently low temperatures ($T<0.2J/k$), even a monolayer film will be ferromagnetic. (A result analogous to this has been found by Osborne[10] in a study of the two-dimensional ideal Bose-Einstein gas, a closely related problem.)

In addition to its dependence on T and G_z shown in Fig. 1 and discussed above, the spontaneous magnetization depends on G, the linear dimension of the film expressed in units of the lattice parameter. When conditions are such that all terms beyond the first term of the sum in Eq. (5) can be neglected, this dependence is very simple, and we find:

$$\partial(M/M_0)/\partial \ln G=-(kT/J)(1/\pi G_z). \quad (8)$$

The condition for the validity of Eq. (8) is that the excitation energy of a state with nonzero z-wave number $2\pi\lambda_z/G_z$ be large compared to kT; i.e., $(J/kT)4\pi^2/G_z^2)\gg 1$. When this condition is satisfied, M/M_0 is a linear function of $\ln G$: M/M_0 decreases as $\ln G$ increases, T and G_z (film thickness) held constant.

When Eq. (8) is not valid, one can still obtain some information on the dependence of M/M_0 on G; namely, by considering the full sum in Eq. (5), it can be shown that for $G>G_z^2$, $\partial(M/M_0)/\partial \ln G<0$, implying that for sufficiently large G, M/M_0 goes to zero. (The bound $G>G_z^2$ is merely a convenient one in estimating the partial derivative since the functional dependence is quite complicated.)

III. DISCUSSION

Let us now give a qualitative physical discussion which may help to clarify the results which have been derived above. Consider the energy levels of the system as given by the spin-wave theory. They have the form:[7]

$$E(n_{\boldsymbol{\lambda}})=C+J\sum_{\lambda_x,\lambda_y,\lambda_z}\left[\sum_{i=x,y,z}\left(1-\cos\frac{2\pi\lambda_i}{G_i}\right)\right]n_{\boldsymbol{\lambda}}, \quad (9)$$

where C is a constant and $n_{\boldsymbol{\lambda}}$ is an integer which gives the number of spin-wave quanta in the state characterized by λ_x, λ_y, λ_z.

When $G_z\ll G(=G_x=G_y)$, these energy levels correspond to a spectrum in which the spacing of states differing in their λ_x- or λ_y-values but having the same value of λ_z is very small compared to the spacing of states which differ only in their λ_z-values. In particular there are G^2 states with $\lambda_z=0$ (which may be called two-dimensional states); and, since for $\lambda_z\neq 0$ the lowest energy level is ($\lambda_x=\lambda_y=0$, $\lambda_z=1$), for which the excitation energy is $\cong J(2\pi^2/G_z^2)$, it is easy to show that there are $\cong\pi(G/G_z)^2$ two-dimensional states having energies lower than the first state with $\lambda_z\neq 0$. (Similarly, between the states ($\lambda_x=\lambda_y=0$, $\lambda_z=1$) and ($\lambda_x=\lambda_y=0$, $\lambda_z=2$) there are approximately $3\pi(G/G_z)^2$ states, etc.)

These remarks indicate, therefore, that when G_z is sufficiently small compared to G, i.e., when the film thickness is sufficiently small compared to its linear dimension, only the states determined by the first few values of λ_z make any important contribution in the relevant low temperature region. In the calculations given above this means that only the first few terms of the sum in Eq. (5) are appreciable. As a consequence, when $G_z/G\ll 1$, the magnetic properties are essentially determined by the two-dimensional states, giving rise to the results discussed quantitatively in Sec. II above.

The authors would like to thank the referee for several valuable suggestions.

APPENDIX

We shall now discuss the omission of the states with $\lambda_x=\lambda_y=\lambda_z=0$. These states of zero spin-wave vector have a simple classical interpretation: they correspond to all spins being parallel with the spin system aligned in an arbitrary direction. In the absence of an external magnetic field, these states have no excitation energy, as may be verified from Eq. (9). The contribution of these states to the magnetization is infinite as can be seen from Eq. (1).

The origin of this infinite term in the magnetization can be traced to the following circumstance. The sum of the $n_{\boldsymbol{\lambda}}$ (the occupation numbers of the spin-wave states) is a measure of the number of reversed spins in the lattice. Consequently, this sum has a maximum value. In carrying out the partition sum (from which Eq. (1) is derived) one should therefore impose a restriction on the possible values of the $n_{\boldsymbol{\lambda}}$; namely, their sum should be less than a fixed number, proportional to N. Actually the partition sum is evaluated without imposing this restriction: the $n_{\boldsymbol{\lambda}}$ are allowed to take on all integer values from zero to infinity. This (incorrect) method of evaluating the partition sum leads directly to the infinity in question.

We have not been able to perform the calculation of the partition sum rigorously, but we have made another type of approximate calculation. We have restricted the occupation numbers $n_{\boldsymbol{\lambda}}$ by setting their sum equal to one fixed value determined to fit experimental data for the spontaneous magnetization. While this method is only an *a posteriori* one, the result is of interest: the troublesome states, with $\lambda_x=\lambda_y=\lambda_z=0$, make a completely negligible contribution to the magnetization, rather then the infinite one obtained by the usual method.

The result of this approximate calculation and the physical unreality of the infinite term in question have been our justification for omitting the zero wave number states from our treatment. A rigorous calculation would, of course, settle the subject conclusively.

[10] M. F. M. Osborne, Phys. Rev. 76, 396 (1949).

Nuclear Recoils Resulting from the Decay of Be^{7}*

PHILIP B. SMITH† AND JAMES S. ALLEN
Physics Department, University of Illinois, Urbana, Illinois
(Received October 3, 1950)

Be^{7} was deposited as a thin film on a Ta foil. The energy spectrum of the Li^{7} recoils from the reaction $Be^{7}+e_K \rightarrow Li^{7}+\nu+Q$ was studied. The observed spectra did not exhibit the monoenergetic character predicted by theory. The maximum energy of the recoils was 56.6 ± 1.0 ev, corresponding to a $Be^{7}-Li^{7}$ mass difference of 860 ± 8 kev. This mass difference, in combination with the best value of the $Li^{7}(p,n)Be^{7}$ threshold, yields 785 ± 8 kev for $n-H$. Coincidence measurements were made which indicated that monolayer surfaces were probably produced. Auger electrons following the K-capture were observed. The variation of the shape of the recoil energy spectrum was studied as a function of the temperature of the backing foil.

I. INTRODUCTION

As was first pointed out by Wang[1] it seems likely that an investigation of the recoil energy spectrum in the decay of Be^{7} will yield an excellent verification of the neutrino hypothesis. Since the decay scheme of Be^{7} is well known and quite simple, the results of such an experiment should be relatively unambiguous. In the 90 percent branch of the decay scheme a neutrino carries off practically the entire energy difference between Be^{7} and the ground state of Li^{7}. In this case the recoiling Li^{7} nucleus should have a well-defined momentum, and a corresponding unique energy. In the 10 percent branch a gamma-ray of 478 kev follows K-capture to the first excited state of Li^{7}. The recoiling nucleus in this branch will not be monoenergetic; however, if a coincidence technique is utilized to define the directions of both the recoil and the gamma-ray, the recoil momentum can have one of two possible values. In the hope of verifying the aforementioned theoretical conclusions the earlier work on this problem by one of the authors[2] has been repeated under more favorable conditions. In the earlier work the recoil energy spectrum from a thin layer of Be^{7} was investigated using a retarding potential method with an Allen-type electron multiplier as detector. In the present work better separation techniques were available, and a more refined retarding grid structure permitted a more precise determination of the maximum energy of the recoils. Preliminary results of these measurements have been reported previously.[3]

II. PREPARATION OF Be^{7} SURFACES

Selective evaporation was used to achieve the high order of separation required to prepare sufficiently thin Be^{7} surfaces. Several of the sources were obtained from the University of Illinois cyclotron, and one from the University of Chicago cyclotron. These were produced by both the $Li^{6}(d,n)Be^{7}$ and $Li^{7}(p,n)Be^{7}$ reactions. In addition, a separated cyclotron produced source was purchased from the AEC. The unseparated sources were in the form of metallic Li. These were converted to dry LiCl and then separated by selective evaporation. The separated source was supplied as a solution which was then dried and further separated as already mentioned. The general method of separation was the same as that developed by Sherwin.[4] The first step in the process was to determine the rate of transfer of activity as a function of temperature. This was done in a vacuum system provided with means of monitoring the activity transferred from the initial "hot" foil (3 mil Ta) to a catcher. It was found in the case of the untreated sources that the activity transferred to about 1400°C, as measured with an optical pyrometer. This confirms the conclusion reached by Allen[2] that the Be^{7} remained in its elemental state. The separated source from the AEC unfortunately showed an appreciable transfer rate over a wide range of temperatures. A high temperature fraction (about 1200–1400°C) of this source was used in the experiment. Actually, to prepare a source, a catcher foil was placed near the initial foil when it had reached the predetermined temperature of transfer. In some cases this catcher foil was then transferred to the final system and the recoil energy spectrum observed. In several other cases the catcher foil was moved to the final system and some of its activity was then transferred by a second evaporation to another catcher foil which could be moved into position in front of the detector without breaking the vacuum. In all cases the final foil was $\frac{1}{2}$ mil Ta. Surprisingly enough, the quality of surfaces prepared in the more complicated manner was no better than that of those prepared by the simple one-step process.

III. ENERGY SPECTRA OF NUCLEAR RECOILS

Figure 1 is a schematic diagram showing the arrangement of the grids and multiplier tube used to study the recoil energy spectra. The recoil counting rate was measured as a function of the potential of the retarding grid. The plot of these data is the integral energy spectrum of the recoils, except for the distortions introduced by the grid structure. Since these distortions

* This work was supported in part by the joint program of the AEC and ONR.
† Address: Physics Department, University of São Paulo, Caixa Postal 219-B, São Paulo, Brazil.
[1] K. C. Wang, Phys. Rev. **61**, 97 (1942).
[2] J. S. Allen, Phys. Rev. **61**, 692 (1942).
[3] P. B. Smith and J. S. Allen, Phys. Rev. **77**, 747 (1950).
[4] C. W. Sherwin, Phys. Rev. **73**, 216, 1173, 1799 (1949).

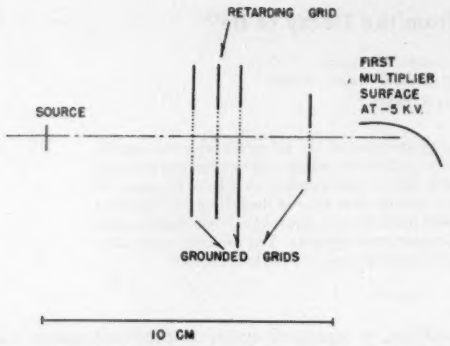

FIG. 1. Schematic diagram showing the location of the source, grids, and detector used to obtain the retarding potential curves for the Be^7 decay. The source was held at ground potential during the retarding potential measurements.

are almost impossible to calculate analytically, the grid system was calibrated by monoenergetic ions. A broad beam of ions was produced by surrounding the source holder with a cylindrical grounded grid and replacing the sources with a spodumene ion source on a Pt foil. The Pt foil was held at the desired positive voltage and then heated until the spodumene emitted ions.

Figure 2 shows the extreme high energy end of a retarding potential curve taken with a Be^7 surface and also a typical curve taken with a Pt-spodumene source. The curves were normalized at 58.75 retarding volts. This particular Pt-spodumene curve, corresponding to a positive ion energy of 56.6 ev, is shown because it matched the end point of the Be^7 curve so well. On the basis of this comparison, the value of 56.6 ± 1.0 ev was assigned to the upper end point of the Be^7 recoil spectrum. While it is clear from Fig. 2 that the end point could be assigned more accurately than ±1.0 ev, since there was no information on the difference between the contact potential of the Pt-spodumene source and the contact potential of the backing material of the Be^7 source, an error of ±1.0 ev was assigned which was thought to be large enough to take care of such a difference. The mass difference, Be^7-Li^7 calculated using this end point is 860 ± 8 kev. A neutrino mass of 10 kev would introduce an error of only 60 ev in this calculation, and, in view of the fact that recent measurements indicate that the neutrino mass is probably considerably less than 10 kev, it can be stated that the Be^7-Li^7 mass difference as measured by this method is essentially independent of neutrino mass. Using the Q value of $Li^7(p,n)Be^7$ as measured by Shoupp[5] *et al.* of (-1.645 ±0.002 Mev) and the reaction equation:

$$(n-H)=-Q-(Be^7-Li^7), \qquad (1)$$

$n-H$ is 785 ± 8 kev. In Table I are presented some recent values of $n-H$ with the corresponding values of the Be^7-Li^7 mass difference and the expected recoil energy. In each example the Be^7-Li^7 mass difference has been calculated using the Q value of the $Li^7(p,n)Be^7$ reaction as determined by Shoupp[5] *et al.*

Figure 3 presents the retarding potential curves for three surfaces and also the theoretically predicted curve D. This latter curve has not been corrected for grid distortion since the error introduced by the grids is very small compared to the difference between the theoretical curve and the measured curves. Table II summarizes the important characteristics of these surfaces. In the next section the method of obtaining the source strength and surface efficiencies is described.

Surface efficiency is defined as the ratio of the number of recoils which escape from the surface as ions to the total number of recoils occurring from the source. The efficiency is then a measure of the quality of a surface. Presumably, if all the recoils are able to escape from the surface the source is a monolayer. Since in the case of surface C the surface efficiency is 93 ± 42 percent, it is presumed that this source was a monlayer. The shape of the retarding potential curve C above 20 v indicates the emission of relatively more high energy recoils from this surface than from either of the thicker surfaces A or B. However, the counting rates in the case of surface C were so small that the statistical accuracy of the data was very poor. Although addi-

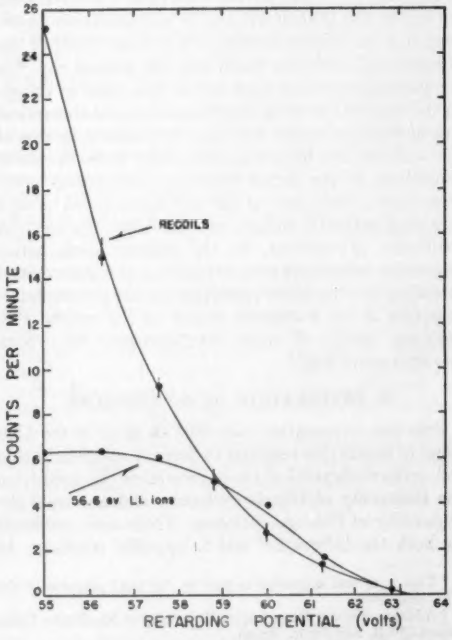

FIG. 2. The retarding potential curves for the recoils from the decay of Be^7 and for singly charged Li ions from a spodumene source.

[5] Shoupp, Jennings, Jones, and Garbuny, Phys. Rev. **75**, 336 (1949); Shoupp, Jennings, and Jones, Phys. Rev. **76**, 502 (1949).

tional data could have been obtained by counting for a longer period of time, the increasing importance of instrumental errors would have limited the accuracy of the data. We conclude from these results that very little improvement is to be expected if weaker sources on Ta substrata are used. It is of course possible that other substrata may produce less interference with the recoils. It seems unlikely that a very marked difference will occur, however, and thus the authors feel that the investigation of K-capture recoils with a gaseous source is a more fruitful field of investigation than the continuation of experiments with surface sources.[6]

TABLE I. Values of the $n-H$ and Be^7-Li^7 mass differences.

$n-H$ (kev)	Be^7-Li^7 (kev)	Recoil energy (ev)	Reference
783±5	863±5	57.2±0.7	Stephens[a]
782±1	864±3	57.2±0.3	Taschek *et al.*[b]
800±4	846±5	55.0±0.5	Tollestrup *et al.*[c]
804±9	842±9	54.4±1.1	Bell & Elliott[d]
785±8	860±8	56.6±1.0	Present measurements

[a] W. E. Stephens, Phys. Rev. **76**, 181 (1949).
[b] Taschek, Jarvis, Argo, and Hemmendinger, Phys. Rev. **75**, 1268 (1949).
[c] Tollestrup, Jenkins, Fowler, and Lauritsen, Phys. Rev. **76**, 181 (1949).
[d] R. E. Bell and L. G. Elliott, Phys. Rev. **74**, 1552 (1948).

IV. COINCIDENCE MEASUREMENTS

For coincidence measurements the experimental arrangement was the same as for retarding potential measurements (Fig. 1) except that a scintillation crystal counter was placed behind the source. The crystal was so located that it detected the gamma-rays from the 10 percent branch at an angle of 180° from the direction of the recoils. The signal from the scintillation counter, indicating that a gamma-ray had been stopped in the crystal, was used as "zero-time" for the decay. The recoil traveled a known distance through field-free space to the grounded grid in front of the electron multiplier and was accelerated from there into the first dynode. The time of flight spectrum was recorded by a 20-channel delayed coincidence circuit. Details of this circuit will appear in another publication.

A detailed analysis of the factors causing the true and chance coincidence rates shows that the absolute source strength is given to a high degree of accuracy by

$$N_0=(N_c/N_t)(\alpha/\tau), \qquad (2)$$

where N_0 is the source strength in disintegrations per sec and N_c/N_t is the ratio of chance to true coincidence rates, α is a constant of the apparatus which can be evaluated and τ is the resolving time of the delayed coincidence apparatus.

A 70-hr coincidence run was taken on surface B. The coincidence counting rate was so low that not much can be said about the shape of the energy spectrum, except that it is in rough agreement with the retarding potential measurements for this surface shown in Fig. 3. However, it was possible to obtain an estimate of the rates of the true to chance counting rates which is accurate to about ±35 percent. This ratio was 23 for surface B and the source strength computed from Eq. (2) was 0.25 μc. A recoil counting rate of 5.4/sec was expected if the surface efficiency were 100 percent. Since the observed recoil rate was 3.2/sec, the actual surface efficiency was 59 percent. The source strengths and surface efficiencies of surfaces A and C were determined by measuring their gamma-ray and recoil counting rates under the same conditions as used for surface B. The characteristics of these three surfaces are shown in Table II.

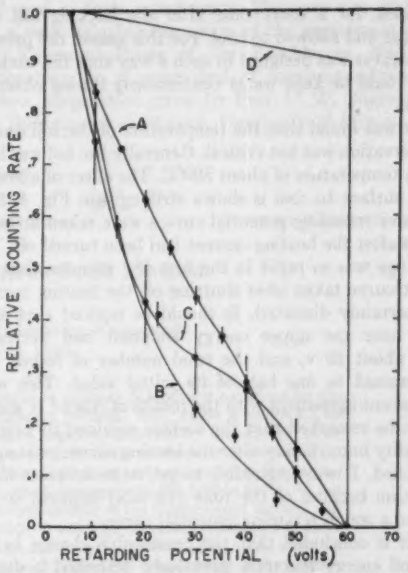

FIG. 3. A, B, and C are retarding potential curves for Be^7 surfaces of decreasing thickness. Curve D is the predicted curve for the recoils. The decrease in the relative counting rate as the retarding potential is increased is due to the distribution of recoil energies resulting from the nearly simultaneous emission of a gamma-ray and a neutrino.

TABLE II. Characteristics of the activated surfaces.

Surface	Gamma-count (counts/min)	Recoil count (counts/min)	Source strength	Source efficiency (percent)
A	3×10^4	2350	0.12±0.04 mc	1±0.35
B	61	189	0.25±0.09 μc	59±20
C	9	43.7	0.037±0.013 μc	93±32

V. HEATING OF SURFACES

In the earlier work of Allen[2] it was found that more recoils were observed and the maximum energy in-

[6] Since the conclusion of these experiments the authors have been informed that R. Davis of Brookhaven National Laboratory has obtained considerably better results with a somewhat different technique.

creased, for a short time after the backing foil was heated and allowed to cool. For this reason the present apparatus was designed in such a way that the backing foil could be kept warm continuously during observations.

It was found that the temperature of the foil during observation was not critical. Generally the foil was held at a temperature of about 500°C. The effect of allowing the surface to cool is shown strikingly in Fig. 4. Successive retarding potential curves were taken at intervals after the heating current had been turned off. The change was so rapid in the first few minutes that the first curve taken after shutting off the heating current is certainly distorted. It should be noticed that after an hour the upper energy endpoint had decreased by about 10 v, and the total number of recoils had decreased to one half of its initial value. This is in excellent agreement with the results of Allen.[2] It should also be remarked that the surface regained its original quality immediately after the heating current was again applied. It was impossible to get more accurate information because of the time (10 min) required to get even a rough retarding potential curve.

It is concluded that the remarkable change in the recoil energy spectrum previously described is due to the absorption of a layer of gas on the surface. Apparently, this layer forms very quickly when the surface is allowed to cool, and is rapidly driven off when the surface is reheated.

VI. OBSERVATION OF AUGER ELECTRONS

Ta was used as the substratum for all the surfaces made in this experiment. It is easy to handle, easy to clean, and can be heated well above the Be melting point without danger of melting or evaporating. Since its work function is somewhat smaller than the first ionization potential of Li (the recoiling atom), there is a very small probability of surface ionization. It was therefore desirable to show that Auger emission followed K-capture, since this would provide a mechanism for ionization. By running the first dynode of the multiplier at $+500$ v it was possible to detect these very low energy electrons. A retarding potential curve was taken on these electrons and it was found that they had a maximum energy of 36 ± 5 ev. This value agrees with the expected energy of Auger electrons from Li. In addition, the total number of electrons was in rough agreement with the number of recoils observed. It was also found, when counting either ions or electrons, that if a sufficient retarding potential was applied to stop the most energetic particles, the counting rate fell to the same value as when the source was completely removed. This result indicated that x-rays from Li were almost entirely absent, since the multiplier should count these with high efficiency.

We conclude that Auger emission occurs in almost 100 percent of the decays, and that this is the probable explanation of the existence of charged recoils when Ta is used as the substratum.

VII. CONCLUSION

This experiment has shown that the reaction energies of the K-capture type of decay can be determined with good accuracy by measurement of the maximum energy of the recoiling ions. We have succeeded in measuring the Be^7-Li^7 mass difference in this way, and have found the value 860 ± 8 kev. From this and the Q value of the reaction $Li^7(p,n)Be^7$ we have arrived at a value of 785 ± 8 kev for the $n-H$ mass difference which agrees closely with the value 782 ± 1 kev of Taschek *et al.*[7]

The experiment would also have provided convincing corroboration of the neutrino hypothesis if monoenergetic recoils had been observed. The coincidence measurements described above prove that, although very nearly monolayer surfaces were produced, the recoil energy spectra observed were in sharp disagreement with the predictions of the neutrino hypothesis. It must be concluded that either the Ta substrata distorted the recoil energy spectra, or else that the predictions of

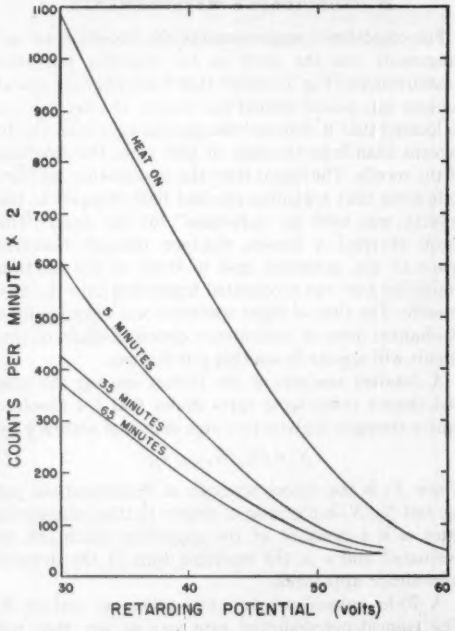

FIG. 4. Retarding potential curves for the recoils from Be^7. The top curve was obtained with the source at 500°C. The lower curves were taken at various intervals of time after the source had returned to room temperature.

[7] Taschek, Jarvis, Argo, and Hemmendinger, Phys. Rev. 75, 1268 (1949).

beta-decay theory are not fulfilled in this decay process. Certainly all other experimental results support the former conclusion.

The authors wish to express their appreciation to the crews of the University of Illinois and the University of Chicago cyclotrons, who provided most of the Be^7 used in these experiments. They are also grateful for a very valuable discussion of the experiment with Dr. Raymond Davis of the Brookhaven National Laboratory, to a great deal of excellent advice on surface preparation given by Prof. C. W. Sherwin of the Department of Physics, University of Illinois.

PHYSICAL REVIEW VOLUME 81, NUMBER 3 FEBRUARY 1, 1951

A Simplification of the Hartree-Fock Method

J. C. SLATER
Massachusetts Institute of Technology, Cambridge, Massachusetts*
(Received September 28, 1950)

It is shown that the Hartree-Fock equations can be regarded as ordinary Schrödinger equations for the motion of electrons, each electron moving in a slightly different potential field, which is computed by electrostatics from all the charges of the system, positive and negative, corrected by the removal of an exchange charge, equal in magnitude to one electron, surrounding the electron whose motion is being investigated. By forming a weighted mean of the exchange charges, weighted and averaged over the various electronic wave functions at a given point of space, we set up an average potential field in which we can consider all of the electrons to move, thus leading to a great simplification of the Hartree-Fock method, and bringing it into agreement with the usual band picture of solids, in which all electrons are assumed to move in the same field. We can further replace the average exchange charge by the corresponding value which we should have in a free-electron gas whose local density is equal to the density of actual charge at the position in question; this results in a very simple expression for the average potential field, which still behaves qualitatively like that of the Hartree-Fock method. This simplified field is being applied to problems in atomic structure, with satisfactory results, and is adapted as well to problems of molecules and solids.

I. INTRODUCTION

THE Hartree-Fock equations[1] furnish the best set of one-electron wave functions for use in a self-consistent approximation to the problem of the motion of electrons in the field of atomic nuclei. However, they are so complicated to use that they have not been employed except in relatively simple cases. It is the purpose of the present paper to examine their meaning sufficiently closely so that we can see physically how to set up a simplification, which still preserves their main features. This simplified method yields a single potential in which we can assume that the electrons move, and we shall show the properties of this field for problems not only of single atoms but of molecules and solids, showing that it leads to a simplified self-consistent method for handling atomic wave functions, easy enough to apply so that we can look forward to using it even for heavy atoms.

II. THE HARTREE-FOCK EQUATIONS AND THEIR MEANING

It is well known that the Hartree equations are obtained by varying one-electron wave functions $u_1(x)$, $u_2(x)$, $\cdots u_n(x)$, in such a way as to make the energy $\int u_1^*(x_1)\cdots u_n^*(x_n)Hu_1(x_1)\cdots u_n(x_n)dx_1\cdots dx_n$ an extreme, where H is the energy operator of a problem involving n electrons in the field of certain nuclei, and where the functions u_i are required to be normalized. Similarly the Hartree-Fock equations, as modified by Dirac,[2] are obtained by varying the u_i's so as to make the energy

$$\frac{1}{n!}\int\begin{vmatrix} u_1^*(x_1)\cdots u_1^*(x_n) \\ \cdots\cdots\cdots\cdots \\ u_n^*(x_1)\cdots u_n^*(x_n)\end{vmatrix} H \begin{vmatrix} u_1(x_1)\cdots u_1(x_n) \\ \cdots\cdots\cdots\cdots \\ u_n(x_1)\cdots u_n(x_n)\end{vmatrix} dx_1\cdots dx_n$$

an extreme, where in this latter expression the u's are assumed to be functions depending on coordinates and spin, and where the integrations over the dx's are interpreted to include summing over the spins. The Hartree-Fock equations can then be written in the form

$$H_1u_i(x_1)+\left[\sum_{k=1}^{n}\int u_k^*(x_2)u_k(x_2)(e^2/4\pi\epsilon_0r_{12})dx_2\right]u_i(x_1)$$
$$-\sum_{k=1}^{n}\left[\int u_k^*(x_2)u_i(x_2)(e^2/4\pi\epsilon_0r_{12})dx_2\right]u_k(x_1)$$
$$=E_iu_i(x_1). \quad (1)$$

Here H_1 is the kinetic energy operator for the electron of coordinate x_1, plus its potential energy in the field of

* The work described in this paper was supported in part by the Signal Corps, the Air Materiel Command, and the ONR, through the Research Laboratory of Electronics of M.I.T.

[1] J. C. Slater, Phys. Rev. 35, 210 (1930); V. Fock, Z. Physik 61, 126 (1930); L. Brillouin, *Les Champs Self-Consistents de Hartree et de Fock*, Actualités Scientifiques et Industrielles No. 159 (Hermann et Cie., 1934); D. R. Hartree and W. Hartree, Proc. Roy. Soc. A150, 9 (1935); and many other references.

[2] P. A. M. Dirac, Proc. Cambridge Phil. Soc. 26, 376 (1930).

all nuclei; $e^2/4\pi\epsilon_0 r_{12}$ is the Coulomb potential energy of interaction between electrons 1 and 2, expressed in mks units; to get the corresponding formula in Gaussian units we omit the factor $4\pi\epsilon_0$, and to get it in atomic units we replace $e^2/4\pi\epsilon_0$ by 2. The u_i's as before are assumed to depend on spin as well as coordinates, and the integrations over dx_2 include summation over spin, so that the exchange terms, the last ones on the left side of Eq. (1), automatically vanish unless the functions u_i and u_k correspond to spins in the same direction.

The Hartree-Fock equations in the form given present an appearance which seems to differ from the ordinary one-electron type of Schrödinger equation, and for this reason it is ordinarily thought that they cannot be given a simple physical interpretation. This assumption arises partly from the paper of Dirac[3], in which they are interpreted in a rather involved way. The second term on the left of (1) is simple: it is clearly the Coulomb potential energy, acting on the electron at position x_1, of all the electronic charge, including that of the ith wave function whose wave equation we are writing. The last term on the left, the exchange term, however, is peculiar, in that is is multiplied by $u_k(x_1)$ rather than by $u_i(x_1)$. It must somehow correct for the fact that the electron does not act on itself, which it would be doing if this term were omitted. In the Hartree, as opposed to the Hartree-Fock, equations, this is obvious. There the last term differs from that in the Hartree-Fock equations only in that all terms in the summation are omitted except the ith; the exchange term in that case then merely cancels the term in $k=i$ from the Coulomb interaction found in the second term. The main point of our discussion is to show that an equally simple interpretation of this term can be given in the Hartree-Fock equations.

Let us first state in words what the interpretation proves to be; then we can more easily describe the way in which the equations lead to it. We can subdivide the total density of all electrons into two parts, ρ_+ from those with plus spins, ρ_- from those with minus spins; the two together add to the quantity $-e\sum(k=1\cdots n)\times u_k^*(x)u_k(x)$, where e is the magnitude of the electronic charge. Then we can show that the Hartree-Fock Eq. (1) for a wave function u_i which happens to correspond to an electron with a plus spin is an ordinary Schrödinger equation for an electron moving in a perfectly conventional potential field. This field is calculated by electrostatics from all the nuclei, and from a distribution of electronic charge consisting of the whole of ρ_-, but of ρ_+ corrected by removing from the immediate vicinity of the electron, whose wave function we are finding, a correction or exchange charge density whose total amount is just enough to equal a single electronic charge. That is, this corrected charge distribution equals the charge of $n-1$ electrons, as it should. The exchange charge density equals just ρ_+ at the position of the electron in question, gradually falling off as we go away from that point. We can get a rough idea of the distance in which it has fallen to a small value by replacing it by a constant density ρ_+ inside a sphere of radius r_0, zero outside the sphere. We have $\frac{4}{3}\pi r_0^3|\rho_+| = e$, or

$$r_0 = (3e/4\pi|\rho_+|)^{\frac{1}{3}}. \tag{2}$$

The situation is then much as if the corrected charge density equaled the actual total electronic charge density outside this sphere, but was only ρ_- within the sphere; there is a sort of hole, sometimes called the Fermi[3] or exchange hole, surrounding the electron in question, consisting of a deficiency of charge of the same spin as the electron in question. Actually, of course, this exchange hole does not have a sharp boundary, but the charge density of the same spin as the electron in question gradually builds up as we go away from this electron. Similar statements hold for the field acting on an electron of minus spin.

The exchange hole clearly is different for wave functions of the two spins, provided ρ_+ and ρ_- are different; examination proves further that it is different for each different wave function u_i. It is this difference which leads to the complicated form of the Hartree-Fock equation; and the simplification which we shall introduce in a later section is that of using sort of an averaged exchange hole for all the electrons. The difference between the exchange charge for two wave functions u_i corresponding to the same spin is not great, however. We have already seen that the radius r_0 which we obtain by assuming a hole of constant density depends only on ρ_+ (for a plus spin), and hence is the same for all u_i's of that spin. Thus the exchange holes for different u_i's of the same spin will only show small differences. We shall later examine these differences for the case of a free electron gas, and show that they are really not large. It is this small dependence on u_i which will make it reasonable to use an averaged exchange charge in the simplified method which we shall suggest later.

To agree with the qualitative description which we have just given, we then expect the exchange charge density at point x_2, producing a field acting on the electron at x_1 whose wave function $u_i(x_1)$ we are determining by the Hartree-Fock Eq. (1), to integrate over dx_2 to $-e$ (a single electronic charge), and to be equal when x_2 approaches x_1 to the quantity

$$-e \sum_{\substack{k=1 \\ \text{spin } k=\text{spin } i}}^{n} u_k^*(x_1)u_k(x_1). \tag{3}$$

We shall now show that this is the case.

[3] E. Wigner and F. Seitz, Phys. Rev. 43, 804 (1933); *ibid.* 46, 509 (1934). The discussion of Wigner and Seitz was one of the first to show a proper understanding of the main points taken up in the present paper, which must be understood to represent a generalization and extension of previously suggested ideas, rather than an entirely new approach. See also L. Brillouin, J. de Phys. et le Radium, 5, 413 (1934) for a discussion somewhat similar to the present one.

To show it, we rewrite (1) in the equivalent form[4]

$$H_1u_i(x_1)+\left[\sum_{k=1}^{n}\int u_k^*(x_2)u_k(x_2)(e^2/4\pi\epsilon_0 r_{12})dx_2\right]u_i(x_1)$$

$$-\left[\sum_{k=1}^{n}\frac{\int u_i^*(x_1)u_k^*(x_2)u_k(x_1)u_i(x_2)(e^2/4\pi\epsilon_0 r_{12})dx_2}{u_i^*(x_1)u_i(x_1)}\right]u_i(x_1)$$

$$=E_iu_i(x_1). \quad (4)$$

The exchange term now appears as the product of a function of x_1, times the function $u_i(x_1)$; thus it has the standard form of a potential energy term in a one-electron Schrödinger equation. This exchange potential energy is the potential energy, at the position of the first electron, of the exchange charge density,

$$-e\sum_{k=1}^{n}\frac{u_i^*(x_1)u_k^*(x_2)u_k(x_1)u_i(x_2)}{u_i^*(x_1)u_i(x_1)}, \quad (5)$$

located at the position x_2 of the second electron. We note as we expect that the exchange charge density depends on the position of the first electron, as well as the second, and also on the quantum state i in which this first electron is located. We note, furthermore, that the total charge is that of a single electron. To show this, we integrate the exchange charge density (5) over dx_2, and find at once, on account of the orthogonality of the u_i's (which follows from the Hartree-Fock equations) that the integral over all space is $-e$. Furthermore, as x_2 approaches x_1, we see at once that the exchange charge density approaches the correct value (3), where the restriction that the spins of i and k must be equal arises from (1), where an exchange term $u_k^*(x_2)u_i(x_2)$ is automatically zero unless this condition is satisfied. Thus we have shown that the exchange charge density (5) satisfies all the conditions necessary to justify our qualitative discussion of its behavior. In a later section, where we work out detailed values for the free-electron case, we can examine its properties more in detail.

The great difference between the Hartree and the Hartree-Fock methods is the fact that in the Hartree-Fock method the exchange hole or correction charge appropriate for an electron at x_1 moves around to follow that electron; in the Hartree method it does not, the correction charge depending only on the index i of the wave function u_i. If our problem is a single atom, this is not very important, but in a crystal, for instance a metal, the difference is profound. Thus consider a periodic lattice, in which the one-electron functions u_i are modulated plane waves, corresponding to $1/N$ of an electronic charge on each of the N atoms of the crystal. In the Hartree scheme, the potential acting on the electron in the wave function u_i is that of all electrons, minus this charge corresponding to $1/N$ of an electron on each atom. This correction charge is so spread out that its effect on the potential field is completely negligible, and each electron acts as if it were in the field of all electrons, thus finding itself in the field of a neutral atom when near any of the nuclei of the metal. On the other hand, with the Hartree-Fock equations, the exchange charge is located near the position x_1 of the electron in question, moving around with it, so that when this electron is on a given atom, the exchange charge is removed largely from that atom, leaving it in the form of a positive ion, which, as our physical intuition tells us, is the correct situation.

III. AVERAGED EXCHANGE CHARGE

We have seen that the exchange charges for different wave functions u_i corresponding to the same spin are not very different from each other, since in every case they reduce to the same value when $x_2=x_1$, and integrate to the same value over all space. Furthermore, in a system containing equal or approximately equal numbers of electrons with both spins, ρ_+ and ρ_- will be at least approximately the same, so that exchange charges for different u_i's even of opposite spins will be nearly the same. It then seems clear that we shall make no very great error if we use a weighted mean of the exchange charge density, weighting over i, for each value of x_1. The result of this will be that we shall have a single potential field to use for the Schrödinger equation for each u_i, simplifying greatly the application of the Hartree-Fock method. Let us first set up this average exchange charge and the consequent averaged exchange potential, then give some discussion of their properties and uses.

The probability that an electron at x_1 should be in the state i is evidently $u_i^*(x_1)u_i(x_1)/[\sum_j u_j^*(x_1)u_j(x_1)]$. We can then use this quantity as a weighting factor to weight the exchange charge density (5). When we do this, we find as the average exchange charge density the quantity[5]

$$-e\frac{\sum_{j=1}^{n}\sum_{k=1}^{n}u_j^*(x_1)u_k^*(x_2)u_k(x_1)u_j(x_2)}{\sum_{j=1}^{n}u_j^*(x_1)u_j(x_1)}. \quad (6)$$

Using this average exchange charge density, we come to the following Schrödinger equations for the u_i's, as

[4] J. C. Slater and H. M. Krutter, Phys. Rev. 47, 559 (1935); particularly p. 564, where this same method is used in discussing the Thomas-Fermi method.

[5] J. C. Slater, Rev. Mod. Phys. 6, 209 (1934), particularly p. 267, where this same expression is used for similar purposes, but without pointing out that it is the weighted mean of the exchange charge density found in the Hartree-Fock equations.

substitutes for the Hartree-Fock equations:

$$H_1 u_i(x_1) + \left[\sum_{k=1}^{n} \int u_k^*(x_2) u_k(x_2) (e^2/4\pi\epsilon_0 r_{12}) dx_2 - \frac{\sum_{j=1}^{n} \sum_{k=1}^{n} \int u_j^*(x_1) u_k^*(x_2) u_k(x_1) u_j(x_2) (e^2/4\pi\epsilon_0 r_{12}) dx_2}{\sum_{j=1}^{n} u_j^*(x_1) u_j(x_1)} \right] u_i(x_1) = E_i u_i(x_1). \quad (7)$$

The wave functions u_i, and energy values E_i, as determined from these equations, will not be quite so accurate as those determined from the Hartree-Fock equations; but they will at least be much better than those found from the Hartree equations, particularly for the case of the crystal, and they have the great advantage that they are all solutions of the same potential problem. This automatically brings one good feature, which the solutions possess in common with solutions of the Hartree-Fock equations, but which solutions of the Hartree equations do not have: the functions u_i are all orthogonal to each other.

There is one aspect of Eqs. (7) which is very important. In the last few years there has been a great development of the energy-band theory of semiconductors. This is all based on the hypothesis that we can build up a model of a solid in which each electron moves independently in a potential field which is made up from the nuclei, and all other electrons except the one in question. The electric field derived from this potential is sometimes called the motive field acting on the electron. Each wave function corresponds to a definite energy level, and the Fermi statistics are applied to the distribution of the electrons in these levels. The soundest way to set up this potential acting on each electron is by the Hartree-Fock method, but we see by our present discussion that this implies a different potential energy or motive for each electron, or each u_i. If we wish to have a single motive field appropriate for all electrons, the best thing we can do is to use the weighted mean suggested in the present section. Thus Eqs. (7) may well be taken to be the basis of the ordinary form of the energy-band theory of solids.

In many problems, we are interested in cases of degeneracy, not merely in evaluating the wave function of a single nondegenerate stationary state. Thus we may be solving a problem of multiplet structure in an atom or molecule, or discussing ferromagnetism in a solid. In such a case we start with a number of degenerate or approximately degenerate energy levels, corresponding to different orientations of orbit or spin, or in some cases (as in the hybridization of atomic orbitals) corresponding to different total or azimuthal quantum numbers, and then carry out perturbations. If we take the Hartree-Fock scheme literally, we shall use different potentials for finding the u_i's of each of these various unperturbed functions. It is highly desirable in such cases, in the interests of simplicity, to modify the method so as to use the same potential function for the calculation of each wave function. This may involve even more averaging than is contemplated in setting up Eqs. (6) and (7). As one illustration, Hartree's use of a spherical potential for discussing atomic structure is an example of this procedure; this involves averaging over all orientations of the various orbital angular momenta of electrons which are not in closed shells. Whether we are using the Hartree scheme or the present simplification of the Hartree-Fock scheme, such averaging over orientations seems certainly desirable. Again, in studying ferromagnetism, the potentials to use, according to the scheme of the present paper, will depend on the net magnetization, or on the number of electrons of each spin. It is much simpler to handle such a problem, however, by using a single potential function, and that will usually be chosen to be that representing the unmagnetized state, with equal numbers of plus and minus spins.

In all these cases which we have just been discussing, we use one-electron wave functions which are slightly less accurate than those found by the Hartree-Fock scheme. When we apply perturbation methods, we must remember this, computing the matrix components of the exact energy operator with respect to these somewhat incorrect wave functions, remembering the wave equation (for instance (7)) which they actually satisfy. Nondiagonal matrix components of energy between these somewhat inaccurate wave functions will be somewhat larger than those between exact Hartree-Fock functions. Nevertheless they will still not be very large, for the wave functions are still quite accurate; the slight decrease in exactness is much more than made up by the simplicity of the method. The energy values computed by averaging the exact energy operator over the wave function will be very nearly the same as for Hartree-Fock functions, on account of the theorem that the mean value of energy over an in-

correct wave function has errors only of the second order of small quantities.

IV. THE EXCHANGE CHARGE FOR THE FREE-ELECTRON CASE

The calculations of exchange charge and exchange potential which we have been describing in general language can be carried out exactly for the case of a free-electron gas, as is well known. In this section we shall give the results, as an illustration of the general case. Then we shall point out in the next section that by using a free-electron approximation we can get an exchange potential much simpler than that of Eq. (7), which still is accurate enough for many purposes.

Let us have a free-electron gas with n electrons in the volume V, half of them of each spin; the volume is assumed to be filled with a uniform distribution of positive charge, just enough to make it electrically neutral. The electrons are assumed to obey the Fermi statistics. Then by elementary methods we find that they occupy energy levels with uniform density in momentum space, out to a level whose energy is $P^2/2m=(h^2/2m)(3n/8\pi V)^{\frac{2}{3}}$, corresponding to a maximum momentum $P=h(3n/8\pi V)^{\frac{1}{3}}$. The de Broglie wavelength

$$d=h/P=(8\pi V/3n)^{\frac{1}{3}} \tag{8}$$

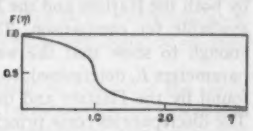

FIG. 1. $F(\eta)$ as function of η (from Eq. (11)).

associated with this maximum momentum is clearly related to the radius r_0 of the exchange hole, which we introduced in Eq. (2). When we notice that $|\rho_+|$ which appeared there equals $ne/2V$, we see that

$$d=(4\pi/3)^{\frac{1}{3}}r_0. \tag{9}$$

We can now state some of the principal results of the application of this model to the exchange charge density and exchange energy. The exchange potential energy can be conveniently stated in terms of the ratio $\eta=p/P$ of the magnitude of the momentum of the electron to the maximum momentum corresponding to the top of the Fermi distribution. It is[5]

$$\text{exchange potential energy}=(e^2/4\pi\epsilon_0)(4P/h)F(\eta)$$
$$=(6/\pi)^{\frac{1}{3}}(e^2/4\pi\epsilon_0 r_0)F(\eta), \tag{10}$$

where

$$F(\eta)=\frac{1}{2}+\frac{1-\eta^2}{4\eta}\ln[(1+\eta)/(1-\eta)]. \tag{11}$$

The function $F(\eta)$ is shown in Fig. 1. It goes from unity when $\eta=0$, for an electron of zero energy, to $\frac{1}{2}$ when $\eta=1$, at the top of the Fermi distribution. We see that this exchange potential energy is of the form which we should expect. If we had a sphere of radius r_0, filled

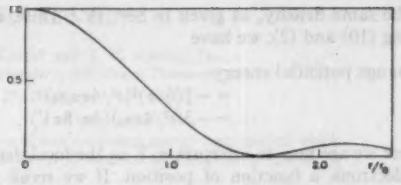

FIG. 2. Exchange charge density (divided by $\rho/2$) plotted as a function of r/r_0, from Eq. (12), where r_0 is given by Eq. (9).

with uniform charge density $|\rho_+|=ne/2V$, the potential energy of an electronic charge at the center of the sphere would be $\frac{3}{2}(e^2/4\pi\epsilon_0 r_0)$, while the value from Eq. (10) is $1.54(e^2/4\pi\epsilon_0 r_0)$ at the bottom of the Fermi band, half this value at the top. Thus this simple model of an exchange hole of constant charge density gives a qualitatively correct value for the exchange potential, and rather accurate quantitative value; and the extreme difference between top and bottom of the band corresponds only to a factor of 2 in the exchange potential.

If now we average over-all wave functions, we find that the properly weighted average of $F(\eta)$ is $\frac{3}{4}$. Thus the exchange potential energy of the averaged exchange charge[6] is $(\frac{3}{4})(6/\pi)^{\frac{1}{3}}(e^2/4\pi\epsilon_0 r_0)$. This can also be found from the averaged exchange charge density. This charge density is[5]

$$\frac{\rho}{2}\left[\frac{3\sin(r/d)-(r/d)\cos(r/d)}{(r/d)^3}\right]^2, \tag{12}$$

where ρ is the total charge density of electrons, d is given by Eqs. (8) and (9), and r is the distance from point x_1, where the electron whose wave function we are computing is located, to x_2, where we are finding the exchange charge density. This function (12) is shown in Fig. 2, plotted as a function of r/r_0, and we see that it does in fact represent a density which equals $\rho/2$ when $r=0$, and falls to small values at approximately $r=r_0$. The potential energy of an electron at the center of this averaged exchange charge distribution is just the value $(\frac{3}{4})(6/\pi)^{\frac{1}{3}}(e^2/4\pi\epsilon_0 r_0)$ previously given.

V. USE OF THE FREE-ELECTRON APPROXIMATION FOR THE EXCHANGE POTENTIAL

From the argument of Sec. III, it is clear that the exchange charge density (6), and the corresponding potential appearing in (7), must depend on the density of electronic charge, but not greatly on anything else. Thus in no case will we expect it to be very different from what we should have in a free-electron gas of the same charge density. We may then make a further approximation and simplification, beyond that of Sec. III; we may approximate the averaged exchange potential by what we should have in a free-electron gas

[6] F. Bloch, Z. Physik **57**, 545 (1929) gave the first derivation of this value.

of the same density, as given in Sec. IV.[7] Thus, combining (10) and (2), we have

$$\text{exchange potential energy} = -\tfrac{3}{4}(6/\pi)^{\frac{1}{3}}(e^2/4\pi\epsilon_0 r_0) = -3(e^2/4\pi\epsilon_0)(3n/8\pi V)^{\frac{1}{3}}, \quad (13)$$

where we are now to interpret n/V as the local density of electrons, a function of position. If we recall that this is $\sum(k)u_k^*(x)u_k(x)$, we finally have as our simplified Schrödinger equation for the one-electron functions u_i, to replace (7),

$$H_1u_i(x_1)+\left[\sum(k)\int u_k^*(x_2)u_k(x_2)(e^2/4\pi\epsilon_0 r_{12})dx_2 - 3(e^2/4\pi\epsilon_0)\left\{\frac{3}{8\pi}\sum(k)u_k^*(x_1)u_k(x_1)\right\}^{\frac{1}{3}}\right]u_i(x_1) = E_iu_i(x_1). \quad (14)$$

This equation is in practice a very simple one to apply. We solve it for each of the wave functions u_i, then find the total charge density arising from all these wave functions, and can at once calculate the potential energy, including the exchange term, to go into (14), so as to check the self-consistency of the solution. Here, as before, we change to Gaussian units by omitting $4\pi\epsilon_0$, and atomic units by changing $e^2/4\pi\epsilon_0$ to 2.

One result of this formulation of the self-consistent problem is of immediate interest. In a periodic potential problem such as a crystal, it is obvious that the total charge density will have the same periodicity as the potential. Thus the corrected potential of Eq. (14) will also be periodic, and hence the functions u_i will be modulated according to Block's theorem. In other words, such modulated functions are the only type which can follow from a proper application of our simplification of the Hartree-Fock method to a periodic potential problem.

Our general method is applicable to any problem of atoms, molecules, or solids. It is easy to give it a very explicit formulation for the case of atoms, which can then be used for the self-consistent treatment of atomic structure. Let the electrostatic potential of the nucleus, and of all electrons, at distance r from the nucleus of a spherical atom, be $Z_p(r)e/4\pi\epsilon_0 r$. Then the charge density is given by Poisson's equation as $\rho=-\epsilon_0\nabla^2(Z_pe/4\pi\epsilon_0 r)$. When we express the Laplacian in spherical coordinates, this gives at once $\rho=-(e/4\pi)(1/r)d^2Z_p/dr^2$. This is the quantity which is expressed as $-e\sum(k)u_k^*(x)u_k(x)$. Thus the exchange potential energy becomes $-3(e^2/4\pi\epsilon_0)[(\frac{3}{2}\pi^2)(1/r)d^2Z_p/dr^2]^{\frac{1}{3}}$, and, finally, the total potential energy, for use in the Schrödinger equation for $u_i(x_1)$, is

$$-\frac{e^2}{4\pi\epsilon_0 r}\left[Z_p+3\left(\frac{3}{32\pi^2}\right)^{\frac{1}{3}}\left(r^2\frac{d^2Z_p}{dr^2}\right)^{\frac{1}{3}}\right]. \quad (15)$$

To carry out a self-consistent solution for an atom, using this simplified method, we then find a Z_p such that the wave functions u_i, determined from a single Schrödinger equation using the potential energy (15), determined from Z_p, add to give a charge density which would lead by Poisson's equation to a potential energy $-e^2Z_p/4\pi\epsilon_0 r$.

In order to check the applicability of the method Mr. George W. Pratt is carrying out a self-consistent solution of the ion Cu^+ by this method. This ion was chosen, as being the heaviest one for which solutions by both the Hartree and the Hartree-Fock methods are available for comparison. The solution has gone far enough to show that the wave functions and energy parameters E_i determined from it are not far from those found by the Hartree and the Hartree-Fock methods. The discrepancies come principally from large values of r, where the charge density is small, and our free-electron approximation for exchange is not very good. Over most of the range of r, however, the approximation seems very satisfactory. Detailed results will be reported later. The great advantages of this method for numerical calculation are clear from this example which has been worked out. Actual calculation is simpler than for the original Hartree scheme, since only one potential function need be computed, and can be used for all wave functions. The wave functions have the advantage of being orthogonal; and they possess a considerable part of the accuracy which the solutions of the Hartree-Fock equations possess, in contrast to the Hartree equations. It is to be hoped that they will make enough simplification so that it will be possible to carry out calculations for more complicated atoms than have yet been attempted by the Hartree-Fock method. At the same time the method should prove valuable in setting up solutions for molecules and solids.

[7] This method of treating the exchange potential as if the electrons formed part of a free-electron gas is similar to what is done in the Thomas-Fermi method with exchange (see Dirac (reference 2), Slater and Krutter (reference 4), and L. Brillouin, *L'Atome de Thomas-Fermi et la Méthode du Champ "Self-Consistent,"* Actualités Scientifiques et Industrielles No. 160 (Hermann et Cie., 1934)).

Characteristics of Ni^{59} and Ni^{63}

A. R. Brosi, C. J. Borkowski, E. E. Conn* and J. C. Griess, Jr.
Chemistry Division, Oak Ridge National Laboratory, Oak Ridge, Tennessee
(Received September 28, 1950)

Separated stable isotopes of Ni have been used to assign a 67-kev maximum energy beta-emitter which decays with an 85-yr half-life to Ni^{63}. Ni^{59} was found to decay by K electron capture with a half-life of 7.5×10^4 yrs.

I. INTRODUCTION

CAMAC and Brown[1] produced long-lived nickel activities by (d,p) and (n,γ) radiations on nickel and by an (α,n) reaction on iron. They identified the radiations as 50-kev electrons and x-rays. From yield data the radiations were estimated to decay with a half-life of 12 ± 6 yrs. Assignment of both radiations to Ni^{59} was based partly on production by an (α,n) reaction on iron and partly on the previous assignment of a 2.6-hr period to Ni^{63}. Later Swartout[2] showed by (n,p) reactions on separated copper isotopes that the 2.6-hr period should be assigned to Ni^{65}. This mass assignment was confirmed by Conn[3] from (n,γ) yields on separated nickel isotopes. In confirming the mass assignment of the 2.6-hr isotope, evidence was found for assignment of the x-radiations reported by Camac and Brown to Ni^{59} as they had proposed. The (n,γ) yields indicated, however, that the soft beta-radiation should be assigned to Ni^{63}.

An attempt has been made to determine the decay constants of Ni^{59} and Ni^{63} by measuring the x-radiation and the soft beta-radiation separately over a period of 3 yrs. Since these measurements were started, Pomerance[4] has measured the isotopic absorption cross sections of the nickel isotopes. These cross sections were used to make preliminary estimates of the Ni^{59} and Ni^{63} half-lives for the Table of Isotopes.[5] Further work has been done to eliminate a large and uncertain correction for self-absorption of the Ni^{63} beta-ray. Quantitative data are presented on (n,γ) yields from which mass assignments have been made and half-lives calculated.

II. MASS ASSIGNMENT OF Ni^{63}

When nickel with the natural isotopic composition is activated in the Oak Ridge National Laboratory reactor, two types of radiation are found associated with the long-lived nickel activities. Using a G-M counter with a mica end window several mg/cm² in thickness, an x-ray component only is observed. When a windowless counter is used, a soft beta-component also is observed with a counting rate several hundred times that of the x-ray component as shown by the aluminum absorption curve in Fig. 1.

In order to assign these radiations to the proper isotopes, (n,γ) yields from separated nickel isotopes** have been measured. In preliminary work it was found that repeated purification of the nickel was necessary in order to remove iron and cobalt activities formed by (n,α) and (n,p) reactions, respectively. It was also found necessary to prepare very thin uniformly spread samples in order to eliminate errors caused by absorption of the soft beta-radiation within the samples. Samples prepared by electrodeposition of nickel on platinum gave reproducible data as shown by the self-absorption curves for three different specific activities in Fig. 2. Further evidence that errors from self-absorption could be made small was obtained by deposition of a mass of nickel equivalent to a monatomic layer on a platinum plate. This sample gave the same value for the counting

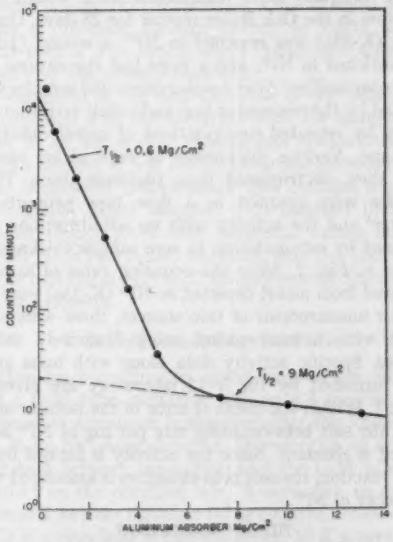

FIG. 1. Aluminum absorption curve of Ni^{63} beta-radiation.

* Present address: Department of Biochemistry, University of Chicago, Chicago, Illinois.

[1] M. Camac and L. Brown, Metallurgical Project Report CP-2407, Oct., 1944, unpublished.

[2] J. A. Swartout *et al.*, Phys. Rev. **70**, 232 (1946).

[3] E. E. Conn *et al.*, Phys. Rev. **70**, 768 (1946).

[4] H. S. Pomerance, Phys. Rev. **76**, 195 (1949).

[5] G. T. Seaborg and I. Perlman, Rev. Modern Phys. **20**, 585 (1948).

** Obtained from the Y-12 plant, Carbide and Carbon Chemicals Division, Oak Ridge, Tennessee.

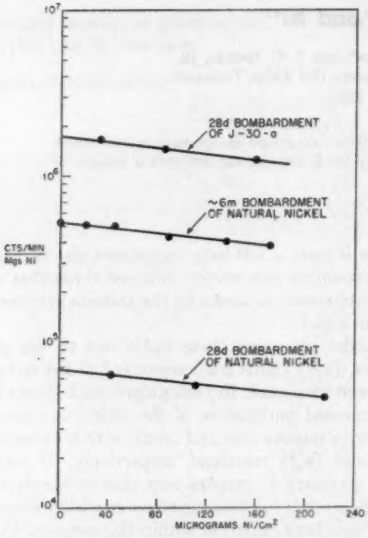

FIG. 2. Self-absorption curves of Ni^{63} beta-radiation.

rate per mg of nickel as the extrapolation to zero mg/cm² of the self-absorption curve of nickel with the same specific activity.

When preliminary data indicated that errors from self-absorption could be made negligibly small, three nickel samples were bombarded with cobalt flux monitors in the Oak Ridge reactor for 28 days. One of these (K-33a) was enriched in Ni^{58}, a second (J-30a) was enriched in Ni^{62}, and a third had the natural isotopic composition. After bombardment the samples were purified by the removal of iron and cobalt activities and finally by repeated precipitations of nickel dimethylglyoxime. Various thicknesses of each nickel sample were then electroplated onto platinum discs. These samples were counted in a flow type proportional counter[6] and the activity with no self-absorption was obtained by extrapolation to zero sample thickness as shown in Fig. 2. Since the counting rates of samples prepared from nickel depleted in Ni^{62} (K-33a) were too low for measurement of thin sources, these were compared with natural nickel using "infinitely thick" sources. Specific activity data along with mass assay data furnished by the Y-12 laboratory are given in Table I. Within the limits of error of the isotopic assay data, the soft beta-counting rate per mg of Ni^{62} bombarded is constant. Since the activity is formed by an (n,γ) reaction, the soft beta-radiation is associated with the decay of Ni^{63}.

III. Ni^{63} RADIATION

Magnetic deflection experiments showed that the radiation from Ni^{63} was soft electrons. The absence of annihilation radiation from 100 microcurie sources showed that negatrons rather than positrons were emitted by Ni^{63}. Feather analysis of aluminum absorption curves gave a range of 6.6 mg/cm² corresponding to an energy of about 65 kev.

A more precise measurement of the maximum beta-energy has been made using a proportional counter spectrometer.[7] For these measurements the nickel was electroplated on platinum to a thickness of 10 μg/cm². The pulse height distribution in the form of a Kurie plot is shown in Fig. 3. The energy scale was calibrated using the K x-radiations of Co, Xe, and Eu. Data on soft beta-emitters such as Tm^{171} and S^{35} that have been measured with both the thin lens spectrometer and the proportional counter spectrometer show that, although the shape of the Kurie plot is somewhat changed by the platinum backing, the end point is not appreciably affected. Hence no special significance is attached to the shape of the Kurie plot, but the maximum energy of 67±2 kev is thought to be reliable and is in fair agreement with the value of 63±2 kev given by Wilson and Curran.[8]

TABLE I. Comparison of (n,γ) yields of soft beta-emitter with Ni^{63} assay.

Nickel sample	Ni (β counts/min/mg)	Ni^{63} (%)	Ni^{63} (β counts/min/mg)
J-30a	1.75×10^{5}	94.25±0.5	1.86×10^{5}
Natural	6.80×10^{4}	3.66±0.01	1.86×10^{6}
K-33a	3.08×10^{3}	0.13±0.05	$2.37\pm0.9\times10^{6}$

IV. Ni^{63} DECAY CONSTANT

In order to use the activation data in Table I to calculate a half-life from the neutron absorption cross section, it is necessary to know the counting yield of the counter. Since the counting yield might be expected to vary with maximum beta-energy the counting yields for several soft beta-emitters with known decay schemes

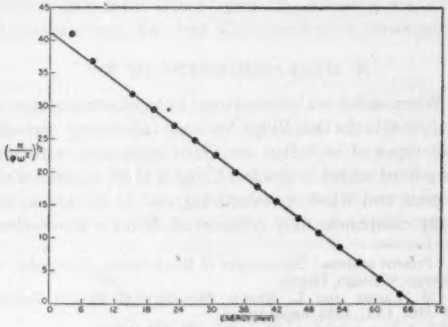

FIG. 3. Kurie plot of Ni^{63} beta-energy spectrum.

[6] C. J. Borkowski, Anal. Chem. 21, 348 (1949).

[7] C. J. Borkowski and E. Fairstein, Phys. Rev. 77, 759 (1950).

[8] H. W. Wilson and S. C. Curran, Phil. Mag. 40, 631 (1949).

were determined. These were Ru^{106}, Nb^{95}, and Co^{60} with maximum beta-energies[9] of 0.039 Mev, 0.147 Mev, and 0.31 Mev, respectively. Ru^{106} decays to 30 sec Rh^{106} which has a known decay scheme.[10,11] Co^{60} and Nb^{95} have been investigated by numerous[5] workers who are in essential agreement concerning the decay schemes. Since all these decay schemes have gamma-rays in coincidence with the beta-ray, it is possible to determine disintegration rates of these isotopes by coincidence methods. The counting yield is the ratio of the observed counting rate and the disintegration rate.

All sources were counted under the same conditions as was Ni^{63} using essentially weightless samples mounted on "infinitely thick" platinum. The cobalt and ruthenium sources were prepared by electroplating and the niobium sources were prepared by adsorption. In each case reduction in counting rate from self-absorption was shown to be negligible by counting samples which varied in thickness by a factor of five. The agreement in counting yield between sources of the same radiation was within the counting error of 2 percent. The counting yield data for the proportional counter used are given in Table II.

Although reproducible counting yields were found for the beta-emitters measured, there is still some uncertainty concerning the correct counting yield for Ni^{63} beta-radiation. Factors contributing to this uncertainty are the effect of differences in electron energy distributions and the correct method of interpolation between the beta-energies given in Table II. Graphical interpolation from a smooth curve gives a counting yield of 56 percent for beta-radiation with a maximum energy of 67 kev.

TABLE II. Counting yields of low energy beta-emitters.

Beta-emitter	Maximum energy (kev)	Counting yield (%)
Ru^{106}	39	53.5
Nb^{95}	147	62.1
Co^{60}	310	68.8

The activation data in Table I have been converted to disintegration rates using 56 percent as the counting yield. From these data and the disintegration rate of the Co^{60} activity induced in the neutron flux monitor the half-life of Ni^{63} can be calculated using the equation

$$T_1 = \sigma_1 N_1 D_2 T_2 / \sigma_2 N_2 D_1, \qquad (1)$$

where T is the half-life, σ the cross section, N the number of atoms bombarded, and D the induced disintegration rate. The subscripts 1 and 2 refer to $Ni^{63}(n,\gamma)Ni^{63}$ and $Co^{59}(n,\gamma)Co^{60}$ reactions, respectively. Numerical values of the variables used to calculate a Ni^{63} half-life are given in Table III along with estimated probable errors.

TABLE III. Calculation of a Ni^{63} half-life.

Variable	Numerical value	Probable error
σ_1	14.8 barns	20%
σ_2	34.5 barns	5
D_1	3.32×10^6 d/m/mg Ni^{63}	5
D_2	1.31×10^6 d/m/mg Co^{60}	2
T_2	5.3 yrs	5
T_1	85 yrs	20 yrs

The half-life of 85 yrs for Ni^{63} calculated from the data in Table III is considerably shorter than values previously estimated[12] from activation data. Since the neutron energy distribution for the activation experiments was somewhat different from that used in measuring the cross sections, resonance absorption could lead to an error in the half-life. Therefore, nickel enriched in Ni^{62} and a Co^{59} flux monitor were activated in the pile oscillator where the cross sections had been measured. The uncertainty with respect to the correct cross section was removed since these activation data also gave a half-life of 85 yrs for Ni^{63}.

Ionization currents, produced by two electroplated nickel samples containing Ni^{63} and by uranium and RaD standards, have been measured over a period of 3 yrs. Other Ni^{63} samples have been counted along with standards on a proportional counter for shorter periods. Although the relative probable errors in the half-life measurements of individual samples are of the order of 20 percent, the apparent half-lives vary from 35 to 60 yrs. Because of the low half-thickness of the Ni^{63} beta-particle (0.5 mg/cm²) oxidation of a few hundred lattice layers or diffusion through twenty or thirty lattice layers over a 3-yr period could reduce the apparent activity by the amount observed.

Comparison of the beta-spectrum of Ni^{63} when first electroplated with the spectrum after the sample had stood in air for several months has shown that the relative number of low energy electrons decreases with time. Because of this evidence that changes occur in electroplated nickel samples, it is believed that the apparent decay gives only minimum values for the half-life. It is concluded, therefore, that the best value for the half-life of Ni^{63} is 85 yrs as given by the activation experiments.

V. MASS ASSIGNMENT OF Ni^{59}

When reactor activated nickel samples are counted with a G-M tube, radiation with an 8.8 mg/cm² half-thickness in aluminum is observed after the 2.6-hr Ni^{65} and 36-hr Ni^{67} have decayed. Introduction of a magnetic field between the sample and the G-M tube has no effect on the counting rate. X-rays with an energy of about 7 kev are therefore being counted. These could be Co K x-rays from K capture decay, Ni K x-rays from internal conversion in a metastable state or Ni x-rays

[9] H. M. Agnew, Phys. Rev. 77, 655 (1950).
[10] W. C. Peacock, Phys. Rev. 72, 1049 (1947).
[11] E. T. Jurney, Phys. Rev. 76, 290 (1949).
[12] G. T. Seaborg and I. Perlman, Revs. Modern Phys. 20, 585 (1948); G. Friedlander, BNL-AS 2, p. 49 (1949) (to be published).

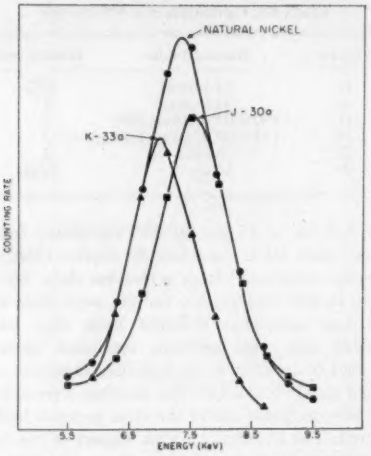

FIG. 4. Automatically recorded proportional counter spectrometer curves of the x-rays emitted by neutron bombarded nickel samples of different isotopic composition. Points are indicated for identification only.

produced by bombardment of Ni in the sample with the soft Ni^{63}-electrons.

In order to establish the origin and the energy of the x-rays, proportional counter spectrometer measurements were made on nickel samples of different isotopic composition after a 28-day bombardment in the ORNL reactor. The spectrometer curves in Fig. 4 show that the x-rays in Ni^{58} rich sample K-33a were almost pure Co K x-rays. Both Co and Ni K x-rays were found in the natural nickel sample, while the x-rays in Ni^{62} rich J-30a were Ni x-rays plus a continuum of harder x-radiation.

The Ni K x-rays probably originate from the bombardment of nickel by the Ni^{63} beta-radiation. The yield of about 2 Ni K x-ray quanta per 1000 Ni^{63} β disintegrations is consistent with yields quoted by Compton and Allison[13] for the efficiency of x-ray production by electron bombardment.

The Co x-rays are associated with Ni^{58} in the bombarded sample and must therefore result from K capture decay of Ni^{59}. Additional evidence that Ni^{59} decays by K capture was found with the nickel fraction from a group of essentially nickel-free cobalt targets bombarded with 14-Mev deuterons in the MIT cyclotron.† This nickel is of interest because a $d,2n$-reaction on Co^{59} gives Ni^{59}. The x-rays from this nickel were found to be essentially pure Co K x-rays.

VI. Ni^{59} DECAY CONSTANT

If it is assumed that the x-radiation is produced by the beta-radiation from Ni^{63} and by K capture decay of Ni^{59} and by no other means, the observed counting rate will be given by the relationship,

$$\text{x-ray counts/min} = A_1 k_1(\beta^- \text{ d/m}) + A_2 k_2(\text{mg Ni}^{58}). \quad (2)$$

Here A_1 and A_2 correct for the absorption in the nickel sample of Ni K x-rays and Co K x-rays, respectively. The term k_1 is the product of the Ni K x-ray production efficiency of Ni^{63} beta-particles and the counting yield of Ni K x-rays. The term k_2 is the product of the K capture disintegration rate per mg of Ni^{58} bombarded, the fluorescent yield of Co K x-rays and the counting yield of Co K x-rays. In cases where the samples are thin, an additional term correcting for the fraction of Ni^{63} beta-energy absorbed in the sample is required.

X-ray counting data on nickel samples of different isotopic composition which were bombarded in the ORNL reactor for 28 days, then purified and counted after decay of the short-lived nickel isotopes, are given in Table IV. The value of k_2 obtained from these data using Eq. (2) is 6.0 with a probable error of about 10 percent because of uncertainties in the analyses of absorption curves.

Since the fluorescent yield of Co K x-rays is known, it is necessary to know only the counting yield of the counter for Co K x-rays to determine the K capture disintegration rate from k_2. This counting yield was measured using a standard sample of Ni^{59} produced in the MIT cyclotron. It was prepared by electroplating about 10 mg/cm² of nickel onto platinum and was covered with a one mil aluminum foil. From the ionization current measured when the sample was placed at the center of a spherical ionization chamber, from the chamber radius, gas density, mass absorption coefficients, x-ray energy and the energy to produce an ion pair, the number of quanta per minute radiated from the surface was calculated. The probable error in the number of quanta calculated from measurements with different gases at several different pressures was about 5 percent.

TABLE IV. X-ray counting data.

Sample	β^- d/m/mg Ni	Amount of Ni (mg)	Amount of Ni^{58} (mg)	A_1	A_2	X-ray (counts/min)
K-33a	5.49×10^5	23.45	23.2	0.79	0.74	106
Natural Ni	1.21×10^6	29.1	19.7	0.74	0.69	185
J-30a	3.12×10^6	22.2	0.5	0.80	0.76	2100

Another determination of the number of quanta per minute leaving the source was made with a 2π geometry proportional counter filled with xenon to a pressure such that 95 percent of the x-rays were absorbed. The counting rate was in good agreement with that expected from the ionization chamber measurements. The Gold integral[14] was used to make corrections for absorption in the one-mil aluminum and self-absorption in the

[13] A. H. Compton and S. K. Allison, *X-Rays in Theory and Experiment* (D. Van Nostrand Company, Inc., New York, 1935).

† The authors wish to thank Prof. J. W. Irvine for this sample of nickel activity.

[14] E. Gold, Proc. Roy. Soc. (London) **A82**, 62 (1908).

nickel to obtain the total Co K x-ray emission rate in the standard.

The counter used to obtain the data in Table IV was found to have a counting yield of 0.016. Since the fluorescent yield of Co K x-rays is 0.33, the K capture disintegration rate per mg of Ni^{58} bombarded is 1130 $\pm$170 per min. Equation (1) can now be used to calculate the Ni^{59} half-life with subscript 1 referring to the $Ni^{58}(n,\gamma)Ni^{59}$ reaction and subscript 2 to the (n,γ) reaction on Co^{59} as before. The data used in the calculation are given in Table V along with estimated probable errors. These data give $7.5\pm1.3\times10^4$ yrs for the K electron capture half-life of Ni^{59}.

TABLE V. Calculation of Ni^{59}-half-life.

Variable	Numerical value	Probable error
σ_1	4.2 barns	5%
σ_2	34.5 barns	5
D_1	1130 d/m/mg Ni^{58}	15
D_2	1.31×10^8 d/m/mg Co^{59}	2
T_2	5.3 yrs	5
T_1	7.5×10^4 yrs	1.3×10^4 yrs

PHYSICAL REVIEW VOLUME 81, NUMBER 3 FEBRUARY 1, 1951

Diffusion of High Energy Gamma-Rays through Matter. I. Fundamental Equations*

L. L. FOLDY
Case Institute of Technology, Cleveland, Ohio
(Received September 11, 1950)

The fundamental processes, photoelectric absorption, Compton scattering, and pair production, leading to the modification of the energy spectrum and angular distribution of gamma-rays diffusing through matter are discussed in relation to the problem of penetration of gamma-rays through matter. The transport equation describing the diffusion is derived in the approximation in which radiation from the secondary electrons produced by the photoelectric effect and pair production is neglected. By limiting one's interest to gamma-rays of energy greater than a few Mev, further approximations may be made which reduce the transport equation to a much more simple form. An elementary proof is given for the following theorem: If monoenergetic gamma-rays are incident normally on a slab of material, then after the gamma-rays have undergone many Compton scatterings, the gamma-rays of a given energy are distributed Gaussian-wise in angle about their original direction with the breadth of the distribution being simply related to the energy and increasing with decreasing energy.

I. INTRODUCTION

IN many experiments and applications involving gamma-rays one is confronted with the problem of how the energy spectrum of a beam of gamma-rays is modified in passing through a given thickness of a particular material.[1] Important examples of applications which may be quoted are the design of shields for gamma-rays, the determination of depth-dosage relations in radiology, and the design of gamma-ray filters (differential absorbers). The *elementary* processes[2] by which the spectrum is modified in a material are very well known. In the low energy region the principal process is the *photoelectric effect* in which the gamma-ray is absorbed by an atom with the ejection of an electron from the atom. For higher energies, *Compton scattering* of the gamma-rays by electrons surpasses the photoelectric effect in importance. In the Compton scattering process, the scattered gamma-ray has a lower energy than does the incident gamma-ray, with the remainder of the energy going to the electron. At still higher energies, the *production of positron-electron pairs* by gamma-rays in the Coulomb field of a nucleus surpasses the Compton effect in importance. The energy of the gamma-rays passes into the positron-electron pair. In both the Compton effect and pair production the secondary electrons resulting from the process may produce further gamma-rays by impact with nuclei (bremsstrahlung) before they are stopped by ionization energy loss.

The energy region in which each of these processes is dominant depends strongly on the atomic number of the material being traversed by the gamma-ray. In light materials (carbon, aluminum, water) the photoelectric effect becomes unimportant at relatively low energies and pair production does not become important until relatively high energies are reached, so that Compton scattering is the dominant process over a wide energy range. On the other hand, in heavy materials (lead) the energy above which the photoelectric effect

* This work has been supported in part by the AEC and by a grant-in-aid from the Scientific Research Society of America.

[1] Previous studies of the diffusion of high energy gamma-rays through matter have been reported in the following papers: Hirschfelder, Magee, and Hull, Phys. Rev. 73, 852 (1948); J. O. Hirschfelder and E. N. Adams II, Phys. Rev. 73, 863 (1948); W. R. Faust and M. H. Johnson, Phys. Rev. 75, 467 (1949); U. Fano and P. R. Karr, Phys. Rev. 75, 1303 (1949); Bethe, Fano, and Karr, Phys. Rev. 76, 538 (1949); U. Fano, Phys. Rev. 76, 739 (1949); P. R. Karr and J. C. Lamkin, Phys. Rev. 76, 1843 (1949); L. V. Spencer and F. Jenkins, Phys. Rev. 76, 1885 (1949); Fano, Hurwitz, and Spencer, Phys. Rev. 77, 425 (1950).

[2] See, for example, W. Heitler, *The Quantum Theory of Radiation* (Oxford University Press, London, 1944).

TABLE I. Competition of gamma-ray processes.

Z	Material	Energy region in which indicated processes dominate			Critical energy	Critical length
		Photoelectric effect	Compton effect	Pair production	E_c	λ_c
6	carbon (C)	<0.025 Mev	0.025–25 Mev	>25 Mev	100 Mev	20 cm
15	aluminum (Al)	<0.050 Mev	0.050–15 Mev	>15 Mev	50 Mev	10 cm
29	copper (Cu)	<0.150 Mev	0.150–9 Mev	>9 Mev	25 Mev	1.5 cm
82	lead (Pb)	<0.55 Mev	0.55–4.5 Mev	>4.5 Mev	7 Mev	0.5 cm

is unimportant and the energy below which pair production is unimportant lie very close together leaving only a small range of energies in which the Compton effect is important. In Table I are given the energy intervals in which each of the three processes is dominant for a number of representative materials.

The importance of radiation by the secondary electrons produced in the photoelectric effect and pair production may be gauged by the relative probability that the secondaries will produce an energetic gamma-ray in a collision before they are stopped by ionization. In Table I are also given the critical energies E_c for each material where E_c is the electron energy below which it is more likely that the electron will be stopped by ionization before radiating than that it will radiate a high energy gamma-ray, and the critical lengths λ_c, where λ_c is the mean free path for an electron to make a radiative collision in which a high energy gamma-ray is produced. From this table it is apparent that the effects of the secondary electrons are small in light materials except at energies above say 30 Mev.

An examination of the table further shows that if one is primarily interested in gamma-rays with energies lying in the range from 3 to 30 Mev, and in light materials, then the most important process in modifying the gamma-ray spectrum is the Compton effect. If the layer of material through which the gamma-ray passes is sufficiently thin, then the probability of the gamma-ray undergoing more than one Compton scattering is negligible and the problem of calculating the spectral transition becomes relatively simple. As the thickness increases, however, and becomes more than a mean free path for Compton scattering, multiple scattering becomes important and the problem becomes much more difficult. Since the mean free path for Compton scattering is of the order of 2 g/cm², one sees that multiple scattering is important for thicknesses of more than 2 cm of water, 1 cm of carbon, 0.7 cm of aluminum, and 2 mm of lead. Hence in a great many practical cases multiple Compton scattering must be taken fully into account.

The problem which we have posed above is further complicated by important correlation effects between the energy and direction of travel of gamma-rays which have traversed a certain amount of material. If one has a beam of monoenergetic gamma-rays incident normally on one face of a slab of material, then after one Compton scattering the rays which have been scattered through larger angles have less energy than the rays which have been scattered through smaller angles. This effect leads to an energy-dependent collimation of the gamma-rays as they traverse the slab, even after many scatterings, so that the higher energy gamma-rays leaving the slab are confined to a narrower cone about the normal to the surface than are the less energetic gamma-rays. It is obvious that this correlation may be of very great importance in the applications mentioned above. It is in the attempt to take proper account of these correlation effects at high energies that the work reported here and in succeeding papers of this series differs considerably from some other attacks on the problem of the penetration of gamma-rays through matter.

The primary problem with which we shall be concerned may be stated precisely as follows. A slab of material of thickness t has incident normally on one of its faces a beam of gamma-rays of given energy. What is the distribution in energy and angle (with the normal to the surface of the slab) of the gamma-rays emerging from the other side of the slab as a function of the energy of the incident gamma-rays, the properties of the material traversed, and the thickness t of the slab? Obviously, if this problem can be solved, the solution for any distribution in energy and angle of the incident gamma-rays can be obtained by integration.

II. COMPTON SCATTERING

We begin with a brief resume of the required formulas for the investigation of Compton scattering. We measure the energy of the gamma-ray, $E=h\nu=\hbar\omega$, in units of the rest energy of the electron by writing

$$\epsilon=E/mc^2. \tag{1}$$

Then if a gamma-ray of energy ϵ is scattered through an angle Θ by an electron (at rest), its energy ϵ' after the scattering is given by

$$\epsilon'=\epsilon/[1+\epsilon(1-\cos\Theta)]. \tag{2}$$

The energy transferred to the electron is $\epsilon-\epsilon'$.

The differential cross section for scattering through the angle is given by the Klein-Nishina formula

$$d\Phi=\pi r_0^2 d\phi=\frac{r_0^2 d\Omega}{2}\left(\frac{\epsilon'}{\epsilon}\right)\left[\frac{\epsilon}{\epsilon'}+\frac{\epsilon'}{\epsilon}-\sin^2\Theta\right]. \tag{3}$$

Here r_0 is the classical electron radius e^2/mc^2. The total

cross section for Compton scattering is obtained by integration:

$$\Phi=\pi r_0^2\phi=\frac{\pi r_0^2}{\epsilon^2}\left[\left(\epsilon-2-\frac{2}{\epsilon}\right)\ln(1+2\epsilon)+\frac{2\{\epsilon^2(\epsilon+1)+2(1+2\epsilon)^2\}}{(1+2\epsilon)^2}\right]. \quad (4)$$

For $\epsilon\ll 1$, that is gamma-ray energies much less than 0.5 Mev, this reduces to the Thomson cross section:

$$\Phi_{Th}=\pi r_0^2\phi_{Th}=(8\pi/3)r_0^2. \quad (5)$$

For $\epsilon\gg 1$, the cross section becomes

$$\Phi=\pi r_0^2\phi=(\pi r_0^2/\epsilon)[\tfrac{1}{2}+\ln(1+2\epsilon)] \quad (6)$$

and so decreases as $\ln(\epsilon)/\epsilon$ at very high energies.

In the work which is to follow it will be convenient to use in place of the energy ϵ, its reciprocal

$$\sigma=1/\epsilon. \quad (7)$$

Since we shall often have occasion to refer to this quantity it will be convenient to attach a name to it, and for lack of any better term we shall call it the "softness" of the gamma-ray. In terms of the softness, Eq. (2) becomes

$$\sigma'=\sigma+1-\cos\Theta. \quad (8)$$

Hence in a single Compton scattering, the softness of a gamma-ray is simply increased by one minus the cosine of the angle of scattering. The Klein-Nishina formula expressed in terms of the softness takes the form

$$d\Phi=\pi r_0^2 d\phi=\frac{r_0^2 d\Omega}{2}\left(\frac{\sigma}{\sigma'}\right)^2\times\left[\frac{\sigma'}{\sigma}+\frac{\sigma}{\sigma'}-2(\sigma'-\sigma)+(\sigma'-\sigma)^2\right], \quad (9)$$

and the total cross section becomes

$$\Phi=\pi r_0^2\phi=\pi r_0^2\sigma\left[(1-2\sigma-2\sigma^2)\ln\left(\frac{\sigma+2}{\sigma}\right)+2\frac{1+\sigma+\sigma(\sigma+2)^2}{\sigma(\sigma+2)^2}\right] \quad (10)$$

which at high energies simplifies to

$$\Phi=\pi r_0^2\phi=\pi r_0^2\sigma\left[\frac{1}{2}+\ln\left(\frac{\sigma+2}{\sigma}\right)\right]. \quad (11)$$

An examination of the Klein-Nishina formula reveals that scattering through small angles is somewhat favored over scattering through large angles at high primary gamma-ray energies, but large losses of energy of the gamma-rays are favored over small losses of energy at high primary energies. Furthermore, gamma-rays scattered through more than 90° have energies less than 0.5 Mev regardless of primary energy, and gamma-rays scattered through more than 60° have energies less than 1 Mev regardless of primary gamma-ray energy. Hence all gamma-rays which are back scattered have energies less than 0.5 Mev and are relatively soft.

III. TOTAL CROSS-SECTION

In addition to the Compton effect, the photoelectric absorption and pair production by gamma-rays also contribute to the modification of the gamma-ray spectrum as it traverses matter. We will require later the total gamma-ray cross section; that is, the sum of the cross sections for the photoelectric effect, the Compton effect, and pair production. The theoretical expressions for these quantities are too unwieldy to be of direct value and we shall not present them here. Instead we give in Fig. 1 graphs of the total cross section as a function of gamma-ray energy for several materials of interest. It may be noted that particularly in light materials at the higher energies there is a relatively large energy region in which the total cross section is approximately constant. In such regions, as will be seen later, the solution of the equations for the spectral transition problem is made much easier.

IV. COLLIMATION OF HIGH ENERGY MULTIPLY-SCATTERED GAMMA RAYS

Consider a beam of monoenergetic gamma-rays incident normally on a slab of material. As mentioned earlier, the fact that the larger the angle of scattering of a gamma-ray in a Compton collision, the lower is the energy of the secondary gamma-ray leads to a collimation of high energy gamma-rays within a narrower cone of angles as they traverse the material. We may make an approximate calculation of this effect as follows. If a high energy gamma-ray with original softness σ_0 makes n Compton collisions, each through a small angle $\Delta\Theta$, then its softness after these collisions, according to Eq. (8) will be

$$\sigma_n=\sigma+n(1-\cos\Delta\Theta)\simeq\sigma+\tfrac{1}{2}n(\Delta\Theta)^2.$$

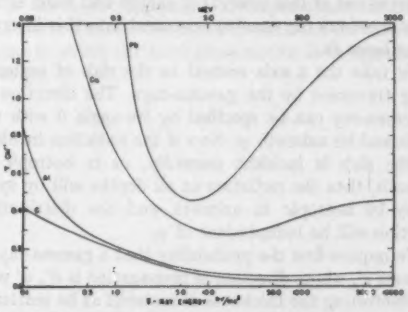

FIG. 1. Total gamma-ray absorption coefficients for carbon (C), aluminum (Al), copper (Cu), and lead (Pb).

After these scatterings, the maximum change in direction of the gamma-ray with respect to its original direction will be $\theta_{max}=n\Delta\Theta$. However, it will be relatively improbable that a gamma-ray which makes n scatterings will have the successive scatterings so arranged that this maximum deviation will be obtained. In fact, because of the "random walk" character of successive scatterings, it will be relatively improbable for the change in direction of the gamma-ray to be greater than $\theta_{max}/n^{\frac{1}{2}}=n^{\frac{1}{2}}\Delta\Theta$. Hence gamma-rays of softness σ_n will be largely confined in a cone of half-angle θ_0 about the original direction where θ_0 is given by

$$\sigma_n=\sigma_0+\tfrac{1}{2}n(\Delta\Theta)^2=\sigma_0+\tfrac{1}{2}\theta_0^2. \tag{12}$$

The fact that n is not explicitly involved in this equation shows that this collimation effect will be independent of the number of scatterings which the gamma-ray has undergone. It is actually not necessary to require all the angles of scattering to be equal; the same result will hold essentially provided only that the angles of scattering are small.

One may anticipate further that after a great many scatterings an originally monoenergetic beam of gamma rays will be distributed approximately Gaussian-wise about the original direction; more precisely, one would expect that at great depth in the material, gamma-rays of softness σ will be distributed in angle according to the distribution

$$\exp[-\theta^2/2(\sigma-\sigma_0)], \tag{13}$$

where σ_0 is their original energy. This result will be verified by more rigorous calculations later.

V. DERIVATION OF THE TRANSPORT EQUATION

In order to obtain the distribution in energy and angle of the gamma-rays at any depth in a material we must set up the transport equation expressing the change in the distribution function with depth. What we require is an equation which expresses the fact that the change in the number of gamma-rays having energies and angles in a given range in going from a depth z to a depth $z+dz$ is equal to the number of gamma-rays scattered out of this interval of energy and angle in the layer dz minus the number scattered into this interval in the layer dz.

We take the z axis normal to the slab of material being traversed by the gamma-rays. The direction of a gamma-ray can be specified by its angle ϑ with the z-axis and its azimuth φ. Now if the radiation incident on the slab is incident normally, or is isotropic in azimuth, then the radiation at all depths will by symmetry be isotropic in azimuth and the distribution function will be independent of φ.

We require first the probability that a gamma-ray of softness σ', whose direction of propagation is ϑ', φ' will, in penetrating the thickness of material dz be scattered so that its angle with the z-axis lies in the element of solid angle $\sin\vartheta d\vartheta d\varphi$. The angle of scattering, Θ, is given by

$$\cos\Theta=\cos\vartheta\cos\vartheta'+\sin\vartheta\sin\vartheta'\cos(\varphi-\varphi').$$

The required probability is then given by

$$N\pi r_0^2 p(\sigma',\vartheta',\varphi',\vartheta,\varphi)\sin\vartheta d\vartheta d\varphi\left|\frac{dz}{\cos\vartheta'}\right|$$

$$=\frac{N\pi r_0^2 d\phi(\sigma',\Theta)|dz|}{|\cos\vartheta'|}, \tag{14}$$

where N is the number of electrons per unit volume in the material and $\pi r_0^2 d\phi$ the Klein-Nishina cross section:

$$\pi r_0^2 d\phi(\sigma',\Theta)=\frac{r_0^2\sin\vartheta d\vartheta d\varphi}{2}\left(\frac{\sigma'}{\sigma}\right)^2\left[\frac{\sigma'}{\sigma}+\frac{\sigma}{\sigma'}-\sin^2\Theta\right]$$

with

$$\sigma=\sigma'+1-\cos\Theta.$$

Now let $f(\sigma,\vartheta,\varphi,z)\sin\vartheta d\vartheta d\varphi d\sigma$ be the number of gamma-rays passing through the plane z with direction in the element of solid angle $\sin\vartheta d\vartheta d\varphi$ and softness in the range $\sigma,\sigma+d\sigma$. To obtain the equation satisfied by f we consider what happens to the gamma-rays entering the region bounded by the planes z and $z+dz$. Making use of the fact that all gamma-rays entering this region also leave this region (neglecting for the moment photoelectric absorption and pair production), we have for $\vartheta<\pi/2$:

$$f(\sigma,\vartheta,\varphi,z+dz)\sin\vartheta d\vartheta d\varphi d\sigma$$

$$=f(\sigma,\vartheta,\varphi,z)\sin\vartheta d\vartheta d\varphi d\sigma\left[1-\frac{N\pi r_0^2\phi(\sigma)}{\cos\vartheta}\right]$$

$$+N\pi r_0^2\int_0^{\frac{1}{2}\pi}\int_0^{2\pi} f(\sigma',\vartheta',\varphi',z)\sin\vartheta' d\vartheta' d\varphi' d\sigma'$$

$$\times p(\sigma',\vartheta',\varphi',\vartheta,\varphi)\sin\vartheta d\vartheta d\varphi(dz/\cos\vartheta')$$

$$+N\pi r_0^2\int_{\frac{1}{2}\pi}^{\pi}\int_0^{2\pi} f(\sigma',\vartheta',\varphi',z+dz)\sin\vartheta' d\vartheta' d\varphi' d\sigma'$$

$$\times p(\sigma',\vartheta',\varphi',\vartheta,\varphi)\sin\vartheta d\vartheta d\varphi(dz/|\cos\vartheta'|)$$

or

$$\frac{\partial f(\sigma,\vartheta,\varphi,z)}{\partial z}+N\pi r_0^2\phi(\sigma)|\sec\vartheta|f(\sigma,\vartheta,\varphi,z)$$

$$=N\pi r_0^2\int_0^{\pi}\int_0^{2\pi} f(\sigma',\vartheta',\varphi',z)p(\sigma',\vartheta',\varphi',\vartheta,\varphi)$$

$$\times|\sec\vartheta'|\sin\vartheta' d\vartheta' d\varphi'. \tag{15}$$

The same equation is obtained for $\vartheta>\pi/2$. Now one can see readily that to take into account *absorption* of gamma-rays by the photoelectric effect and pair production, it is only necessary to replace $\pi r_0^2\phi(\sigma)$ by the

total gamma-ray cross section which we shall write as $\pi r_0^2 \phi_T(\sigma)$. After this substitution, the equation above is the desired transport equation. In the form given above it is extremely complicated and it is unlikely that useful solutions can be obtained from it directly. Resort to approximations simplifying the equation are therefore indicated.

VI. HIGH ENERGY-SMALL ANGLE APPROXIMATION: INTRODUCTION OF NEW VARIABLES

In our study of the problem of gamma-ray diffusion through matter we shall be primarily interested in high energy gamma-rays of say greater than 2-Mev energy. In this case one can limit one's study of the transport process to gamma-rays contained within a small cone of angles about the original direction of the gamma-rays. The reason for this is apparent from the discussion in Section IV above. Since σ for a 2-Mev gamma-ray is approximately $\frac{1}{4}$, it follows from the arguments of the preceding section that gamma-rays of this energy, even after many scatterings, are confined largely to a cone about the original direction of half-angle about 40°. Higher energy gamma-rays will be confined to even narrower cones about the original direction. Furthermore, if a gamma-ray of any energy is scattered even once through an angle greater than 40°, then the energy of the resulting gamma-ray will be less than 3 Mev. Hence, as long as we are interested in only the high energy gamma-rays we can employ small-angle approximations (such as replacing $\sin\vartheta$ by ϑ, etc.) with the introduction of only relatively small errors in the results.

To exploit fully the advantages of working with small angles, it is convenient to introduce new variables to describe the direction of a gamma-ray in place of the usual angles ϑ and φ. If we define

$$\xi=\frac{2\sin\vartheta\cos\varphi}{1+\cos\vartheta},\quad \eta=\frac{2\sin\vartheta\sin\varphi}{1+\cos\vartheta} \tag{16}$$

then ξ and η have many of the advantages of rectangular coordinates, particularly for small angles. From their definitions above, one readily finds

$$\xi^2+\eta^2=\frac{4\sin^2\vartheta}{(1+\cos\vartheta)^2}=4\frac{1-\cos\vartheta}{1+\cos\vartheta},$$

$$\cos\vartheta=\frac{1-\tfrac{1}{4}(\xi^2+\eta^2)}{1+\tfrac{1}{4}(\xi^2+\eta^2)},\quad \sin\vartheta=\frac{(\xi^2+\eta^2)^{\frac{1}{2}}}{1+\tfrac{1}{4}(\xi^2+\eta^2)},$$

$$\cos\Theta=\cos\vartheta\cos\vartheta'+\sin\vartheta\sin\vartheta'\cos(\varphi-\varphi')$$

$$=1-\frac{\tfrac{1}{2}[(\xi-\xi')^2+(\eta-\eta')^2]-\tfrac{1}{4}(\xi^2+\eta^2)(\xi'^2+\eta'^2)}{[1+\tfrac{1}{4}(\xi^2+\eta^2)][1+\tfrac{1}{4}(\xi'^2+\eta'^2)]},$$

$$d\Omega=\sin\vartheta\,d\vartheta\,d\varphi=d\xi\,d\eta/[1+\tfrac{1}{4}(\xi^2+\eta^2)].$$

When ϑ is small, ξ and η are also small and we can write

$$\vartheta^2\simeq\xi^2+\eta^2,\quad d\omega\simeq d\xi\,d\eta, \tag{17}$$
$$1-\cos\Theta\simeq\tfrac{1}{2}\{(\xi-\xi')^2+(\eta-\eta')^2\}.$$

Inserting these results into our transport equation and expression for the Klein-Nishina cross section, the transport equation takes the form:

$$\frac{\partial f(\sigma,\xi,\eta,\zeta)}{\partial\zeta}+\phi_T(\sigma)f(\sigma,\xi\ \eta\ \zeta)$$

$$=\frac{1}{2\pi}\int\int f(\sigma',\xi',\eta',\zeta)\left(\frac{\sigma'}{\sigma}\right)^2\left[\frac{\sigma'}{\sigma}+\frac{\sigma}{\sigma'}\right]d\xi'd\eta', \tag{18}$$

$$\sigma'=\sigma-\tfrac{1}{2}\{(\xi-\xi')^2+(\eta-\eta')^2\},\quad \zeta=N\pi r_0^2 z. \tag{18}$$

This is considerably simpler in mathematical structure than is Eq. (15). We have in the transport equation dropped the term in $\sin^2\Theta$ from the Klein-Nishina formula and also replaced $\sec\vartheta$ and $\sec\vartheta'$ by unity. We introduce no further error by taking the limits on the integrals over ξ' and η' in Eq. (18) above to be $-\infty$ to ∞.

In the work which follows we shall take Eq. (18) to be our fundamental equation. The approximations involved in its derivation lead to negligible errors for high energy gamma-rays and the errors are still not extreme even at energies of 2 Mev. The neglect of radiation from secondary electrons, however, places a limitation on the energies to energies below the critical energy E_c, discussed in the introduction, for thickness of material greater than λ_c.

In the succeeding paper, an approximate solution of the above transport equation is obtained for the energy range in which the total cross section is independent of energy.

Diffusion of High Energy Gamma-Rays through Matter.* II. Solution of the Diffusion Equation

L. L. FOLDY AND R. K. OSBORN
Case Institute of Technology, Cleveland, Ohio
(Received September 11, 1950)

An approximate solution of the diffusion equation derived by Foldy has been obtained for the case in which the total gamma-ray cross section is independent of energy. This is the case for essentially all materials in the energy region in which the derived diffusion equation is valid. For monoenergetic gamma-rays incident normally on a slab of material, the distribution in angle of gamma-rays of a given energy after traversing a large thickness of material is shown to be Gaussian with a breadth depending on the energy in accordance with a theorem derived by Foldy. Some numerical calculations for the case of 17-Mev gamma-rays incident on water are presented to illustrate the nature of the results.

I. INTRODUCTION

IN the preceding paper[1] (hereinafter referred to as I) an equation was derived describing the diffusion of high energy gamma-rays through matter. This equation is applicable in the energy region extending from a few Mev to the critical energy at which radiation by the secondary electrons arising from the photoelectric effect and (more importantly) from pair production by the gamma-rays became important. In light materials the region of validity is a fairly wide energy range.

In the present paper a solution of this equation will be derived applicable to the energy region in which the total gamma-ray cross section is approximately independent of energy. Since there is always a minimum in the gamma-ray cross section as a function of energy, there is in all materials an energy region in which the total cross section will be substantially constant. The breadth of this region varies greatly from material to material, but an examination of the total cross-section curves given in I shows that actually, for each material over the energy range for which the derived transport equation is valid, the cross section may legitimately be regarded as approximately independent of energy. Hence the assumption of a constant total cross section represents really no further approximation to the diffusion equation.

Unfortunately, even with this simplification, the solution of the transport equation presents a formidable problem. Indeed, it will be necessary to make a further approximation with considerably less justification than any made previously. The exact nature of the approximation is described below; it consists in replacing a varying factor under the integral in the transport equation by a constant value. The factor actually varies from the value 2 at small angles to a value 1 at large angles. In replacing it by the constant value 2, the results will be correspondingly inaccurate but only for gamma-rays much softer than the incident gamma-rays; for gamma-rays only slightly softer than the incident gamma-rays, there is no significant impairment of the results.

II. SOLUTION OF THE TRANSPORT EQUATION

The transport equation derived in I can be written as

$$\partial f(\sigma,\xi,\eta,\zeta)/\partial\zeta+\phi_T f(\sigma,\xi,\eta,\zeta)$$
$$=\frac{1}{2\pi}\int_{-\infty}^{\infty}\int_{-\infty}^{\infty} f(\sigma',\xi',\eta',\zeta)(\sigma'/\sigma)^2 \times[\sigma/\sigma'+\sigma'/\sigma]d\xi'd\eta', \quad (1)$$

with

$$\sigma'=\sigma-\tfrac{1}{2}\{(\xi-\xi')^2+(\eta-\eta')^2\}, \quad (2)$$

where the total cross section, ϕ_T, may, in accordance with the discussion in the introduction above, be regarded as constant. (For definitions of the symbols, reference should be made to I). We first transform the dependent variable by the transformation (σ_0 is a constant to be defined later)

$$g(\sigma,\xi,\eta,\zeta)=(\sigma/\sigma_0)f(\sigma,\xi,\eta,\zeta), \quad (3)$$

which reduces Eq. (1) to the simpler form:

$$\partial g(\sigma,\xi,\eta,\zeta)/\partial\zeta+\phi_T g(\sigma,\xi,\eta,\zeta)$$
$$=\frac{1}{2\pi}\int_{-\infty}^{\infty}\int_{-\infty}^{\infty} g(\sigma',\xi',\eta',\zeta)[1+(\sigma'/\sigma)^2]d\xi'd\eta'. \quad (4)$$

The approximation which we now make consists in replacing the term $[1+(\sigma'/\sigma)^2]$ under the integral sign by the constant value 2 which reduces the equation to the form:

$$\partial g(\sigma,\xi,\eta,\zeta)/\partial\zeta+\phi_T g(\sigma,\xi,\eta,\zeta)$$
$$=\frac{1}{\pi}\int_{-\infty}^{\infty}\int_{-\infty}^{\infty} g(\sigma',\xi',\eta',\zeta)d\xi'd\eta'. \quad (5)$$

The method of solution which we shall employ makes use of Fourier transformations on the variables ξ and η and a Laplace transformation on the variable σ:

$$g(\sigma,\xi,\eta,\zeta)=\int_{-\infty}^{\infty}\int_{-\infty}^{\infty}\int_{-i\infty}^{i\infty}\gamma(s,\alpha,\beta,\zeta) \times\exp(i\alpha\xi+i\beta\eta+s\sigma)ds d\alpha d\beta. \quad (6)$$

* This work was supported in part by the AEC and by a grant-in-aid to one of the authors (L.L.F.) from the Scientific Research Society of America.
[1] L. L. Foldy, Phys. Rev. **80**, 395 (1950), preceding paper.

Inserting this expression into Eq. (4), one finds that the transform function γ must satisfy the equation

$$\partial\gamma/\partial\zeta+\{\phi_T-(2/s)\exp[-(\alpha^2+\beta^2)/2s]\}\gamma=0, \quad (7)$$

with solution

$$\gamma=G(\alpha,\beta,s)\exp\{-\phi_T\zeta+(2\zeta/s)\times\exp[-(\alpha^2+\beta^2)/2s]\}, \quad (8)$$

where $G(\alpha, \beta, s)$ is an arbitrary function of its arguments.

The form of G is fixed by the initial conditions, that is, the distribution function of the gamma-rays incident on the face of the slab of material, $\zeta=0$. We assume that the incident gamma-rays fall normally on the slab and are monoenergetic with softness σ_0. These conditions can be stated mathematically by writing

$$g(\sigma,\xi,\eta,0)=\delta(\sigma-\sigma_0)\delta(\xi)\delta(\eta), \quad (9)$$

and this condition, in turn, will be satisfied provided we take G to have the form

$$G(\alpha,\beta,s)=e^{-s\sigma_0}/(2\pi)^2 i. \quad (10)$$

The remainder of the problem then consists in substituting (8) and (10) into (6) and carrying out the integrations. We have

$$g(\sigma,\xi,\eta,\zeta)=\frac{1}{(2\pi)^2 i}\int_{-\infty}^{\infty}\int_{-\infty}^{\infty}\int_{-i\infty}^{i\infty}\times\exp\left\{-\phi_T\zeta+s(\sigma-\sigma_0)+i\alpha\xi+i\beta\eta+\frac{2\zeta}{s}\exp[-(\alpha^2+\beta^2)/2s]\right\}ds\,d\alpha\,d\beta$$

$$=\exp(-\phi_T\zeta)\cdot\sum_{m=0}^{\infty}g_m. \quad (11)$$

$$g_m=\frac{1}{(2\pi)^2 i\,m!}\int_{-\infty}^{\infty}\int_{-\infty}^{\infty}\int_{-i\infty}^{i\infty}\left(\frac{2\zeta}{s}\right)^m\times\exp\{s(\sigma-\sigma_0)+i\alpha\xi+i\beta\eta-m(\alpha^2+\beta^2)/2s\}ds\,d\alpha\,d\beta. \quad (12)$$

The evaluation of the g_m can be accomplished without difficulty. One has immediately

$$g_0=\delta(\sigma-\sigma_0)\delta(\xi)\delta(\eta), \quad (13)$$

and

$$g_1=\frac{1}{(2\pi)^2 i}\int_{-\infty}^{\infty}\int_{-\infty}^{\infty}\int_{-i\infty}^{i\infty}\frac{2\zeta}{s}\exp\{s(\sigma-\sigma_0)+i\alpha\xi+i\beta\eta-(\alpha^2+\beta^2)/2s\}ds\,d\alpha\,d\beta$$

$$=\frac{\zeta}{2\pi^2 i}\int_{-i\infty}^{i\infty}\exp\left\{s\left(\sigma-\sigma_0-\frac{\xi^2+\eta^2}{2}\right)\right\}ds$$

$$=\frac{\zeta}{\pi}\delta\left(\sigma-\sigma_0-\frac{\xi^2+\eta^2}{2}\right). \quad (14)$$

For $m\geq 2$, the integrations of α and β are easily carried out. The further integration on s can be carried out by the use of Jordan's lemma and the method of residues; one obtains

$$g_m=\frac{1}{4\pi^2 i\,m!}\int_{-i\infty}^{i\infty}s\left(\frac{2\zeta}{s}\right)^m\times\exp\left[s\left(\sigma-\sigma_0-\frac{\xi^2+\eta^2}{2m}\right)\right]ds$$

$$=\frac{(m-1)(2\zeta)^m}{2\pi(m!)^2}\left(\sigma-\sigma_0-\frac{\xi^2+\eta^2}{2m}\right)_*^{m-2}, \quad (15)$$

where the asterisk subscript on the parenthesis indicates that the quantity inside the parenthesis is to be replaced by zero if it is negative.

The solution which we have obtained is, apart from the over-all exponential absorption factor, in the form of a power series in the thickness of material traversed. Each of the terms in the series has a rather simple physical interpretation. The first term represents the original gamma-rays which have filtered through to any depth without undergoing scattering or absorption. The second term, as can be seen from the correlation between energy and angle, corresponds to gamma-rays which have undergone only a single Compton scattering. The succeeding terms represent gamma-rays which have undergone 2, 3, etc. Compton scatterings in reaching the indicated depth.

An examination of the quantities g_m for large m reveals that they are closely related to the terms in the power series expansion of the zeroth-order Bessel function of imaginary argument. We write g_m as

$$g_m=-\frac{\partial^2}{\partial\sigma\,\partial(\vartheta^2)}\left\{\frac{[2\zeta(\sigma-\sigma_0)]^m}{\pi(m!)^2}\left[1-\frac{\vartheta^2}{2m(\sigma-\sigma_0)}\right]_*^m\right\},$$

and note that for large m it may be approximated by

$$g_m\sim-\frac{\partial^2}{\partial\sigma\,\partial(\vartheta^2)}\left\{\frac{(\rho/2)^{2m}}{\pi(m!)^2}\exp[-\vartheta^2/2(\sigma-\sigma_0)]\right\}, \quad (16)$$

where

$$\rho=[8\zeta(\sigma-\sigma_0)]^{\frac{1}{2}}. \quad (17)$$

Now the zeroth-order Bessel function of imaginary argument, $I_0(\rho)$ has the power series expansion

$$I_0(\rho)=\sum_{m=0}^{\infty}(\rho/2)^m/(m!)^2.$$

We can exploit this close relationship between the two

series by writing

$$\sum_{m=2}^{\infty} g_m = -\frac{1}{\pi}\frac{\partial^2}{\partial\sigma\partial(\vartheta^2)}\{[I_0(\rho)-1-\rho^2/4]$$
$$\times\exp[-\vartheta^2/2(\sigma-\sigma_0)]\}$$
$$+\sum_{m=2}^{\infty}\frac{(\rho/2)^m}{(m!)^2}\{[1-\vartheta^2/2m(\sigma-\sigma_0)]_*^m$$
$$-\exp[-\vartheta^2/2(\sigma-\sigma_0)]\}$$
$$=\frac{1}{\pi}\frac{\partial}{\partial\sigma}\left\{\zeta\left[\frac{I_0(\rho)-1}{\rho^2/4}-1\right]\right.$$
$$\left.\times\exp[-\vartheta^2/2(\sigma-\sigma_0)]\right\}$$
$$-\frac{1}{\pi}\frac{\partial^2}{\partial\sigma\partial(\vartheta^2)}\sum_{m=2}^{\infty}\frac{(\rho/2)^m}{(m!)^2}$$
$$\times\{[1-\vartheta^2/2m(\sigma-\sigma_0)]_*^m$$
$$-\exp[-\vartheta^2/2(\sigma-\sigma_0)]\}. \quad (18)$$

Inserting these results into (11) and (3) we obtain two equivalent forms for the distribution function:

$$f(\sigma,\xi,\eta,\zeta)=\left[\delta(\sigma-\sigma_0)\delta(\xi)\delta(\eta)+\frac{\zeta\sigma_0}{\pi\sigma}\delta(\sigma-\sigma_0-\tfrac{1}{2}\vartheta^2)\right.$$
$$\left.+\frac{\sigma_0}{\sigma}\sum_{m=2}^{\infty}\frac{(m-1)(2\zeta)^m}{(m!)^2}\right.$$
$$\left.\times(\sigma-\sigma_0-\vartheta^2/2m)_*^{m-2}\right]\exp(-\phi_T\zeta)$$
$$=\left[\delta(\sigma-\sigma_0)\delta(\xi)\delta(\eta)+\frac{\zeta\sigma_0}{\pi\sigma}\delta(\sigma-\sigma_0-\tfrac{1}{2}\vartheta^2)\right.$$
$$+\frac{\zeta\sigma_0}{\pi\sigma}\frac{\partial}{\partial\sigma}\left\{\left[\frac{I_0(\rho)-1}{\rho^2/4}-1\right]\right.$$
$$\left.\left.\times\exp[-\vartheta^2/2(\sigma-\sigma_0)]\right\}\right]\exp(-\phi_T\zeta)$$
$$+\left[\frac{\sigma_0}{\pi\sigma}\frac{\partial^2}{\partial\sigma\partial(\vartheta^2)}\left\{\sum_{m=2}^{\infty}\frac{(\rho/2)^m}{(m!)^2}\right.\right.$$
$$\times\{\exp[-\vartheta^2/2(\sigma-\sigma_0)]$$
$$\left.\left.-[1-\vartheta^2/2m(\sigma-\sigma_0)]_*^m\}\right\}\right]$$
$$\times\exp(-\phi_T\zeta). \quad (19)$$

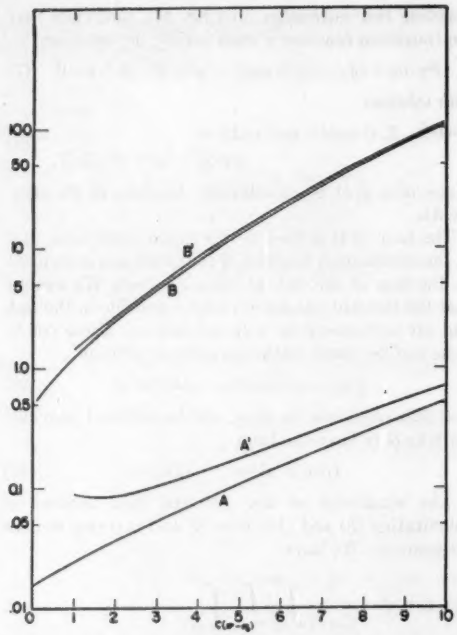

FIG. 1. Functions representing energy spectrum of multiply scattered gamma-rays apart from factor σ_0/σ. (A) Spectrum on axis, (A') asymptotic approximation for spectrum on axis, (B) spectrum integrated over all angles, (B') asymptotic approximation for spectrum integrated over all angles.

The second form has the advantage that in two important cases the last term (the summation) can be neglected compared to the other terms. First, if $\vartheta^2/2(\sigma-\sigma_0)\ll 1$ then the expression in braces in the summation is very small for every term and the summation can be neglected. Secondly, for large values of $\zeta(\sigma-\sigma_0)$, one finds that most of the contributions to the series $\sum_{m=2}^{\infty} g_m$ comes from terms where $m\sim[2\zeta(\sigma-\sigma_0)]^{\frac{1}{2}}$; hence if $\vartheta^2/2(\sigma-\sigma_0)\ll[2\zeta(\sigma-\sigma_0)]^{\frac{1}{2}}$, the use of the approximate expression (16) for g_m is justified and the summation can again be neglected. Hence in these cases

$$f(\sigma,\xi,\eta,\zeta)=\left[\delta(\sigma-\sigma_0)\delta(\xi)\delta(\eta)+\frac{\zeta\sigma_0}{\pi\sigma}\delta(\sigma-\sigma_0-\tfrac{1}{2}\vartheta^2)\right.$$
$$\left.+\frac{\zeta\sigma_0}{\pi\sigma}\frac{\partial}{\partial\sigma}\left\{\left[\frac{I_0(\rho)-1}{\rho^2/4}-1\right]\right.\right.$$
$$\left.\left.\times\exp[-\vartheta^2/2(\sigma-\sigma_0)]\right\}\right]$$
$$\times\exp(-\phi_T\zeta). \quad (20)$$

On the axis, $\vartheta=0$, the distribution function takes the simpler form

$$f(\sigma, 0, 0, \zeta)=\left[\delta(\sigma-\sigma_0)\delta(0)\delta(0)+\frac{\zeta\sigma_0}{\pi\sigma}\delta(\sigma-\sigma_0)\right.$$
$$\left.+\frac{32\zeta^2\sigma_0}{\pi\sigma}\left\{\frac{1-I_0(\rho)+\frac{1}{2}\rho I_1(\rho)}{\rho^4}\right\}\right]\exp(-\phi_T\zeta). \quad (21)$$

To show the distribution in energy of the multiply scattered gamma-rays on the axis, we have plotted in Fig. 1 as curve A the factor in braces in (21) as a function of $\zeta(\sigma-\sigma_0)$. Aside from the additional factor σ_0/σ this shows the relative distribution in energy.

The distribution of the gamma-rays per unit *energy* interval (rather than unit softness interval) can be obtained from the above formulas by simply multiplying by σ^2.

III. ASYMPTOTIC DISTRIBUTION

If $\rho=[8\zeta(\sigma-\sigma_0)]^{\frac{1}{2}}$ is not only large compared to $\vartheta^2/2(\sigma-\sigma_0)$ but is also large compared to unity, then it is permissible to replace the Bessel function occurring in (20) by its asymptotic form. Furthermore, after the differentiation with respect to σ has been carried out, one can obtain the asymptotic form of the distribution function by neglecting all terms but the one which is dominant when $[8\zeta(\sigma-\sigma_0)]^{\frac{1}{2}}$ is very large. The resultant asymptotic form is found to be

$$f(\sigma, \xi, \eta, \zeta)\sim\frac{32\zeta^2\sigma_0}{\pi\sigma}\exp[-\vartheta^2/2(\sigma-\sigma_0)]$$
$$\times\left\{\frac{\frac{1}{2}e^\rho}{(2\pi)^{\frac{1}{2}}\rho^{3/2}}\right\}\exp(-\phi_T\zeta), \quad (22)$$

with the validity condition

$$\rho=[8\zeta(\sigma-\sigma_0)]^{\frac{1}{2}}\gg 1+\vartheta^2/2(\sigma-\sigma_0).$$

It will be noted that the distribution in angle of gamma-rays of a given softness is just the Gaussian distribution derived by elementary arguments in I. The distribution in energy on the axis (except again for the factor σ_0/σ) according to this asymptotic formula is given by the curve A' in Fig. 1.

IV. INTEGRATION OVER ANGLES

To obtain the flux of gamma-rays at any depth independent of the direction in which they are travelling one may simply integrate the distribution (19) over all angles. One obtains the result:

$$F(\sigma, \zeta)=\int\int f d\xi d\eta=\delta(\sigma-\sigma_0)\exp(-\phi_T\zeta)$$
$$+\frac{4\zeta\sigma_0\exp(-\phi_T\zeta)}{\sigma}\left\{\frac{I_1(\rho)}{\rho}\right\}. \quad (23)$$

It is easily found that the integration over angles of the approximate formula (20) gives exactly the same result, so that the approximation involved in dropping the last summation in (19) corresponds only to a redistribution in angle of gamma-rays of given energy at any depth without a change in their total number.

The first term in (23) represents, of course, the gamma-rays which have reached the depth ζ unscattered and unabsorbed, while the second term represents the scattered gamma-rays. The distribution in energy of the latter as given by the factor in braces (neglecting again the factor σ_0/σ) is plotted as curve B in Fig. 1 as a function of $\zeta(\sigma-\sigma_0)$. When $\zeta(\sigma-\sigma_0)$ is very large compared with unity, the Bessel function can be replaced by its asymptotic form giving the distribution function

$$F(\sigma, \zeta)\sim\frac{4\zeta\sigma_0\exp(-\phi_T\zeta)}{\sigma}\left\{\frac{e^\rho}{(2\pi)^{\frac{1}{2}}\rho^{\frac{1}{2}}}\right\}. \quad (24)$$

The factor here in braces is also plotted in Fig. 1 as curve B'.

V. CALCULATIONS OF ANGULAR DISTRIBUTION

In order to see in greater detail the angular distribution of the multiply scattered gamma-rays, some

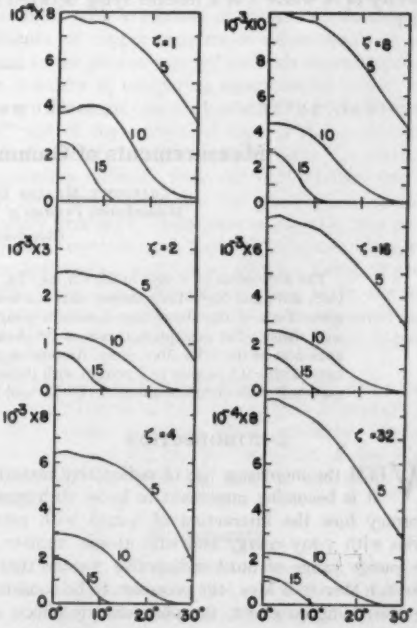

FIG. 2. Distribution in angle of multiply scattered gamma-rays of energies of 5, 10, and 15 Mev at various depths in material for 17-Mev gamma-rays incident on water. Note variations in vertical scales which represent the number of gamma-rays per unit solid angle per Mev energy interval per incident gamma-ray.

numerical calculations on the basis of Eq. (20) have been performed for incident gamma-rays of 17-Mev energy diffusing through water. The curves of angular distribution as given by the number of gamma-rays per unit *energy* interval (energy measured in Mev) and per unit solid angle are plotted in Fig. 2 for energies of 15, 10, and 5 Mev and $\zeta=1$, 2, 4, 8, 16, and 32. It will be noted that the angular distribution is very close to Gaussian even for relatively small thicknesses of material.

For a complete picture of the energy and angular distribution one must add to the above curves the contributions of the two terms containing delta-functions in (20) representing the unscattered and singly scattered gamma-rays.

VI. CONCLUDING REMARKS

The principal source of error in the solution obtained above results from the approximation made in going from Eq. (4) to Eq. (5). Going back to the fundamental equations, this corresponds to approximating the factor $\frac{1}{2}(\epsilon'/\epsilon)^2[\epsilon/\epsilon'+\epsilon'/\epsilon]$ in the Klein-Nishina formula [I, Eq. (3)] by ϵ'/ϵ (neglecting the term in $\sin^2\Theta$). The extent of this error is shown in Fig. 3 where both factors are plotted. Some improvement in the results might be obtained if one used in place of ϵ'/ϵ, the quantity $c\epsilon'/\epsilon$ where c is a number lying between 0.5 and 1.

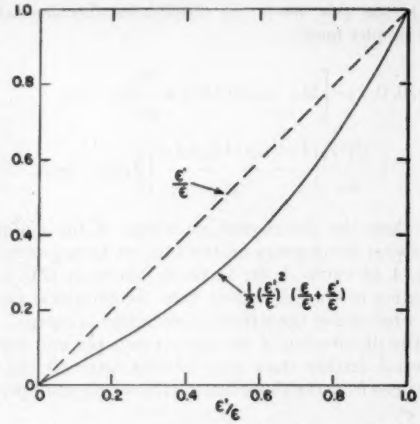

FIG. 3. Extent of approximation to Klein-Nishina formula involved in solution of the diffusion equation.

It would be of value to determine the corrections due to the difference between the approximate expression used and the correct expression by a perturbation treatment. A calculation of this type is planned for the future.

We wish to express our thanks to Mr. G. F. Bing for his aid with the numerical calculations.

PHYSICAL REVIEW VOLUME 81, NUMBER 3 FEBRUARY 1, 1951

Measurements of Gamma-Ray Absorption Coefficients*†

CHARLOTTE MEAKER DAVISSON‡ AND ROBLEY D. EVANS
Massachusetts Institute of Technology, Cambridge, Massachusetts

(Received December 5, 1949)

The absorption of γ-rays in Al, Cu, Sn, Ta, and Pb was measured using γ-rays from I^{131}, Cu^{64}, Mn^{54}, Co^{60}, Zn^{65}, and Na^{24}. Tests showed that scattering from nearby objects and from the absorber were negligible. Tests of the absorption of radium γ-rays in Pb showed good agreement with other workers and with theory. The absorption curves of I^{131} showed the presence of a 0.65-Mev γ-ray about 15 percent as abundant as the 0.367-Mev γ-ray. Absorption coefficients measured with the other sources showed agreement within 0.5 percent to 2 percent with theory. An anomalous absorption coefficient (5 percent less than expected) with tantalum absorber ($Z=73$) and Zn^{65} and Co^{60} sources ($h\nu\sim1.2$ Mev) needs reinvestigation.

I. INTRODUCTION

WITH the increasing use of radioactive materials, it is becoming important to know with greater accuracy how the interaction of γ-rays with matter varies with γ-ray energy and with atomic number. In the energy range of most radioactive γ-rays, that is, from 0.1 Mev to 6 Mev, the processes to be considered are the Compton effect, the photoelectric effect, and pair production. Theoretical analyses of these processes have been made, and from them values of absorption coefficients can be found for comparison with experiment. A summary of most of these theories has been given by Heitler.[1] We have made a detailed study of the results of the theories and shall publish elsewhere[2] our calculations in the form of equations, tables, and curves.

Early experimental studies of absorption coefficients

* Assisted by the joint program of the ONR and AEC.

† Presented at the April, 1948, meetings of the American Physical Society.

‡ Present address: care of Dr. J. W. Davisson, Crystal Branch, Naval Research Laboratory, Washington 20, D. C.

[1] W. Heitler, *The Quantum Theory of Radiation* (Oxford University Press, London, 1936), pp. 119 *et seq.*

[2] C. M. Davisson and R. D. Evans, Revs. Modern Phys. (to be published).

were made with sources of radium, RdTh, and x-rays. Recently, strong sources of artificially radioactive substances have been made available; and with these it is now possible, with single energy γ-rays, to extend absorption studies beyond the energy range practicable with x-rays.

II. PRESENT EXPERIMENT

With absorbers of aluminum, copper, tin, tantalum, and lead we have rechecked the results of other workers with sources of Zn^{65} (1.14 Mev), Co^{60} (1.16 and 1.31 Mev), and Na^{24} (1.38 and 2.76 Mev), and in addition have studied the absorption of the γ-rays from I^{131} (0.367-Mev and others), Cu^{64} (annihilation radiation), and Mn^{54} (0.835 Mev).

A. Sources

The sources of I^{131}, Cu^{64}, Zn^{65}, and Na^{24} were obtained from the Atomic Energy Commission at Oak Ridge, while the Mn^{54} and Co^{60} sources were prepared in the M.I.T. cyclotron by deuteron bombardment of chromium and cobalt, respectively. The decay curves of I^{131}, Cu^{64}, and Na^{24} showed the characteristic half-lives of each isotope, and corrections were made for decay during the readings. The Mn^{54} sample was allowed to stand for several months before being used, so that the 6.5-day activity of Mn^{52} was less than 0.1 percent of the activity of Mn^{54} at the time of the measurements.

The sources were placed in 10-mm Pyrex tubing, sealed off, and placed in an aluminum container which fitted into a brass-lined hole in the lead source block (Fig. 1). In the case of long sources which emitted two γ-rays (Co^{60}, I^{131}, and Na^{24}), correction was made for different self-absorption in the source before comparing results with theory.

B. Absorbers

The five absorbers, aluminum, copper, tin, tantalum, and lead, were chosen because they could be obtained easily in pure form and because they covered the full range of Z values in satisfactory steps. They were carefully machined to the desired lengths, and their densities determined from measurements of length, diameter, and weight. In addition spectroscopic analyses were made of the tantalum and lead absorbers; and their densities were measured at the National Bureau of Standards.

The qualitative spectroscopic analysis of Ta, made by the M.I.T. Spectroscopy Laboratory, showed traces (<0.01 percent) of Al, Ca, Cu, Fe, K, Mn, and Na; and Si as a minor constituent (>0.01 percent). Calculations showed that the presence of these contaminations, even at abundances greater or less by a factor of 10, should not affect the measured absorption coefficient by more than 0.5 percent. A further chemical analysis by Mr. D. Guernsey of the M.I.T. Metallurgy Department showed that at least 99.5 percent of the sample was tantalum.

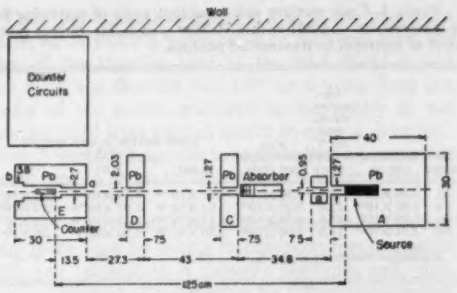

FIG. 1. Schematic plan view of apparatus and collimating system, approximately to scale. All dimensions are shown in cm.

An analysis of one of the lead absorbers by the New England Spectrochemical Laboratories showed that the absorber contained from 0.1 to 10 percent of bismuth. The measured density of 11.29 gm/cc would indicate that about 4 percent of the sample was bismuth. Calculations show, however, that even if the sample were 10 percent bismuth, the absorption coefficients expected theoretically would not differ from those we have used for pure lead by more than 0.5 percent.

C. Detectors

The counters used had copper mesh cathodes and were filled with a mixture of argon and alcohol. The efficiency of copper counters is substantially proportional to the photon energy,[3] and this was assumed for our counters in comparing experimental results with theory. The single counter used for I^{131}, Cu^{64}, Mn^{54}, and Co^{60} was of the cylindrical type, 2 cm in diameter, with an effective length of about 8 cm. To eliminate annihilation radiation from the Zn^{65} readings and the 1.38-Mev γ-rays from the Na^{24} readings, coincidence counters were used. These were of the bell type geometry with very thin glass "bubble" windows. They were 2 cm in diameter, and had an effective length of about 3 cm. They were arranged end on, with the thin windows facing each other, in an arrangement such that thin copper absorbers could be placed between them.

The voltage supplies were well regulated, and a daily check was made to be sure the counters were operating on their voltage plateaus. When necessary, counting rates were corrected for the deadtime of the single counter and the resolving time of the coincidence counters.

D. Geometry

The geometry of apparatus for measuring absorption coefficients must be such that the scattered radiation which reaches the detector is either negligible or can be quantitatively determined.

[3] See, e.g., Roberts, Elliott, Downing, Peacock, and Deutsch, Phys. Rev. 64, 268 (1943); and Bradt, Gugelot, Huber, Medicus, Preiswerk, and Scherrer, Helv. Phys. Acta 19, 77 (1946).

TABLE I. Cross sections and maximum angle of scattering for a transmission of 0.001 with 2.76-Mev γ-rays, for various ratios S/B of scattered to transmitted photons.

Element	Electrons per cc	Absorber thickness for T =0.001 (cm)	$N_e x_0$ (electrons per cm^2)	Cross section in cm^2/electron if S/B is 0.001	0.01	0.1
Al	7.86×10^{23}	69.7	5.48×10^{25}	1.82×10^{-29}	1.82×10^{-28}	1.82×10^{-27}
Cu	2.46×10^{24}	21.2	5.20×10^{25}	1.92×10^{-29}	1.92×10^{-28}	1.92×10^{-27}
Sn	1.85×10^{24}	25.5	4.72×10^{25}	2.12×10^{-29}	2.12×10^{-28}	2.12×10^{-27}
Pb	2.71×10^{24}	14.8	4.00×10^{25}	2.50×10^{-29}	2.50×10^{-28}	2.50×10^{-27}
Maximum scattering angle, θ_0				0.5°	1.6°	5°–6°

A diagram of our geometry is shown in Fig. 1. To prevent radiation scattered from nearby objects from reaching the detector, we surrounded both the source and the detector with lead. The least a scattered ray could pass through was 15 cm, which would reduce the intensity of 2.76-Mev γ-rays to 0.1 percent, and softer scattered rays to negligible proportions. That they were negligible was shown by the following tests with the Co^{60} source. With 20 cm or more of lead in the absorber position, the counting rate was the same as the background, within the experimental error of 1.5 percent. Addition of a large aluminum sheet placed parallel to and at different distances from the γ-ray beam, with the 20 cm of lead in the absorber position, produced no change from the background counting rate.

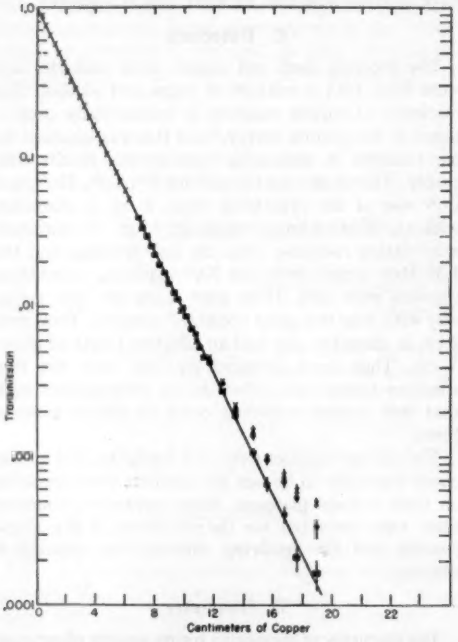

FIG. 2. Transmission of γ-rays of Co^{60} through copper, as measured with different degrees of final collimation. The solid line represents the values expected theoretically if no secondary quanta reach the detector. Crosses: with counter at near end (a) of lead block (E), no collimation after absorber. Solid circles: with counter withdrawn 13.5 cm into lead block (E), no collimation after absorber. Solid squares: with counter in lead block, and collimators C and D of Fig. 1 in place.

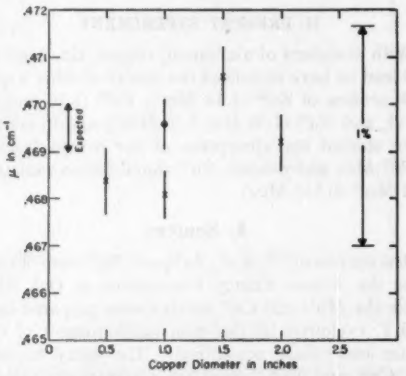

FIG. 3. Absorption coefficient of γ-rays of Co^{60} in copper absorbers of various diameters, showing that multiple scattering is effectively excluded by the collimation shown in Fig. 1. Crosses: data calculated using a deadtime of 149 μsec. Solid circle: data calculated using 119 μsec deadtime.

Compton singly scattered radiation is the most important of the secondary radiations produced in the absorber itself which might reach the detector. An analysis of the amount reaching the detector has been made by Tarrant.[4] If it is assumed that the angles involved are small, that the absorber is not very close to either the source or the detector, and that the efficiency of the detector is proportional to the energies of the photons, then the ratio of the number of scattered photons, S, to the number of transmitted photons, B, actuating the detector is

$$S/B = N_e x_0 \, {}_e\sigma_s^{\theta_0}, \tag{1}$$

where N_e is the number of electrons per unit volume in the absorber, x_0 is the length of the absorber, and ${}_e\sigma_s^{\theta_0}$ is the cross section for the total photon energy scattered between 0 and θ_0. The equation for ${}_e\sigma_s^{\theta_0}$ will be published elsewhere.[2] For small angles it is[5]

$${}_e\sigma_s^{\theta_0} = \pi r_0^2 \theta_0^2 [1-(\theta_0^2/12)(9\alpha+4)], \tag{2}$$

where α is $h\nu/m_0c^2$, and r_0 is e^2/m_0c^2.

From Eq. (2) we can estimate the maximum allowable angle, θ_0, for any arbitrarily chosen value of S/B. This

[4] G. T. P. Tarrant, Proc. Camb. Phil. Soc. 28, 475 (1932).

[5] This does not agree with the equation given by Tarrant, which is

$${}_e\sigma_s^{\theta_0} = \pi r_0^2 \theta_0^2 \{1+(\theta_0^2/4)[(11/2)\alpha-1]\}.$$

We can find no mistake in our algebra. Also, values calculated from his equation deviate from the correct values more than the still poorer approximation

$${}_e\sigma_s^{\theta_0} = \pi r_0^2 \theta_0^2.$$

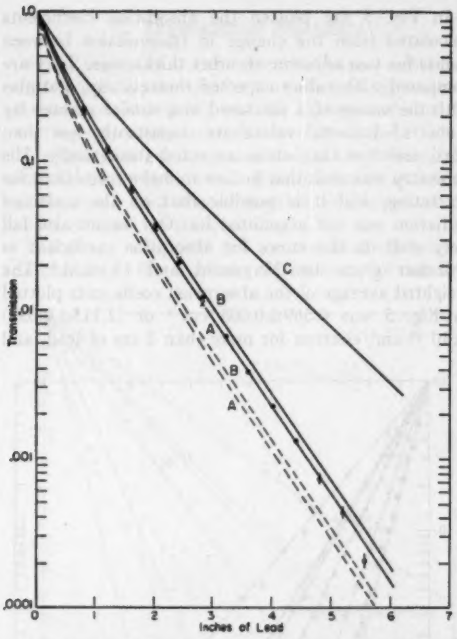

FIG. 4. Transmission of γ-rays of radium, in equilibrium with its decay products, through lead, in very narrow-beam geometry. *Crosses:* Experimental points using 1.76 mg Ra salt in glass tube. *Solid circles:* Experimental points using 27.7 mg Ra in a platinum cylinder of unknown wall thickness. Various theoretical transmission curves are shown, each calculated using the transmission through 0.5-mm Pt as unity. *Dashed curves:* Assume detector sensitivity is independent of photon energy. *Solid curves:* Assume detector sensitivity is linearly proportional to photon energy. *Curves A:* the number *vs* energy distribution in the γ-ray spectrum is taken from the data of C. D. Ellis and M. A. Aston (Proc. Roy. Soc. **129A**, 180 (1930)) as compiled by R. D. Evans (Nucleonics **1**, No. 2, 32 (1947)). For each individual γ-ray component, the effective absorption coefficient is taken as $(\tau+\kappa+\sigma)$. *Curves B:* The γ-ray spectrum is a blend of Ellis and Aston for the low energy components up to 1.12 Mev, and of G. D. Latyshev (Revs. Modern Phys. **19**, 132 (1947)) for the high energy components. Individual absorption coefficients $(\tau+\kappa+\sigma)$. *Curve C:* Spectrum of Ellis and Aston: effective absorption coefficients taken as $(\tau+\kappa+\sigma-\sigma_s)$, i.e., as broad-beam with no scattered radiation excluded from the counter. The best fit is with the solid curve *A*; i.e., all scattered radiation assumed excluded from the counter, counter sensitivity proportional to photon energy, and Ellis and Aston spectrum. The transmission curve is not strongly sensitive to the assumed γ-ray spectrum, as shown by the position of the solid curve *B*.

is done in Table I for 2.76-Mev γ-rays and a transmission of 0.1 percent. With available source strengths it is unlikely that a transmission of 0.001 could be measured to better than 1 percent, so with a scattering angle of 1.5° to 2°, no correction would need to be made for single scattering.[6]

[6] Analysis of multiply scattered photons, or of secondary radiation due to annihilation radiation or bremsstrahlung which reach the detector is more difficult. We have made no estimate of this for our geometry, but our scattering tests indicate that it must be negligible.

From the dimensions given in Fig. 1, the maximum angle, θ_0, at which a γ-ray could be scattered from the edge of the absorber next to the lead shield *C* and still reach the detector was 1.3° for a γ-ray from the center of the source scattered to the center of the detector (2.6° from edge of source to edge of detector). Thus, it seemed reasonable to suppose that no correction would need to be made for radiation scattered from the absorber.

Tests for such radiation scattered from the absorbers were made both by taking transmission measurements with lead collimators in different positions, and, with the final amount of collimation, by taking transmission measurements with different diameters of copper absorbers. Transmission curves for different amounts of lead collimation are shown in Fig. 2. Without the lead collimation after the absorber (*C* and *D* in Fig. 1), some scattered radiation was reaching the detector; but with this shielding the measurements agree with the expected values to transmissions as low as 0.0002. The average absorption coefficients measured with copper absorbers of different diameters are plotted in Fig. 3. The results show no consistent variation with absorber diameter, are the same within 1 percent, and show excellent agreement with the value expected theoretically.

As a further scattering check, and for comparison of our results with previous workers, a study was made of the absorption of radium γ-rays in lead. Our measured transmissions are plotted in Fig. 4, where they are compared with the transmissions to be expected theoretically, making different assumptions as to γ-ray spectra, counter sensitivity, and amount of scattered radiation reaching the detector. Our results agree well with the curves for no scattering, indicating again that in our geometry scattered radiation was negligible.

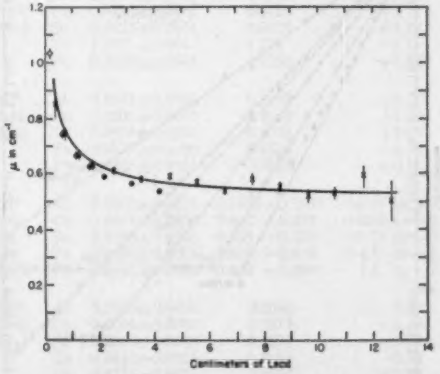

FIG. 5. Theoretical and experimental dependence of the absorption coefficients for the γ-rays of radium (and its decay products) on Pb filtration. Initial filtration 0.5 mm Pt. *Solid Curve:* derived from the slope of the solid curve *A* of Fig. 4. *Crosses:* values from slope between adjacent experimental points of Fig. 4. *Solid Circles:* experimental values of Roberts (reference 7).

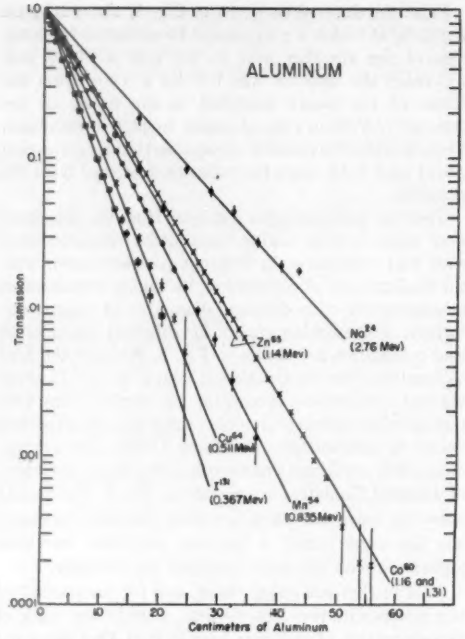

FIG. 6. Transmission of γ-rays from various radionuclides through Al. Solid curves: theoretical transmission for the γ-ray energy shown opposite each curve.

However, our measurements were not accurate enough to show which of the radium γ-ray spectra is the better.

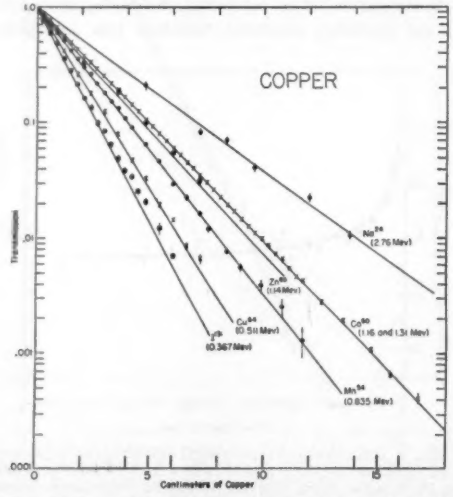

FIG. 7. Transmission of γ-rays from various radionuclides through Cu. Solid curves: theoretical transmission for the γ-ray energy shown opposite each curve.

In Fig. 5 are plotted the absorption coefficients calculated from the change in transmission between points for two adjacent absorber thicknesses. They are compared with values expected theoretically, and also with the values of μ measured in a similar manner by Roberts.[7] Roberts' values are consistently less than ours, and less than those expected theoretically. His geometry was such that he had to make corrections for scattering, and it is possible that all the scattered radiation was not accounted for. Our values also fall very well on the curve for absorption coefficient *vs* absorber given by Mayneord and Cipriani.[8] The weighted average of the absorption coefficients plotted in Fig. 5 was 0.569 ± 0.008 cm^{-1} or $(2.115\pm0.030)\times10^{-25}$ cm^2/electron for more than 2 cm of lead, and

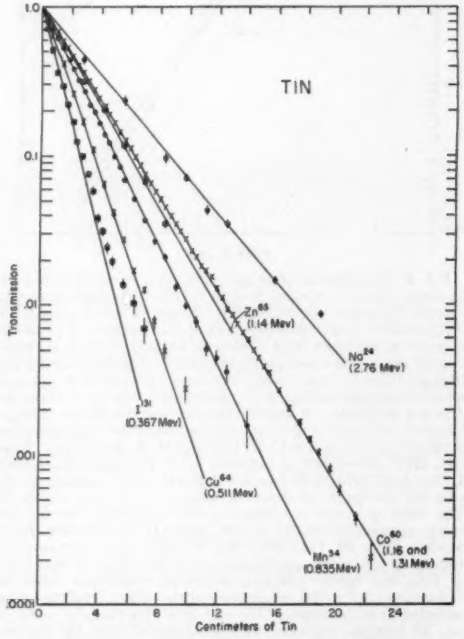

FIG. 8. Transmission of γ-rays from various radionuclides through Sn. Solid curves: theoretical transmission for the γ-ray energy shown opposite each curve.

was 0.556 ± 0.008 cm^{-1} or $(2.065\pm0.028)\times10^{-25}$ cm^2/electron for more than 5 cm of lead. These are in reasonable agreement with those of other workers.[9]

[7] J. E. Roberts, Proc. Roy. Soc. **183A**, 338 (1945).
[8] W. V. Mayneord and A. J. Cipriani, Can. J. Research **25A**, 303 (1947).
[9] See, e.g., K. W. F. Kohlrausch, Sitzber. Akad. Wiss. Wien **126IIa**, 441, 683, 887 (1917); Handbuch Exp. Phys. **15**, 78 (1928); J. S. Rogers, Proc. Phys. Soc. London **44**, 349 (1932); I. Zlotowski, J. phys. rad. **6**, 242 (1935); Ketelaar, Piccard, and Stahel, J. phys. rad. **5**, 385 (1934); and L. Meitner and H. H. Hupfeld, Z. Physik **67**, 147 (1931).

E. Experimental Procedure

At the beginning and end of each day, and sometimes more frequently, the circuits were checked, the counter plateau was determined, and the background and the counting rate without absorber were measured.

The transmission was calculated as the ratio of the corrected counting rate with the absorber to that with no absorber, and the absorption coefficients were calculated from the transmissions.

The errors calculated are the standard deviations, and combine in the usual way the errors in the counting rate and in the measured counter deadtime. In averaging the absorption coefficients the values were weighted according to the inverse of their errors, and the standard deviation of the average calculated from the equations given in the *Handbook of Chemistry and Physics*.

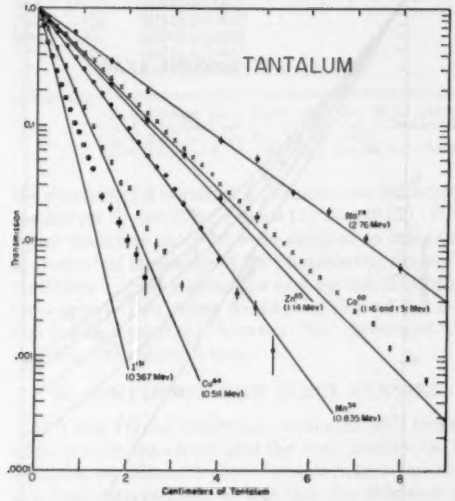

FIG. 9. Transmission of γ-rays from various radionuclides through Ta. Solid curves: theoretical transmission for the γ-ray energy shown opposite each curve.

III. EXPERIMENTAL RESULTS

Our measured transmissions in each absorber are shown in Figs. 6 to 10; the average absorption coefficients are summarized in Table II; and the measured electronic coefficients, plotted against atomic number, are shown in Fig. 11. The solid lines in these figures indicate the results expected according to existing theories. The measurements were made in 1947.

The I^{131} results were unexpected, since in 1947 the highest energy which I^{131} was known to emit was 0.367 Mev.[10] The transmissions in lead could be repeated

[10] Downing, Deutsch, and Roberts, Phys. Rev. **61**, 686 (1942).

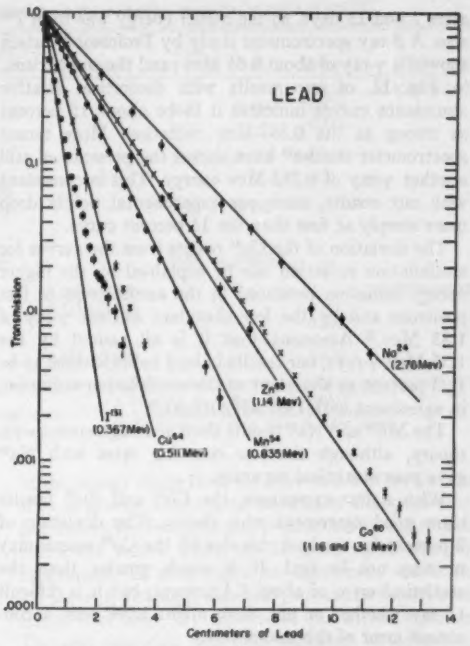

FIG. 10. Transmission of γ-rays from various radionuclides through Pb. Solid curves: theoretical transmission for the γ-ray energy shown opposite each curve.

TABLE II. Measured absorption coefficients compared with those expected theoretically.[a]

Source	Element	Meas. μ (cm^{-1})	Theor. μ (cm^{-1})	% difference
Mn^{54}	Al	0.1823±0.0003	0.1820	+0.16
(0.835	Cu	0.5782±0.0013	0.5718	+1.12
Mev)	Sn	0.4683±0.0014	0.4628	+1.19
	Ta	1.210 ±0.004	1.228	−1.47
	Pb	0.9368±0.0041	0.9256	+1.21
Zn^{65}	Al	0.1571±0.0022	0.1559	+0.77
(1.14	Cu	0.4862±0.0070	0.4914	−1.06
Mev)	Sn	0.3923±0.0054	0.3858	+1.69
	Ta	0.9127±0.0100	0.9536	−4.30
	Pb	0.7068±0.0051	0.7057	+0.11
Co^{60}	Al	0.1502±0.0001	0.1495−0.1501	+0.47 to +0.07
(1.16	Cu	0.4693±0.0003	0.469 −0.470	+0.06 to −0.15
and	Sn	0.3686±0.0003	0.369 −0.372	−0.11 to −0.92
1.31	Ta	0.8694±0.0007	0.910 −0.916	−4.5 to −5.1
Mev)	Pb	0.6497±0.0006	0.659 −0.669	−1.4 to −2.9
Na^{24}	Al	0.0956±0.0026	0.1001	−4.50
(2.76	Cu	0.3164±0.0080	0.3273	−3.33
Mev)	Sn	0.2668±0.0045	0.2692	−0.89
	Ta	0.6433±0.0055	0.6467	−0.53
	Pb	0.4776±0.0045	0.4644	+2.84

[a] Use of the more recent values (Lind, Brown, and DuMond, Phys. Rev. **76**, 591 (1949)) of 1.17 and 1.33 Mev for the energies of the gamma-rays of Co^{60} would decrease the theoretical values of μ by about 1 percent, and would slightly improve the over-all agreement between theory and experiment. The newer value[10] of 1.12 Mev for the gamma-ray energy of Zn^{65} would increase the theoretical absorption coefficients for this nuclide by an average of about 1.5 percent.

after 7 and 13 days, so the higher energy was from I^{131} also. A β-ray spectrometer study by Professor Deutsch showed a γ-ray of about 0.65 Mev; and the comparison, in Fig. 12, of our results with theoretical relative abundance curves indicates it to be about 15 percent as strong as the 0.367-Mev radiation. More recent spectrometer studies[11] have shown the presence of still another γ-ray of 0.283-Mev energy. This is consistent with our results, since our experimental points drop more steeply at first than the 15 percent curve.

The deviation of the Cu^{64} results from the curves for annihilation radiation can be explained by the higher energy radiation produced in the annihilation of fast positrons and by the low abundant nuclear γ-ray of 1.35 Mev.[12] Assuming that it is all caused by the 1.35-Mev γ-rays, our results in lead indicate them to be 1.23 percent as abundant as the annihilation radiation, in agreement with Deutsch's report.[12]

The Mn^{54} and Na^{24} results show good agreement with theory, although the low counting rates with Na^{24} gave poor statistical accuracy.

With a few exceptions, the Co^{60} and Zn^{65} results show good agreement with theory. The deviation of 2 percent for the lead values with the Co^{60} source may or may not be real. It is much greater than the statistical error of about 0.1 percent, but it is difficult to say whether or not there might have been a consistent error of this magnitude.

The disagreement of 5 percent with Co^{60} and tantalum, however, is far outside the statistical experimental error of 0.1 percent which was based on the variations among 60 independent measurements. Measurements made at different times, and calculations using a counter deadtime greater by 25 percent do not differ from each other by more than the experimental error. The results with Zn^{65} and tantalum also differ from theory. The coincidence counting rate was low, but the measured absorption coefficient was less than theory by 3 times the standard deviation of the average value (obtained from 7 independent observations). It is improbable that this deviation would be due purely to statistical fluctuations. Assuming the Zn^{65} energy[13] to be 1.12 Mev, our results would still agree with theory within 2 percent except for tantalum, which would deviate by 5 percent. An error in the physical conversion coefficients for tantalum would have caused deviations at other energies. We have checked the possible presence of inner x-rays[14] but find the energies and intensities of these to be much too small to affect our results. If the deviation we have found in tantalum is real, it indicates the presence of anomalously small absorption in tantalum of γ-rays of about 1.2-Mev energy. At this energy

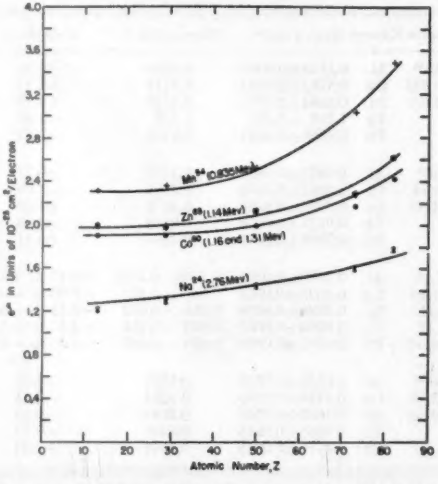

FIG. 11. Experimental and theoretical (narrow-beam) total absorption coefficients ($_e\tau + _e\kappa + _e\sigma$), in 10^{-25} cm²/electron.

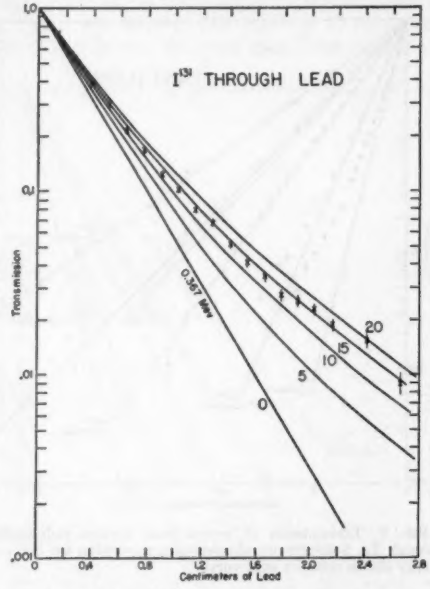

FIG. 12. Experimental and theoretical transmission of the γ-rays of I^{131} through Pb. Solid curves: expected transmission for homogeneous 0.367-Mev photons (marked 0), and for 5, 10, 15, and 20 photons of 0.65 Mev per 100 photons of 0.367 Mev. Initial filtration 0.122-cm Pb taken as unit transmission. These data were the first evidence for the presence of the 0.638-Mev γ-ray component in I^{131}, and their curvature at low filtration is consistent with the presence of the weak 0.283-Mev component as found subsequently by Metzger and Deutsch (reference 11).

[11] F. Metzger and M. Deutsch, Phys. Rev. 74, 1640 (1948).
[12] Martin Deutsch, Phys. Rev. 72, 729 (1947).
[13] Jensen, Laslett, and Pratt, Phys. Rev. 76, 430 (1949).
[14] J. K. Knipp and G. E. Uhlenbeck, Physica 3, 425 (1936); F. Block, Phys. Rev. 50, 272 (1936); C. S. Wu, Phys. Rev. 59, 481 (1941); S. E. Edwards and M. L. Pool, Phys. Rev. 69, 549 (1946).

TABLE III. Measured absorption coefficients compared with those of other workers (in units of cm^{-1}).

Source	Element	Meas.	Groetzinger and Smith[a]	Mayneord and Cipriani[b]	Alburger[c]	Cork and Pidd[d]	Cork[e]	Cowan[f]	Parkinson[g]
Zn^{65}	Al	0.1571±0.0022						0.155	0.156 ±0.001
(1.14	Cu	0.4862±0.0070				0.51	0.460	0.478	
Mev)	Sn	0.3923±0.0054						0.372	
	Ta	0.9127±0.0100							
	Pb	0.7068±0.0051				0.72	0.678	0.724	
Co^{60}	Al	0.1502±0.0001		0.150±0.002					
(1.16	Cu	0.4693±0.0003		0.475±0.005		0.46	0.440		
and	Sn	0.3686±0.0003							
1.31	Ta	0.8694±0.0007							
Mev)	Pb	0.6497±0.0006		0.651±0.007		0.64	0.610		
Na^{24}	Al	0.0956±0.0026			0.088±0.001				0.0996±0.0008
(2.76	Cu	0.3164±0.0080			0.311±0.005				
Mev)	Sn	0.2668±0.0048						0.265	
	Ta	0.6433±0.0055							
	Pb	0.4776±0.0045	0.467±0.009		0.454±0.004			0.479	

[a] G. Groetzinger and L. Smith, Phys. Rev. 67, 53 (1945).
[b] W. V. Mayneord and A. J. Cipriani, Can. J. Research 25A, 303 (1947).
[c] D. E. Alburger, Phys. Rev. 73, 344 (1948).
[d] J. M. Cork and R. W. Pidd, Phys. Rev. 66, 227 (1944).
[e] J. M. Cork, Phys. Rev. 67, 53 (1945).
[f] C. L. Cowan, Phys. Rev. 74, 1841 (1948).
[g] W. C. Parkinson, Phys. Rev. 76, 1348 (1949).

the absorption in tantalum is primarily due to Compton encounters ($\sigma/\mu=0.84$; $\tau/\mu=0.15$; $\kappa/\mu=0.01$), If the entire deviation observed were assigned to inaccuracy in theoretical knowledge of the photoelectric absorption coefficient τ, then a reduction of τ by one-third would be required. This seems unlikely in view of the more reasonable agreement between the theoretical and experimental values in lead.

IV. COMPARISON WITH OTHER WORKERS

In Table III our results are compared with those of other workers who have used the same sources. On the whole the agreement is good. In most cases where there is a large disagreement we feel that the difference can be attributed to poorer shielding which allowed appreciable scattered radiation to reach the detector,[15–17] or to the method of separating the Na^{24} energies.[15]

V. CONCLUSION

Our results with the γ-rays from Cu^{64}, Mn^{54}, Zn^{65}, Co^{60}, and Na^{24} show that experiment agrees with theory in the energy range from 0.5 Mev to 2.8 Mev, and thus that in general the present theories of Compton effect, photoelectric effect, and pair production give absorption coefficient values which are in good agreement with experiment. In most cases our agreement was within 1.5 percent, although with Na^{24}, where the experimental errors were large, the agreement was within 4 percent. The one exception was with tantalum absorbers and the 1.14-Mev radiation of Zn^{65} and the 1.16- and 1.31-Mev radiation of Co^{60}. We could find no experimental cause for this deviation. However, in view of the anomalous absorption in magnesium which was found by Meitner and Hupfeld,[9] but could not later be duplicated,[18,19] we hesitate to state that this anomalous result is real. Further tests should be made with a stronger source of Zn^{65}, and with an entirely different tantalum absorber.

The authors wish to express their appreciation to Professor Martin Deutsch for his helpful discussions and suggestions. They are indebted to Dr. E. L. Brady, Miss Dorothy Kelly, and Miss Jane Drury for their advice concerning sources and for chemical separations.

[15] D. E. Alburger, Phys. Rev. 73, 344 (1948).
[16] J. M. Cork and R. W. Pidd, Phys. Rev. 66, 227 (1944).
[17] J. M. Cork, Phys. Rev. 67, 53 (1945).
[18] J. C. Jacobsen, Z. Physik 103, 747 (1936).
[19] W. Gentner, Physik. Z. 38, 836 (1937).

On the Displacement of Corresponding Energy Levels of C^{13} and N^{13}

JOACHIM B. EHRMAN*
Princeton University, Princeton, New Jersey
(Received July 17, 1950)

It is investigated to what extent the change in boundary conditions at the nuclear surface due to Coulomb wave function distortion in the external region can explain the relative displacement of the first excited states of C^{13} and N^{13}. It is found that the calculated displacement is in the right direction and of a sufficiently large magnitude, but rather sensitively dependent on the definition of nuclear radius.

I. INTRODUCTION

IT is well known that the energy differences between the ground states of the members of a pair of mirror nuclei can be explained, apart from the neutron-hydrogen mass difference, as due to the Coulomb repulsion existing between a pair of protons. This means that the nuclear radii as calculated from the Coulomb energy differences can be expressed by an equation of the form

$$r = r_0 A^{\frac{1}{3}}, \tag{1}$$

where A is the mass number of the nucleus, and r_0 is fairly constant for all mirror nuclei, being equal[1] to about 1.45×10^{-13} cm. Moreover, the spins and parities are presumed to agree for both mirror nuclei, and there seems to be no definite experimental evidence to contradict this assumption.

These circumstances may be explained by assuming that the force between two protons is the same as that between two neutrons except for the Coulomb repulsion. From this assumption it would then seem to be plausible to anticipate that also in the excited states of mirror nuclei there will be a similar correspondence in the positions of energy levels, provided that the radii in the excited states are the same as in the ground states. Now, while in the ground states the energy differences can be fitted with the above-indicated variation of the nuclear radius to within 100 kev (except in the case of $Al^{27}-Si^{27}$, where[2] it is 150 kev), in the excited states there appear some very large discrepancies.

In the case of $C^{13}-N^{13}$, the first two excited levels[3] of the two nuclei lie at about 3.10 Mev and 3.91 Mev for C^{13}, and at 2.35 Mev and 3.49 Mev for N^{13} (Fig. 1). A level in C^{13} at 0.8 Mev found by the reaction $B^{10}(\alpha,p)C^{13}$ has not been found by other reactions and will not be considered here. If we now make the tentative assumption that the above mentioned levels are really corresponding levels in the two nuclei, then, at first sight, it would appear that not only must the nuclear radius be considered to be larger in the excited states than in the ground states, but this change of radius would not even be monotonic in going from one level to the next.

However, a more careful analysis indicates that the displacement between the corresponding energy levels should not be due entirely to a Coulomb energy difference varying inversely as the nuclear radius and otherwise independent of energy. It is postulated that the elements of the dispersion-theoretic R-matrix on the nuclear surface as a function of energy may be the same for both mirror nuclei, once the ordinary Coulomb energy difference has been taken into account. If there were no Coulomb repulsion between a proton pair, and exact equality of n-n and p-p forces, then the nuclear levels would occur at the same energies (except for the constant neutron-hydrogen mass difference displacement) and the two nuclei would be described by the same wave functions at any energy, the Hamiltonian being symmetric in the exchange of a neutron with a proton. In this case, the R matrix would certainly be the same function of energy for both mirror nuclei. Now, for light nuclei the Coulomb forces inside the nucleus are very much smaller than are the purely nuclear forces, so that they will hardly influence the nuclear wave function inside the nucleus. Their only

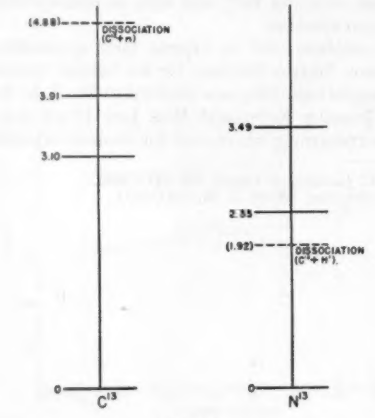

FIG. 1.

* AEC Predoctoral Fellow.

[1] J. M. Blatt, *On the Interpretation of Energy Levels in Light Nuclei*, unpublished.

[2] Barkas, Creutz, Delsasso, Sutton, and White, Phys. Rev. **58**, 382 (1940). G. Kuerti and S. N. Van Voorhis, Phys. Rev. **58**, 614 (1940).

[3] W. F. Hornyak and T. Lauritsen, Revs. Modern Phys. **20**, 191 (1948). T. Lauritsen, *Energy Levels of Light Nuclei*, Preliminary Report No. 5, Nuclear Science Series, Nat. Res. Council.

appreciable effect will be a constant displacement of the energy levels. This will result in a displacement of the R matrix curves along the energy axis by a constant amount. If the assumption is made that the protons are distributed uniformly throughout a sphere of radius r, then the above displacement,

$$\Delta = 6Ze^2/5r, \tag{2}$$

where Z and $Z+1$ are the numbers of protons in the two mirror nuclei. The radius thus obtained has about the $A^{\frac{1}{3}}$ dependence on mass number, as discussed below. This postulate is therefore a reasonable form in which to express an assumption concerning the equality of n-n and p-p forces, without using any model to discuss wave functions in the interior of the nucleus. (In the case of the shell model this would mean that the shapes of the potentials in the nuclear interior are the same, the potential for the proton being displaced upward by a constant amount with respect to that for the neutron.)

On the basis of the above assumption, a calculation has been carried out to determine to what extent the 750-kev discrepancy between the first excited states of C^{13} and N^{13} can be explained while adhering to the assumption that the excited state radius is equal to the ground state radius. In applying the above mentioned postulate there is some ambiguity as to the exact value which ought to be taken for the radius of the nuclear surface along that channel of the configuration space which is of interest. For a system which, in the dissociated state, consists of two nuclei, of mass numbers A_1 and A_2, it may be most reasonable to take $r=r_0(A_1^{\frac{1}{3}}+A_2^{\frac{1}{3}})$. In the present case, $A_1=12$ and $A_2=1$. However, there may be effects which tend to decrease or increase this value, for example, taking some sort of auxiliary potential in the interior of the nucleus to represent electrostatic repulsion in the case of the proton, and polarization of the C^{13} core, respectively. Moreover, the results obtained here depend rather critically on the value taken for the radius. The calculations were carried out for a very low value, $r=r_0(12)^{\frac{1}{3}}$, and for the higher value $r=r_0[(12)^{\frac{1}{3}}+(1)^{\frac{1}{3}}]$. Here r_0 was taken to be 1.40×10^{-13} cm, which is a rather low value, and also as 1.46×10^{-13} cm in the only important case, to show the critical dependence on the radius. The value $r=r_0(12)^{\frac{1}{3}}$ will turn out to be quite unusable.

The boundary condition postulate predicts a shift in the positions of the energy levels of C^{13} with respect to the corresponding levels of N^{13}, in addition to the ordinary Coulomb energy difference and the neutron-hydrogen mass difference, especially for states near the dissociation energy. It turns out that for the first excited state this shift is in the right direction to explain the experimentally observed results. The ground state, however, shows a shift in the same direction, although a smaller one, thus reducing the energy discrepancy between the first excited states which this consideration is able to explain. This means that the ordinary Coulomb energy difference is smaller than the actual energy difference, the remainder constituting a "boundary condition energy difference" which arises as a result of the Coulomb wave function distortion, as compared with the neutron case, in the external region of configuration space. If the ordinary Coulomb energy difference is still to be given by the old formula, a somewhat larger than the usual value of the nuclear radius must be assumed in the ground state.

II. FORMALISM OF THE R MATRIX FORMALISM

The following derivation employs the results of the article of Wigner and Eisenbud,[4] and that of Feshbach, Peaslee, and Weisskopf.[5] In a system having two channels of disintegration, let φ denote r times the radial part of the wave function. Now in each channel let radial wave functions D and V be defined so that

$$\begin{aligned} &(rD)|_{r=a}=0 \qquad &&(d/dr)(rD)|_{r=a}=(M/\hbar)^{\frac{1}{2}}, \\ &(rV)|_{r=a}=(M/\hbar)^{\frac{1}{2}} \qquad &&(d/dr)(rV)|_{r=a}=0, \end{aligned} \tag{3}$$

where M is the reduced mass for the channel, and a is the nuclear radius. Then, for each channel, equations of the form[6]

$$\varphi_1=(rD)_1+R_{11}(rV)_1+R_{12}(rV)_2 \tag{4a}$$

$$\varphi_2=(rD)_2+R_{21}(rV)_1+R_{22}(rV)_2 \tag{4b}$$

can be used to define an R matrix. It can easily be shown that, like the R matrix of Wigner and Eisenbud, our R matrix also can be written as

$$R=\sum_\lambda(\gamma_\lambda\times\gamma_\lambda)/(E_\lambda-E), \tag{5}$$

where γ_λ, E_λ are independent of energy. One then defines the quantities

$$\begin{aligned} &B=k^{\frac{1}{2}}(F'^2+G'^2)^{\frac{1}{2}}, \qquad &&A=(i)^l k^{-\frac{1}{2}}(G+iF), \\ &\omega=(-i)^l(F'+iG')(F'^2+G'^2)^{-\frac{1}{2}}, \qquad &&C=-GG'-FF', \end{aligned} \tag{6}$$

where the prime means $d/d(kr)$; l is the orbital angular momentum; and F and G represent the regular and irregular confluent hypergeometric functions defined according to the convention of Yost, Wheeler, and Breit.[7] All functions are to be evaluated for the argument equal to ka. Let u and v be incoming and outgoing waves with the asymptotic behavior $s^{-\frac{1}{2}}\exp(\mp ikr)$ at infinity, s being the velocity at infinity. If φ is to represent that function which has an incoming and an outgoing wave in channel 1, but only an outgoing wave in channel 2, then one can write $\varphi=\varphi_1+\mathfrak{C}\varphi_2$, and obtain $\mathfrak{C}$ by equating to zero the coefficient of u_2 on

[4] E. P. Wigner and L. Eisenbud, Phys. Rev. **72**, 29 (1947).
[5] Feshbach, Peaslee, and Weisskopf, Phys. Rev. **71**, 145 (1947).
[6] In Eq. (4a) and below, suitably normalized functions of the angular and of the internal variables have been omitted for the sake of brevity of notation, since no confusion arises. In detail, Eq. (4a) should read

$$\varphi_1=[(rD)_1+R_{11}(rV)_1]\omega_1+[R_{12}(rV)_2]\omega_2,$$

where ω_1 depends on the internal and angular variables of channel 1, and similarly for ω_2.
[7] Yost, Wheeler, and Breit, Phys. Rev. **49** 174 (1936).

the right-hand side of the following equation:

$$\begin{aligned}\varphi=&[(rD)_1+R_{11}(rV)_1+R_{12}(rV)_2]\\&+\mathfrak{C}[(rD)_2+R_{21}(rV)_1+R_{22}(rV)_2]\\=&\tfrac{1}{2}i[A_1(-i)^{l_1}u_1-A_1^*(+i)^{l_1}v_1]\\&+\tfrac{1}{2}R_{11}[B_1\omega_1^*(-i)^{l_1}u_1+B_1\omega_1(+i)^{l_1}v_1]\\&+\tfrac{1}{2}R_{12}[B_2\omega_2^*(-i)^{l_2}u_2+B_2\omega_2(+i)^{l_2}v_2]\\&+\tfrac{1}{2}i\mathfrak{C}[A_2(-i)^{l_2}u_2-A_2^*(+i)^{l_2}v_2]\\&+\tfrac{1}{2}R_{21}\mathfrak{C}[B_1\omega_1^*(-i)^{l_1}u_1+B_1\omega_1(+i)^{l_1}v_1]\\&+\tfrac{1}{2}R_{22}\mathfrak{C}[B_2\omega_2^*(-i)^{l_2}u_2+B_2\omega_2(+i)^{l_2}v_2].\end{aligned}\tag{7}$$

Therefore,

$$\mathfrak{C}=-R_{12}[R_{22}+iA_2(B_2\omega_2^*)^{-1}]^{-1}.\tag{8}$$

In the application to be made here, the second channel will refer to the emission of a photon. Since the γ-ray width will be extremely small compared with the width for channel 1 (elastic proton or neutron scattering), it will be sufficient for the present derivation to treat the photon as if it were described by the Schrödinger equation for zero angular momentum and no Coulomb field. (It will turn out that the exact nature of this assumption will not enter the final result. Only the smallness of the γ-ray width and γ-ray wave number (compared with a nuclear wave number) will be employed.) Hence, $C_2=0$, $A_2A_2^*=k_2^{-1}$, k_2 being the γ-ray wave number. If one next defines φ to be that part of the previously defined φ referring to channel 1 only, and $f(E)=a\varphi^{-1}d\varphi/dr$, then it follows by straightforward calculation that

$$f(E)=a/(R_{11}-R_{12}^2(R_{22}+ik_2^{-1})^{-1}),\tag{9}$$

or, since $k_2^{-1}\gg R_{22}$,

$$f(E)=a(R_{11}+ik_2R_{12}^2)^{-1}.\tag{10}$$

If $f(E)=f_0(E)-ih(E)$, where f and h are real, then

$$f_0(E)=aR_{11}(R_{11}^2+k_2^2R_{12}^4)^{-1}\cong aR_{11}^{-1}\tag{11a}$$

$$h(E)=k_2aR_{12}^2(R_{11}^2+k_2^2R_{12}^4)^{-1}\cong k_2a(R_{12}/R_{11})^2.\tag{11b}$$

The absorption cross section (transition from channel 1 to channel 2) becomes, on noting that $k_2(R_{12}/R_{11})^2\ll k(G^2+F^2)^{-1}$:

$$\sigma_{abs}=\frac{4\pi}{k^2}(2l+1)ka\frac{k_2a(R_{12}/R_{11})^2(G^2+F^2)^{-1}}{[ka(G^2+F^2)^{-1}]^2+[(a/R_{11})-ka(GG'+FF')(G^2+F^2)^{-1}]^2},\tag{12}$$

l being the orbital angular momentum in channel 1. (The confluent hypergeometric functions are, of course, to be evaluated for the argument ka.) For low kinetic energies and high potential barrier (Coulomb and centrifugal), F and F' are negligible compared with G and G', and the expression for $(1/R_{11})_{res}$ becomes the same as the one which would be obtained for resonance if only elastic scattering were considered,

$$(1/R_{11})_{res}=(kG'/G)_{res},\tag{13a}$$

the F and F' having already been neglected. However, the variation of k, G, and G' between E_{res} and $E_{res}+\frac{1}{2}\Gamma$ cannot be neglected[8] in the computation of the variation of R. Hence,

$$\left[\left(\frac{1}{R}-\frac{kG'}{G}\right)^2+\frac{k^2}{G^4}\right]_{E_{res}+\frac{1}{2}\Gamma}=\left(\frac{2k^2}{G^4}\right)_{E_{res}}.$$

TABLE I. R values and calculated energy displacements for first excited states.

	$-R_{res}$	$-R_{res+\frac{1}{2}\Gamma}$	$-R_{Cis}$	Displacement for R linear in E (kev)	Displacement for R^{-1} linear in E (kev)
$l=0$ $r=0.48$	0.55814	0.55338	0.355	750	1160
$l=0$ $r=0.46$	0.53720	0.53417	0.355	1050	1570
$l=0$ $r=0.32$	0.42423	0.42494	0.355	...	...
$l=1$ $r=0.46$	0.32027	0.32178	0.266	...	...
$l=1$ $r=0.32$	0.23446	0.23526	0.224	...	...

$f(E)$ is proportional to the logarithmic derivative of the wave function in channel 1, while the R matrix has elements referring to all channels. Equation (9) shows the relation between them. The absorption cross section, of course, could have been obtained directly from the ratio of the coefficients of v_2 and u_1 in Eq. (7).

From these equations and a knowledge of the location of the maximum and of the width of the absorption resonance, it is possible to determine R_{11} for two values of the energy. The matrix element R_{12} is not necessary for this consideration for the reasons already mentioned above, while R_{22} is even more negligible.

For a bound state, R_{11} is easily determined by using the Schrödinger wave functions, whose asymptotic behavior for large r is similar to $\exp(-\beta r)$. In the neutron case, these functions are of the form $\exp(-\beta r)\cdot P(\beta r)$, where $P(\beta r)$ is a polynomial in $(\beta r)^{-1}$. In the proton case, these functions are the functions $W_{k,m}(z)$ given by Whittaker and Watson,[9] where $z=2\beta r$, $m=l+\frac{1}{2}$, and $k=-ZZ'e^2M/\hbar^2\beta^2$, Ze and $Z'e$ being the charges, M the reduced mass of the system, and $-\hbar^2\beta^2/2M$ its energy.

If a diagonal element of the R matrix given by Eq. (5) is approximated by summing only over those terms for which E_λ is smaller than a given value E_0, the result will be algebraically smaller than the correct value,

[8] The author wishes to thank Mr. R. G. Thomas, whose work parallels the present discussion in some respects, for bringing this essential point to his attention (see Phys. Rev. 80, 136 (1950)).

[9] Whittaker and Watson, *Modern Analysis* (Cambridge University Press, 1927), fourth edition, p. 340.

and will increase less rapidly as a function of E than the correct function as long as E is less than E_0. In particular, in an energy range in which only one E_λ lies below E, a one-level approximation to R with that E_λ gives an increase of R with E slower than the correct one. This turns out to be important in interpreting the results of the calculation given in the next section.

III. RESULTS

Table I lists the values of R_{11} in units of 10^{-12} cm corresponding to the N^{13} nucleus at 2.35 Mev (E_{res}) and at (2.35+0.0175) Mev, which is $E_{res}+\frac{1}{2}\Gamma$, and to the C^{13} nucleus at 3.10 Mev. The cases considered are $l=0$ with $r=0.32$, 0.46, and 0.48×10^{-12} cm, and $l=1$ with $r=0.32$ and 0.46×10^{-12} cm. The cases in $l=1$ and the case $l=0$, $r=0.32\times10^{-12}$ cm must be ruled out, since they make dR_{11}/dE negative. If, for N^{13}, R_{11} were known to be a function of E involving only two parameters, these two could then be determined from the two known points of the curve, for $E=2.35$ Mev and $E=(2.35+0.0175)$ Mev. The energy at which R_{11} for N^{13} attains the value which it actually has for C^{13} at 3.10 Mev is then called the position of the energy level predicted for C^{13}, since this value of R_{11} is the boundary condition which is experimentally known to be required for a level. (R_{11} will henceforth be written as R.)

Table I shows that the calculated correction depends quite sensitively on the value taken for the "radius." Since the 2.35-Mev level of N^{13} is of even parity ($l=0$), while the ground state is generally assumed to have odd parity, the 2.35-Mev level may be assumed to be the lowest level of its kind (even parity, $J=\frac{1}{2}$). Hence, a one-level approximation for the form of the R matrix allows one to obtain an upper bound for the amount by which the C^{13} level is calculated to lie above the N^{13} level. Figure 2 indicates schematically the form of R as a function of energy (dotted curve), its intersection with the full curve indicating the position of (s-proton) resonances for the case of positive energy and of bound states for negative energy (of which there are none in this case). The value of γ^2 calculated from such a one-level formula is about equal to the quantity given by the sum rule over processes,[10,11] $\sum_s \gamma_{\lambda s}^2 \cong 3\hbar^2/2Ma$, where s represents modes of disintegration, whether energetically allowed or not at the energy considered, and λ may be considered to refer to the E_λ most closely connected with this resonance. As a matter of fact, for $r=0.46\times10^{-12}$ cm, γ^2 is 1.13 times $3\hbar^2/2Ma$, while for $r=0.48\times10^{-12}$ cm, it is 0.81 times $3\hbar^2/2Ma$. This means that if the compound nucleus picture is to be used at all, the one-level approximation can hardly be a valid one here. Moreover, the γ^2 obtained[12] from the one-level equation $\Gamma=2k\gamma^2A^{-2}$ (where A^{-2} is the penetrability) does not agree with the above γ^2 but is smaller by a factor of about 4, proving again that a one-level approximation is not valid in this case. The possibility of $l=1$ could have been ruled out previously from the result of the experiment of Hall and Fowler[13] on the radiative capture of protons of energy near 100 kev by C^{12}. Their cross section is larger than the one calculated theoretically from the assumption $l=0$ for the 2.35-Mev level of N^{13} by a factor of less than 2 (not unsatisfactory, because of the approximations in their calculations), but is of much larger order of magnitude than would be calculated from $l=1$. Moreover, the sum rule would be even more seriously infringed by the $l=1$ assumption, in addition, of course, to dR/dE being negative at the 2.35-Mev resonance. The one-level correction indicated in Table I (R^{-1} linear in E) is therefore only to be considered as an upper bound to the correction resulting from the use of the true function of energy $R(E)$. The example R linear in E is given as an illustration.

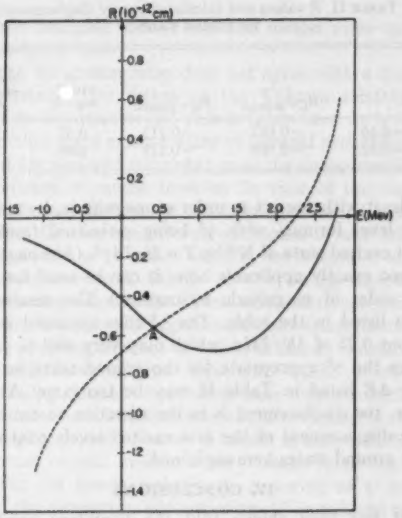

FIG. 2. Schematic graph of R for N^{13} as a function of energy (broken curve). Point A corresponds to the 2.35-Mev level in N^{13}; i.e., to the proton-C^{12} resonance at about 430 kev. If at any energy R has the value given by the solid curve, there is a bound state of N^{13} at that energy if $E<0$ and a virtual state if $E>0$. The whole figure refers to $L=0$, $r=0.48\times10^{-12}$ cm. Both curves are schematic.

One must remember, however, that in order to calculate a displacement which can be compared with the experimentally determined value, it is necessary to make the same boundary condition adjustment for the ground states as was done for the first excited states, since the experimental values are referred to a ground state displacement zero. Table II lists the values of R for the ground states, $l=1$. In this case, since both states involved are bound states, there is no experimentally determined width. The energy displacement implied by the difference in R values can be estimated,

[10] T. Teichmann, Ph.D. Thesis, Princeton University (1949).
[11] E. P. Wigner, Am. J. Phys. 17, 99 (1949).
[12] L. Eisenbud, Ph.D. Thesis, Princeton University (1948).
[13] R. N. Hall and W. A. Fowler, Phys. Rev. 77, 197 (1950).

TABLE II. R values and calculated energy displacements for ground states.

	$R_{C^{13}}$ ground	$R_{N^{13}}$ ground	γ^2 (10^{-13} erg-cm)	ΔE (one-level estimate) (kev)
$r=0.46$	−0.187	−0.212	0.57	195
$r=0.32$	−0.169	−0.178	0.96	155

at least with respect to order of magnitude, by using a one-level formula with γ^2 being estimated from the first excited state of N^{13} by $\Gamma=2k\gamma^2A^{-2}$. (Although this is not exactly applicable here, it can be used for such an order of magnitude estimation.) The results are also listed in the table. The γ^2 thus obtained is still about 0.25 of $3\hbar^2/2Ma$, which may very well be larger than the γ^2 appropriate for the ground state, so that the ΔE listed in Table II may be too large. At any rate, the displacement is in the direction to cut down the displacement of the first excited levels relative to the ground states here explained.

IV. CONCLUSIONS

It has been shown that the boundary condition postulate introduced here predicts a displacement of the first excited levels of C^{13} with respect to N^{13} in the right direction, and of sufficient magnitude to explain the experimentally known displacement. The critical dependence on the nuclear radius rules out any very definite result. It may be, of course, that there exist as yet undiscovered levels in C^{13} and N^{13} which would alter the whole analysis, and that the 3.10-Mev level of C^{13} is not really the one which corresponds to the 2.35-Mev level in N^{13}. Recent experiments on the elastic scattering of protons by C^{12} up to a proton energy of about 4 Mev (with energy resolution of order 1 kev) have failed to reveal additional N^{13} levels in the range in question here.[14]

It is a pleasure to thank Professor Wigner for suggesting this problem, and for continued advice and encouragement. I also wish to thank Professor Sherr for his interesting discussions of the experimental aspects of this problem, and Professor Breit for making available to me his tables of confluent hypergeometric functions.

[14] The author wishes to thank G. Goldhaber and R. Williamson for informing him of their results prior to publication.

PHYSICAL REVIEW VOLUME 81, NUMBER 3 FEBRUARY 1, 1951

Internal Excitation and Apparent Range of Nuclear Forces in Scattering Experiments

G. BREIT AND M. C. YOVITS*
Yale University,† New Haven, Connecticut
(Received October 9, 1950)

The effect of a speculatively considered internal excitation of nucleons on the scattering of elementary particles is examined by means of a schematic model. It is found that the relation between the integral of the square of the wave function describing the normal nucleonic state and the apparent range of force differs from that expected on the ordinary potential energy description. The effect is of the order of eight percent if one assumes the excitation to be 275 mc^2. The direction of the effect is such as to decrease the apparent range as though the meson mass were increased, somewhat as indicated by a comparison of the mass of a pi-meson with experiments on scattering. A possible necessity of corrections for the velocity dependence of nuclear forces which is considered above is briefly discussed in connection with the correlation of data on scattering with that on binding energies.

I. INTRODUCTION

IT has become customary to describe interactions between nuclear particles by means of potential energies. That such a description is of a provisory character has been well realized since the first introduction of exchange forces by Heisenberg[1] and Majorana.[2] These forces can, of course, be introduced by means of certain additive terms in the Hamiltonian without any reference to their origin. Nevertheless, Heisenberg's arguments were partly based on an expected analogy to interactions between atoms which take place in molecules. The same general feature is present in meson theories of nuclear forces.[3] According to these theories the origin of the force is not the interaction between nucleons with each other but a more primary type of process consisting in the production of mesons by nucleons. Only in special cases can the static part of the nuclear potential be split off from the relativistic part by a definite transformation. In the general Møller-Rosenfeld mixture, the potential employed in attempts to explain scattering or binding energies is only a part of a more general interaction which has not been evaluated on

* AEC predoctoral fellow.
† Assisted by the joint program of the ONR and AEC.
[1] W. Heisenberg, Z. Physik **77**, 1 (1932).
[2] E. Majorana, Z. Physik **82**, 137 (1933).
[3] H. Yukawa, Proc. Phys. Math. Soc. Japan **17**, 48 (1935). C. Møller and L. Rosenfeld, Proc. Cop. **17**, No. 8. G. Wentzel, *Einführung in die Quantentheorie der Wellenfelder* (Franz Deuticke, Wien, 1943).

account of internal inconsistencies of meson field theories. On the other hand the usual interpretations by means of potential energies without any other velocity dependence than that implied in the use of exchange forces lead to an apparently simple picture. The hypothesis of charge independence of nuclear forces appears to be verified rather accurately by the more recent experimental[4] and theoretical work[5] provided a long tail[6] is assumed to exist in the nuclear potential, as is expected from the meson theory of nuclear forces. Thus on the one hand one starts out with a field theoretic description of nuclear forces which is mathematically inconsistent and on the other hand success results from an application of partial results of the theory to experimental material in a rather detailed and literal manner. The situation appears to be still more paradoxical if it is remembered that the agreement of the observed mass of the pi-meson with the apparent range of nuclear force as derived from proton-proton scattering is not very good. It may be permissible, therefore, to regard the successes of the empirical approach as being due, at least in part, to an accidental inclusion in present treatments of some essential features of the correct explanation. It appears reasonable to attempt to look into other approaches to the bridging of the gap between the field theoretic formalism and the potentials used for the treatment of experiments on scattering. In view of the possibility of relating information on scattering to that on binding energies of the lighter nuclei it appears especially desirable to consider whether the features of the nuclear interaction determined by scattering are necessarily related to binding energies in the same manner as the potential energy viewpoint appears to indicate. It has been known[7] very early in the development of scattering theory that the rate of change of the phase shift with energy is essentially determined by

$$\int_0^\infty u^2 dr,$$

where u is r times the radial wave function and r is the distance between the particles. This integral determines the rate of change of the logarithmic derivative of the wave function with energy and its value is therefore one of the main data derivable from scattering experiments on the assumption of a potential energy curve explanation. It is clear, on the other hand, that such a relationship cannot hold for general velocity dependent potentials because with such general assumptions one can vary the logarithmic derivative in an arbitrary way and produce arbitrary changes in the phase shift. It appears desirable to look into this matter more quantitatively.

Since the meson mass does not agree with a literal interpretation by means of the Yukawa relation a slight modification of the view is taken here. It is supposed that there exists a state of internal excitation of one of the nucleons somewhat as in the strong coupling formulation of meson theories. In view of the many unsatisfactory features of the existing forms of strong coupling theories the internal excitation is here introduced *ad hoc* so as not to confuse the feature of such an hypothesis with details of the strong coupling theories. It appears to the writers that an internal excitation may have physical significance quite apart from the strong coupling theories and that it merits consideration also from another viewpoint. While there is practically no doubt[8] that mesons have some connection with nucleon-nucleon interactions the evidence for considering the primary process to consist in the production of virtual or real mesons is very weak. Were one to consider the meson emission as occurring at a later stage, the divergence difficulties would be reduced and possibly eliminated. For then an isolated nucleon would not have to be supposed as capable of producing mesons; this property could in fact be assigned to special nucleonic states which arise only as a consequence of nucleon-nucleon interactions. There would then be no mesic self-energy of a nucleon. In order to have such a theory in a satisfactory form, one would have to formulate it relativistically and the presence of nucleons in states of negative energy would offer a possible difficulty. The interactions responsible for the formation of internally activated states would have to be treated in such a way as not to introduce the self-energy difficulty over again through collisions with particles in negative energy states. The fact, however, that the separation of states in accordance with the sign of energy is relativistically invariant makes it possible to postulate that the property of activation is peculiar to collisions between particles having energies with the same sign. It is realized that there would be some difficulty in avoiding a divergence on account of collisions of particles in negative energy states with each other. The reduced probability of these particles occupying the same volume in phase space is of help at this point, however. Also the situation is different from that in the non-activation types of field theories because the meson field is produced only by activated nucleonic states having a smaller density than that of nucleons in normal states. No attempt is being made to develop such a theory in the present paper. That it may be possible to do so has been one of the reasons for carrying through the calculations, however.

[4] E. Melkonian, Phys. Rev. **76**, 1744 (1949). Hughes, Burgy, and Ringo, Phys. Rev. **77**, 291 (1950).

[5] J. Schwinger, Phys. Rev. **78**, 135 (1950).

[6] L. Rosenfeld, at the International Colloquium on Nuclear Physics and Fundamental Particles, Paris, April, 1950. J. M. Blatt and J. D. Jackson, Phys. Rev. **76**, 18 (1949).

[7] Breit, Condon, and Present, Phys. Rev. **50**, 825 (1936). Breit, Thaxton, and Eisenbud, Phys. Rev. **55**, 1018 (1939). G. Breit and W. G. Bouricious, Phys. Rev. **75**, 1029 (1949).

[8] Burfening, Gardner, and Lattes, Phys. Rev. **75**, 382 (1949). W. H. Barkas, Phys. Rev. **75**, 1467 (1949). S. B. Jones and R. S. White, Phys. Rev. **75**, 1468 (1949); **76**, 588 (1949). Kaplon, Peters, and Bradt, Phys. Rev. **76**, 1735 (1949). Smith, Gardner, and Bradner, Phys. Rev. **77**, 562 (1950).

The model used is highly schematic. A state of internal excitation of the composite system consisting of two nucleons is introduced. It is supposed that the chance of formation of such a state exists only when the two particles are sufficiently close to each other. No attempt is made to derive the law which determines the manner with which the transition probability to activated states depends on the internucleonic distance. For purposes of simplicity it is supposed in most of the calculations presented here that the matrix element responsible for the transition is energy independent and in most of the work this value is taken as independent of r for $r<b$ and to have the value 0 for $r>b$. It is found that the integral over the square of the radial function is no longer quite so simply related to the apparent range of force, and that there is an appreciable correction arising from this circumstance. The effect of taking the correction into account is to increase the apparent meson mass by roughly ~ 9 percent if the internal excitation energy is $\sim 275\ mc^2$ where m is the electronic mass and c is the velocity of light. Such a correction cannot be of direct quantitative significance, there being other possible modifications in the theory. For example there might be more than one state of internal excitation, the assumptions concerning the variation of the transition probability with distance may be in error etc. The fact that the meson mass corresponding to observation for proton-proton scattering ($\sim 320\ m$) agrees somewhat better with the corrected rather than the uncorrected apparent range of force has presumably only qualitative significance. The existence of the correction and its approximate magnitude may be, however, more pertinent to the physical situation. The finite extension of the region within which the interaction matrix element has a nonvanishing value is not in itself in contradiction with relativity since it would be possible to assign the law of formation for the activated state arbitrarily in the rest frame and to derive from it the behavior of the system in other frames. It is admittedly objectionable, however, to introduce this law in the arbitrary manner in which this is done below.

The general nature of the range correction considered can be seen from the fact that if the interaction could be treated by second-order perturbation theory, a velocity dependence would be brought in through the variation of the energy differences occurring in the denominators of usual formulas. The estimates of these effects made on p. 1062 of the paper by Breit, Thaxton, and Eisenbud[7] indicate that a progressive increase in depth of roughly 1.6 percent per $2.4\ mc^2$ change in the energy of relative motion is approximately equivalent to a shortening of the range by the factor $(21.6/16)^{\frac{1}{2}} = 1.16$, which corresponds to a 16 percent effect. A nine percent effect on range should correspond, therefore, roughly to a progressive increase in depth of 0.9 percent in $2.4\ mc^2$. An energy difference of $2.4\ mc^2$ is 0.87 percent of the meson mass energy, $275\ mc^2$, in agreement with estimates of velocity dependence effects on range made below. The effect is thus approximately such as though it were caused by variations in the energy denominators. It appeared worth while nevertheless to make somewhat more systematic and independent calculations because the accuracy of the second order perturbation approximation is somewhat uncertain in this case.

II. GENERAL RELATIONS

In order to estimate the possible effect of the internal excitation of nucleons the following schematic treatment will be used. The state of the system will be described by

$$\Psi = \psi_0(\mathbf{r})u_0 + \psi_1(\mathbf{r})u_1 + \cdots, \tag{1}$$

where $u_1, u_2, \cdots$ are functions of internal coordinates while $\mathbf{r}$ is the relative displacement vector of the nucleons. The internal coordinates refer to states of mesons. These will be denoted schematically by x_{In}. The Hamiltonian contains operators acting on the $\mathbf{r}$ and x_{In}. Phenomenologically one is sure that in the part of configuration space corresponding to large distances,

$$r = |\mathbf{r}|,$$

there are well defined functions $u_j(x_{In})$ which represent internal states of excitation of the nucleons and that the corresponding ψ_j are then solutions of the free particle equations for two bodies. In regions of configuration space within which the nucleons interact the functions u_j will be taken to be the same as for the larger r. The Hamiltonian will be supposed to have the form

$$H = -\frac{\hbar^2}{2\mu}\Delta_r + H_{In} + H', \tag{1.1}$$

where μ = reduced mass $= M/2$, M = mass of nucleon, H_{In} = Hamiltonian describing the formation of mesons around individual nucleons, and H' = remainder of the Hamiltonian which is, therefore, responsible for the specific nuclear interaction.

The operator H_{In} is such that

$$H_{In}u_j = E_j u_j, \tag{1.2}$$

where E_j is the internal excitation energy of nucleons when they are well separated. The functions u_j form a complete orthonormal set for the x_{In}. Substitution of Eq. (1.1) into Eq. (1) gives

$$\Sigma_j u_j\left[-\frac{\hbar^2}{2\mu}\Delta_r - E + E_j\right]\psi_j + \Sigma_j H'\psi_j u_j = 0,$$

so that

$$-\frac{\hbar^2}{2\mu}\Delta_r\psi_i + E_i\psi_i + \Sigma_j(u_i, H'\psi_j u_j)_\pi = E\psi_i. \tag{1.3}$$

The scalar products in the last term do not contain the internal coordinates of the meson system and are functions of $\mathbf{r}$ only. The symbol π is used in the subscript because π-mesons are presumably connected or possibly

responsible for the interaction. For a fixed $\mathbf{r}$

$$(u_i(x_{In}), H'(\mathbf{r}, x_{In})\psi_j(\mathbf{r})u_j(x_{In}))_x$$
$$=\psi_j(\mathbf{r})(u_i(x_{In}), H'(\mathbf{r}, x_{In})u_j(x_{In}))_x=H_{ij}'(\mathbf{r})\psi_j(\mathbf{r}).$$

The last scalar product is a function of $\mathbf{r}$ and of i, j only. One has, therefore,

$$-\frac{\hbar^2}{2\mu}\Delta\psi_i+E_i\psi_i+\Sigma_jH_{ij}'(\mathbf{r})\psi_j(\mathbf{r})=E\psi_i, \quad (1.4)$$

a coupled system of equations involving interaction matrix elements H_{ij}' which themselves depend on $\mathbf{r}$ and functions $\psi_j(\mathbf{r})$ which have to be determined by solving Eq. (1.4). The subscript r in Δ will be dropped from now on.

The diagonal elements of $\|H_{ij}'\|$ contribute terms of the potential energy type. If only such terms were present one would have independent solutions for each i. This situation is analogous to the behavior of a diatomic molecule when its motion of vibration is describable by a potential energy curve. The presence of nondiagonal terms produces coupling between states of motion along different potential energy curves.

In order to simplify the treatment only two potential energy curves will be considered. The system is then described by

$$\left[-\frac{\hbar^2}{2\mu}\Delta+H'_{00}(\mathbf{r})\right]\psi_0(\mathbf{r})+H'_{01}(\mathbf{r})\psi_1(\mathbf{r})=E\psi_0(\mathbf{r}),$$
$$\left[-\frac{\hbar^2}{2\mu}\Delta+H'_{11}(\mathbf{r})\right]\psi_1(\mathbf{r})+H'_{10}(\mathbf{r})\psi_0(\mathbf{r})=(E-E_1)\psi_1(\mathbf{r}). \quad (2)$$

The internal energy is here standardized by $E_0=0$.

By employing different assumptions about H_{00}', H_{01}', H_{11}' one can obtain a variety of conditions intermediate between the extreme situation of the strict potential energy curve description and that of the interaction being caused mainly by H_{01}'. The latter condition is farthest from the usual assumptions and will, therefore, be considered first. The notation

$$H_{01}'(\mathbf{r})=H'D(\mathbf{r})$$

will be used. Here H' is a constant which is in general complex while $D(\mathbf{r})$ is a real function. Since ψ_0, ψ_1 must satisfy standard regularity conditions at $r=0$ and $r=\infty$, one may solve the second line of Eq. (2) for ψ_1 by the formula

$$\psi_1(\mathbf{r})=-(MH'^*/4\pi\hbar^2)\int D(\mathbf{r}')|\mathbf{r}-\mathbf{r}'|^{-1}$$
$$\times[\exp(-\kappa|\mathbf{r}-\mathbf{r}'|)]\psi_0(\mathbf{r}')d\mathbf{r}' \quad (2.1)$$

and the problem becomes describable by an integro-differential equation in one variable:

$$-(\hbar^2/M)\Delta\psi_0(\mathbf{r})-D(\mathbf{r})(M|H'|^2/\hbar^2)$$
$$\times\int G(\mathbf{r}, \mathbf{r}')D(\mathbf{r}')\psi_0(\mathbf{r}')d\mathbf{r}'=E\psi_0(\mathbf{r}), \quad (2.2)$$

where the Green's function

$$G(\mathbf{r}, \mathbf{r}')=\{\exp[-\kappa|\mathbf{r}-\mathbf{r}'|]\}/[4\pi|\mathbf{r}-\mathbf{r}'|] \quad (2.3)$$

with

$$\kappa=[M(E_1-E)/\hbar^2]^{\frac{1}{2}} \quad (2.4)$$

is such that

$$[\Delta-\kappa^2+\delta(\mathbf{r}-\mathbf{r}')]G(\mathbf{r}, \mathbf{r}')=0. \quad (2.5)$$

It is assumed here that κ is real which implies that $E<E_1$.

By means of the Fourier representation

$$e^{-\kappa r}/r=(1/2\pi^2)\int[e^{i\mathbf{k}\mathbf{r}}/(\kappa^2+k^2)]d\mathbf{k}$$

and the expansion

$$e^{i\mathbf{k}\mathbf{r}}=\Sigma_Li^L(2L+1)P_L(\mathbf{k}\mathbf{r}/kr)F_L(kr)/(kr),$$

where the P_L are Legendre functions and the F_L are standard expressions in Bessel functions of half-integral order, one obtains

$$G(\mathbf{r}, \mathbf{r}')=(1/2\pi^2)\Sigma_L(-)^L(2L+1)P_L(\mathbf{r}\mathbf{r}'/rr')$$
$$\cdot\int_0^\infty[F_L(kr)F_L(kr')/rr'](k^2+\kappa^2)^{-1}dk \quad (2.6)$$

which gives the expansion of G in terms of Legendre functions of the cosine of the angle between $\mathbf{r}$ and $\mathbf{r}'$. For $L=0$ the sum on the right of Eq. (2.6) contributes the spherically symmetric part

$$\langle G(\mathbf{r}, \mathbf{r}')\rangle=(e^{-\kappa r}/4\pi\kappa rr')\sinh(\kappa r'), \quad (r>r'), \quad (2.7)$$

the latter expression being readily obtainable directly from the definition of G.

Assuming for simplicity that ψ_0 is spherically symmetric and introducing

$$F=r\psi_0$$

one has

$$d^2F/dr^2+k^2F-\int_0^\infty v(r, r')F(r')dr'=0, \quad (3)$$

$$k^2=(M/\hbar^2)E, \quad (3.1)$$

with the convention that F stands for $F(r)$ unless otherwise specified. The quantity v is given by

$$v(r, r')=-A^2D(r)D(r')[\exp(-\kappa|r-r'|)$$
$$-\exp(-\kappa|r+r'|)]/(2\kappa), \quad (3.2)$$

where

$$A^2=(M/\hbar^2)^2|H'|^2. \quad (3.3)$$

For scattering at $E<E_1$ the function F has to be continued from $r=0$ to $r=\infty$. According to Eq. (2.1) the corresponding $\psi_1(\mathbf{r})$ is spherically symmetric and vanishes rapidly at $r=\infty$. With the simplifying assumptions made here the solution of the scattering problem reduces, therefore, to the determination of the logarithmic derivative of F at a value of r, $r=b$ beyond which the last term in Eq. (3) is negligible. One finds

by a repetition of the usual[9] Green's theorem proof type of calculation that

$$[\partial(\partial F/F\partial r)/\partial(k^2)]_{r=b}=-F^{-2}(b)\int_0^b F^2dr$$

$$+F^{-2}(b)\int_0^b\int_0^b F(r)[\partial v(r,r')/\partial(k^2)]F(r')drdr'. \quad (3.4)$$

The presence of the last term is characteristic of the velocity dependence of v which is caused by the dependence of κ on the energy of the system.

In order to apply this result to the scattering of protons by protons it suffices to introduce

$$u=C_0\mathfrak{F}/\sin K_0, \quad u^s=C_{0i}\mathfrak{F}^s/\sin K_0^s,$$

where K_0 is the phase shift and the notation is as in Breit and Hatcher.[10] The function $\mathfrak{F}$ now replaces F of the charge free case while $\mathfrak{F}^s$, K_0^s are the modifications of $\mathfrak{F}$ and K_0 for the standard reference potential which is eventually made to have zero range. In terms of the function

$$f=(C_0^2/\eta)\cot K_0+q_0/\eta-2\ln\eta \quad (4)$$

of Breit, Condon, and Present[7] in the notation of Yost, Wheeler, and Breit[11] a combination of the argument which led to Eq. (3.4) with the steps contained between Breit and Hatcher's Eqs. (2.7), (5) yields

$$[\partial(f-f^s)/\partial(k^2)]_b=(\hbar^2/\mu\epsilon^2)\left\{\int_0^\infty[(u^s)^2-u^2]dr\right.$$

$$\left.+\int_0^\infty\int_0^\infty u(r)[\partial v(r,r')/\partial(k^2)]u(r')drdr'\right\}, \quad (4.1)$$

where the right side is to be evaluated for $E=0$. Since $\partial f^s/\partial(k^2)=0$ the right side of Eq. (4.1) gives the slope of the f curve plotted against E.

III. EFFECT ON APPARENT RANGE

Since $\partial f/\partial(k^2)$ is approximately proportional to the range parameter and since without velocity dependence the first (single) integral alone gives the whole effect the ratio of the double to the single integral in Eq. (4.1) gives an effect characteristic of the velocity dependence. This ratio will now be estimated. To do so the equation determining $F(r)$ which is also satisfied by $u(r)$ will first be changed into a more transparent form. This is accomplished by noting that the second of the two terms in Eq. (3.2) can be obtained from the first by changing the sign of the first term and changing the sign of one of the two quantities r or r'. This suggests extending the problem to negative r and defining

$$D(-r)=D(r), \quad F(-r)=-F(r). \quad (5)$$

[9] G. Breit and E. Wigner, Phys. Rev. **53**, 998 (1938).
[10] G. Breit and R. D. Hatcher, Phys. Rev. **78**, 110 (1950).
[11] Yost, Wheeler, and Breit, Phys. Rev. **49**, 174 (1936).

Instead of Eqs. (3), (3.2) one has then the equivalent

$$d^2F/dr^2+k^2F-\int_{-\infty}^{+\infty}v_1(r,r')F(r')dr'=0, \quad (5.1)$$

$$v_1(r,r')=-A^2D(r)D(r')[\exp(-\kappa|r-r'|)]/(2\kappa). \quad (5.2)$$

The advantage of Eq. (5.1) is that for sufficiently large κ the contributions to the integral are more obviously localized near r. Accordingly the integro-differential equation can be approximated by a differential equation. Expansion of $D(r')F(r')$ in a Taylor series around r and integration term by term give

$$d^2F/dr^2+k^2F+A^2D(r)[1/\kappa^2+d^2/\kappa^4dr^2$$
$$+d^4/\kappa^6dr^4+\cdots]D(r)F(r)=0, \quad (5.3)$$

which may be also written symbolically as

$$d^2F/dr^2+k^2F+(A^2D/\kappa^2)(1-\kappa^{-2}d^2/dr^2)^{-1}DF=0. \quad (5.4)$$

To a first approximation the interaction is such as though the potential energy were

$$-[A^2D^2(r)/\kappa^2](\hbar^2/M). \quad (5.5)$$

The correction term to the equivalent range is obtainable from

$$\int_0^\infty\int_0^\infty u(r)v(r,r';\kappa)u(r')drdr'$$
$$=-(A^2/4\kappa)\int_{-\infty}^{+\infty}\int_{-\infty}^{+\infty}D(r)D(r')$$
$$\times e^{-\kappa|r-r'|}u(r)u(r')drdr' \quad (5.6)$$

so that taking into account the relation $\partial/\partial(k^2)=-\partial/(2\kappa\partial\kappa)$ one has

$$\int_0^\infty\int_0^\infty u(r)[\partial v(r,r';\kappa)/\partial(k^2)]u(r')drdr'$$
$$=(A^2/8\kappa)\int_{-\infty}^{+\infty}\int_{-\infty}^{+\infty}D(r)D(r')$$
$$\times\{\partial[\kappa^{-1}\exp(-\kappa|r-r'|)]/\partial\kappa\}u(r)u(r')drdr'. \quad (5.7)$$

On expanding $D(r')u(r')$ in a Taylor's series and integrating over r' this expression becomes

$$-(A^2/2)\int_{-\infty}^{+\infty}D(r)u(r)[1/\kappa^4+2d^2/\kappa^6dr^2$$
$$+3d^4/\kappa^8dr^4+\cdots]D(r)u(r)dr, \quad (5.8)$$

and hence for large κ

$$\int_0^\infty\int^\infty u(r)[\partial v(r,r';\kappa)/\partial(k^2)]u(r')drdr'$$
$$\cong-(A^2/2\kappa^4)\int_{-\infty}^{+\infty}[D(r)u(r)]^2dr. \quad (5.9)$$

On the other hand, it follows from Eq. (5.3) that

$$(A^2/\kappa^2)[D(r)]^2u(r)\cong -d^2u(r)/dr^2-k^2u(r) \quad (6)$$

and hence, according to Eq. (5.9),

$$\int_0^\infty\int_0^\infty u(r)[\partial v(r,r';\kappa)/\partial(k^2)]u(r')drdr' \cong(1/2\kappa^2)\int_{-\infty}^{+\infty} u[d^2u/dr^2+k^2u]dr. \quad (6.1)$$

The two terms on the right side of Eq. (4.1) can be thus expressed in terms of single integrals involving $u(r)$ and a factor $1/\kappa^2$. Except for this factor, the quantity κ^2 enters implicitly in the present approximation. It will be noted that for $E=0$, the term k^2u on the right side of Eq. (6.1) vanishes.

An approximate evaluation of the two terms can be carried through readily for a square well in the absence of Coulomb interaction *i.e.* for proton-neutron scattering. For zero energy the wavelength inside the well will be denoted by $2\pi/K$, the radius of the well will be referred to by b and the notation $z=Kb$ will be used. For $r>b$ the function $u(r)$ varies linearly with r and can be expressed as

$$u(r)=1+r/a_1, \quad (k=0), \quad (7)$$

since the absolute value of $u(r)$ does not matter in the comparison of the two terms. The homogeneous logarithmic derivative at $r=b$ has the value

$$Y=(rdF/Fdr)_{r=b}=z\cot z \quad (7.1)$$

and one finds that

$$a_1/b=(1-Y)/Y \quad (7.2)$$

and

$$u^{-2}\int_0^b (u^0)^2dr=(a_1/3)[1+b/a_1-(1+b/a_1)^{-2}] =(b/3Y)[1-(1-Y)^3]. \quad (7.3)$$

The other two integrals on the right side of Eq. (4.1) are

$$u^{-2}\int_0^b u^2dr=(z-\sin z\cos z)/(2K\sin^2 z), \quad (7.4)$$

$$u^{-2}\int_0^\infty\int_0^\infty u(r)[\partial v(r,r';\kappa)/\partial(k^2)]u(r')drdr' \cong -K(z-\sin z\cos z)/(2\kappa^2\sin^2 z). \quad (7.5)$$

Substitution of numbers corresponding to a square well depth of the ordinary potential theory $D=11.33$ Mev, an internal excitation $E_1=275\ mc^2$, a square well width $b=e^2/mc^2$ gives $z=1.471$, $Y=0.1472$

$$\int_0^b (u^0)^2dr\Big/\int_0^b u^2dr=1.83$$

and

$$\int_0^\infty\int_0^\infty u(r)[\partial v/\partial(k^2)]u(r')drdr'\Big/\int_0^\infty [(u^0)^2-u^2]dr \cong -0.098$$

and the effect may be expected to vary approximately inversely with the internal excitation energy.

The estimate made above is subject to various objections some of which are concerned with the approximations made in Eq. (6.1). Without further calculation it is especially unsatisfactory not to have available some estimate of the effect of the change in the shape of the function $u(r)$, produced by the coupling of the function without excitation, ψ_0, to that with excitation, ψ_1. The expansion in powers of $1/\kappa^2$ is not a good one for $|b-r|/b\ll 1$ because of the discontinuity in $D(r)$ at $r=b$. For these reasons more accurate calculations have also been made by means of two independent methods.

The first method amounts to an exact solution for the special case of $D(r)$ having the value 0 when $r>b$ and a constant nonvanishing value for $r<b$. The constant value of $AD(r)$ in $0<r<b$ will be referred to as V so that

$$V=AD(r), \quad (r<b). \quad (8)$$

The coupled system of equations already dealt with under Eq. (2) assumes the form

$$\begin{aligned}(d^2/dr^2+k^2)F(r)+VG(r)&=0,\\ VF(r)+(d^2/dr^2-\kappa^2)G(r)&=0,\end{aligned} \quad (8.1)$$

where $F(r)$, $G(r)$ replace ψ_0, ψ_1. The general solution of these equations subject to $F=G=0$ at $r=0$ is

$$\begin{aligned}F&=C_1\sin(\omega_1 r)+C_2\sinh(|\omega_2|r),\\ G&=[C_1(\omega_1^2-k^2)\sin(\omega_1 r) \quad (r<b) \quad (8.2)\\ &\quad +C_2(\omega_2^2-k^2)\sinh(|\omega_2|r)]/V,\end{aligned}$$

where

$$\begin{aligned}\omega_1^2-k^2&=-\kappa_0^2/2+[(\kappa_0^2/2)^2+V^2]^{\frac{1}{2}},\\ \omega_2^2-k^2&=-\kappa_0^2/2-[(\kappa_0^2/2)^2+V^2]^{\frac{1}{2}},\end{aligned} \quad (8.3)$$

and where only the case

$$\omega_2^2<0 \quad (8.4)$$

is being considered. The quantity

$$\kappa_0^2=k^2+\kappa^2=ME_1/\hbar^2 \quad (8.5)$$

is independent of the energy E. For $r>b$ the function G is of the form const $\exp(-\kappa r)$ and the continuity of the logarithmic derivative of G at $r=b$ gives the condition

$$-\kappa=[C_1(\omega_1^2-k^2)\omega_1 c_1+C_2(\omega_2^2-k^2)|\omega_2|ch_2]/[C_1(\omega_1^2-k^2)s_1+C_2(\omega_2^2-k^2)sh_2], \quad (8.6)$$

where

$$\begin{aligned}c_1&=\cos(\omega_1 b), \quad s_1=\sin(\omega_1 b),\\ sh_2&=\sinh(|\omega_2|b), \quad ch_2=\cosh(|\omega_2|b).\end{aligned} \quad (8.7)$$

The condition just mentioned gives the ratio C_1/C_2

and determines the solution within a constant factor. A reasonably lengthy calculation yields

$$\int_0^\infty\int_0^\infty F(r)[\partial v/\partial(k^2)]F(r')drdr'$$
$$=(V^2/4\kappa)\Big\{-\frac{2\kappa C_1^2}{(\kappa^2+\omega_1^2)^2}\Big(b-\frac{\sin(2z_1)}{2\omega_1}\Big)$$
$$-\frac{4\kappa C_1C_2}{\omega_1^2+|\omega_2|^2}\Big[\frac{1}{(\kappa^2+\omega_1^2)^2}+\frac{1}{(\kappa^2+\omega_2^2)^2}\Big]$$
$$\times[|\omega_2|s_1ch_2-\omega_1c_1sh_2]$$
$$-\frac{2\kappa C_2^2}{(\kappa^2+\omega_2^2)^2}\Big(-b+\frac{\sinh(2z_2)}{2|\omega_2|}\Big)+\Xi\Big\}, \quad (8.8)$$

in the notation

$$z_1=\omega_1b, \quad z_2=|\omega_2|b \quad (8.81)$$

and with

$$\Xi=-2\Big[C_1\frac{(\kappa-\omega_1^2\kappa^{-1})s_1+2\omega_1c_1}{(\kappa^2+\omega_1^2)^2}$$
$$+C_2\frac{(\kappa-\omega_2^2\kappa^{-1})sh_2+2|\omega_2|ch_2}{(\kappa^2+\omega_2^2)^2}\Big]$$
$$\times\Big[C_1\frac{\omega_1c_1}{\kappa^2+\omega_1^2}+C_2\frac{|\omega_2|ch_2}{\kappa^2+\omega_2^2}\Big]. \quad (8.82)$$

Similarly

$$\int_0^b F^2dr=\tfrac{1}{2}C_1^2\Big(b-\frac{\sin(2z_1)}{2\omega_1}\Big)$$
$$+2C_1C_2\frac{|\omega_2|s_1ch_2-\omega_1c_1sh_2}{\omega_1^2+|\omega_2|^2}$$
$$+\tfrac{1}{2}C_2^2\Big(-b+\frac{sh(2z_2)}{2|\omega_2|}\Big), \quad (8.9)$$

$$\int_0^b F_s^2dr=(C_1s_1+C_2sh_2)^2[(b^3/3)+a_1b(a_1+b)]/(a_1+b)^2. \quad (8.91)$$

In applying these formulas a simplification results from the fact that z_2 is a number of the order of 5 so that one may set $\tanh z_2=1$. In this approximation it is convenient to introduce the quantity

$$q=(C_2/C_1)\sinh z_2, \quad (9)$$

which has the significance of the ratio of the contribution to the wave function F at $r=b$ arising from the term in $\sinh(|\omega_2|b)$ to the amplitude of the sinusoidal part of F. One has some further simplifications arising in the case $k^2=0$ on account of the relation

$$\omega_2^2+\omega_1^2+\kappa^2=k^2=0 \quad (9.1)$$

which enable a simplification to be made in the form of the denominators in Eqs. (8.8), (8.82). It is thus found for $k^2=0$, in the limit of $\exp(-z_2)\ll 1$ that

$$\int_0^\infty\int_0^\infty F(r)[\partial v/\partial(k^2)]F(r')drdr'$$
$$\cong C_1^2b[(Vb^2)^2/(4\zeta)][-2\zeta z_2^{-4}(1-s_1c_1/z_1)$$
$$-4\zeta q(z_1^{-4}+z_2^{-4})(z_2s_1-z_1c_1)/(z_1^2+z_2^2)$$
$$-2\zeta q^2/(z_1^4z_2)+\Xi/C_1^2b^4], \quad (9.2)$$

where

$$\Xi/(C_1^2b^4)\cong-2\{[(\zeta-z_1^2\zeta^{-1})s_1+2z_1c_1]/z_2^4$$
$$+q(\zeta+z_2)^2/(\zeta z_1^4)\}[z_1c_1/z_2^3-qz_2/z_1^3], \quad (9.3)$$

and

$$\zeta=\kappa b. \quad (9.31)$$

The remaining integrals simplify as follows,

$$[1/(C_1^2b)]\int_0^b F^2dr\cong\tfrac{1}{2}(1-s_1c_1/z_1)$$
$$+2q(z_2s_1-z_1c_1)/(z_1^2+z_2^2)+q^2/(2z_2), \quad (9.4)$$

$$[1/(C_1^2b)]\int_0^b F_s^2dr$$
$$\cong(s_1+q)^2[(b^2/3)+a_1(a_1+b)]/(a_1+b)^2. \quad (9.5)$$

In order to apply these relations for preassigned Y, ζ and z_1, it is necessary to be able to determine z_2 and q from ζ and z_1. This may be done by means of

$$z_2=(z_1^2+\zeta^2)^{\frac{1}{2}}, \quad (10)$$

$$q\cong(z_1^2/z_2^2)(\zeta s_1+z_1c_1)/(\zeta+z_2), \quad (10.1)$$

$$Y\cong(z_1c_1+qz_2)/(s_1+q) \quad (10.2)$$

and

$$(Vb^2)^2=z_1^2z_2^2. \quad (10.3)$$

Equations (10), (10.1) supply all the quantities on the right side of Eq. (10.2) as functions of z_1. The left side of Eq. (10.2) is known from experiment and hence z_1 can be determined by adjusting it so that Eq. (10.2) is satisfied. An alternative procedure is to introduce

$$Y_1=z_1\cot z_1. \quad (10.4)$$

It follows from Eqs. (10), (10.1), (10.2) that

$$Y_1\cong[Y+z_1^2\zeta(Yz_2^{-2}-z_2^{-1})/(\zeta+z_2)]/$$
$$[1+z_1^2(z_2^{-1}-Yz_2^{-2})/(\zeta+z_2)] \quad (10.5)$$

which is suitable for the determination of z_1 by successive approximations. A trial value of z_1 on the right side gives a value of Y_1 which determines an improved z_1 which may again be used on the right side of Eq. (10.4).

Corresponding to $D=11.33$ Mev, $b=e^2/mc^2$, $E_1=275\,mc^2$, $Y=0.1472$, is the value $\zeta=5.17$. Equation (10.5),

for the above values, is satisfied for $s_1=1.62$ and $Y_1=-0.079$. Substitution of these numbers in the above equations gives

$$\int_0^b (u')^2dr \Big/ \int_0^b u^2dr = 1.76,$$

and

$$\int_0^\infty \int_0^\infty u(r)[\partial v/\partial(k^2)]u(r')drdr' \Big/ \int_0^\infty [(u')^2-u^2]dr = -0.088$$

corresponding to an 8.8 percent decrease in $f^{(0)}$ and therefore approximately to the same fractional amount in the value of the range parameter.

In the second of the two methods supplementing Eq. (6.1) the potential is adjusted so as to represent by means of u the wave function for a square well of the ordinary, potential energy curve, theory. The physical model is thus different from that just considered. A comparison of numerical results obtained by the two methods will be seen to show that the value of the correction for energy dependence is relatively insensitive to the details of the model. The representation of the square well wave function is carried out only approximately. At each stage in the process the function u is approximated by a function u_n consisting of a number of straight line segments joining each other continuously at a set of preassigned values r denoted here as r_i, $(i=1, 2, \cdots, n)$. The function u_n is continuous everywhere but the derivative du_n/dr is discontinuous at the points r_i. The possibility of employing straight line segments in the representation of u owes its origin to the fact that it suffices to make the evaluations for $E=0$. The discontinuities in du_n/dr are treated as the limiting forms of conditions approached by functions having very high curvature in the vicinity of the values $r=r_i$. Such a condition can be reproduced by making $D(r)$ have the value zero except in the vicinity of the values $r=r_i$, where $D(r)$ is made to have very large values. The limiting form of $D(r)$ leading to the desired behavior of u_n is

$$D(r)=\Sigma_i a_i\delta(r-r_i), \tag{11}$$

where δ is Dirac's δ function and the a_n are a set of adjustable parameters. In accordance with Eq. (3.2)

$$v(r, r')=-A^2\Sigma_{i,j}a_ia_j\delta(r-r_i)\delta(r'-r_j)U(r, r'), \tag{11.1}$$

where

$$U(r, r')=[\exp(-\kappa|r-r'|)-\exp(-\kappa|r+r'|)]/(2\kappa). \tag{11.2}$$

Equation (3) assumes the form

$$[d^2/dr^2+k^2]u_n(r) + A^2\Sigma_{i,j}a_ia_j\delta(r-r_i)U(r, r_j)u_n(r_j)=0. \tag{11.3}$$

According to this equation u_n is a sine function with wavelength $2\pi/k$ except at the values $r=r_i$, where

$$du_n/dr\Big|_{r_i-0}^{r_i+0} = -A^2a_i\Sigma_j U(r_i, r_j)a_ju_n(r_j). \tag{11.4}$$

For $E=0$ this equation can be used to determine the quantities a_i in such a way as to represent a preassigned set of values of the $u_n(r_i)$. In fact the $u_n(r_i)$ determine the left side of Eq. (11.4) and hence one is dealing with n simultaneous quadratic equations in the n unknowns a_i. Denoting temporarily by Σ the sum occurring in Eq. (11.4), one may regard these equations as n linear equations with Σ entering as a parameter. The solution of these equations gives the a_i as expressions proportional to $1/\Sigma$ and their substitution into the formula giving Σ as a linear expression in the a_i furnishes a value of Σ^2. The a_i are, therefore, determined to within a sign common to all of them. The correction term for velocity dependence which enters Eq. (4.1) is not affected by a change of sign of all of the a_i, however, and is, therefore, uniquely determined by the choice of $u_n(r)$. The value of A is seen to be immaterial in this procedure because the whole matter can be put entirely in terms of the products Aa_i. Explicitly

$$\int_0^\infty \int_0^\infty u(r)[\partial v(r, r'; \kappa)/\partial(k^2)]u(r')drdr' = -A^2\Sigma_{i,j}a_ia_jU(r_i, r_j)u(r_i)u(r_j) \times[1+\kappa r_>-\kappa r_<\coth\kappa r_<]/(2\kappa^3), \tag{11.5}$$

where $r_<$, $r_>$ are respectively the smaller and greater of the pair of values r_i, r_j. For $n=1$ the function u_n is uniquely determined by the value of du/dr for $r>b$ and by the requirement

$$\int_0^\infty (u_n^2-u^2)dr=0.$$

For $n>1$ these requirements alone are not sufficient to determine u_n. However u_n is chosen so as to approximate u as closely as possible for a preassigned n.

For $n=1$ calculation shows a decrease in range of about five percent. For $n=2$ one obtains a decrease in range of between about five percent and seven percent depending on the r_i chosen. These figures are of the same order of magnitude as those obtained above but are smaller.

It may be shown however that this difference is not unexpected. It is seen from Eq. (5.7) that

$$\partial[\exp(-\kappa|r-r'|)/\kappa]/\partial\kappa$$

is the desired quantity. Differentiation yields

$$-(1+\kappa[r-r'|)\exp(-\kappa|r-r'|)/\kappa^2.$$

In the applications of the method just presented, which have been carried out, the term $\kappa|r-r'|$ is not given

a full chance to appear because for the relatively small number of segments chosen the importance of contributions due to $r=r'$ is exaggerated as a consequence of the rapid decay of the exponential function containing κ. In fact for $n=1$ the term is totally lacking. Since

$$\int_0^\infty [\exp(-\kappa|r-r'|)]d|r-r'| = \int_0^\infty (\kappa|r-r'|)\exp(-\kappa|r-r'|)d|r-r'| = \kappa^{-1},$$

one would expect this term to give an effect of close to a factor of 2. The fact that the limits go from 0 only to b modifies this figure somewhat.

A rough evaluation of this effect for $n=1$ can be made making use of the fact that if the term in $\kappa|r-r'|$ were neglected the contributions to the integral representing the correction for range would have relative weights $\sin^2 z dr$ where z is the phase of the internal function. A numerical estimate shows that about half of $\int_0^b \sin^2 z dr$ is caused by contributions arising in $0<r<3b/4$. Through most of this range of values of r the value of $\exp\{-\kappa|\pm b-r|\}$ is small compared to unity and the inclusion of $\kappa|r-r'|$ in addition to 1 in the factor multiplying the exponential may be expected practically to double this contribution, since the limits of integration for r' may be replaced by $\pm\infty$. In the range $3b/4<r<b$ the contributions arising from $-b<r'<r$ may again be treated approximately as though the lower limit of integration were $-\infty$ giving rise to a doubling of a quarter of the whole effect. Contributions from $r<r'<b$ are harder to refine by this consideration and will be left out of account. The expected correction factor is thus $2(1/2)+2(1/4)=1.5$ which would lead to an effect on $f^{(1)}$ and approximately on the range parameter of $5(1.5)=7.5$ percent in reasonably good agreement with other estimates. These considerations indicate that the effect is relatively insensitive to the choice of $D(r)$, this choice having been made in one of the calculations so as to have $D(r)$ constant in $0<r<b$ and in another so as to reproduce the square well wave function.

IV. DISCUSSION

The general viewpoint of the present paper could perhaps be objected to on the grounds that in some forms of meson theories it is possible to eliminate a set of variables by a contact transformation and that the static interaction occurs then in the equations without velocity dependence. To take into account the energy of meson formation would appear to be superfluous, therefore. The method of removing field variables is not capable of dealing with the whole interaction, however, and is applicable only in special cases. This objection to the consideration of velocity dependence would appear to be especially inapplicable if the formation of mesons involves the excitation of a nucleon as a preliminary step.

It appears to be very desirable to emphasize that the calculations made in the present paper cannot be interpreted as indicating in a definite way an improved agreement between the range of nuclear force derived from proton-proton scattering and the mass of the pi-meson through the Yukawa formula. In the tentative form of theory attempted above the connection of the meson field with the shape of the nuclear potential is replaced by the introduction of the function $D(r)$ which might itself be explained perhaps as in the strong coupling forms of meson theory. Without a more complete view regarding the origin of $D(r)$ a quantitative comparison is not meaningful. It appears reasonable to claim on the other hand that if one adjusts $D(r)$ so as to reproduce the Fermi intercept expected for the Yukawa potential by means of the function called F in the present paper then the velocity dependence of the force gives rise to an apparent shortening of the range of force when the latter is inferred from scattering experiments.

The equations considered above are not equivalent to the ordinary way of describing nucleons. There is present an additional component of the wave functions for each spin direction and in terms of the component describing relative motion in the unactivated state the differential equation is not an ordinary differential equation of the second order as is clear from Eqs. (5.3), (5.4). Scattering experiments and observations on binding energies will be connected, therefore, in a somewhat different way from that expected for standard types of forces. Exact adjustments of potential well parameters to fit both sets of phenomena would not be adequate for obtaining a true picture and such phenomenologic parameters would not even be expected to be obtainable quite consistently from different data.

In view of the qualitative rather than quantitative interest of the present problem the values of the parameters employed for the nuclear potential well were only approximate and the effects for proton-proton scattering were inferred from the somewhat similar situation for the proton-neutron case.

Scattering and Absorption of Scalar and Pseudoscalar Mesons by Nucleons

MURRAY PESHKIN*
Cornell University, Ithaca, New York
(Received September 11, 1950)

Cross sections have been calculated for scattering of pi-mesons by nucleons and for absorption of the charge of the meson in the scattering process. Computations are carried out to second order in g^2, using scalar and pseudoscalar fields with scalar and pseudoscalar coupling, respectively. It is found that there are strong qualitative differences in the cross sections depending upon field type and upon the type of mixture where neutral mesons are concerned.

I. INTRODUCTION

THE present status of the weak-coupling meson theories of nuclear forces is far from satisfactory. Many theories agree qualitatively with the experimental information, but no theory has yet been devised which presents a consistent quantitative interpretation of all the well established observations. It is most reasonable to attribute the failures of the theories to large coupling constants. However, it has not yet been possible to formulate a strong coupling theory in a relativistic manner, and in the absence of any other model of action-at-a-distance forces, it seems useful to investigate further the consequences of the weak-coupling theories in the hopes of finding some clearcut agreement or disagreement.

It is entirely possible that the difficulties encountered in the past are a result of considering the relatively complicated problem of forces between nucleons and then deducing the properties of the mesons in an indirect way. This hypothesis could be tested by performing experiments dealing directly with mesons. Such experiments, while characteristically more difficult to carry out in the laboratory, show at least some prospect of unambiguous theoretical interpretation. The purpose of this paper is to study the theoretically simplest problem of the latter kind; the second order scattering of mesons by nucleons.

We shall assume that pi-mesons of mass $276m_e$ are the only field particles interacting with nucleons, regarded as Dirac particles of mass $1836m_e$. We shall be concerned primarily with charged mesons, and shall assume that neutral mesons differ from them only in their lack of charge. Finally, we shall deal with spinless mesons (i.e., scalar and pseudoscalar fields) whose coupling constant will be assumed to be small in spite of the indirect experimental evidence to the contrary.

II. THE MATRIX ELEMENTS

We shall use the following notation. Three-vectors are represented in ordinary boldface, 4-vectors in italics. The time component is real, and we use the convention $a\cdot b=a_4b_4-\mathbf{a}\cdot\mathbf{b}\cdot a$ is the length of the three-vector $\mathbf{a}$. We treat the matrices $\gamma_\mu=\beta\alpha_\mu$ ($\mu=1, 2, 3, 4$) as a four-vector. $\gamma_\mu\gamma_\nu+\gamma_\nu\gamma_\mu=2g_{\mu\nu}$ where $g_{44}=1$, $g_{11}=g_{22}=g_{33}=-1$, and all other $g_{\mu\nu}=0$. Thus by our convention $\gamma_\mu\gamma_\mu=+4$. $\gamma_5=\gamma_1\gamma_2\gamma_3\gamma_4$ and its adjoint $\bar{\gamma}_5=\gamma_4\gamma_3\gamma_2\gamma_1=+\gamma_5$. If a is an ordinary four-vector, $\mathfrak{a}=a_\mu\gamma_\mu=a_4\gamma_4-a_1\gamma_1-a_2\gamma_2-a_3\gamma_3$. Boldface capitals like $\mathbf{M}$ will denote transition matrix elements. In the scattering problem, $k=(\mathbf{k}, \omega)$ is the momentum-energy vector of the incident meson, $k'=(\mathbf{k}', \omega')$ that of the scattered meson, and similarly $p=(\mathbf{p}, E)$ and $p'=(\mathbf{p}', E')$ for the nucleon. We use natural units throughout, i.e. $\hbar=c=1$, g in esu.

The Feynman diagrams for the scattering process are shown in Fig. 1. Picture 1 refers to the scattering of a positive meson by a neutron or of a negative meson by a proton. Picture 2 is for scattering of a negative meson by a neutron or a positive meson by a proton. For scattering of a neutral meson or for conversion of a charged to a neutral meson in the scattering process, the amplitudes for the two diagrams must be added with the appropriate relative phase.

The matrix elements for these diagrams are given by Feynman[1] for pseudoscalar and scalar mesons respectively as[2]

$$\mathbf{M}_1{}^P=\bar{u}'\bar{\gamma}_5\frac{1}{\mathfrak{p}+\mathfrak{k}-M}\gamma_5 u, \tag{1}$$

$$\mathbf{M}_2{}^P=\bar{u}'\bar{\gamma}_5\frac{1}{\mathfrak{p}-\mathfrak{k}'-M}\gamma_5 u, \tag{2}$$

$$\mathbf{M}_1{}^S=\bar{u}'\frac{1}{\mathfrak{p}+\mathfrak{k}-M}u, \tag{3}$$

$$\mathbf{M}_2{}^S=\bar{u}'\frac{1}{\mathfrak{p}-\mathfrak{k}'-M}u, \tag{4}$$

where M is the nucleon mass, u, u' the Dirac spinors (normalized so $\bar{u}u=1$) of the initial and final state and $\bar{u}$, $\bar{u}'$ their adjoints ($\bar{u}=u^*\beta$). μ is used for the pi-meson mass.

* AEC Predoctoral Fellow. Now at Northwestern University, Evanston, Illinois. This research was supported by the AEC predoctoral Fellowship Program.

[1] R. P. Feynman, Phys. Rev. 76, 769 (1949).

[2] The absolute sign of the matrix element does not enter the problem to second order, and will not be elaborated upon here. Actually, if the expansion coefficient $-ig^2$ is used, following the formalism of quantum electrodynamics, it becomes necessary to use γ_5 for emission and $\bar{\gamma}_5$ for absorption in the pseudoscalar theory, and 1 and -1 in the scalar theory.

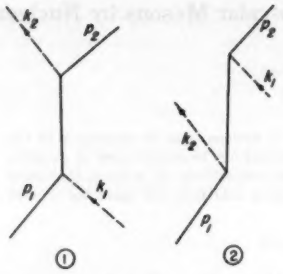

FIG. 1. The Feynman diagrams for second-order scattering. Picture 1 refers to scattering of π^+ by N or π^- by P, while Picture 2 refers to scattering of π^+ by P or π^- by N. For any process involving neutral mesons, the amplitudes for the two processes must be added.

By using the momentum conditions ($p^2=p'^2=M^2$, $k^2=k'^2=\mu^2$, $p+k=p'+k'$) and the Dirac equation ($(\not{p}-M)u=(\not{p}'-M)u'=0$), the matrix elements can be simplified to read

$$\mathbf{M}_1^P=+(\bar{u}'\not{k}u)(\mu^2+2k\cdot p)^{-1} \tag{5}$$

$$\mathbf{M}_2^P=-(\bar{u}'\not{k}u)(\mu^2-2k'\cdot p)^{-1} \tag{6}$$

$$\mathbf{M}_1^S=(\bar{u}[2M+\not{k}]u)(\mu^2+2k\cdot p)^{-1} \tag{7}$$

$$\mathbf{M}_2^S=(\bar{u}[2M-\not{k}]u)(\mu^2-2k'\cdot p)^{-1}. \tag{8}$$

The cross sections are proportional to $|\mathbf{M}|^2$, and since we are not interested in the spin states of the nucleons (which can never be turned over by a spinless meson), it will be most convenient to calculate one-half the trace of the operator $\bar{\mathbf{M}}\Lambda'\mathbf{M}\Lambda$, where the projection operator $\Lambda=(\not{p}+M)/2M$ and $\Lambda'=(\not{p}'+M)/2M$.

The traces are readily evaluated to give the invariant forms

$$T_1^P=\frac{\mu^2(\mu^2-k\cdot k')+2(p\cdot k)(p\cdot k')}{2M^2(\mu^2+2p\cdot k)^2}, \tag{9}$$

$$T_2^P=\frac{\mu^2(\mu^2-k\cdot k')+2(p\cdot k)(p\cdot k')}{2M^2(\mu^2-2p\cdot k')^2}, \tag{10}$$

$$T_1^S=\frac{2(2M^2+p\cdot k)(2M^2+p\cdot k')-(4M^2-\mu^2)(\mu^2-k\cdot k')}{2M^2(\mu^2+2p\cdot k)^2}, \tag{11}$$

$$T_2^S=\frac{2(2M^2-p\cdot k)(2M^2-p\cdot k')-(4M^2-\mu^2)(\mu^2-k\cdot k')}{2M^2(\mu^2-2p\cdot k')^2}, \tag{12}$$

where

$$T=\tfrac{1}{2}\,\mathrm{Trace}\{\bar{\mathbf{M}}\Lambda'\mathbf{M}\Lambda\}.$$

III. THE DIFFERENTIAL CROSS SECTIONS

The relation between differential cross sections and the matrix elements in the Feynman notation is most usefully written in the covariant form

$$\frac{d\sigma}{d\Omega}=\frac{1}{v}\cdot\frac{g^4}{\omega\omega'}\cdot\frac{M}{E}\cdot\frac{M}{E'}k'^2\left[\frac{k'}{\omega'}-\frac{\mathbf{p}'\cdot\mathbf{k}'}{E'k'}\right]^{-1}T. \tag{13}$$

v is the velocity difference and $d\Omega$ is the element of solid angle corresponding to the scattering angle θ.

Relation (13) can be derived from the Lagrangian method[3] or from the relation to the S-matrix.[4] It is easily understood in terms of the ordinary perturbation theory, since T is proportional to the usual $|H|^2$. The factors ω^{-1} and M/E arise from normalization of the initial state, and all the rest, except $1/v$ for the initial state, is proportional to the density of normalized final states per energy interval. The numerical coefficient can be obtained by requiring conservation of probability.

[3] R. P. Feynman, Phys. Rev. **80**, 440 (1950).
[4] F. J. Dyson, Phys. Rev. **75**, 1736 (1949).

In the laboratory system, Eq. (13) reads

$$\frac{d\sigma}{d\Omega}=g^4\frac{k'}{k}\frac{M}{\omega'}T\left[\frac{M}{\omega'}+\frac{\omega}{\omega'}-\frac{k}{k'}\cos\theta\right]^{-1}, \tag{14}$$

and

$$kk'\cos\theta=\omega\omega'-M(\omega-\omega')-\mu^2.$$

Equations (9) through (12) can be put into (14) to give the differential cross sections in the laboratory system.

$$\frac{d\sigma_1^P}{d\Omega}=\frac{g_P^4}{2}\frac{k'^2}{k}\times\frac{2M\omega\omega'-\mu^2(\omega-\omega')}{(\mu^2+2M\omega)^2[M\omega\omega'-\mu^2(M+\omega-\omega')]}, \tag{15}$$

$$\frac{d\sigma_2^P}{d\Omega}=\left(\frac{2M\omega+\mu^2}{2M\omega'-\mu^2}\right)^2\frac{d\sigma_1^P}{d\Omega}, \tag{16}$$

$$\frac{d\sigma_1^S}{d\Omega}=\left(\frac{g_S}{g_P}\right)^4\left(1+\frac{8M^2(M+\omega)}{2M\omega\omega'-\mu^2(\omega-\omega')}\right)\frac{d\sigma_1^P}{d\Omega}, \tag{17}$$

$$\frac{d\sigma_2^S}{d\Omega}=\left(\frac{g_S}{g_P}\right)^4\left(1+\frac{8M^2(M-\omega')}{2M\omega\omega'-\mu^2(\omega-\omega')}\right)\frac{d\sigma_2^P}{d\Omega}. \quad (18)$$

It is instructive to examine the limiting forms of the differential cross sections for very high and very low energies. In the nonrelativistic limit, the cross sections are most conveniently written in terms of the fractional momentum transfer $\mathbf{q}=(\mathbf{k}-\mathbf{k}')/k$, which is related to the scattering angle by

$$\cos\theta=[1-\tfrac{1}{2}(1+\mu/M)q^2][1-(\mu/M)q^2]^{-\frac{1}{2}}.$$

Then Eq. (14) takes the form

$$d\sigma/d\Omega=L(q)T, \quad (19)\text{N.R.}$$

where

$$L(q)=g^4(1-0.150q^2)^{\frac{1}{2}}(1-0.0862q^2)^{-1} \quad (20)\text{N.R.}$$

and

$$T_1^P=0.216M^{-2}[1+0.070(k/\mu)^2-0.081(k/\mu)^2q^2] \quad (21)\text{N.R.}$$

$$T_2^P=0.292M^{-2}[1-0.081(k/\mu)^2+0.0815(k/\mu)^2q^2] \quad (22)\text{N.R.}$$

$$T_1^S=\mu^{-2}[1-0.860(k/\mu)^2-0.0004(k/\mu)^2q^2] \quad (23)\text{N.R.}$$

$$T_2^S=\mu^{-2}[1-1.16(k/\mu)^2+0.18(k/\mu)^2q^2]. \quad (24)\text{N.R.}$$

In the extreme relativistic limit, virtually all the mesons come out in the forward direction because of the motion of the center of gravity. In this case it is more useful to look at the energy distribution of the scattered meson, which can be obtained from Eq. (14) and reads

$$\frac{d\sigma}{d\omega'}=2\pi\frac{d\cos\theta}{d\omega'}\frac{d\sigma}{d\Omega}=2\pi r_0^2\left(\frac{M}{\omega}\right)^2T, \quad (25)\text{E.R.}$$

where $r_0=g^2/M$, the effective nucleon radius for mesons. Then

$$d\sigma_1^P=d\sigma_1^S=\tfrac{1}{2}\pi r_0^2\omega^{-3}\omega' d\omega' \quad (26)\text{E.R.}$$

$$d\sigma_2^P=d\sigma_2^S=\tfrac{1}{2}\pi r_0^2\omega^{-1}\omega'^{-1}d\omega'. \quad (27)\text{E.R.}$$

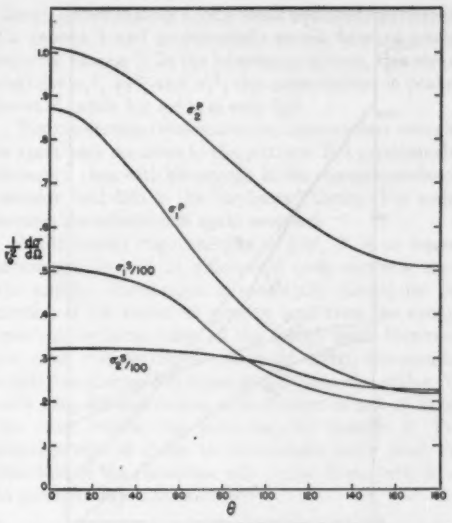

FIG. 2. Angular distributions in the laboratory system for $\omega=2\mu$.

It should be noted that r_0 depends upon g and will be different for the scalar and pseudoscalar cases, and that these equations are valid only for $\omega'\gg M$, so that (27) must not be integrated down to low energies.

The angular distributions for $\omega=2\mu$ are displayed in Fig. 2.

IV. THE TOTAL CROSS SECTIONS

The total cross sections are obtained most easily by carrying out the integration in the center-of-mass system, where Eq. (13) reads

$$d\sigma_c/d\Omega_c=g^4M^2(\omega_c+E_c)^{-2}T.$$

The subscript, c, refers to the center-of-mass system. T, and the total cross section, σ, are invariants. We have then the following relations.

$$\sigma_1^P=\frac{2\pi g_P^4}{(\omega_c+E_c)^2}\cdot\frac{2\omega_c^2E_c^2+(2\omega_cE_c-\mu^2)(\omega_c^2-\mu^2)}{[(\omega_c+E_c)^2-M^2]^2}, \quad (28)$$

$$\sigma_2^P=\frac{\pi g_P^4}{(\omega_c+E_c)^2}\cdot\left[\frac{\mu^4}{(2\omega_cE_c-\mu^2)^2-4(\omega_c^2-\mu^2)^2}+\frac{2\omega_cE_c+2\omega_c^2-\mu^2}{4(\omega_c^2-\mu^2)}\ln\frac{2\omega_cE_c+2\omega_c^2-3\mu^2}{2\omega_cE_c-2\omega_c^2+\mu^2}\right], \quad (29)$$

$$\sigma_1^S=\frac{2\pi g_S^4}{(\omega_c+E_c)^2}\cdot\frac{2\omega_c^2E_c^2+(2\omega_cE_c-\mu^2)(\omega_c^2-\mu^2)+8M^2E_c(\omega_c+E_c)}{[(\omega_c+E_c)^2-M^2]^2}, \quad (30)$$

$$\sigma_2^S=\frac{\pi g_S^4}{(\omega_c+E_c)^2}\cdot\left[\frac{(4M^2-\mu^2)^2}{(2\omega_cE_c-\mu^2)^2-4(\omega_c^2-\mu^2)^2}+\frac{(\omega_c+E_c)^2-9M^2}{4(\omega_c^2-\mu^2)}\ln\frac{2\omega_cE_c+2\omega_c^2-3\mu^2}{2\omega_cE_c-2\omega_c^2+\mu^2}\right]. \quad (31)$$

These results can be taken over into the laboratory system, making use of the following formulas

$$\omega_c+E_c=(M^2+\mu^2+2M\omega)^{\frac{1}{2}},$$
$$\omega_c=(\mu^2+M\omega)/(\omega_c+E_c).$$

In the extreme cases they become, for $\omega\gg M$,

$$\sigma_1^P=\sigma_1^S=\tfrac{1}{4}\pi r_0^2\omega^{-1}, \quad (32)\text{E.R.}$$

$$\sigma_2^P=\sigma_2^S=\tfrac{1}{4}\pi r_0^2\omega^{-1}\ln[2M\omega/(M^2-\mu^2)], \quad (33)\text{E.R.}$$

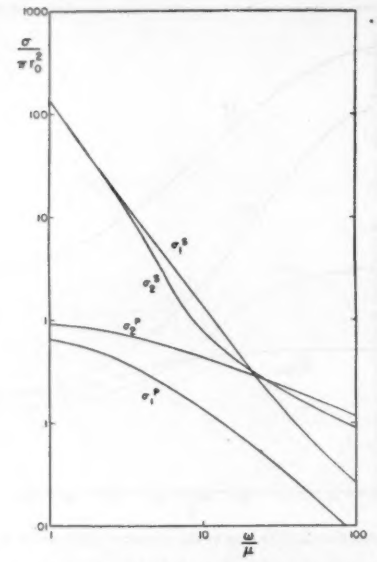

FIG. 3. Total cross section (in units of the nucleon "area") for nuclear scattering *vs.* energy of the incident meson (in units of its mass) for processes 1 and 2, using scalar and pseudoscalar theories. The effect of Coulomb forces has been neglected.

and for $\omega-\mu\ll\mu$,

$$\sigma_1^P=\pi r_0^2[0.654-0.216(\omega-\mu)/\mu], \quad (34)\text{N.R.}$$

$$\sigma_2^P=\pi r_0^2[0.889-0.127(\omega-\mu)/\mu], \quad (35)\text{N.R.}$$

$$\sigma_1^S=\pi r_0^2[136-265(\omega-\mu)/\mu], \quad (36)\text{N.R.}$$

$$\sigma_2^S=\pi r_0^2[136-272(\omega-\mu)/\mu]. \quad (37)\text{N.R.}$$

The behavior of the total cross sections as functions of ω are shown in Fig. 3.

V. CONVERSION PROCESSES

There is also the possibility that a charged meson will lose its charge to the nucleon in the scattering process and be re-emitted as a neutral meson. To calculate the cross section for this conversion it is necessary to include both Feynman diagrams of Fig. 1. The matrix element will then be $M_a=M_1+aM_2$, where a depends on the coupling assumed between mesons and nucleons of the two kinds. In Kemmer's charge-symmetric theory, where the coupling constant of the neutron is equal and opposite to that of the proton, $a=-1$. On the other hand, if we assume "ordinary" neutral mesons (i.e., nucleons having the same coupling constants for neutral and for charged mesons), then $a=+1$. Values other than ±1 are very unlikely, since they would make the neutron-neutron force different from the proton-proton force, contrary to the experience with mirror nuclei.

The differential cross section for the mixed field is given by $\sigma_a=[\sigma_1^{\frac{1}{2}}\pm a\sigma_2^{\frac{1}{2}}]^2$. The relative sign follows from Eqs. (5) through (8), and is negative in the scalar but positive in the pseudoscalar theory. The cross term is integrated in the manner discussed in Sec. IV to yield the result

$$\sigma_a^P=\sigma_1^P+a^2\sigma_2^P+a\frac{2\pi g_P^4}{(\omega_c+E_c)^2}\times\left[1+\frac{\mu^4}{4[(\omega_c+E_c)^2-M^2](\omega_c^2-\mu^2)}\times\ln\frac{2\omega_cE_c+2\omega_c^2-3\mu^2}{2\omega_cE_c-2\omega_c^2+\mu^2}\right], \quad (38)$$

$$\sigma_a^S=\sigma_1^S+a^2\sigma_2^S-a\frac{2\pi g_S^4}{(\omega_c+E_c)^2[(\omega_c+E_c)^2-\mu^2]}\times\left[(\omega_c+E_c)^2-9M^2+\frac{(4M^2-\mu^2)^2}{4(\omega_c^2-\mu^2)}\times\ln\frac{2\omega_cE_c+2\omega_c^2-3\mu^2}{2\omega_cE_c-2\omega_c^2+\mu^2}\right]. \quad (39)$$

These results are plotted as functions of ω in Fig. 4. In every case $\sigma_a=a^2\sigma_2$ in the limit of very high energies, but at low energies there are great differences.

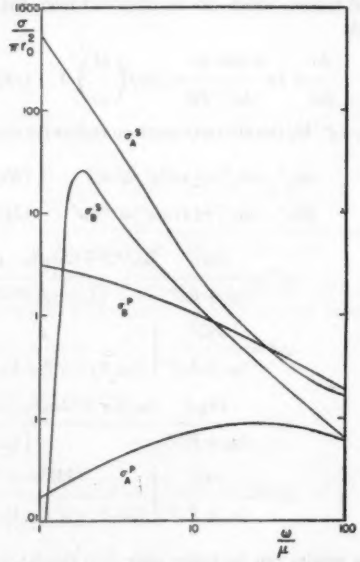

FIG. 4. Total cross section (in units of the nucleon "area") for charge absorption in the scattering process *vs.* energy of the incident meson (in units of its mass), using scalar and pseudoscalar theories. Subscript A refers to the charge-symmetric mixture, B to the "ordinary" mixture.

The "ordinary" mixture leads to cross sections given by the formulas

$$\sigma^P = \pi r_0^2[3.06 - 0.76(\omega-\mu)/\mu], \quad (40)\text{N.R.}$$

$$\sigma^S = \pi r_0^2[1.4(\omega-\mu)^2/\mu^2], \quad (41)\text{N.R.}$$

while the charge-symmetric theory gives

$$\sigma^P = \pi r_0^2[0.0174 + 0.0176(\omega-\mu)/\mu], \quad (42)\text{N.R.}$$

$$\sigma^S = \pi r_0^2[544 - 1077(\omega-\mu)/\mu]. \quad (43)\text{N.R.}$$

VI. RESULTS

There are certain strong qualitative differences among the cases calculated. By comparison of these results with scattering and conversion data, it should be possible to determine whether charged mesons are scalar or pseudoscalar and to find how the neutral mesons are coupled to nucleons of both kinds, provided that neutral and charged mesons are of the same type.

The difference between scalar and pseudoscalar mesons are most striking at low energies. The absolute cross sections will be nearly the same in the two theories despite the apparent disparity because the coupling constants must be adjusted to fit the binding energy of the deuteron. However, it will be about proportional to ω^{-2} for scalar mesons and to $\omega^{-0.2}$ for pseudoscalar. An additional possible distinction is that the total scattering cross sections for scattering of positive and negative mesons by the same type of nucleon are equal for scalar, but differ by about 14 percent for pseudoscalar mesons.

The influence of the mixture on the conversion cross sections is very great at very low energies. The most important feature is that for pseudoscalar theory, the "ordinary" mixture leads to a conversion cross section of four times the scattering cross section, while the charge-symmetric mixture predicts virtually no production of neutral mesons. In the scalar theory, the situation is reversed. This is a particularly useful result since it provides a sensitive measurement of a in case the mixture is of neither of these limiting types.

At intermediate energies, like $\omega = 2\mu$, it becomes possible to get information from the angular distribution as well as the total cross section. Then the total cross section for scattering is still an appreciable fraction of the zero-energy cross section for pseudoscalar, but is very much smaller for scalar mesons. While the differential cross section at zero energy is in every case isotropic in the center of gravity system, at somewhat higher energies the pseudoscalar theory gives a stronger backward cross section for process 1 and an equally stronger forward cross section for process 2. The scalar theory shows instead a very weak backward preference for process 1 and an extremely strong forward preference for process 2. In the laboratory system, this means that for σ_1^P, σ_2^P, and σ_1^S, the cross section is peaked forward, while for σ_2^S it is very flat.

The conversion cross section at intermediate energies is again very sensitive to the mixture. For pseudoscalar mesons it rises with the energy in the charge-symmetric mixture, and falls in the "ordinary" theory. For scalar mesons the situation is again reversed.

At extremely high energies, $\omega \gg M$, it is no longer interesting to look at differential cross sections, since the angular distribution is essentially caused by the motion of the center of gravity, and even the energy spectrum is independent of the theory used. However, the total cross section is now most useful, the pseudoscalar being over 100 times larger than the scalar. In each case the conversion cross section is just a^2 times the cross section for scattering by process 2. The absolute sign of a can be determined easily from the direction of the correction due to the linear term in a, as given by Eqs. (38) and (39).

VII. LIMITATIONS

The two principal modifications of these results will arise from radiative corrections and Coulomb effects, the former being both more important and much more difficult to obtain than the latter.

The scattering of charged mesons by protons must, of course, be modified by the Coulomb scattering. Except for very low energies, this will only add some forward scattering. The sign of the interference term between Coulomb and nuclear scattering, if observable, might be of interest because the nuclear scattering of negative mesons by protons (process 1) has the opposite sign for scalar and pseudoscalar theories.

The main limitation of our theory is the neglect of radiative corrections. Some fourth-order corrections have been calculated in the nonrelativistic limit.[5] These indicate that the corrections will be considerable at low energies if g^2 is of the order of unity. Unfortunately there is not at present any estimate of what influence the fourth order has at intermediate or high energies. Higher orders than the fourth, even in the Thomson limit, would be extremely difficult to obtain.

The author wishes to thank Professor Hans A. Bethe of Cornell University, who suggested the problem, for his continued assistance and encouragement.

[5] Ashkin, Simon, and Marshak, Prog. Theo. Phys. (to be published). The author is indebted to them for a comparison of some results.

Transmission of Gamma-Rays through Large Thicknesses of Heavy Materials

GLENN H. PEEBLES,
RAND Corporation, Santa Monica, California

AND

MILTON S. PLESSET*
California Institute of Technology, Pasadena, California

(Received July 24, 1950)

A study has been made of the feasibility of accurate numerical determinations of the transmission of gamma-rays through large thicknesses of materials. The first procedure investigated consists in regarding the total probability of photon transmission, N_t, as the sum of the probabilities N_n, where N_n is the probability of photon transmission with exactly n scatterings. The total expected transmitted energy, E_t, is similarly considered to be given by ΣE_n. A numerical calculation of N_n and E_n has been made for $n=0, 1, 2, 3$ for a slab of uranium 20 cm thick, upon which photons are incident normally with energy $\alpha=10\ mc^2$. The maximum value of N_n/N_0 occurs at $n=2$ and of E_n/E_0 at $n=1$. These calculations are also adapted to a slab of lead 35 cm thick. Consideration has been given to the behavior of N_n and E_n for large n, and estimates are thereby made for N_t and E_t. The second procedure consists in deriving the transmission through a thick slab from a succession of transmissions through thin slabs. The transformation of an incident photon distribution into the distribution transmitted through a thin slab is conveniently expressed as a matrix, and the total transmission is then given by the iteration of the matrix on the successive transmitted distributions. Numerical results obtained by this procedure for particular incident photon distributions are presented.

I. INTRODUCTION

THE purpose of the present investigation has been a study of the feasibility of straightforward numerical determinations of the transmission of gamma-rays through large thicknesses of materials containing heavy elements. The limitation of the discussion to heavy elements makes possible some simplifications essentially because of the large probability of absorption by the photoelectric effect of photons which are degraded to low energy. The present approach to the gamma-ray transmission problem is based on the notion that one need consider only those transmitted gamma-rays which have suffered relatively few scatterings even for thicknesses of materials of approximately 20 mean free paths. The validity of this view is demonstrated by the results which are presented in the following sections. Specific calculations have been made of the attenuation of gamma-rays with incident energy $10\ mc^2$ through thicknesses of uranium up to 20 cm. These calculations are adjusted to give the attenuation through thicknesses of lead up to 35 cm.

The elementary processes of gamma-ray interaction with matter that are taken into account are the photoelectric effect, Compton scattering, and pair-production. Since the numerical results for gamma-ray transmission will depend upon the values taken for the absorption coefficients for these processes, a partial table of the values for uranium and lead used in the present calculations is given in Table I. If a minor alteration is made in these values, the effect on the transmission values given here could be determined without great difficulty. The probability of Compton scattering is assumed to be given by the Klein-Nishina formula, in which the effects of polarization of the radiation have been averaged out. Thus, the partial polarization which arises upon scattering of originally unpolarized radiation and the alteration in the probability of further Compton scattering has been disregarded. The gamma-ray energies of present concern are sufficiently high so that these polarization effects are believed to be unimportant. The possible contribution to the transmitted radiation from bremsstrahlung produced by Compton recoil electrons is not included in the present calculations; the range of gamma-ray energies considered here is known to be too low for this contribution to be significant.

Two methods for the determination of the probability of transmission of a photon through a slab of material of thickness a will be considered. In the first method, the total probability of transmission is taken as the sum of the probability of transmission with no scattering, plus the probability of transmission with one scattering, plus the probability of transmission with two scatterings, etc. In the second method, the slab of thickness a is divided into a series of thin slabs and the transmission through the total thickness is determined from the transmission through the series of thin slabs in succession.

II. SUCCESSIVE SCATTERED CONTRIBUTIONS TO THE TRANSMITTED RADIATION

Consider a homogeneous slab of material which has infinite extent in the y- and z-directions and which has thickness a in the x-direction, $0 \leq x \leq a$. One can readily give an integral expression for the probability that a gamma-ray incident on the face $x=0$ is not absorbed in the slab and emerges after exactly n collisions from the face $x=a$. Let the gamma-ray enter with the energy α_0 in a direction making an angle ψ_0 with the normal to the face of the slab, travel a distance s_0 within the slab

* Consultant to RAND Corporation.

TABLE I. Values for the absorption coefficients for lead and uranium which were used in the calculations: α=photon energy in units of mc^2; μ_U=total absorption coefficient for uranium; μ_{Pb}=total absorption coefficient for lead.

α	μ_U	μ_{Pb}
0.2	68.8	57.0
0.5	12.0	6.10
1.0	3.07	1.686
2.0	1.339	0.768
4.0	0.890	0.514
6.0	0.824	0.477
8.0	0.847	0.479
10.0	0.868	0.494

to the first collision, scatter (if it is not absorbed) into a direction making an angle θ_1 with the original direction and an angle ψ_1 with the normal to the slab face, travel a distance s_1 to a second collision, scatter into a direction specified by θ_2 and ψ_2, and so on (see Fig. 1). After n collisions, the path angles are θ_n and ψ_n, and s_n is the distance traveled from the $(n-1)$th collision to the exit face of the slab at $x=a$. The path line after the kth collision is characterized by an azimuthal angle ϕ_k in addition to the angles θ_k and ψ_k; these angles are connected by the familiar relation,

$$\cos\psi_{k+1}=\cos\psi_k\cos\theta_{k+1}+\sin\psi_k\sin\theta_{k+1}\cos\phi_{k+1};$$

$k=0, 1, 2, \cdots, (n-1)$. The energy of the photon between the kth and the $(k+1)$th collision is α_k in units of mc^2, and the value of the total absorption coefficient for this energy α_k will be denoted by μ_k. The successive values of the energy α_k are related by the Compton formula:

$$\alpha_k=\alpha_{k-1}/[1-\alpha_{k-1}(1-\cos\theta_k)].$$

The probability, N_n, that the photon will be transmitted after exactly n collisions by any possible path is

$$N_n=\left(\frac{\nu r^2}{2}\right)^n\int\int_S\cdots\int e^{-\mu_n s_n}\prod_{k=0}^{n-1}e^{-\mu_k s_k}\times q_{k+1}\,ds_k\,d\phi_{k+1}\,d\theta_{k-1}, \quad (1)$$

where ν is the number of electrons per cm³ in the slab material, r is the electron radius, e^2/mc^2, and q_{k+1} is obtained from the Klein-Nishina differential cross section as

$$q_{k+1}=\frac{\sin\theta_{k+1}}{[1+\alpha_k(1-\cos\theta_{k+1})]^2}\times\left[1+\cos^2\theta_{k+1}+\frac{\alpha_k^2(1-\cos\theta_{k+1})^2}{1+\alpha_k(1-\cos\theta_{k+1})}\right].$$

The $3n$-dimensional space S over which the integration in Eq. (1) must be performed needs detailed description. A point $(s_0, \theta_1, \phi_1, s_1, \theta_2, \phi_2, \cdots, s_{n-1}, \theta_n, \phi_n)$ represents a path followed by the photon in reaching the nth collision and is a possible path or a point in S if all these collisions are within, or at the boundary of, the slab. Any value of ϕ_k and θ_k is possible as long as

$$0\leq\phi_k\leq 2\pi, \quad 0\leq\theta_k\leq\pi. \quad k=1, 2, \cdots, n.$$

The first collision, however, will not be in the slab unless

$$0\leq s_0\cos\psi_0\leq a.$$

Further, the value of the angle ψ_1 determines whether the first collision has given forward or backward scattering. If the scattering is forward,

$$0\leq\psi_1\leq\pi/2,$$

then the second collision will be possible only if

$$0\leq s_1\cos\psi_1\leq a-s_0\cos\psi_0.$$

If the scattering is backward,

$$\pi/2<\psi_1\leq\pi,$$

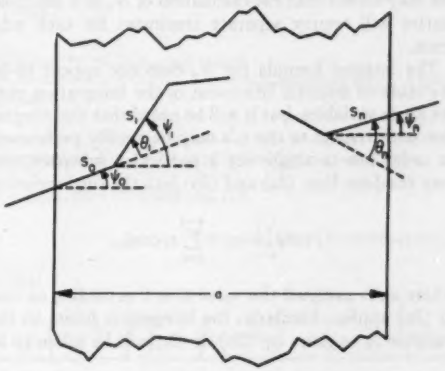

FIG. 1. Geometric parameters of a typical photon path through a slab.

then the inequality

$$0\geq s_1\cos\psi_1\geq -s_0\cos\psi_0$$

must hold. Continuing in this way, one sees that the space S is defined by the inequalities:

$$0\leq\phi_k\leq 2\pi; \quad 0\leq\theta_k\leq\pi; \quad (2a)$$

$$0\leq s_{k-1}\cos\psi_{k-1}\leq a-\sum_{i=0}^{k-2}s_i\cos\psi_i, \quad \text{if } 0\leq\psi_{k-1}\leq\tfrac{1}{2}\pi; \quad (2b)$$

$$0\geq s_{k-1}\cos\psi_{k-1}\geq -\sum_{i=0}^{k-2}s_i\cos\psi_i, \quad \text{if } \tfrac{1}{2}\pi<\psi_{k-1}\leq\pi. \quad (2c)$$

For each inequality of Eq. (2), $k=1, 2, \cdots, n$. It is to be noted that for $k=1$, one replaces

$$\sum_{i=0}^{k-2}s_i\cos\psi_i$$

by zero; the last inequality (2c), which gives the range

of $s_{k-1}\cos\psi_{k-1}$, is trivial; and the inequality defining the range of ψ_{k-1} loses significance.

The space S divides naturally into 2^{n-1} subspaces, where each subspace represents a particular sequence of forward and backward scatterings. The scatter forward or backward on the last, or nth, collision does not figure in these inequalities, but does enter by way of the integrand. For transmission, s_n is defined by the relation,

$$s_n\cos\psi_n = a - \sum_{i=0}^{n-1} s_i\cos\psi_i, \quad \text{if } 0\leq\psi_n\leq\tfrac{1}{2}\pi, \tag{3a}$$

and for reflection by

$$s_n\cos\psi_n = -\sum_{i=0}^{n-1} s_i\cos\psi_i, \quad \text{if } \tfrac{1}{2}\pi<\psi_n\leq\pi. \tag{3b}$$

Hence, the number of subspaces is increased to 2^n, and one may expect that the calculation of N_n as a practical matter will require separate treatment for each subspace.

The integral formula for N_n does not appear to be tractable to analytic treatment of the integration over the angle variables, but it will be noted that the integration with respect to the s_k's may be readily performed. In order not to single out a particular subspace, one may combine Eqs. (3a) and (3b) into the single relation

$$s_n\cos\psi_n = a_n - \sum_{i=0}^{n-1} s_i\cos\psi_i,$$

where a_n is assigned the value a or 0 according as (3a) or (3b) applies. Similarly, the integration limits on the variable s_k as given by (2b) or (2c) will be taken to be 0 and

$$a_k - \sum_{i=0}^{k-2} s_i\cos\psi_i,$$

where a_k has the value a or 0 according as the subspace defined by (2b) or (2c) applies. Then Eq. (1) requires the integration of the function,

$$\exp\left[\frac{\mu_n}{\cos\psi_n}\left(a_n - \sum_{i=0}^{n-1} s_i\cos\psi_i\right)\right]\cdot\exp\left[-\sum_{i=0}^{n-1}\mu_i s_i\right],$$

first with respect to s_{n-1} over the interval

$$\left(0, a_{n-1} - \sum_{i=0}^{n-2} s_i\cos\psi_i\right),$$

then with respect to s_{n-2} over the interval

$$\left(0, a_{n-2} - \sum_{i=0}^{n-3} s_i\cos\psi_i\right), \text{ etc.}$$

This series of operations has a recursive nature which can be made evident by the following device. Let

$$F_{j,k} = \begin{cases} \exp\left[-\lambda_j\left(a_j - \sum_{i=0}^{k} s_i\cos\psi_i\right)\right]\cdot\exp\left[-\sum_{i=0}^{k}\mu_i s_i\right], & \text{for } k\geq 0; \\ \exp[-\lambda_j a_j], & \text{for } k=-1. \end{cases}$$

Then, if J_k represents the operation of integrating with respect to s_k between the limits 0 and

$$a_k - \sum_{i=0}^{k-1} s_i\cos\psi_i,$$

one has

$$J_k(F_{j,k}) = [F_{j,k-1} - e^{-\lambda_j(a_j-a_k)}F_{k,k-1}]/(\lambda_k-\lambda_j)\cos\psi_k, \tag{4a}$$

$$J_{k-1}[J_k(F_{j,k})] = \frac{[F_{j,k-2} - e^{-\lambda_j(a_j-a_{k-1})}F_{k-1,k-2}]/(\lambda_{k-1}-\lambda_j)\cos\psi_{k-1} - e^{-\lambda_j(a_j-a_k)}[F_{k,k-2} - e^{-\lambda_k(a_k-a_{k-1})}F_{k-1,k-2}]/(\lambda_{k-1}-\lambda_k)\cos\psi_{k-1}}{(\lambda_k-\lambda_j)\cos\psi_k}. \tag{4b}$$

Further iterations proceed similarly. It is evident that the s-integrations in Eq. (1) are the end of a sequence of these operations of which (4a) and (4b) are the first two; the sequence in N_n is obtained from Eq. (4) by these substitutions: $k=n-1$, $j=n$, $\lambda_n=\mu_n/\cos\psi_n$. For $n=1$, one has

$$N_1(a_1) = \tfrac{1}{2}\nu r^2\int\int_{S_1}[e^{-\lambda_1 a_1} - e^{-\lambda_1(a_1-a)}e^{-\lambda_0 a}]q_1 d\theta_1 d\phi_1/(\lambda_0-\lambda_1)\cos\psi_0, \tag{5}$$

and for $n=2$,

$$N_2(a_1,a_2) = \left(\frac{\nu r^2}{2}\right)^2\int\int\int\int_{S_2}\frac{\dfrac{e^{-\lambda_2 a_2} - e^{-\lambda_2(a_2-a)}e^{-\lambda_0 a}}{(\lambda_0-\lambda_2)\cos\psi_0} - e^{-\lambda_2(a_2-a_1)}\dfrac{e^{-\lambda_1 a_1} - e^{-\lambda_1(a_1-a)}e^{-\lambda_0 a}}{(\lambda_0-\lambda_1)\cos\psi_0}}{(\lambda_1-\lambda_2)\cos\psi_1} q_1 q_2 d\phi_1 d\theta_1 d\phi_2 d\theta_2. \tag{6}$$

Thus, the probability of a photon passing through the slab with exactly one collision is given by Eq. (5) as $N_1(a)$, and the probability of being reflected out through the incident face of the slab with one collision is $N_1(0)$. The probability of transmission with exactly two collisions is given by Eq. (6) as the sum of the two probabilities $N_2(a,a)$ and $N_2(0,a)$, and the probability of reflection out through the incident face with two collisions is the sum

of the two probabilities $N_2(a,0)$ and $N_2(0,0)$. If one defines $v_i=\lambda_i a$, then these probabilities may be written as follows:

$$N_1(a)=\tfrac{1}{2}\pi r^2 a\varepsilon^{-v_0}\int\int_{S_1(a)}[1-\varepsilon^{-(v_0-v_1)}]q_1 d\phi_1 d\theta_1/(v_0-v_1)\cos\psi_0; \tag{7}$$

$$N_1(0)=\tfrac{1}{2}\pi r^2 a\int\int_{S_1(0)}[1-\varepsilon^{-(v_0-v_1)}]q_1 d\phi_1 d\theta_1/(v_0-v_1)\cos\psi_0; \tag{8}$$

$$N_2(a,a)=\left(\frac{\pi r^2 a}{2}\right)^2\varepsilon^{-v_0}\int\int\int\int_{S_2(a,a)}\frac{[1-\varepsilon^{-(v_2-v_0)}]/(v_2-v_0)\cos\psi_0-[1-\varepsilon^{-(v_2-v_1)}]/(v_1-v_0)\cos\psi_0}{(v_1-v_2)\cos\psi_1}q_1q_2 d\phi_1 d\theta_1 d\phi_2 d\theta_2; \tag{9a}$$

$$N_2(0,a)=\left(\frac{\pi r^2 a}{2}\right)^2\varepsilon^{-v_0}\int\int\int\int_{S_2(0,a)}\frac{[1-\varepsilon^{-(v_2-v_1)}]/(v_2-v_1)\cos\psi_0-[1-\varepsilon^{-(v_2-v_0)}]/(v_2-v_0)\cos\psi_0}{(v_1-v_0)\cos\psi_1}q_1q_2 d\phi_1 d\theta_1 d\phi_2 d\theta_2; \tag{9b}$$

$$N_2(a,0)=\left(\frac{\pi r^2 a}{2}\right)^2\int\int\int\int_{S_2(a,0)}\frac{[1-\varepsilon^{-(v_1-v_2)}]/(v_1-v_2)\cos\psi_0-[1-\varepsilon^{-(v_0-v_2)}]/(v_0-v_2)\cos\psi_0}{(v_0-v_1)\cos\psi_1}q_1q_2 d\phi_1 d\theta_1 d\phi_2 d\theta_2; \tag{10a}$$

$$N_2(0,0)=\left(\frac{\pi r^2 a}{2}\right)^2\int\int\int\int_{S_2(0,0)}\frac{[1-\varepsilon^{-(v_0-v_2)}]/(v_0-v_2)\cos\psi_0-[1-\varepsilon^{-(v_0-v_1)}]/(v_0-v_1)\cos\psi_0}{(v_2-v_1)\cos\psi_1}q_1q_2 d\phi_1 d\theta_1 d\phi_2 d\theta_2. \tag{10b}$$

One notes that ε^{-v_0} appears as a factor in all the transmission probabilities; ε^{-v_0} is, of course, the probability that a photon is transmitted through the slab without absorption or scattering.

In heavy materials, the probability of photoelectric absorption increases very rapidly as the photon energy decreases. As a consequence, the transmission probability for a path which includes two or more backward scatterings will be unimportant compared with the transmission probability for a path with the same number of collisions all of which are in the forward direction; e.g., $N_2(0,a)\ll N_2(a,a)$. In terms of the integration spaces, the subspace corresponding to $a_1=a_2=\cdots=a_n=a$ is the important one that need be considered of all the types N_n. This particular sequence of probabilities has the form

$$N_n(a,a,\cdots,a)=\left(\frac{\pi r^2 a}{2}\right)^n\int\int\cdots\int_{S_n(a,a,\cdots,a)}f_n(v_n,v_{n-1},\cdots,v_0)\times\prod_{k=0}^{n-1}q_{k+1}d\phi_{k+1}d\theta_{k+1}, \tag{11}$$

where

$$f_0(v_0)=\varepsilon^{-v_0},$$
$$f_1(v_1,v_0)=[f_0(v_1)-f_0(v_0)]/(v_0-v_1)\cos\psi_0,$$
$$f_2(v_2,v_1,v_0)=[f_1(v_2,v_0)-f_1(v_1,v_0)]/(v_1-v_2)\cos\psi_1,$$
$$f_3(v_3,v_2,v_1,v_0)=[f_2(v_3,v_1,v_0)-f_2(v_2,v_1,v_0)]/(v_2-v_3)\cos\psi_2,$$

etc.

The expected energy, E_n, say, which is carried by a photon transmitted or reflected is obtained if the integrand in Eq. (1) is multiplied by α_n, where

$$\alpha_n=\alpha_{n-1}/[1-(1-\cos\theta_n)\alpha_{n-1}]=\alpha_0/\prod_{k=0}^{n-1}[1-(1-\cos\theta_{k+1})\alpha_k],$$

so that

$$E_n=\alpha_0\left(\frac{\pi r^2}{2}\right)^n\int\int\cdots\int_{S_n}\varepsilon^{-\mu_0 s_0}\times\prod_{k=0}^{n-1}\varepsilon^{-\mu_{k+1}s_{k+1}}p_{k+1}ds_k d\phi_{k+1}d\theta_{k+1}, \tag{12}$$

In Eq. (12)

$$p_k=q_k/[1-(1-\cos\theta_{k+1})\alpha_k].$$

Every formula developed for N_n has its counterpart for E_n.

The formulas summarized in Eqs. (11) and (12) do not appear at all amenable to analytic evaluation.

TABLE II. Transmission values for photons incident normally with energy 10 mc^2 ($\alpha_0=10$, $\psi_0=0$). The values for uranium apply to a plane slab of thickness $a=20$ cm; the values for lead apply to a slab of thickness $a=35$ cm. N_n is the number of photons transmitted with exactly n scatterings. E_n is the expected energy transmitted with exactly n scatterings.

	Transmission values for U: $\alpha_0=10$, $\psi_0=0$, $a=20$ cm		Transmission values for Pb: $\alpha_0=10$, $\psi_0=0$, $a=35$ cm	
n	N_n/N_0	E_n/E_0	N_n/N_0	E_n/E_0
0	1.0	1.0	1.0	1.0
1	2.6	1.7	2.8	1.85
2	3.0	1.5	3.6	1.8
3	2.2	0.88	2.85	1.15

Numerical integration, on the other hand, cannot be carried out for large values of n in a reasonable length of time. It would be of great interest, however, to have a quantitative notion of how many collisions contribute significantly to the number of photons and the energy transmitted through a large thickness of a heavy material. A numerical calculation was therefore carried out for a slab of uranium 20 cm thick upon which photons are incident normally ($\psi_0=0$) with energy $\alpha_0=10$. The results through the third scattered beam are given in Table II. It is estimated that these values may be in error by as much as 10 percent. The error is greatest, of course, for N_3 and E_3; and for these the error may be pessimistically estimated to be as large as 20 percent.

These results can be used to obtain transmission values through a slab of lead for photons incident under the same conditions: $\psi_0=0$, $\alpha_0=10$. It may be noted (see Table I) that the total absorption coefficient, $\mu(\alpha)$, for uranium is larger than that for lead in the energy range from 1 to 10 mc^2 by an almost constant factor of approximately 1.75. Consequently, integrals (7), (8), (9), (10), etc. evaluated for 20 cm of uranium should have about the same values for 1.75×20 cm $=35$ cm of lead except for the factor $(\nu^2 a/2)^n$. The quantity in this factor which varies in going from uranium to lead is νa, and the ratio of νa for lead to its value for uranium is 1.09. In this way, one gets the transmission values for lead shown in Table II.†

These results point to the interesting conclusion that the major portion of the photons and of the energy transmitted through a slab of heavy material of the order of 20 mean free paths thick is contained in the contributions from the first four or five scattered beams. If an extrapolation is made in a reasonable geometric fashion to higher values of n, one gets for the total energy and total number of photons transmitted through a slab of uranium

$$E_t\approx 5.5E_0, \tag{13a}$$

$$N_t\approx 10.8N_0, \tag{13b}$$

with the transmitted photons having the average energy

$$E_t/N_t\approx 5mc^2. \tag{13c}$$

Corresponding values for the slab of lead are

$$E_t\approx 6.4E_0, \tag{14a}$$

$$N_t\approx 12.7N_0, \tag{14b}$$

$$E_t/N_t\approx 5mc^2. \tag{14c}$$

This extrapolation is not so daring as might appear. One would expect that once $E_n(a)$ and $I_n(a)$ begin to fall, they would decrease ever more rapidly as n increases. This inference is strengthened by a qualitative examination of the integrals for E_n and I_n, which indicates for large a a trend for a behavior of the following type:

$$E_n(a)/E_0\approx(ka)^n/n!, \tag{15a}$$

$$I_n(a)/I_0\approx(ca)^n/n!, \tag{15b}$$

where k and c do not vary strongly with n. The first four values of E_n/E_0 given in Table II agree fairly well with Eq. (15a) with the value $k=0.087$ cm^{-1}; the value $c=0.12$ cm^{-1} in Eq. (15b) gives a rough fit to the tabulated values for N_n/N_0. Corresponding values for the slab of lead are $k=0.054$ cm^{-1}; $c=0.075$ cm^{-1}. It should be noted that Eqs. (15a) and (15b) are of the form which would be obtained from a one-dimensional calculation of the transmission probabilities. Although the values for k and c derived from a one-dimensional calculation would depend on the kind of approximation made, one would not expect that the one-dimensional form would underestimate the general trend of the contributions to the transmission from large values of n. One may, therefore, argue that one gets rapid convergence in E_n and I_n, and that an extrapolation made with k and c chosen for the best fit over the first few values of n which go beyond the maxima in E_n and I_n would be reasonably safe. Such an extrapolation, which uses Eqs. (15) to get the contributions for n beyond those calculated, gives essentially the same results for E_t and N_t as does the geometric extrapolation mentioned above.

No effort was made to improve the accuracy of the computed values of E_n and I_n presented in Table II because of the difficulty involved in this straightforward approach to the calculation. The functions involved have a behavior unsuited to numerical methods; and, furthermore, the number of numerical quadratures which must be performed, for example, in the case $n=3$, prohibits the use of more than a few points in each integration. The present results were obtained by using from three to five points for each integration. So few points would indicate a poorer accuracy than stated if one were to assume the use of an unadorned Simpson's rule. The worst function behavior, however, is found with the functions $p_k(\theta_k)$ and $q_k(\theta_k)$, which are all of one class, so that they may be considered together. Further, the functions of θ_k and ψ_k arising from $f_n(v_n,v_{n-1},\cdots,v_0)$ are also more or less of a class; of these, the greatest difficulty for the numerical integrations comes from a variation in which the function rises to a maximum and then falls rapidly in roughly exponential manner.

A typical integral which must be evaluated is of the form

$$\int_0^{\theta_k^*} f(\theta_k)q_k(\theta_k)d\theta_k. \tag{16}$$

Now if the function $f(\theta_k)$ is approximated by a polynomial $c_0+c_1\theta_k+\cdots+c_n\theta_k^n$ which passes through n

† *Note added in proof:* A direct calculation for a 35-cm slab of Pb has been made for $\alpha_0=10$ with the following results: $N_1/N_0=2.6$, $N_2/N_0=3.4$; $E_1/E_0=1.85$, $E_2/E_0=1.83$. The agreement of these values with the Pb values in Table II is very good.

points of $f(\theta)_k$ and if the integrals

$$\int_{\theta_{k'}}^{\theta_{k''}} \theta_k{}^j q_k(\theta_k) d\theta_k, \quad j=0, 1, 2, \cdots, n,$$

are evaluated, then an approximate value of Eq. (16) is obtained in which the number of points required depends on the behavior of $f(\theta_k)$ and very little on that of $q_k(\theta_k)$. Such a procedure is useful since the functions q_k (and p_k) are amenable to the required analysis. A complete study of a few typical integrals of the type (16) showed that three points can be used to approximate $f(\theta_k)$ with sufficient accuracy to give an error of

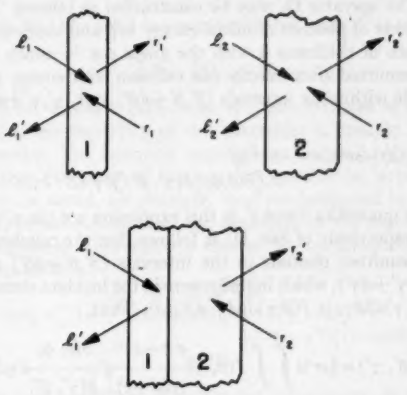

FIG. 2. A schematic representation of the incident, reflected, and transmitted photon distributions for two component slabs 1 and 2 and for the combined slab.

about 5 percent in the integrated value. It is essentially such a procedure which was followed with some care and control to give the results of Table II in a reasonable time.

III. TOTAL TRANSMISSION AS SUCCESSIVE TRANSMISSION THROUGH A SERIES OF THIN SLABS

It is clear from the preceding results that the transmission through a slab one or two mean free paths thick should not require the evaluation of scattered contributions beyond the two-collision beam. Indeed, the twice scattered photons would then constitute only a small portion of the total transmission. The calculation of the unscattered and singly scattered transmission beams is a simple matter, and the calculation of the doubly scattered transmission beam is also not difficult if high accuracy in its numerical value is not required. With a practicable method of evaluating the transmission through a thin slab, one might propose to obtain the transmission through a thick slab by considering it to be composed of a number of thin slabs. This procedure may readily be examined in a formal manner.

Let $\mathbf{O}$ be the operator which transforms a distribution of photons incident upon one face of a slab into the distribution of photons leaving the second face, and let $\mathbf{S}$ be the operator which transforms the incident distribution into the distribution leaving the incident face of the slab. It is plausible, in view of the physical situation, to assume for any distributions l and r that the operational relations

$$\mathbf{O}(l+r)=\mathbf{O}l+\mathbf{O}r,$$
$$\mathbf{O}l+\mathbf{S}l=(\mathbf{O}+\mathbf{S})l, \quad \mathbf{O}(\mathbf{S}l)=\mathbf{O}\mathbf{S}l,$$

are valid. Consider two slabs in contact (Fig. 2) and let l_1 be the distribution entering the left face of the first slab, r_1 the distribution entering the right face, and l_1' and r_1' the distributions leaving the left and right faces, respectively. Let l_2, r_2, l_2', r_2' be the corresponding distributions for the second slab. The two slabs, for the general discussion, need not be identical either in material or thickness, so that the first slab has operators $\mathbf{O}_1$, $\mathbf{S}_1$ and the second slab has corresponding operators $\mathbf{O}_2$, $\mathbf{S}_2$. Then the following relations hold:

$$r_1'=\mathbf{O}_1l_1+\mathbf{S}_1r_1, \quad l_1'=\mathbf{S}_1l_1+\mathbf{O}_1r_1,$$
$$r_2'=\mathbf{O}_2l_2+\mathbf{S}_2r_2, \quad l_2'=\mathbf{S}_2l_2+\mathbf{O}_2r_2,$$

and, since the distributions which leave one inner face must enter the other,

$$r_1'=l_2, \quad r_1=l_2'.$$

These six equations reduce to

$$\begin{aligned} r_1'&=\mathbf{O}_1l_1+\mathbf{S}_1r_1, \quad l_1'=\mathbf{S}_1l_1+\mathbf{O}_1r_1, \\ r_2'&=\mathbf{O}_2r_1'+\mathbf{S}_2r_2, \quad r_1=\mathbf{S}_2r_1'+\mathbf{O}_2r_2. \end{aligned} \tag{17}$$

Substitution of the fourth of these equations into the first leads to

$$r_1'=\mathbf{O}_1l_1+\mathbf{S}_1\mathbf{O}_2r_2+\mathbf{S}_1\mathbf{S}_2r_1',$$

and this relation when applied to itself gives

$$r_1'=(\mathbf{O}_1+\mathbf{S}_1\mathbf{S}_2\mathbf{O}_1)l_1+(\mathbf{S}_1\mathbf{O}_2+\mathbf{S}_1\mathbf{S}_2\mathbf{S}_1\mathbf{O}_2)r_2+(\mathbf{S}_1\mathbf{S}_2)^2r_1';$$

repetition of this process k times yields the relation

$$\begin{aligned} r_1'=&[\mathbf{O}_1+\mathbf{S}_1\mathbf{S}_2\mathbf{O}_1+(\mathbf{S}_1\mathbf{S}_2)^2\mathbf{O}_1+\cdots+(\mathbf{S}_1\mathbf{S}_2)^k\mathbf{O}_1]l_1 \\ &+[\mathbf{S}_1\mathbf{O}_2+\mathbf{S}_1\mathbf{S}_2\mathbf{S}_1\mathbf{O}_2+(\mathbf{S}_1\mathbf{S}_2)^2\mathbf{S}_1\mathbf{O}_2+\cdots \\ &+(\mathbf{S}_1\mathbf{S}_2)^k\mathbf{S}_1\mathbf{O}_2]r_2+(\mathbf{S}_1\mathbf{S}_2)^{k+1}r_1'. \end{aligned} \tag{18}$$

If one substitutes the first of Eqs. (17) into the fourth, and iterates in a similar way, one finds

$$\begin{aligned} r_1=&[\mathbf{S}_2\mathbf{O}_1+\mathbf{S}_2\mathbf{S}_1\mathbf{S}_2\mathbf{O}_1+(\mathbf{S}_2\mathbf{S}_1)^2\mathbf{S}_2\mathbf{O}_1+\cdots \\ &+(\mathbf{S}_2\mathbf{S}_1)^k\mathbf{S}_2\mathbf{O}_1]l_1+[\mathbf{O}_2+\mathbf{S}_2\mathbf{S}_1\mathbf{O}_2+\cdots \\ &+(\mathbf{S}_2\mathbf{S}_1)^k\mathbf{O}_2]r_2+(\mathbf{S}_2\mathbf{S}_1)^{k+1}r_1. \end{aligned} \tag{19}$$

The quantities $(\mathbf{S}_1\mathbf{S}_2)^{k+1}r_1'$ and $(\mathbf{S}_2\mathbf{S}_1)^{k+1}r_1$ represent a distribution of photons which have been reflected back and forth between the slabs $k+1$ times. For k sufficiently large, these terms may be neglected. If Eqs. (18) and (19) so simplified are substituted into the second and

third of Eqs. (17), one finds

$$I_1' = [S_1 + O_1S_2O_1 + O_1S_2S_1S_2O_1 + O_1(S_2S_1)^2S_2O_1 + \cdots]I_1 + [O_1O_2 + O_1S_2S_1O_2 + O_1(S_2S_1)^2O_2 + \cdots]r_2; \quad (20)$$

$$r_1' = [O_2O_1 + O_2S_1S_2O_1 + O_2(S_1S_2)^2O_1 + \cdots]I_1 + [S_2 + O_2S_1O_2 + O_2S_1S_2S_1O_2 + O_2(S_1S_2)^2S_1O_2 + \cdots]r_2. \quad (21)$$

Equations (20) and (21) give the two distributions emerging from the two outer faces of the combined slabs in terms of the two entering distributions. Each sum of operator products in the brackets of these equations represents an operator (**S** or **O**) for the composite slab in terms of the operators for the two constituent slabs. It is clear that, if a third slab is brought into the system, the foregoing process could be repeated to obtain the operators for the combination of three slabs, and this process may be extended for any number of component slabs. In any such extension, the operator coefficient of I_1 will either be the transformation of the distribution incident on the left face of the composite slab into the distribution transmitted out of the last face on the right, or it will be the transformation which reflects this distribution back from the incident face. The behavior in a general case of any number of component slabs is illustrated well enough by Eqs. (20) and (21). The coefficient of I_1 in Eq. (21) consists of the following operators: $\mathbf{O_2O_1}$, which represents the operator for direct transmission through the two slabs; $\mathbf{O_2S_1S_2O_1}$, which represents transmission through the first slab, a reflection from the second slab, a reflection from the first slab, and finally a transmission through the second slab; etc. As would be expected, this operator sum represents all possible successions of transmissions and reflections which end finally in transmission. The other operator brackets have similar interpretations.

The number of photons in the distributions $\mathbf{O_2O_1}I_1$, $\mathbf{O_2S_1S_2O_1}I_1$, $\cdots$ must be decreasing. Indeed, for a material with an appreciable absorption cross section, one would expect that the important contribution to the transmission would be accurately represented by $\mathbf{O_2O_1}$. With this assumption, the transmission through k identical slabs is given by the simple operator $\mathbf{O}^k$.

This operational process is a promising approach and has the advantage of giving details about the photon distribution at a succession of thicknesses of material. In this way a rather complete history of the attenuated beam is obtained.

The formulation in Sec. II gives the necessary basis for the construction of the operator **O**. The distribution of photons incident upon a slab may be specified in terms of the initial energy, α_0, and the angle of incidence, ψ_0. The variables $\beta = 1/\alpha_0$ and $\gamma = \cos\psi_0$ are somewhat more convenient, so that the incident frequency distribution will be $I(\beta,\gamma)$. Then, for the transmitted distribution, one has

$$I'(\beta',\gamma') = \mathbf{O}I(\beta,\gamma).$$

Now **O** may be considered to be the sum of the operators $\mathbf{O}_0$, $\mathbf{O}_1$, $\mathbf{O}_2$, $\cdots$, where $\mathbf{O}_k$ transforms $I(\beta,\gamma)$ into $I_k'(\beta',\gamma')$, and $I_k'(\beta',\gamma')$ is the function for those photons which are transmitted with exactly k collisions. The first of these operators, $\mathbf{O}_0$, is found at once. Those photons in the incident distribution element $I(\beta,\gamma)d\beta d\gamma$, which are transmitted without collision, have unaltered energy and direction of travel and are diminished in number of the factor $\exp[-a\mu(\beta)/\gamma]$, where $\mu(\beta)$ is the total cross section of the material for photons of energy β and a is the slab thickness. Hence, $\mathbf{O}_0$ is defined exactly by the relation

$$I_0'(\beta',\gamma') = \exp[-a\mu(\beta)/\gamma]I(\beta,\gamma).$$

The operator $\mathbf{O}_1$ may be constructed as follows. The number of photons of initial energy $1/\beta$ and incident on a slab of thickness a with the angle $\cos^{-1}\gamma$ which are transmitted after exactly one collision with energy and angle within the intervals $(\beta',\beta'+d\beta')$ and $(\gamma',\gamma'+d\gamma')$ is

$$dN_1(a) = \nu\pi^2 a(e^{-v} - e^{-v'})q' \times [\partial(\theta,\phi)/\partial(\gamma',\beta')]d\gamma' d\beta'/2\gamma(v'-v).$$

The quantities v and v' in this expression are the v_0 and v_1 respectively of Sec. II. It follows that the number of transmitted photons in the intervals $(\beta',\beta'+d\beta')$ and $(\gamma',\gamma'+d\gamma')$, which initially were in the incident element $I(\beta,\gamma)d\beta d\gamma$, is $I(\beta,\gamma)d\beta d\gamma \cdot dN_1(a)$. Thus,

$$I_1'(\beta',\gamma') = \tfrac{1}{2}\nu\pi^2 a \int\int I(\beta,\gamma)\frac{e^{-v} - e^{-v'}}{\gamma(v'-v)}q'\frac{\partial(\theta,\phi)}{\partial(\gamma',\beta')}d\gamma d\beta$$

$$= \tfrac{1}{2}\nu\pi^2 a \int\int I(\beta,\gamma)\frac{e^{-v} - e^{-v'}}{v'-v}\frac{\beta}{\beta'^3} \times \frac{\beta'\beta^2 + (1+2\beta'-2\beta'^2)\beta^2 + (\beta'^3 - 2\beta'^2)\beta + \beta'^2}{\gamma(1-\cos^2\theta_1 - \gamma'^2 + 2\cos\theta_1\gamma'\gamma - \gamma^2)^{\frac{1}{2}}}d\gamma d\beta, \quad (22)$$

where $\cos\theta_1 = 1+\beta-\beta'$. It is evident that the operator $\mathbf{O}_1$ is a multiplication by a function followed by an integration over the proper space in the variables β, γ.

The operators $\mathbf{O}_2$, $\mathbf{O}_3$, etc. can be defined in the same way. There remains, however, the problem of performing the indicated transformations with sufficient accuracy and speed. The essential features of one approach to this problem will be illustrated with the operator $\mathbf{O}_1$. The incident distribution $I(\beta,\gamma)$ is represented in the range of interest or significance by a set of discrete points, $i \cdot k$ in number, taken from i values of β: $\beta_1 < \beta_2 < \cdots < \beta_i$, and k values of γ: $\gamma_1 < \gamma_2 < \cdots < \gamma_k$. These values of $I(\beta_s,\gamma_t)$ are arranged in a column matrix $\|I_{st}\|$. Then $I'(\beta',\gamma')$ as determined by Eq. (22) can be evaluated at a given point (β',γ') by performing i numerical integrations over γ (β successively fixed at $\beta_1, \beta_2, \cdots, \beta_i$) followed by a numerical integration over β. This procedure can consist in multiplying each discrete value of $I(\beta,\gamma)$ in the column

matrix by a suitable coefficient and accumulating the products. It is, thus, readily suggested that one form a square matrix $\|\mathbf{O}_1\|$ of order $i \cdot k$ in which the elements in the first, second, third, etc. rows are respectively the coefficients for obtaining $I_1'(\beta_1,\gamma_1)$, $I_1'(\beta_1,\gamma_2)$, $I_1'(\beta_1,\gamma_3)$, etc. One has, consequently, a matrix representation for the transformation $\mathbf{O}_1$. A matrix representation $\|\mathbf{O}_2\|$ for $\mathbf{O}_2$ can also be found, and its derivation is entirely similar to the above. The operator $\mathbf{O}_0$, which is merely a multiplication by a function with no integrations, is represented by a diagonal matrix. For a slab which is sufficiently thin so that the higher operators are negligible, one has the total matrix

$$\|\mathbf{O}\| = \|\mathbf{O}_0\| + \|\mathbf{O}_1\| + \|\mathbf{O}_2\|,$$

such that the total transmitted distribution I' is given by

$$\|I'\| = \|\mathbf{O}\| \times \|I\|.$$

If an accurate calculation requires matrices of high order, the feasibility of this procedure is brought into question. The functions involved are not well behaved so that the order of the matrices tend to be large. It may be noted, for example, that the integrand in Eq. (22) becomes infinite at the boundary of the region of integration. This region is defined by the simultaneous inequalities:

$$\beta' - 2 \leq \beta \leq \beta',$$
$$\gamma' \cos\theta_1 - [(1-\gamma'^2)(1-\cos^2\theta_1)]^{\frac{1}{2}} \leq \gamma \leq \gamma' \cos\theta_1 + [(1-\gamma'^2)(1-\cos^2\theta_1)]^{\frac{1}{2}},$$
$$\gamma \geq 0.$$

The area so defined is clearly not rectangular, so that there is the difficulty of ending the numerical integration with respect to γ (β fixed) on the boundary when no discrete point falls on the boundary. These difficulties, however, are not insuperable and can be so treated as to make the method feasible.

The transmission of four different distributions incident on a slab of uranium was calculated by this iterative method. The results are presented in Tables III, IV, V, VI, and VII. Case A in these tables represents the first attempt with this procedure and is largely an exploratory calculation. The incident, or initial, distribution is constant in the reciprocal energy range $0.1 \leq \beta \leq 0.15$ and is also constant over the range of cosine of incident angle $0.8 \leq \gamma \leq 1.0$; the incident distribution is zero elsewhere. A net of 49 points was used in the computation and their values are given by $\beta = 0.1, 0.125, 0.15, 0.20, 0.25, 0.35, 0.45$ and $\gamma = 0, 0.2, 0.4, 0.6, 0.8, 0.9, 1.0$. As the calculations proceeded, it became clear that the accuracy could be improved by a different arrangement of points without a great increase in their number. The improvement consists in taking a closer spacing of γ-values for small β and a larger spacing of γ-values for large β. Since the distributions which are operated on vary rapidly for small β and slowly for large β, it is clear that this nonuniform net is advantageous. The improved net was incorporated

TABLE III. Ratios of the total number of photons transmitted, N_t, to the number incident, N_i, for various thicknesses, a, of plane slabs of uranium. The four cases, A, I, II, III, for which N_t/N_i is tabulated, represent various incident photon distributions in energy and angle and are specified in the text.

a (cm)	A	I	II	III
0	1	1	1	1
2	2.36×10^{-1}	2.22×10^{-1}	2.34×10^{-1}	2.42×10^{-1}
4	5.20×10^{-2}	4.68×10^{-2}	5.21×10^{-2}	5.50×10^{-2}
6	1.12×10^{-2}	9.80×10^{-3}	1.14×10^{-2}	1.23×10^{-2}
8	2.40×10^{-3}	2.05×10^{-3}	2.46×10^{-3}	2.69×10^{-3}
10	5.07×10^{-4}	4.29×10^{-4}	5.28×10^{-4}	5.85×10^{-4}
12	1.07×10^{-4}	8.97×10^{-5}	1.13×10^{-4}	1.26×10^{-4}
14	2.24×10^{-5}	1.87×10^{-5}	2.40×10^{-5}	2.71×10^{-5}
16	4.70×10^{-6}	3.91×10^{-6}	5.08×10^{-6}	5.79×10^{-6}
18	9.83×10^{-7}	8.14×10^{-7}	1.07×10^{-6}	1.23×10^{-6}
20	2.06×10^{-7}	1.70×10^{-7}	2.26×10^{-7}	2.61×10^{-7}

in the matrix operator for the incident distributions, which are labelled Cases I, II, and III. For each of these, the incident beam is monoenergetic, $\beta = 0.1$, and the distributions over γ are, respectively, 1, $5(\gamma-0.8)$, 25 $(\gamma-0.8)^2$ in the interval $0.8 \leq \gamma \leq 1.0$, and zero

TABLE IV. Ratios of the total expected energy transmitted, E_t, to the incident energy, E_i, for the conditions of Table III.

a (cm)	A	I	II	III
0	1	1	1	1
2	2.05×10^{-1}	1.85×10^{-1}	1.97×10^{-1}	2.03×10^{-1}
4	4.14×10^{-2}	3.45×10^{-2}	3.86×10^{-2}	4.09×10^{-2}
6	8.34×10^{-3}	6.50×10^{-3}	7.63×10^{-3}	8.25×10^{-3}
8	1.69×10^{-3}	1.24×10^{-3}	1.52×10^{-3}	1.67×10^{-3}
10	3.42×10^{-4}	2.42×10^{-4}	3.04×10^{-4}	3.40×10^{-4}
12	6.95×10^{-5}	4.74×10^{-5}	6.10×10^{-5}	6.92×10^{-5}
14	1.42×10^{-5}	9.38×10^{-6}	1.23×10^{-5}	1.41×10^{-5}
16	2.89×10^{-6}	1.87×10^{-6}	2.50×10^{-6}	2.88×10^{-6}
18	5.93×10^{-7}	3.75×10^{-7}	5.08×10^{-7}	5.91×10^{-7}
20	1.22×10^{-7}	7.56×10^{-8}	1.04×10^{-7}	1.21×10^{-7}

elsewhere. This choice of angular distributions was motivated by several considerations. Some distribution of the incident beam over a finite range of γ is indicated for the practical reason that a monoangular entering beam adds greatly to the computational difficulties. On the other hand, an incident distribution with appreciable magnitude at or near $\gamma = 0$ would tend to increase the importance of the matrix $\|\mathbf{S}\|$, which is neglected. The incident distribution of Case I is precisely the distribution from an isotropic point source out of which radiation in a cone of half-angle 36° 52′ is accepted. The successive distributions of Case I, II, and III may be regarded as the first three elements of an infinite sequence of incident distributions which converges to the monoenergetic and monoangular beam ($\gamma = 1$, $\alpha = 10$) considered in Sec. II.

The thickness of the slab element, i.e., the "thin" slab associated with $\|\mathbf{O}\|$, has always been held at 2 cm. This thickness is less than 2 mean free paths, and reduces the contribution of the twice scattered beam to a few percent of the total. The ratio of the total number of photons transmitted to the number incident

TABLE V. Ratios of the total number of photons transmitted, N_t, to the number transmitted without scattering, N_u, for the conditions of Table III.

a (cm)	A	I	II	III
0	1.0	1.0	1.0	1.0
2	1.49	1.53	1.51	1.50
4	2.06	2.19	2.14	2.12
6	2.73	3.07	2.95	2.91
8	3.55	4.24	4.00	3.91
10	4.49	5.78	5.36	5.19
12	5.60	7.78	7.08	6.82
14	6.87	10.4	9.28	8.87
16	8.35	13.6	12.0	11.4
18	9.98	17.8	15.5	14.6
20	11.8	23.0	19.9	18.6

is given in Table III for thicknesses of uranium from 2 to 20 cm in 2 cm intervals. The expected energy transmitted is similarly tabulated in Table IV. It is clear that, for the sequence of Cases I, II, and III, the mean angle of the initial distribution with the normal to the slab decreases; and, therefore, the transmission should increase. One may examine the question as to how rapidly this sequence of cases is approaching the monoangular transmission values. For $\beta=0.1$, $\gamma=1.0$, and a total slab thickness of 20 cm of uranium, one has for the ratio of the number transmitted without scatter to the number incident, $N_0/N_i=\exp[-\mu_0 a]=2.89\times10^{-8}$. This ratio and Eqs. (13) give for the monoangular distribution

$$N_t/N_i=3.12\times10^{-7};\quad E_t/E_i=1.59\times10^{-7}.$$

These values compared with those of the sequences in Tables III and IV show slow convergence to the monoangular values. This same slow convergence is found in the unscattered transmission, which can be calculated simply and accurately. For 20 cm of uranium, the sequence of monoenergetic cases considered here gives for the unscattered transmitted number, N_u, and the unscattered transmitted energy, E_u, the successive values

$$N_u/N_i=E_u/E_i=7.36\times10^{-9};\quad 1.14\times10^{-8};\quad 1.40\times10^{-8}.$$

The limit value 2.89×10^{-8} indicates the convergence of

TABLE VI. Ratios of the total energy transmitted, E_t, to the energy transmitted without scattering, E_u, for the conditions of Table III.

a (cm)	A	I	II	III
0	1.0	1.0	1.0	1.0
2	1.31	1.28	1.27	1.26
4	1.65	1.61	1.59	1.58
6	2.05	2.03	1.98	1.96
8	2.53	2.57	2.47	2.43
10	3.08	3.25	3.08	3.01
12	3.72	4.11	3.84	3.73
14	4.45	5.18	4.78	4.61
16	5.24	6.53	5.94	5.69
18	6.16	8.20	7.36	7.02
20	7.18	10.3	9.12	8.63

TABLE VII. The mean energy in the transmitted beam, E_t/N_t, for the conditions of Table III.

a (cm)	A	I	II	III
0	8.10	10.0	10.0	10.0
2	7.05	8.36	8.39	8.39
4	6.45	7.36	7.42	7.43
6	6.03	6.63	6.72	6.73
8	5.71	6.07	6.18	6.21
10	5.46	5.63	5.74	5.80
12	5.27	5.28	5.42	5.47
14	5.12	5.01	5.15	5.20
16	4.99	4.79	4.92	4.98
18	4.88	4.61	4.74	4.80
20	4.80	4.46	4.59	4.64

the unscattered transmission is fully as slow as the convergence of the total transmission.

Tables V and VI summarize the values for the ratio of the total transmission to the unscattered transmission. These ratios express the transmission in a convenient manner. The unscattered transmission N_u and E_u (or N_0 and E_0 for the monoenergetic, monoangular initial distributions) are obtained by an elementary calculation which is subject to no computational inaccuracy; further, N_u and E_u give a rough order of magnitude of the transmission. One may compare the behavior of the sequence of values of N_t/N_u, E_t/E_u for Cases I, II, and III with the monoangular values of Sec. II. The values in Tables V and VI stand in the proper relationship with each other and with the limit. Again, the slow convergence of the sequence of angular distributions toward the values for the monoangular case is evident. It is worthy of note that the effects of an initial angular distribution, even though it is fairly sharp, are very evident in the trans-

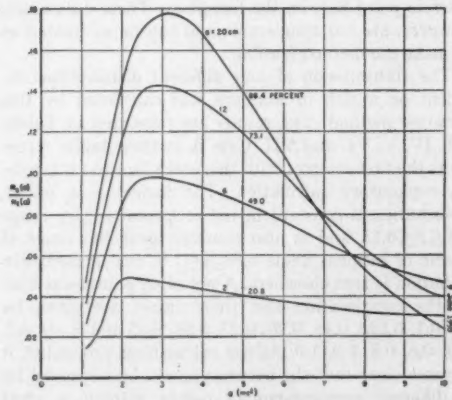

FIG. 3. The ratio of scattered transmitted photons $N_s(\alpha)$ to the total transmitted photons N_t is plotted as ordinate against the photon energy α in units of mc^2 for the incident distribution of Case III. The curves are given for various thicknesses, a, of plane slabs of uranium, and these curves are normalized so that the area under each curve equals the fraction of the total transmitted number which consists of scattered photons. These fractions are indicated as percentages on each curve.

mission values, and these effects persist as the angular distribution is sharpened. Another such effect is to be noted in the behavior of the average energy of the photons transmitted. These values are tabulated in Table VII. For 20 cm, these average photon energies for the sequence are in proper relationship with each other and with the limit value for 5 mc^2 for the mono-angular case.

The distributions for Case III of the scattered photons emerging from slabs of various thicknesses are shown in Fig. 3. For purposes of comparison, these distributions have been divided by the total number of photons transmitted for the given thickness. Therefore, the area under each distribution curve gives the percentage of the total transmission which comes from photons which suffered at least one collision. For slab

TABLE VIII. Ratios of the total number of photons transmitted, N_t, to the number transmitted without scattering, N_u, for various thicknesses, a, of plane slabs of lead. The four cases, A, I, II, III, represent the same incident distributions as were used to obtain the results of Table III.

a (cm)	A	I	II	III
0	1.0	1.0	1.0	1.0
3.5	1.54	1.59	1.56	1.55
7.0	2.19	2.34	2.29	2.26
10.5	2.98	3.39	3.24	3.19
14.0	3.96	4.8	4.5	4.4
17.5	5.1	6.7	6.2	6.0
21.0	6.5	9.3	8.4	8.1
24.5	8.1	12.7	11.3	10.7
28.0	10.0	17.1	14.9	14.1
31.5	12.2	22.6	19.6	18.4
35.0	14.6	30.2	25.8	24.0

thicknesses of 2, 6, 12, and 20 cm, these percentages are 20.8, 49.0, 73.1, and 88.4, respectively.

The results for uranium may be adjusted to give estimates for transmission through lead (Tables VIII and IX). The method follows closely the one used in Sec. II. It is clear from the discussion given in that section that one can write

$$\frac{N_t}{N_u}=\sum_{k=0}^{\infty}\frac{N_k}{N_u}=\sum_{k=0}^{\infty}(\nu a)^k I_k,$$

where I_k is the appropriate integral. The ratio of the absorption coefficient for uranium to that for lead, it will be remembered, is roughly 1.75 in the interval $1.0\leq\alpha\leq 10.0$. Therefore, I_k for a cm of uranium has approximately the same value for $1.75a$ cm of lead. However, because of the differences in the value of ν

TABLE IX. Ratios of the total expected energy, E_t, to the energy transmitted without scattering, E_u, for the conditions of Table VIII.

a (cm)	A	I	II	III
0	1.0	1.0	1.0	1.0
3.5	1.34	1.31	1.30	1.29
7.0	1.72	1.68	1.66	1.64
10.5	2.18	2.16	2.10	2.08
14.0	2.74	2.79	2.67	2.63
17.5	3.40	3.60	3.40	3.31
21.0	4.2	4.6	4.3	4.2
24.5	5.1	6.0	5.5	5.3
28.0	6.0	7.7	6.9	6.6
31.5	7.2	9.8	8.8	8.3
35.0	8.5	12.6	11.0	10.4

for lead and uranium, one must correct the kth term by multiplying it by the factor $(1.09)^k$. In Sec. II, where the first few terms in this sum were evaluated explicitly, this correction was straightforward; but here one is given only the sum. Suppose, however, one assumes that for a cm of uranium $N_k/N_u=K^k/k!$, as Eqs. (15a) and (15b) suggest. Then, if one selects K so that

$$\sum_{k=0}^{\infty}\frac{K^k}{k!}=e^K=\frac{N_t}{N_u},$$

one has for $1.75a$ cm of lead $N_t/N_u=e^{1.09K}$. The assumption basic to this easy transformation of results is probably not, in view of its purpose, too seriously in error, since the transformed result is not very sensitive to the manner in which N_k/N_u is distributed over the terms of the series. The greatest divergence from the assumption occurs for thin slabs; but for these, the first term, which needs none of this correction, gives most of the total transmission.

As a general remark concerning the tabulated values, the use of three significant figures might be taken as indicative of over-optimism regarding the accuracy of the computations, because of their extent and complexity. However, it is estimated that a numerical result from one matrix iteration is accurate to 2 percent or better. Since the error may be cumulative, it might be implied that 10 iterations, which carry the transmission through 20 cm of uranium, could have an error of 20 percent. Such an accumulation of errors cannot be dismissed merely by saying that it is improbable. However, the results of the various calculations support each other with notable consistency; and this behavior has led the writers to the view that the results and the procedure have very acceptable accuracy.

Interaction Between the *d* Shells in the Transition Metals*

C. ZENER
Institute for the Study of Metals, University of Chicago, Chicago, Illinois
(Received October 9, 1950)

It is assumed (1) that the interaction between the incomplete *d* shells of the transition elements is insufficient to disrupt the coupling between the *d* electrons in the same shells, and (2) that the exchange interaction between adjacent *d* shells always has the same sign irrespective of distance of separation. The direct interaction between adjacent *d* shells then invariably leads to a tendency for an antiferromagnetic alignment of *d* spins. The body-centered cubic structure of the transition metals V, Cr, Cb, Mo, Ta, and W is thereby interpreted, as well as more complex lattices of certain alloys. It is demonstrated that the spin coupling between the incomplete *d* shells and the conduction electrons leads to a tendency for a ferromagnetic alignment of *d* spins. The occurrence of ferromagnetism is thereby interpreted in a much more straightforward manner than through the *ad hoc* assumption of a reversal in sign of the exchange integral. The occurrence of antiferromagnetism and of ferromagnetism in various systems is readily understood, and certain simple rules are deduced for deciding which type of magnetism will occur in particular alloys.

I. INTRODUCTION

A REVIEW of the crystal structure and of the magnetism of the transition elements has led the author to very simple principles which appear to govern the interaction between the incomplete *d* shells of neighboring atoms.

The first principle is that, at least in the fourth column (V, Cb, Ta) and beyond, the spin correlation between the electrons in the incomplete *d* shell of a single atom is essentially the same when the atom forms part of a solid as when it is isolated in the gaseous state. In the isolated atom the lowest energy state is given by that electron configuration in which the incomplete *d* shell has the highest net electron spin, i.e., in which all unpaired electrons have spins pointing in the same direction. As has been shown by Slater,[1] the physical basis for this rule of highest net electron spin is that electrons with similar spin automatically avoid close proximity. According to this first principle the incomplete *d* shell of an atom in a metal also has the highest net electron spin consistent with the number of electrons therein.

The second principle is that the exchange integral between *d* shells of adjacent atoms has always the same sign as in the H_2 molecule. The direct interaction between *d* shells of adjacent atoms is thus of such a sign as tends, in all circumstances, to lead to an antiferromagnetic configuration of the *d* shell spins. This principle is contradictory to the usual *ad hoc* assumption that within a certain range of the ratio (radius of *d* shell/closest distance of approach) the exchange integral is of reversed sign.

The third principle is that the spin of an incomplete *d* shell is strongly coupled to the spin of the conduction electrons. This coupling tends to align the spins of the incomplete *d* shells in a ferromagnetic manner. It is only when this indirect coupling dominates over the direct coupling between adjacent *d* shells that ferromagnetism is possible.

In the present paper no attempt will be made to deduce these principles from theory. As has been pointed out by Hartree,[2] the electron distribution in the outer regions of the *d* shells is extremely sensitive to small changes in the potential. A theoretical deduction of the interaction between *d* shells will therefore be very difficult. The purpose of the present paper is to point out the many diverse observations of structure and of magnetic properties which may be correlated by these three principles. They will, however, be supported by considerations of orders of magnitude.

The physical basis for the first principle, the retention of the spin coupling of the electrons in an incomplete *d* shell, must reside in the large magnitude of this coupling compared with the band width of the *d* shell. In Cr 2.5 ev (58,000 cal/mole) are required to reverse the spins of two of the five electrons in the 3*d* shell.[3] This coupling is smaller than the computed *d* band width in[4] Fe and in[5] W. However, when similar computations are carried out by the Hartree-Fock method under the assumption of highest net electron spin, the computed radius of the *d* shell must automatically contract, for the correlations thereby introduced will allow the *d* electrons to come closer to the nucleus without at the same time coming closer to one another. Such a contraction in radius will of course lower the computed band width.

The second principle has a purely empirical basis. Heisenberg[6] and others have demonstrated that it is not unreasonable to expect the exchange integral to reverse sign as the quantum number increases. However, in no cases other than in the ferromagnetism of the metals in the first transition period have effects been observed which are attributable to a reversal in the sign of this integral. Not even an attempt at a theoretical justi-

* This research has been partially supported by the ONR.
[1] J. C. Slater, Phys. Rev. 34, 1293 (1929).
[2] D. R. Hartree, Proc. Roy. Soc. 141, 282 (1950).
[3] R. F. Bacher and S. Goudsmit, *Atomic Energy States* (McGraw-Hill Book Company, Inc., New York, 1932).
[4] J. C. Slater, Phys. Rev. 49, 537 (1936).
[5] M. F. Manning and M. I. Chodorow, Phys. Rev. 56, 787 (1939).
[6] W. Heisenberg, Z. Physik 49, 619 (1928).

TABLE I. Correlation of binding energy with electronic structure of isolated atoms.

Ni($3d^{8}4s^{2}$) 98,000*	Cu($3d^{10}4s$) 82,000	Zn($3d^{10}4s^{2}$) 31,000
Pd($4d^{10}$)	Ag($4d^{10}5s$) 69,000	Cd($4d^{10}5s^{2}$) 27,000
Pt($5d^{9}6s$) 125,000	Au($5d^{10}6s$) 91,000	Hg($5d^{10}6s^{2}$) 14,000

* Latent heat of vaporization in cal/mole.

fication can be given for the usual assumption for a reversal in sign restricted to a given range of atomic separation. The persistence of this concept of a reversal in the sign of the exchange integral is a consequence solely of the absence of a better theory of ferromagnetism.

The third principle is based upon a firm foundation. In the isolated atoms a single electron in the outer s shell is always coupled fairly strongly to the spin of the inner incomplete d shell, the lowest energy always corresponding to the spin of the s electron being parallel to that of the d shell. Thus in the first transition group this coupling varies from a maximum of 0.93 ev for Mn to a minimum[3] of 0.39 ev for Ni. This coupling is proportional to the density of the s electron in that region of the atom where the radial charge density of the d electrons is a maximum. Now in the isolated atom the outer s electron spends only about one-third of its time within the radius r_a associated with the atomic volume in the condensed state. As the atoms condense from a gaseous to a metallic state the s electrons will therefore increase by about a factor of three the time spent in the vicinity of the d electrons, and hence their coupling with these electrons will be increased by the same factor.

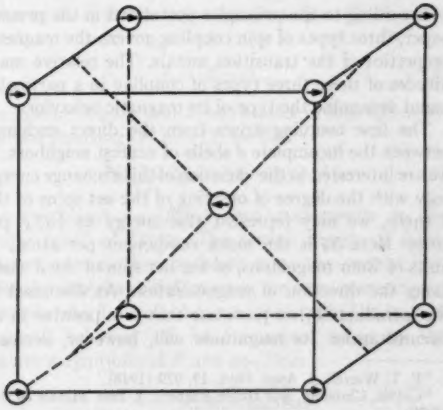

FIG. 1. Postulated antiferromagnetic spin arrangement in V, Cr, Cb, Mo, Ta, W.

TABLE II. Crystal structure of the transition metals.

Ca	Sc	Ti	V	Cr	Mn	Fe	Co	Ni
fcc hcp	fcc hcp	bcc hcp	bcc	bcc	4 types	fcc bcc	fcc hcp	fcc
Cr	Y	Zr	Cb	Mo	Ma	Ru	Rh	Pd
fcc	hcp	bcc hcp	bcc	bcc	*	hcp	fcc	fcc
Yb	Lu	Hf	Ta	W	Re	Os	Ir	Pt
*	hcp	hcp	bcc	bcc	hcp	hcp	fcc	fcc

* Structure unknown.

II. CRYSTAL STRUCTURE

According to the first two principles, the direct exchange interaction tends to align the spins of the incomplete d shell in an antiferromagnetic manner, and this tendency will be stronger the larger the spin of the d shells. A rough but not exact correlation exists between the magnitude of the spins of the d shell of an atom in the isolated gaseous state and in the condensed solid state. Some transition atoms have two outer s electrons when isolated. We can be quite sure from the data in Table I that two electrons will not stay in the outer shell when these atoms are condensed. The great drop in the heat of vaporization in passing from Cu to Zn, from Ag to Cd, and from Au to Hg is due primarily to the inability of the second s electron in the latter atoms to be demoted to an inner d shell and thereby avoid the necessity of acquiring the large Fermi kinetic energy associated with the second conduction electron per atom. If we tentatively assume that one electron remains in the outer s state, or more correctly in the conduction band, we find that Cr, Mo, and W will have 5 electrons in the incomplete d shell. This is just the number which will give the greatest d shell spin. Hence of all the transition elements, Cr, Mo, and W will have the greatest tendency to form a lattice structure in which all nearest neighbors have anti-parallel spins. The most common crystal lattices of the elements are fcc (face-centered cubic) and hcp (hexagonal close-packed). No arrangement of spins on these two types of lattices can satisfy the requirement that all nearest neighbors have antiparallel spins, for some of the nearest neighbors of a particular atom are nearest neighbors of one another. As may be seen in Fig. 1 this requirement is, however, satisfied by the bcc (body-centered cubic) lattice in which Cr, Mo, and W do in fact crystallize. While W may be obtained by electrolysis in another modification, this element has no stable allotropic modification.

From the value of the saturation magnetization in Fe, Co, and Ni it is commonly accepted that the conduction band has less than one electron per atom, the precise number being 0.2, 0.7, 0.6 for the above three elements, respectively. If we generalize these findings and assume that the number of electrons in the conduction band is always less than unity for the transition metals, we arrive at the conclusion that next to Cr, Mo,

and W the transition elements which have the greatest number of unpaired electrons are V, Cb, and Ta. The observation that these three metals likewise crystallize in the bcc lattice, with no stable allotropic form, is a strong vindication of our postulated principles. No transition metals other than these six are stable only in the bcc lattice. As seen from Table II, Ti, Zr, and Fe also exist as bcc lattices, but they have other stable modifications.

The unstable modification of W, formed by electrolysis, has the structure illustrated in Fig. 2. Here one-fourth of the atoms, those occupying the bcc lattice positions, have no close neighbors. The remaining W atoms are closely packed along linear rows. Exchange repulsion within these rows is presumably avoided by the spins of the d shells alternating in sign. This same lattice type, A15, has been found elsewhere only in V_3Si and in Cr_3Si.* In these silicides the Si atoms occupy the bcc lattice positions, while the V and Cr atoms occur only in the close packed rows. The limitation of the A15 structure to the transition elements in the fourth and fifth columns is again a strong confirmation of our postulated principles.

Many ordered d spin arrangements will at least partially minimize the exchange repulsion between the d shells. Thus suppose that alternate (001) planes in a fcc lattice had d shell spins of alternating direction, as illustrated in Fig. 3. Then each d shell would have a full repulsive interaction with only four of its twelve nearest neighbors, leading to a lower energy than given by a random distribution of spin. Since the exchange repulsion will be between nearest neighbors in the same (001) plane, the ordered spin arrangement postulated in Fig. 3 would lead to a tetragonal lattice, the c/a ratio being less than unity. The γ-phase of Mn has all the earmarks of being such an ordered phase. As quenched

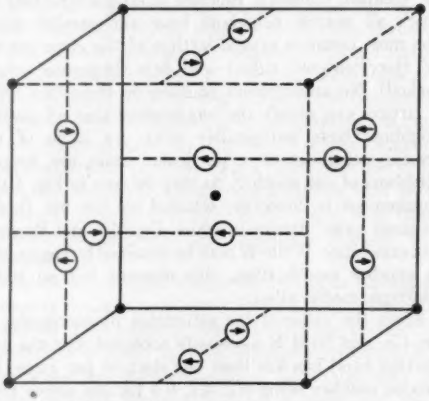

FIG. 2. Postulated antiferromagnetic spin arrangement in V_3Si, Cr_3Si: ● silicon atom. ○ transition metal atom.

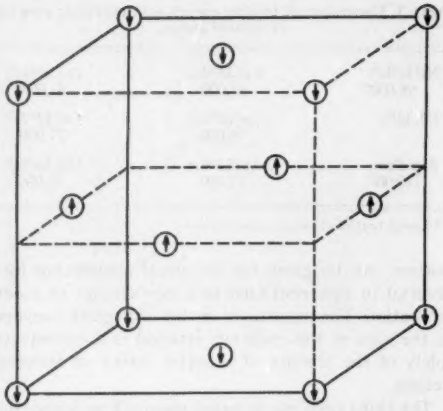

FIG. 3. Postulated antiferromagnetic spin arrangement in fct Mn.

its structure is face-centered tetragonal, with a c/a ratio of 0.94. Since the high temperature γ-phase is very difficult to retain in pure manganese, investigations are usually carried out with deliberate additions of some impurity, such as Cu. Worrell[7] has found that such alloys (containing about 12 percent Cu) when quenched have a microstructure apparently consisting of finely spaced twins. A similar twin-like microstructure has later been reported[8] in quenched Mn with additions of Cr. The author[9] has interpreted this structure as indicating that at the higher temperature the lattice was cubic, and became tetragonal only on cooling. Due to the constraints of neighboring grains, a given grain can become tetragonal only if it becomes heavily twinned. Only in this manner can the grains avoid a large free energy of elastic strain.

III. MAGNETIC PROPERTIES

According to the principles postulated in the present paper, three types of spin coupling govern the magnetic properties of the transition metals. The relative magnitudes of these three types of coupling in a particular metal determine the type of its magnetic behavior.

The first coupling arises from the direct exchange between the incomplete d shells of nearest neighbors. If we are interested in the variation of this exchange energy only with the degree of ordering of the net spins of the d shells, we may represent this energy as $\frac{1}{2}\alpha S_d^2$ per atom. Here S_d is the mean component per atom, in units of Bohr magnetons, of the net spin of the d shells along the direction of magnetization. As discussed in the introduction, we postulate that α is positive in all circumstances. Its magnitude will, however, decrease

* *Note added in proof:* A further example of the A15 structure is Mo_3Si (Templeton and Dauben, Acta Cryst. 3, 261 (1950)).

[7] F. T. Worrell, J. Appl. Phys. 19, 929 (1948).
[8] Carlile, Christian, and Hume-Rothery, J. Inst. Metals 76, 169 (1949).
[9] C. Zener, *Elasticity and Anelasticity of Metals* (University of Chicago Press, Chicago, 1948), pp. 160–163.

rapidly with a decreasing amount of overlap of the d shells of adjacent atoms. Its magnitude will therefore be smallest for those elements in the upper right corner of Table II.

The second spin coupling arises from the exchange between the conduction electrons and the inner d electrons. This coupling energy we may represent as $-\beta S_d S_c$ per atom. Here S_c is the net magnetization of the conduction electrons, expressed in units of Bohr magnetons per atom. The coefficient β is always positive. In the introduction we have seen that the value of β can be estimated from spectroscopic data of the isolated atoms, and is of the order of magnitude of one electron volt.

The third spin coupling arises from the Fermi kinetic energy of the conduction electrons. This kinetic energy is a minimum when the same number of conduction electrons have spins pointing along as pointing against the direction of magnetization. Under these conditions S_c is zero. Since the increase in Fermi kinetic energy associated with an unbalanced distribution of the conduction electrons must be an even function of S_c, we may represent this increase in kinetic energy by $\frac{1}{2}\gamma S_c^2$ per atom provided the inbalance is small. The coefficient γ may be expressed in terms of the kinetic energy at the top of the Fermi distribution ϵ, and in terms of the number of conduction electrons per atom, n. This relation is

$$\gamma = 2\epsilon/3n.$$

The magnitude of γ is several electron volts.

Upon combining the above three types of spin coupling, we obtain for the spin energy

$$E_{\text{spin}} = \tfrac{1}{2}\alpha S_d^2 - \beta S_d S_c + \tfrac{1}{2}\gamma S_c^2. \tag{1}$$

Since the contribution of the conduction electrons to the entropy of the system is negligible, the equilibrium value of S_c is that which minimizes E_{spin}. We thereby obtain

$$S_c = (\beta/\gamma) S_d. \tag{2}$$

We thus anticipate that S_c has a value of several tenths.

Upon inserting (2) into (1) we find

$$E_{\text{spin}} = \tfrac{1}{2}\{\alpha - (\beta^2/\gamma)\} S_d^2. \tag{3}$$

The coefficient $\{\alpha - \beta^2/\gamma\}$ thus corresponds to the "inner field" of Weiss. The formal theory of ferromagnetism may thus be based upon the present postulated principles as well as upon the more conventional concepts which also lead to an inner field. The type of magnetic behavior will be determined solely by the relative magnitudes of β^2 and $\alpha\gamma$. Thus

$$\beta^2 \gtrless \alpha\gamma \text{ for } \begin{matrix} \text{ferromagnetism} \\ \text{antiferromagnetism.} \end{matrix} \tag{4}$$

Since it is not the purpose of the present paper to develop the quantitative theory of ferromagnetism, it will be sufficient to note that the ferromagnetic coupling term $\frac{1}{2}(\beta^2/\gamma)S_d^2$ is of the right order of magnitude. From the above estimates we deduce that this coupling energy is of the order of magnitude of a tenth of an ev per atom while the observed magnetization energies of Fe, Co, and Ni are 0.07, 0.05, and 0.01 ev per atom, respectively.

The value of our theory in its present qualitative stage lies in its simple interpretation of the various observed types of magnetic properties without the aid of *ad hoc* hypotheses, and of its power in predicting the magnetic properties of systems as yet not investigated. Ferromagnetism will be observed in all systems for which the first inequality of (4) is satisfied, i.e., in which the neighboring incomplete d shells are sufficiently far apart so that the indirect ferromagnetic coupling through the conduction electrons dominates over the direct antiferromagnetic coupling. Among the pure transition metals this condition is most likely to occur in the last elements of the first transition group. An interesting possibility occurs in alloys. Suppose we have a material in which transition atoms are dissolved in a metal or alloy otherwise containing only completed inner shells, and that the transition atoms have ordered positions such that they are not nearest neighbors of one another. In such an alloy there would be no direct exchange between incomplete d shells. The ferromagnetic coupling via the conduction electron must, therefore, give rise to ferromagnetism at a sufficiently low temperature. The Heusler alloys are one example of the above postulated structure. Here the transition atoms, namely, Mn, occupy ordered positions which are next next nearest neighbors of one another.[10] The other constitutents of the Heusler alloys have only completed inner shells. The ferromagnetism of the Heusler alloys disappears upon disordering.[11] While in the ordered lattice no Mn atom has another Mn atom as nearest neighbor, or even as a next nearest neighbor, in the disordered bcc lattice each Mn atom has on the average two other Mn atoms as nearest neighbors. The resulting direct exchange coupling must, therefore, considerably reduce the ferromagnetic Curie temperature.

A large distance of separation between incomplete d shells insures ferromagnetic behavior only when conduction electrons are present to provide the necessary ferromagnetic coupling. In $MnCl_2$ the neighboring Mn ions are comparatively far apart, 40 percent further than in metallic Mn. $MnCl_2$ does not, however, have any conduction electrons. The small direct exchange, therefore, gives rise to the observed antiferromagnetism. The Mn ions occur in linear chains, so the antiferromagnetic structure may be obtained simply by alter-

[10] C. S. Barrett, *Structure of Metals* (McGraw-Hill Book Company, Inc., New York, 1943), p. 234.

[11] The author is indebted to Professor C. S. Smith for this observation.

nating spins along the chains,[12] just as in the case of V_3Si, Cr_3Si and in the β-phase of W.

The antiferromagnetic direct coupling between d shells, and the ferromagnetic indirect coupling via the conduction electrons, are not the only possible types of spin coupling between the incomplete d shells. Another indirect spin coupling, called superexchange, is possible through intervening nonmagnetic atoms. This coupling has recently been discussed in full by Anderson.[13]

[12] The author is indebted to Professor W. Stout for this observation.

[13] P. W. Anderson, Phys. Rev. 79, 350 and 705 (1950).

PHYSICAL REVIEW VOLUME 81, NUMBER 3 FEBRUARY 1, 1951

Pressure Dependence of Second Sound Velocity in Liquid Helium. II*

R. D. MAURER AND MELVIN A. HERLIN
Research Laboratory of Electronics, Massachusetts Institute of Technology, Cambridge, Massachusetts*

(Received October 13, 1950)

The velocity of second sound as a function of pressure and temperature has been measured to 0.95°K by a pulse method. The quantitative dependence of the rise in velocity upon pressure is found to support the role of the phonons in contributing to the normal fluid flow alone.

I. INTRODUCTION

THE properties of liquid He II have been explained most satisfactorily by the "two fluid" concept advanced in the theories of Tisza[1] and Landau.[2] Each theory regarded liquid helium as composed of a "normal fluid" fraction and a "superfluid" fraction, although the origin of these two fluids was assigned to different molecular mechanisms. In the temperature range just below the lambda-point Tisza, following the suggestion of London, considered the transverse excitations to be similar to those of a Bose-Einstein gas, appropriately modified by the liquid state. Experiments showing no superfluidity in He^3 have borne out this view, as opposed to the roton model of Landau. On the other hand, Landau considered the longitudinal excitations, the Debye phonons, as a component of the normal fluid flow only, rather than as associated with the fluid as a whole, which was Tisza's view. The phonons are masked by the Bose-Einstein excitations at higher temperatures, but below about 1.1°K their effect is evident. The rise in second sound velocity [3–5] at low temperature and the sustained existence of the waves without undue attenuation tends to bear out the hypothesis that the new type of excitation predominant below 1°K is associated with the normal fluid flow only, and not with the superfluid. The present experiment takes advantage of the large pressure dependence of first sound velocity in liquid helium to investigate whether this low temperature excitation is indeed a phonon effect.

II. EXPERIMENT

Second sound is a type of wave motion most easily excited by the heating of liquid helium. Pellam has developed a pulse method [4,6] which was used by the authors to measure the velocity to below 1°K at vapor pressure.[3] Peshkov has created standing waves to determine the velocity at vapor pressure[5] down to 1° and at higher pressures[7] down to 1.3°.

A pulse method of exciting second sound similar to that formerly used in this work[3,6] was employed again. The chief innovation was the installation of a delay line in the timing mechanism. This permitted a view of the pulse on a faster, continuous sweep and hence a more accurate determination of its leading edge. A DuMont 246 oscillograph was used to trigger the pulse generator and to actuate the delay line. The pulse generator excited the carbon resistor of the second sound chamber. Another carbon resistor, acting as a resistance thermometer, received the second sound pulse, which was amplified and fed into the vertical deflection plates of a second 246D oscillograph. This last oscillograph was triggered by the delay line. The movable marker of the receiver oscillograph could be adjusted on the sweep so that it coincided with the edge of the pulse. By reading the marker dial and by knowing the delay, one could obtain the transit time for the pulse. The capacitative pick-up within the Dewar from the transmitting pulse could be amplified easily to give a sharp leading edge when viewed on the final oscillograph. In doing this, we could not detect any instrumental delay caused by the timing system.

The second sound chamber itself was sealed with solder for immersion in a liquid helium bath. Inside the chamber a thin sleeve separated the carbon resistors and determined the fixed path of 4.23 cm. Four capillaries with an inner diameter of 0.020 in. led to the chamber. Two of these acted as electrical shields for the wires while the other two were pressure lines, one to

[1] L. Tisza, Phys. Rev. 72, 838 (1947).
[2] L. Landau, J. Phys. USSR 5, 71 (1941).
[3] R. D. Maurer and M. A. Herlin, Phys. Rev. 76, 948 (1949).
[4] J. R. Pellam and R. B. Scott, Phys. Rev. 76, 869 (1949).
[5] V. Peshkov, J. Phys. USSR 10, 389 (1946); JETP USSR 18, 1951 (1948).
[6] J. R. Pellam, Phys. Rev. 75, 1183 (1949).
[7] V. Peshkov and K. N. Zinovyeva, JETP USSR 18, 438 (1948).

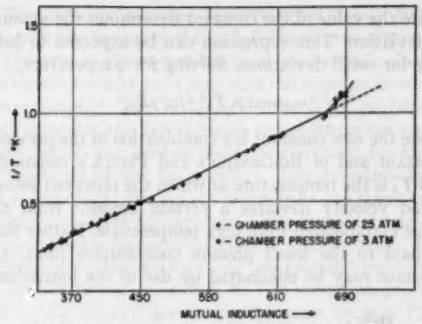

FIG. 1. Plot of the mutual inductance of the salt in the dummy chamber *versus* the reciprocal of the temperature as obtained from McLeod gauge readings. Values were taken with the liquid helium in the chamber at two different pressures. The extrapolated broken line gives the true temperature in terms of that obtained from McLeod gauge readings.

condense in helium gas from a tank and the other to observe pressure equilibrium with a check gauge. Liquid helium exists under a temperature gradient in the capillaries so that the heat leak from the lambda-temperature to the chamber is limited only by the inner diameter. The size of these pressure capillaries was a compromise between this heat leak and the persistent clogging of the line by frozen materials. The pressure values of the experiment were determined on the input side by an Ashcroft Laboratory test gauge. A Distillation Products MB200 diffusion pump with three Kinney VSD forepumps was used to remove vapor from the liquid helium bath.

Temperature measurements were made with a McLeod gauge through a tube in the pumping line above the Dewar arrangement as described formerly.[3] The equivalence of temperatures obtained from the McLeod gauge and those inside the chamber was established by constructing a dummy chamber of the same dimensions as the real one but filled with iron ammonium alum. Liquid helium under pressure was supplied to this chamber. A mutual inductance bridge was used to measure the relative paramagnetic susceptibility of the salt at different McLeod gauge values and at two different chamber pressures. The susceptibility of the salt, and hence the mutual inductance, varies as $1/T$. Figure 1 shows that the mutual inductance gives a straight line, except at low temperatures, when plotted against this variable obtained from the McLeod values. The deviation below 1° is attributed to the pumping pressure drop from the bath as observed previously[3] and is not due to any radical change in heat conductivity of the helium in the capillaries. The data below 1° were corrected from this curve.

III. RESULTS AND CONCLUSIONS

The data for the second sound velocity as a function of temperature and pressure are shown in Fig. 2. They agree, to within experimental error, with the measurements down to 1.3°K by Peshkov.[7] The velocity of second sound along the vapor pressure line as previously reported[3] was remeasured with the present apparatus and is also shown. The maximum deviation of the points is ±1 percent from the curves drawn through them.

Landau's proposal that the phonons contribute to the normal fluid flow implies that at the absolute zero of temperature the second sound velocity must approach the value $c_1/\sqrt{3}$, where c_1 is the velocity of ordinary (first) sound.[2] The value of c_1 at the vapor pressure is

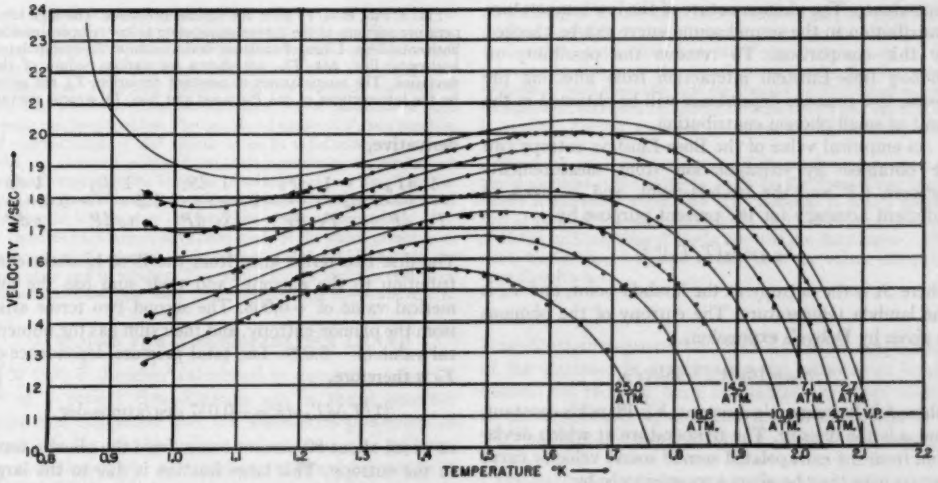

FIG. 2. The velocity of second sound as a function of temperature and pressure. Experimental points for the vapor pressure curve are not shown.

about 250 m/sec, which is an order of magnitude larger than the velocity of second sound. The second sound velocity must therefore rise rapidly as the temperature is lowered. The first sound velocity increases with pressure, so that the second sound curves at various pressures must cross somewhere in the temperature region below 0.95°K, if they are to arrive at Landau's value of velocity.

It has been found, however, that a computation based on a linear superposition of the terms giving the entropy and normal fluid fraction for the Bose-Einstein and phonon contributions to the excitations does not agree quantitatively with the observed velocity. The experimental curve shows no indication of the phonon term down to 1.2°K, but is rising rapidly at 1.0°. A phonon term simply added to the Bose-Einstein term extrapolated from higher temperature does not show an appreciable rise until about 0.6°. Landau gets the rise at 1° by using a roton expression which decreases more rapidly (exponentially instead of algebraically), but the phonon term is then too large in comparison to be absent at 1.2° as observed. The suddenness of the onset of the phonon contribution below 1.2° suggests the possibility that an interaction between the Bose-Einstein excitations and the phonons is removing the former rapidly as the latter becomes sufficiently large in comparison.

Nevertheless, the temperature at which this rise must begin corresponds to the point at which the entropy of the phonons begins to be of the same order of magnitude as the entropy of the Bose-Einstein excitations as the temperature is lowered. The pressure dependence of this temperature can be computed from the known pressure dependence of the first sound velocity, and compared with the observed pressure dependence. The phonon nature of the low temperature contribution to the second sound curve can be checked by this comparison. To remove the possibility of phonon Bose-Einstein interaction from affecting the result, this pressure dependence will be obtained in the limit of small phonon contribution.

An empirical value of the Bose-Einstein entropy can be obtained by extrapolation from measurements between 1.2° and the lambda-point, and is given to sufficient accuracy for the present purpose by,

$$S_{BE}=S_\lambda(T/T_\lambda)^{5.5},$$

where S_λ is the entropy at the lambda point, and T_λ is the lambda temperature. The entropy of the phonons is given by Debye's expression,

$$S_{ph}=16\pi^5k^4T^3/45h^3c_1^3\rho,$$

where k is Boltzmann's constant, h is Planck's constant, and ρ is the density. The temperature at which deviation from the extrapolated second sound velocity curve occurs may then be given approximately by,

$$S_{ph}=\text{const}\times S_{BE},$$

where the value of the constant determines the amount of deviation. This expression can be expected to hold only for small deviations. Solving for temperature,

$$T_d^{2.5}=\text{const}\times T_\lambda^{5.5}/c_1^3\rho S_\lambda,$$

where the new constant is a combination of the previous constant and of Boltzmann's and Planck's constants, and T_d is the temperature at which the observed second sound velocity deviates a certain amount from the value extrapolated from high temperature. Rather than to pass to the small phonon contribution limit, the constant may be eliminated by use of the logarithmic

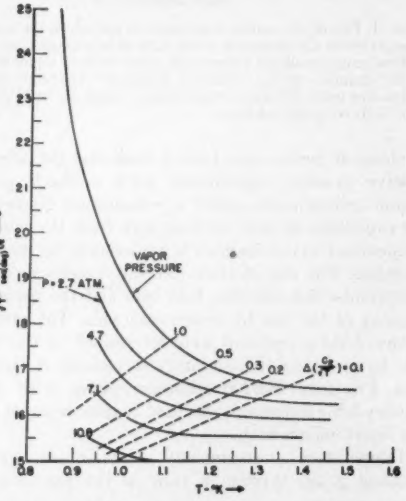

FIG. 3. Plot of c_2/T^3 *vs.* T for various pressures. The high temperature portions of the curves extrapolate to low temperatures as horizontal lines. Lines, of constant deviation from the extrapolated horizontal line, $\Delta(c_2/T^3)$, are shown for various values of the deviation. The temperatures of constant deviation, T_d, are given by the intersections of the $P=$const and $\Delta(c_2/T^3)=$const curves.

derivative,

$$\frac{1}{T_d}\frac{dT_d}{dP}=2.2\frac{1}{T_\lambda}\frac{dT_\lambda}{dP}-0.4\frac{1}{S_\lambda}\frac{dS_\lambda}{dP}-1.2\frac{1}{c_0}\frac{dc_1}{dP}-0.4\frac{1}{\rho}\frac{d\rho}{dP}.$$

The first two terms arise from the Bose-Einstein contribution to the entropy, and their sum has the numerical value of -0.008. The second two terms arise from the phonon entropy, and their sum has the numerical value of -0.029. The total pressure dependence of T_d is therefore,

$$(1/T_d)dT_d/dP=-0.037 \text{ deg/atmos-deg},$$

of which about 80 percent comes from the phonon term in the entropy. This large fraction is due to the large pressure dependence of first sound velocity in liquid helium.

The observed pressure dependence of T_d can be obtained from the curves of Fig. 3. If the phonon term were not present in the expression for second sound velocity, the velocity would go to zero with the square root of the temperature.[1,2] The ratio c_2/T^3 therefore exhibits a horizontal straight line at higher temperature but somewhat below the lambda-point, which may be easily extrapolated to low temperature. The deviation from the extrapolated line is then taken from the rising part of the curve at low temperature. Lines of constant deviation are shown for various values of the deviation. The corresponding values of dT_d/dP are plotted against the amount of deviation in Fig. 4. The values of dT_d/dP and $(1/T_d)\ dT_d/dP$ are nearly the same because T_d is near 1°K. The extrapolated value at zero deviation is in good agreement with the value computed above.

This agreement supports the hypothesis that the phonons contribute to the normal fraction of fluid only and are responsible for the rise of second sound velocity at low temperature. The phonons do not, however, combine linearly with the Bose-Einstein excitations, unless the Bose-Einstein spectrum is greatly different from what has been assumed heretofore.

The authors are indebted to Messrs. R. P. Cavileer and W. B. Wilbur for the manufacture of liquid helium and to Mr. A. R. Sears for assistance with the electronics. Messrs. H. H. Kolm and E. H. Jacobson contributed notably to the early phases of the experiment.

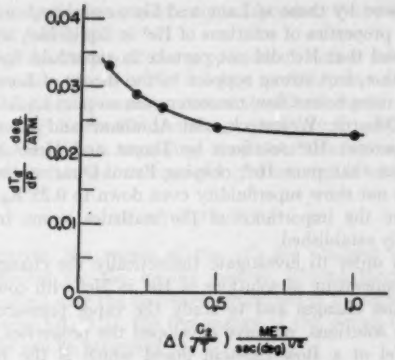

FIG. 4. Pressure derivative of the temperature of constant deviation, (dT_d/dP), as a function of the amount of deviation, $\Delta(c_2/T^3)$, taken from Fig. 3. Since T_d is near 1°K, dT_d/dP is nearly the same as $(1/T_d)dT_d/dP$. The value expected from the phonon contribution to the normal fluid flow at small deviations is about 0.037.

PHYSICAL REVIEW VOLUME 81, NUMBER 3 FEBRUARY 1, 1951

A Contribution to the Theory of Bose-Einstein Liquids

C. V. HEER AND J. G. DAUNT
Mendenhall Laboratory, Ohio State University, Columbus, Ohio

(Received June 29, 1950)

Smoothed potential models for liquid He^4 and liquid He^3 in which each are considered as ideal Bose-Einstein and Fermi-Dirac gases situated in potential wells of potential $-\chi_4^0$ and $-\chi_3^0$, respectively, are considered. It is shown that the degeneracy temperature, T_0 of pure liquid He^4 on this model can be deduced and that the λ-transition temperatures, T_λ, of solutions of such liquids can be calculated. The calculated values of T_λ as a function of concentration of He^3 appear to be in satisfactory agreement with the observed values. From these considerations, predictions are made regarding the behavior of solutions of two Bose-Einstein liquids; e.g., He^6 in He^4. It is shown, moreover, that solutions of such model liquids obey the third law of thermodynamics.

Detailed calculations have been made of the vapor pressures of such smoothed potential liquid models of He^4 and He^3 both in the pure state and in solution. The results for the vapor pressures of the solutions indicate that, in the temperature range above 1°K for solutions of not too high concentration of He^3, the total vapor pressure would be higher than that given by Raoult's law for temperatures both above and below the λ-temperature of the solution. In this way the experimental results for the vapor pressure of such solutions, first emphasized by Taconis, *et al.*, can be explained, and good agreement between theory and experiment is evident. Explicit formulas are given for further numerical evaluation.

Finally the results of calculations of the total vapor pressure of model solutions of He^3 in He^4 in which the He^3 Fermi-Dirac liquid model is extremely degenerate are discussed. It would appear that at very low temperatures (<0.5°K) the partial vapor pressure of He^3 in such solutions of He^3 in He^4 and the distribution coefficient, C_v/C_L should become *smaller* than the values calculable from Raoult's law.

I. MODEL FOR A BOSE-EINSTEIN LIQUID

IN 1938 F. London[1] calculated in detail the behavior of a perfect Bose-Einstein gas in the degenerate state and suggested that the anomalous properties of liquid He II could be understood, at least qualitatively, by considering the λ-transition in liquid helium as a Bose-Einstein degeneration. Such a possible significance of the statistics in determining the behavior of liquid helium has recently been the subject of study owing to the availability of the rarer isotope of helium, He^3. The preliminary experiments of Daunt and others,[2]

[1] F. London, Nature **141**, 643 (1938); Phys. Rev. **54**, 947 (1938); J. Phys. Chem. **43**, 1 (1939).

[2] Daunt, Probst, Johnston, Aldrich, and Nier, Phys. Rev. **72**, 502 (1947). Daunt, Probst, and Johnston, J. Chem. Phys. **15**, 759 (1947).

followed by those of Lane and his co-workers,[3] on the flow properties of solutions of He^3 in liquid He^4, which showed that He^3 did not partake in superfluid flow in solution, lent strong support to the theory of London. The more recent flow measurements on pure liquid He^3 by Osborne, Weinstock, and Abraham[4] and those on 90 percent He^3 solutions by Daunt and Heer[5] have shown that pure He^3, obeying Fermi-Dirac statistics, does not show superfluidity even down to 0.25°K, and hence the importance of the statistics seems to be firmly established.

In order to investigate theoretically the change of λ-temperature of solutions of He^3 in He^4 with concentration changes and to study the vapor pressures of such solutions, we have developed the properties of a model of a Bose-Einstein liquid which is the Bose-Einstein analog of a free-electron gas in a metal. The model adopted here treats tentatively liquid He^4 as a perfect Bose-Einstein gas in a potential well, of potential χ_4^0. This smoothed potential model assumes that the volume of the liquid, V, can be written as

$$V=NV_4^0, \tag{1.1}$$

where N is the number of particles and V_4^0 the atomic volume per atom. The free energy of such a liquid can be written as

$$F=-kTZ+N_4kT\ln\lambda_4, \tag{1.2}$$

where Z is given by:[6]

$$Z=\sum_r \tilde{\omega}_r \ln[1-\lambda_4\exp(-\epsilon_r/kT)]^{-1},$$

where the energy ϵ is written as $\epsilon=(p^2/2m_4)-\chi_4^0$ and where λ_4 is determined by the general condition for maintaining a constant number of particles, as discussed below.

For the situation below the condensation temperature, T_0, of the Bose-Einstein system, the term Z can be written in two parts, as has been pointed out by London,[1] the first of which concerns the number of particles which are "condensed." One can therefore write the free energy, F_4, as

$$F_4=-kT\Big\{-\ln[1-\lambda_4\exp(\chi_4^0/kT)]$$
$$-N_4\ln\lambda_4-N_4V_4^0 2\pi\left(\frac{2m_4kT}{h^2}\right)^{\frac{3}{2}}$$
$$\times\int_0^\infty \ln\left[1-\lambda_4\exp\left(\frac{\chi_4^0}{kT}-y\right)\right]y^{\frac{1}{2}}dy\Big\}. \tag{1.3}$$

For this model, therefore, the onset of extreme degeneracy will be determined when the term

$$\lambda_4^*\equiv\lambda_4\exp(\chi_4^0/kT)\simeq 1. \tag{1.4}$$

On this simple model the introduction of the potential well does not affect the condensation temperature T_0 of the system in first approximation.[7]

The conservation of the total number of particles requires as is pointed out by Fowler and Guggenheim,[8] that:

$$\left(\frac{\partial F_4}{\partial\lambda_4}\right)_{TV}=0=\left(\frac{\partial F}{\partial\lambda_4^*}\right)_{TNV^0}, \tag{1.5}$$

a condition which evaluates λ_4^*. If one now introduces, as is general in the two fluid theories of liquid He II, a parameter, x, defining the fraction of noncondensed particles, given by

$$x=(1/N_4)(\text{number of uncondensed particles})=N_4^n/N_4$$

and putting with London[9]

$$\lambda_4^*=1-\frac{1}{(1-x)N_4}, \tag{1.6}$$

then one finds from Eqs. (1.3), (1.4), (1.5), and (1.6) that the temperature T_0, at which almost all the particles are noncondensed, is given by

$$T_0=(h^2/2\pi m_4k)(1/2.612V_4^0)^{\frac{2}{3}}, \tag{1.7}$$

which is the same value of the degeneracy temperature as that given by London[1] for a perfect Bose-Einstein gas. When $\mathfrak{N}V_4^0$ is taken to be 27.6 cc, the numerical value of T_0 calculated in this way[1] is 3.13°K.

From Eqs. (1.5) and (1.6) it will be seen that the very general statistical requirement given by Eq. (1.5), which is the requirement of constant number of particles, can in the case of our *liquid* model be written

$$(\partial F_4/\partial\lambda_4)_{TV}=0=(\partial F_4/\partial\lambda_4^*)_{TNV^0}\simeq(\partial G_4/\partial x)_{T_p} \tag{1.8}$$

hence showing that the equilibrium evaluation of G, given when $(\partial G/\partial x)_{T_p}=0$ as used in Gorter's treatment,[10] follows directly from the statistics provided the pressures are small, a condition necessary for Eq. (1.8) to hold.

Examination of Eqs. (1.3), (1.5), and (1.8) indicates that in any experiment on a degenerate Bose-Einstein liquid which attempts to count the total number of particles; i.e., the number given by the total mass, an operation equivalent to $(\partial F/\partial\lambda)$ is performed and the number of particles contributing is the same as the total number of atoms. For experiments which do not

[3] Lane, Fairbank, Aldrich, and Nier, Phys. Rev. 73, 256 (1948).
[4] Osborne, Weinstock, and Abraham, Phys. Rev. 75, 988 (1949).
[5] J. G. Daunt and C. V. Heer, Phys. Rev. 79, 46 (1950).
[6] The notation is the same as that used by Fowler in Statistical Mechanics (Cambridge University Press, London, 1936). See for example this reference, p. 72.
[7] Variations in χ_4^0 with variation in volume V will, however, give further (second order) variations in T_0. See footnote 16 for further discussion of this.
[8] R. H. Fowler and E. A. Guggenheim, *Statistical Thermodynamics* (Cambridge University Press, London, 1936), p. 62.
[9] See also E. Schrödinger, *Statistical Thermodynamics* (Cambridge University Press, London, 1946), p. 77.
[10] C. J. Gorter, Physica 15, 523 (1949).

depend on the operation $(\partial F/\partial\lambda)$, e.g., specific heat measurements, the term $\ln(1-\lambda_4^*)$ can be neglected, and hence the free energy F, and the entropy, S, and etc., will appear to depend only on some number N_4^*; i.e., on the number of active particles. Such measurements would appear to include viscosity experiments, for which, therefore, only the number of normal atoms would be active and take part in producing a viscous term.

II. SOLUTIONS OF He³ IN THE BOSE-EINSTEIN LIQUID AND THEIR LAMBDA-TEMPERATURES

In order to investigate the change in lambda-temperature of He³ and He⁴ solutions the treatment given in Sec. I of a Bose-Einstein liquid is extended to include a solution composed of such a Bose-Einstein liquid model and a similar but statistically independent Fermi-Dirac liquid model.

For calculation of the properties of such a solution the molar volume of He³ is taken as $\mathfrak{N}V_3^0$, and of He⁴ as $\mathfrak{N}V_4^0$, and we assume potential wells of depth $-\chi_3^0$, and $-\chi_4^0$ for the He³ and He⁴, respectively. In addition, the assumptions regarding ideal solutions are made; i.e., that the total volume of such a solution is assumed to be

$$V=N_3V_3^0+N_4V_4^0. \tag{2.1}$$

Moreover, the values of the χ^0's are assumed to be unaffected by the mixing process. Mixing therefore will affect only the statistical properties of the mixture.

Using Eq. (1.2), the free energy of the Fermi-Dirac liquid can be expressed as

$$F_3=-kT\left\{4\pi\left(\frac{2m_3kT}{h^2}\right)^{\frac{3}{2}}N_3V_3^0\int_0^\infty \ln\left[1+\lambda_3\exp\left(\frac{\chi_3^0}{kT}-y\right)\right]y^{\frac{1}{2}}dy-N_3\ln\lambda_3\right\}, \tag{2.2}$$

where the statistical weight of each level is for a known spin[11] of $\frac{1}{2}$ for He³. Combining this with Eq. (1.3) for the free energy of the Bose-Einstein liquid, the free energy of the solution is written as:

$$\begin{aligned}F&=F_3+F_4=F_3^0+F_4^0+\Delta F\\&=-kT\left\{4\pi\left(\frac{2m_3kT}{h^2}\right)^{\frac{3}{2}}(N_3V_3^0+N_4V_4^0)\right.\\&\quad\times\int_0^\infty \ln[1+\lambda_3\exp(\chi_3^0/kT-y)]y^{\frac{1}{2}}dy\\&\quad-N_3\ln\lambda_3-\ln(1-\lambda_4^*)-N_4\ln\lambda_4\\&\quad-2\pi\left(\frac{2m_4kT}{h^2}\right)^{\frac{3}{2}}(N_3V_3^0+N_4V_4^0)\\&\quad\left.\times\int_0^\infty \ln(1-\lambda_4^*e^{-y})y^{\frac{1}{2}}dy\right\}\cdots,\end{aligned} \tag{2.3}$$

where λ_4^* is given by Eq. (1.4), F_3^0 and F_4^0 are the free energies in the unmixed state, and ΔF is the free energy of mixing.

The conservation of the total number of particles requires that

$$(\partial F/\partial\lambda_3)_{TV_4^0V_4^0N_3N\lambda_4}=0, \tag{2.41}$$

$$(\partial F/\partial\lambda_4)_{TV_3^0V_4^0N_3N\lambda_3}=0, \tag{2.42}$$

and so λ_3 and λ_4 are determined from Eqs. (2.41) and (2.42). For $\lambda_4^*\simeq 1$, this leads to

$$\frac{\lambda_4^*}{1-\lambda_4^*}-N_4+\left(\frac{2\pi m_4kT}{h^2}\right)^{\frac{3}{2}}\times(N_3V_3^0+N_4V_4^0)(2.612)=0. \tag{2.5}$$

[11] H. L. Anderson, Phys. Rev. 76, 1460 (1949).

Defining $\lambda_4^*=1-1/(1-x)N_4$ as in Eq. (1.6), where xN_4 is the number of He⁴ atoms in the noncondensed state, the temperature at which condensation begins is given by

$$T_\lambda=\frac{h^2}{2\pi m_4k}\left(\frac{N_4}{N_3V_3^0+N_4V_4^0}\right)^{\frac{2}{3}}\left(\frac{1}{2.612}\right)^{\frac{2}{3}}. \tag{2.6}$$

By combining Eq. (2.6) with Eq. (1.7) one obtains

$$T_\lambda/T_0=[N_4V_4^0/(N_3V_3^0+N_4V_4^0)]^{\frac{2}{3}} \tag{2.7}$$

as the equation of the λ-line for solutions of He³ and He⁴.

In terms of the concentration of He³ atoms in He⁴, $C_3=N_3/(N_3+N_4)$, Eq. (2.7) can be written:

$$T_\lambda/T_0=\left[\frac{1-C_3}{1+C_3(V_3^0/V_4^0-1)}\right]^{\frac{2}{3}}. \tag{2.8}$$

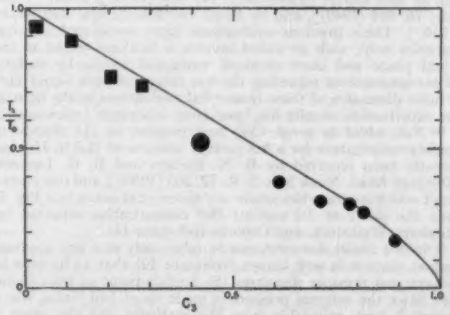

FIG. 1. Plot of the λ-temperature, T_λ, of solutions of He³ in He⁴ (as a fraction of the λ-temperature, T_0, of pure liquid He⁴) against He³ concentration, C_3. The full curve is the theoretical evaluation (Eq. (2.8)). The points marked with circles are the experimental results of Daunt and Heer (reference 5). The points marked with squares are the experimental results of Abraham, Weinstock, and Osborne (reference 14).

In order to estimate T_λ numerically, the molar volumes $\mathfrak{N}V_4^0$ and $\mathfrak{N}V_3^0$ of liquid He^4 and liquid He^3, respectively, have been taken to be[12,13] 27.6 cc and 37.6 cc. Using these values, and putting $T_0=2.18°K$, the experimentally determined[12] λ-point of pure liquid He^4, rather than the theoretical value of 3.13°K, the calculated variation of T_λ for the solutions according to Eq. (2.8) has been plotted against C_3 in Fig. 1.

Experimental observations have been made of the lambda-temperatures, T_λ, of He^3 solutions by Abraham, Weinstock, and Osborne[14] in the concentration range C_3 up to 28 percent and by Daunt and Heer[5] in the concentration range C_3 up to 89 percent. The observations are also shown in Fig. 1, and it will be seen that, except for the point at $C_3=42$ percent, there is good agreement with the theoretical values deduced from Eq. (2.8) as has been previously briefly pointed out.[5,15] The observed point at $C_3=42$ percent, however, was open to considerable error of observation (see Daunt and Heer, reference 5).[15a]

It might be concluded, therefore, that the assumptions made earlier, namely that we are dealing with perfect solutions of smoothed potential liquid models may in first approximation be applicable and that the change in T_λ with change in C_3 is due largely to the effect of the accompanying changes in the number density of the Bose-Einstein gas, rather than by the potential of the liquid well in which it is contained.[16]

These considerations also lead to the conclusion that a solution of two Bose-Einstein liquids, e.g., He^6 in He^4, should show two lambda-points (if each separately in the pure phase shows a lambda-transition), the T_λ for each concentration being given by Eq. (2.8). For very dilute solutions the lambda-temperature of the solute (e.g., He^6) would not be reached at temperatures of 1°K up, and hence one would not expect the solute to take part in superflow.[17] On such a model, therefore, an observed lack of superfluidity of Bose-Einstein particles in *dilute* solution could be taken as a strong support of the original thesis of London.[1]

III. ENTROPY AND FREE ENERGY OF MIXING OF DEGENERATE BOSE-EINSTEIN AND FERMI-DIRAC LIQUID MODELS

Assuming the models for Bose-Einstein and Fermi-Dirac liquids outlined in Secs. I and II above, the free energy of mixing can be written:

$$\Delta F=-kT\Big\{4\pi\Big(\frac{2m_3kT}{h^2}\Big)^{\frac{3}{2}}\Big[(N_3V_3^0+N_4V_4^0)\times\int_0^\infty \ln[1+\lambda_3\exp(\chi_3^0/kT-y)]y^{\frac{1}{2}}dy-N_3V_3^0\int_0^\infty \ln[1+\lambda_3^0\exp(\chi_3^0/kT-y)]y^{\frac{1}{2}}dy\Big]-N_3\ln\lambda_3/\lambda_3^0-\ln\Big(\frac{1-\lambda_4^*}{1-\lambda_4^{0*}}\Big)-N_4\ln\lambda_4/\lambda_4^0-2\pi\Big(\frac{2m_4kT}{h^2}\Big)^{\frac{3}{2}}\Big[(N_3V_3^0+N_4V_4^0)\times\int_0^\infty \ln(1-\lambda_4^*e^{-y})y^{\frac{1}{2}}dy-N_4V_4^0\int_0^\infty \ln(1-\lambda_4^{0*}e^{-y})y^{\frac{1}{2}}dy\Big]\Big\}+\cdots. \quad (3.1)$$

It can be shown that only in the completely classical case; i.e., far from degeneracy, where $\lambda_3\exp(\chi_3^0/kT)\ll 1$ and $\lambda_4\exp(\chi_4^0/kT)\ll 1$ that the expression (3.1) reduces to the more familiar formulation.[18]

$$\Delta F=-kT\Big\{N_3\ln\frac{N_3+N_4}{N_3}+N_4\ln\frac{N_3+N_4}{N_4}\Big\}. \quad (3.2)$$

At sufficiently low temperatures it can be assumed that in the case of He^3 and He^4 solutions, both the Fermi-Dirac and the Bose-Einstein liquids will be very degenerate, and in this situation Eq. (3.1) leads to the

[12] W. H. Keesom, *Helium* (Elsevier Publishing Company, Inc., New York, 1942).

[13] Grilly, Hammel, and Sydoriak, Phys. Rev. **75**, 1103 (1949).

[14] Abraham, Weinstock, and Osborne, Phys. Rev. **76**, 864 (1949).

[15] Other theoretical evaluations of the λ-line for solutions of He^3 in He^4 have been made by deBoer [Phys. Rev. **76**, 852 (1949)], deBoer and Gorter [Phys. Rev. **77**, 569 (1950)], Stout [Phys. Rev. **76**, 864 (1949)], and by Engel and Rice [Phys. Rev. **78**, 55 (1950)]. These previous evaluations have considered classical statistics only, such as would involve a localized model of the liquid phase and have obtained numerical results by making *ad hoc* assumptions regarding the free energy of pure liquid He^4. A fuller discussion of these theoretical evaluations in the light of the experimental results has been given elsewhere (reference 5).

[15a] *Note added in proof.* One measurement on the change in lambda-temperature for a 1.5 percent solution of He^3 in He^4 has recently been reported by B. N. Eselson and B. G. Lazarew [Doklady Akad. Nauk S. S. S. R. **72**, 265 (1950)], and this gives a result which is somewhat nearer our theoretical curve (see Fig. 1) than the point at 2.4 percent He^3 concentration reported by Abraham, Weinstock, and Osborne (reference 14).

[16] Such a model, however, can be taken only as a first approximation, since it is well known (reference 12) that an increase in the external pressure decreases the lambda-point of pure liquid He^4. Since the external pressure is made up of two terms, one a "kinetic" term calculable from the statistics and the other a statical pressure due to variation of χ_4^0 with volume, one must conclude that $\partial\chi(V^0)/\partial V^0$ must in second approximation for our model affect T_0. Such a difficulty is a natural consequence for any smoothed potential model in which the gas-like quality of the liquid is emphasized. See for example Fowler and Guggenheim, *Statistical Thermodynamics* (Cambridge University Press, London, 1949), p. 486.

[17] This conclusion has been arrived at by Landau and Pomeranchuk [Compt. rend. acad. sci. U.R.S.S. **59**, 669 (1948)] starting from different initial assumptions.

[18] The resolution to this form requires the usual assumption that the difference between the arithmetic mean and the geometric mean of the molar volumes is small: i.e.,

$$\frac{N_3V_3^0+N_4V_4^0}{N_3+N_4}\simeq[(V_3^0)^{N_3}(V_4^0)^{N_4}]^{1/(N_3+N_4)}.$$

following value for the entropy of mixing, ΔS:

$$\Delta S=-\left(\frac{\partial \Delta F}{\partial T}\right)=-\frac{\partial}{\partial T}[\tfrac{3}{5}N_3(\epsilon^{0*}-\epsilon^*)+O(T^2)] \quad (3.3)$$

where ϵ^* and ϵ^{0*} are the Fermi-Dirac degeneracy energies in the mixed and unmixed states respectively. Equation (3.3) shows that the entropy of mixing ΔS tends to zero as $T\to 0$, in conformity with the third law, a result which does not hold for the classical expression derivable from Eq. (3.2). Thus the models postulated herewith for liquid He^3 and He^4 indicate an "unmixing" as $T\to 0$.

IV. VAPOR PRESSURES OF SOLUTIONS OF He^3 IN THE BOSE-EINSTEIN LIQUID ABOVE AND BELOW THE LAMBDA-TEMPERATURE

A. Below the Lambda-Temperature

The partial vapor pressures of He^3 and He^4 in equilibrium with a solution of He^3 and He^4 can be computed by equating the partial potentials $\mu_3{}^L$, $\mu_4{}^L$ in the liquid phase to the partial potentials in the vapor phase $\mu_3{}^v$ and $\mu_4{}^v$.

The Gibbs function G for the liquid is

$$G=F+pV=F+p(N_3V_3{}^0+N_4V_4{}^0)\simeq F$$

at ordinary pressures. With this approximation the partial potentials are given by

$$\mu_3{}^L=\left(\frac{\partial G}{\partial N_3}\right)_{Tp}=\left(\frac{\partial G}{\partial N_3}\right)_{TV_3{}^0V_4{}^0}\simeq\left(\frac{\partial F}{\partial N_3}\right)_{TV_3{}^0V_4{}^0}, \quad (4.1)$$

etc.

In the first instance the He^3 liquid model, pure and diluted, will be considered as essentially Boltzmannian in the temperature region above 1°K. Using Eqs. (1.3), (2.2), and (2.3) the partial potentials become, for the pure liquids He^3 and He^4 separately:

$$\mu_3{}^{0L}=-\chi_3{}^0-kT-kT\ln V_3{}^0-kT\ln 2\left(\frac{2\pi m_3kT}{h^2}\right)^{\frac{3}{2}} \quad (4.2)$$

$$\mu_4{}^{0L}=-\chi_4{}^0-0.514\left(\frac{2\pi m_4kT}{h^2}\right)^{\frac{3}{2}}(2.612)V_4{}^0kT \quad (4.3)$$

and for the solutions:

$$\mu_3{}^L=-\chi_3{}^0-\frac{N_3V_3{}^0kT}{N_3V_3{}^0+N_4V_4{}^0}-kT\ln 2\left(\frac{2\pi m_3kT}{h^2}\right)^{\frac{3}{2}}+kT\ln\frac{N_3}{N_3V_3{}^0+N_4V_4{}^0}-\left(\frac{2\pi m_4kT}{h^2}\right)^{\frac{3}{2}}(1.341)V_3{}^0kT \quad (4.4)$$

$$\mu_4{}^L=-\chi_4{}^0-\frac{N_3V_4{}^0kT}{N_3V_3{}^0+N_4V_4{}^0}-(1.341)\left(\frac{2\pi m_4kT}{h^2}\right)^{\frac{3}{2}}V_4{}^0kT. \quad (4.5)$$

Applying the condition of equilibrium, i.e., the partial potential in the vapor phase is equal in each case to the partial potential in the liquid phase, we obtain, assuming the vapor to be a perfect gas,

$$\begin{aligned}\mu_3{}^L-\mu_3{}^{0L}&=\mu_3{}^v-\mu_3{}^{0v}=kT\ln(p_3/p_3{}^0)\\ \mu_4{}^L-\mu_4{}^{0L}&=\mu_4{}^v-\mu_4{}^{0v}=kT\ln(p_4/p_4{}^0)\end{aligned} \quad (4.6)$$

where the superscripts v refer to the vapor phase, and where p_3 and p_4 are the *partial* vapor pressures and $p_4{}^0$ and $p_4{}^0$ the full vapor pressures of liquid He^3 and He^4 respectively.[19]

Combining Eqs. (4.2) to (4.6) the partial vapor

---

[19] Adopting the same equilibrium conditions, the smoothed potential models of liquid He^4 and liquid He^3 allow immediate calculation of the vapor pressures, $p_4{}^0$ and $p_3{}^0$, of the pure liquids. *At sufficiently low temperatures*, where the effect of degeneracy predominates, the vapor pressure formulas can be written as:

For the He^4 liquid model

$$\ln p_4{}^0=-\chi_4{}^0/kT+5/2\ln T-0.514(T/T_0)^{\frac{3}{2}}+\ln(2\pi m_4/h^2)^{\frac{3}{2}}k^{5/2},$$

i.e.,

$$\log_{10}p_4{}^0(\text{cm})=-U_4{}^0/RT+2.5\log_{10}T-0.069T^{\frac{3}{2}}+1.196.$$

This equation is similar to the equations put forward by Bleaney and Simon and by Lingac and Kistemaker (see H. Van Dijk, Proceedings of International Conference on the Physics of Very Low Temperatures. M.I.T. 1949, p. 117, for a discussion of vapor pressure data). The third (specific heat) term in the above equation however gives a variation of T to the three halves power, rather than to higher powers of T (three or six) as previously assumed.

For the He^3 liquid model.

$$\ln p_3{}^0=-\frac{(\chi_3{}^0-\frac{3}{5}\epsilon^{0*})}{kT}+\frac{5}{2}\ln T-\frac{\pi^2}{4}\frac{kT}{\epsilon^{0*}}+\ln 2\left(\frac{2\pi m_3}{h^2}\right)^{\frac{3}{2}}k^{3/2}$$

or

$$\log_{10}p_3{}^0(\text{cm})=-\frac{U_3{}^0}{RT}+2.5\log_{10}T-0.511T+1.31.$$

For He^3 the smoothed potential model leads to an additional factor of 2 in the vapor pressure constant due to the spin. The coefficient of the third (specific heat) term in the above equation has been calculated assuming that the degeneracy temperature of the liquid He^3 is the same (4.85°K) as that for a perfect Fermi-Dirac gas with the liquid density. However it is expected that the degeneracy temperature would be somewhat lower, as in the case of He^4, and consequently the term in T would require slight modification. It should be emphasized moreover, that strictly the vapor pressure formula given above would be accurate only for *temperatures less than one quarter of the degeneracy temperature.* The chief differences between the above equation and that first proposed by deBoer and Lunbeck [Physica 14, 510 (1948)] are (a) the inclusion of the spin in the vapor pressure constant, as has previously been adopted for the smoothed potential model of electrons in metals and (b) the inclusion here of a specific heat term proportional to T. This term may remain important even at low temperatures due to its slow dependence on T. For a limited temperature range above 1°K, it is reasonable to allow for the conditions being nearer the degeneracy temperature by reducing the coefficient in the specific heat term. If this specific heat term in the vapor pressure formula given above is put equal to $0.170T$ and if $U_3{}^0$ is put equal to $1.16R$, a value in agreement with that proposed by deBoer and Lunbeck, the calculated vapor pressures are within 2.5 percent of the observed values given in the preliminary measurements of Sydoriak, Grilly, and Hammel (reference 23), up to 1.8°K. Modifications should, of course, be made to the above formulations for the non-ideality of the vapor [see Kranendonk, Compaan, and deBoer, Phys. Rev. 76, 1728 (1949)] but in view of the approximate character of our liquid models this has not been considered worth while.

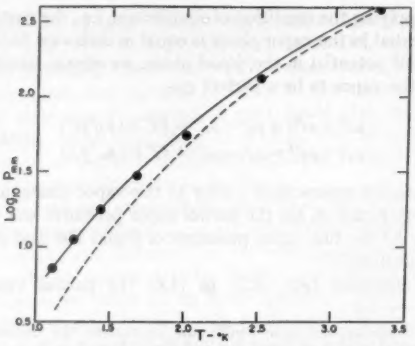

FIG. 2. Plot of the vapor pressure of a 20 percent solution of He^3 in liquid He^4 against temperature. The full curve is the theoretical evaluation [Eqs. (4.13) to (4.16)]. The dashed curve is the result of assuming Raoult's law. The points marked with circles are the experimental results of measurement of a 20.3 percent mixture of He^3 in He^4 by Weinstock, Osborne, and Abraham (reference 21).

pressures ratios can be expressed as

$$p_3/p_4=C_3'p_3^0/p_4^0\exp\left\{C_3'V_4^0/V_3^0+C_4'-0.514\frac{N_4^nV_3^0}{N_3V_3^0+N_4V_4^0}\right\}\cdots, \quad (4.7)$$

where

$$C_4'=\frac{N_4V_4^0}{N_3V_3^0+N_4V_4^0} \text{ and } C_3'=\frac{N_3V_3^0}{N_3V_3^0+N_4V_4^0}\cdots, \quad (4.8)$$

and where N_4^n is the number of "normal" (uncondensed) He^4 atoms, given for the perfect Bose-Einstein fluid by:

$$N_4^n=(T/T_0)^{\frac{3}{2}}N_4.$$

For dilute solutions, $N_4\gg N_3$, formulas (4.7) can be written, as:

$$\frac{C_v}{C_L}=(V_3^0/V_4^0)(p_3^0/p_4^0)\times\exp\left[1-0.514\left(\frac{T}{2.18}\right)^{\frac{3}{2}}\frac{V_3^0}{V_4^0}\right], \quad (4.9)$$

where the concentration in the liquid phase is given by $C_L=N_3/N_4$ and the concentration in the vapor phase by $C_v=N_3^v/N_4^v=p_3/p_4$. This result, as will be discussed later, gives values of C_v/C_L higher than those obtained from Raoult's law, such as has been experimentally observed by Taconis *et al.*[20]

[20] Taconis, Beenakker, Nier, and Aldrich, Physica **15**, 733 (1949).

B. Above the Lambda-Temperature

Following the procedure adopted in Sec. IVA, similar calculations for the vapor pressure ratios above the lambda point have been made.

The equation for the free energy above the λ-point is given by London.[1]

$$F_4=-N_4\chi_4^0-N_4kT\ln(T/T_\lambda)^{\frac{3}{2}}-N_4kT(1-\ln 2.612)-0.462N_4kT(T_\lambda/T)^{\frac{3}{2}}-0.108N_4kT(T_\lambda/T)^3\cdots \quad (4.10)$$

where T_λ is given by Eq. (2.6).

Applying the conditions of equilibrium to the liquid and gaseous phases, the latter being assumed perfect, the vapor pressure equation, for example, for the dilute model solutions reduces to

$$p_3/p_4=(p_3^0/p_4^0)(N_3V_3^0/N_4V_4^0)\times\exp[1-V_3^0/V_4^0+0.462(V_3^0/V_4^0)(T_0/T)^{\frac{3}{2}}+0.022(V_3^0/V_4^0)(T_0/T)^3+\cdots], \quad (4.11)$$

or in terms of the concentrations,

$$C_v/C_L=(V_3^0/V_4^0)\exp\{1-V_3^0/V_4^0+0.462(V_3^0/V_4^0)(T_0/T)^{\frac{3}{2}}+0.022(V_3^0/V_4^0)(T_0/T)^3+\cdots\}. \quad (4.12)$$

These results for the model solutions indicate that p_3, dp_3/dT, and C_v/C_L are continuous across the λ-point, even for concentrated solutions which are discussed in more detail below.

C. Discussion of Vapor Pressure Results

Numerical evaluations have been made of the total vapor pressures (p_3+p_4) of two model solutions of He^3 and He^4 as a function of temperature using the following formulas from which formulas (4.7) and (4.11) were obtained:

Above T_λ

$$p_3/p_3^0=C_3'\exp\left\{\left(1-\frac{V_3^0}{V_4^0}\right)C_4'+0.462\left(\frac{V_3^0}{V_4^0}\right)\left(\frac{T_\lambda}{T}\right)^{\frac{3}{2}}C_4'+0.022\left(\frac{V_3^0}{V_4^0}\right)\left(\frac{T_\lambda}{T}\right)^3C_4'+\cdots\right\}, \quad (4.13)$$

$$p_4/p_4^0=C_4'\exp\left\{\left(1-\frac{V_4^0}{V_3^0}\right)C_3'-0.462\left[1+C_3'-\frac{1}{C_4'}\right]\left(\frac{T_\lambda}{T}\right)^{\frac{3}{2}}-0.011\left[1+2C_3'-\frac{1}{(C_4')^2}\right]\left(\frac{T_\lambda}{T}\right)^3-\cdots\right\}. \quad (4.14)$$

Below T_λ

$$p_3/p_3^0=C_3'\exp\left\{C_4'-0.514\left(\frac{V_3^0}{V_4^0}\right)\left(\frac{T}{T_\lambda}\right)^{\frac{3}{2}}C_4'\right\}, \quad (4.15)$$

$$p_4/p_4^0=\exp\left[-\left(\frac{V_4^0}{V_3^0}\right)C_3'\right]. \quad (4.16)$$

The two solution concentrations chosen for calculation were with C_3 of 20 and 25.5 percent. These values were chosen because experiments have been made by Weinstock, Osborne, and Abraham[21] on the vapor pressures of such solutions. The result of our computations, giving the vapor pressure ($p=p_3+p_4$) plotted against temperature for the 20 percent solution is given in Fig. 2 by the full curve. The dashed line indicates the vapor pressure curve calculated from Raoult's law. The experimental points[21] for a 20.3 percent He^3 mixture are shown by the circled points in Fig. 2, and it will be seen that their agreement with our calculation is good, particularly below the lambda-temperature (calculated $T_\lambda=1.79$). The deviations of the experimental points from the full curve at the higher temperatures are in a direction which would be expected, since experimentally at the higher temperatures the quantity of He^3 in the vapor increases and consequently the concentration, C_3, in the liquid phase becomes smaller than that (20.3 percent) for the unrefrigerated gas. The general agreement between theory and experiment for the vapor pressures of the 25.5 percent concentration solution is as good as that shown for the 20 percent solution of Fig. 2. It is concluded that Eqs. (4.13) to (4.16) are adequate in first approximation to account for the vapor pressure of strong or dilute solutions above or below their lambda-temperatures. It is to be noticed moreover that Eqs. (4.13) and (4.14), as is shown in Fig. 2, indicate that even *above* T_λ Raoult's law is inadequate, as has been noticed experimentally by Weinstock, Osborne, and Abraham[21] and by Lane and his co-workers.[22]

It would be of interest to have more detailed measurements of the vapor pressures, or of the distribution coefficient C_v/C_L, above the lambda-temperatures of the solutions concerned.

Although it is considered that many of the measurements of the distribution coefficient, C_v/C_L, for He^3 in He^4 do not have the accuracy of a direct vapor pressure, measurement, it was thought worth while to calculate numerically C_v/C_L for the case of very dilute solutions, since the experimental work on the measurement of C_v/C_L has been carried out so far using only dilute solutions. ($C_3<1$ percent.) A numerical evaluation therefore has been made of C_v/C_L for dilute model solutions using Eqs. (4.9) and (4.12) for below and above the λ-temperature respectively. In the calculations it was assumed that the He^3 concentration, C_3, in the solution was so small that $T_\lambda \simeq T_0=2.18°K$, and the measured values of the vapor pressures p_3^0 and p_4^0 of the pure-components were adopted (see Sydoriak, Grilly, and Hammel[23] for vapor pressures of liquid He^3 and Van Dijk and Shoenberg[24] for vapor pressure of liquid He^4). The result of this computation is given by the full curve of Fig. 3.

Also in Fig. 3, the dashed curve gives the calculated value of C_v/C_L, obtained by assuming Raoult's law, being given by

$$C_v/C_L=p_3^0/p_4^0. \tag{4.17}$$

It will be seen that the values of C_v/C_L for our model lie at all temperatures above those given by Eq. (4.17). Below the lambda-temperature, experiments have shown that, in conditions where the He^3 was well mixed in the liquid phase, the observed values of C_v/C_L, also lie well above the values calculated from Eq. (4.17), as has been demonstrated by Taconis[20] *et al.* and by Lane and his co-workers,[25] and as is indicated by the points plotted in Fig. 3.[26]

It has been suggested[20] by Taconis that formula (4.17) could be modified to fit the observations *below* the lambda-temperature by assuming that the He^3 dissolves in the "normal" fraction (N_4^n) of the liquid He^4 only. Such a postulate would leave the theoretical evaluation of C_v/C_L *above* the lambda-temperature as being determined with good approximation by Eq.

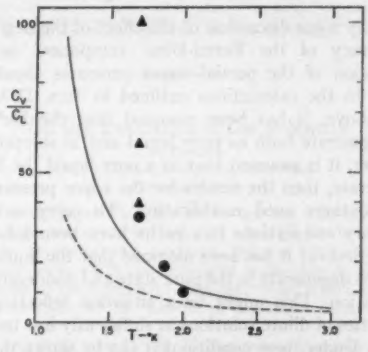

FIG. 3. Plot of the distribution coefficient, C_v/C_L, for dilute solutions ($C_3\leq 1$ percent) of He^3 in liquid He^4 against temperature. The full curve is the theoretical evaluation [Eqs. (4.9) and (4.12)]. The dashed curve is the result of assuming Raoult's law [Eq. (4.17)]. The points marked with circles are the measurements of Taconis and co-workers (reference 20). The triangular points are the measurements of Lane and co-workers (reference 25).

[21] Weinstock, Osborne, and Abraham, Phys. Rev. **77**, 400 (1950).
[22] Fairbank, Reynolds, Lane, McInteer, Aldrich, and Nier, Phys. Rev. **74**, 345 (1948).
[23] Sydoriak, Grilly, and Hammel, Phys. Rev. **75**, 303 (1949). See also Abraham, Osborne, and Weinstock, Phys. Rev. **80**, 366 (1950).
[24] H. Van Dijk and D. Shoenberg, Nature **169**, 151 (1949).
[25] Lane, Fairbank, Aldrich, and Nier, Phys. Rev. **75**, 46 (1949).
[26] The results of measurement of C_v/C_L by Taconis *et al.* (reference 20) lie between the extremes presented on the one hand by the work of Daunt and others (reference 27) and of Lane and co-workers [Phys. Rev. **73**, 729 (1948)] and on the other hand by Rollin and Hatton [Phys. Rev. **74**, 508 (1948)] and by Lane and co-workers (reference 25). This is largely due to the improved method of stirring the solution adopted by Taconis whereby strong concentration gradients within the liquid were avoided. (See Daunt and Heer, reference 5, for further discussion of this point.) It has been suggested (reference 5) that these difficulties of observation of equilibrium values of C_v/C_L would be largely avoided by measurement on solutions with higher He^3 concentration, and further experiments with $C_3>1$ percent would be of value.

(4.17). In our model, however, C_v/C_L should lie above the values calculated by the simple theory of Eq. (4.17) even *above* the lambda-temperature.

The measurements below the lambda-temperature of C_v/C_L are in moderate agreement with our calculations, as is shown in Fig. 3. Too great a reliance, however, cannot be placed on the accuracy of the existing experimental data, as is evident from the large scatter of the results (see also footnote 26). The direct vapor pressure measurements of more concentrated solutions provides, as is indicated earlier, a more satisfactory test of the adequacy of the calculations.

Above the lambda-temperature there are indications in the work of Lane and co-workers[22] and of Weinstock *et al.*[21] that discrepancies exist between the observations of C_v/C_L and the simple theory [Eq. (4.17)]; although the older results[27,28] on extremely dilute solutions do not permit a conclusion to be made. It would be valuable to have further measurements of C_v/C_L above the lambda-temperature in order to check whether the high values of C_v/C_L can be explained in the manner outlined above.[28a]

D. The Vapor Pressures of Solutions Where Both He^3 and He^4 Are Degenerate

Finally some discussion of the effect of the degree of degeneracy of the Fermi-Dirac component on the calculation of the partial vapor pressures should be made. In the calculations outlined in Secs. IVA and IVB above, it has been assumed that the He^3 was nondegenerate both as pure liquid and in solution. If, however, it is assumed that as a pure liquid the He^3 is degenerate, then the results for the vapor pressures of the solutions need modification. To carry out the necessary calculations two paths have been followed. In the first (a) it has been assumed that the liquid He^3 model is degenerate in the pure state and nondegenerate in solution. This might be a situation reflecting the properties of dilute solutions at sufficiently low temperatures. Under these conditions it can be shown that:

$$p_3/p_3^0 = C_3'(4/3(\pi)^{\frac{1}{2}})(\epsilon^{0*}/kT)^{\frac{1}{2}} \times \exp\{-\tfrac{3}{2}(\epsilon^{0*}/kT) + \pi^2/4(kT/\epsilon^{0*}) - C_3' - 0.514(T/T_\lambda)^{\frac{1}{2}}C_4'(V_3^0/V_4^0)\}. \quad (4.18)$$

At sufficiently low temperatures the term $\exp[-\frac{3}{2}(\epsilon^{0*}/kT)]$ predominates and results in a reduction of the partial vapor pressure even below the value calculable from Raoult's law. If the degeneracy temperature of the pure Fermi-Dirac liquid model, $T^{0*}=\epsilon^{0*}/k$, were equal to 4.85°K, i.e., the value calculable for a perfect gas of He^3 with the liquid density, the value of p_3/p_3^0, as given by Eq. (4.18), would already be less than the value predicted by Raoult's law at 1°K. The experimental results however (see Fig. 2) for the measured vapor pressures indicate that down to 1°K values are obtained in good agreement with our theory on the basis of nondegeneracy of the Fermi-Dirac liquid, as given in Sec. IVA. It must in consequence be assumed that $T^{0*}<4.85$°K (see footnote 19) and moreover it can be shown from Eq. (4.18) that for $T^{0*}\leq 2$°K, the non-degenerate evaluation of p_3/p_3^0 given in Eq. (4.15) is an adequate approximation down to the lowest temperatures to which measurements have been made, i.e. down to 1°K.

The evaluation of C_v/C_L under the degenerate conditions assumed above involves not only (4.18) for p_3/p_3^0 but also a knowledge of p_3^0/p_4^0. It can be shown that, if the known vapor pressure formulas for He^4 (Bleaney and Simon[29]) and for He^3 (Sydoriak, Grilly, and Hammel[22]) are extrapolated below 1°K, then the distribution coefficient C_v/C_L will always continue to increase with decreasing temperature. This is due to the fact that the ratio of the vapor pressure of He^3 to that of He^4 increases with decreasing temperature more rapidly than the ratio of the partial vapor pressures p_3/p_4. Nevertheless C_v/C_L would in these circumstances be below the values calculable from Raoult's law [Eq. (4.17)]. It would appear therefore that the results given in Sec. IVA, which showed that the partial vapor pressure of He^3 in model solutions of He^3 and He^4 and the value of the distribution coefficient, C_v/C_L, were greater than the values given by Raoult's law, are limited to a temperature range above some critical temperature which is estimated to be about 0.5°K.

The second case of interest (b) would occur when both the pure liquid He^3 and the He^3 in solution are degenerate. In this case the general results are the same as for case (a), i.e. values for p_3 and C_v/C_L less than those calculable from Raoult's law are obtained. This situation is probably of less importance than the case (a) above, since at easily attainable temperatures it would involve only strong solutions of He^3. The value of p_3 which has been obtained for case (b) is given by:

$$\ln p_3/p_3^0 = 3/5(1/kT)(\epsilon^*-\epsilon^{0*}) - \frac{\pi^2}{4}\left(\frac{1}{\epsilon^*}-\frac{1}{\epsilon^{0*}}\right)kT + 2/5(\epsilon^*/kT)C_4' - \frac{\pi^2}{6}\frac{kT}{\epsilon^*}C_4' - 0.514\left(\frac{T}{T_\lambda}\right)^{\frac{1}{2}}C_4'\frac{V_3^0}{V_4^0}. \quad (4.19)$$

[27] Daunt, Probst, and Smith, Phys. Rev. **74**, 495 (1948).

[28] Fairbank, Lane, Aldrich, and Nier, Phys. Rev. **71**, 911 (1947).

[28a] *Note added in proof.* We have recently carried out experimental measurements of C_v/C_L above and below the λ-temperature of a one percent He^3 solution in He^4 and find results in close agreement with our theoretical evaluations given in this paper, even *above* the λ-temperature. Details of this work will be published shortly. We note also that recent experimental values of C_v/C_L quoted by Taconis, Beenakker, and Dokoupil [(Phys. Rev. **78**, 171 (1950)] for He^3 in He^4 solutions varying from 0.11 to 0.22 percent He^3 concentration average about a value of C_v/C_L equal to 75 at 1.38°K. This is in moderate agreement with our calculated value of 50 at the same temperature, whereas Taconis' empirical solubility law (reference 20) predicts a value of C_v/C_L equal to 300 at this temperature.

[29] B. Bleaney and F. Simon, Trans. Faraday Soc. **35**, 1205 (1939).

Letters to the Editor

PUBLICATION of brief reports of important discoveries in physics may be secured by addressing them to this department. The closing date for this department is five weeks prior to the date of issue. No proof will be sent to the authors. The Board of Editors does not hold itself responsible for the opinions expressed by the correspondents. Communications should not exceed 600 words in length.

The r-Unit at 320 and 160 Mev*

EDWIN M. MCMILLAN, WADE BLOCKER, AND ROBERT W. KENNEY
Radiation Laboratory, Department of Physics, University of California, Berkeley, California
December 7, 1950

THE r-unit is used today in at least two different ways: as a measure of radiation dosage, and as a measure of x-ray intensity. The meaning of the former is fairly well defined in terms of energy absorbed per gram of tissue, and the standard thimble chambers are calibrated to read in these terms. The meaning of the latter is much less clear. As originally defined, the r-unit referred to the ionization in air due to secondary electrons in equilibrium with the primary beam of x-rays. With low energy x-rays equilibrium is easily attained since the range of the secondaries is small compared with the absorption distance of the primaries in air, but with high energy x-rays this is no longer true. Since a clearly defined equilibrium no longer exists, the old definition must be abandoned and the question remains: what should the r-unit mean in connection with the intensity of a beam of high energy x-rays?

It would seem that the definition must be arbitrary, that is, it must apply to some specified setup of the ionization chamber and its surroundings. Because of their convenience in use and universal availability, the Victoreen thimble chambers have been most widely used as measuring devices. Some workers have used these bare; some, in a block of plastic; some, inside a lead cylinder; and some, behind a lead sheet. Because of this ambiguity the r-unit has lost much of its value for x-ray measurements in the range of many Mev, and we believe that it should be replaced by absolute measurements in terms of energy flux or "effective number of quanta" (energy flux divided by upper limit quantum energy). However, it would be convenient to retain the r-unit, with a suitable arbitrary definition, for rough measurements and for intercomparison of various x-ray sources.

Therefore we would like to suggest that a standard setup should be adopted, consisting of a Victoreen thimble chamber inside an open-ended lead cylinder with $\frac{1}{4}$-inch wall thickness, $\frac{1}{2}$-inch inside diameter, and at least 2 inches length. This arrangement was chosen because it is easily reproducible and because there is already considerable precedent for the use of similar setups. It should be placed with its axis transverse to the beam direction and at a sufficient distance from the x-ray source that the intensity is reasonably uniform over a region at least an inch wide. The r-unit so specified can be calibrated in terms of absolute x-ray energy per unit area. To do this, a beam is defined by an aperture in a thick lead wall; the total energy flux in this beam is measured, and the Victoreen thimble reading in the center of the same beam is determined. The flux divided by the area of the beam at the Victoreen thimble gives the average intensity of the beam at this distance; this is multiplied by a factor, computed from the measured angular distribution in the beam, to get the central intensity.

Calibrations of this sort have been carried out for two energies, using the method of Blocker, Kenney, and Panofsky[1] for the flux measurements. The apertures are holes in a 9.57-inch thick lead wall placed 56.5 inches from the target; they are tapered to follow rays of the beam, and hole diameters of $\frac{1}{4}$, 1, and $1\frac{1}{2}$ inches (at the small end) were used, with good internal consistency. Victoreen thimbles of 250 r, 100 r, and 25 r ratings (also with good agreement) were placed 337 inches from the target. A thin-walled integrating monitor chamber permanently mounted between the target and the aperture was useful in making the intercomparisons.

The results are given in Table I. The x-ray energies are accurate to about two percent, the calibrations to about ten percent. We find that our Victoreen setup, for a given exposure, reads 1.5 times as high as that used by Kerst (thimble behind $\frac{1}{4}$-inch lead sheet), and if allowance is made for this our result for 320 Mev is in good agreement with the absolute calorimetric measurement of Kerst and Price.[2] The r-unit mentioned in reference 1 was defined in terms of Zeus meter readings, and was included only to show the order of magnitude of intensities used; it is in very poor agreement with thimble chamber readings and should not be used again.

TABLE I. Calibration data.

X-ray energy	Ergs/cm² r	Mev/cm² r	"Effective quanta"/cm² r
320 Mev	5.3×10^{8}	3.3×10^{8}	1.04×10^{7}
160 Mev	3.5×10^{8}	2.2×10^{8}	1.38×10^{7}

The thimble chamber readings (in the standard setup) obtained in the course of the calibration, reduced to a standard distance by the inverse square law, indicate that the time average output of the Berkeley synchrotron is 1000 r/min at one meter under best operating conditions. This is at full energy and with a pulse rate of six per second. Operation at this level has been maintained for periods of many hours.

* This work was done under the auspices of the AEC.
[1] Blocker, Kenney, and Panofsky, Phys. Rev. 79, 419 (1950).
[2] D. W. Kerst and G. A. Price, Phys. Rev. 79, 725 (1950).

On the Evaluation of the S-Matrix

F. COESTER
State University of Iowa, Iowa City, Iowa
December 5, 1950

IN a recent paper Wick[1] has shown how the S-matrix can be expanded into a sum of "ordered" terms by purely algebraic methods. In general this procedure yields a large number of equivalent terms which can be reduced to one term by changing the names of the integration variables. Using Wick's methods general formulas for the number of equivalent terms can be obtained.

The n'th order term $S^{(n)}$ of the S-matrix of quantum electrodynamics can be written as[2]

$$S^{(n)}=\frac{(-ie)^n}{n!}\int dx_n\int dx_{n-1}\cdots\int dx_1 P[j^{\mu_n}(x_n)\cdots j^{\mu_1}(x_1)]\times P[A_{\mu_n}(x_n)\cdots A_{\mu_1}(x_1)], \quad (1)$$

where $-ej^{\mu}(x)$ is the electric current density and A_{μ} is the vector potential. In a previous paper[3] a formula has been derived for the number of equivalent terms which are obtained by expanding the P-product of the vector potentials only, leaving the P-product of the currents unchanged. For most purposes, however, it is more convenient to expand the P-product of the currents first, collect equivalent terms before expanding the product of the vector potentials, and carry out desired contractions between vector potentials afterwards.

An ordered term obtained in the expansion of $P(j^{\mu_n}\cdots j^{\mu_1})$ contains a number of typical factors, each of which would be represented in a Feynman-Dyson graph by an open polygon or by a closed loop of electron-lines containing m vertices respectively. All terms having the same number of open polygons and the same number of closed loops for every m are equivalent. A set of equivalent terms is completely specified, if for every m, $1\leq m\leq n$, the

number of open polygons with m vertices k_m and the number of closed loops with m vertices l_m are given. l_1 vanishes by definition. The k_m and l_m are subject to the restriction

$$\Sigma_m m(k_m+l_m)=n. \tag{2}$$

Let $F_n(k_1\cdots k_n,\ l_2\cdots l_n)$ be the number of equivalent terms. F_n will be zero by definition if (2) is not satisfied. From Wick's theorems[1] follows the recursion formula

$$F_n(k_1\cdots,l_2\cdots)=F_{n-1}(k_1-1,\cdots,l_2\cdots)$$
$$+\sum_{m=1}^{n-1}(k_m+1)\{2F_{n-1}(\cdots k_m+1,k_{m+1}-1\cdots,l_2\cdots)$$
$$+F_{n-1}(\cdots k_m+1\cdots,\cdots l_{m+1}-1\cdots)\}. \tag{3}$$

Hence

$$F_n(k_1\cdots,l_2\cdots)=n!\prod_{m=1}^{n}2^{(m-1)k_m}2^{(m-1)l_m}/k_m!l_m!(m!)^{k_m+l_m}. \tag{4}$$

The validity of (4) for $n=2$ is easily verified directly. For arbitrary n, Eq. (4) follows by mathematical induction from (3).

[1] G. C. Wick, Phys. Rev. **80**, 268 (1950).
[2] F. J. Dyson, Phys. Rev. **75**, 492, 1737 (1949).
[3] F. Coester and J. M. Jauch, Phys. Rev. **78**, 154 (1950).

Note on the Fluorescence Yield of Argon*

D. L. Dexter and W. W. Beeman
Department of Physics, University of Wisconsin, Madison, Wisconsin
December 5, 1950

An atom, ionized in one of its inner shells, may either radiate or emit an Auger electron in a nonradiative transition. The fluorescence yield for the K shell, r, is defined as the transition probability for all radiative transitions that quench the K-ionized state divided by the total transition probability; the internal conversion coefficient α equals $1-r$. Fluorescence yields have been measured for many elements by x-ray workers.[1] The internal conversion coefficient for chlorine has been measured[2] more recently using argon, A^{37}, which undergoes nuclear K-capture. The α values obtained for the K shell of Cl are inconsistent, being about 0.89 as determined by the x-ray methods and 0.96 ± 0.03 by the other.

It is believed that the fluorescence yield can be calculated accurately for argon by using precise experimental data of Parratt[3] and wave functions determined by solving Fock's equations. Parratt measured the x-ray absorption coefficient of argon gas in the vicinity of the K edge, and found the width of the resonance absorption line corresponding to the $1s-4p$ transition to be 0.58 ev. (The probable error in this width[4] is 0.01 or 0.02 ev.) Thus the total transition probability for filling the K shell of the argon atom is 0.58 ev divided by $\hbar$, or 8.8×10^{14} sec^{-1}, which, as stated above, is equal to the sum of the transition probabilities for Auger and radiative transitions. We neglect the contribution of the multiplet structure of the line to the line width because an estimation shows the multiplet separation to be only 0.01 or 0.02 ev, and a structure separation of 0.06 ev would result in an error in the internal conversion coefficient of only 1 percent. The transition probability for radiative transitions can be calculated easily and accurately, since it involves only bound state wave functions that are accurately known. The calculation of Auger transition probabilities is more difficult, and in particular requires the use of continuum wave functions, which are not accurately known. Thus Parratt's measurement makes an important contribution to the accuracy of this calculation, obviating as it does the calculation of Auger transition probabilities.

The radial part of the dipole matrix element between a $2p$ and a $1s$ argon wave function has been found by numerical integration to be $R_{1s}^{2p}=0.0615a_0$ where $a_0=\hbar^2/me^2$, and between a $3p$ and a $1s$ wave function $R_{1s}^{3p}=0.0146a_0$. The wave functions used were ground-state argon wave functions, calculated by Hartree and Hartree[5] from solutions of the Fock equations including exchange.

The wavelength of the $K\alpha$ line is 4.20A and that of the $K\beta$ line 3.88A; so the total radiative transition probability from the excited K state is $W_r=1.13\times10^{14}$ sec^{-1}. The transition probability of all other radiative transitions is less than one percent of this value and will be ignored. The fluorescence yield of the K shell is then $r=0.129$.

When a $1s$ electron is removed from the argon atom, of course, the wave functions of all the other electrons are changed, becoming more like potassium wave functions. The above matrix elements have also been determined using corresponding wave functions[6] for potassium and it is found in this case that $W_r=1.02\times10^{14}$ sec^{-1}, and $r=0.116$.

Although the $2p$ and $3p$ wave functions in the excited argon atom are very similar to potassium wave functions, the $1s$ function is not as much affected by the removal of the electron, and will be roughly half-way between a potassium and an argon $1s$ function. Using this interpolated $1s$ function and potassium $2p$ and $3p$ functions, we find $R_{1s}^{2p}=0.0602a_0$, $R_{1s}^{3p}=0.0156a_0$, and $r=0.123$.

The plot of the internal conversion coefficient of the K shell against atomic number is a smooth curve, both experimentally and theoretically. Burhop[6] has calculated α as a function of atomic number, using screened hydrogen-like wave functions. The shape of the theoretical curve is very similar to that of the experimental curve, but is displaced toward higher atomic number. Burhop[6] believes the disagreement to be a result of his somewhat arbitrary choice of wave functions. His calculations predict that for argon $\alpha=0.94$. The value of α for argon read from the experimental curve[1,6] is $\alpha=0.87$ or 0.88, in agreement with the present calculation, and 0.89 for Cl.

The agreement between the results of the simple calculation described in this note and the experimental data indicates that for argon α is very close to 0.88, and for chlorine, 0.89. Thus the disagreement between the x-ray and nuclear measurements has become more pronounced. Weimer, Kurbatov, and Pool[2] have already commented on the unlikelihood that this disagreement can be due to the method of ionizing the K shell.

* Research supported in part by ONR.
[1] A. H. Compton and S. K. Allison, *X-Rays in Theory and Experiment*, (D. Van Nostrand Company, Inc., New York, 1935), p. 488.
[2] Weimer, Kurbatov, and Pool, Phys. Rev. **66**, 209 (1944).
[3] L. G. Parratt, Phys. Rev. **56**, 295 (1939).
[4] L. G. Parratt, private communication.
[5] D. R. Hartree and W. Hartree, Proc. Roy. Soc. **A166**, 457 (1938).
[6] E. H. S. Burhop, Proc. Roy. Soc. **A148**, 272 (1935).

Erratum: Study of the Multiple Scattering of Fast Charged Particles in a Gas and Its Role in the Interpretation of Cloud-Chamber Tracks

[Phys. Rev. **77**, 584 (1950)]

Gerhart Groetzinger, Martin J. Berger, and Fred L. Ribe
Institute for Nuclear Studies, University of Chicago, Chicago, Illinois

The following errors occurred in the text of this paper. In line 4, paragraph 2, left column, page 587, and in line 4, right column, page 594, the word "initial" should be changed to "final".

The Cross Section Ratio $\sigma[B^{10}(n,\alpha)Li^7]/\sigma[B^{10}(n,\alpha)Li^{7*}]$ as a Function of Energy

H. Bichsel, W. Hälg, P. Huber, and A. Stebler
Physikalisches Institut der Universitaet Basel, Basel, Switzerland
December 6, 1950

The (n,α) reaction in B^{10} leads, for not too large neutron energies, to a lithium nucleus in either the ground state (Li^7) or the excited state (Li^{7*}) at 0.48 Mev above the ground state. The ratio of the cross sections,

$$K=\sigma[B^{10}(n,\alpha)Li^7]/\sigma[B^{10}(n,\alpha)Li^{7*}],$$

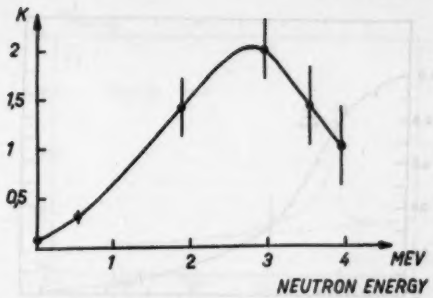

FIG. 1. Dependence of the cross section ratio on neutron energy.

has been measured for thermal neutrons and neutrons with 0.5-, 1.9-, 2.9-, 3.5-, and 3.9-Mev energy. The reactions were generated in an ionization chamber filled with 8 atmos argon and 1 atmos BF_3; and the events were registered in the usual fashion,[1] by means of a photographic pulse spectrograph. The neutrons of 0.5-Mev energy originated in the $C^{13}(d, n)N^{13}$ reaction, a thin graphite layer (0.07 mg/cm²) serving as the target. The higher energy neutrons were generated in the $D(d, n)He^3$ reaction using a thick heavy-ice target.

The measured values of K are given in Fig. 1. The errors to be associated with each measurement are indicated.

A detailed report of this work will appear in the Helvetica Physica Acta.

[1] A. Stebler and P. Huber, Helv. Phys. Acta 21, 59 (1948).

Rayleigh Afterglow in Hydrogen Discharges

ROBERT J. LEE AND RICHARD G. FOWLER
Department of Physics, University of Oklahoma, Norman, Oklahoma
November 13, 1950

IN 1943 Lord Rayleigh[1] induced an electrodeless hydrogen discharge in a continuous tube, or discharge ring, to which a side tube, or neck, was attached. He observed that the luminosity extended several centimeters into the neck, and determined with a rotating mirror that it advanced along the neck, out of the exciting field, with a velocity of the order of 4×10^6 cm/sec, as some sort of afterglow. Coupling this with photometric measurements at two points along the flame, he concluded that approximately 10^{-4} sec represented the time interval during which the luminosity moving along the neck decreased in intensity by a factor of $1/e$. This

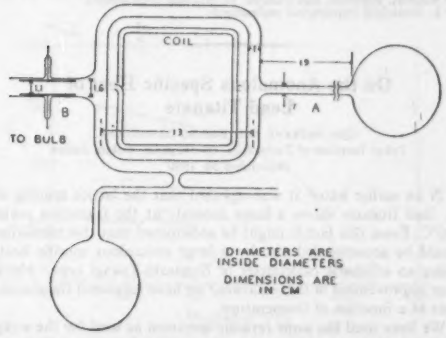

FIG. 1. Schematic design of electrodeless discharge to be used in observing Rayleigh phenomenon.

afterglow time is several hundred times the lifetimes of the excited states, so that some process other than relaxation of the atoms must occur to account for the total duration. At present, the process is not completely explained. We have undertaken to investigate this afterglow, in an attempt to discover as much as possible about the processes involved.

The tube was similar to that used by Rayleigh. The discharge ring was bent from 1-cm diameter glass tubing as shown in Fig. 1. Two side tubes were attached to opposite sides of the discharge ring, terminating in large bulbs, and the tube was pumped out through a side tube joined to a third side. One of the two opposite necks was 0.7 cm in diameter, and the other was 1.6 cm in diameter with copper plates built in as shown. Rotating mirror pictures were taken of neck A in Fig. 1 through a 0.7-mm slit parallel to the axis of the neck. The exciting circuit consisted of a 10-kv transformer in series with a spark gap of about 7 mm and an exciting coil of 11.5 turns of 4.5-mm outside diameter copper tubing, bent square, 10 cm on a side, with $0.1\mu f$ across the secondary terminals of the transformer. The frequency of the circuit was about 1.5×10^5 cps. The rotating mirror turned at 50 rps, and rotating mirror pictures were recorded with an f:4.5 camera on Super XX film.

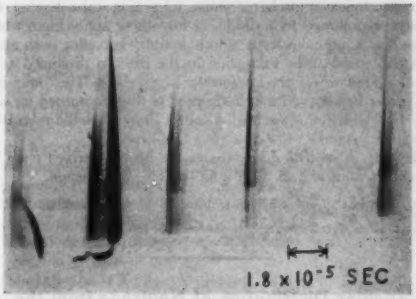

FIG. 2. A group of rotating mirror records of luminosity present in side tube A of Fig. 1 subsequent to discharges in the main tube. Note angle of inclination between stationary trace and moving mirror records.

Hydrogen was used in the discharge tube at pressures varying from 0.1 to 0.8 mm Hg, values which constituted limits on the operation of this particular circuit. The velocity of the advance of luminosity along neck A, calculated from rotating mirror measurements, was about 2×10^6 cm/sec, and showed a tendency to increase with lower pressure. The afterglow times were about 3×10^{-4} sec.

Figure 2 is a sample mirrorgram, taken at 0.40 mm Hg. The very dark trace is taken with the mirror stationary and the striated traces are taken with the mirror turning. The angle between a striation and the stationary trace provides the basis for calculating the velocity of advance. The striations were caused by the condenser oscillations, and the discontinuity in intensity near the base is due to a $1/e$ filter. Since lines of the mirrorgram parallel to the dark trace represent instantaneous slit images, it is apparent from Fig. 2 that the luminosity is highly concentrated in a series of advancing fronts, rather than ejected as a tongue or jet.

Ions were shown to exist in the afterglow by completion of a circuit between the plates in side tube B through a milliameter, and discharging the tube with a small U magnet hanging over neck B between the plates and the discharge ring. The ammeter showed a small deflection; and when the magnet was reversed, the ammeter deflected in the opposite direction, showing that ions were deflected to the plates by the magnet.

It was also observed that the luminosity went much farther along the large side tube than along the smaller, going far beyond the plates in the large tube, whether or not the plates were grounded.

The striations evident in Fig. 2 did not appear in Rayleigh's mirrorgrams. This is apparently because the frequency in his circuit was so great that the mirror did not separate the successive oscillations. Rayleigh suggested that the gas excited in the discharge ring and heated to a very high temperature expanded into the neck, remaining luminous for 10^{-4} sec; and Zanstra[2] showed theoretically that ions expanding into the neck and recombining all along its length might account for Rayleigh's observations. It appears that if either of these processes were the major process in the neck, an instantaneous photograph of the tube should show a tongue rather than a front of luminosity. The front which is observed is more suggestive of an exciting process occurring in the neck, concurrently with the emission of radiation, such as a shock wave producing excitation or ionization as it proceeds along the neck. Such an exciting process is further suggested by the order of magnitude of the velocity of advance.

No experiments have been performed as yet which will enable us to decide whether recombination is active in the discharge. Rayleigh and Zanstra showed that the energy delivered to the discharge is adequate to produce a high average degree of ionization, yet how much of this energy is actually available in the excitation process in the neck is not so far known.

An electrodeless discharge pulse in a ring tube having appendages is followed by a discharge into these appendages which proceeds as a luminous front of local activity traveling with ultra-acoustical speeds. The excitation in the front is produced at or near the point where the luminosity is perceived. The "long lifetime of the Balmer series in hydrogen" is thus accounted for as a delay in production of excitation rather than a belated relaxation of excited systems.

The authors wish to acknowledge the benefit derived from the concurrent work of J. S. Goldstein on this phenomenon.

[1] R. J. Strutt (Lord Rayleigh), Proc. Roy. Soc. (London) **183**, 26 (1944–45).
[2] H. Zanstra, Proc. Roy. Soc. (London) **186**, 236 (1946).

Angular Distribution of Neutrons from the Bombardment of Be by 340-Mev Protons*

JAMES DEJUREN
Radiation Laboratory, Department of Physics, University of California, Berkeley, California
October 9, 1950

IN conjunction with the measurements of Miller, Sewell, and Wright[1] of the angular distribution of the neutrons produced by the bombardment of various targets with 330-Mev protons, a measurement was made using bismuth fission chambers[2,3] as detectors instead of the carbon $(n, 2n)$ reaction employed by the above group. Bismuth fission has its threshold at a neutron energy of about 50 Mev compared to 20 Mev for the C$(n, 2n)$ reaction. The data from 15° to 27° were taken using the neutrons produced from the bombardment of a 2.8-inch Be target with 330-Mev protons inside the cyclotron immediately after the C$(n, 2n)$ measurements. Shallow fission chambers containing two 4.5-inch diameter bismuth coated plates were employed as monitor and detector. The 8° result was obtained from the bombardment of a 2-inch Be target with 350-Mev protons at the standard probe position.

To extend the angular range, measurements were made with the neutrons knocked out of a 1¼-inch diameter beryllium rod by the electro-magnetically deflected, external 345-Mev proton beam. Since the fission counting rate was only about 70 counts per hour at 12°, it was necessary to find the fission pulse height distribution by means of a pulse height analyzer[4] to insure that "pile-ups" were not occurring during the 0.1 μsec deflected proton pulse. Satisfactory plateaus were obtained with the long bismuth fission counters previously employed for the 95- and 270-Mev neutron energy measurements of nuclear cross sections.[5]

The distance from detector to target was such that the angular resolution was within ±1° of the indicated setting except at 62° and 85° where it was ±2°. No attempt has been made to correct for neutron background scattered into the detector or produced by protons at regions other than the beryllium target. Four inches of lead was placed in front of the detector to prevent protons from entering it.

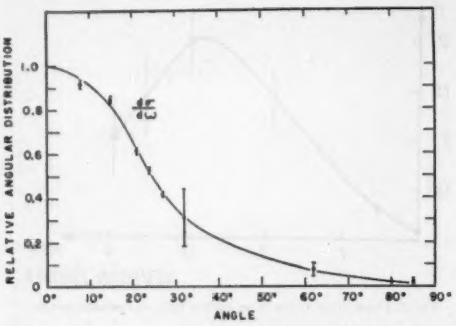

FIG. 1. Angular distribution of neutrons from the bombardment of Be by 340-Mev protons.

The measured angular distribution is shown in Fig. 1, and the statistical errors indicated are standard deviations based on counting. The full width at half maximum is 49° with an estimated probable error of 1° due to the scatter of the experimental points and statistical errors. By comparison, Miller, Sewell, and Wright[1] obtained for beryllium a width of 54±1 degrees using the lower threshold carbon $(n, 2n)$ detection.

If the angular distribution is graphically integrated the resultant total cross section for production of a high energy neutron is

$$\sigma_t = 1.05(d\sigma/d\omega)_0.$$

The neutron yield in the forward direction has been measured by Knox[6] for the neutrons knocked out of Be with 350-Mev protons using the same fission chambers. His result is $(d\sigma/d\omega) = 42.2\times10^{-27} \times\sigma_{p,\,pn}(350\text{ Mev})/\sigma_{n,\,2n}(270\text{ Mev})$ where the indicated cross sections are for carbon. When 38 and 17 millibarns are used for the carbon (p, pn)[6] and $(n, 2n)$[7] cross sections, respectively, the value of the total cross section is 100 millibarns (with an estimated accuracy of 50 percent). The total collision cross section for 270-Mev neutrons and a Be nucleus is 230 millibarns, as measured with bismuth fission detectors.

* This work was performed under the auspices of the AEC.
[1] Miller, Sewell, and Wright, Phys. Rev. **81**, 374 (1951).
[2] C. Wiegand, Rev. Sci. Instr. **19**, 790 (1948).
[3] J. DeJuren and N. Knable, Phys. Rev. **77**, 606 (1950).
[4] I am indebted to Clyde Wiegand for the loan of this analyzer.
[5] W. Knox, UCRL-440, unpublished.
[6] Aamodt, Peterson, and Phillips, UCRL-526, unpublished.
[7] L. Baumhoff (theoretical estimation).

On the Anomalous Specific Heat of Lead Titanate

GEN SHIRANE AND ETSURO SAWAGUCHI
Tokyo Institute of Technology, Oh-okayama, Tokyo, Japan
November 30, 1950

IN an earlier letter[1] it was reported that the lattice spacing of lead titanate shows a large anomaly at the transition point 490°C. From this fact it might be anticipated that this transition would be accompanied also by a large anomalous specific heat. Using an adiabatic calorimeter of Nagasaki-Takagi type,[2] which is an improvement of that of Sykes,[3] we have measured the specific heat as a function of temperature.

We have used the same ceramic specimen as used for the x-ray analysis, which was prepared by sintering the mixture of PbO and TiO_2 at about 1100°C. The powdered specimen of about 25 g was

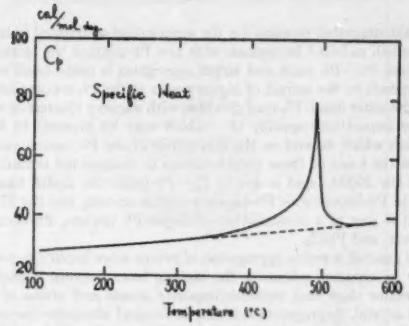

FIG. 1. Specific heat as a function of temperature.

heated in a glass vessel, 2g in weight, at a rate of about 2°C/min. The heat capacity of the empty calorimeter was calibrated with KCl as a standard substance. The specific heat vs temperature curve is shown in Fig. 1.

As is seen in Fig. 1, there is a rather large anomaly of the specific heat in the transition region. The specific heat curve shows a sharp peak at 490°C, corresponding to the anomalies of permittivity and lattice spacing. Attention must be paid to the fact that the specific heat shows an anomaly over a wide temperature range. Though it is difficult to estimate the transition energy accurately from such a curve, we have tentatively assumed that the normal specific heat corresponds to the broken line shown in the figure. We thus obtain the transition energy as 1150 cal/M in the range 340 to 540°C. The accompanying entropy change is about $0.80R$. This large anomaly is to be compared with the small transition energy in $BaTiO_3$,[4] which is about 20 to 40 cal/M.

According to the theory of barium titanate proposed by Devonshire,[6] the anomalous internal energy associated with the spontaneous polarization can be written as

$$E = A \cdot T_c \cdot P^2 + \cdots = B \cdot T_c \cdot (c/a - 1) + \cdots, \qquad (1)$$

where T_c represents the Curie temperature and B depends on the piezoelectric and elastic constants. This relation between polarization and crystal strain has been confirmed experimentally by Merz[6] in the case of barium titanate. Though the value of the spontaneous polarization of lead titanate has not been estimated, we have found that c/a, which is 1.063 at 30°C, begins to decrease considerably from a temperature far below the Curie point. Taking account of this fact, it seems to be reasonable to assume that the specific heat also has an anomaly in the same temperature range. Utilizing the normal specific heat shown in Fig. 1, we have calculated the anomalous internal energy E, as is shown in Fig. 2.

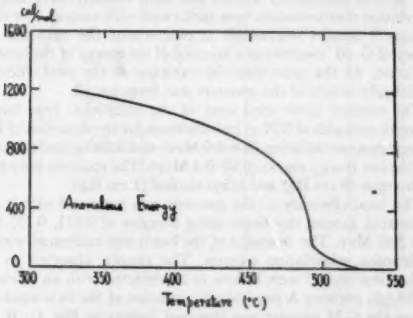

FIG. 2. Anomalous internal energy estimated from the specific heat curve.

This curve is quite similar to the temperature dependence of the axial ratio c/a, shown in the previous letter.[1] It is found that Eq. (1) holds approximately in this temperature range with $B=40$ cal/M. On the other hand, we have estimated that B is about 15 cal/M in the case of $BaTiO_3$.

It is difficult at present to determine whether there is a latent heat at the transition point.

We wish to express our sincere thanks to Professor Y. Takagi for his kind guidance and also to Mr. S. Nagasaki for his helpful advice on our work.

[1] Shirane, Hoshino, and Suzuki, Phys. Rev. 80, 1105 (1950).
[2] S. Nagasaki and Y. Takagi, J. Appl. Phys. Japan 17, 104 (1948).
[3] C. Sykes, Proc. Roy. Soc. (London) A143, 422 (1935).
[4] Harwood, Popper, and Rushman, Nature 160, 58 (1948); Blattner, Känzig, and Merz, Helv. Phys. Acta. 22, 35 (1949); S. Sawada and G. Shirane, J. Phys. Soc. Japan 4, 52 (1949).
[5] A. F. Devonshire, Phil. Mag. 11, 1040 (1949).
[6] W. J. Merz, Phys. Rev. 76, 1221 (1949).

A Note on the Distribution of Impurities in Alkali Halides

E. BURSTEIN, J. J. OBERLY, B. W. HENVIS, AND J. W. DAVISSON
Crystal Branch, Metallurgy Division, Naval Research Laboratory, Washington, D. C.
November 10, 1950

THE manner in which impurities are distributed in a crystal is not readily determined by direct measurement. In the absence of specific information it is frequently assumed, particularly for small concentrations, that the impurities are distributed at random. Large deviations from a random distribution may result, however, from the formation of stable aggregates of two or more impurity atoms as in the aggregation of trapped electrons and trapped holes in the alkali halides.[1] The purpose of this note is to present evidence from optical data for the formation of impurity aggregates in NaCl crystals containing Pb^{++} and to discuss the conditions under which such deviations from random distribution may, in general, be expected.

Although NaCl, KCl, and RbCl crystals containing Pb all exhibit absorption bands at approximately 2730 and 1960A, variations in the character of these bands have been noted by earlier investigators.[2] The present study has revealed additional bands in NaCl:Pb which vary with the growth and thermal history of the specimen.[3] Similar variations with growth history have been observed in the absorption bands of other impurities in alkali halides, particularly in NaCl:Cu and KCl:Cu.[4]

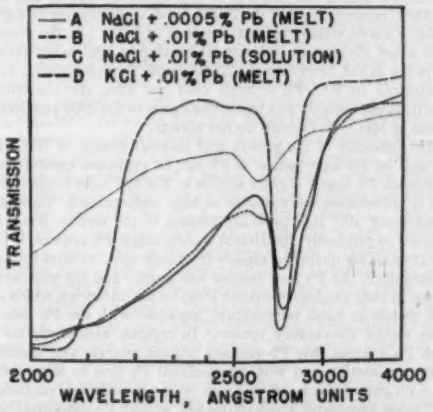

FIG. 1. Transmission curves of NaCl:Pb crystals, grown from the melt and from solution, contrasted with a curve for a melt-grown KCl:Pb crystal. The concentrations of Pb shown are those in the melt and solution. The corresponding concentrations in the crystals are lower.

Transmission curves for several NaCl:Pb crystals grown from the melt and from solution are shown in Fig. 1, together with a curve for a melt-grown KCl:Pb crystal.[5] The NaCl:Pb curves are markedly different from the KCl:Pb curve in every case. Absorption bands appear at 2900 and 2600A in NaCl:Pb which are absent in KCl:Pb, while bands appear at 2050, 2100, 2300, and 2450A in KCl:Pb which are absent in NaCl:Pb. In one curve, which is typical of a number of NaCl:Pb crystals with low Pb content, only the 2600A band appears. The curves for NaCl:Pb crystals with high Pb content (not shown), on the other band, resemble those for $PbCl_2$ films.

The effect of various heat treatments (always followed by rapid quenching to room temperature) on the absorption bands of two of the melt-grown NaCl:Pb crystals is shown in Fig. 2. In each

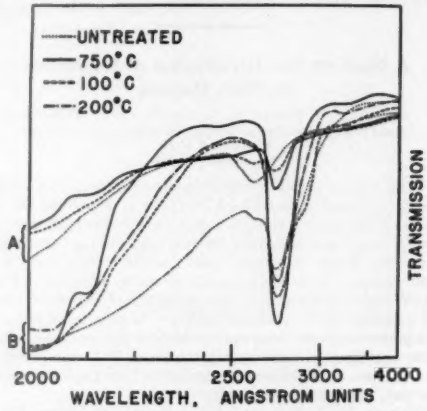

FIG. 2. The influence of various heat-treatments followed by rapid quenching to room temperature on the Pb absorption spectrum of two melt-grown NaCl:Pb crystals, specimens *A* and *B* of Fig. 1.

case heating at 750° yields curves which are similar to the KCl:Pb curve of Fig. 1. After several days at room temperature, the 2730A band in the crystal with high Pb content weakens and a new band appears at 2900A. The same result is obtained by heating the crystal for only a few minutes at approximately 100°C. Heating at 200°C removes most of the 2900A band, while heating at 400°C yields a curve similar to that obtained at 750°C. In the crystal with a low Pb content, subsequent heating at 100° partly reconverts the 2730A band into the 2600A band. Applying similar heat treatments to KCl:Pb crystals does not alter the absorption spectrum appreciably and bands analogous to the 2900 and 2600A bands in NaCl:Pb crystals do not appear.

The influence of the growth and thermal history of NaCl:Pb crystals on the aggregation of Pb can be explained qualitatively as follows. Pb is only slightly soluble in NaCl at room temperature but is appreciably more soluble at high temperatures. Above approximately 400° it is probably present in the various NaCl:Pb crystals as randomly distributed mobile single Pb centers. When the crystals are quenched rapidly from high temperatures to room temperature, the Pb ions become less mobile and are practically frozen in their random positions. Positive ion vacancies, which are still mobile at room temperature, associate with the Pb ions to form mobile Pb-vacancy centers.[6] In crystals with moderate or high Pb content, the Pb-vacancy centers migrate and combine with one another and with unassociated Pb ions to form stable Pb—Pb pairs (associated with one or two positive ion vacancies) and larger aggregates which ultimately, at high Pb concentrations, precipitate out as a $PbCl_2$ phase. The rate at which these processes occur depends on the Pb concentration, the mobility of the Pb-vacancy centers, and the stability of the various clusters. The mechanism for the aggregation of Pb in NaCl is thus very similar to that suggested recently for the aggregation of trapped holes in the alkali halides.[1] In crystals with low Pb content the tendency to form Pb—Pb pairs and larger aggregates is quite small since it depends on the second or higher power of the Pb concentration. On the other hand, Pb may combine with vacancy clusters or with other impurities (possibly O^{--} which may be present) to form centers which depend on the first power of the Pb concentration.

On the basis of these considerations it is suggested tentatively that the 2900A band is due to Pb—Pb pairs, the 2600A band is due to Pb-impurity or Pb-vacancy cluster centers, and the 2730A band is due to a combination of single Pb centers, Pb-vacancy centers, and $PbCl_2$.

In general, a stable aggregation of two or more impuritity atoms may be expected whenever the binding force between impurities is greater than that between impurity atoms and atoms of the host crystal. Aggregation will also be favored whenever the strain energy associated with the distortion of the lattice in the vicinity of the impurity cluster is smaller than that caused by the single impurity atoms. Lattice defects in the form of vacancies and dislocations also play an important role in impurity aggregation.[7] The lattice distortion is probably a dominant factor in the aggregation of Pb in NaCl. Thus, cluster formation occurs readily in NaCl where Pb^{++} ($r=1.32$A) is larger than Na^+ ($r=0.98$A), but not in KCl, where Pb^{++} is the same size as K^+ ($r=1.33$A). The same factor is probably also dominant in the aggregation of Cu in NaCl and in KCl.

[1] F. Seitz, Phys. Rev. **79**, 529 (1950); E. Burstein and J. J. Oberly Phys. Rev. **79**, 903 (1950).
[2] R. Hilsch, Z. Physik **44**, 860 (1927).
[5] Analogous variations in the Pb excitation spectrum have been observed by Schulman, Ginther, and Klick (private communication).
[6] A. M. MacMahon, Z. Physik **52**, 336 (1928); R. Hilsch, Proc. Phys. Soc. (London) **49**, (extra part) 40 (1937).
[5] These crystals were kindly supplied by L. R. Johnson and W. Zimmerman of the Crystal Growing Section of the Crystal Branch.
[6] Mapother, Crooks, and Maurer, J. Chem. Phys. **18**, 1231 (1950).
[7] A. H. Cottrell, *Report of a Conference on Strength of Solids* (The Physical Society, London, 1948), p. 30; F. Seitz, Acta Crys. **3**, 355 (1950).

Quantum Efficiency of Bismuth Counters for Electromagnetic Radiation of 0.07-Mev to 2.8-Mev Energy*

R. J. HART, K. RUSSEL, AND R. M. STEFFEN
Department of Physics, Purdue University, Lafayette, Indiana
December 6, 1950

THE absolute quantum efficiency of Geiger-Müller counters has been measured by several authors using the coincidence method.[1] This method presupposes a knowledge of the decay schemes of the radioactive isotopes used and of the angular correlation of successively emitted radiations. It has only been in the last few years, however, that an appreciable number of decays has become completely known and only recently have angular correlation measurements been performed with success. For these reasons it seemed worthwhile to redetermine the quantum efficiency of G.-M. counters as a function of the energy of the incident radiation. At the same time the variation of the local efficiency at different points of the counters was investigated.

The counter tubes used were of the cylindrical type having bismuth cathodes of 0.77-g/cm² thickness for the detection of high energy gamma-radiation (0.4–3.0 Mev) and 0.080-g/cm² thickness for the low energy region (0.07–0.4 Mev). The counters were filled with argon (9 cm Hg) and ethyl alcohol (1 cm Hg).

The local efficiency of the counters was measured with a well collimated gamma-ray beam using energies of 0.511, 0.73, 1.25, and 2.62 Mev. The intensity of the beam was calibrated with an anthracene scintillation counter. The quanta absorbed in the anthracene crystal were known to be detected with an efficiency of (96±6) percent. A considerable variation of the local efficiency across the G-M counter was observed (points in Fig. 1). It was found, however, that this variation can be well described by assuming that all secondary electrons counted are produced in an

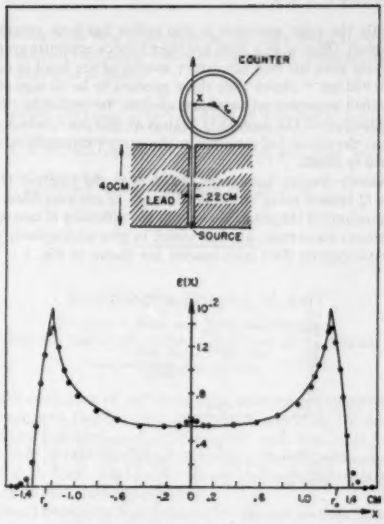

FIG. 1. Variation of the local efficiency across the diameter of the counters. The open circles represent the measured values. The solid line is calculated for a γ-beam of 0.22 cm width.

"effective layer" of the counter cathode and that all electrons produced in this layer reach the sensitive volume. The thickness of this hypothetical layer depends, of course, on the quantum energy of the radiation to be measured. The local efficiency is then simply given by the fraction of the radiation absorbed in this layer (solid curve in Fig. 1). From the local efficiency, an average efficiency for infinitely large source distance can be computed (double circles in Fig. 2).

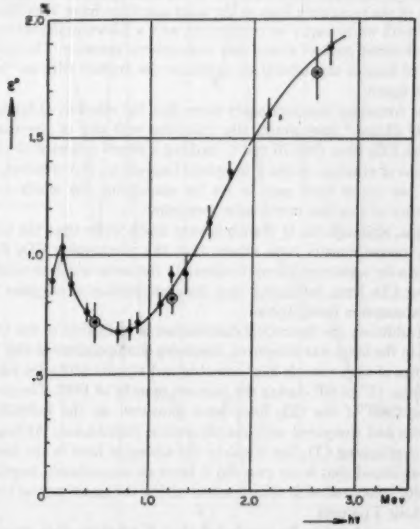

FIG. 2. Practical efficiency of γ-counters with bismuth cathodes plotted as a function of quantum energy.

A convenient definition of a *practical* efficiency is the following:

$$\epsilon^*(h\nu) = (4\pi/\Omega)\cdot(D(h\nu)/\bar{A}(h\nu)),$$

where $D(h\nu)$ is the detection probability for electromagnetic radiation of energy $h\nu$, Ω is the solid angle subtended by the counter volume at the source and $\bar{A}(h\nu)$ is a factor describing the absorption of the radiation in the counter wall. Neglecting the variation of the local efficiency as far as attenuation of the radiation in the counter wall is concerned, we write for $\bar{A}$: $\bar{A}(h\nu) = \int_\Omega \epsilon^{-\mu d} d\Omega/\Omega$. The variation of the local efficiency makes it doubtful that a practical efficiency, as defined above, exists which is independent of the distance between the counter and the source. Measurements made at source distances from 4.0 cm up to 150 cm showed, however, that the practical efficiency varied less than 4 percent. It was also found that the error involved by calculating $\bar{A}$ using the above mentioned simplification was less than 2 percent for $\bar{A} > 0.5$.

The detection probability $D(h\nu)$ for a particular counter arrangement was determined from gamma-gamma and beta-gamma coincidence data for electromagnetic radiation of different quantum energies. The data were obtained from measurements on Sc^{46}, Co^{60}, Rh^{106} (obtained from the Isotopes Division of the U. S. AEC, Oak Ridge) and Na^{24}, Al^{28}, Cl^{38}, Mn^{56}, In^{111}, Hg^{197}, and Au^{198} (produced by deuteron bombardment in the Purdue cyclotron). Corrections were applied for the angular correlation of the gamma-rays[3] and for coincidence losses due to the intrinsic time lag of the counters. In Fig. 2 the practical efficiency for counters with bismuth cathodes calculated from the measured detection probability is plotted as a function of the quantum energy.

* Supported by contract with ONR.

[1] Bradt *et al.*, Helv. Phys. Acta **19**, 77 (1946); F. Norling, Arkiv för Matematik, Astronomi och Fysik **27A**, No. 27 (1941); H. Maier, Leibnitz, Zeits. f. Naturforschung **1**, 243 (1946).

[2] E. L. Brady and M. Deutsch, Phys. Rev. **78**, 558 (1950); R. M. Steffen ibid. **80**, 115 (1950).

The Beta-Spectrum of Tc^{99}

S. I. TAIMUTY
University of Southern California, Los Angeles, California*
December 4, 1950

MANY observers[1] have reported success in fitting the spectra of forbidden beta-transitions into the theory of beta-decay. Tc^{99}, with a half-life[2] of 2.12×10^5 yr. and an endpoint[3] of 300 kev, falls into the forbidden classification, and should provide another useful test of the theory. Since the only published spectrum[3] was obtained with a 10 mg/cm² source, it was felt that the spectrum should be remeasured with a thinner source.

The present investigation was undertaken with a sample of Tc^{99} in the form NH_4TcO_4 supplied by the Isotope Division of the AEC at Oak Ridge. The measurements were made in a double thin lens magnetic spectrometer described elsewhere.[4] The sources were mounted on 0.02 mg/cm² Nylon films coated with Aquadag. A 0.03 mg/cm² Nylon counter window, which produced no significant absorption above 30 kev, was used in all of the measurements.

Because of the low specific activity of the sample, the spectrometer was adjusted to 6.5 percent resolution, and the spectra were corrected for resolution by the method of Owen and Primakoff.[5] For the same reason, sources thinner than 0.17 mg/cm² could not be used. In order to determine the energy at which distortion due to source thickness would become effective, measurements were made on sources varying in thickness from 0.17 to 1.3 mg/cm². In addition, supplemental runs were made with sources of Pm^{147} varying in thickness from 0.025 to 0.17 mg/cm². For these runs, the spectrometer adjustments were identical with those used for the technetium sources. The sources were also examined for non-uniformities in thickness by autoradiographic methods. In particular, microdensitometer measurements on an autoradiograph of the thinnest Tc^{99} source showed that the thickness varied from 0.05 to 0.29 mg/cm². The thickest portion covered approximately 10 percent of the source area, the remaining area being divided in the ratio of about 6:4 between fairly uniform

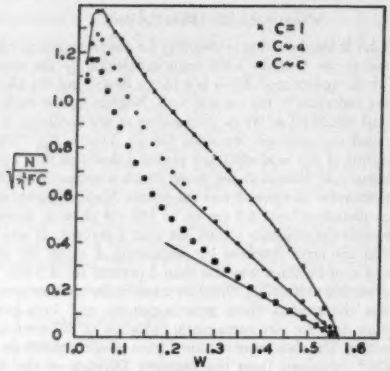

FIG. 1. Fermi plots for Tc^{99}.

deposits of thicknesses 0.17 and 0.05 mg/cm². Taking account of the large errors inherent in this type of determination, the results of this work showed that for the thinnest Tc^{99} source used, distortion due to source thickness should probably be negligible at energies greater than 125 to 150 kev.

Fermi plots of the thin source data are shown in Fig. 1. The end-point energy was determined to be 0.292±0.003 Mev from runs on four different sources. Using this value and the half-life quoted above, an *ft* value of 2.3×10^{13} is obtained. Empirically, this figure would make the transition at least second-forbidden. In addition, the nuclear shell model[2] predicts a probable spin change of 3 units and no parity change, thus classifying the transition as second-forbidden under the G-T selection rules. In such a case, the correction factor $c\sim3p^4+10p^2q^2+3q^4$ should apply. Examination of Fig. 1 shows that this factor yields a straight line plot down to approximately 200 kev. The results obtained with the other second-forbidden correction factors having a definite energy dependence were in all cases worse. (No attempt was made to apply the correction factors containing a combination of matrix elements.) Application of the correction factor $a\sim p^2+q^2$ produced a fairly good straight line down to approximately 140 kev. As noted above, this is the region in which distortion due to source thickness might be expected for a source of the thickness used. It seems plausible to conclude, then, that the correction factor *a* applies, and that the transition is probably first-forbidden, $\Delta J=\pm2$ (yes), under the G-T selection rules. This conclusion leaves the large *ft* value unexplained. Because of the source thickness used, however, these results should be verified with a thinner source when higher specific activity material becomes available.

I would like to thank Drs. C. M. Van Atta and S. D. Warshaw for their advice and encouragement during the course of this work.

* This work was supported by the joint program of the ONR and the AEC.

[1] H. M. Agnew, Phys. Rev. **77**, 655 (1950); Hughes, Eggler, and Alburger, Phys. Rev. **77**, 726 (1950).
[2] Jaffey, Fried, Hall, and Glendenin, Phys. Rev. to be published.
[3] B. H. Kettelle and J. W. Ruch, Phys. Rev. **77**, 565 (1950).
[4] Van Atta, Warshaw, Chen, and Taimuty, Rev. Sci. Instr. **21**, 985 (1950).
[5] G. E. Owen and H. Primakoff, Phys. Rev. **74**, 1406 (1948); see also discussion in reference 4.
[6] E. Feenberg and K. C. Hammack, Phys. Rev. **75**, 1877 (1949).

The Absence of Atmospheric Ethylene*

J. H. SHAW AND H. H. CLAASSEN
Mendenhall Laboratory, Ohio State University, Columbus, Ohio
December 6, 1950

SUTHERLAND and Callendar[1] have suggested resemblances between the atmospheric spectrum taken by Adel[2] with a grating spectrometer and the spectrum of ethylene near 950 cm^{-1}.

Recently the solar spectrum in this region has been remapped at Columbus, Ohio, with a 3600 line/inch replica echelette grating. Comparison with our own laboratory spectra of the band of ethylene near 950 cm^{-1} shows that there appears to be no sign of the ethylene fine structure on our solar spectra. In particular, there is no indication of the intense Q branch at 950 cm^{-1}, which suggests that the amount of ethylene in the earth's atmosphere must be extremely small.

Laboratory spectra have been taken near the position of the ethylene Q branch using an absorption cell 15 cm long filled with known amounts of ethylene. Because of the difficulty of measuring low pressures accurately, air was added to give atmospheric pressure for all spectra. Two such spectra are shown in Fig. 1.

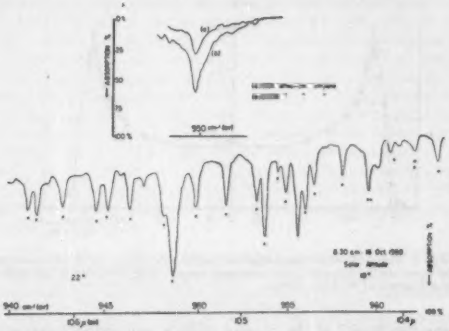

FIG. 1. Upper Curves: Laboratory spectra of ethylene showing Q branch at 949.76 cm^{-1}. Lower Curve: Solar spectrum from 940 to 960 cm^{-1}.

Beneath these is a solar spectrum taken at low solar altitudes to enhance atmospheric lines in this region. The regularly spaced series of weak lines marked with a dot belong to the band of CO_2 centered at 961 cm^{-1} which has been measured in the laboratory by Barker and Adel[3] and observed in the solar spectrum by Adel.[4] Most of the remaining lines in the solar spectrum have been identified with water vapor by comparison with a laboratory spectrum of an 8-meter path of steam near atmospheric pressure. The positions of lines in this laboratory spectrum are marked with an "x" in the figure.

Our frequency measurements show that the ethylene Q branch at 949.75 cm^{-1} (air) practically coincides with one of the most intense CO_2 lines (949.76 cm^{-1}), making a direct estimate of the amount of ethylene in the atmosphere impossible. Nevertheless, a very low upper limit may be set by considering the width and intensity of this line in the solar spectrum.

Thus, although the Q branch is very much wider than the CO_2 lines, measurements have shown that the overlapping CO_2 line in the solar spectrum has approximately the same width as neighboring CO_2 lines, indicating that the contribution of ethylene to this absorption is negligible.

In addition, the theoretical distribution of intensities of the CO_2 lines in the band was computed, assuming a temperature of 250°K. A series of solar records has been obtained at solar altitudes varying from 15° to 60° during the summer months of 1950. The peak absorptions of the CO_2 lines were measured on the individual records and compared with the theoretical distribution. Although the overlapping CO_2 line is one of the strongest lines in the band, it was found that in no case did it show an anomalously large intensity compared with other lines to within the experimental error of about 3 percent.

It must therefore be concluded that if ethylene does exist in the atmosphere, the amount present must be much smaller than the 0.01 atmos.-cm giving the absorption in the figure.

From the work now in progress on the solar spectrum from 7 to 13μ it is hoped that upper limits will be set to a series of other suspected atmospheric gases.

* This work was supported in part by contract between the U. S. Air Force and the Ohio State University Research Foundation, through sponsorship of the Geophysical Research Directorate, Air Force Cambridge Research Laboratories.

[1] G. B. B. M. Sutherland and G. S. Callendar, Rep. Prog. Phys. IX, 18 (1943).
[2] A. Adel, Astrophys. J. 94, 451, 1941.
[3] E. F. Barker and A. Adel, Phys. Rev. 44, 185, 1933.
[4] A. Adel, Astrophys. J. 94, 379, 1941.

Scintillation Spectra of As^{76}

JOE KRAGY BAIR AND FRED MAIENSCHEIN
Fairchild Engine and Airplane Corporation, NEPA Division, Oak Ridge, Tennessee
November 20, 1950

THE radiations of As^{76} have been investigated extensively in the past. Gamma-rays of approximately 0.57, 1.2, and 1.75 Mev have been reported by Siegbahn[1] and Wu, *et al.*,[2] while Miller and Curtiss[3] have found, in addition to the above, a gamma-ray at 2.15 Mev. The present investigation also indicates the presence of this fourth gamma-ray.

Radioactive arsenic was prepared by thermal neutron bombardment of part of the National Bureau of Standards sample No. 83a (>99.99 percent purity) of arsenic trioxide. The resulting activity had a half-life of 27.6±1 hours with no indication of the presence of any other period. Figure 1 shows the spectra obtained with a single one-inch sodium iodide crystal. The high energy peaks were obtained with a stronger source. The observed energies are listed in Table I.

Further investigation of the spectra was made with a Hofstadter type two-crystal spectrometer.[4] The energies so determined are also listed in Table I. All energy determinations were based on calibrations with Cs^{137} and Co^{60}. The two crystal spectra, Fig. 2, clearly indicates the presence of four gamma-rays.

TABLE I. Gamma-rays from As^{76}.

Number	Energy from single crystal Mev	Energy from coincidences Mev
1	0.59	0.58
2	1.19	1.20
3	1.73	1.76
4	1.99	2.02

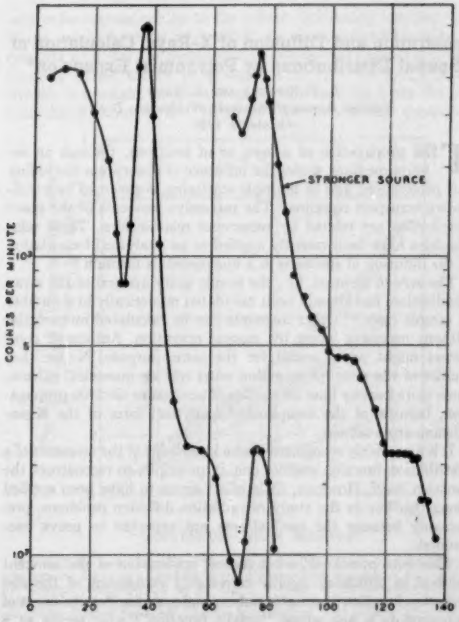

FIG. 1. Single crystal spectrum of As^{76}.

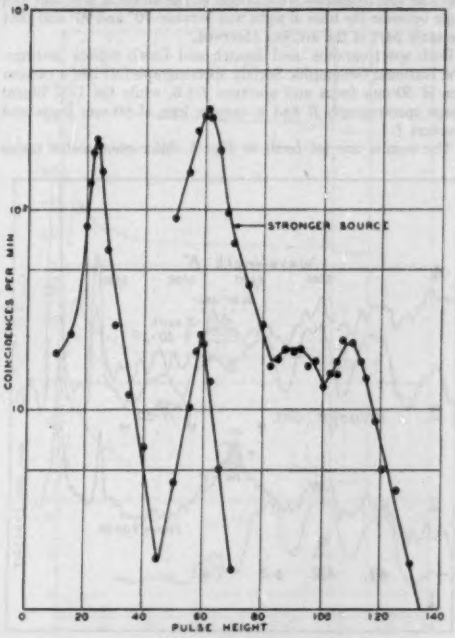

FIG. 2. Hofstadter-type two-crystal spectrum of As^{76}.

The two crystal curves were taken with the geometry described by the authors.[5] The gamma-ray energies were calculated from the observed recoil-electron energies together with the known degraded crystal geometry. If there is a cross-over gamma-ray of between 2.3 and 2.7 Mev as indicated by Myers and Wattenberg,[6] its intensity must be less than 10^{-4}.

[1] K. Siegbahn, Arkiv Fysik, 34A, No. 7 (1947).
[2] Wu, Havens, and Rainwater, Phys. Rev. 74, 1248 (1948).
[3] L. C. Miller, and L. F. Curtiss, Phys. Rev. 70, 983 (1946).
[4] R. H. Hofstadter and J. A. McIntyre, Phys. Rev. 78, 619 (1950).
[5] Bair, Maienschein, and Baker, Phys. Rev. 81, 283 (1951).
[6] U. Myers and A. Wattenberg, ANL-4174, 33 (1948), unpublished.

Protons and the Aurora*

C. W. GARTLEIN
Physics Department, Cornell University, Ithaca, New York
December 4, 1950

AT the conference on Ionospheric Physics at Pennsylvania State College in July, D. F. Martyn presented a theory of magnetic storms and aurora which assigned a primary role to

protons ejected by the sun. Since previous work[1] had shown the hydrogen lines in auroral spectra to be broadened, the writer and D. F. Berkey determined at that time to make a critical test of the hydrogen using two spectrographs. One spectrograph was set up at the airport at Arnprior, Ontario, 330 km north of the second spectrograph at Ithaca, New York.

On the night of September 30, 1950, a moderate aurora appeared with homogeneous arcs and later rayed arcs at elevations of about 10° and 20° above the northern horizon as seen from Ithaca.

The spectrograph (called *B*) at Ithaca was aimed at the arc at 20°, while H. Stevinson of the Flight Research Section at Arnprior operated spectrograph *A* so that it pointed between the zenith and 10° north of the zenith. Telephone communication assured that the spectrographs were aimed at *the identical arc*, that the angle between the lines of sight was between 70° and 90° and that the same part of the arc was observed.

Both spectrographs used Bausch and Lomb replica gratings. The National Geographic Society spectrograph (*A*) had a camera lens of 50-mm focus and aperture *f*:1.6, while the U.S. Signal Corps spectrograph *B* had a camera lens of 90-mm focus and aperture *f*:1.

The results are set forth in Fig. 1. Microphotometer traces

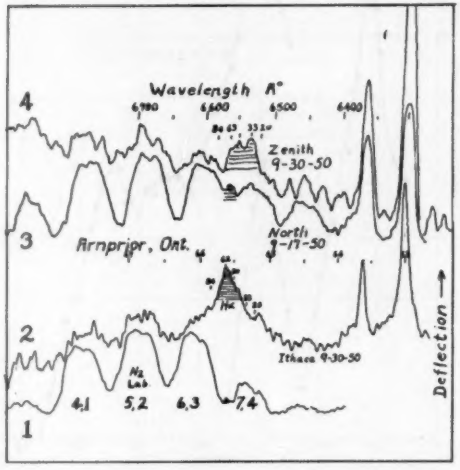

FIG. 1. Microphotometer traces of three aurora spectrograms. Spectra 2 and 4 taken simultaneously. Curves displaced in deflection direction.

were made of the several plates, and these were photographed so that the dispersions were brought to a common scale. Trace 1 is the spectrum of a nitrogen discharge in the laboratory. Trace 3 is from an aurora at elevation 20° above the north horizon at Arnprior. Trace 2 from Ithaca and trace 4 from Arnprior are from the simultaneous spectra of this experiment. In trace 2 the $H\alpha$ line is an outstanding feature and of the same intensity as OI 6363A. The $H\alpha$ is centered on 6562A and is nearly symmetric. The extension on the blue side is presumed to be due to superposition on N_2 band 7,4. The cross lines indicate the wavelength range over which $H\alpha$ was probably spread, that is, from about 6580 to 6535. In trace 4 the $H\alpha$ peak rises sharply from about 6575 to the peak at 6563 and spreads to shorter wavelength to approximately 6520. Thus, there is a clear shift to shorter wavelength on the Arnprior spectrum which is consistent with motion of the hydrogen in spiralling down the lines of magnetic force. The graininess of the records and interference from N_2 bands prevents precision in velocity determination, but preliminary conclusions can be drawn. Trace 2 gives an $H\alpha$ broadening to red and violet of about 10A, indicating a velocity 450 km/sec in the line of sight. This is either the velocity of the scattered hydrogen or the line of sight component of the spiralling velocity. From trace 4 we estimate a mean shift of 15A and a maximum of at least 30A, giving a mean velocity of 675 km/sec and maximum velocity of 1350 km/sec. The experiment will be repeated.

Thus, this experiment establishes that the auroral hydrogen is coming into the earth's atmosphere from outside. Since our previous spectra taken about at right angles to the auroral rays (earth's field) show only a broadening, even when the spectrograph was aimed eastward, while this spectrum taken along the rays shows a broadened shift, we see that there is a strong influence of the earth's field and that the particles are charged; therefore, they must be protons.

Similar results have been obtained by Meinel[2] with two exposures by the same spectrograph, on the great aurora of August 19 (cloudy at Ithaca). His two pictures from the same station show the broadening and a much greater shift. The maximum velocity found was 3200 km/sec. These high velocities occurred during a great aurora (magnetic disturbance $K=9$) while the velocities we find, about 1350 km/sec occurred during a moderate aurora, $K=5$. This suggests that there is a relation between the incoming velocities and the size of aurora, and also that protons may be the immediate cause of the aurora. That the hydrogen behaves in this manner is attested by the broadness of $H\beta$ on all our plates taken since 1940 and by the shift of $H\alpha$ appearing in two auroras at widely separated points at different times.

Thanks are here expressed to D. W. R. McKinley of the National Research Council of Canada and G. S. Levy of the Flight Research Section for use of the facilities at Arnprior and to H. Stevinson for operating the spectrograph.

* This research was supported in part by the National Geographic Society and by the U. S. Signal Corps.

[1] C. W. Gartlein, Document T124 Intern. Assoc. Terr. Magn. Elec. U.G.G.I., Oslo assembly, 1948; C. W. Gartlein, Phys. Rev. **74**, 1208 (1948); C. W. Gartlein, Trans. Am. Geophys. Union **31**, 18 (1950).

[2] A. B. Meinel, private communication; Science **112**, November (1950); Phys. Rev. **80**, 1096 (1950).

Penetration and Diffusion of X-Rays. Calculation of Spatial Distributions by Polynomial Expansion*

L. V. SPENCER AND U. FANO
National Bureau of Standards, Washington, D. C.
October 9, 1950

THE propagation of x-rays, or of neutrons, through an infinite medium, under the influence of absorption (including pair production) and of multiple scattering, is governed by a well-known transport equation.[1] The successive moments of the space distribution are related by recurrence relationships. These relationships have been recently applied to an analytical formulation of the diffusion of electrons in a homogeneous medium.[2]

The zero-*th* moment, i.e., the simple space integral of the x-ray distribution, has already been calculated numerically in a number of sample cases.[3,4] Other moments can be calculated numerically without excessive labor, by manual operation. Automatic computers might prove useful for the same purpose. Notice that studies of the x-ray propagation must rely on numerical calculations more heavily than do studies of neutron or electron propagation, because of the complicated analytical form of the Klein-Nishina cross section.

It is also widely recognized that a knowledge of the moments of a distribution function enables one, in principle, to reconstruct the function itself. However, little effort seems to have been applied along this line in the study of radiation diffusion problems, presumably because the method was not expected to prove convenient.

This note points out a convenient application of the moment method in obtaining rapidly convergent expansions of the distribution function in suitable polynomial systems. A suitable set of polynomials is one whose "weight function"[5] $w(x)$ serves as a

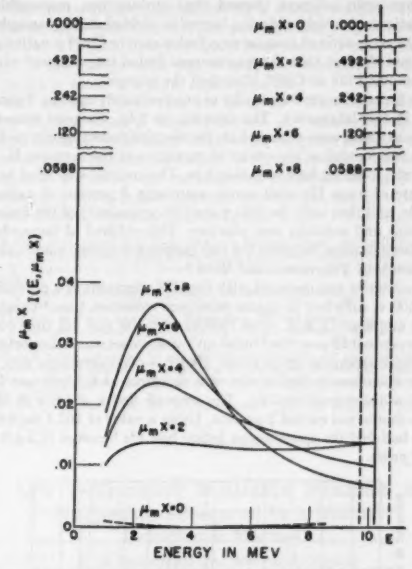

FIG. 1. Differential spectra $I(E, \mu_m x)$ of the x-ray intensity at various distances from a plane monodirectional 10.2-Mev source in Pb. The position of the source spectrum is indicated by the solid vertical line, its intensity by the area of the dotted rectangle. The scale of ordinates is normalized to unit strength of the source at $x=0$; at greater depths it discounts an exponential decay corresponding to the absorption coefficient μ(3.2 Mev) $=\mu_m=0.469$ cm^{-1} of the most penetrating component. The dotted line for $x=0$ departs from the base line only because of the approximations made.

zero-order approximation to the actual distribution function $f(x)$. If the weight function $w(x)$ which one chooses should happen to coincide with $f(x)$ the corresponding polynomial expansion of this function would reduce to a single term $[f(x)=w(x)\cdot 1]$. Even though the weight function departs substantially from the actual distribution, a few terms of the polynomial expansion

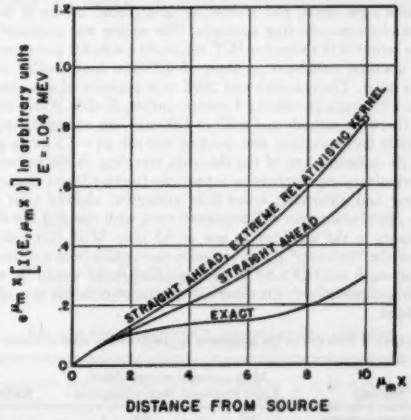

FIG. 2. Differential intensity $I(E, \mu_m x)$ of the 1.04-Mev component of the spectrum of Fig. 1 as a function of the distance from the source, calculated by different methods: (a) as in Fig. 1 ("exact"), (b) disregarding the deflection of scattered photons ("straight ahead"), (c) using the extreme relativistic form of the Klein-Nishina cross section. The point at the end of the top curve is the result of an asymptotic calculation by Karr and Hurwitz (unpublished).

$[f(x)\sim w(x)[1+P_1(x)+P_2(x)+\cdots]]$ appear to compensate the departures effectively over a wide range of values of x.

This procedure has been tested by application to standard (Bessel and confluent hypergeometric) mathematical functions. A simple exponential decay proves to be quite adequate as a choice of weight function for the distribution of x-rays up to fairly deep penetration into a material (10 to 15 mean free paths of the primary radiation).

A full report on these calculations will be given in the *Journal of Research* of the National Bureau of Standards.

Two initial numerical applications have been made:

(a) *Plane monodirectional source of 10.2-Mev x-rays in lead.*—This calculation was extended only down to an energy of 1.04 Mev.

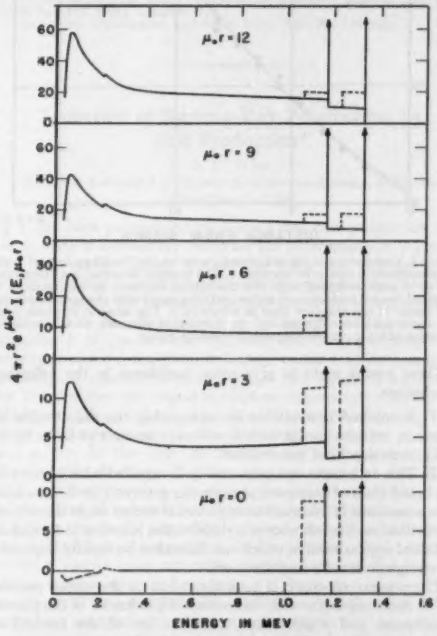

FIG. 3. Differential spectra $I(E, \mu r)$ of the x-ray intensity at various distances r from a Co^{60}-point isotropic source in water. The positions of the two lines of the source spectrum are indicated by the solid vertical lines, their intensities by the area of the dotted rectangles. The scales of ordinates are normalized to unit intensity of the 1.33-Mev component of the source; $\mu_o=0.0612$ cm^{-1} is the narrow-beam absorption coefficient of this component.

Therefore backscattering could be disregarded and one could use an ordinary expansion in Laguerre polynomials. Four terms of the expansion were used. The results tre shown in Figs. 1 and 2.

(b) *Co^{60} isotropic point source of x-rays in water.*—This calculation has been extended down to energies at which the photoelectric absorption suppresses the secondary radiation, so that comparisons could be made with the experimental results.[6] This application required the development of special non-self-adjoint polynomial expansions which utilize only even- or odd-order moments. Four terms of the expansion were used. The results are shown in Figs. 3 and 4.

Analytical formulas have also been developed for plane monodirectional, plane isotropic, and point monodirectional source geometries. The latter geometry is the basic one, in that any source may be resolved into a combination of point monodirectional sources. Sample numerical applications of these formulas are in progress.

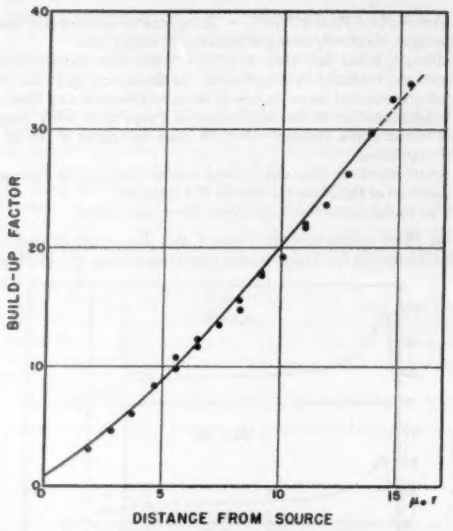

FIG. 4. Comparison of the calculated curve for the "build-up factor" with the experimental results of reference 6. The spectral distributions illustrated in Fig. 3 were weighted with the theoretical response in roentgens of a standard free air ionization chamber and then again with the specific correction factor of the chamber used in reference 6. The integral response over the whole spectrum divided by the calculated response to the primary radiation alone gives the theoretical build-up factor.

These results seem to give some confidence in the following conclusions.

(1) A method is available for calculating the distribution of x-rays in uniform media with a moderate amount of labor up to fairly large depths of penetration.

(2) This technique can presumably be applied with success to the broad class of transport phenomena governed by Boltzmann-type equations. It takes advantage even of rather crude theoretical predictions on the behavior of a distribution function to formulate an initial approximation which can thereafter be rapidly improved by straightforward numerical work.

The present approach is complementary to the earlier papers[7] which dealt primarily with the asymptotic behavior of the photon distribution and which made extensive use of the method of Laplace transforms. The work reported in those papers has now been developed into a more comprehensive treatment which will be the object of a separate report.

We wish to thank Mrs. F. A. Stinson for carrying out most of the numerical work.

* Work supported by the ONR, Applied Mathematics Branch.

[1] R. E. Marshak, Revs. Modern Phys. **19**, 201 (1947), Eq. (63); the kernel of the equation depends on the pertinent physical mechanism of scattering.
[2] H. W. Lewis, Phys. Rev. **78**, 526 (1950).
[3] P. R. Karr and J. C. Lamkin, Phys. Rev. **76**, 1843 (1949).
[4] L. V. Spencer and Fannie Jenkins, Phys. Rev. **76**, 1885 (1949).
[5] D. Jackson, *Fourier Series and Orthogonal Polynomials*, (Mathematical Ass. of Amer. Monograph, 1941), p. 149.
[6] G. R. White, Phys. Rev. **80**, 154 (1950).
[7] U. Fano, Phys. Rev. **76**, 739 (1949); Fano, Hurwitz, and Spencer, Phys. Rev. **77**, 425 (1950).

Spontaneous Fission in Cm^{242}

G. C. HANNA, B. G. HARVEY, N. MOSS, AND P. R. TUNNICLIFFE*
Atomic Energy Project, National Research Council of Canada, Chalk River, Ontario, Canada
December 4, 1950

SPONTANEOUS fission has been observed in Cm^{242}. It was detected initially in samples of Am^{241} irradiated with slow neutrons in the Chalk River pile. Chemical separation in ion-exchange resin columns showed that curium was responsible. Irradiations of widely differing intensity yielded curium samples with the same ratio of spontaneous fission rate to Cm^{242} α-activity. This, and the fact that the spontaneous fission rate decayed with the same half-life as Cm^{242}, identified the isotope.

The fission counter was similar to one previously used by Tunnicliffe[1] in this laboratory. The samples, on 1-in. diameter smooth platinum disks, were mounted on the electron collecting electrode, which was located at the center of curvature of the negative H.T. electrode, a hemisphere of radius 2 in. The counter was filled to a pressure of 8 cm Hg with argon containing 5 percent of carbon dioxide, and thus only the first $\frac{1}{4}$ cm (air equivalent) of the fission fragment and α-tracks was effective. This method of improving the discrimination between the two particles was first used in this laboratory by Pontecorvo and West.[2]

The counter was operated with the H.T. electrode at a potential of -400 v, sufficient to ensure minimum collection time.[3] Using a linear amplifier (T.R.E. type 1008A) with rise and fall time constants set to 0.15 μsec the "build-up" of α-pulses was unimportant for source strengths up to about 3×10^3 α-disintegrations/min.

The spontaneous fission rate was measured as 6.2/min per 10^3 Cm^{242} α-disintegrations/min. The over-all limits of error in this figure should not exceed 2 percent. Using a value of 162.5 days for the α half-life[4] the spontaneous fission half-life becomes $(7.2\pm0.2)\times10^6$ years.

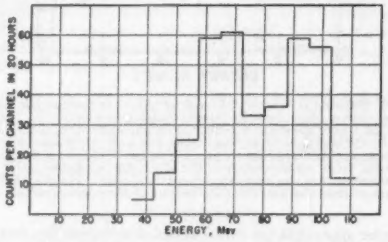

FIG. 1. Energy distribution of the fission pulses.

A rough measurement was made of the energy distribution of the spontaneous fission fragments in an ionization chamber rather similar to that described by Bunemann, Cranshaw, and Harvey.[5] The ion chamber contained two plane parallel electrodes 10 cm square 4.3 cm apart, and a shielding grid placed 1.5 cm in front of the electron-collecting electrode. The source was mounted in in the center of the negative H.T. electrode (cathode) and covered with a simple collimator, a sheet of 0.37-mm brass drilled with 3-mm holes. The chamber was filled to a pressure of one atmosphere with argon containing 5 percent carbon dioxide. A collecting field (between cathode and grid) of 470 volts/cm was used, amply adequate for saturation, and the grid was run at -1.5 kv to prevent its collecting any of the electrons traveling to the collector.

Preliminary experiments on α-particles (using a larger electrode spacing and somewhat lower field strengths) showed that the pulse distribution was well preserved even with rise and fall time constants in the amplifier as low as 0.5 μsec. With this fast response the "build-up" pulses of fission energy size from a source of the strength used (5×10^6 α-disintegrations/min) would be negligible compared with the observed spontaneous fission rate of 18 per hour.

TABLE I. Energies of the fragments in the fission of several nuclei.

Nucleus	Most probable energy (Mev) Light fragment	Heavy fragment	Ratio
Spontaneous fission in Cm^{242}	95	65	
	97, 94	68, 66	1.43
	91	65	
$Pu^{239}+n$	94.6	65.2	1.45
$U^{235}+n$	94.5	60.2	1.57
$U^{233}+n$	93.0	56.6	1.64

The fission pulses were sorted by a simple ten-channel pulse analyzer and recorded on a ten-pen Esterline Angus operation recorder. The distribution obtained in one of the runs is shown in Fig. 1. The energy scale was obtained by comparison with the α-pulses in terms of a pulse signal-generator.[6]

The results of three runs are given in Table I together with data on slow neutron fission.[7] Before any detailed comparison could be made, much longer runs with finer pulse analyzer resolution would be required. Moreover, a thinner source would also be desirable. However, the investigation aimed at seeing if there were any major difference between spontaneous and slow neutron induced fission. Apparently there is not.

* Now at the Atomic Energy Research Establishment, Harwell, England.
[1] P. R. Tunnicliffe, Chalk River report CRG-449, unpublished.
[2] B. Pontecorvo and D. West, Chalk River report MP-210 (1945), unpublished.
[3] B. Rossi and H. Staub, *Ionization Chambers and Counters* (McGraw-Hill Book Company, Inc., New York, 1949), p. 14.
[4] Hanna, Harvey, and Moss, Phys. Rev. **78**, 617 (1950).
[5] Bunemann, Cranshaw, and Harvey, Can. J. Research **A27**, 191 (1948).
[6] Because of the very high α-counting rate the α-pulses were compared with the signal generator on a triggered oscilloscope. In spite of the short distance between the source and the grid, enough α-particles left the source sufficiently obliquely to give a well-resolved trace corresponding to the total α-energy.
[7] D. C. Brunton and W. B. Thompson, Can. J. Research **A28**, 498 (1950).

Low Temperature Resistance Minimum in Magnesium Measured by a Mutual Inductance Method*

H. E. Rorschach and Melvin A. Herlin
Research Laboratory of Electronics, Massachusetts Institute of Technology, Cambridge, Massachusetts
November 17, 1950

SOME experiments performed recently by the authors to investigate the low temperature resistance of magnesium have utilized a method which may prove to be useful for many types of low temperature resistance measurements. Owing to the strong influence of impurities and crystal structure on low temperature resistivities, a method was developed which makes it possible to use a bulk sample of material rather than a drawn wire. The principle utilized in this method is that the complex mutual inductance of two coaxial coils surrounding a sample depends on the conductivity of the sample. The mutual inductance is measured with a bridge. The calculations can be easily carried out for cylindrical

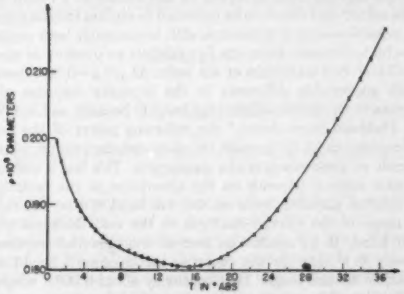

FIG. 1. A plot of resistivity *vs* temperature for a cylindrical sample of magnesium.

symmetry[1] (two coaxial coils containing a cylindrical core of conductivity σ), yielding a relation between the mutual inductance and the core conductivity. Refinements to the calculation can be introduced to correct for the finite length of the coil and the core.

This method has several advantages over the customary measurements made with wires and resistance bridges. No connections to the sample are necessary, thus eliminating contact effects and the possibility of a heat leak down the connecting wires. Single crystal samples can be easily made in a shape suitable for use in conductivity measurements. Further, the bulk resistivity comes fully into play, making small imperfections, which might greatly influence wire measurements, of little importance.

The resistivity of magnesium has been measured by this method in order to study the resistance minimum reported by Garfunkel, Dunnington, and Serin.[2] An illustration of the results is shown in Fig. 1.

At the present time, measurements are under way at this Laboratory to investigate the effect of impurity content and crystal structure on the resistance minimum.

* This work was supported in part by the Signal Corps, the Air Materiel Command, and ONR.
[1] N. W. McLachlan, *Bessel Functions for Engineers* (Oxford University Press, London, 1941), Chapter IX.
[2] Garfunkel, Dunnington, and Serin, Phys. Rev. **79**, 1 (1950).

Detection of Gamma-Ray Polarization by Pair Production*

G. C. Wick
Radiation Laboratory, University of California, Berkeley, California
December 12, 1950

IT has been pointed out by Yang,[1] that pair production may provide a method for detecting the polarization of γ-rays in the high energy range: $h\nu \gg mc^2$ (m being the electron mass) where the usual Compton recoil method becomes insensitive. The idea is to utilize the azimuthal dependence of the pair production cross section $d\sigma$, the azimuth ϕ being measured around the direction $\mathbf{k}$ of the incident quantum and from the plane containing $\mathbf{k}$ and the electric polarization vector $\boldsymbol{\varepsilon}$ of the quantum. Actually, of course, one must consider two azimuths ϕ_+ and ϕ_- for the positive and negative electron respectively. Berlin and Madansky,[2] from whose paper our notation is borrowed, have made a careful study of the dependence of $d\sigma$ on ϕ_- when $\phi_+ = \phi_- + \pi$. In this case the plane of the pair contains *exactly* the direction $\mathbf{k}$ of the incident quantum, and one can speak simply of the azimuth $\phi = \phi_-$ of the plane of the pair with respect to the plane of polarization. From the experimental standpoint it will be practically impossible to select the pairs which satisfy the Berlin-Madansky condition. Both electrons will be emitted within a narrow cone around $\mathbf{k}$, and the plane of the pair will always make a very small angle with $\mathbf{k}$. No matter whether pairs are observed in a photographic emulsion or produced in a thin target and detected with counters, scattering within the emulsion or target will unavoidably distort the initial directions to a considerable extent. It seems more reasonable, therefore, to set as our goal the measurement of the angle between the plane of the pair and the plane of polarization without any selection. The question then arises whether the case considered by Berlin and Madansky is sufficiently representative to permit a rough prediction of what is to be expected in the general case. The result of the following calculation may indicate that it is not.

The Bethe-Heitler formula for $d\sigma$ has a quite complicated dependence on the various parameters involved, so that the sign and magnitude of the effect to be expected can be seen only at the end of a laborious integration. In order to find a simpler picture we have used the Weizsäcker-Williams approximation.[3] In order to deal with pair production, Williams makes a Lorentz-transformation parallel to $\mathbf{k}$ with velocity $v = c(\xi-1)/(\xi+1)$, with $\xi = h\nu/mc^2$. In the new system the quantum has an energy $h\nu_1 = mc^2$. The method can be applied if $\xi \gg 1$ so that v is very close to c; the field of the nucleus can then be approximately substituted by a spectrum $\sim(C/\nu)d\nu$ of virtual quanta, C being a slowly variable function of ν, which we shall treat as a constant. These quanta move in the direction $-\mathbf{k}$, and if one of them, having an energy $h\nu_2 > mc^2$, collides with the real quantum, a pair may be produced. It is characteristic of the Weizsäcker-Williams

method that the transfer of momentum to the nucleus is represented by the removal of a virtual quantum from the field, and is hence parallel to **k**. Consequently the planes of all pairs produced contain **k** exactly. The difference between this statement and the apparently similar language of the Berlin-Madansky condition may be understood as follows. Presumably in the more accurate theory the probable values of the difference $\phi_+ - \phi_- - \pi$ are rather small; if this is true the procedure we follow is equivalent to averaging the Bethe-Heitler cross section over the previously difference, rather than considering the case when the difference is equal to zero. The virtual quanta are, on the whole, unpolarized. Hence we need the pair production cross section for two quanta moving in opposite directions, one of them linearly polarized, one unpolarized. This is known[4] to be, in the center of mass of the two quanta:

$$d\sigma = (\beta r_0^2/2x^3)\{(1-\beta^2\cos^2\theta)^{-1} - \tfrac{1}{2} + 2\beta^2(1-\beta^2) \times (1-\beta^2\cos^2\theta)^{-2}\sin^2\theta\cos^2\phi\}\sin\theta d\theta d\phi,$$

where βc is the velocity of either electron, $r_0 = e^2/mc^2$, $x = h\nu/mc^2 = (1-\beta^2)^{-\frac{1}{2}}$, θ is the angle between the electrons and the photons, while ϕ is the azimuth of the plane containing electrons and photons measured from the plane of polarization of the polarized photon. We integrate over θ since we are only interested in the dependence on ϕ. Finally we must transform the frequencies to the system in which one of the quanta has an energy $h\nu_1 = mc^2$, and integrate over a spectrum $Cd\nu_2/\nu_2$ for the other quantum. The result is:

$$d\sigma = \tfrac{3}{4}Cr_0^2(1+\tfrac{1}{3}\cos^2\phi)d\phi,$$

which exhibits an azimuthal dependence of comparable magnitude to that found by Berlin-Madansky in their special case. The sign, however, is the opposite: the plane of the pair prefers to be parallel to the electric vector.

The applicability of the Weizsäcker-Williams method to the present problem may be doubted; in particular one may fear that the transverse momentum transfer to the nucleus, which is neglected in this method, might affect the directions of the particles in such a way as to alter the correlation between polarization and directions of motion entirely. It may be pointed out, however, that the transverse momenta of the pair are of the order of mc, while the momentum transfer to the nucleus is much smaller than mc in a majority of the collisions[5] (if $h\nu \ll mc^2$). We believe, therefore, that the Berlin-Madansky conclusions apply only if the condition they postulate ($\phi_+ = \phi_- + \pi$) is strictly satisfied. An investigation of the Bethe-Heitler formula under more general conditions is under way.

* This work was performed under the auspices of the AEC.

[1] C. N. Yang, Phys. Rev. **77**, 722 (1950).
[2] T. H. Berlin and L. Madansky, Phys. Rev. **78**, 623 (1950).
[3] C. F. von Weizsäcker, Z. Physik **88**, 612 (1934). E. J. Williams, Kgl. Danske Videnskab. Selskab. Mat.-fys. Medd. **13**, Nr. 4 (1935) and Phys. Rev. **45**, 729 (1934).
[4] G. Breit and J. A. Wheeler, Phys. Rev. **46**, 1087 (1934).
[5] H. A. Bethe, Proc. Camb. Phil. Soc. **30**, 524 (1934). Jost, Luttinger, and Slotnick, Phys. Rev. **80**, 189 (1950).

The Masses of the Negative and Positive Electrons*

JESSE W. M. DUMOND
California Institute of Technology, Pasadena, California
December 7, 1950

BECAUSE of its far-reaching theoretical consequences, great importance attaches to the question whether positive electrons differ in mass from negative electrons and the writer has recently been urged[1] to present such experimental evidence as now exists on this point. With E. R. Cohen, he has been engaged for the last several months in the preparation of a completely new least-squares evaluation of all of the atomic constants in the light of a number of new and very precise measurements in the microwave and other fields. These results will soon be released in the form of a preprint. It appears from this study that the present "best" value of the Compton wavelength $h/(mc)$ is

$$\lambda_c = h/(mc) = (2.426067 \pm 0.000032) \times 10^{-10} \text{ cm}. \quad (1)$$

In this equation, m is clearly the mass of the negative electron because the measurements used involved negative electrons only.

On the other hand, a recent direct measurement[2] by DuMond, Lind, and Watson with the 2-meter curved crystal gamma-ray spectrometer at this Institute of the wavelength λ_A of the annihilation radiation from Cu^{64} yielded the result

$$\lambda_A = (2.4271 \pm 0.0010) \times 10^{-10} \text{ cm} \quad (2)$$

larger than λ_c by about four parts in 10^4 with an *assigned* uncertainty of about the same order as the difference, $\lambda_A - \lambda_c$.

The uncertainty of the measurement of the annihilation radiation wavelength was very conservatively, perhaps *too* conservatively, estimated with a large allowance for unknown systematic errors. On the basis of only *the internal consistency* of the seven measurements, a calculation of the probable error yields

$$\lambda_A = (2.4271 \pm 0.00012) \times 10^{-10} \text{ cm}, \quad (3)$$

which is only about one-eighth the error claimed in the paper. In fixing our assigned uncertainty at the higher value, $\pm 0.001 \times 10^{-10}$ cm, two considerations determined our estimate. (1) We were aware of a discrepancy of this order between our observed λ_A and the value of λ_c from the DuMond and Cohen[3] 1947 least-squares evaluation of the constants. (The new reevaluation of the constants has not materially changed this discrepancy.) (2) The uncertainty we assigned (and the discrepancy) correspond to a motion of our source carriage and precision wavelength screw of only 0.01 mm and this did not seem to be an unreasonable safe *upper limit of systematic* error although *we have no direct evidence that errors this large exist*. The difference between λ_c and λ_A corresponds to a quantum energy difference of a little over 200 ev.

Three possible theoretical sources of difference between λ_A and λ_c have been considered and rejected as probably[4] insufficient to explain the discrepancy. Two of these were discussed briefly (pages 1226 and 1237) in the DuMond, Lind, and Watson paper: (1) A possible shift because of the potential energies and (2) a possible shift because of the kinetic energies of the members of the recombining pairs. The low kinetic energies, which we derived from our own observation of the Doppler broadening of the annihilation line itself, have since been further verified in a beautiful independent method by De Benedetti, Cowan, and Konneker[5] with results in accord with ours. The third possible source of shift from Compton modified scattering in the source material has also been analyzed by the author in a recent letter to the editor[6] and shown to be too small to explain the discrepancy.

A possible source of systematic shift has recently been suggested to us by L. Alvarez. Since the line exhibits an observable spectral breadth at half-maximum of the order $\Delta\lambda_A/\lambda_A = 0.004$ there will be an appreciable difference in the intensity response of the instrument on the two sides of the line, (1) because, as Lind, West, and DuMond have shown,[7] the reflecting power of the crystal varies about as λ^3, (2) because the multi-cellular counter efficiency depends on some power of the wavelength. This last is difficult to estimate since it depends on the absorption of the radiation in the counter partition walls on the one hand and on the ratio of the range of the ejected electrons to the wall thickness on the other hand. If we assume an over-all instrumental response increasing as λ^9 then the line center at half-maximum height would be shifted toward longer wavelengths by about $0.009a$, where a is the half-breadth at half-maximum, or by a proportionate wavelength shift, $\delta\lambda/\lambda = 3.8 \times 10^{-5}$ which is a ten times smaller quantity than the discrepancy in question. For an instrumental response obeying a higher power of λ then the cube, $\delta\lambda/\lambda$ would only be increased in proportion to the exponent, and it seems very unlikely that this will account for the discrepancy.

The annihilation radiation line, since it results from the recombination of positive with negative electrons, should have a wavelength

$$\lambda_A = h[\tfrac{1}{2}(m^+ + m^-)c]^{-1}. \quad (4)$$

From the difference between λ_A and λ_c therefore one can readily calculate the relative difference in the masses m^+ and m^- of positive and negative electrons. If our observed discrepancy is to be so interpreted in its entirety then

$$(m^- - m^+)/m^- = 2(\lambda_A - \lambda_c)/\lambda_A = 0.82\times 10^{-4}. \quad (5)$$

The probable error to be assigned to this number we believe lies somewhere between an estimated upper "limit of error" of $\pm 0.82\times 10^{-4}$ and a probable error by internal consistency of the individual measurements themselves of $\pm 0.1\times 10^{-4}$. The direction of the discrepancy is consistent with a heavier mass for negative than for positive electrons.

We wish to emphasize that the evidence for this discrepancy $(\lambda_A - \lambda_c)$, *depends entirely on the possibility of calibrating the 2-meter curved crystal gamma-ray spectrometer with high absolute accuracy by means of x-rays.* Other nuclear physics laboratories equipped with β-ray spectrometers may (and we hope will) attempt to verify with all the precision available the *ratios* of the energies of the various lines we have recently measured such as Au^{198}, Cu^{64}, Co^{60}, Ta^{183}, and since our measurements on some of these such as Au^{198} are at present somewhat more accurate than our work to date on Cu^{64} it may be possible in this way to improve our knowledge of λ_A *but the absolute value of* λ_A for comparison with λ_c must at present *rest on the calibration of our instrument alone.*

We plan in the near future to repeat the measurements of λ_A with higher accuracy. Recent very considerable improvements in the sensitivity of our instrument through the use of a crystal scintillation counter and an improved collimator will, we hope, make possible a considerable improvement in resolving power. We plan also to study the effect of changing the atomic number of the substance in which the annihilation takes place. Plans are also under way for a direct precision comparison of the charge-to-mass ratios e/m^+ and e/m^- by a new method involving the new homogeneous field axial focusing β-ray spectrometer[8] whose construction at this Institute is now nearing completion.

* Assisted by the joint program of the ONR and AEC.
[1] I am indebted to W. K. H. Panofsky for pointing out to me the importance of this question.
[2] DuMond, Lind, and Watson, Phys. Rev. 75, 1226 (1949).
[3] J. W. M. DuMond and E. R. Cohen, Revs. Modern Phys. 20, 82 (1948).
[4] The shift because of the potential energies of the recombining pair members has only been estimated roughly. For this reason, our program includes study of the annihilation radiation in substances of different atomic numbers.
[5] De Benedetti, Cowan, and Konneker, Phys. Rev. 76, 440 (1949).
[6] J. W. M. DuMond, Phys. Rev. 75, 1226 (1949).
[7] Lind, West, and DuMond, Phys. Rev. 77, 475 (1950).
[8] No description of the design of this new instrument has, as yet, been published. Its design exploits the ideas of the author for obtaining optimum luminosity and energy resolution set forth in a recent paper in Rev. Sci. Instr. 20, 160 (1949).

The Half-Life of Na^{24}

J. H. Sreb
Nucleonics Division, Naval Research Laboratory, Washington, D. C.
December 11, 1950

BEING concerned with the development of precise methods of measuring half-lives, we have used Na^{24} as one of the isotopes for checking our approach to the problem. We have obtained a value of 15.060 ± 0.039 hr. This is in accord with the result, 15.04 ± 0.04 hr reported by Solomon.[1] Wilson and Bishop[2] have reported a value of 14.90 ± 0.02 hr, which is at variance with our determination. It appears that an error in their analysis is responsible for the discrepancy. They indicated correctly that the points on the semilogarithmic plot of the activity *versus* time as obtained in their experiment must be weighted according to the square of the measured activity. For a decaying activity the weighting factors thus decrease with time. Instead of analyzing the decay directly, they compare the activity of the Na^{24} source with that of a relatively long-lived source by considering the ratio of the activities. The ratio that they formed inadvertently was that of the long-lived activity to the Na^{24} activity. This function increases with time and thus cannot properly be considered the "activity" as far as the application of the weighting factors in their analytical treatment is concerned. Using their published data we have recalculated the runs, taking as the activity function to be analyzed the ratio $u = (Na^{24}\ \text{activity})/(\text{reference activity})$.

With t the elapsed time in hours, the resulting linear logarithmic equations are:

Series I	$\log u = -1.32143 - 0.04576t$
Series II	$\log u = -0.89174 - 0.04667t$
Series III	$\log u = -1.27935 - 0.04590t$

giving, respectively, a half-life of:

15.150 ± 0.070 hr, 14.852 ± 0.041 hr and 15.102 ± 0.076 hr.

The average half-life is thus 14.96 ± 0.10 hr which falls within the range of our measurement. It should be noted that the error in measurement due to statistical variation of the reference activity was considered to be negligible.

The interest and encouragement of Dr. F. N. D. Kurie in this work is gratefully acknowledged, and the verification of our calculations by Dr. G. R. Bishop[3] is appreciated.

[1] A. K. Solomon, Phys. Rev. 79, 403 (1950).
[2] R. Wilson and G. R. Bishop, Proc. Phys. Soc. London A62, 457 (1949)
[3] G. R. Bishop (private communication, November 20, 1950).

Choice of Gauge in London's Approach to the Theory of Superconductivity

J. Bardeen
Bell Telephone Laboratories, Murray Hill, New Jersey
December 11, 1950

IT has been pointed out by London[1] that it is possible to derive the phenomenological equation of superconductivity:

$$\text{curl}(\Lambda \mathbf{j}) = \mathbf{B}, \quad (1)$$

from quantum theory if it is assumed that the superconducting state is such that the wave function, Ψ, of the conduction electrons is not altered very much by the magnetic field. The expression for Ψ depends on the choice of gauge in the vector potential, A. London assumes that Ψ is approximately equal to the wave function for zero field, Ψ_0, if the gauge is chosen in such a way that

$$\text{div}\mathbf{A}_s = 0; \quad \mathbf{A}_{s\perp} = 0 \text{ on surface}. \quad (2)$$

The subscript s will indicate this particular choice. For a simply connected region, these conditions determine the gauge uniquely.[2] The current density, j, is then proportional to $\mathbf{A}_s$;

$$\mathbf{j} = \mathbf{A}_s/\Lambda, \quad (3)$$

and the curl of this relation gives (1). While this procedure is reasonable, it seems desirable to derive (2) from a gauge invariant formulation of the theory.

Let A be the vector potential for arbitrary choice of gauge. Terms in the Hamiltonian which involve the magnetic field are

$$H_m = (1/2m)\sum_{n=1}^{n} \{[p_n + e\mathbf{A}(\mathbf{r}_n)/c]^2 - p_n^2\}, \quad (4)$$

where $-e$ is the charge on an electron and the sum is over all electrons. Let us consider the class of wave functions of the form

$$\Psi = \exp[(ie/\hbar c)\Sigma_n \varphi(\mathbf{r}_n)]\Psi_0(\mathbf{r}_1 \cdots \mathbf{r}_n). \quad (5)$$

The exponential factor is of the type which is introduced when a gauge transformation

$$\mathbf{A} \rightarrow \mathbf{A} + \text{grad}\varphi$$

is made, and is required when the gauge is chosen arbitrarily. We shall choose φ in such a way as to make the first-order energy,

W_m, arising from the magnetic field a minimum. This energy is

$$W_m=\int \Psi^* H_m \Psi d\tau=\frac{1}{2m}\Sigma_a \int \Psi_0^*\left[-\frac{ie\hbar}{c}\operatorname{div}(\mathbf{A}_a+\operatorname{grad}\varphi_a)\right]$$

$$-\frac{2i\hbar e}{c}(\mathbf{A}_a+\operatorname{grad}\varphi_a)\operatorname{grad}_a+\frac{e^2}{c^2}(\mathbf{A}_a+\operatorname{grad}\varphi_a)^2\Psi_0 d\tau_1\cdots d\tau_n. \quad (6)$$

After an integration by parts, (6) can be written in the form

$$W_m=\frac{i}{c}\int (\mathbf{A}+\operatorname{grad}\varphi)\cdot\mathbf{j}_0(\mathbf{r})d\tau-\frac{2}{2mc^2}\int (\mathbf{A}+\operatorname{grad}\varphi)^2\rho_0(\mathbf{r})d\tau, \quad (7)$$

where $\mathbf{j}_0$ and ρ_0 are the current and charge densities in the absence of a field:

$$\mathbf{j}_0(\mathbf{r})=(i\hbar e/2m)\Sigma_a\int (\Psi_0^*\operatorname{grad}_a\Psi_0-\Psi_0\operatorname{grad}_a\Psi_0^*)\times\delta(\mathbf{r}-\mathbf{r}_a)d\tau_1\cdots d\tau_n,$$

$$\rho_0=-e\Sigma_a\int \Psi_0^*\Psi_0\delta(\mathbf{r}-\mathbf{r}_a)d\tau_1\cdots d\tau_n. \quad (8)$$

We shall assume that $\mathbf{j}_0=0$ and $\rho_0=$const. The condition that W_m be invariant for small changes $\Delta\varphi$ in φ is then

$$\delta W_m=-(e\rho_0/mc^2)\int [(\mathbf{A}+\operatorname{grad}\varphi)\cdot\operatorname{grad}\Delta\varphi]d\tau=0,$$

or, after an integration by parts

$$\int \Delta\varphi\operatorname{div}(\mathbf{A}+\operatorname{grad}\varphi)d\tau-\int \Delta\varphi(\mathbf{A}+\operatorname{grad}\varphi)_\perp dS=0. \quad (9)$$

The second integral is over the surface, S. If (9) is to be satisfied for all $\Delta\varphi$ we must have

$$\operatorname{div}(\mathbf{A}+\operatorname{grad}\varphi)=0;\quad (\mathbf{A}+\operatorname{grad}\varphi)_\perp=0 \text{ on } S. \quad (10)$$

Choosing φ in this way is equivalent to choosing the gauge so that (2) is satisfied and taking $\Psi=\Psi_0$.

We have used[3] this approach in a theory of superconductivity based on interactions between electrons and lattice vibrations.[4]

[1] F. London, Proc. Roy. Soc. **A152**, 24 (1935); Phys. Rev. **74**, 562 (1948).
[2] London (reference 1) has considered the extension of the theory to cover multiply connected regions.
[3] J. Bardeen, Phys. Rev. **80**, 567 (1950).
[4] J. Bardeen, Phys. Rev. **79**, 167 (1950).

Crystalline Magnetic Anisotropy in Zinc Manganese Ferrite

J. K. Galt, W. A. Yager, J. P. Remeika, and F. R. Merritt
Bell Telephone Laboratories, Murray Hill, New Jersey
December 11, 1950

We have grown crystals of zinc manganese ferrite whose composition is approximately $Zn_{0.35}Mn_{0.65}Fe_2O_4$. From the saturation magnetization, M_s, and from ferromagnetic resonance data, we have determined the crystalline magnetic anisotropy, K, of these crystals. The measurements were made at room temperature, by essentially the same procedure as the earlier measurements on nickel ferrite.[1,2] The value of M_s was measured by comparison with nickel ferrite in a hysteresis loop tracer; M_s for nickel ferrite has been measured by Guillaud and Roux[3] as well as by us.[2]

The crystals were grown in a manner similar to that by which nickel ferrite crystals were grown earlier.[2] A mix of 15 g borax, 6.4 g Fe_2O_3, 1.6 g ZnO, 1.4 g MnO was heated to 1325°C in a platinum crucible and held for 5½ hours. It was then cooled at approximately 100°C/hr simply by turning off the furnace. The resulting crystals ranged in size up to octahedra 1 mm on an edge. Most of them were not mechanically sound, but one good one was found which showed cubic symmetry magnetically. Chemical analysis showed that this material is approximately $Zn_{0.35}Mn_{0.65}Fe_2O_4$. There were no significant impurities.

The value of K/M for these materials at room temperature was determined from the variation with crystallographic direction of the magnetic field required to produce ferromagnetic resonance[4,5] at 24,160 Mc. The width of the resonance line, ΔH, and the g factor[5] were also observed. The variations in ΔH with crystallographic direction were not large enough to be significant. The results are given in Table I.

Table I. Measurements on zinc manganese ferrite.

K/M	M(cgs units)	K(erga/cc)	ΔH(oe)	g
−21 ±5%	181 ±10%	−3800 ±15%	70	1.997

Check measurements were made on a second sample. This sample did not show cubic symmetry magnetically but the magnitude of the variations in the field required for resonance was the same.

Snoek[6] has suggested that the effect field due to magnetocrystalline anisotropy acting on a material in no external field will cause resonance or perhaps relaxation behavior in the initial permeability of the material; this behavior should occur at the frequency of the Larmor precession in the effective field. This effective internal field when the magnetization is along an easy direction ([111] in these crystals) is:[7]

$$H_{eff}=-1.33K/M.$$

This leads us to expect this behavior at 78 Mc in this material. This frequency may be increased if the effective field is increased by the presence of free poles due to the domain pattern; it is therefore a lower limit in practice.

The authors wish to express their gratitude to Dr. E. A. Wood for x-ray assistance and to H. G. Hopper for technical assistance.

[1] Yager, Galt, Merritt, and Wood, Phys. Rev. **80**, 744 (1950).
[2] Galt, Matthias, and Remeika, Phys. Rev. **79**, 391 (1950).
[3] C. Guillaud, and M. Roux, Compt. rend. **229**, 1133 (1949).
[4] C. Kittel, Phys. Rev. **73**, 155 (1948).
[5] C. Kittel, Phys. Rev. **76**, 743 (1949).
[6] J. L. Snoek, Nature **160**, 90 (1947); Physica **14**, 207 (1948).
[7] L. R. Bickford, Jr., Phys. Rev. **78**, 449 (1950).

The Absence of Cross-Over Transitions in Tellurium Isomers

R. D. Hill
Physics Department, University of Illinois, Urbana, Illinois
December 8, 1950

A MODIFIED estimate of multipole radiation probabilities has been put forward recently by Weisskopf.[1] According to this theory, the probability λ of electric 2^ϵ pole radiation is given by

$$\lambda=\frac{2(\epsilon+1)}{\epsilon}[1\cdot 3\cdot 5\cdots(2\epsilon+1)]^{-2}\frac{K^{2\epsilon+1}}{\hbar}e^2R^{2\epsilon},$$

and the probability of magnetic 2^ϵ pole radiation is lower than that of electric 2^ϵ pole by a factor $\sim(\hbar/McR)^2$. K is the wave number, $2\pi\nu/c$, of the radiation, M is the nucleon mass, and R is the nuclear radius. It is to be realized that this formula, like previous ones based on older estimates, is claimed to be valid only to within a factor $\sim 10^{\pm 2}$. In the following note it is pointed out that Weisskopf's formula, unlike earlier ones, is consistent with the absence of cross-over transitions in the decay of several long-lived tellurium isomers.

Isomers of $Te^{123,125,125}$ have been observed[2] to decay in two successive transitions, the first being preponderantly magnetic 2^4 pole and the second being magnetic dipole. It was puzzling, on the basis of the older radiation formulas, that no cross-over transitions of an electric 2^3 character, between the long-lived and the ground states, were observed experimentally.

Relative probabilities of magnetic 2^4 and electric 2^3 transitions have been calculated and are tabulated in Table I. Columns 2 and 3 give, respectively, the energies of the long-lived magnetic

TABLE I. Transition probabilities in long-lived tellurium isomers.

Isomer	2^4m (kev)	2^4el (kev)	$\lambda 2^5/\lambda 2^4$ (old)	$\lambda 2^5/\lambda 2^4$ (new)	$t_{\frac{1}{2}}$ (sec) (new)	$t_{\frac{1}{2}}$ (sec) (exp)
Te^{121}	82	295	3.5×10^{6}	0.4	3.7×10^{7}	1.33×10^{7}(154d)
Te^{123}	88.5	247.5	7.0×10^{6}	7.0×10^{-3}	2.7×10^{7}	9.0×10^{6}(104d)
Te^{125}	109.7	145.1	1.0	2.0×10^{-4}	1.2×10^{7}	5.0×10^{6}(58d)

2^4 transitions and of the expected cross-over electric 2^5 transitions. Column 4 gives the ratios of the total transition probabilities based on older formulas, as, for example, that used by Axel and Dancoff[3] in their classification of nuclear isomers. The same ratios, based on the new formula of Weisskopf, are given in column 5. Total transition probabilities include corrections required to take into account internal conversions, the coefficients of which were obtained from Rose's accurate tables,[4] either directly or by extrapolation. Values of K to L ratios were also required, and these were taken from the graphs of Lowen and Tralli.[5] Uncertainties involved in the knowledge of theoretical K to L ratios at this stage will not significantly change the transition probabilities of Table I.

Experimentally, all electric 2^5 transitions can be excluded at present to within approximately 5 percent of the magnetic 2^4 transitions. From Table I it is clear that although the older estimates would indicate the cross-over 2^5 transitions to be more probable than the 2^4, the new estimates of transition probabilities are essentially in agreement with experiment.

Theoretical lifetimes for the converted magnetic 2^4 transitions are listed in column 5. The new values are again in significantly better agreement with experimental lifetimes than are the older values.

It is interesting also to compare estimated lifetimes of the intermediate tellurium states with the upper limits established experimentally for these lifetimes. Theoretical estimates based on old and new formulas are shown in columns 3 and 4, respectively, of Table II. In one case, the 35.4-kev excited state of Te^{125}, the

TABLE II. Lifetimes of intermediate states of tellurium isomers.

Isomer	2^4m (kev)	$t_{\frac{1}{2}}$ (sec) (old)	$t_{\frac{1}{2}}$ (sec) (new)	$t_{\frac{1}{2}}$ (sec) (exp)
Te^{121}	213	7.65×10^{-10}	1.3×10^{-11}	$<3\times10^{-9}$ [a]
Te^{123}	159	3.05×10^{-9}	2.55×10^{-11}	$<2\times10^{-8}$ [b]
Te^{125}	35.4	4.6×10^{-7}	1.85×10^{-10}	$<5\times10^{-8}$ [c]

[a] M. Deutsch and W. E. Wright, Phys. Rev. 77, 139 (1950).
[b] S. Frankel (thesis, University of Illinois, 1949).
[c] K. McGowan, Phys. Rev. 77, 138 (1950).

present experimental evidence decides strongly in favor of the new estimates as opposed to the old.

Valuable criticism of this investigation by John M. Blatt is gratefully acknowledged.

[1] Privately circulated notes, to appear as part of a book on nuclear physics.
[2] R. D. Hill, Phys. Rev. 76, 333 (1949); J. C. Bowe and G. Scharff-Goldhaber, Phys. Rev. 76, 438 (1949); Katz, Hill, and Goldhaber, Phys. Rev. 78, 9 (1950).
[3] P. Axel and S. M. Dancoff, Phys. Rev. 76, 892 (1949).
[4] Rose *et al.*, *Tables of K-Shell Conversion Coefficients*.
[5] N. Tralli and I. S. Lowen, Phys. Rev. 76, 1541 (1949).

Multiple Scattering of Electron Pairs from (Li, p) Gamma-Rays in Photographic Emulsions

L. VOYVODIC AND E. PICKUP
Physics Division, National Research Council, Ottawa, Canada
November 20, 1950

IN order to check multiple Coulomb scattering results obtained for high energy cosmic-ray particles with photographic emulsions,[1] we have made scattering measurements on electron pairs observed in emulsions exposed to Be^8 γ-rays from the bombardment of an evaporated lithium target with a 450-kev resolved proton beam. Ilford G5 emulsions 400μ thick were irradiated with about 10 milliroentgens of γ-radiation.

The scattering method follows that developed by Fowler,[2] in which the perpendicular coordinates of a track are recorded at equal intervals along the axis of motion of the microscope stage to which the track is made approximately parallel. The arithmetic mean $\langle|D|\rangle_{Av}$ of the second differences of the perpendicular coordinates is related to the projected mean angle between successive chords at intervals q by the expression $\langle\alpha(q)\rangle_{Av}=\langle|D|\rangle_{Av}/q$. From the multiple scattering theory of Williams,[3] as formulated by Rossi and Greisen,[4] $\langle\alpha(q)\rangle_{Av}=(K/p\beta)(q/100)^{\frac{1}{2}}$ degrees[5] where $K=32.7$, p is the particle momentum in units Mev/c, β is the velocity in units of c, and q is in microns of emulsion.

Observations have been made on a total of 100 electron pairs at intervals of 20 divisions (1 div$=0.88\mu$) for about 700μ along each track. Figure 1 shows the scattering distribution for one of

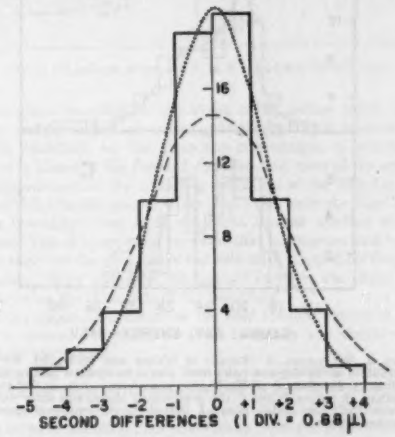

FIG. 1. Distribution of second differences for the tracks of an electron pair with equal energy division. The histogram represents 71 combined values for overlapping intervals of 40 div, and the dotted curve is a Gaussian with the same arithmetic mean ($\langle|D|\rangle_{Av}=1.09\pm0.09$ div).

the pairs which represents a case of almost equal energy division from the incident γ-ray. Using the observed value for $\langle|D|\rangle_{Av}$ the calculated total energy of each electron is 12.7 Mev, which corresponds to a γ-ray energy of 25.4 ± 2 Mev. This is to be compared with the maximum Be^8 γ-ray energy[6] (17.6 Mev). It would appear from this example that the experimental scattering distribution is approximately Gaussian, but K is too big.

The γ-ray energies deduced from the experimental values of $\langle|D|\rangle_{Av}$ for 100 electron pairs are shown in Fig. 2. Curve A is the Be^8 γ-ray spectrum as given by Walker and McDaniel[6] for a thin lithium target at 460-kev proton energy with a magnetic pair spectrometer. This shows the pronounced 17.6-Mev line and a very broad lower energy line. Curve B shows our results for 70 pairs observed in a plate exposed to γ-rays in the forward proton direction. Besides a shift of the spectrum to higher energies, this curve shows some evidence for two peaks, whose relative intensities differ considerably from those shown by Walker and McDaniel. It is difficult to attribute the shape of curve B as being a distortion of curve A due to some feature of the scattering method. We have therefore exposed plates at 90° to the proton beam direction to test for any noticeable angular asymmetry in the relative intensities of the two γ-ray lines.[7,8] Curve C shows preliminary results for 30 electron pairs from this irradiation, in which there is an indication of two γ-ray groupings which more

nearly resemble the spectral distribution shown in curve *A*. It may be noted that the relative positions of the two groups in curves *B* and *C* are about the same as that given by the results of Walker and McDaniel.

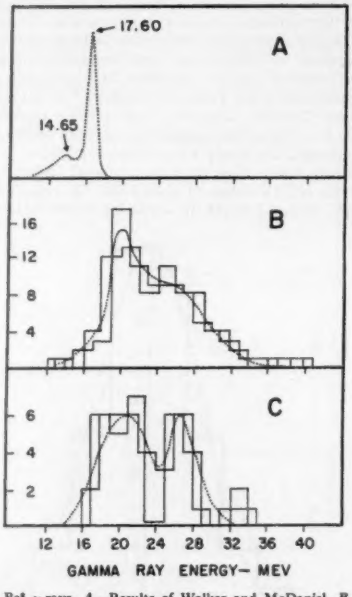

FIG. 2. Be^8 γ-rays. *A*—Results of Walker and McDaniel. *B*—Energy distribution of 70 electron pairs from γ-rays in forward proton direction. *C*—Energy distribution of 30 electron pairs from γ-rays at 90° to proton direction. In curves *B* and *C* the overlapping histograms show number of electron pairs per 2-Mev interval, dotted curves represent approximate smoothed results.

If we assume that the apparent groupings at energies 21 ± 1 and 26 ± 1 Mev in curves *B* and *C* are due to the 14.65- and 17.60-Mev γ-rays, and if we correct for energy losses by the electrons ($\sim$0.4 Mev) and spurious experimental scattering ($\sim$3 percent), then the constant K is reduced from 32.7 to a value 21.3, with an estimated probable error of 5 percent. This result is in agreement with recent measurements by Corson[9] on 115-Mev electrons.[10] Thus it would appear that energy values obtained by this scattering method using $K=32.7$ may be too high by about 35 percent.

It will be of interest to test the scattering of particles other than electrons. Further work will be done on the Be^8 electron pairs to investigate the apparent asymmetry of the spectrum and to establish the resolution of the multiple scattering method.

We are indebted to Mr. E. H. McLaren for the H.T. set irradiations and to Miss S. W. Young for searching the emulsions for electron pairs.

[1] Camerini, Fowler, Lock, and Muirhead, Phil. Mag. **41**, 413 (1950); E. Pickup and L. Voyvodic, Phys. Rev. **80**, 89 (1950). Camerini, *et al.* used $K=32.7$ determined from a proton calibration and we used their value.
[2] P. H. Fowler, Phil. Mag. **41**, 169 (1950).
[3] E. J. Williams, Proc. Roy. Soc. **169**, 531 (1939).
[4] B. Rossi and K. Greisen, Revs. Modern Phys. **13**, 240 (1941).
[5] This was calculated using a radiation length of 2.86 cm of emulsion.
[6] R. L. Walker and B. D. McDaniel, Phys. Rev. **74**, 315 (1948).
[7] The γ-ray orientation in reference 6 was not specified.
[8] S. Devons and M. G. N. Hine, Phys. Rev. **74**, 976 (1948) observe a small asymmetry (near resonance) in the Be^8 γ-radiation and mention that observations on this asymmetry, as a function of γ-energy, indicate that the 17-Mev component is mainly responsible.
[9] D. R. Corson, Phys. Rev. **80**, 303 (1950).
[10] It is also in fair agreement with the detailed statistical theory of Williams (reference 3) as will be discussed in a subsequent note.

Electron Bombardment Induced Conductivity in Germanium Point Contact Rectifiers

A. R. MOORE AND F. HERMAN
RCA Laboratories Division, Radio Corporation of America, Princeton, New Jersey
December 7, 1950

ELECTRON bombardment experiments on insulators and semiconductors using electrons in the kev range have been reported. Some of this work dealt with the currents induced in the solid by the electron beam.[1-4] This is called electron bombardment induced conductivity (EBIC). Some workers have employed α-particles of several Mev energies, and were principally interested in the corresponding current pulses in insulators or semiconductor rectifiers as crystal counters.[5,6] This is a report of preliminary experiments on the bombardment of germanium rectifiers with electrons of several kev energy.

The technique employed here involves scanning the surface of the germanium crystal with an electron beam magnetically deflected in a standard 525 line television raster. The ac component of the current flowing in the probe circuit is used as a video signal which either modulates the grid of a kinescope which is being synchronously deflected, or modulates the vertical deflection of an ordinary oscilloscope. In the first case a two dimensional plot of the EBIC is obtained which shows immediately the effects of nonhomogeneity on the surface; in the second case a quantitative measure of the diode current is obtained.

The diodes studied consisted of $2.5\times2.5\times0.5$ mm pieces of Ge, large area heavily gold-plated base electrodes, and phosphor bronze probes inclined 45° to the Ge surface and to the beam, which strikes normally.

Figures 1a and b show the result on the kinescope of bombarding an *N*-type crystal biased in the back and forward direction respectively. The black level signal corresponds to an electron current from the probe into the Ge in the diode circuit; the white signal is the reverse. Thus the effect of the electron beam is always to increase the conductivity for both directions of bias. The sensitive region in the neighborhood of the point can be measured with accuracy by the scanning method, and a suitable scale is shown. The diameter of this sensitive region increases with increasing positive or negative bias. The size shown on the figure agrees with the rough estimate made by McKay[4] using α-particles and negative bias.

The magnitude of the EBIC effect can be seen from Fig. 2. Here δ is the ratio of the change of crystal probe current to beam current, given as a function of bias for three different beam voltages. The values plotted are maximum currents, obtained when the beam sweeps within 0.001" of the point contact. Note that δ reaches saturation in the forward and reverse directions, but the values of δ_{sat} are not the same. Table I gives the ratio of

TABLE I. Saturation values of δ.

Beam voltage	δ_{+sat}	δ_{-sat}	$\delta_{-sat}/\delta_{+sat}$
5 kv	0.54×10^3	0.55×10^4	10.2
7.5	1.5	1.5	10.0
10	1.9	1.8	9.5

δ_{-sat} (back direction) to δ_{+sat} (forward direction) for the beam voltages of Fig. 2. The ratio $\delta_{-sat}/\delta_{+sat}$ is constant within experimental error. Since the barrier at the contact is present in the back but not in the forward direction, $\delta_{-sat}/\delta_{+sat}$ has been tentatively interpreted as the current multiplication at the barrier, analogous to the "excess" values of α obtained in transistor experiments.[7] However, it is not yet certain whether some of this factor of 10 must be assigned to the normal current gain accompanying hole injection.

The advantage of the scanning technique in uncovering surface or subsurface effects as well as evidence for the motion of holes can be seen in Fig. 1c. The *N*-type crystal under bombardment

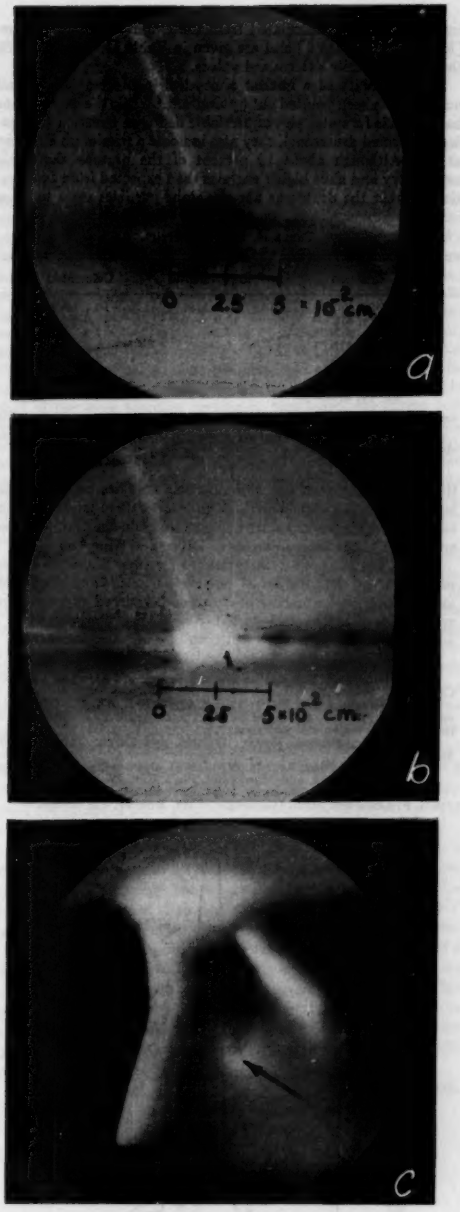

FIG. 1. Kinescope photographs of EBIC. (a) *N*-type crystal, biased −1 volt in back direction. (b) Same crystal, biased +0.2 volt in forward direction. Electron beam 10 kv for both cases. (c) *N*-type crystal, biased +0.1 volt, showing grain boundary effects. Electron beam 14 kv.

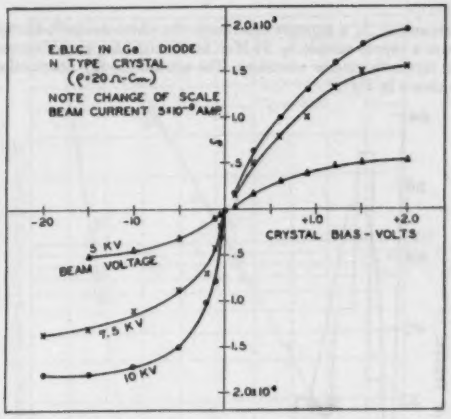

FIG. 2. Magnitude of the EBIC in *N*-type Ge as crystal bias.

had a grain boundary in the shape of an obtuse angle (135°) easily visible under an optical microscope. This boundary is readily identified on the kinescope photograph, in which the crystal is biased in the forward direction and most of the applied bias appears across the spreading resistance of the bulk Ge. The arrow indicates the point contact. Note that only the edge of the grain boundary away from the point contact appears sharply defined. This is interpreted to mean that holes generated by the beam travel in the direction of the field until stopped by the grain boundary. Were electrons the current carriers, the sharp edge would be on the other side of the boundary.

In the upper right corner of the field another barrier of some sort is observed, although no grain boundary was visible under the light microscope.

Additional evidence of hole flow has been obtained by confining the scanning raster to the sensitive area around the point and then blanking the electron beam for 1 μsec during each scanning line. As successive scanning lines move away from the point contact a progressive increase in the delay time of the crystal probe signal corresponding to the blank with respect to the horizontal synchronizing pulse can be easily measured. The values are in satisfactory agreement with the delay calculated from known values of the hole mobility in Ge.

[1] E. S. Rittner, Phys. Rev. **73**, 1212 (1948).
[2] K. G. McKay, Phys. Rev. **74**, 1606 (1948).
[3] L. Pensak, Phys. Rev. **75**, 472 (1949).
[4] K. G. McKay, Phys. Rev. **77**, 816 (1950).
[5] P. J. Van Heerden, *The Crystal Counter* (Amsterdam, 1945).
[6] K. G. McKay, Phys. Rev. **76**, 1537 (1949).
[7] W. Shockley, Phys. Rev. **78**, 294 (1950).

Photo-Disintegration of Copper*

P. R. BYERLY, JR.† AND W. E. STEPHENS
Physics Department, University of Pennsylvania, Philadelphia, Pennsylvania

December 11, 1950

THE protons ejected from a copper foil irradiated with the bremsstrahlung from a 24-Mev betatron were observed in nuclear emulsions. In the process of determining the photo-proton energy distribution, several anomalies suggested the possibility of the presence of photo-deuterons. By grain counting the end of the tracks, it was possible to differentiate deuterons from protons and a considerable number of deuterons were found. Using this identification, the energy, angular distribution and relative numbers of protons, deuterons, and also alpha-particles were

determined. In a separate experiment the photo-neutrons ejected from a copper sample by 24-Mev bremsstrahlung were observed by recoils in nuclear emulsions. The neutron energy distribution is shown in Fig. 1.

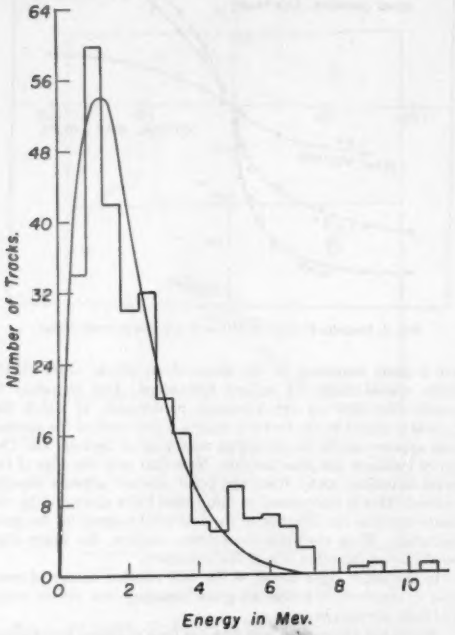

FIG. 1. Comparison of neutron energy distribution with theory (solid curve W and E).

From this data, the relative numbers of neutrons, protons, deuterons, and alpha-particles ejected from copper by 24 Mev bremsstrahlung were ascertained to be 280:100:31:3. As is indicated in Table I, the n/p ratio is in reasonable agreement with the

TABLE I. Particles emitted from Cu by γ-radiation.

Particle ratio	Exp.	W. and E.[a]	Schiff[b]	Courant[c] (Proton)	Courant[c] (Alpha)	LeCouteur[d]
n/p	2.8	1.76	1.83	1.02	0.37	3.15
d/p	0.31	0.0005	0.0007	0.036	0.103	0.002
α/p	0.03	0.007	0.020	0.004	0.022	0.013

[a] Reference 1.
[b] L. I. Schiff, Phys. Rev. 73, 1311 (1948), the value of "a" used was 1/2.
[c] Reference 3.
[d] K. J. LeCouteur, Proc. Phys. Soc. London 63A, 259 (1950).

value predicted by the various theoretical formulations of the statistical model of the compound nucleus.

The concept that these particles are evaporated from a nucleus excited by the betatron photons is also supported by the fact that about 90 percent of the protons and neutrons have energies to be expected from the Weisskopf-Ewing[1] formulas (see Fig. 1 for the neutrons). Even the deuterons have an energy distribution well described by the Weisskopf-Ewing model as shown in Fig. 2. However, the number of deuterons seems to be orders of magnitude greater than that expected on an evaporation model. While this ratio is sensitive to the binding energies assumed for the particles, it does not seem uncertain to this extent. The binding energies used were calculated from the empirical mass equation [Eq. (21), reference 2] and are given in Table II, together with the experimentally determined values.

The possibility of a nuclear photoelectric effect on individual nucleons has been pointed out by Courant.[3] While the calculations based on his formulas give appreciable deuteron emission (assuming preformed deuterons), they also indicate a maximum emission at 90°. Although about 10 percent of the protons show this asymmetry and have higher energies than expected from evaporation, neither the deuterons nor the alpha-particles seem to show

TABLE II. Binding energies.

Reaction	Experimental	Calculated
$Cu^{65}(\gamma, n)Cu^{64}$	10.2 Mev	10.1 Mev
$Cu^{63}(\gamma, n)Cu^{62}$	10.9	11.0
$Cu^{65}(\gamma, p)Ni^{64}$	7.7[a]	7.4
$Cu^{63}(\gamma, p)Ni^{62}$	6.2[a]	6.1
$Cu^{65}(\gamma, d)Ni^{63}$	—	14.7
$Cu^{63}(\gamma, d)Ni^{61}$	—	14.6
$Cu^{65}(\gamma, \alpha)Co^{61}$	—	5.7
$Cu^{63}(\gamma, \alpha)Co^{59}$	—	6.3

[a] These values were determined from observed (γ, n) thresholds and observed beta-ray energies.

these effects. In fact, the alpha-particle energies are somewhat lower than those expected from an evaporation model, as was also found in cosmic-ray stars.[4] These results on the photo-protons are similar to the measurements of Diven and Almy[5] on silver.

Although the photo-disintegration of copper seems to consist mainly in the evaporation of nuclear particles from an excited nucleus, the large numbers of deuterons observed suggest either an additional mechanism (possibly a "pick-up" process[6]) or a large error in the calculated deuteron binding energies.

* Assisted by the joint program of the ONR and AEC.
† Now at the Radiation Laboratory, University of California, Berkeley, California.
[1] V. F. Weisskopf and D. H. Ewing, Phys. Rev. 57, 472 (1940); the value of "a" used was 8. We are indebted to Professor V. F. Weisskopf for the latest penetration cross sections.
[2] McElhinney, Hanson, Becker, Duffield, and Diven, Phys. Rev. 75, 542 (1949).
[3] E. D. Courant, Phys. Rev. 74, 1226 (1948), also private communication.
[4] Bernardini, Cortini, and Manfredini, Phys. Rev. 79, 952 (1950).
[5] B. C. Diven and G. M. Almy, Phys. Rev. 80, 407 (1950).
[6] G. F. Chew and M. L. Goldberger, Phys. Rev. 77, 470 (1950).

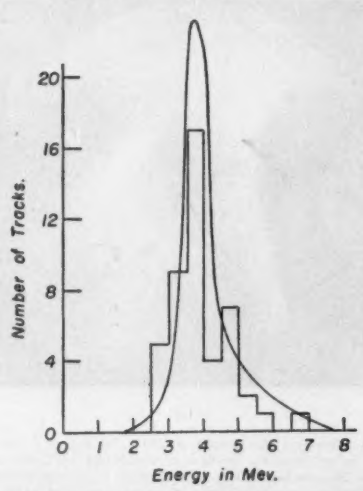

FIG. 2. Comparison of deuteron energy distribution with theory (solid curve W and E).

Measurement of Hole Diffusion in *n*-Type Germanium

F. S. Goucher
Bell Telephone Laboratories, Murray Hill, New Jersey
December 11, 1950

A HOLE-ELECTRON pair is generated in a filament of *n*-type germanium for each photon of light absorbed, as previously discussed.[1] For densities of holes small in comparison with that of electrons only small electric fields are present and the holes move mainly under the influence of diffusion in a manner similar to that discussed in connection with carriers injected across the junction in a $p-n$ junction rectifier.[2] The presence of a hole density in excess of the equilibrium value can be detected by "the internal contact potential" developed at a rectifying point contact made with the surface.[3] This potential can be measured as a difference in potential between the contact point and another contact, such as one at the end of the filament, sufficiently far removed from the region of light absorption that the hole concentration in its neighborhood has substantially its equilibrium value. According to the theory, which is similar to that of the $p-n$ junction previously mentioned, the excess hole density produced by the light should decay as $\exp(-|x|/L)$, where $L=(D\tau)^{\frac{1}{2}}$ is the diffusion length, D the diffusion constant, and τ the hole lifetime in the filament. If then a small light spot is moved with respect to the rectifying contact or probe, the logarithm of the voltage response as a function of distance from the plane of the probe should plot as a straight line from the slope of which L can be calculated.

Figure 1 illustrates the essential features of our experimental set-up. The test specimen was a rectangular rod of *n*-type single-crystal germanium with electroplated end electrodes and of dimensions approximately $0.05\times0.05\times2.0$ cm. A potential probe P was brought into contact with one side of the rod in a fixed position about 1 cm from one electrode. A small light spot L in the focal plane of two crossed exit slits of a monochromator made normal incidence on the top surface at an adjustable distance x from the probe location. The light ($\lambda=1.5\mu$) was pulsed and the voltage V between the end electrode and the probe P was measured by means of a high impedance electronic voltmeter. A scan of the intensity of the light spot in the x-direction by means of a detector small in comparison with its width enables one to determine the extent of the region near p which was activated by light in the direct beam.

Figure 2 shows the results of our measurements. Curve A is semilogarithmic plot of V *vs* x for both positive and negative values of x. The straight line determined by the plotted points for values of x in excess of about 0.07 cm shows that on the average V falls off exponentially with distance from the plane of the probe. Curve B is a normalized response *vs* distance in the direction of x showing the variation of light intensity in the light spot from its maximum value for both positive and negative values of x. This shows a drop of intensity to one percent of its maximum value in a distance of about 0.05 cm. It is therefore reasonable to ascribe the exponential portion of curve A for distances in excess of 0.05 cm to the diffusion of holes.

From the slope of A, the diffusion distance L_D is 0.028 cm,

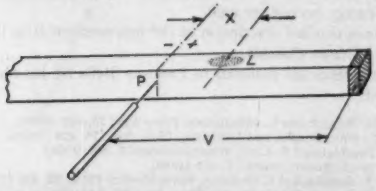

FIG. 1. Schematic of experimental arrangement.

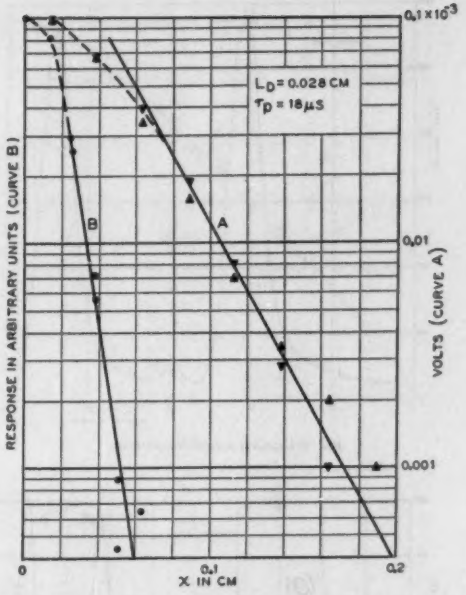

FIG. 2. Curve A—Photo-voltage V *vs* distance x (both positive and negative values). Curve B—Variation of light intensity in direction x measured from the center of the light spot L.

from which we can calculate a hole lifetime τ_p of 18 μsec, using the value 44 cm²/sec for the diffusion constant D. This value is based on the most recent determination of the hole mobility,[4] μ_p, as 1700 cm²/volt sec and the Einstein relationship.

That this is the correct interpretation was established by a direct measurement of mean lifetime[5] over the same portion of the specimen as that covered by the scanning curve A. A further check was also obtained by the photo-current method through the illumination of the same portion of the specimen with a known number of quanta, correction being made for reflection loss and unit quantum efficiency being assumed.[1] Each of these checks gave $\tau_p=18$ μsec within experimental error.

Thanks are due W. Shockley who suggested the experiment, to J. R. Haynes for the direct measurement of τ_p, and to H. B. Briggs for collaboration in making the optical measurements.

[1] F. S. Goucher, Phys. Rev. **78**, 816 (1950).
[2] W. Shockley, Bell System Tech. J. **28** (3), 435 (1949).
[3] See Shockley (reference 2) for $n-p$ junctions. The theory has been extended by J. Bardeen, Bell System Tech. J. **29** (4), 469 (1950).
[4] Pearson, Haynes, and Shockley, Phys. Rev. **78**, 295 (1950).
[5] Shockley, Pearson, and Haynes, Bell System Tech. J. **28** (3), 344 (1949).

The $Li^6(n, \alpha)H^3$ Reaction Spectrum

Ugo Facchini, Emilio Gatti, and Elio Germagnoli
Laboratori C.I.S.E., Piazzale Cimitero Monumentale, Milan, Italy
November 24, 1950

A MEASUREMENT of the energy of the α and H^3 particles emitted in the $Li^6(n, \alpha)H^3$ nuclear reaction for slow neutrons is of considerable interest. Only measurements of the ranges of these particles[1] and evaluations of the energy released in the above reaction from known values of the Q's of other reactions[2] have been made thus far. A direct energy determination, if com-

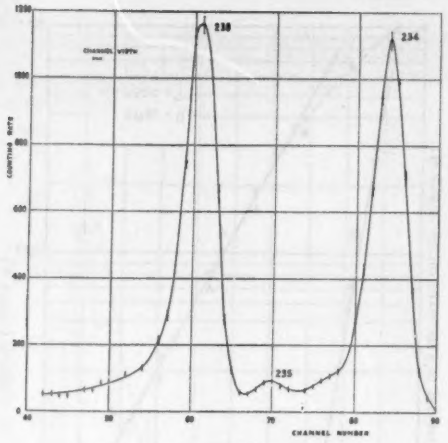

FIG. 1. Uranium α-particle spectrum.

1 to 2 μsec (α-particles) and 4 μsec (H^3). Pulse heights are analyzed by a 99-channel impulse spectrograph.[4]

Figure 1 shows a spectrum of uranium α-particles as a test of the whole apparatus.

In Fig. 2 two spectra of the pulses obtained from fission of lithium and α-particles of uranium are represented. These are used as an absolute energy standard. The dashed lines show artificial peaks obtained by feeding calibration pulses into the grid of the ionization chamber. By this means, linearity and stability are checked. Deviations from ideal behavior of the whole apparatus are in any case less than 3 percent. A correction was made in order to take into account both the shift of the maximum of the peaks owing to the finite thickness of layers and the measured spreading of pulses due to noise in the amplifier.

Taking 4.180 Mev and 4.763 Mev as values of the energy of the uranium α-particles,[5] the energies of the particles generated from lithium fission are

$$E_\alpha = 2.051 \pm 0.017 \text{ Mev}, \quad E_{H^3} = 2.748 \pm 0.014 \text{ Mev}.$$

Consequently, we obtain for the Q-values

$$Q_\alpha = 4.786 \pm 0.043 \text{ Mev}, \quad Q_{H^3} = 4.809 \pm 0.024 \text{ Mev}.$$

The average value of $\bar{Q}$ is

$$\bar{Q} = 4.804 \pm 0.022 \text{ Mev}.$$

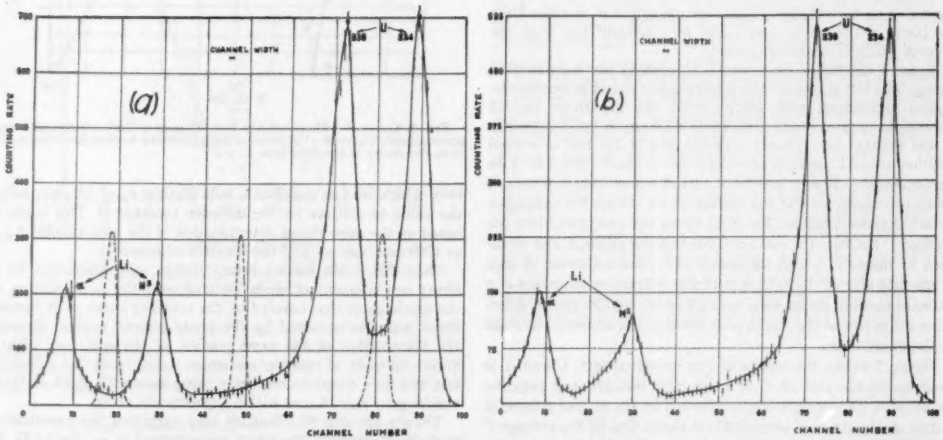

FIG. 2. Complete spectrum of the $Li^6(n, \alpha)H^3$ reaction and of the uranium α-particles. (a) Chamber filled at 6 atmos; -1800 v on the emitting electrode and -1200 v on the grid. (b) Pressure reduced to 3 atmos; voltages reduced to -900 v and -600 v, respectively, in order to maintain E/p ratio. The H^3 line is distorted because the H^3's pass through the emitting electrode-grid area. The peaks corresponding to uranium and lithium α-particles are not displaced: thus evidence is obtained of the independence of the gain by rise time and of the negligibility of electron capture by impurities in the argon.

pared with range measurements, will also give a point on each of the two range-energy curves of both H^3 and α particles.

We have observed the α and H^3 energy spectrum with a grid ionization chamber for electron collection,[3] filled with argon purified by circulation over hot calcium.

A thin LiF layer, obtained by evaporation in vacuum, and a thin UO_3 layer, obtained by electrolytic deposition, are present simultaneously on the emitting electrode, both layers being deposited on a stainless steel support, worked to optical smoothness. The thickness of both layers is about 0.02 mg cm^{-2}. The ionization chamber, placed in a paraffine box, is exposed to a flux of slow neutrons, obtained from a 500-mc Ra $\alpha-$Be source.

The collecting electrode is connected to a conventional amplifying system, whose rise time is 0.6 μsec, provided with a reflection line having a rise time of 0.2 μsec and a reflection time of 3 to 6 μsec for the clipping of pulses, which have a rise time of about

These values were obtained by averaging 15 measurements, obtained under different conditions of pressure and voltage, and the errors were calculated from the standard deviation.

The α and H^3 energy values agree with those obtained by Böggild and Minnhagen[1] by range measurements, when corrected range-energy curves[6] are used.

A more detailed description of the measurement is to be published in *Nuovo Cimento*.

The authors are indebted to Professor Bolla for his continued interest.

[1] J. K. Böggild and L. Minnhagen, Phys. Rev. 75, 782 (1949).
[2] Tollestrup, Fowler, and Lauritsen, Phys. Rev. 76, 428 (1949).
[3] U. Facchini and E. Gatti, Nuovo Cimento 7, 589 (1950).
[4] E. Gatti, Nuovo cimento 7, 655 (1950).
[5] G. T. Seaborg and I. Perlman, Revs. Modern Phys. 20, 585 (1948).
[6] W. P. Jesse and J. Sadauskis, Phys. Rev. 78, 1 (1950).

Ferromagnetic Resonance in Various Ferrites

W. A. YAGER AND F. R. MERRITT
Bell Telephone Laboratories, Murray Hill, New Jersey
AND
CHARLES GUILLAUD
C.N.R.S. Laboratories, Bellevue (S. et O.), France
November 30, 1950

THE results of ferromagnetic resonance experiments at room temperature and at a frequency of 24,164 Mc/sec on spherical polycrystalline specimens of magnesium, nickel, cobalt, manganese, and manganese-zinc ferrites are summarized in Table I. Data showing the effect of sphere size ("size effect") on the apparent g-factor, line width, and magnetic energy absorption for a typical semiconducting ferrite are presented in the figures.

TABLE I. The g-factor and line width observed in various polycrystalline ferrite spheres.

Ferrite	Sphere diam. ~0.05 cm ΔH(oe.)[a]	Sphere diam. ~0.05 cm Apparent g	Sphere diam. →0 g[b]
Mg	1030	2.01	2.03
Mg	870	2.04	2.06
Ni	520	2.18	2.21
Co	Extremely broad line	—	—
$Mn_{0.1}Zn_{0.9}$	520	2.005	2.02
$Mn_{0.3}Zn_{0.7}$	455	2.005	2.01
$Mn_{0.4}Zn_{0.6}$	465	2.01	2.03
$Mn_{0.45}Zn_{0.55}$	685	2.02	2.05
$Mn_{0.55}Zn_{0.45}$	550	2.01	2.02
$Mn_{0.9}Zn_{0.1}$	1675	2.07	2.05
$Mn_{0.9}Zn_{0.1}$	1263	2.07	2.06
Mn	618	2.02	2.05

[a] ΔH = Line width between half-power points.
[b] Estimated extrapolation to zero diameter.

The sphere diameter of each specimen was in most cases varied from 0.020 to 0.070 cm in order to take account of the "size effect" discussed below. The apparent line width and g-factor for a 0.050-cm sphere obtained by interpolation of the data are recorded in the second and third columns of Table I and the estimated extrapolation of the apparent g-factor to zero diameter is given in the last column. The precision of the measurements is in general about 0.5 percent.

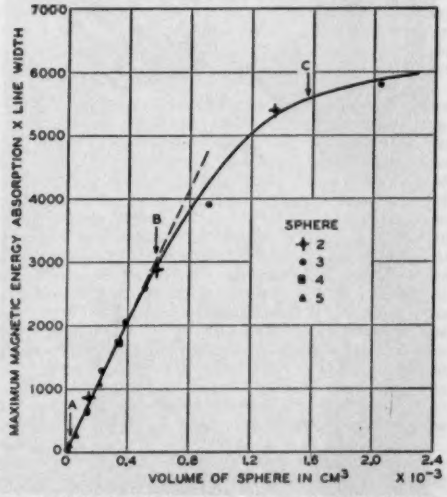

FIG. 1. (a) The effect of sphere size on the apparent g-factor of a specimen of polycrystalline manganese-zinc ferrite. (b) The effect of sphere size on the apparent line width of a specimen of polycrystalline manganese-zinc ferrite.

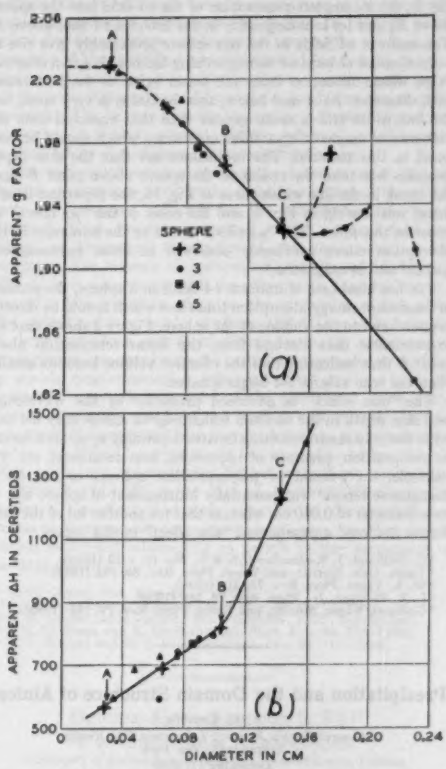

FIG. 2. The effect of sphere size on the magnetic energy absorption of a specimen of polycrystalline manganese-zinc ferrite.

The saturation magnetization (magnetic moment per gram at 0°K and infinite field) for the two specimens of Mg-ferrite in Table I having the same nominal composition but prepared at different temperatures is 41.1 and 29.3 respectively. One of us[1] has shown that they correspond to incompletely inversed ferrites. The magnitude of the g-factors obtained in these experiments indicates that the magnetic moment of Mg-ferrite and of the whole series of Mn-Zn ferrites is due almost entirely to the spin moments of the Fe^{+++} and Mn^{++} ions and that the contribution from the orbital moment is essentially zero in these materials. The fact that the g-factor and saturation moment[1] of Ni-ferrite are both considerably greater than the spin only values shows that the orbital moment contribution *is* important in Ni-ferrite. The g-factor of Co-ferrite could not be determined because of the extremely broad absorption line associated with its very high magnetic crystalline anisotropy.

The effect of sphere size on the apparent g-factor, line width, and magnetic energy absorption as determined from measurements on four spheres of a specimen of polycrystalline $Mn_{0.1}Zn_{0.9}Fe_2O_3$ is shown in Figs. 1 and 2. The observed behavior is at least qualitatively consistent with the hypothesis that the "size effect" is caused by one or more factors depending on the size of the test sphere relative to the wavelength and skin depth in the medium. The principal factors contributing to the "size effect" appear to be: (a) electromagnetic cavity-type resonance[2] above point C,

Fig. 1; (b) incomplete penetration of the r-f field into the sphere above B; and (c) inhomogeneity in the internal r-f field above A. Non-uniform r-f fields in the test sphere presumably give rise to a distribution of local r-f demagnetizing factors about an effective value whose deviation from the static value of $4\pi/3$ increases with diameter. At A and below, this deviation is very small but the line width still is much greater than that expected from the influence of magnetic crystalline anisotropy which should be very small in this material. The indications are that the skin depth becomes less than the radius of the sphere above point B since the break in the line width curve of Fig. 1b, the departure from a linear relationship in Fig. 2, and the onset of the "μ_R effect" all occur at this point. The "μ_R effect" refers to the minimum in the absorption curve previously observed in some ferromagnetic metals[3] and in magnetite.[4]

For the ideal case of uniform r-f fields in a sphere, the product of maximum energy absorption times line width should be directly proportional to the volume of the sphere. Figure 2 shows that the experimental data deviate from the linear relationship above point B thus indicating that the effective volume becomes smaller than the true volume for larger spheres.

The "size effect" is governed primarily by the wavelength and skin depth in the medium which may of course vary between wide limits in semiconducting ferrites depending upon such factors as composition, presence of impurities, heat treatment, etc. For example, the g-factor of polycrystalline spheres of one lot of manganese ferrite[5] was essentially independent of sphere size up to a diameter of 0.060 cm whereas that for another lot of the same ferrite disclosed a pronounced "size effect" in this region.

[1] C. Guillaud, J. Recherches C.N.R.S., No. 12, 1–10 (1950).
[2] Yager, Galt, Merritt, and Wood, Phys. Rev. 80, 744 (1950).
[3] W. A. Yager, Phys. Rev. 75, 316 (1949).
[4] L. R. Bickford, Jr., Phys. Rev. 78, 449 (1950).
[5] Guillaud, Yager, Merritt, and Kittel, Phys. Rev. 79, 181 (1950).

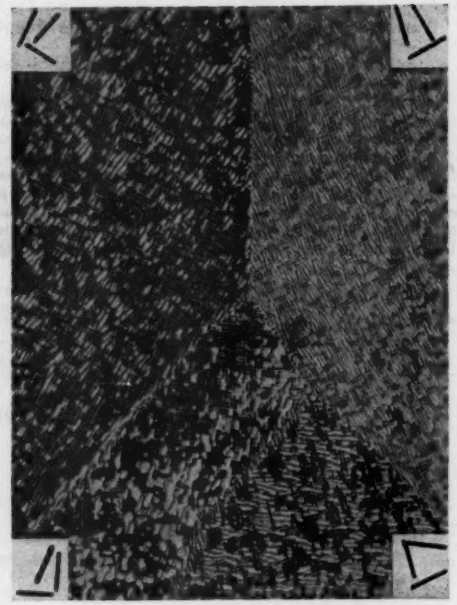

FIG. 1. Microstructure of Alnico 2 aged 300 hr at 800°C. ×500. Traces of the precipitate plates in the four crystals are indicated in the white squares at the corners.

Precipitation and the Domain Structure of Alnico 5

A. H. GEISLER
General Electric Research Laboratory, The Knolls, Schenectady, New York
December 11, 1950

THE good magnetic properties of many permanent magnet materials originate in the precipitation from solid solution of a ferromagnetic phase. In the Alnico alloys during the precipitation heat treatment plate-like particles of an iron-rich phase form in a matrix which becomes rich in the intermetallic compound NiAl. The particles are parallel to {100} planes of the parent matrix. Thus, they present a maximum of three trace directions in any one crystal on a polished and etched surface of the polycrystalline alloy as shown by Fig. 1.

Alnico 5 has the somewhat unique characteristic of exhibiting anisotropic properties when precipitation is initiated during cooling in a magnetic field. The residual induction is especially high in the direction of the field that is applied during cooling. Two years ago the author attributed this behavior to the preferential formation of precipitate particles on certain but not all of the three {100} planes.[1] Later Kittel, Nesbitt, and Shockley[2] showed that anisotropic properties are present immediately after the controlled cooling in the magnetic field and prior to the precipitation heat treatment. This indicates that the preferred orientation of nuclei is established during the cooling and that merely growth on these nuclei occurs during the subsequent aging treatment.

Kittel and his co-workers[2] attributed the preferred orientation to a minimum demagnetization energy for nuclei which have their surface closely parallel to the field direction. Recently, the author published further microscopic evidence that confirmed this expected preferred orientation: a single crystal which had been cooled with the field along the [001] direction and then reheated to 800°C and held for 16 hr to grow the precipitate

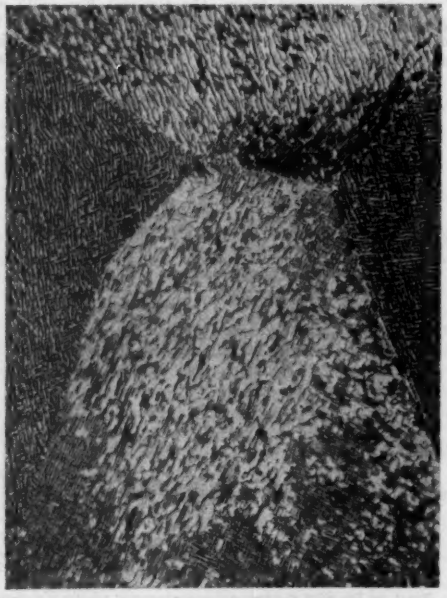

FIG. 2. Microstructure of Alnico 5 aged 300 hr at 800°C. ×500.

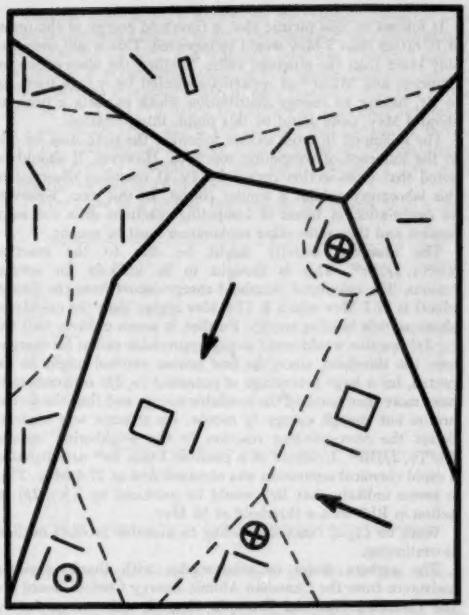

FIG. 3. Tracing of Fig. 2 showing crystal boundaries as heavy lines, approximate domain boundaries as broken lines, the traces of precipitate particles, and field direction in each domain of the largest crystal.

particles exhibited plates on (010) and (100) planes but none on (001) planes.[3] An elaboration of the author's theory that the magnetostriction energy of the matrix supplies part of the strain energy for nucleation of the favored orientations of the precipitate is included in the latter report.

Goldman and Smoluchowski[4] propose that the preferred orientations are those in which the direction of minimum strain energy due to magnetostriction is closely parallel to the field direction. From work on single crystals of Fe-Co alloys they show that the minimum magnetostriction in the precipitate would be expected to occur in ⟨100⟩ directions.

When an applied field is capable of influencing the precipitation process one would expect that the field due to spontaneous magnetization of the magnetic domains would promote a similar effect. The micrograph in Fig. 2 is presented as evidence for this effect. The micrograph is for Alnico 5 which had been oil quenched from the solution heat treating temperature and then aged for 300 hr at 800°C to grow the particles to a microscopically resolvable size. No external field had been applied during any part of the treatment. The micrograph shows that within each of the four crystals there are domains in which two of the three possible orientations of the precipitate predominate. The extent of the domains and the traces of the precipitate plates are sketched in Fig. 3. The direction of spontaneous magnetization in the domains can be determined by the criterion that the direction of the field must have been parallel to the two different orientations of precipitate plates. These directions have been designated in Fig. 3 for the largest crystal which has been sectioned with a (100) type plane approximately parallel to the plane of polish.

The non-uniform distribution of the precipitate in Fig. 2 is thus a manifestation of the magnetic domain structure of the matrix which has been revealed also by the usual powder technique.[5] In the presence of an applied field each crystal would be a single domain and those favored orientations of the precipitate would be nucleated throughout the crystal. In contrast to the macro-domain structure of the parent matrix, the micro-domain structure of the individual precipitate particles and the cooperative interaction between particles in the less ferromagnetic matrix are the more important considerations in producing the magnetic hardening. The increased residual induction provided by preferred nucleation most likely originates in the enhancement of particles in orientations of minimum demagnetization energy.

The main contribution of this note is the observation that the internal spontaneous fields in the domain structure of the matrix exert an important influence on the precipitation process in Alnico 5. Thus, the requirement of a high external field considered in theoretical treatments of the phenomenon is not necessary. The absence of preferential precipitation in Alnico 2 (Fig. 1) is in accordance with the observation that cooling in a magnetic field has little effect on the properties of this alloy. The author's theory would attribute the difference in behavior of these two alloys mainly to differences in the anisotropy of strain energy associated with the precipitation process as modified by matrix magnetostriction, whereas others[4] attribute it to differences in magnetic properties of the precipitate. Both alloys contain precipitate particles of a plate-like shape necessary for anisotropy of demagnetization energy; however, the spontaneous field in the Alnico 2 sample would be expected to be low, for the 800°C aging temperature is only 25° below the Curie temperature of Alnico 2 while 90° below that of Alnico 5. Metallographic studies of the effect of domain structure on the precipitation process at lower temperatures is now in progress, and they should provide additional information to permit further evaluation of the three theories.

[1] A. H. Geisler, Elec. Eng. **69**, 37 (1950).
[2] Kittel, Nesbitt, and Shockley, Phys. Rev. **77**, 839 (1950).
[3] A. H. Geisler, ASM Preprint No. 9 (October, 1950), unpublished.
[4] J. E. Goldman and R. Smoluchowski, Phys. Rev. **80**, 302 (1950).
[5] E. A. Nesbitt and H. J. Williams, Phys. Rev. **80**, 112 (1950).

Gamma-Alpha-Reaction in Rb^{87}

R. N. H. HASLAM AND H. M. SKARSGARD
University of Saskatchewan, Saskatoon, Saskatchewan, Canada
November 20, 1950

USING 100-Mev betatron x-rays, Baldwin and Klaiber[1] have obtained multiple photo-nuclear disintegrations in which alpha-particles were observed in cloud-chamber photographs to be ejected from nuclei. Gaerttner and Yeater[2] have also observed disintegrations in N and O which they believe may be due to (γ, α) reactions. To date the most extensive examination of (γ, α) processes has been carried out by the use of photographic emulsion techniques.[3-6] This letter describes a study of the (γ, α) processes by an entirely different method; namely, by the study of the activity in an unstable product nuclide.

Samples of $RbNO_3$ of 10 g were irradiated in the University of Saskatchewan betatron at peak energies ranging from 15 to 27.4 Mev. The samples were placed very close to the donut target for high dosage rates. Irradiation times ranged from a few minutes to several hours. Tantalum strips were used to monitor the dosage rate. The reaction $Ta^{181}(\gamma, n)Ta^{180}$ gives a pure 8.2-hr activity which has a low threshold and whose activation curve has been measured carefully in this laboratory.[6] After irradiation the active Br was extracted from $RbNO_3$ by precipitation with $AgNO_3$, and the resulting activity counted in standard geometry. For irradiation energies up to 27 Mev a pure 140-min activity, arising from Br^{82}, was observed. After appropriate corrections for geometry, self-absorption, back-scattering, etc., the activation curve of Fig. 1 was obtained. This shows the number of active atoms formed per minute per 100r per minute per Rb^{87} atom bombarded, as a function of maximum betatron energy. Here 100 percent efficiency of chemical separation has been assumed.

Analysis of the activation curve by a method described pre-

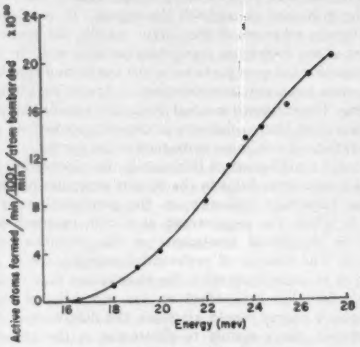

FIG. 1. Activation curve, $Rb^{87}(\gamma, \alpha)Br^{83}$.

viously[6] yields the cross-section curve reproduced in Fig. 2. This curve has a maximum at 22.5 Mev, a half-width of 6.6 Mev, and the integrated cross section is 4×10^{-4} Mev-barn. Presumably the reason that the cross section starts at a finite value is that a threshold has been assumed which is actually too high and consequently, near the threshold, activity which is actually due to photons of lower energy has been credited to photons of energy in the immediate vicinity of the apparent threshold. The observed threshold (16 Mev) may be considerably higher than the actual threshold. The experimental point at 16.5 Mev corresponds to a measured activity of only 1.5 counts/min above background of 32 counts/min over a two-hour counting period. The length of irradiation was 1.5 hr. To obtain points at lower betatron energies would have necessitated much longer irradiations than were thought feasible. The binding energy of the alpha-particle in Rb^{87} calculated from the Feenberg formula[7] in the form given by Stern[8] (with the obvious corrections) is only 5.3 Mev. The discrepancy between this value and the observed value is very large but it may be explained partially by the barrier effect. It should be expected that in order to compete with de-excitation by gamma-emission the half-life for alpha-emission must be of the order of 10^{-12} sec at the most. According to calculations based on the simple one-body theory of Bethe[9] the half-life for alpha-emission from Rb^{87} as a function of alpha-energy is as follows:

α-particle energy (Mev)	4	5	6	8
Half-life (sec)	3.8×10^{-10}	4.8×10^{-13}	2.8×10^{-15}	4.3×10^{-18}

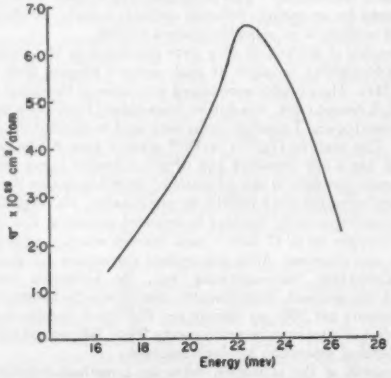

FIG. 2. Cross-section curve for the reaction $Rb^{87}(\gamma, \alpha)Br^{83}$.

It follows on this picture that a threshold energy of the order of 10 rather than 5 Mev would be expected. This is still considerably lower than the observed value. Further, the observation by Cameron and Millar[10] of α-particles ejected by γ-rays from Ag or Br, having an energy distribution which exhibits a peak at about 4 Mev, casts doubt on this simple interpretation.

The falling-off in cross section following the peak may be due to the influence of competing reactions. However, it should be noted that cross-section curves for (γ, n) reactions observed in this laboratory exhibit a similar course. In this case, however, an explanation in terms of competing reactions does not seem feasible and thus some other explanation must be sought.

The observed activity might be due to the reaction $Rb^{85}(\gamma, 2p)Br^{83}$. This is thought to be unlikely for several reasons. The calculated threshold energy (apart from the barrier effect) is 17.7 Mev which is 12.4 Mev higher than the calculated alpha-particle binding energy. Further, it seems unlikely that the $(\gamma, 2p)$ reaction would occur to any appreciable extent for energies near the threshold, since the first proton emitted might be expected, for a large percentage of potential $(\gamma, 2p)$ occurrences to have more than one-half the available energy and thus the second proton not enough energy to escape. An attempt was made to detect the corresponding reaction in the neighboring isotope, $Rb^{87}(\gamma, 2p)Br^{85}$. Evidence of a possible 3-min Br^{85} activity after a rapid chemical separation was obtained first at 27.4 Mev. Thus it seems unlikely that Br^{83} would be produced by a $(\gamma, 2p)$ reaction in Rb^{85} with a threshold at 16 Mev.

Work on (γ, α) reactions leading to unstable product nuclides is continuing.

The authors desire to acknowledge with thanks financial assistance from the Canadian Atomic Energy Control Board and the Canadian National Research Council, and several helpful discussions with Mr. A. G. W. Cameron.

[1] G. C. Baldwin and G. S. Klaiber, Phys. Rev. **70**, 259 (1946).
[2] E. R. Gaerttner and M. L. Yeater, Phys. Rev. **79**, 401 (1950).
[3] C. H. Millar and A. G. W. Cameron, Phys. Rev. **78**, 78 (1950).
[4] Hanni, Telegdi, and Zunti, Helv. Phys. Acta **21**, 203 (1948).
[5] Goward, Telegdi, and Wilkins, Proc. Phys. Soc. London **A63**, 402 (1950)
[6] Johns, Katz, Douglas, and Haslam, Phys. Rev. **80**, 1061 (1950).
[7] E. Feenberg, Revs. Modern Phys. **19**, 239 (1947).
[8] M. O. Stern, Revs. Modern Phys. **21**, 316 (1949).
[9] H. A. Bethe, Revs. Modern Phys. **9**, 161 (1937).
[10] A. G. W. Cameron, private communication.

The First Excited State of Be^7 from the $Li^7(p, n)Be^7$ Reaction*

HARVEY B. WILLARD AND WILLIAM M. PRESTON
Laboratory for Nuclear Science and Engineering, Massachusetts Institute of Technology, Cambridge, Massachusetts

November 20, 1950

THE existence of an excited state in Be^7 at about 430 kev has been confirmed by several methods: (a) the reaction[1-3] $B^{10}(p, \alpha)Be^7$, (b) the reaction[1] $Li^6(d, n)Be^7$, (c) scattering of neutrons from a $Li^7(p, n)Be^7$ source[4] by He, (d) photographic plate analysis of recoil protons from a $Li^7(p, n)Be^7$ neutron source.[5-6] Of these methods, (a) and (b) are the most accurate, the results[1] being 429 ± 5 kev from γ-ray measurements, and from magnetic analysis of α-particles,[2,3] 434 ± 5 and 431 ± 5 kev. Method (d) has shown the presence of a low energy neutron group with about ten percent of the total neutron intensity at bombarding energies $E_p = 2.7$ to 4.0 Mev (well above the expected threshold for the second group at 2.38 Mev).

With a thin target and a neutron counter subtending a small angle on the beam axis, the yield curve just above threshold shows a "geometrical peak"[7,8] due to forward concentration of neutrons in the laboratory reference frame. By taking advantage also of the greater sensitivity of a bare BF_3 counter for the low energy second group neutrons, it should be possible to detect the group at its threshold unless its relative intensity is very small. We are not aware that this has been done previously.[10]

Protons from the MIT Rockefeller electrostatic generator were used to bombard a thin Li target. The beam was bent magnetically and analyzed by slits. The magnetic field was stabilized and its magnitude H at one point measured by a proton resonance method which permits a reading accuracy on a standard oscillator of one part in 10^4. The $Li^7(p, n)Be^7$ threshold[11] at $E_p = 1.882$ was taken as a calibration point and it was assumed that the proton energy $E_p \propto H^2$. This relation has been checked so far only by measuring the $B^{11}(p, n)C^{11}$ threshold, which agreed within 2 kev with Richards' value[12] of 3.015 Mev.

Figure 1 shows a plot of the ratio of the counts from a one-

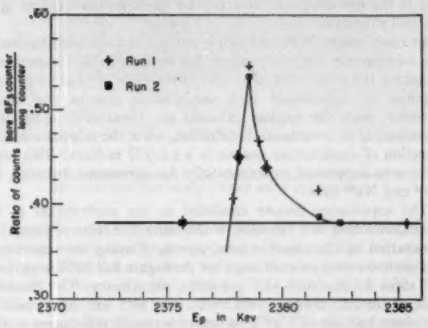

FIG. 1. Ratio of counts from a BF_3 counter to those from a "long counter."

inch diameter BF_3 counter, on the beam axis eight inches from the target and shielded by ½ inch of B_4C, to those from a paraffin moderated "long counter" whose efficiency is nearly independent of neutron energy.[13] The curve is flat in the neighborhood of the expected threshold except for the peak shown, which is attributed to the second neutron group. The measured threshold is 2.378 Mev and the Q value 2.081 Mev. From the ground state $Q = 1.647$ Mev, the excited state in Be^7 is at 434 kev. The statistical and reading errors appear to be within ±1 kev, but the extent of possible systematic errors in the calibration has not been explored. It is satisfactory to note that the eight determinations in the papers referred to above, as well as an additional photographic determination (unpublished) by P. Stelson of our group, all agree with this value within the authors' stated errors. The ratio of the height of the "geometrical peak" of the second group (above "background") to that of the corresponding first group peak is about 0.03.

* This work was jointly supported by the ONR and Bureau of Ships.
[1] T. Lauritsen and R. G. Thomas, Phys. Rev. 78, 88 (1950).
[2] Brown, Chao, Fowler, and Lauritsen, Phys. Rev. 78, 88 (1950).
[3] Van Patter, Sperduto, Strait, and Buechner, Phys. Rev. 79, 900 (1950).
[4] T. A. Hall, Phys. Rev. 77, 411 (1950).
[5] Johnson, Laubenstein, and Richards, Phys. Rev. 77, 413 (1950).
[6] J. C. Grosskreutz, Phys. Rev. 77, 580 (1950).
[7] B. Hamermesh and V. Hummel, Phys. Rev. 78, 73 (1950).
[8] Freier, Stratton, and Rosen, Phys. Rev. 79, 721 (1950).
[9] R. Taschek and A. Hemmendinger, Phys. Rev. 74, 373 (1948).
[10] Freier, Lampi, and Williams, Phys. Rev. 75, 901 (1949).
[11] Herb, Snowdon, and Sala, Phys. Rev. 75, 246 (1949).
[12] H. T. Richards, Phys. Rev. 77, 732 (1950).
[13] A. O. Hanson and J. L. McKibben, Phys. Rev. 72, 673 (1947).

Inelastic Scattering of Deuterons by C^{12}

K. K. KELLER, J. B. NIEDNER, C. F. WANG, AND F. B. SHULL
Physics Department, Washington University, St. Louis, Missouri*
December 4, 1950

A HEAVY-PARTICLE magnetic spectrometer has been used to determine the momentum distribution of deuterons scattered by thin carbon targets. The spectrometer produces a uniform field within an annular region which has approximately 84 cm mean diameter and 7 cm width. Charged particles which emerge from the target in a direction perpendicular to the incident beam are focused magnetically (180°) and fall at grazing incidence upon Ilford C-2 nuclear emulsions. Rapid and positive identification of particles is based on a combination of measured track lengths and experimental momentum ($H\rho$) values. A series of successive exposures with different magnetic fields permits examination of any desired range of momenta up to a maximum of about 6.5×10^5 gauss-cm.

Two types of carbon target were used. One was a 0.2-mil foil of Nylon, which contains mostly hydrogen and carbon, together with some nitrogen and oxygen. The other was a very thin foil of aluminum on which carbon is unavoidably deposited during bombardment. This carbon deposit apparently results from the use of oil diffusion pumps, despite the presence of a liquid nitrogen cold trap. A comparison of the proton spectra from the two targets indicates that little or no nitrogen or oxygen is included in the built-up deposit on the aluminum foil. No signs of $O^{16}(d, p)$ or $N^{14}(d, p)$ reactions were found for the aluminum target.

The carbon targets were bombarded by a collimated beam of 10-Mev deuterons from the Washington University cyclotron. Figure 1(a) shows the spectrum of deuterons scattered from the Nylon target. Three closely spaced groups at high momenta are deuterons scattered elastically by C^{12}, N^{14}, and O^{16}. The relative intensities of the three groups correspond roughly to the 6:1:1 atomic ratio (approx.) of these elements in Nylon. A fourth group of deuterons appears with momenta in the vicinity of 3.7×10^5 gauss-cm. These deuterons have been inelastically scattered by C^{12}, leaving the carbon nucleus in an excited state. It is evident from the width of this peak that the Nylon target is a "thick" one for the inelastic deuterons, whose energy (at 90°) is about 3.3 Mev. Poor resolution results from the rather large energy losses suffered by these slow deuterons as they emerge from the foil.

The inelastic peak was restudied using the aluminum-borne carbon deposit as a target. Figure 1(b) compares results from the two targets for this group. The momentum scale has been expanded for clarity. Some improvement in resolution has been produced through use of the thinner target, so that the inelastic peak now displays a low energy "tail" and somewhat resembles thick-source internal conversion peaks in beta-spectroscopy. If we assume the maximum intensity corresponds to scattering events

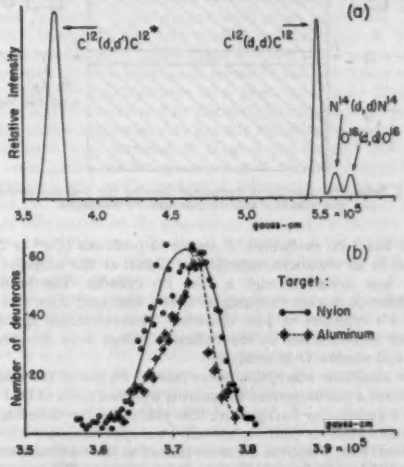

FIG. 1. (a) Momentum spectrum of deuterons scattered by a Nylon target. (b) Momentum distribution of deuterons scattered inelastically by C^{12}, two different targets compared.

which occurred near the front surface of the carbon deposit, the particle momentum is 3.73×10^8 gauss-cm. This leads to $Q=-4.41$ Mev for the inelastic scattering process, which compares favorably with figures quoted elsewhere[1] for the energy (relative to the ground state) of the lowest well-established excited state of C^{13}. The ratio of total intensities for the inelastic and elastic groups is roughly 2.0. No evidence was found for lower excited states of C^{13}.

* Assisted by the joint program of the ONR and AEC.

[1] W. F. Hornyak and T. Lauritsen, Revs. Modern Phys. 20, 191 (1948) have reviewed previous studies which lead to knowledge of the excited states of C^{13}.

The Angular Correlation of Photo-Electrons Ejected by Annihilation Quanta*

FRANK L. HEREFORD
University of Virginia, Charlottesville, Virginia
December 4, 1950

IT was first pointed out by Wheeler[1] that selection rules require that the polarization planes of two quanta emitted in the annihilation of slow positrons be orthogonal. A number of workers[2] have verified the expected cross polarization through coincidence detection of the quanta scattered from antiparallel beams of annihilation radiation at various azimuth angles. These data yield an asymmetry in the coincidence rate as the relative azimuthal orientation of the detecting counters is varied, the preferred scattering being in the planes containing the radiation beams and the electric vectors of the quanta.

Pryce and Ward[3] have suggested that the relative polarization states also could be determined through observation of the photo-electrons ejected by the quanta at various azimuths. In addition to providing a check on the results obtained by detection of the scattered quanta, this method yields information which was previously lacking on the directional distribution of photo-electrons produced by polarized quanta of relatively high energy (0.51 Mev).

By means of the scheme depicted in Fig. 1 the suggested experiment has been performed. A source of positrons (Cu^{64} or Na^{22}) sealed in an aluminum capsule was placed at the midpoint of a ¼-in. hole drilled through a 7-in. Pb cylinder. The beams of annihilation quanta emerging as shown impinged upon two thin wall Pb cylinders of ¼-in. diameter. Photo-electrons ejected in planes perpendicular to the radiation beams were detected by two end window G-M counters.

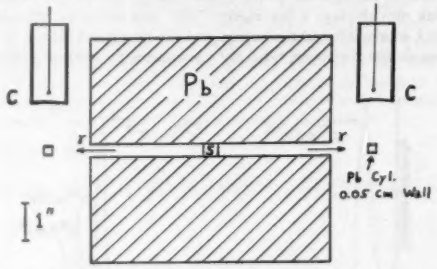

FIG. 1. Schematic drawing of apparatus showing the positron source (S), counters (C), and the thin wall Pb scatterers.

An aluminum absorption curve taken with one of the counters indicated a photo-electron component with end point at 0.51 Mev plus a gamma-ray background. The photo-electron counting rate with zero absorber (end window only) was approximately one-third the total rate. Compton electrons ejected at the minimum angle θ accepted by the finite half-span of the counter (20°) were of insufficient energy to penetrate the end window, and hence did not contribute to the observed counting rate. The majority of the background gamma-rays apparently were those penetrating the large Pb absorber rather than those scattered from the main radiation beams by the thin wall cylinders. This followed from the observation that, with a given orientation of the two counters, the coincidence rate dropped to approximately the cosmic-ray shower plus accidental coincidence background upon insertion of sufficient aluminum to absorb the 0.51-Mev photo-electrons. This apparent suppression of the gamma-gamma-coincidences was due to the fact that the ratio of photoelectric to Compton scattering cross sections for 0.51-Mev gamma-rays in Pb is about 1.3; to the small amount of material presented by the thin wall cylinders; and to the low detection efficiency for gamma-rays incident upon the end windows.

In cases where Na^{22} was employed, a possible contribution to the coincidence rate was present due to the 1.3-Mev gamma-ray following the beta-transition. The probability of observing these gammas in coincidence with annihilation quanta was small, however, since the nuclear gammas are presumably spherically symmetrical in directional distribution, while the relative emission direction of annihilation quanta is $\pi\pm1/137$ radians.[4] This argument was supported experimentally by agreement between the Cu^{64} and Na^{22} data.

The experiment proper consisted in the observation of the coincidence rate as a function of the minimum relative azimuthal orientation of the counter axes, $\phi_2-\phi_1$. During the experiment the counters were rotated together through a full 360° in periodic 90° steps to eliminate any geometric asymmetry. The resolving time of the coincidence circuit was 1.7×10^{-7} sec. As a result of the short half-life of Cu^{64} and source strength differences a wide range of total and accidental coincidence rates were involved. Table I shows the collected data with the genuine coincidence rates normalized to a common source strength. The combined accidental, shower, and gamma-gamma-rates were generally less than one-half of the total rate. The significant aspects of the results involve $C_\perp/C_\parallel$ and are discussed in the following letter. The low coincidence rate at 36° cannot be considered real and is being checked along with other intermediate angles.

TABLE I. Counting rate of genuine coincidences.

$\phi_2-\phi_1$	Coincidences/min	$C_\perp/C_\parallel$
0°	0.33 ±0.019	1.94 ±0.14
90°	0.64 ±0.020	
36°	0.31 ±0.04	
54°	0.43 ±0.03	

The author is indebted to Dr. P. H. Abelson of the Department of Terrestrial Magnetism for supplying the Na^{22}.

* Supported in part by Navy Bureau of Ordnance.
[1] J. A. Wheeler, Ann. N. Y. Acad. Sci. 48, 219 (1946).
[2] E. Bleuler and H. L. Bradt, Phys. Rev. 73, 1398 (1948); R. C. Hanna, Nature 162, 332 (1948); C. S. Wu and I. Shaknov, Phys. Rev. 77, 136 (1950).
[3] M. H. L. Pryce and J. C. Ward, Nature 160, 435 (1947).
[4] DeBenedetti, Cowan, Konneker, and Primakoff, Phys. Rev. 77, 205 (1950).

The Radioactive Decay of I^{131}

J. M. CORK, W. C. RUTLEDGE, A. E. STODDARD, C. E. BRANYAN, AND W. J. CHILDS
University of Michigan, Ann Arbor, Michigan*
December 11, 1950

SPECTROMETRIC studies have been continued in an effort to clarify the currently conflicting information[1] relative to radioactive emission of I^{131}, now so widely used in medicine. Sufficiently strong samples have been employed to make an exhaustive search for previously unreported gamma-rays, and by successive exposures to determine the half-life associated with each gamma-ray. The upper energy limits of the two components of the beta-spectrum have also been redetermined by a double-focusing magnetic spectrometer.

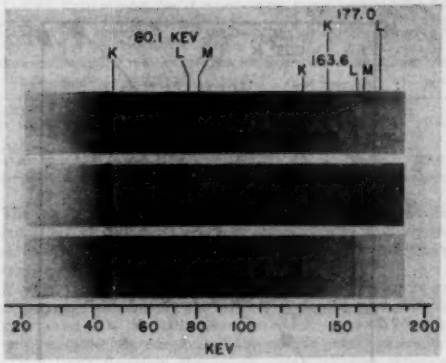

FIG. 1. Successive exposures showing the increased darkness of electron lines due to the 12-day 163.6 gamma-ray.

Using the reported[3] energies of three of the gamma-rays, as measured in a crystal spectrometer by DuMond and his associates, as a calibration standard, the gamma-energies are now found to be: 28.0 (Auger X), 80.1, 163.6, 177.0, 284.1, 364.2, 637, and 723 kev. In every case the conversion electron lines have *K-L* differences characteristic of xenon. The 723-kev gamma-ray, whose conversion electrons were about half as abundant as those for the 637-kev gamma, has not been previously reported.

All gamma-rays except the 163.6 kev are found to decay with a half-life of 8 days. The 163.6-kev gamma-ray has a longer half-life as shown in Fig. 1 and is presumably associated with a 12-day metastable state in xenon as found to exist by Brosi, De Witt, and Zeldes. Figure 1 shows successive exposures for the energy region 20 to 190 kev, with the time of each of the three exposures adjusted so that the electron lines associated with an 8-day half-life should appear equally dark on successive photograms. Electron lines associated with the longer 12-day half-life should then appear relatively stronger in the later exposures. It is evident that the *K*, *L*, and *M* lines for the 163.6-kev gamma-ray do appear to grow stronger relative to the neighboring electron lines of comparable intensity caused by the 177-kev gamma-ray. The upper limits of the two beta-distributions are found to be 600±3 kev and 305±10 kev.

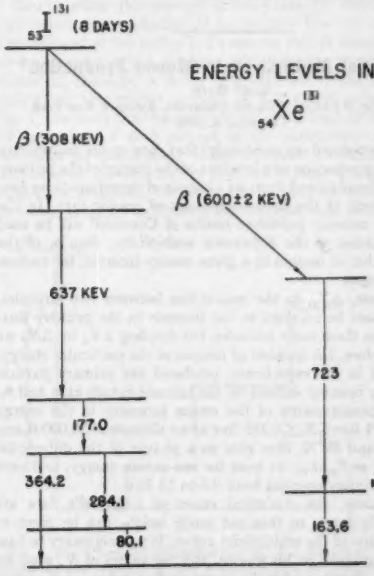

FIG. 2. Possible decay scheme for I^{131}.

It is of interest that these known energies can be accommodated by a level scheme as shown in Fig. 2 in which a branching occurs with exactly the same over-all energy in each branch. While this proposed scheme appears to be highly satisfactory energetically and can also be reconciled with present coincidence measurements, it does not satisfy observations on the relative intensities. The more abundant 600-kev beta-transition is in sequence with the less copious 723-kev gamma-emission and the less intense 305-kev beta is followed by the more intense gamma-emissions. Also, the metastable state in xenon is considered as following the 723-kev gamma-ray since the half-life of this gamma-ray is 8 days. Any alternate scheme must allow isomers of different energy for the parent isotope.

Observations of the beta-spectrum were made by Dr. E. Salmi and will be presented elsewhere.

* This investigation was made possible by the joint support of the AEC and ONR.

[2] G. Tape and J. Cork, Phys. Rev. 53, 676 (1938); J. Livingood and G. Seaborg, Phys. Rev. 54, 775 (1938); F. Metzger and M. Deutsch, Phys. Rev. 74, 1640 (1948); Owen, Moe, and Cook, Phys. Rev. 74, 1879 (1948); Brosi, De Witt, and Zeldes, Phys. Rev. 75, 1615 (1949); Cork, Keller, Sazynski, Rutledge, and Stoddard, Phys. Rev. 75, 1621 (1949); Kern, Mitchell, and Zaffrano, Phys. Rev. 76, 94 (1949); and I. Feister and L. Curtiss, Phys. Rev. 78, 179 (1950).

[3] Lind, Brown, Klein, Muller, and DuMond, Phys. Rev. 75, 1544 (1949).

Magnetic Structure of Magnetite and Its Use in Studying the Neutron Magnetic Interaction

C. G. SHULL, E. O. WOLLAN, AND W. A. STRAUSER
Oak Ridge National Laboratory, Oak Ridge, Tennessee
December 8, 1950

THE interaction of the magnetic moment of a neutron with the atomic magnetic moments existing in magnetic substances has been shown by Bloch,[1] Schwinger,[2] and Halpern and Johnson[3] to give rise to scattering effects comparable in magnitude to those produced by the nuclear short range interaction. This magnetic interaction has been studied experimentally in ferromagnetic substances by means of the so-called single and double-transmission types of experiments for which the most noteworthy and complete descriptions have been given recently by Hughes, Wallace, and Holtzman[4] and by Fleeman, Nicodemus, and Staub.[5] Further studies performed with neutron reflection by magnetized mirrors have been discussed by Hughes and Burgy.[6] We have been investigating the Bragg scattering of neutrons produced by paramagnetic and antiferromagnetic substances and by unmagnetized and magnetized ferromagnetic substances and these have yielded information on the magnetic structure of the samples and on the magnitude and directional properties of the interaction which exists between the neutron's magnetic moment and the atomic magnetic moment.

A study of the magnetic scattering properties of Fe_3O_4 is of interest in that (a) it gives a direct check on the magnetic structure and (b) that its magnetic properties make it very favorable for use in studying the directional properties associated with the magnetic scattering of neutrons. This oxide is a member of the ferrite series and is ferromagnetic. Néel has suggested the magnetic structure to be of *ferrimagnetic* type,[7] that is, that some of the ferrous and ferric ions which make up the lattice are coupled antiferromagnetically. On this picture the balancing of the parallel and antiparallel moments is not complete and Néel has been able to explain quantitatively the resultant ferromagnetism of the lattice. Neutron diffraction studies have been made on several

samples of Fe_3O_4, principally on a very pure powder sample kindly furnished by Professor A. von Hippel. The neutron intensities are sensitive to both the magnetic structure and the chemical crystallographic structure and the observed pattern agrees excellently with that calculated on the basis of Néel's model.

On the basis of this structure the neutron diffraction pattern for Fe_3O_4 gives a (111) reflection which arises almost wholly from magnetic scattering with only about two percent nuclear scattering contribution. This very interesting property of this reflection can be used in studying the directional effects of scattering when the sample is magnetized. Halpern and Johnson[2] have given for the intensity of scattering of unpolarized neutrons by a ferromagnetic material

$$I = b(C^2 + q^2 D^2)$$

with C the nuclear scattering amplitude, D the magnetic scattering amplitude, and b a proportionality constant. The term q^2 is a function of the angle α between the scattering vector and the magnetization vector and is given as $\cos^2\alpha$ in the original theory developed by Bloch[1] and as $\sin^2\alpha$ in the later treatment of Schwinger[2] and Halpern and Johnson.[2] The angular function depends on the assumed form of the magnetic interaction of the neutron with the magnetic medium. This can be related to the question of whether the neutron is affected by H or B on the average in the magnetic medium. Bloch[8] and Ekstein[9] have discussed this angular dependence and although they express themselves in conversation as expecting the Schwinger treatment to be correct, they both suggest that the selection of one or the other, or possibly a composite of the two interactions, should be left to experiment. With this in mind, the (111) powder diffraction ring of Fe_3O_4 was investigated when the sample was magnetized in different directions with typical results shown in Fig. 1. When

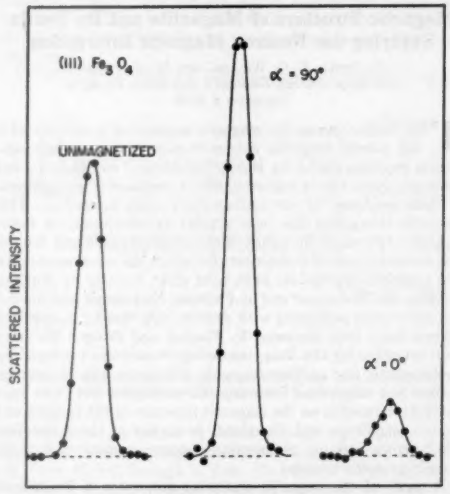

FIG. 1. Effect of sample magnetization in different directions upon the (111) Fe_3O_4 neutron diffraction peak.

$\alpha = 90°$, the intensity has increased over that for the unmagnetized sample and when $\alpha = 0°$, the intensity falls to a very low value. After correcting the intensities for residual nuclear scattering and second-order contaminant (of half-wavelength), values of q^2 have been evaluated for several angles with the result shown in Fig. 2. Within the experimental uncertainty of perhaps two percent the agreement with the Schwinger-Halpern-Johnson theory is quite satisfactory.

The pronounced dependence of neutron scattering intensity

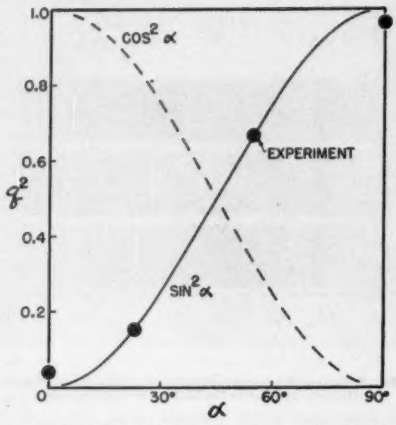

FIG. 2. Variation of q^2 with the angle α between the scattering and magnetization vectors. The experimental points have been normalized to the unmagnetized value of $q^2 = 2/3$.

with magnetization direction suggests that this reflection might have interesting application as a fast neutron shutter. In a single crystal reflection large neutron currents are attainable and rapid field variations with the small fields required for saturation of single crystals can be achieved in this or other members of the ferrite series.

[1] F. Bloch, Phys. Rev. 50, 259 (1936).
[2] J. S. Schwinger, Phys. Rev. 51, 544 (1937).
[3] O. Halpern and M. H. Johnson, Phys. Rev. 55, 898 (1939).
[4] Hughes, Wallace, and Holtzman, Phys. Rev. 73, 1277 (1948).
[5] Fleeman, Nicodemus, and Staub, Phys. Rev. 76, 1774 (1949).
[6] D. J. Hughes and M. T. Burgy, Phys. Rev. 76, 1413 (1949).
[7] L. Néel, Ann. phys. 3, 137 (1948).
[8] F. Bloch, Phys. Rev. 51, 994 (1937).
[9] H. Ekstein, Phys. Rev. 76, 1328 (1949).

Differential Multiplicity in Meson Production*

KURT SITTE
Department of Physics, Syracuse University, Syracuse, New York
December 6, 1950

IT has been pointed out previously[1] that data on the multiplicity of meson production as a function of the energy of the primary particle can be obtained from an analysis of experiments on geomagnetic effects of the hard component of cosmic rays. In the present note recently published results of Conversi[2] will be used for an evaluation of the *differential multiplicity;* that is, of the average number of mesons in a given energy interval, for various primary energies.

The increase, ΔN_μ, in the meson flux between two latitudes, θ_1 and θ_2, must be ascribed to the increase in the primary flux, ΔN_p, between these same latitudes. On dividing ΔN_μ by ΔN_p we obtain, therefore, the number of mesons of the particular energy, E_μ, recorded in the experiment, produced per primary particle of the energy interval defined by the latitude cutoffs at θ_1 and θ_2. Conversi's measurements of the meson intensity in the energy interval $0.224\ \text{Bev} \leq E_\mu \leq 0.255\ \text{Bev}$ at an altitude of 30,000 ft and between 9° and 59°N, thus give us a picture of the differential multiplicity, $m(E_\mu, E_p)$, at least for one meson energy, and over a range of primary energies from 0.5 to 14 Bev.

Unfortunately, the statistical errors of Conversi's data are comparatively large, so that not much weight can be given to the exact shape of the multiplicity curve. It was necessary to base the present analysis on his graphs, and the values of N_μ used are summarized, together with the corresponding values of N_p taken from the paper of Winckler *et al.*[3] in Table I.

TABLE I. Total number, N_μ, of mesons in the energy interval $0.224\ \text{Bev} \leq E_\mu \leq 0.255\ \text{Bev}$ (from Table III and Fig. 2 of reference 2), and total vertical primary intensity N_p near the top of the atmosphere (reference 3) as a function of the geomagnetic latitude.

Latitude	0°	15°	30°	45°	60°
$N_\mu \times 10^5$ $(\text{cm}^2\ \text{sec sterad Mev})^{-1}$	1.97	2.07	2.59	3.32	3.73
$N_p \times 10^2$ $(\text{cm}^2\ \text{sec sterad})^{-1}$	2.6	2.8	4.5	11.5	29.0

The values of $\Delta N_\mu / \Delta N_p$ are shown in Fig. 1 as a function of the primary energy. While the absolute values may be seriously inaccurate, the increase in the multiplicity with increasing primary energy cannot be doubted.

However, the number of mesons produced per incident primary does not represent directly the number of mesons produced per collision, and it is the latter quantity which one would like to determine. Obviously our method favors high energy primaries; they may be able to retain, after one or several collisions, sufficient energy for further meson production. Moreover, their secondaries might also contribute, so that the actual variation of the multiplicities with the primary energy in the region shown above may be considerably smaller than the factor of about 20 indicated in Fig. 1. Still, the corrections do not invalidate the conclusions drawn. The contribution due to shower secondaries can be shown to be very small, and it follows then that also the later collisions of the primaries account for only a fraction of all the mesons produced.

To get a rough estimate of the contribution of the secondaries, we observe first from Fig. 1 that particles of energies below, say, 1 Bev are very inefficient in the production of hard-component mesons. We note, next, that the average multiplicity of relativistic secondaries to primaries of 12 to 14 Bev colliding with air nuclei is not very high; a figure between 4 and 6 is certainly not an underestimate (see Salant *et al.*[6]). We recall, finally, that the energy spectrum of shower secondaries, observed by Rochester and Butler[5] on their predominantly positive particles, shows only 2 out of 16 measured particles with a momentum exceeding 2 Bev/c, while the average primary energy selected in their experiment was probably 10 to 20 Bev (see the estimates of Piccioni[8] and of the author[7]). To assume that in these collisions in air an average of 1.5 particles with energies above 1 Bev are ejected is, therefore, a rather high estimate. Using for the multiplicity at this energy a value of 0.25×10^{-4} as suggested by Fig. 1, one finds that the secondaries of the first collision account for only about 7 to 8 percent of the multiplicity of 5.0×10^{-4} computed for the highest energy interval. Evidently, the contributions of the secondaries from subsequent collisions become completely negligible. The primaries themselves, descending with an energy reduced to about ½ per collision, will become entirely inefficient in about 4 collisions. It follows that, if their multiplicity remained constant during the energy-degrading descent, the observed number of mesons could increase by as much as a factor of about 4, while the actual increase is about 4 to 5 times larger. In order to account for the experimental data, one must thus demand a rather strong energy dependence of the differential multiplicity, even for the comparatively low meson energies recorded in Conversi's experiment.

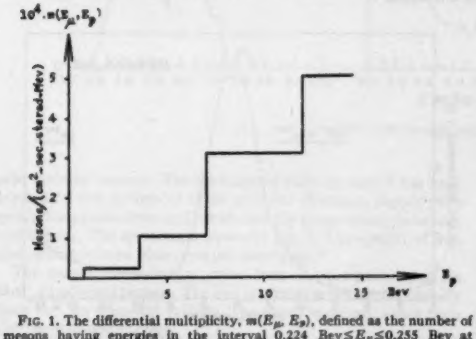

FIG. 1. The differential multiplicity, $m(E_\mu, E_p)$, defined as the number of mesons having energies in the interval $0.224\ \text{Bev} \leq E_\mu \leq 0.255$ Bev at 30,000 ft, produced per primary of energy E_p.

It should be noted that the values N_μ in Table I are not the total number of mesons produced, but the number of mesons reaching the 30,000-ft level. Corrections for decay in flight, analogous to the calculations of Sands,[8] can be made, based on specific assumptions on the "production spectrum" of the mesons. As it is doubtful whether an identical spectrum should be used for all primary energies, the calculations will not be reproduced here, but it is of interest to note that the total number of relativistic mesons computed in this manner, assuming Sands' production spectrum, for primaries of approximately 4 to 5 Bev (near 45°) is very small; less than 0.5 per incident primary.

* Supported in part by the AEC.
[1] K. Sitte, Phys. Rev. 79, 204 (1950); APS Washington Meeting 1950.
[2] M. Conversi, Phys. Rev. 79, 749 (1950).
[3] Winckler, Stix, Dwight, and Sabin, Phys. Rev. 79, 656 (1950).
[4] Salant, Hornbostel, Fisk, and Smith, Phys. Rev. 79, 184 (1950).
[5] G. D. Rochester and C. C. Butler, Proc. Phys. Soc. London 61, 535 (1948).
[6] O. Piccioni, Phys. Rev. 77, 1 (1950).
[7] K. Sitte, Phys. Rev. 78, 714 (1950).
[8] M. Sands, Phys. Rev. 77, 180 (1950).

The Disintegration of As^{77}

ROBERT CANADA AND ALLAN C. G. MITCHELL*
Physics Department, Indiana University, Bloomington, Indiana
December 11, 1950

As^{77} has a period[1,2] of 40 hr and is formed from the decay of both isomers[1,2] of Ge^{77}, *viz.*, the 59-sec and the 12-hr. Since a metastable state of Se^{77} exists,[3-5] whose period is 17.5 sec, there is always the possibility that the beta-ray transition of As^{77} might lead to the metastable rather than the ground state of Se^{77}. Mandeville, Woo, Scherb, Keighton, and Shapiro[6] state that As^{77} emits no gamma-rays. The beta-ray end point, measured by absorption, is given[7] as 0.8 Mev. Nordheim,[8] on the basis of the shell model, classifies the beta-ray transition of As^{77} as $p_{3/2} - p_{1/2}$ on the assumption that the transition is to the metastable rather than the ground state of Se^{77}. Since the transitions of As^{77} are important in order to give information on the correctness of the shell model, the radiations of As^{77} have been investigated.

A source of Ge^{77} containing its daughter As^{77} was obtained by the irradiation of GeO_2 in the Oak Ridge pile for one month. The arsenic was separated from the germanium by a procedure similar to that of Arnold and Sugarman,[2] in which $GeCl_4$ in HCl solution was distilled in an atmosphere of chlorine. The remaining arsenic was reduced to $AsCl_3$ and distilled from an HCl solution. Finally, the arsenic was precipitated as sulfide and sources were prepared from this material.

A beta-ray source of As^{77} was prepared and investigated in a magnetic lens spectrometer. Particular care was taken to search for internal conversion lines which might be attributed to Se^{77m}. *No internal conversion lines were found.* A Fermi plot was made of the data from the beta-ray spectrum and the results are shown in Fig. 1. The end point comes at 0.700 ± 0.007 Mev and the spectrum appears to have an allowed shape.

In addition an absorption curve was taken on a source of As^{77} and no internal conversion lines or gamma-rays were found.

From the results of these experiments it is clear that As^{77} is not the parent of Se^{77m} and that the transition takes place from the ground state of As^{77} to the ground state of Se^{77}. The value of $\log_{10}(ft)$ is 6.1.

The results of this experiment are of interest in the light of the shell model. Mayer[9] points out that for N or Z lying between 29 and 37 spins of 3/2 are measured for every odd number with

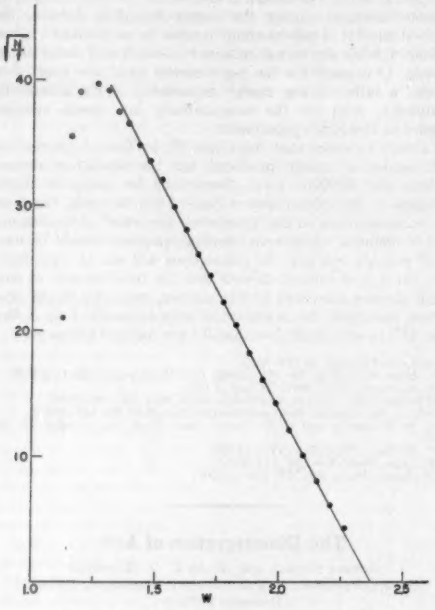

FIG. 1. Fermi plot of beta-ray spectrum of As^{77}.

the exception of $_{37}Rb^{85}$ and $_{30}Zn^{67}$ which show $f_{5/2}$ orbits. For example $_{33}As^{75}$ has a spin of 3/2 and it is presumed that the odd proton is in a $p_{3/2}$ orbit. On these grounds it is supposed that $_{33}As^{77}$ will likewise have a configuration $p_{3/2}$. In the region from 38 to 50, $p_{1/2}$ and $g_{9/2}$ configurations have nearly the same energy. For example $_{32}Ge^{73}$ has a $g_{9/2}$ orbit and spin of 9/2. If one assumes that As^{77} is a $p_{3/2}$ configuration, these experiments show that the ground state of $_{34}Se^{77}$ is $p_{1/2}$ rather than $g_{9/2}$. This follows since no internal conversion line is seen and the *ft*-value indicates an allowed transition. The evidence on the spin of Se^{77} is confusing.[10] There is conflicting evidence showing a spin of 1/2 or one of 7/2. The present experiments lend support to the view that in Se^{77} the $p_{1/2}$ state lies lower than the $g_{9/2}$ state.

The authors wish to thank Messrs. Alan B. Smith and William H. Cuffey for assistance with the measurements and Miss Elma Lanterman for making the chemical separations.

* This research was assisted by the joint program of the ONR and AEC.
[1] Steinberg, Winsberg, and Engelkemeier, as reported in reference (S151) Seaborg and Perlman, Revs. Modern Phys. 20, 585 (1948).
[2] J. R. Arnold and N. Sugarman, J. Chem. Phys. 15, 703 (1947).
[3] Gideon, Miller, and Waldman, Phys. Rev. 75, 329 (1949).
[4] M. Goldhaber and C. O. Muehlhause, Phys. Rev. 74, 1248 (1948).
[5] E. Segré and A. C. Helmholz, Revs. Modern Phys. 21, 271 (1949).
[6] Mandeville, Woo, Scherb, Keighton, and Shapiro, Phys. Rev. 75, 1528 (1949).
[7] G. T. Seaborg and I. Perlman, Revs. Modern Phys. 20, 585 (1948).
[8] L. W. Nordheim, "Tables for beta-decay systematics," privately circulated.
[9] M. G. Mayer, Phys. Rev. 78, 16 (1950).
[10] J. E. Mack, Revs. Modern Phys. 22, 64 (1950).

The Neutron Capture Cross Section of Am^{241}

G. C. HANNA, B. G. HARVEY, AND N. MOSS
Atomic Energy Project, National Research Council of Canada, Chalk River, Ontario, Canada
December 14, 1950

THE 16-hr Am^{242} (Am^{242m}) produced by neutron capture in Am^{241} decays by β-emission to Cm^{242}, by orbital electron-capture to Pu^{242}, and by an isomeric transition to a long-lived ground state (Am^{242} g.s.). Presumably Am^{242} g.s. may also be formed directly. Although a tentative decay scheme of Am^{242m} has recently been published,[1] the relative amounts formed of the various end products are not known accurately.

In a series of irradiations in the NRX pile we have measured the amount of curium produced and, for two of the samples, the amount of americium destroyed.

The samples of Am^{241} for irradiation were deposited on disks of aluminum by evaporation in vacuum from a tantalum filament. Thus, thin deposits were obtained, so that the amount of Am^{241} before and after the irradiation, and the amount of Cm^{242} formed, could be measured accurately by α-pulse analysis, using a low geometry proportional α-counter[2] and a 30-channel pulse analyzer. Since the α-activity of Cm^{242} after the heavier irradiations was about 100 times as great as that of the Am^{241}, accurate estimations of the latter could be achieved in only very thin sources. A typical α-pulse analysis is shown in Fig. 1.

The amount of Am^{241} destroyed was measured with any precision for only the two most heavily irradiated samples (Nos. 3 and 7), since only these would give results of sufficient accuracy. In all cases the Cm^{242} produced was measured and compared with the initial Am^{241} activity.

The measurement of the residual Am^{241} was complicated by the formation of Pu^{238} from the decay of Cm^{242}. The α-particles of Pu^{238} are almost identical in energy with those of Am^{241}; and, therefore, a correction for Pu^{238} has to be made.

A comparison of the Cm^{242} produced with the Am^{241} destroyed gives a value for f, the ratio of the partial cross section of Am^{241} for Cm^{242} production to the total cross section σ_1 for Am^{241} destruction. No knowledge of the neutron flux during the irradiation is required for this estimation of f. Samples 3 and 7 gave values of f equal to 0.66 and 0.62, respectively. The amounts of Am^{241} destroyed were 18 and 25 percent for these two samples, while the Pu^{238} corrections were 15 and 30 percent of the Am^{241} disintegration rates, respectively. Weighing these two results equally gives a value of 0.64 for f. The various errors which may accumulate are difficult to assess, but we feel that this value is correct within ± 10 percent.

By measuring the Cm^{242} produced in all the samples, we obtain a value for the partial cross section of Am^{241} for curium production, i.e., $f\sigma_1$, using the known integrated neutron flux for each sample. This was obtained from the pile operating log and the absolute neutron flux distribution in the pile.[3] The values of the partial cross section are given in Table I. The mean value is 568 barns. The deviations from the mean are within the over-all experimental error, and the absence of any trend toward lower values at high irradiation levels demonstrates that there is no appreciable neutron destruction of Cm^{242}.

This value of $f\sigma_1$, combined with the value of f obtained above, gives for σ_1, the total cross section for Am^{241} destruction, a value of 887 barns.

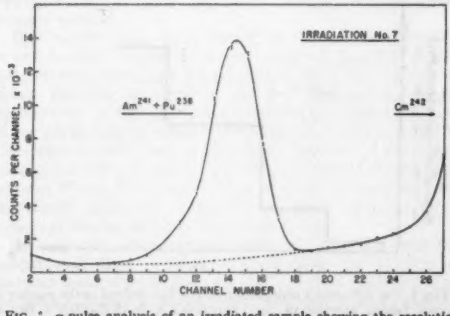

FIG. 1. α-pulse analysis of an irradiated sample showing the resolution obtained between the $Am^{241}+Pu^{238}$ α-group and a Cm^{242} α-group of about 80-fold greater intensity.

TABLE I. Evaluation of the partial cross section for the production of Cm^{243}.
(Mean value $f\sigma_1 = 568$ barns.)

Sample No.	Integrated flux $\int(\rho s)dt$ (10^{25} neutrons/cm^2)	$f\sigma_1\int(\rho s)dt$ from Cm^{243} production	$f\sigma_1$ (barns)	Percent deviation from mean
7	3.24	0.180	555	−2.1
3	2.12	0.123	580	+2.2
6	1.27	0.071	560	−1.3
5	0.365	0.0212	580	+2.1
4	0.162	0.00911	562	−0.9

If no Am^{242} g.s. is formed directly, that is, without intermediate formation of 16-hr Am^{242m}, then f will be identical with b, the β-branching ratio of Am^{242m}. A value of about 0.6 for b has been reported;[1] that is, b and f are approximately equal. This suggests that little, if any, Am^{242} g.s. is formed directly.

It is a pleasure to acknowledge our debt to Mr. Philip B. Aitken for the design of equipment used in the handling of large α-activities.

[1] O'Kelley, Barton, Crane, and Perlman, Phys. Rev. 80, 293 (1950).
[2] Hanna, Harvey, and Moss, Phys. Rev. 78, 617 (1950).
[3] B. W. Sargent, Chalk River Report CRP-403, unpublished.

Odd-Even Effect in Neutron Capture Gamma-Ray Spectra

BERNARD HAMERMESH
Argonne National Laboratory, Chicago, Illinois
November 20, 1950

ADDITIONAL evidence has been obtained showing the dependence of the shapes of the neutron capture gamma-ray spectra on the odd-even character of the compound nuclei formed after neutron capture. The D_2O-soaked plate method[1,2] has been applied to two groups of three adjacent elements, namely, the group manganese, iron, and cobalt and the group silver, cadmium, and indium. The spectra are shown in Fig. 1. The spectra of iron and cadmium have been reported previously.[2]

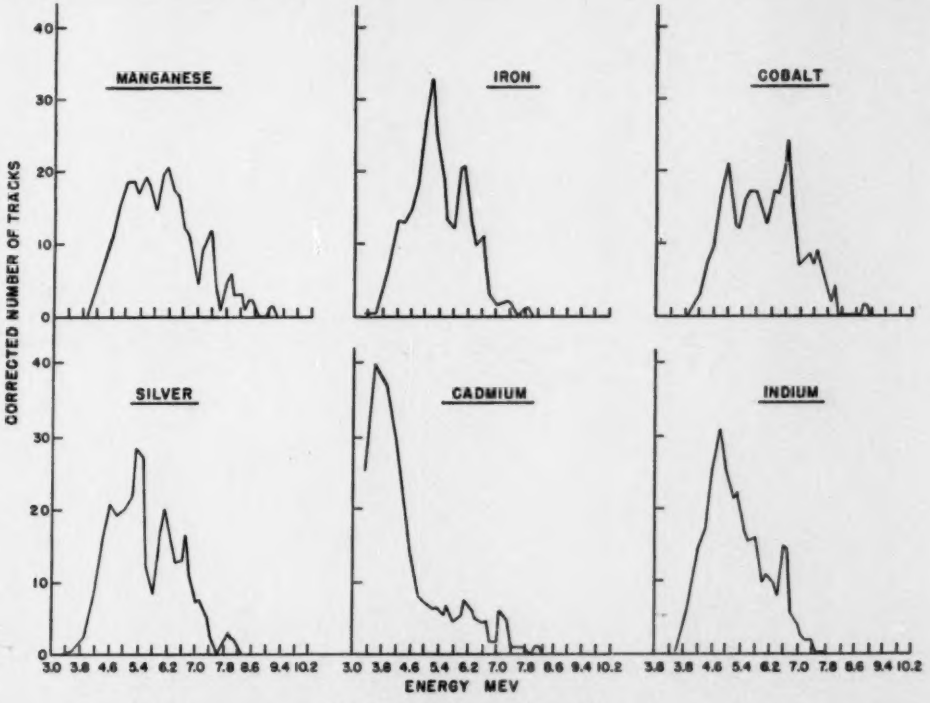

FIG. 1. Neutron capture gamma-ray spectra.

The manganese spectrum arises from the compound nucleus Mn^{56}, an odd-odd nucleus. The iron spectrum arises almost entirely from Fe^{59}, an even-odd nucleus. The cobalt spectrum arises from Co^{60}, an odd-odd nucleus.

The silver spectrum arises from Ag^{108} and Ag^{110}, both odd-odd nuclei. The cadmium spectrum is emitted by Cd^{114}, an even-even nucleus. The indium spectrum is emitted mainly by In^{116}, an odd-odd nucleus.

The evidence shown indicates that in elements of nearly the same Z, the mode of decay from the highly excited state formed on thermal neutron capture is different in nuclei of differing odd-even types. This would indicate a possible dependence of level spacings on odd-even characteristics of nuclei.

[1] B. Hamermesh, Phys. Rev. 76, 182 (1949).
[2] B. Hamermesh, Phys. Rev. 80, 415 (1950).